Ultrasound for Interventional Pain Management

An Illustrated Procedural Guide

Philip Peng
Roderick Finlayson
Sang Hoon Lee
Anuj Bhatia
Editors

Springer

Ultrasound for Interventional Pain Management

Philip Peng • Roderick Finlayson
Sang Hoon Lee • Anuj Bhatia
Editors

Ultrasound for Interventional Pain Management

An Illustrated Procedural Guide

Springer

Editors
Philip Peng
Department of Anesthesia and Pain Management
Toronto Western Hopsital and Mount Sinai Hospital, University of Toronto
Toronto, Ontario
Canada

Sang Hoon Lee
Madi Pain Management Center
Jeonju, Republic of Korea

Roderick Finlayson
Alan Edwards Pain Management Unit, McGill University Health Centre
Montreal, Quebec
Canada

Anuj Bhatia
Department of Anesthesia and Pain Management
Toronto Western Hopsital and Mount Sinai Hospital, University of Toronto
Toronto, Ontario
Canada

ISBN 978-3-030-18370-7 ISBN 978-3-030-18371-4 (eBook)
https://doi.org/10.1007/978-3-030-18371-4

This Springer imprint is published by the registered company Springer Nature Switzerland AG
The registered company address is: Gewerbestrasse 11, 6330 Cham, Switzerland

This book is dedicated to my wife, Carol, for her continued support, encouragement, and understanding;
to my children, Julia and Michael, who fill me with joy and love;
and to my sister, Rita, who keeps reminding me to be strong and assertive.
Without them, this book would be possible.

Philip Peng

Preface

In the last 15 years, we witnessed a rapid surge in interest in applying ultrasound-guided pain intervention. Before 2003, the interest in ultrasound-guided pain intervention was mostly restricted to musculoskeletal system. Since then, many new techniques in ultrasound-guided pain intervention were developed in various peripheral and axial structures among pain specialists. More recently, the field in musculoskeletal (MSK) pain intervention has entered a renaissance. The MSK pain intervention is not restricted to joint injection any more but also includes fenestration of the tendons/ligaments, barbotage in calcific tendinitis, radiofrequency ablation of articular branches of joints, nonsurgical release of the nerve (e.g., carpal tunnel release), nerve release, and intraneural ablation.

As a result, there are a few books published in the arena of ultrasound-guided pain intervention. So, why did we decide to publish another one?

As our book title suggested, it is an illustrated procedural guide. We have 302 illustrations in 27 chapters. The generous numbers of illustration not just help the readers to grasp the concept of the anatomy and the procedure with ease; it also makes the learning enjoyable. We also make the layout easy and practical. A typical chapter started with an introduction of the procedure, the patient selection, and an overview of anatomy. Then, we presented the step-by-step ultrasound scanning procedure with illustrations. We also summarized all the clinical pearls from the expert. The chapter concluded with a brief review of the literature.

I am honored that three experience clinicians were willing to join me as the section editors: Dr. Anuj Bhatia for the peripheral structures, Dr. Rod Finlayson for the axial structures, and Dr. Sang-Hoon Lee for the musculoskeletal intervention. I sincerely thank them for the team effort. We are indebted to the expert contributors for the tireless effort to compose the chapters and invaluable input of their experience. Our hope is to provide clinicians interested in ultrasound-guided pain intervention an enjoyable learning experience and enrich them with the knowledge to benefit the patients suffering in pain.

Toronto, ON, Canada — Philip Peng
Montreal, QC, Canada — Roderick Finlayson
Jeonju, Republic of Korea — Sang Hoon Lee
Toronto, ON, Canada — Anuj Bhatia

Contents

Contributors

Sherif Abbas, MD Department of Anesthesia, UZ Leuven, Leuven, Belgium

Farah Musaad M. Alshuraim, MBBS Department of Anesthesia, Mount Sinai Hospital, Toronto, ON, Canada

Geoff A. Bellingham, MD, FRCPC Department of Anesthesia & Perioperative Medicine, St. Joseph's Health Care London, London, ON, Canada

Anuj Bhatia, MBBS, MD Department of Anesthesia and Pain Management, Toronto Western Hopsital and Mount Sinai Hospital, University of Toronto, Toronto, Ontario, Canada

Marko Bodor, MD Physical Medicine and Rehabilitation, University of California Davis, and Bodor Clinic, Napa, CA, USA

Robert S. Burnham, MSc, MD, FRCPC Central Alberta Pain & Rehabilitation Institute, Lacombe, AB, Canada

Yu M. Chiu, DO Department of Anesthesiology, Division of Pain Medicine, Medical College of Wisconsin, Milwaukee, WI, USA

Sean Colio, MD Bodor Clinic, Napa, CA, USA

John-Paul B. Etheridge, MBChB, DA (SA); CCFP Department of Anesthesia, Kelowna General Hospital, Kelowna, BC, Canada

Roderick Finlayson, MD, FRCPC Alan Edwards Pain Management Unit, McGill University Health Centre, Montreal, Quebec, Canada

David Flamer, MD, FRCPC Anesthesiology and Pain Management, Mount Sinai Hospital – University Health Network, Toronto, ON, Canada

Mauricio Forero, MD, FIPP Department of Anesthesia, McMaster University, Hamilton, ON, Canada

Thiago Nouer Frederico, MD, ASRA-PMUC, WIP-CIPS Department of Anesthesia & Pain, Hospital Sirio Libanes, Sao Paulo, Brazil

Manfred Greher, MD, MBA Department of Anesthesiology, Intensive Care and Pain Therapy, Herz-Jesu Krankenhaus GmbH (Hospital of the Sacred Heart of Jesus), Vienna, Austria

Amitabh Gulati, MD, FIPP CIPS Anesthesiology and Critical Care, Division of Pain Medicine, Memorial Sloan Kettering Cancer Center, New York, NY, USA

Yasmine Hoydonckx, MD, FIPP Department of Anesthesia and Pain Medicine, University of Toronto and Toronto Western Hospital, University Health Network, Toronto, ON, Canada

Ashutosh Joshi, MBBS, MD Department of Anaesthesia, Khoo Teck Puat Hospital, Singapore, Singapore

Jameel Khan, MD Bodor Clinic, Napa, CA, USA

Pranab Kumar, FRCA, FFPMRCA Department of Anesthesia & Pain, Toronto Western Hospital, Toronto, ON, Canada

María Francisca Elgueta Le-Beuffe, MD Department of Anesthesia, Pontificia Universidad Católica de Chile, Santiago, Chile

Sang Hoon Lee, PhD Madi Pain Management Center, Jeonju, Republic of Korea

Eldon Loh, MD, FRCPC Department of Physical Medicine and Rehabilitation, Schulich School of Medicine and Dentistry, Western University, London, ON, Canada

Parkwood Institute, St. Joseph's Health Care London, London, ON, Canada

Anthony J. Mazzola, MD Department of Rehabilitation and Human Performance, Mount Sinai Hospital, New York, NY, USA

Jennifer Kelly McDonald, BScH, MD, FRCPC The Ottawa Hospital, Physical Medicine and Rehabilitation, The Ottawa Hospital Rehabilitation Centre, Ottawa, ON, Canada

Samer Narouze, MD, PhD Center for Pain Medicine, Western Reserve Hospital, Cuyahoga Falls, OH, USA

Zachary Pellis Pain Diagnostics and Interventional Care, Sewickley, PA, USA

Philip Peng, MBBS, FRCPC Department of Anesthesia and Pain Management, Toronto Western Hopsital and Mount Sinai Hospital, University of Toronto, Toronto, Ontario, Canada

David Anthony Provenzano, MD Pain Diagnostics and Interventional Care, Sewickley, PA, USA

Marc Raj, DO Bodor Clinic, Napa, CA, USA

Vicente Roqués Department of Anesthesia, Intensive Care and Pain Treatment, University Hospital Virgen de la Arrixaca, Murcia, Spain

Jay M. Shah, MD SamWell Institute of Pain Management, Woodbridge, NJ, USA

Neilesh Soneji, MD, FRCPC Department of Anesthesia, University of Toronto, Toronto, ON, Canada

Department of Anesthesia and Pain Management, University Health Network – Toronto Western Hospital, Women's College Hospital, Toronto, ON, Canada

Dmitri Souza, MD, PhD Ohio University, Heritage College of Osteopathic Medicine, Athens, OH, USA

Center for Pain Medicine, Western Reserve Hospital, Cuyahoga Falls, OH, USA

David A. Spinner, DO, RMSK, CIPS, FAAPMR Department of Rehabilitation and Human Performance, Mount Sinai Hospital, New York, NY, USA

Agnes Stogicza, MD, FIPP, CIPS Anesthesiology and Pain Management, Saint Magdolna Private Hospital, Budapest, Hungary

Athmaja R. Thottungal, MBBS Department of Anaesthesia & Pain, Kent and Canterbury Hospital, Canterbury, UK

John Tran, HBSc Division of Anatomy, Department of Surgery, 1 King's College Circle, Toronto, ON, Canada

Nestor Jose Trujillo-Uribe, MD Universidad Autónoma de Bucaramanga, Bucaramanga, Colombia

Department of Anesthesia and Pain Medicine, Fundación Oftalmológica de Santander, Clínica Carlos Ardila Lule, Clínica del Dolor y Cuidado Paliativo ALIVIAR LTDA, Floridablanca, Colombia

Juan Felipe Vargas-Silva, MD Department of Surgery and Image Guided Therapy, Pain Clinic, Hospital Pablo Tobón Uribe, Medellin, Colombia

About the Editor

Philip Peng is a full professor in the Department of Anesthesia and Pain Management of the University of Toronto and is currently the director of Anesthesia Pain Program in Toronto Western Hospital and interim director of Wasser Pain Management Center.

He has played an important role in the education of the pain medicine and established major teaching courses for pain in Canada such as the National Pain Refresher Course, Canadian Pain Interventional Course, and Ultrasound for Pain Medicine Course. The Royal College of Physicians and Surgeons of Canada (RCPSC) honored him with founder designation in pain medicine for his role in establishing pain medicine subspecialty in Canada. Besides, he currently serves as the chair of the Exam Committee in Pain Medicine in RCPSC and previously served as the chair of the Education Special Interest Group (SIG) of Canadian Pain Society and the founding executive of Pain Education SIG of International Association for the Study of Pain (IASP). He has been honored with numerous teaching awards at national and regional level.

Dr. Philip Peng is also a leader and pioneer in the application of ultrasound for pain medicine. Being one of the founding fathers for Ultrasound for Pain Medicine (USPM) SIG for ASRA (American Society of Regional Anesthesia), he was involved in the establishment of the guideline for Education and Training for USPM, which was adopted by five continents. He is the chair for the new Ultrasound for Pain Medicine Exam Certificate and chair for the Musculoskeletal Pain Ultrasound Cadaver workshop for ASRA and has been the chair or main organizer for various major teaching courses for USPM, including satellite meeting of the World Congress on Pain, International Pain Congress, combined Canadian and British Pain Society Conference, International Symposium of Ultrasound for Regional Anesthesia (ISURA), and Canadian Pain Interventional Course.

Furthermore, he has edited 7 books and published more than 150 peer-reviewed publications and book chapters.

Basic Principles and Physics of Ultrasound

1

Sherif Abbas and Philip Peng

Understanding the Physics of Ultrasound and Image Generation

Characteristic of Sound Wave

Audible sound wave lies within the range of 20–20,000 Hz. Ultrasound is a sound wave beyond audible range (>20,000 Hz). Ultrasound system commonly used in clinical settings incorporates transducers generating frequencies between 2 and 17 MHz. Some special ultrasound system even generates frequencies between 20 and 55 MHz. Sound waves do not exist in a vacuum, and propagation in gases is poor because the molecules are too widely spaced, which explains the use of gel couplant between the skin of the subject and the transducer interface to eliminate the air-filled gap.

Sound wave is a form of mechanical energy that travels through a conducting medium (e.g., body tissue) as a longitudinal wave producing alternating compression (high pressure) and rarefaction (low pressure) (Figs. 1.1 and 1.2). Sound propagation can be represented in a sinusoidal waveform with a characteristic pressure (P), wavelength (λ), frequency (f), period (T), and velocity. See Table 1.1 for details.

The speed of sound varies for different biological media, but the average value is assumed to be 1540 m/s for most human soft tissues. It can vary greatly, being as low as 330 m/s in air and as high as 4000 m/s through bone.

The wavelength (λ) is inversely related to the frequency (f). Thus, sound with a high frequency has a short wavelength and vice versa.

S. Abbas
Department of Anesthesia, UZ Leuven, Leuven, Belgium

P. Peng (✉)
Department of Anesthesia and Pain Management, Toronto Western Hopsital and Mount Sinai Hospital, University of Toronto, Toronto, Ontario, Canada
e-mail: Philip.peng@uhn.ca

P. Peng et al. (eds.), *Ultrasound for Interventional Pain Management*,
https://doi.org/10.1007/978-3-030-18371-4_1

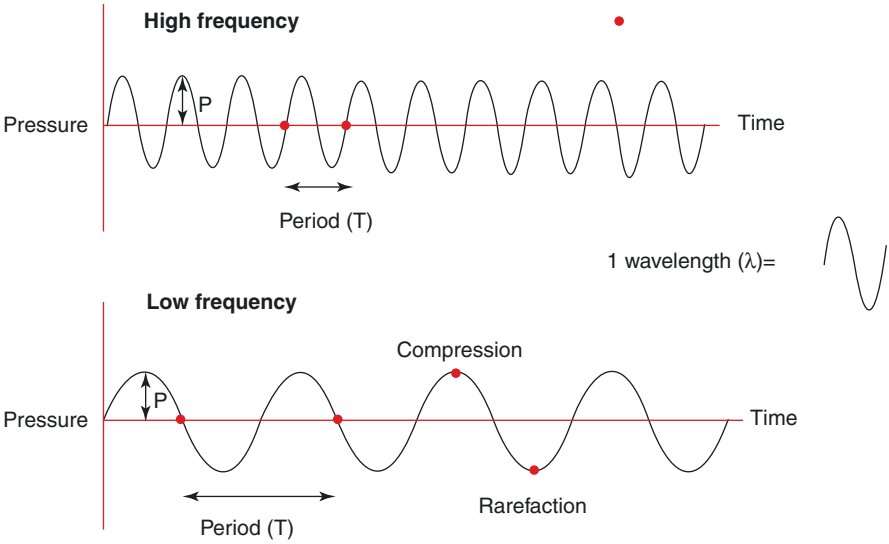

Fig. 1.1 Comparison of high-frequency and low-frequency waveform. (Reprinted with permission from Philip Peng Educational Series)

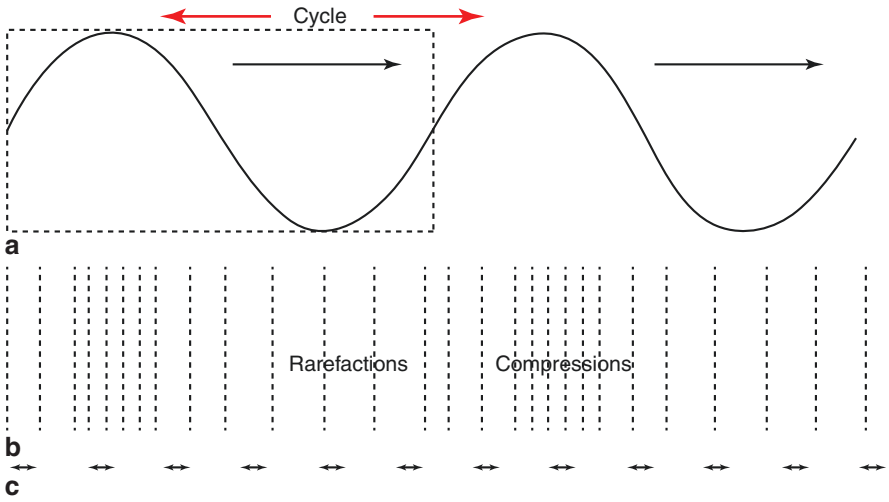

Fig. 1.2 A longitudinal wave showing alternating compression and rarefaction. (Reprinted with permission from Philip Peng Educational Series)

Generation of an Ultrasound Wave

An ultrasound wave is generated when an electric field is applied to an array of piezoelectric crystals located on the transducer surface. Electrical stimulation causes mechanical distortion of the crystals resulting in vibration and production of sound waves (i.e., mechanical energy). The conversion of electrical to mechanical

Table 1.1 Basic terminology

Terminology	Definition
Wavelength (λ)	The spatial period of the wave, and is determined by measuring the distance between two consecutive corresponding points of the same phase. It is expressed in meters (m)
Amplitude (A)	A measure of the height of the wave, i.e., maximal particle displacement. It is expressed in meters (m)
Period (T)	The time taken for one complete wave cycle to occur. The unit of period is seconds (s)
Frequency (f)	The number of completed cycles per second. Thus, it is the inverse of the period (T) of a wave. The unit of frequency is hertz (Hz). Medical imaging uses high-frequency waves (1–20 MHz)
Velocity (c)	The speed of propagation of a sound wave through a medium (m/s). It is the product of its frequency (f) and wavelength (λ)
Energy (E)	The energy of a sound wave is proportional to the square of its amplitude (A). This means that as the amplitude of a wave decreases (such as with deeper penetration), the energy carried by the wave reduces drastically
Power (P)	Defines as the energy (E) delivered per unit time (t)

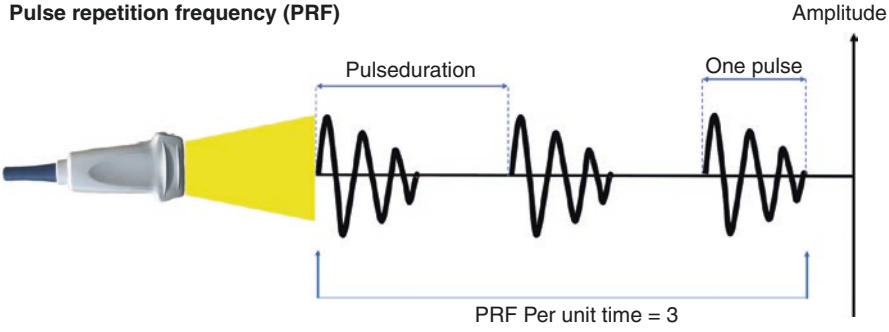

Fig. 1.3 Pulse repetition frequency. (Reprinted with permission from Philip Peng Educational Series)

(sound) energy is called the converse piezoelectric effect. Each piezoelectric crystal produces an ultrasound wave. The summation of all waves generated by the piezoelectric crystals forms the ultrasound beam. Ultrasound waves are generated in pulses (intermittent trains of pressure waves), and each pulse commonly consists of two or three sound cycles of the same frequency.

The pulse length (PL) is the distance traveled per pulse. Waves of short pulse lengths improve axial resolution for ultrasound imaging. The PL cannot be reduced to less than 2 or 3 sound cycles by the damping materials within the transducer.

Pulse repetition frequency (PRF) is the rate of pulses emitted by the transducer (number of pulses per unit time) (Fig. 1.3). Ultrasound pulses must be spaced with enough time between pulses to permit the sound to reach the target of interest and return to the transducer before the next pulse is generated. The PRF for medical imaging ranges from 1 to 10 kHz. For example, if the PRF = 5 kHz and the time between pulses is 0.2 ms, it will take 0.1 ms to reach the target and 0.1 ms to return to the transducer. This means the pulse will travel 15.4 cm before the next pulse is emitted (1540 m/s × 0.1 ms = 0.154 m in 0.1 ms = 15.4 cm).

Generation of an Ultrasound Image

An ultrasound image is generated when the pulse wave emitted from the transducer is transmitted into the body, reflected off the tissue interface, and returned to the transducer. The schematic diagram above showed the transducer waits to receive the returning wave (i.e., echo) after each pulsed wave (Fig. 1.4). The transducer transforms the echo (mechanical energy) into an electrical signal which is processed and displayed as an image on the screen. The conversion of sound to electrical energy is called the piezoelectric effect.

The image can be displayed in a number of modes (Fig. 1.5):

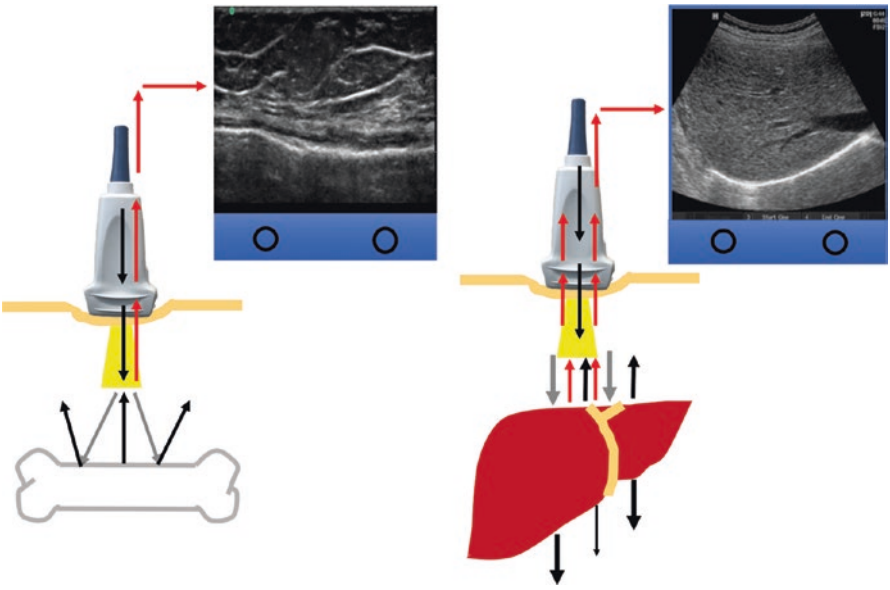

Fig. 1.4 Ultrasound wave interaction with body tissue. (Reprinted with permission from Philip Peng Educational Series)

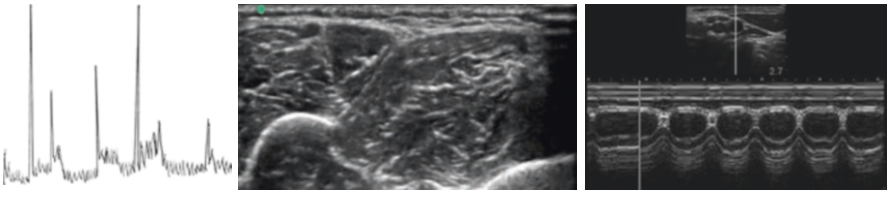

Fig. 1.5 Three different modes of ultrasound. (Reprinted with permission from Philip Peng Educational Series)

- *Amplitude (A)* mode is the display of amplitude spikes in the vertical axis and the time required for the return of the echo in the horizontal axis.
- *Brightness (B)* displays a two-dimensional map of the data acquired and is most commonly used for ultrasound guided intervention.
- *Motion (M)* mode, also called time motion or TM mode, displays a one-dimensional image usually used for analyzing moving body parts. This mode records the amplitude and rate of motion in real time and is commonly used in cardiovascular imaging.

Ultrasound Tissue Interaction

As the ultrasound beam travels through tissue layers, the amplitude of the original signal becomes attenuated as the depth of penetration increases (Fig. 1.6).

Attenuation (energy loss) is due to:

1. Absorption (conversion of acoustic energy to heat)
2. Reflection
3. Scattering at interfaces

In soft tissue, 80% of the attenuation of the sound wave is caused by absorption resulting in heat production. Attenuation is measured in decibels per centimeter of

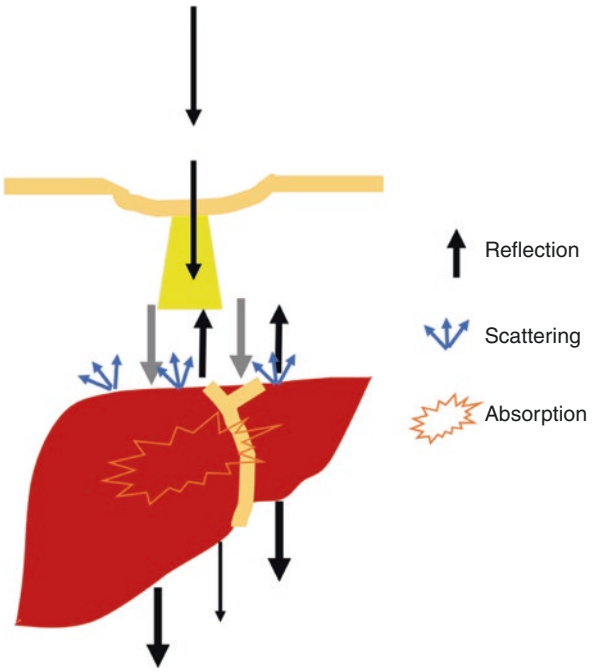

Fig. 1.6 Different types of attenuation. (Reprinted with permission from Philip Peng Educational Series)

tissue and is represented by the attenuation coefficient of the specific tissue type. The higher the attenuation coefficient, the more attenuated the ultrasound wave is by the specified tissue.

Absorption

Absorption is the process of transfer of the ultrasound beam's energy to the medium through which it travels through heat generation and it accounts for most of the wave attenuation. The quality of the returning sound waves depends on the attenuation coefficient of different tissue.

The degree of attenuation also varies directly with the frequency of the ultrasound wave and the distance traveled (Fig. 1.7 and Table 1.2). Generally speaking,

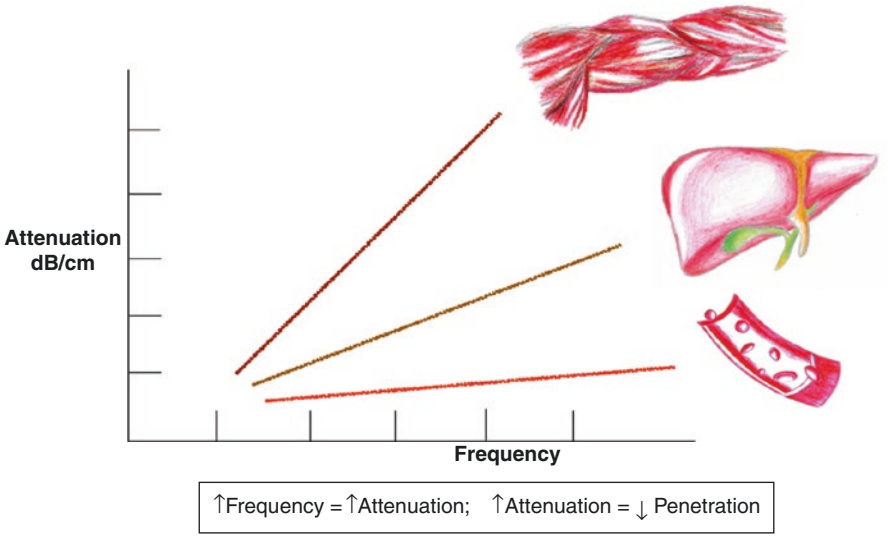

Fig. 1.7 Variation of attenuation with frequency in different organs. (Reprinted with permission from Philip Peng Educational Series)

Table 1.2 Attenuation coefficient of various tissues

Material	α (dB/cm)
Blood	0.18
Fat	0.6
Muscle (across fibers)	3.3
Muscle (along fibers)	1.2
Aqueous and vitreous humor of the eye	0.1
Lens of the eye	2.0
Skull bone	20
Lungs	40
Liver	0.9
Brain	0.85
Kidney	1.0
Spinal cord	1.0
Water	0.0022
Castor oil	0.95
Lucite	2.0

a high-frequency wave is associated with high attenuation, thus limiting tissue penetration, whereas a low-frequency wave is associated with low tissue attenuation and deep tissue penetration.

To compensate for attenuation, it is possible to amplify the signal intensity of the returning echo. The degree of receiver amplification is called the gain. Increasing the gain will amplify only the returning signal and not the transmit signal. An increase in the overall gain will increase brightness of the entire image, including the background noise. Preferably, the time gain compensation (TGC) is adjusted to selectively amplify the weaker signals returning from deeper structures.

Reflection

Attenuation also results from reflection and scattering of the ultrasound wave. The extent of reflection is determined by the difference in acoustic impedances of the two tissues at the interface, i.e., the degree of impedance mismatch.

Acoustic impedance is the resistance of a tissue to the passage of ultrasound. The higher the degree of impedance mismatch, the greater the amount of reflection (Table 1.3). The degree of reflection is high for air because air has an extremely low acoustic impedance (0.0004) relative to other body tissues. The bone also produces a strong reflection because its acoustic impedance is extremely high (7.8) relative to other body tissues. For this reason, it is clinically important to apply sufficient conducting gel (an acoustic coupling medium) on the transducer surface to eliminate any air pockets between the transducer and skin surface. Otherwise, much of the ultrasound waves will be reflected limiting tissue penetration.

The angle of the incidence is also a major determinant of reflection. An ultrasound wave hitting a smooth mirror-like interface at a 90° angle will result in a perpendicular reflection. An incident wave hitting the interface at an angle <90° will result in the wave being deflected away from the transducer at an angle equal to the angle of incidence but in the opposite direction (angle of reflection). When this happens, the signal of the returning echo is weakened, and a darker image is displayed (Fig. 1.8). This explains why it is difficult to visualize a needle inserted at a steep angle (>45° to the skin surface).

Specular reflection occurs at flat, smooth interfaces where the transmitted wave is reflected in a single direction depending on the angle of incidence. Examples of specular reflectors are fascial sheaths, the diaphragm, and walls of major vessels

Table 1.3 Acoustic impendence of various tissues

Body tissue	Acoustic impedance (10^6 RayIs)
Air	0.0004
Lung	0.18
Fat	1.34
Liver	1.65
Blood	1.65
Kidney	1.63
Muscle	1.71
Bone	7.8

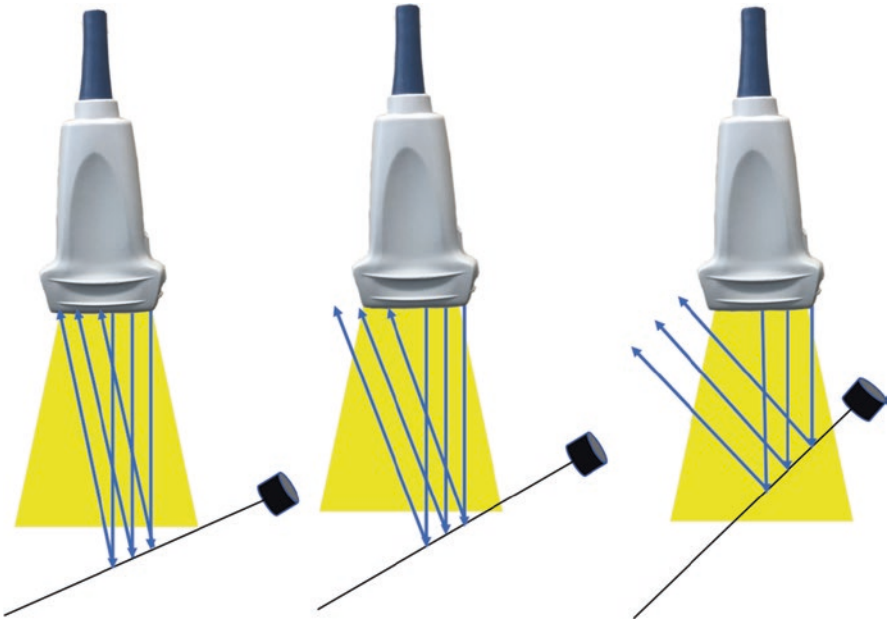

Fig. 1.8 Angle of incidence. (Reprinted with permission from Philip Peng Educational Series)

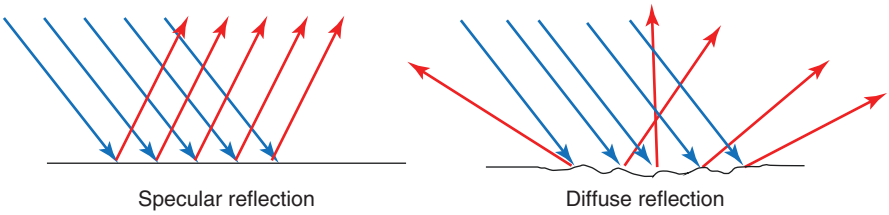

Fig. 1.9 Different types of reflection. (Reprinted with permission from Philip Peng Educational Series)

(Fig. 1.9). Block needles are also strong specular reflectors. For specular reflection to occur, the wavelength of the ultrasound wave must be smaller than the reflective structure. Otherwise, scattering will occur.

Scattering

Reflection in biological tissues is not always specular. Scattering (diffuse reflection) occurs when the incident wave encounters an interface that is not perfectly smooth (e.g., surface of visceral organs). Echoes from diffuse reflectors are generally weaker than those returning from specular reflectors. Scattering also occurs when the wavelength of the ultrasound wave is larger than the dimensions of the reflective structure (e.g., red blood cells). The reflected echo scatters in many different

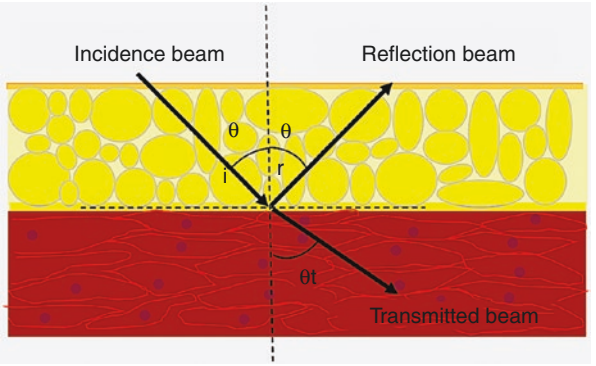

Fig. 1.10 Transmission of beam. (Reprinted with permission from Philip Peng Educational Series)

directions resulting in echoes of similar weak amplitudes. Ultrasonic scattering gives rise to much of the diagnostic information we observe in medical ultrasound imaging.

Transmission

After reflection and scattering, the remainder of the incident beam is refracted with a change in the direction of the transmitted beam (Fig. 1.10). Refraction occurs only when the speeds of sound are different on each side of the tissue interface. The degree of beam change (bending) is dependent on the change in the speed of sound traveling from one medium on the incident side to another medium on the transmitted side (Snell's Law). With medical imaging, fat causes considerable refraction and image distortion, which contributes to some of the difficulties encountered in obese patients. Refraction encountered with bone imaging is even more significant leading to a major change in the direction of the incident beam and image distortion.

The final image on the screen of an ultrasound machine is the result of the interaction of ultrasound waves with the tissues being examined. As the ultrasound wave travels through the tissues, it loses amplitude, and hence energy (attenuation), which is the summative effect of absorption, reflection, and refraction of ultrasound waves.

Image Acquisition and Processing

Transducer Basic

An ultrasound transducer has a dual functionality. It is responsible for both the production of ultrasound waves and, after a set period of time, the reception of waves reflected from the tissues. This is called pulsed ultrasound. The pulse repetition frequency (PRF) is the number of pulses emitted by the transducer per unit of time. The PRF for medical imaging devices ranges from 1 to 10 kHz

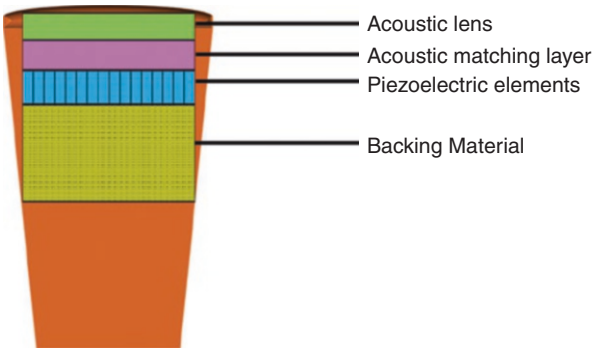

Fig. 1.11 Anatomy of a transducer. (Reprinted with permission from Philip Peng Educational Series)

The ultrasound transducer has the following layers (Fig. 1.11):

(a) Backing material: located behind the piezoelectric element, it serves to prevent excessive vibration. This causes the element to generate ultrasonic waves with a shorter pulse length, improving axial resolution in images.
(b) Piezoelectric elements: they generate ultrasonic waves and also generate images. Piezoelectric ceramic (PZT: lead zirconate titanate) is most commonly used because of their high conversion efficiency.
(c) Acoustic matching layer: this reduces the acoustic impedance mismatch between the transducer and the object and thus minimizes reflection off the interface. This is usually made up of a resin.
(d) Acoustic lens: the acoustic lens prevents the ultrasonic waves from spreading and focuses them in the slice direction to improve the resolution.

Transducer Selection

The choice of which transducer should be used depends on the depth of the structure being imaged. The higher the frequency of the transducer crystal, the less penetration it has but the better the resolution. Therefore, if more penetration is required, you need to use a lower-frequency transducer with the sacrifice of some resolution.

Transducer characteristics, such as frequency and shape, determine ultrasound image quality. For simplicity, there are three types of transducers.

The linear transducer frequencies used for superficial structures and peripheral nerve blocks range from 6 to 15 MHz (Fig. 1.12). Curvilinear (or curved) transducers are most useful for deeper structures or imaging requiring a wide field of view (e.g., spine). Microconvex is commonly used for small acoustic window such as cardiac scanning.

For superficial structures (e.g., nerves in the interscalene region), it is ideal to use high-frequency transducers in the range of 10–15 MHz, but depth of penetration is often limited to 2–3 cm below the skin surface (Fig. 1.13). For visualization of

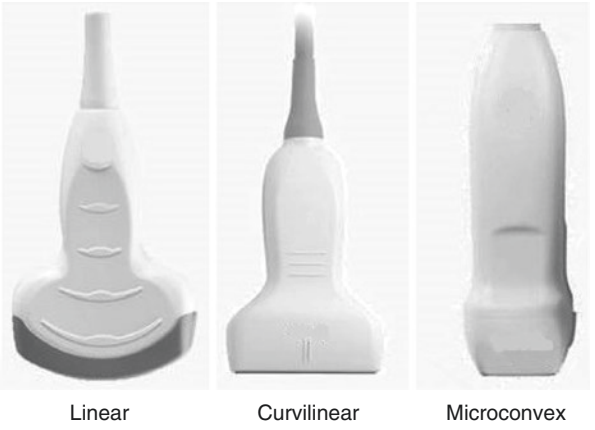

Fig. 1.12 Different types of transducer. (Reprinted with permission from Philip Peng Educational Series)

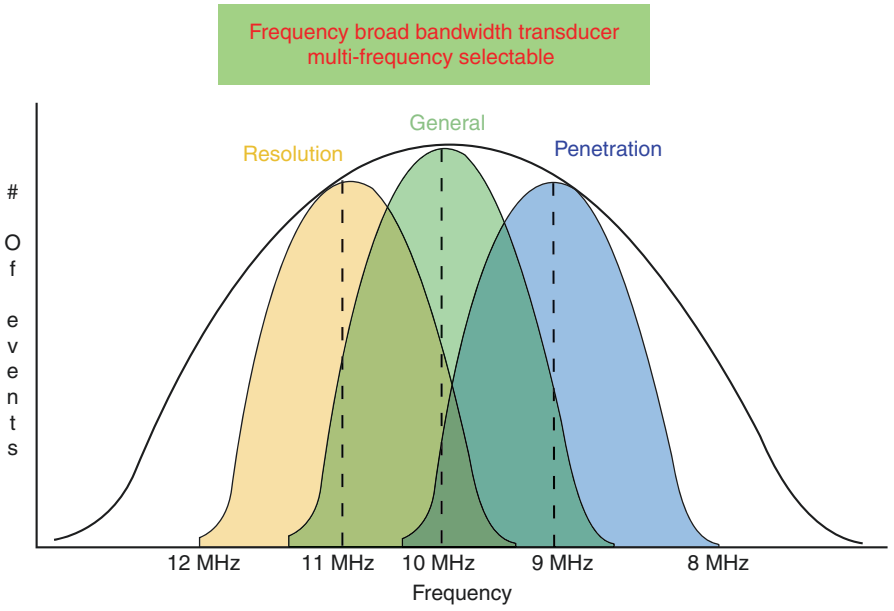

Fig. 1.13 Frequency, resolution, and penetration. (Reprinted with permission from Philip Peng Educational Series)

deeper structures (e.g., in the gluteal region) or when a wider field of view is required, it may be necessary to use a lower-frequency transducer (2–5 MHz) because it offers ultrasound penetration of 4–5 cm or more below the skin surface. However, the image resolution is often inferior to that obtained with a higher-frequency transducer.

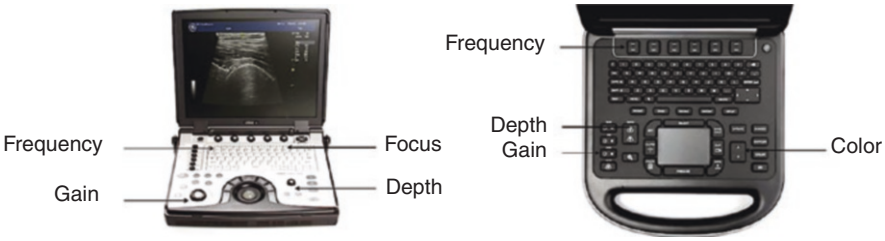

Fig. 1.14 Basic button of ultrasound machine. (Reprinted with permission from Philip Peng Educational Series)

Basic Operation of Ultrasound Machine

To obtain a good ultrasound picture, clinician should be familiar with the basic function and buttons in the ultrasound machine: gain, depth, color (Doppler), and focus (Fig. 1.14).

Gain

The echo signals returning from the tissues reach the crystals and produce an electric current (piezoelectric effect). This is then converted to a pixel on the image, with the energy of the returning wave being proportional to the brightness of the pixel dot on the image. The amplitude of the returning echo signals is very small to be properly displayed on a screen. Hence, it needs amplification. Amplification of signal can be adjusted using the GAIN button, but the use of it adds to "background noise."

Time gain compensation It is the preferential enhancement of signals at different depths returning from deeper tissues (Fig. 1.15). Thus, the echoes returning from similar reflectors can be represented by the same shade of gray regardless of their depth.

Depth

The depth of the field should be adjusted to the area of interest (Fig. 1.16). Too shallow may miss the important information from the background in the deep field, and too deep will diminish the quality of the image in the superficial field.

Focus

The shape of the beam varies and is different for each transducer frequency. There is a fixed focused region of the ultrasound beam which is indicated on the system with a small triangle to the right of the image. This indicates the focal zone of that

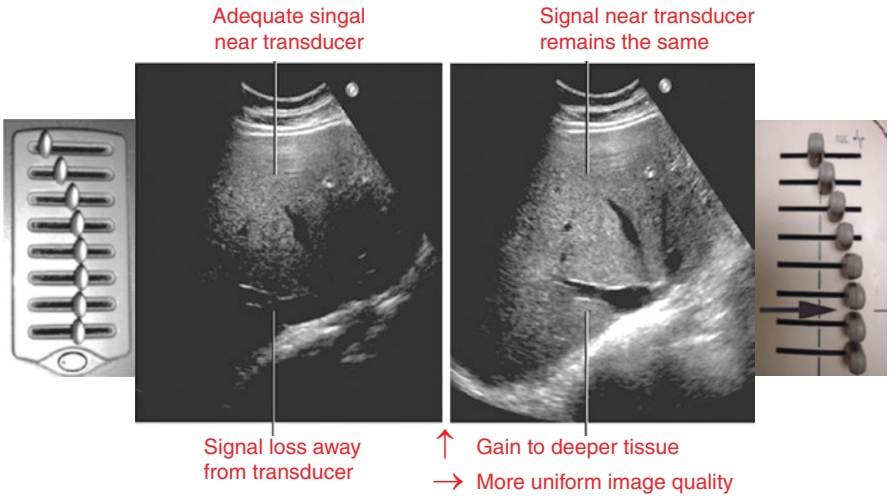

Fig. 1.15 Time gain compensation. (Reprinted with permission from Philip Peng Educational Series)

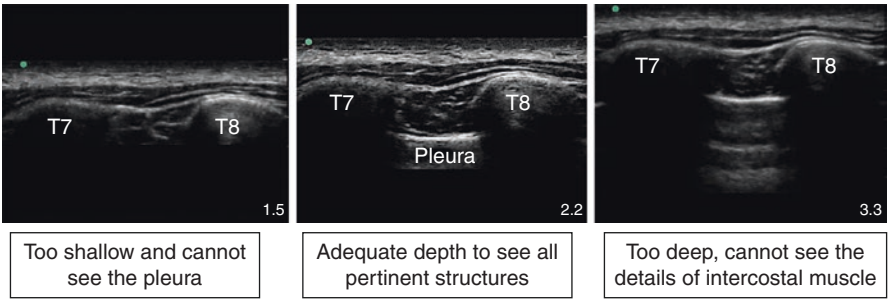

Fig. 1.16 Depth and image acquired. (Reprinted with permission from Philip Peng Educational Series)

transducer and is where the best resolution can be achieved with that particular transducer (Fig. 1.17). Effort should be taken to position the object of interest in the subject to within that focused area to obtain the best detail by adjusting the FOCUS button (Fig. 1.18).

Doppler

The Doppler information is displayed graphically using spectral Doppler, or as an image using color Doppler (directional Doppler) or power Doppler (non-directional Doppler).

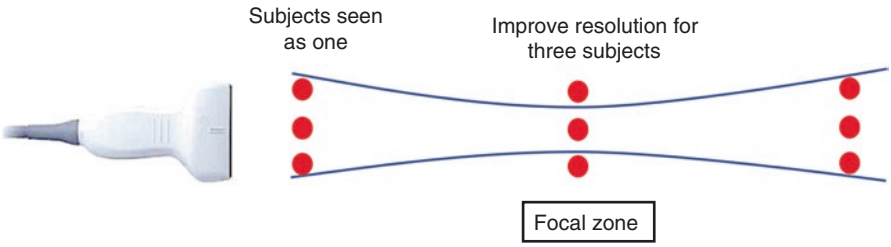

Fig. 1.17 Focus of a beam. (Reprinted with permission from Philip Peng Educational Series)

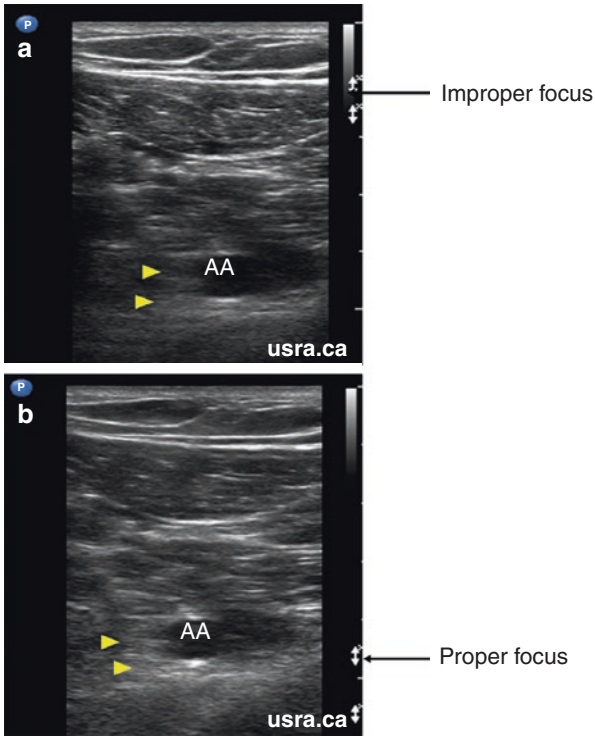

Fig. 1.18 Effect of focus setting and image acquired. (Reprinted with permission from usra.ca)

All modern ultrasound scanners use pulsed Doppler to measure velocity. Pulsed wave machines transmit and receive series of pulses.

In color Doppler, echoes are displayed with colors corresponding to the direction of flow that their positive or negative Doppler shifts represent (toward or away from the transducer). The brightness of the color represents the intensity of the echoes, and sometimes other colors are added to indicate the extent of spectral broadening (Fig. 1.19).

Power Doppler depicts the amplitude or power of Doppler signals rather than the frequency shift. This allows detection of a larger range of Doppler shifts and therefore better visualization of the smaller vessels, but at the expense of directional and velocity information.

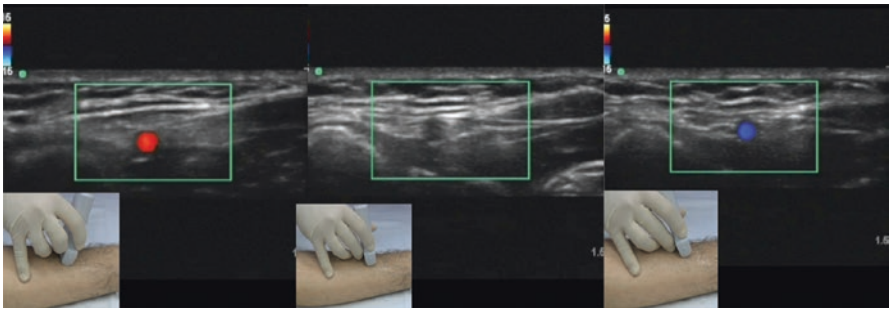

Fig. 1.19 Color Doppler. (Reprinted with permission from Philip Peng Educational Series)

Understanding Sonoanatomy and Artifact

Tissue Echogenicity

When an echo returns to the transducer, its amplitude is represented by the degree of brightness (i.e., echogenicity) of a dot on the display. Combination of all the dots forms the final image. Strong specular reflections give rise to bright dots (hyperechoic), e.g., the diaphragm, gallstone, bone, and pericardium. Weaker diffuse reflections produce gray dots (hypoechoic), e.g., solid organs. No reflection produces dark dots (anechoic), e.g., fluid- and blood-filled structures, because the beam passes easily through these structures without significant reflection. Also, deep structures often appear hypoechoic because attenuation limits beam transmission to reach the structures, resulting in a weak returning echo.

Sonoanatomic Features of Tissue

Vessels

Left sonogram showed a round anechoic artery (A) and an oval-shaped anechoic vein (V) (Fig. 1.20). An artery is pulsatile and not easily compressible. A vein is collapsible and non-pulsatile. Figure 1.21 showed the long axis of vessels with color Doppler on. As discussed in the above section, red color indicates the direction of flow and does not confirm the presence of an artery.

The Adipose, Muscle, and Bone

The left sonogram showed the typical appearance of adipose tissue, which is hypoechoic background with streaks of hyperechoic lines that are often irregular in texture and length (Fig. 1.22). Appearance of muscle is generally hypoechoic. The structure deep to the adipose tissue is the rectus muscle in transverse plane, which has a speckled appearance. The sonogram on the right displayed the muscle in long

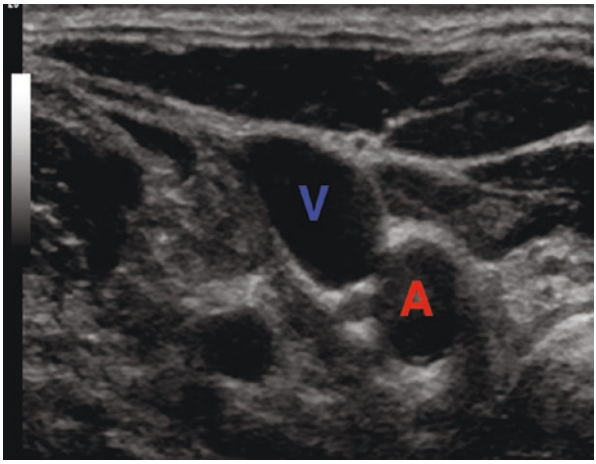

Fig. 1.20 Sonoanatomy of vessels. (Reprinted with permission from Philip Peng Educational Series)

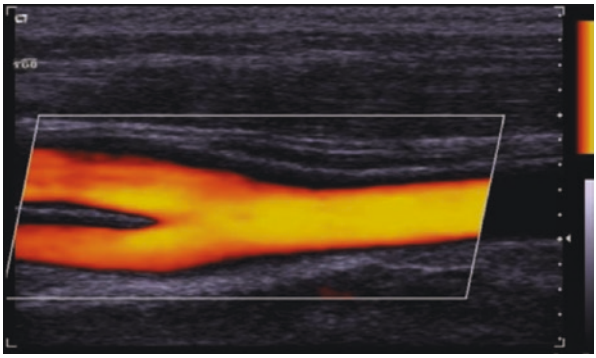

Fig. 1.21 Vessel with color Doppler on. (Reprinted with permission from Philip Peng Educational Series)

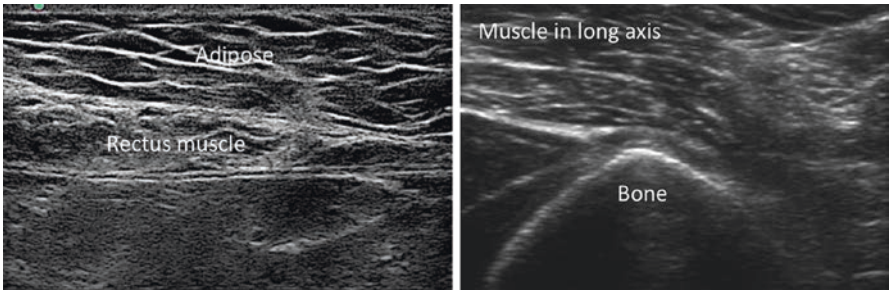

Fig. 1.22 Sonoanatomy of the muscle, adipose tissue, and bone. (Reprinted with permission from Philip Peng Educational Series)

axis, and the perimysial connective tissue is apparent in linear pattern. The bone appears as an hyperechoic line with an anechoic shadow due to lack of beam penetration.

Nerve

The appearance of the nerve (yellow arrows) can be hyperechoic, hypoechoic, or mixed, depending on the location, size, amount of connective tissue, and the angle of the transducer (Fig. 1.23). Above the clavicle, the nerve roots typically appear as hypoechoic (left upper sonogram). As the peripheral nerve picks up more connective tissues, it appears as hyperechoic (femoral nerve in the right upper sonogram). A peripheral nerve can also appear as mixed hyper- and hypoechoic (honeycomb appearance) as shown in the left lower sonogram. In long axis, the nerve appears hypoechoic with fibrillar pattern in the right lower sonogram. However, compared with the tendon in long axis (right sonogram in Fig. 1.24 below), the nerve is more hypoechoic, and the echotexture is coarse.

Tendon

The left sonogram showed the tendon in short axis, which showed densely fibrillar pattern (Fig. 1.24). Comparison of the long axis view of the tendon in the right sonogram with that of the nerve in Fig. 1.23 (right lower sonogram) shows that the tendon is more echogenic and fibrillar in appearance.

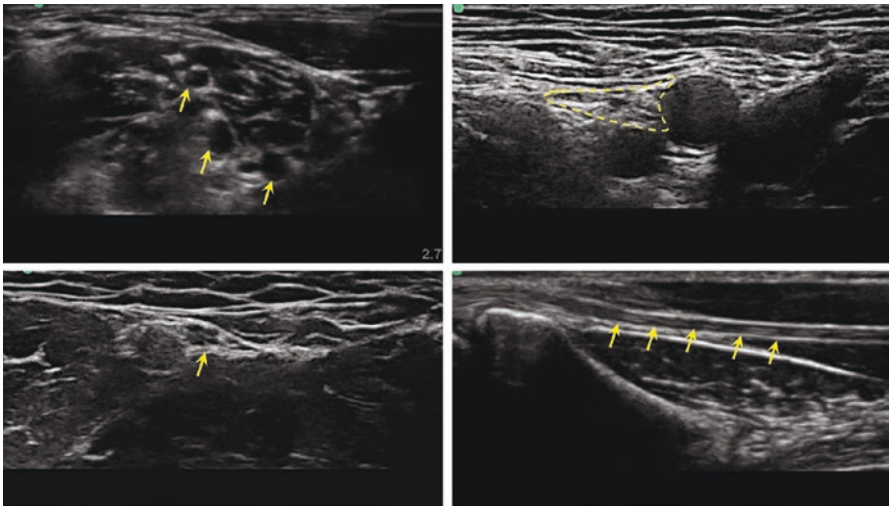

Fig. 1.23 Sonoanatomy of nerves. (Reprinted with permission from Philip Peng Educational Series)

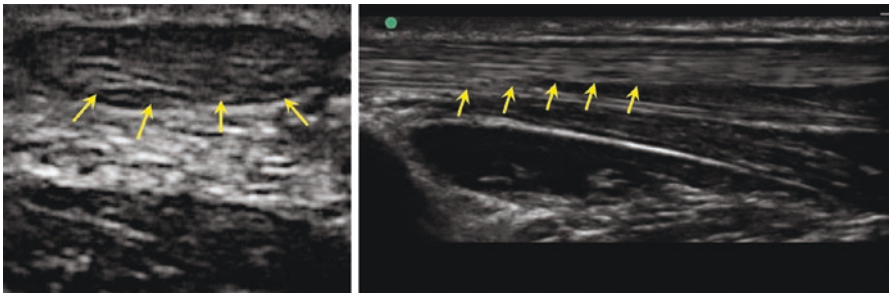

Fig. 1.24 Sonoanatomy of a tendon. (Reprinted with permission from Philip Peng Educational Series)

Artifacts

Reverberation

This is the production of false echoes due to repeated reflections between two interfaces with high acoustic impedance mismatch. The echo from the interface is received by the transducer and displayed on the image. Some of the energy in the returned echo is reflected at the transducer crystals and returns to the reflecting interface as if it was a weak transmitted pulse, returning as a second wave (Fig. 1.25). The time taken for the second wave to arrive is twice that taken by the depth.

This sequence of transmission and reflection can occur many times, with the third wave taking three times as long to return to the transducer and being displayed at three times the depth. These reverberation echoes will be strong because of the high acoustic mismatch.

There are few tricks to reduce reverberation artifact:

1. Increase the amount of gel used
2. Use a standoff pad.
3. Reduce the gain.
4. Adjust the position of the transducer.

Acoustic Shadowing

This appears as an echo-free area behind structures of strongly attenuating tissue. Because of the very high attenuation of the beam at an interface, the transmission is substantially reduced. This artifact can also appear at an interface with large acoustic mismatch such as soft tissue and gas, also at a soft tissue and bone (Fig. 1.26).

Acoustic Enhancement Artifact

This appears as a localized area of increased echo amplitude behind an area of low attenuation. On a scan, it will appear as an area of increased brightness and can commonly be seen distal to fluid-filled structures such as a cyst (Fig. 1.27). This arises due to the application of the time gain compensation (TGC) to areas of low attenuation structure such as fluid. It is caused by the low level of attenuation of the beam as it passes through fluid relative to the greater attenuation of the beam in the adjacent more solid tissue.

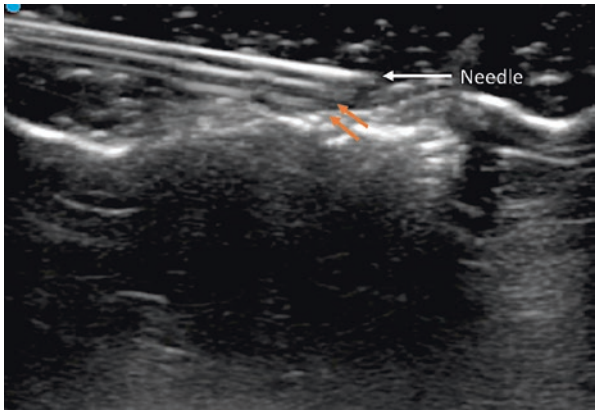

Fig. 1.25 Reverberation artifact. (Reprinted with permission from Philip Peng Educational Series)

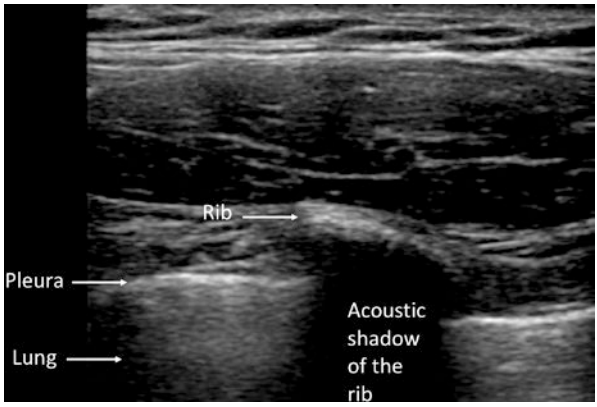

Fig. 1.26 Acoustic shadowing. (Reprinted with permission from Philip Peng Educational Series)

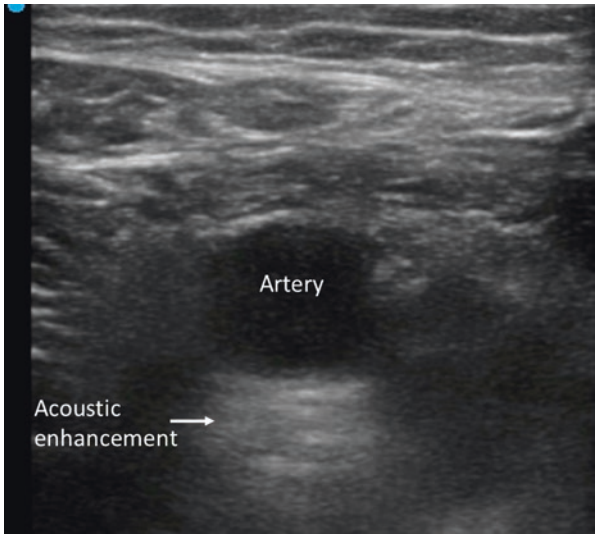

Fig. 1.27 Acoustic enhancement. (Reprinted with permission from Philip Peng Educational Series)

Edge Shadowing

This appears as a narrow hypoechoic shadow line extending down from the edge of a curved reflector (Fig. 1.28). It arises due to refraction of the beam caused by both the curvatures of the rounded edges. When the ultrasound beam races the rounded edge of the structure, reflection will occur, with an angle of incidence equal to the angle of reflection. The outer part of the beam will be totally reflected, but the reminder of the beam passes through the rounded structure and is refracted.

Mirror Imaging Artifact

This artifact results in a mirror image of the structure in an ultrasound display. They arise due to specular reflection of the beam at large smooth interface (Fig. 1.29). An

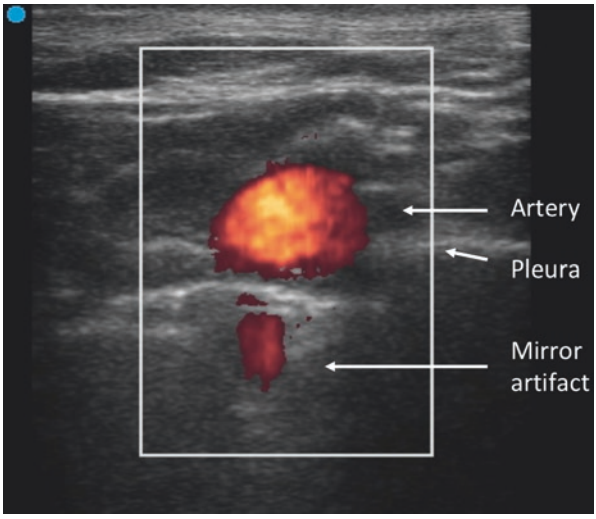

Fig. 1.29 Mirror imaging artifact. (Reprinted with permission from Philip Peng Educational Series)

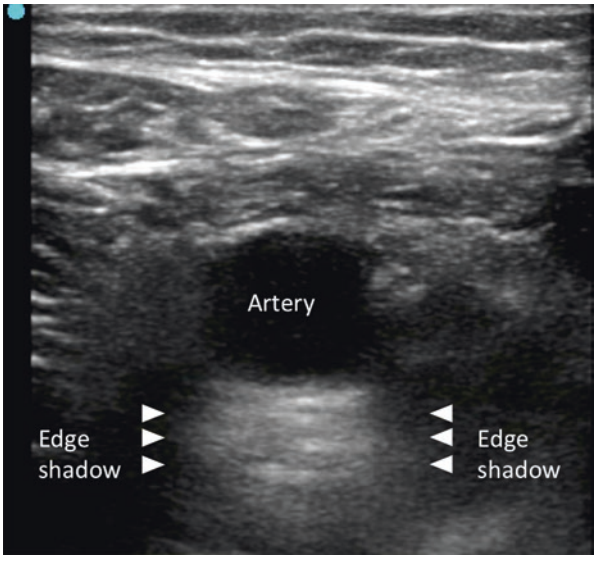

Fig. 1.28 Edge shadowing. (Reprinted with permission from Philip Peng Educational Series)

area close to specular reflector will be imaged twice, once by the original ultrasound beam and once by the beam after it has reflected off the specular reflector. Mirror image artifacts are commonly seen where there is a large acoustic mismatch, such as fluid-air interface. As an example, typically this artifact can occur during the scanning of the subclavian artery on top of the lung (fluid-air interface). It will then have the appearance of a mirror image of the artery within the lung.

Air Artifact

At the transducer skin interface, a large dropout artifact can occur due to a lack of conductive gel and poor transducer to skin contact (Fig. 1.30).

Anisotropy

Anisotropy refers to the angle dependence appearance of a structure (such as tendon) on an image (Fig. 1.31a). When the transducer is perpendicular to the long axis of the object, it results in maximum reception of the signal and optimal image. Tilting the transducing affects the signal and thus the image produced.

This affects the quality of the image because the reflection of sound wave is maximum when the transducer (and the incident waves) is perpendicular to the

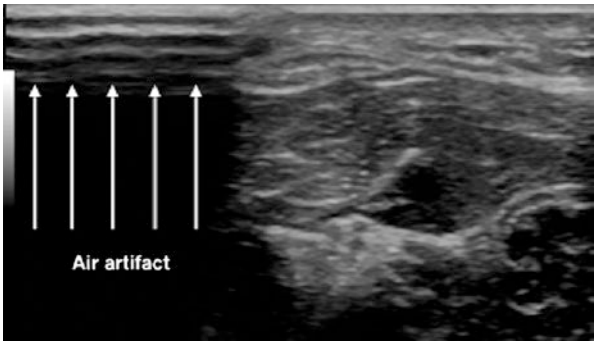

Fig. 1.30 Air artifact. (Reprinted with permission from Philip Peng Educational Series)

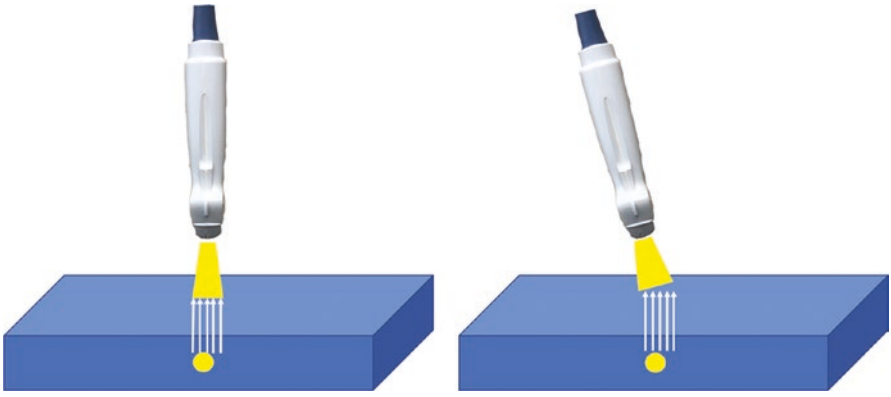

Fig. 1.31a Angle of the ultrasound and the target structure. (Reprinted with permission from Philip Peng Educational Series)

structure (median nerve in this case) under examination (left panel) (Fig. 1.31b). Any change on this incidence angle dramatically reduces the returning echo, causing the structure to "disappear" out of the image (right panel). Manipulation of the transducer (so as to direct the incident beam perpendicular to the structure of interest) and beam-steering can help address anisotropy.

Things to Remember for Optimal Ultrasound Scanning and Performance

Scanning and Positioning Terminology

View and Needle Insertion

Short and long axis is based on the position of the probe with reference to the axis of structure (Fig. 1.32). If the probe is place along the axis of the target structure to be scanned, it is showing the long axis view (Fig. 1.33a).

The approach to insert the needle is described according to the orientation of needle to the plane of ultrasound beam (Fig. 1.33b). If the needle tip and the shaft are inserted in a way such that both are in the ultrasound beam, it is called in-plane. If the axis of needle insertion is right angle to the ultrasound beam, it is out-of-plane.

Transducer Handling

There are four basic transducer handling (mnemonic = "PART") (Fig. 1.34).

- P = Pressure, adjust according to the depth of target for visualization
- A = Alignment, sliding the transducer longitudinally
- R = Rotation, rotating the transducer (clockwise/counterclockwise)
- T = Tilting, tilting or angling the transducer

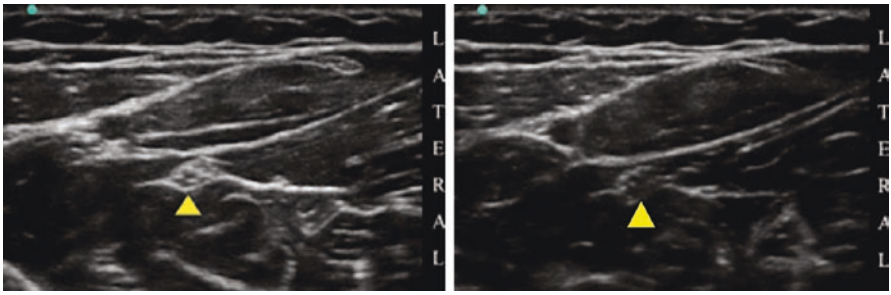

Fig. 1.31b Anisotropy of median nerve. (Reprinted with permission from Philip Peng Educational Series)

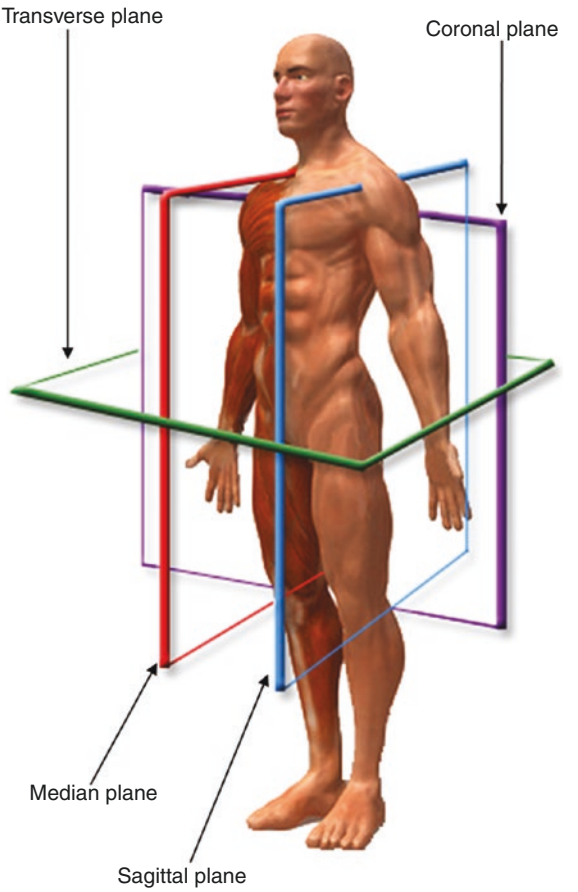

Fig. 1.32 The three different planes. (Reprinted with permission from usra.ca)

Ergonomics

Ergonomics is the study (or science) of the interaction between humans and their working environment. Recent years have witnessed an increasing application of optimal procedural ergonomics in regional anesthesia in an effort to improve outcomes. Poor ergonomics may not only lead to suboptimal performance of a procedure but may contribute to work-related musculoskeletal discomfort.

A sound application of the principles of ergonomics to regional anesthesia and pain management includes the consideration of the following factors:

Positioning and Care of the Patient

Position of patient is important for comfort of patient and for maximal exposure. This position may vary with the type of block being performed. For example, the patient may need a supine position for an upper limb procedure, a prone position for a lower limb procedure, and a sitting position for a neuraxial procedure. Additionally, the position of the limb may be adjusted to assist the procedure.

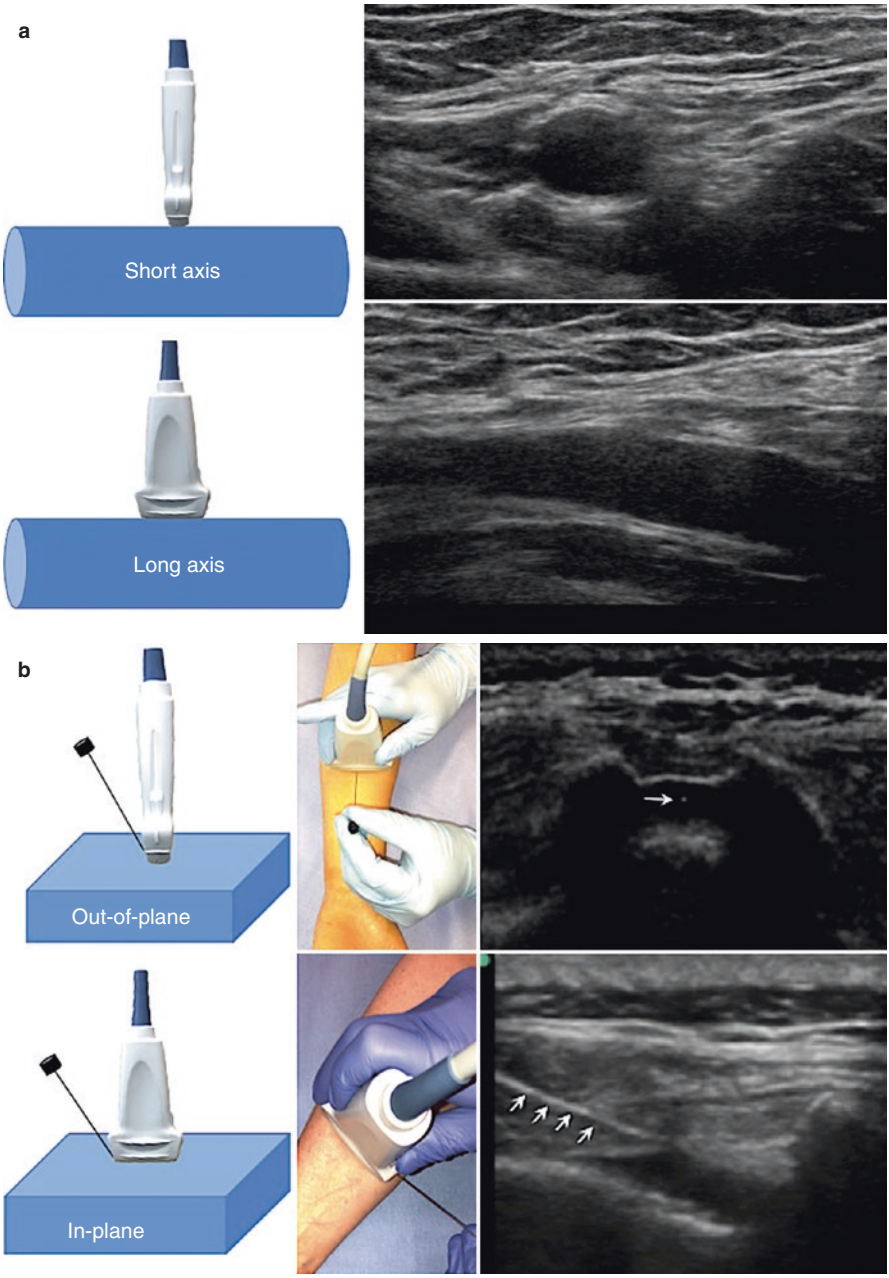

Fig. 1.33 (**a**) Short and long axis. (**b**) In-plane and out-of-plane. (Reprinted with permission from Philip Peng Educational Series)

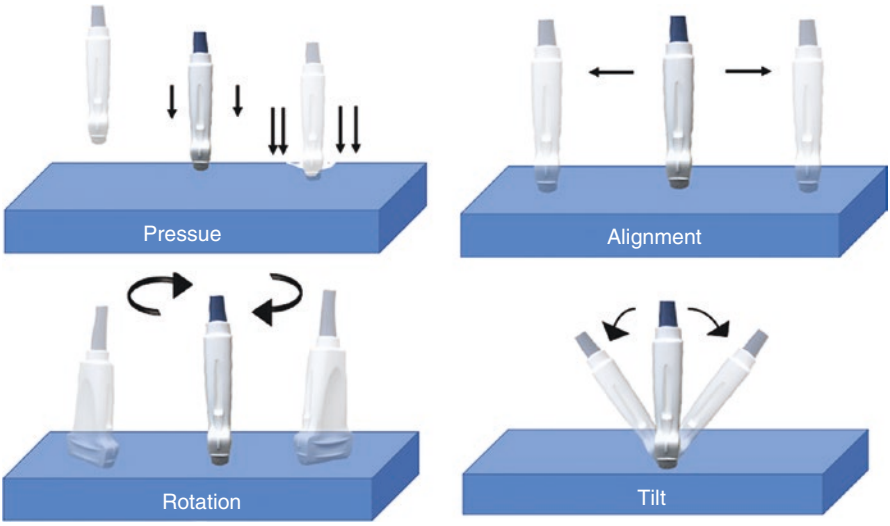

Fig. 1.34 Pressure, alignment, rotation, and tilt. (Reprinted with permission from Philip Peng Educational Series)

Positioning of the Physician

Maintaining a good position with respect to the patient helps to ensure operator comfort and allows optimal procedure performance (Fig. 1.35). This includes the following:

(a) Adjusting the height of patient bed to an appropriate level for the operator.
(b) Assuming a good posture, by choosing to stand or sit down (on a chair).
(c) Performing the procedure from the same target side to avoid reaching over the patient.

Positioning the Equipment

The ultrasound machine is placed in a position so that the operator can view the site of injection and the machine without turning the head. Similarly, the screen of the monitoring equipment must be turned to face the operator during the block to allow a prompt recognition of any significant change of vital signs (Fig. 1.36).

Position of the Assistant

An assistant may be needed both to operate the ultrasound machine and to inject the local anesthetic solution. This may be achieved by standing opposite to the operator and near the ultrasound machine.

Fig. 1.35 Correct and incorrect position of the physician. (Reprinted with permission from Philip Peng Educational Series)

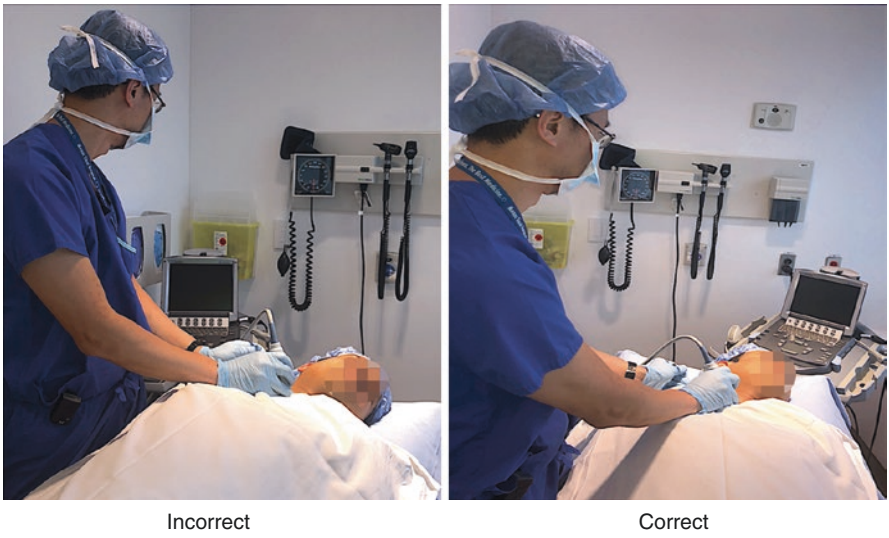

Fig. 1.36 Correct and incorrect position between the operator, patient, and ultrasound machine. (Reprinted with permission from Philip Peng Educational Series)

Fig. 1.37 Correct and incorrect position of holding the ultrasound probe. (Reprinted with permission from Philip Peng Educational Series)

Holding the Probe and Needle Insertion

It is important to have a steady control of the probe position. The probe can be held with 2–3 fingers, and the hand can rest on the body of the patient gently to gain support (Fig. 1.37).

When inserting the needle, make sure your needle is within the field of view of the ultrasound scan, no matter it is in-plane or out-of-plane approach (Fig. 1.38a). Otherwise, the needle is inserted in the wrong plane with reference to the ultrasound field of view and may result in inadvertent tissue puncture (Fig. 1.38b).

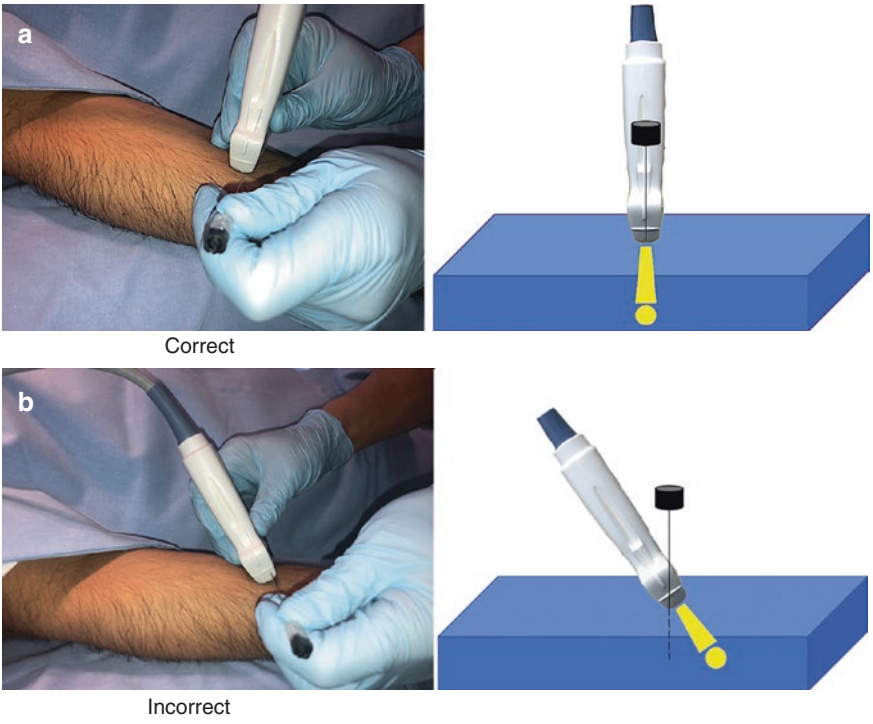

Fig. 1.38 (**a**) Correct angle of insertion of needle. (**b**) Incorrect angle of entry of needle. (Reprinted with permission from Philip Peng Educational Series)

Glossary (Table 1.4)

Table 1.4 Dictionary of terms used in the chapter

Terminology	Definition
Ultrasound	Sound waves of very high frequency (2 MHz or greater)
Absorption	The loss of ultrasound energy when passing through a medium resulting in its conversion to another form of energy such as heat or intracellular mechanical vibration
Acoustic impedance	The resistance to sound transmission through a medium
Acoustic intensity	The concentration of energy in a sound beam; the amount of acoustic power transmitted per unit area
Acoustic power	The amount of acoustic energy generated per unit time
Amplitude	The strength of a sound signal
Artifacts	Display distortions, additions, or errors that can adversely affect ultrasound image acquisition or interpretation
Attenuation	A decrease in amplitude and intensity, as sound travels through a medium. Attenuation occurs with absorption (conversion of sound to heat), reflection (portion of sound returned from the boundary of a medium), and scattering (diffusion or redirection of sound in several directions when encountering a particle suspension or a rough surface)
Axial resolution	The ability to distinguish two structures as separate when the structures are lying close to each other along the same axis as the ultrasound path
Cycle	The combination of one rarefaction and one compression equals one cycle
Diffuse reflection	The reflection that comes off a reflector with an irregular surface
Doppler effect	A change in the frequency of sound as a result of motion between the sound source and the receiver; a positive shift occurs when the source and receiver are approaching each other, and a negative shift occurs when they are moving away from each other
Dynamic range	The ratio of the maximum level of a given parameter to its minimum level; in ultrasound, the dynamic range defines a range of echo intensities that are displayed as a gradient of gray values (minimum value in black and maximum value in white pixels in the final image)
Echogenicity	The degree of brightness of a structure displayed on ultrasound; this is influenced by the amount of beam returning to the transducer (reflection) after encountering the target structure
Enhancement	Increase in reflection amplitude from reflectors that lie behind a weakly attenuating structure, i.e., cysts or solid masses
Frequency	The number of cycles per second; frequency is the inverse of wavelength; the higher the frequency, the shorter the wavelength
Gain	Refers to the amount of amplification of the returning echoes
Gel couplant	A transonic material which eliminates the air interface between the transducer and the animal's skin
Homogenous	Of uniform appearance and texture
Hyperechoic	The image characteristic of a structure that is highly reflective resulting in a brighter displayed image compared to the surrounding structures; the bone and pleura are examples of hyperechoic structures
Hypoechoic	The image characteristic of a structure that is less reflective than the surrounding structure resulting in a darker displayed image compared to the surrounding structures; fluid-filled structures, e.g., vessels and cyst are hypoechoic
Interface	The boundary between two tissue media with different acoustic impedances

(continued)

Table 1.4 (continued)

Lateral resolution	The ability of the system to distinguish two structures as separate when the structures are lying side by side
Longitudinal wave	Movement of particles in the same direction as the direction of the wave propagation
Mechanical probes	Allows the sweeping of the ultrasound beam through the tissues rapidly and repeatedly. This is accomplished by oscillating a transducer. The oscillating component is immersed in a coupling liquid within the transducer assembly. In our case, the coupling fluid is deionized water. It is important that the fluid is bubble free, so that your image is not compromised. Check the water level in the transducer assembly before scanning, and if you see air bubbles, make sure you fill it with the deionized water
M-mode	Is the motion mode displaying moving structures along a single line in the ultrasound beam
Noise	An artifact that is usually due to the gain control being too high
Period	The amount of time required to complete one cycle
Pulsed transducers	Consists of one transducer element which functions as Both the source and receiving transducers
Pulse repetition frequency	The number of pulses occurring in a given time interval; for example, 1 Hz (hertz) is one cycle per second and 10 Hz is ten cycles per second; a lower PRF is required for unambiguous discrimination of structures at deeper imaging depths
Pulse repetition period	Time from the start of one pulse to the start of the next pulse
Pulse duration	The time measured from the start of one pulse to the end of the same pulse
Rayleigh scattering	Scattering of the wave in all directions when the reflector is much smaller than the ultrasound wavelength
Reflection	Mirror-like redirection and return of a propagating sound wave toward the transducer that follows a standard law of reflection; for example, specular reflection results in the reflected angle being equal to the incident angle of the energy propagation
Refraction	A change in the direction of wave propagation when traveling from one medium to another with different propagation speeds according to the Snell's law of refraction
Resolution	The ability to distinguish between two structures that lie close to one another
Reverberation	Multiple reflections commonly seen in the bladder or heart
Scattering	A process by which the ultrasound is forced to deviate from a straight-line reflection and trajectory due to small, localized nonuniformities in the tissue
Shadowing	Created by strong reflectors or attenuating structures, i.e., the bone, gas, calcifications, and air
Speckle	The granular appearance of images and spectral displays that is caused by the interference of echoes from the distribution of scatterers in tissue
Specular reflection	The reflection that comes off a smooth reflector (e.g., a mirror)
Transverse wave	Movement of particles perpendicular to the direction of the wave propagation
Transducers	Convert one form of energy to another. Ultrasound transducers convert electric energy into ultrasound energy and vice versa. Transducers operate on piezoelectricity meaning that some materials (ceramics, quartz) produce a voltage when deformed by an applied pressure and reversely result in a production of pressure when these materials are deformed by an applied voltage

Suggested Reading

Abbas K, Chan V. Basic understanding of ultrasound scanning. In: Peng P, editor. Ultrasound in pain medicine intervention: a practical guide, Philip Peng educational series, vol. I. California: Apple Inc; 2014.

Chin KJ. Needle and transducer manipulation: the art of ultrasound guided regional anesthesia. Int J Ultrasound Appl Technol Periop Care. 2010;1:27–32.

Sehmbi H, Perlas A. Basic of ultrasound imaging. In: Jankovic D, Peng P, editors. Regional nerve blocks in anesthesia and pain therapy. Cham: Springer; 2015.

Greater and Lesser Occipital Nerve

2

Yasmine Hoydonckx and Philip Peng

Introduction

Indication of Blockade

Blockade of the greater and lesser occipital nerves has been implicated in different types of chronic headaches, including primary headaches and secondary headaches (Table 2.1). Patients with these types of headaches often experience good pain relief by targeting the occipital nerves.

The basis of how occipital nerve block works in the primary headache is likely related to the convergence of the functional connection between the sensory inputs from the occipital segments with the nuclei of the trigeminal nociceptive system (the trigeminocervical complex). From there, the neural circuit connects further to thalamus and cortex. Temporary suppression of the inputs from the greater occipital nerve (GON) may lead to modulation of central nociceptive pathways and reducing central sensitization.

Traditionally, the GON block is performed with blinded approach relying on the anatomic landmarks at the level of the superior nuchal line. This approach poses a higher risk to injection in the occipital artery and/or block failure. Complication rates of 5–10% have been reported, including dizziness, blurred vision, and syncope. Use of ultrasound has been shown not only to reduce the risks but also to improve the block efficacy.

Y. Hoydonckx
Department of Anesthesia and Pain Medicine, University of Toronto and Toronto Western Hospital, University Health Network, Toronto, ON, Canada

P. Peng (✉)
Department of Anesthesia and Pain Management, Toronto Western Hopsital and Mount Sinai Hospital, University of Toronto, Toronto, Ontario, Canada
e-mail: Philip.peng@uhn.ca

P. Peng et al. (eds.), *Ultrasound for Interventional Pain Management*,
https://doi.org/10.1007/978-3-030-18371-4_2

Table 2.1 Indications of occipital nerve blocks in headache

	Specific types of headache
Primary	Migraine, cluster headaches, post-concussion headache
Secondary	Cervicogenic headache, occipital neuralgia

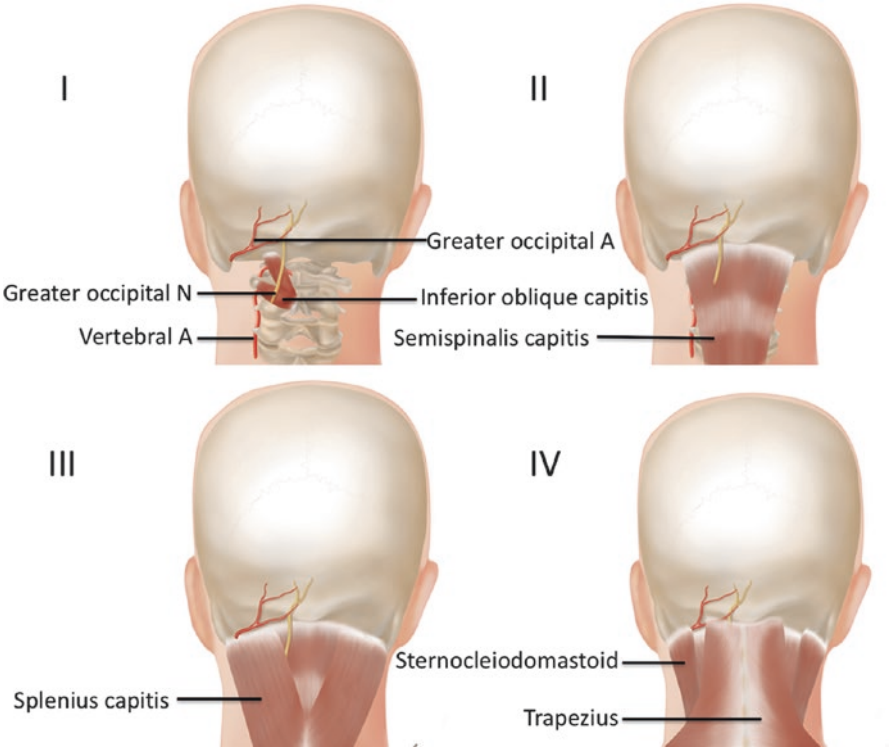

Fig. 2.1 Fours layers of muscles relevant to the greater occipital nerve. N and A-nerve and artery. (Reprint with permission from Philip Peng Educational Series)

Anatomy

The greater occipital nerve (GON) originates from the medial branch of the dorsal ramus of the C2 spinal nerve, with contributions from the C3 dorsal ramus.

The GON exits below the posterior arch of the second cervical vertebra, curves around the inferior oblique capitis (IOC) muscle, and travels cephalad in an oblique trajectory between the inferior oblique capitis and semispinalis capitis (SSC) muscle. At this site, the GON is susceptible to potential entrapment. The GON then perforates the trapezius muscle and ascends medial to the occipital artery to innervate the posterior cutaneous aspect of neck and scalp (Fig. 2.1).

The lesser occipital nerve (LON) is the most cephalad branch of the superficial cervical plexus beneath the sternocleidomastoid muscle. It is formed by fibers of the

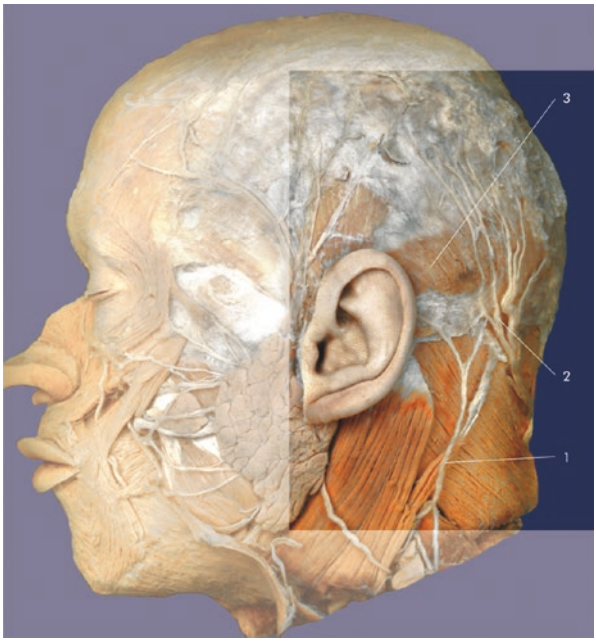

Fig. 2.2 (1) Lesser occipital nerve, (2) greater occipital nerve and occipital artery, and (3) occipital muscle. (Reprinted with permission from Danilo Jankovic)

ventral rami of C2 and C3 and curves around its posterior border to run cranially to the parieto-occipital area where it splits in its terminal branches to innervate the lateral part of the occiput (skin behind and above the ear) (Fig. 2.2).

Patient Selection

The diagnosis of a specific headache type can be made according to the International Head Society (IHS) classification. The occipital nerve block plays a diagnostic role in the diagnosis of occipital neuralgia and cervicogenic headache. For the other aforementioned headaches, the nerve block can be considered in patient's failure to respond to conservative management.

Ultrasound Scanning

The Greater Occipital Nerve: Two Different Target Locations

Proximal Approach at Level of C2

- Position: Prone with head and neck flexed
- Probe: Linear, 12–18 MHz

The key landmarks are the spinous process of C2 and the inferior oblique capitis muscle.

Scan 1: Occipital protuberance (probe in transverse orientation (Fig. 2.3).

Scan 2: Spinous process of C2. It showed a bifid bone structure below the occiput (Fig. 2.4).

Scan 3: The transducer is moved laterally to visualize the inferior oblique capitis (IOC) muscle and semispinalis capitis (SSC) muscle; to maximize the image of this muscle, the lateral end of the probe is rotated slightly in a cranial direction to bring the transducer parallel to the long axis of the muscle (Fig. 2.5). With this movement, the C2 lamina appears boat-shaped, and IOC is cradled within it. The plane between the IOC and SSC is visualized. Greater occipital nerve (GON) is sandwiched between the IOC and SSC muscles. LON-lesser occipital nerve, SCM-sternocleidomastoid.

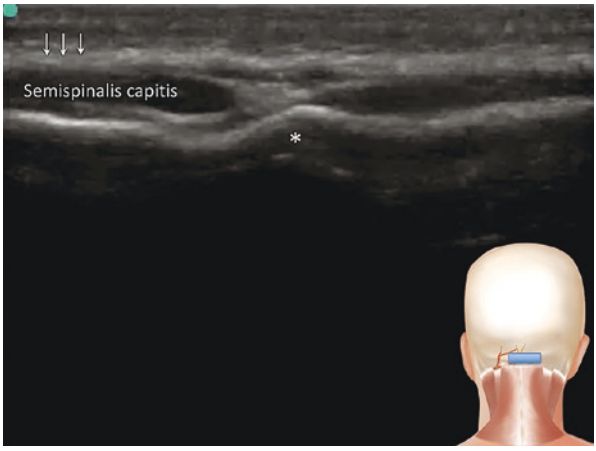

Fig. 2.3 The scan at the occipital protuberance (*). The arrows indicated the superficial fascia of the scalp. The position of the ultrasound probe is shown in the picture in the left lower corner. (Reprinted with permission from Philip Peng Educational Series)

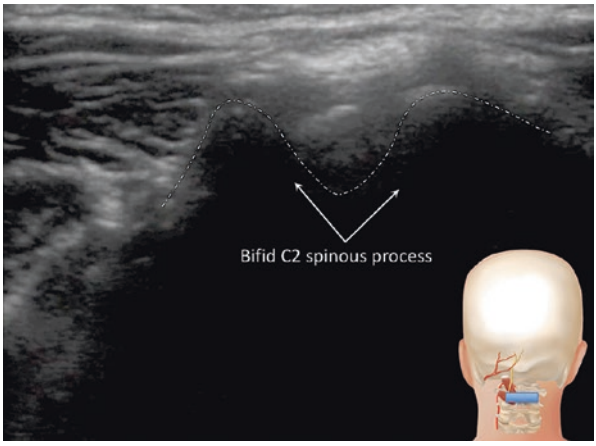

Fig. 2.4 Scan at the C2 level. (Reprinted with permission from Philip Peng Educational Series)

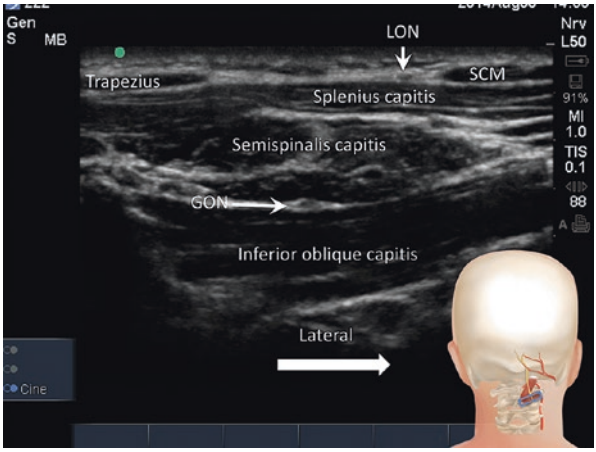

Fig. 2.5 Ultrasound scan at C2 level with the lateral end of the transducer tilted toward C1 lateral mass. (Reprinted with permission from Philip Peng Educational Series)

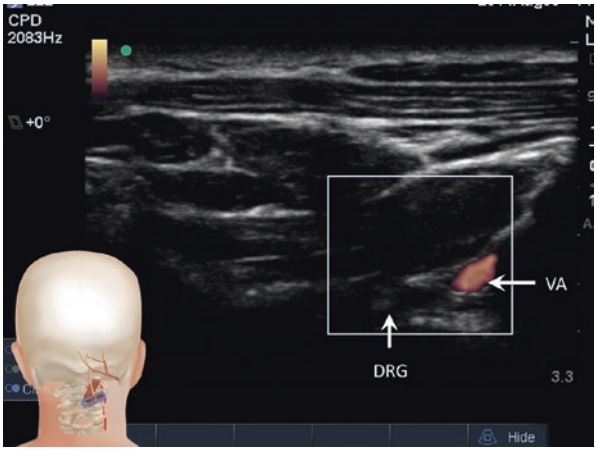

Fig. 2.6 By moving the probe further in the lateral direction as in Fig. 2.5 and applying the Doppler, it revealed the vertebral artery (VA) and the dorsal root ganglion (DRG). (Reprinted with permission from Philip Peng Educational Series)

Scan 4: Doppler scan on the lateral side reveals the vertebral artery (VA) and dorsal root ganglion (DRG) (Fig. 2.6).

Distal Approach at Level of Occiput

- Position: Prone/sitting
- Probe: Linear, 12–18 MHz

The key landmark is the superior nuchal line and occipital protuberance.

Scan 1: Upper sonograph shows the transverse view at superior nuchal line (Fig. 2.7a).

Scan 2: The lower sonograph shows the transducer moved laterally until the greater occipital artery is visualized (Fig. 2.7b). The GON is not commonly

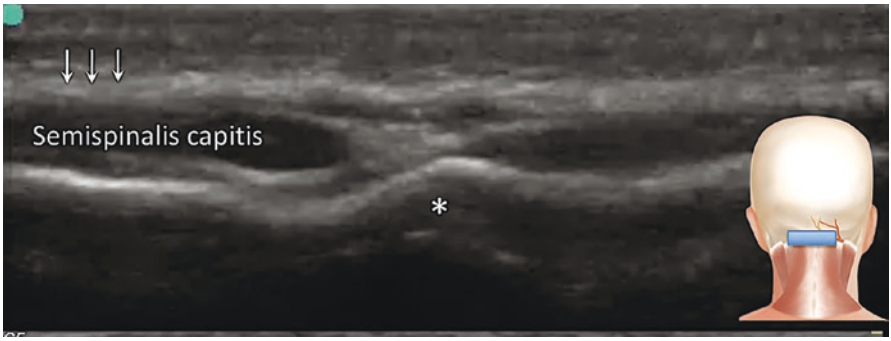

Fig. 2.7a Scan at occipital protuberance (*) and arrows indicated the superficial fascia. (Reprinted with permission from Philip Peng Educational Series)

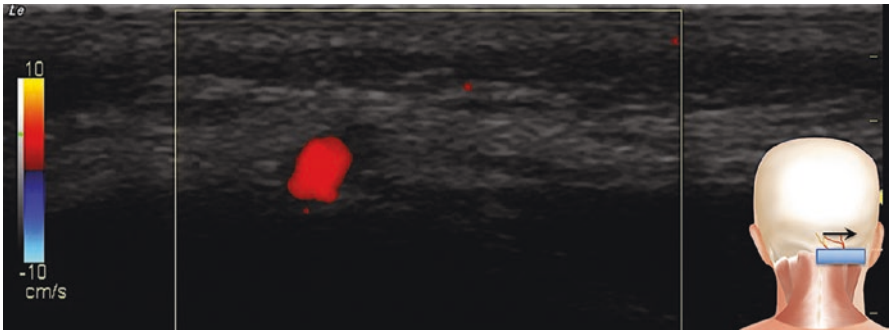

Fig. 2.7b Doppler showed the occipital artery which is in the same fascia plane with the greater occipital nerve. (Reprinted with permission from Philip Peng Educational Series)

visualized as it is usually divided into small branches. However, the visualization of the artery and the plane it is in help to direct the needle to the lateral side of the artery.

The Lesser Occipital Nerve

- Position: Prone/sitting
- Probe: Linear, 12–18 MHz

The key landmark is the posterior border of the sternocleidomastoid muscle, caudal to the mastoid.

Scan 1: The probe is moved cranially and caudally along the posterior border of sternocleidomastoid (SCM) until a nerve structure is identified (Fig. 2.8).

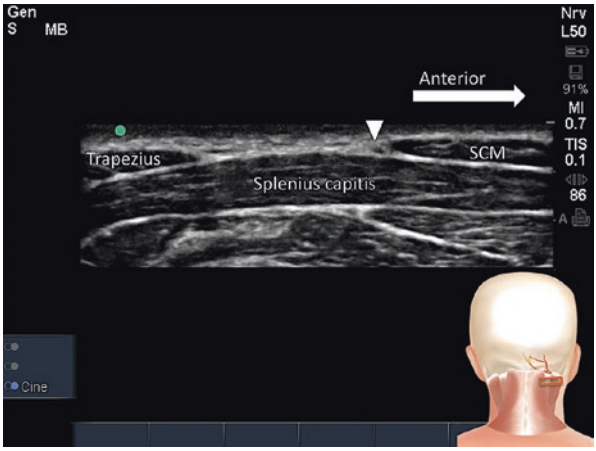

Fig. 2.8 Sonography showed the lesser occipital nerve. SCM-sternocleidomastoid. (Reprinted with permission from Philip Peng Educational Series)

Procedure

- Equipment: 22G 3.5-inch needle
- Drugs: Bupivacaine 0.25% 4 mL with 40 mg Depo-Medrol

Proximal Approach at Level of C2

- A 25G needle infiltrates the skin with 2% lidocaine and then advances in an in-plane technique from lateral to medial (more experienced practitioner may choose out of plane) toward the plane between the inferior oblique capitis muscle and semispinalis capitis muscle (Fig. 2.9).
- Needle tip position is confirmed by using hydrodissection with normal saline (Fig. 2.9).
- Check for absence of vascular structures using Doppler.
- Aspiration is negative prior to injection of therapeutic medication.
- The spread of the injectate is visualized as it surrounds the GON.

Distal Approach at Level of Occiput

- A 25G needle is inserted in an in-plane technique and used to numb the skin with lidocaine 2%.
- The same 25G needle is advanced toward the fascia plane with the greater occipital artery and greater and lesser occipital nerve.
- Aspiration is negative prior to injection of 2 mL of therapeutic medication (4 mL of bupivacaine 0.25% with 40 mg methylprednisolone), medial from the occipital artery.

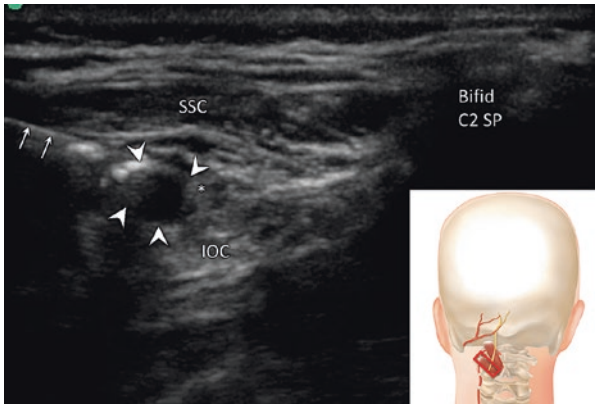

Fig. 2.9 Sonography showed the injection around the greater occipital nerve. SSC semispinalis capitis; IOC inferior obliquus capitis. (Reprint with permission from Philip Peng Educational Series)

- As the artery is dissected free from the surrounding fascia, the needle can be advanced further inferior to the vessel at the lateral side where another 2 mL of the therapeutic medication is injected.

The Lesser Occipital Nerve

- The probe is moved cranially and caudally along the posterior muscle border until a nerve structure is identified, which originated from the superficial cervical plexus beneath the sternocleidomastoid muscle and runs straight upward distally to the lateral occiput.

Clinical Pearls

1. We recommend for less-experienced sonographers to start with the easier distal US-guided GON approach.
2. A block is successful if it creates absence of light-touch sensation in the dermatome of GON.
3. The target area in the proximal approach is not far from vertebral artery and epidural space; constant visualization of the needle and injectate is mandatory.
4. Proximal approach might be the technique of preference for patients with occipital neuralgia, since nerve entrapment is often in proximal location.
5. The GON is usually 3–4 cm from the midline. Quite commonly, another nerve appears in the same plane but much closer to the midline. It is the third occipital nerve.
6. The angle of mandible approximates C3 level. Thus, a simpler way to find the bifid C2 spinous process is to put the transducer in midline at this level and scan in cephalad direction to search for the bifid spinous process.

Literature Review

Several studies have evaluated the efficacy of the greater occipital nerve block in different types of headache. Consistently, these trials showed efficacy that lasted beyond the duration of action of local anesthetics and steroids. A recent published meta-analysis of impact of GON block for migraine patients showed substantial reduction in pain intensity and medication consumption but no impact on headache duration. Both episodic and chronic cluster attacks are suppressed by this block.

Concerning the ultrasound-guided technique, a cadaver study showed that the more precise proximal blockade described above is associated with higher success rate, compared to the distal approach at the superior nuchal line. This was also demonstrated by two recently published case series which demonstrated the feasibility, efficacy, and safety of the proximal ultrasound-guided GON block. However, no clinical trials comparing both US-guided GON approaches (proximal vs. distal) have been published yet.

Some small studies of pulsed radiofrequency treatment of GON have demonstrated better and longer-lasting pain relief comparing to steroid injection in patients with occipital neuralgia, migraine, or cervicogenic headache. This, however, has to be further investigated in better designed study of larger sample size.

Suggested Reading

Ashkenazi A, Blumenfeld A, Napchan U, Narouze S, Grosberg B, Nett R, et al. Peripheral nerve blocks and trigger point injections in headache management – a systematic review and suggestions for future research. Headache. 2010;50(6):943–52.

Cohen SP, Peterlin BL, Fulton L, Neely ET, Kurihara C, Gupta A, et al. Randomized, double-blind, comparative-effectiveness study comparing pulsed radiofrequency to steroid injections for occipital neuralgia or migraine with occipital nerve tenderness. Pain. 2015;156(12):2585–94.

Curatolo M. Greater occipital nerve. In: Peng PWH, editor. Ultrasound for pain medicine intervention: a practical guide. Vol 1. Peripheral Structures. Philip Peng Educational Series. California: iBook, Apple Inc.; 2013. p. 13.

Gaul C, Roguski J, Dresler T, Abbas H, Totzeck A, Gorlinger K, et al. Efficacy and safety of a single occipital nerve blockade in episodic and chronic cluster headache: A prospective observational study. Cephalalgia: Int J Headache. 2017;37(9):873–80.

Greher M, Moriggl B, Curatolo M, Kirchmair L, Eichenberger U. Sonographic visualization and ultrasound-guided blockade of the greater occipital nerve: a comparison of two selective techniques confirmed by anatomical dissection. Br J Anaesth. 2010;104(5):637–42.

Lambru G, Abu Bakar N, Stahlhut L, McCulloch S, Miller S, Shanahan P, et al. Greater occipital nerve blocks in chronic cluster headache: a prospective open-label study. Eur J Neurol. 2014;21(2):338–43.

Naja ZM, El-Rajab M, Al-Tannir MA, Ziade FM, Tawfik OM. Occipital nerve blockade for cervicogenic headache: a double-blind randomized controlled clinical trial. Pain Pract. 2006;6(2):89–95.

Pingree MJ, Sole JS, TG OB, Eldrige JS, Moeschler SM. Clinical efficacy of an ultrasound-guided greater occipital nerve block at the level of C2. Reg Anesth Pain Med. 2017;42(1):99–104.

Platzgummer H, Moritz T, Gruber GM, Pivec C, Wober C, Bodner G, et al. The lesser occipital nerve visualized by high-resolution sonography--normal and initial suspect findings. Cephalalgia: Int J Headache. 2015;35(9):816–24.

Zhang H, Yang X, Lin Y, Chen L, Ye H. The efficacy of greater occipital nerve block for the treatment of migraine: a systematic review and meta-analysis. Clin Neurol Neurosurg. 2018;165:129–33.

Zipfel J, Kastler A, Tatu L, Behr J, Kechidi R, Kastler B. Ultrasound-guided intermediate site greater occipital nerve infiltration: a technical feasibility study. Pain Physician. 2016;19(7):E1027–34.

Cervical Sympathetic Trunk

3

Farah Musaad M. Alshuraim and David Flamer

Introduction

The stellate ganglion block (SGB) is the most common sympathetic block performed today. The sympathetic nervous system plays a prominent role in neuropathic, visceral, and vascular pain. As a result, the SGB can be helpful for a variety of painful and non-painful medical conditions. A temporary blockage of the sympathetic nervous system can help differentiate sympathetically maintained pain (SMP) from sympathetically independent pain (SIP) for conditions of the head, neck, or upper extremity.

Sympathetic fibers supplying the head, neck, and upper limbs arise from the first few thoracic segments and ascend through the sympathetic chains to synapse in the superior, middle, and inferior cervical ganglia, which together form the cervical sympathetic chain (Fig. 3.1). The stellate ganglion (also known as the cervicothoracic ganglion) is formed on each side of the neck by the fusion of the inferior cervical ganglion with the first thoracic ganglion. It lies deep to the prevertebral fascia and medial and posterior to the carotid artery. The ganglion is 1–2.5 cm long and approximately 1 cm wide and may be fusiform, triangular, or oval in shape. At the level of the sixth cervical vertebra (C6), the transverse process has a bony process (termed the "Chassaignac tubercle"), which may be palpated with deep pressure by retracting the carotid artery laterally.

F. M. M. Alshuraim
Department of Anesthesia, Mount Sinai Hospital, Toronto, ON, Canada

D. Flamer (✉)
Anesthesiology and Pain Management, Mount Sinai Hospital – University Health Network, Toronto, ON, Canada
e-mail: david.flamer@uhn.ca

P. Peng et al. (eds.), *Ultrasound for Interventional Pain Management*,
https://doi.org/10.1007/978-3-030-18371-4_3

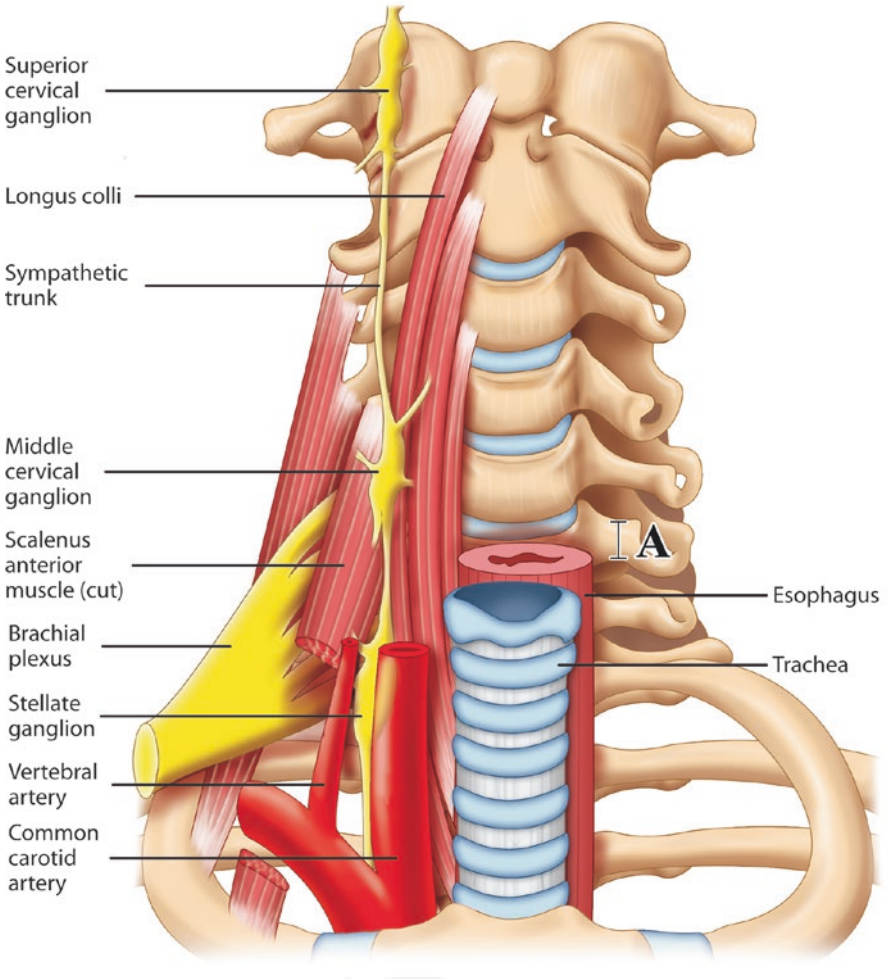

Fig. 3.1 Anatomy of cervical sympathetic chain. (Reprint with permission from Philip Peng Educational Series)

The preganglionic fibers of the head and neck region continue to travel cephalad to the superior and middle cervical ganglion through the cervical sympathetic trunk. Injection of local anesthetic around the stellate ganglion interrupts the sympathetic outflow to the head, neck, and upper limbs through inactivation of both preganglionic and postganglionic fibers (Fig. 3.2). The stellate ganglion is located in close proximity to the pleural and vertebral artery. As a result, the SGB is performed at a more cephalad location, in proximity to the middle cervical ganglion.

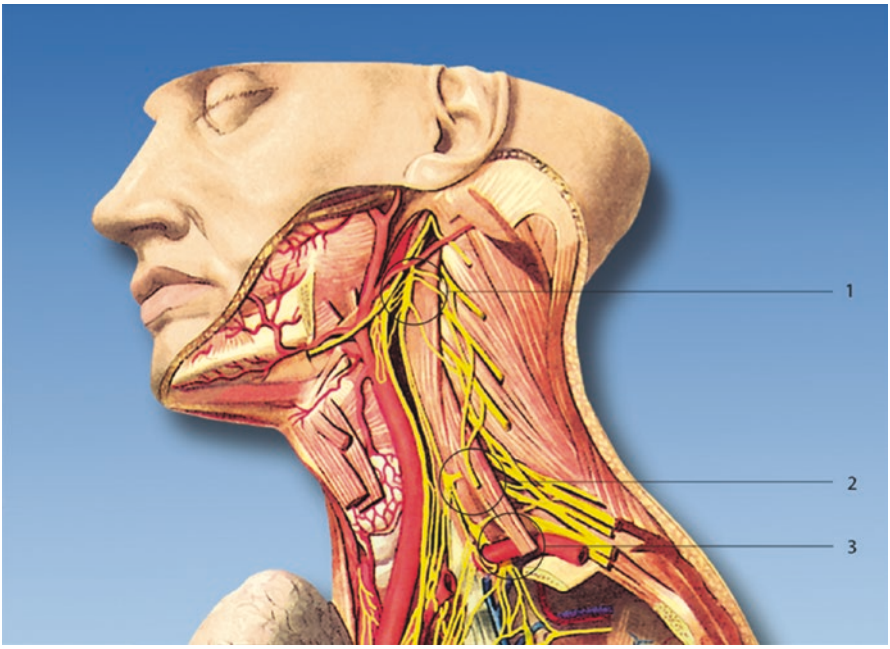

Fig. 3.2 The cervical ganglion trunk: (1) superior cervical ganglion, (2) middle cervical ganglion, and (3) cervicothoracic ganglion. (Reprinted with permission from Danilo Jankovic)

Patient Selection

Stellate ganglion blocks are used for a variety of painful conditions, most notably for sympathetically mediated pain in the context of complex regional pain syndrome. However, the technique is not limited to painful conditions. There is growing evidence for its use in treating numerous non-painful medical conditions.

Indications
Painful medication conditions:
Sympathetically mediated pain of the upper extremity, head, or neck
Acute herpes zoster or postherpetic neuralgia of the head, neck, or upper thorax
Phantom limb pain
Cluster headache or atypical vascular headache
Intractable angina pectoris
Non-painful medication conditions:
Raynaud disease
Obliterative vascular disease
Vasospasm
Hyperhidrosis
Lymphedema
Refractory ventricular arrhythmia
Post-traumatic stress disorders

Contraindications
Anticoagulated patient or coagulopathy
Preexisting contralateral phrenic nerve palsy
Recent myocardial infarction
Cardiac conduction block
Only unilateral blocks should be performed to avoid bilateral recurrent laryngeal nerve block and resulting stridor.

Ultrasound Scanning

- Position: Semi-lateral decubitus position, with the neck turned contralateral
- Probe: Linear 6–13 MHz

- Scan 1: Place the probe at the C6 level (Figs. 3.3 and 3.4). Identify the key landmarks, including the longus colli muscle (LC), longus capitis muscle (LCa), prevertebral fascia (arrows), cervical nerve root (N), carotid artery (C), and internal jugular vein (**). At this level, the transverse process has a prominent anterior tubercle (AT).
- Scan 2: To confirm the level, scan the probe caudally to the C7 level. The transverse process is the key landmark to identify at this level (Fig. 3.5). At this level, the transverse process has a prominent posterior tubercle and vestigial anterior tubercle. Use color Doppler to identify the vertebral artery.

  Note that at the C6 level, the vertebral artery most commonly enters the foramen transversarium. In up to 10% of patients, the vertebral artery travels outside the foramen transversarium at the C6 or even C5 level. The figure showed the presence of vertebral artery anterior to the anterior tubercle at C5 level (Fig. 3.6).

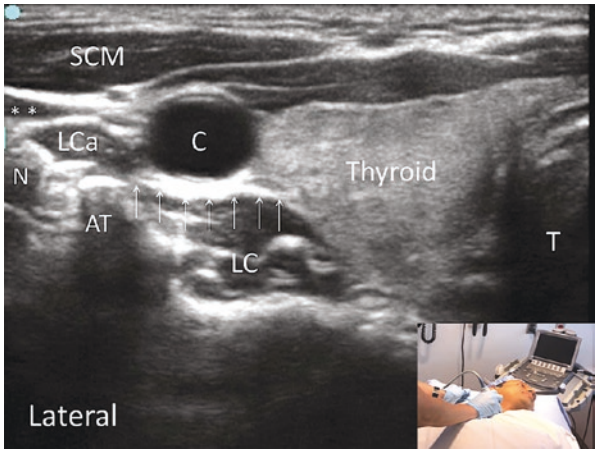

Fig. 3.3 Sonoanatomy at C6. The right lower corner showed the position of the patient. Longus colli muscle (LC), longus capitis muscle (LCa), prevertebral fascia (arrows), cervical nerve root (N), carotid artery (C), and internal jugular vein (**). At this level, the transverse process has a prominent anterior tubercle (AT). (Reprinted with permission from Philip Peng Educational Series)

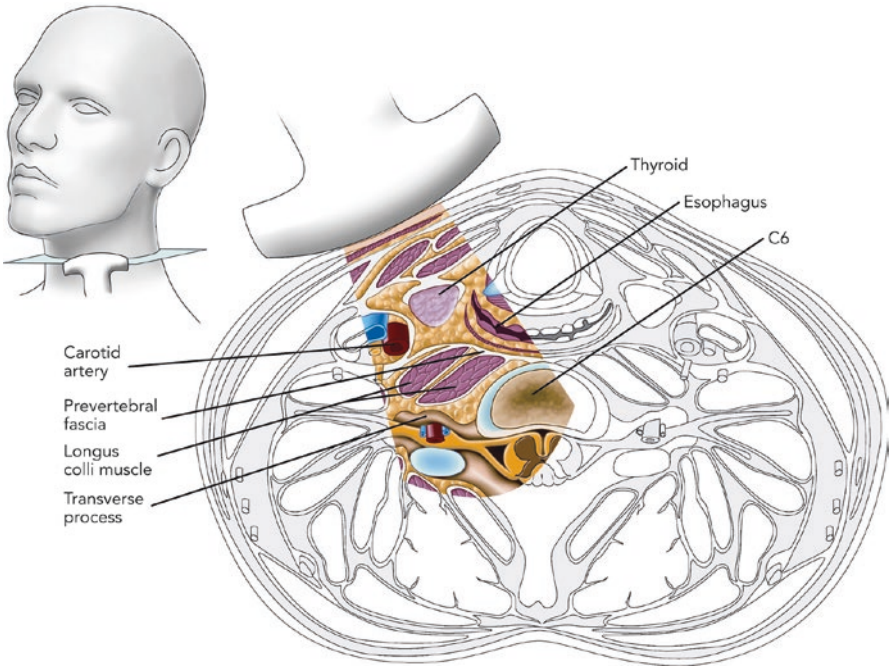

Fig. 3.4 The corresponding anatomic structures revealed at C6. (Reprinted with permission from Philip Peng Educational Series)

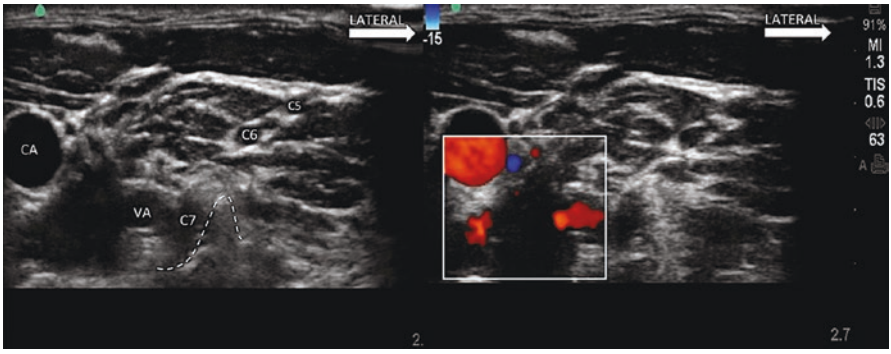

Fig. 3.5 Sonography at C7. VA, vertebral artery; CA, carotid artery. (Reprinted with permission from Philip Peng Educational Series)

- Scan 3: At the C6 level, perform a pre-scan with and without color Doppler (Fig. 3.7). Identifying aberrant vessels and structures such as the esophagus will help plan for the safest approach, which may change in location on swallowing (Fig. 3.7). The location of the esophagus and the vessel may discourage a practitioner from performing a medial or lateral approach (see procedure below).

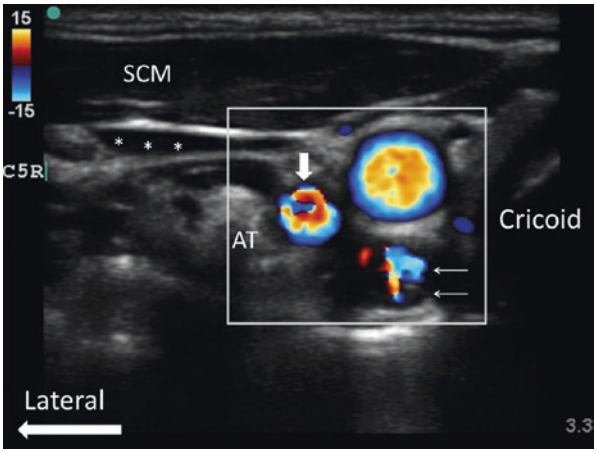

Fig. 3.6 Vertebral artery anterior to the anterior tubercle (AT) at C5. Vertebral artery indicated by bold arrow. The other artery medial to the vertebral artery is the carotid artery with a reflection artifact (arrows). SCM, sternocleidomastoid muscle; ⁎jugular vein. (Reprinted with permission from Philip Peng Educational Series)

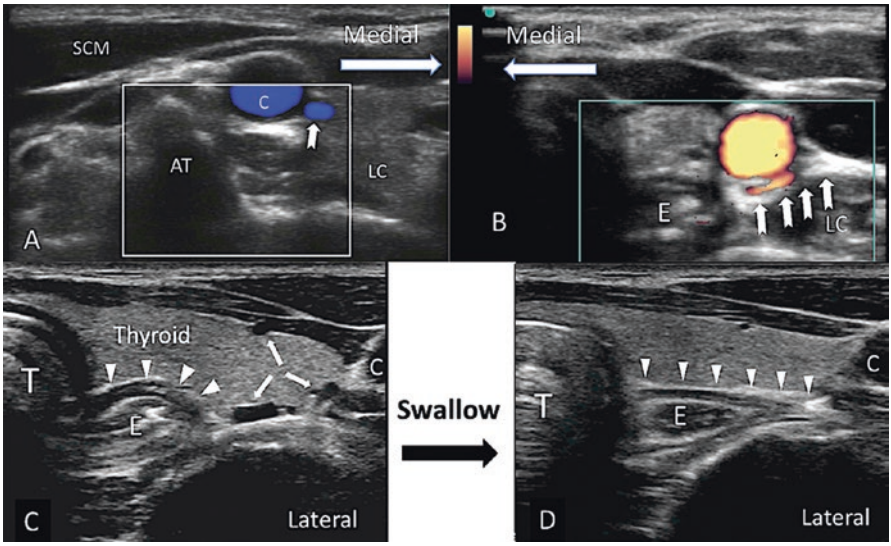

Fig. 3.7 Panels (**a**)–(**c**) showed different aberrant vessels in short axis and long axis (bold arrows). Panels (**b**)–(**d**) showed the presence of the esophagus (E) outlined by arrowheads. (Reprinted with permission from Philip Peng Educational Series)

Procedure

Equipment and Drugs

- Needle: 25G 1.5 inch or 22G 3.5 inch needle
- Drugs: 3–5 mL of local anesthetic (0.25–0.5% bupivacaine)

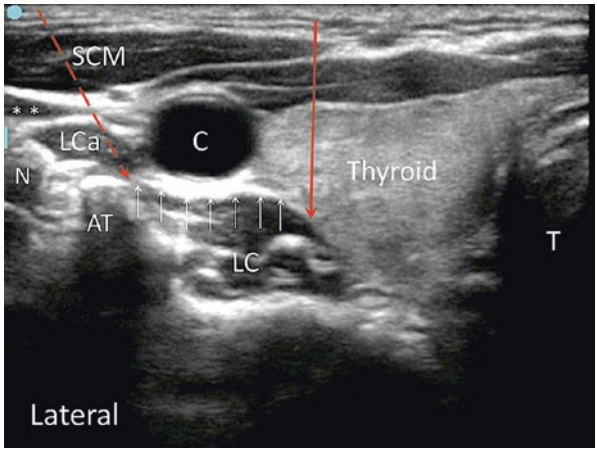

Fig. 3.8 Figure showing the medial (out-of-plane) approach or lateral in-plane approach. The target is the prevertebral fascia (arrows). SCM, sternocleidomastoid muscle; LCa, longus capitis muscle; LC, longus colli muscle; AT, anterior tubercle; T, trachea; solid line, medial out-of-plane approach, dotted line, lateral in-plane approach. *Internal jugular vein (collapsed) (Reprinted with permission from Philip Peng Educational Series)

Both medial and lateral approaches can be utilized for this technique (Fig. 3.8). With both techniques, the needle tip is directed between the prevertebral fascia between the longus colli and capitis muscles. The target is the soft tissue plane between these two layers of prevertebral fascia. The medial approach involves placing the needle medial to the carotid artery, and the needle is advanced toward the target using an out-of-plane technique. The lateral approach involves placing the needle in-plane and lateral to the carotid artery, with the needle tip advanced to the target. Typically, a lateral approach is recommended because of the frequent presence of the esophagus and aberrant vessel medial to the carotid artery.

Care needs to be taken to avoid cervical nerve roots, major blood vessels, and non-vascular structures such as the esophagus and thyroid gland. Continued visualization of the needle tip throughout the technique, coupled with the use of hydrodissection and visualization of local anesthetic spread, will help ensure safe needle placement.

Clinical Pearls

1. When confirming cervical levels, make sure to scan in a caudal and cephalad direction to identify both C6 and C7 levels.
2. In 7–10% of patients, the vertebral artery will be exposed outside of the foramen transversarium at the C6 level.
3. Place a normal saline bag underneath the ipsilateral shoulder to allow more space for the hand holding the needle for the in-plane technique.
4. Always turn the hand to the contralateral side to “move” the carotid artery further away from the anterior or carotid tubercle of C6.
5. Always use color Doppler to assess for the location of the vertebral artery and other major vessels that may lie in the path of the needle.

6. Hydrodissection with normal saline will help minimize the risk of unintended intravascular injection with local anesthetic. Due to the proximity of the central nervous system, small amounts of local anesthetic injected intravascularly can quickly lead complications, such as seizures.
7. Perform only unilateral injections to avoid risk of respiratory complications associated with bilateral injections, such as phrenic nerve palsy and swallowing difficulties.
8. Patients should be made aware of what can be expected postinjection, including but not limited to Horner's syndrome, facial and conjunctival flushing, upper extremity numbness or weakness, hoarseness, and dysphagia. Horner's syndrome following the procedure can be used as a confirmatory sign of successful blockade.

Literature Review

The stellate ganglion block can be useful for both painful and non-painful conditions of the upper extremity, head, neck, and upper thorax. The target is the cervicothoracic ganglion, which is approached by targeting the plane within the prevertebral fascia. This procedure has commonly been performed by using either a landmark-based approach or fluoroscopic-guided approach. These techniques do not allow for identification of the target fascial plane, nor do they help to visualize important vascular structures in the region. Ultrasonography has emerged as a more accurate and potentially safer imaging option for performing an SGB.

Typically, the SGB procedure has involved the injection of local anesthetic for a single sympathetic block; however, other modalities have been used in an attempt to provide a longer duration of blockade. This includes the use of both chemical and thermal neurolysis. Chemical neurolysis for SGB, with the use of phenol, for example, is associated with the risk of serious complications, due to unintended spread to adjacent nerve and vascular structures. Conventional thermal radiofrequency ablation carries the risk of long-term nerve injury due to neural destruction. Pulsed radiofrequency, a variation of thermal radiofrequency that results in less thermal damage, has emerged as a potential treatment for various chronic pain syndromes, including SGB. Evidence is limited, and further research is needed to support its application for the SGB.

Suggested Reading

Abdi S, Zhou Y, Patel N, Saini B, Nelson J. A new and easy technique to block the stellate ganglion. Pain Physician. 2004;7(3):327–31.

Atez Y, Asik I, Ozgencil E, et al. Evaluation of the longus colli muscle in relation to stellate ganglion block. Reg Anesth Pain Med. 2009;34:219–23.

Bhatia A, Peng P. Stellate ganglion block. In: Regional nerve blocks in anesthesia and pain therapy. 4th ed. Cham: Spring Publishing; 2015.

Bhatia A, Flamer D, Peng PW. Evaluation of sonoanatomy relevant to performing stellate ganglion blocks using anterior and lateral simulated approaches: an observational study. Can J Anaesth. 2012;59:1040–7.

Drummond PD, Finch PM, Skipworth S, Blockey P. Pain increases during sympathetic arousal in patients with complex regional pain syndrome. Neurology. 2001;57:1296–303.

Flamer D, Seib R, Peng P. Complications of regional anesthesia in chronic pain therapy. Complications of regional anesthesia. Cham: Spring Publishing; 2017.

Gofeld M, Shankar H, Benzon H. Fluoroscopy and ultrasound-guided sympathetic blocks: stellate ganglion, lumbar sympathetic blocks, and visceral sympathetic blocks. In: Essentials of pain medicine. 4th ed. Philadelphia: Elsevier Publishing; 2016.

Huntoon MA. The vertebral artery is unlikely to be the sole source of vascular complications occurring during stellate ganglion block. Pain Pract. 2010;10:25–30.

Kim ED, Yoo WJ, Kim YN, Park HJ. Ultrasound-guided pulsed radiofrequency treatment of the cervical sympathetic chain for complex regional pain syndrome: a retrospective observational study. Medicine (Baltimore). 2017;96:e5856.

Makharita MY, Amr YM, El-Bayoumy Y. Effect of early stellate ganglion blockade for facial pain from acute herpes zoster and incidence of postherpetic neuralgia. Pain Physician. 2012;15(6):467–74.

Peng P. Peripheral applications of ultrasound for chronic pain. In: Benzon HT, Huntoon MA, Narouze S, editors. Spinal injections and peripheral nerve blocks: interventional and neuromodulatory techniques for pain management. 1st ed. Philadelphia: Elsevier; 2011.

Peng P. Ultrasound for pain medicine intervention: a practical guide. Philip Peng Education Series. 2013. iBooks. https://itunes.apple.com/ca/book/ultrasound-for-pain-medicine-intervention-practical/id643092938?mt=11

Soneji N, Peng P. Ultrasound-guided pain interventions – a review of techniques for peripheral nerves. Korean J Pain. 2013;26(2):111–24.

Suprascapular Nerve

4

Jay M. Shah, Zachary Pellis,
and David Anthony Provenzano

Introduction

Anatomy

The suprascapular nerve (SN) is a mixed sensory and motor nerve that originates from the upper (superior) trunk of the brachial plexus (C5) and innervates the supraspinatus and infraspinatus muscles, as well as the acromioclavicular and glenohumeral joints (Table 4.1 and Fig. 4.1). After passing through the suprascapular notch, inferior to the superior transverse scapular ligament, the suprascapular nerve courses inferolateral in the supraspinous fossa at the periosteal level to reach the lateral border of the spine of the scapula. The nerve then courses around the spinoglenoid notch to reach the infraspinous fossa where if gives off terminal muscular branches to infraspinatus.

The suprascapular artery most commonly passes superficial to the ligament. The SN (stemming from the ventral rami of spinal nerves C4, C5, and C6 and emerging from the upper trunk of the brachial plexus) provides 70% of sensory innervation to the shoulder joint.

Pathophysiology and Clinical Presentation

Shoulder pain can originate from structures (rotator cuff, glenohumeral joint, etc.) innervated by the SN (Table 4.2). In addition, suprascapular neuropathy (SSN) may be considered as a cause of shoulder pain and is seen in individuals who participate in

J. M. Shah
SamWell Institute of Pain Management, Woodbridge, NJ, USA

Z. Pellis · D. A. Provenzano (✉)
Pain Diagnostics and Interventional Care, Sewickley, PA, USA

P. Peng et al. (eds.), *Ultrasound for Interventional Pain Management*,
https://doi.org/10.1007/978-3-030-18371-4_4

Table 4.1 Anatomy of the suprascapular nerve

Origin	A direct branch of the upper trunk of the brachial plexus (C4–6)
General route	Crosses the posterior neck, under the trapezius, travels under the transverse scapular ligament through the suprascapular foramen across the spine of the scapula and then through the spinoglenoid notch
Sensory distribution	Glenohumeral joint Acromioclavicular joint Subacromial bursa Cutaneous innervation of the lateral superior shoulder
Motor innervation	Supraspinatus: Abducts the humerus; especially the initial 20–30 degrees Infraspinatus: Externally rotates the humerus

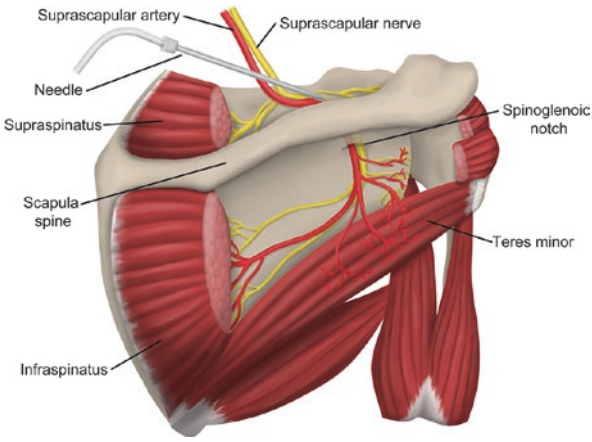

Fig. 4.1 Schematic drawing of the course of the suprascapular nerve. Ultrasound probe needle placement is defined for an ultrasound-guided block along the spine of the scapula. (Reprinted with permission from Pain Diagnostics and Interventional Care. Artwork by Zachary Pellis)

Table 4.2 Differential diagnosis for suprascapular nerve-related shoulder pain

Innervated structures	Differential diagnosis
Supraspinatus	Ganglion cyst at the suprascapular notch Direct compression Trauma Fracture callus
Infraspinatus	Ganglion cyst at the spinoglenoid notch Direct compression Trauma Fracture callus
Superior labrum	SLAP lesion (Superior labrum anterior-posterior tear) Labral cyst
Glenohumeral joint	Adhesive capsulitis and osteoarthritis Poststroke shoulder pain
Acromioclavicular joint	Dislocation Osteoarthritis

repetitive overhead activities. In particular, these are movements that place substantial load on the shoulder in an overhead or abducted and externally rotated position. The SN may also become entrapped at common sites including the suprascapular notch and spinoglenoid notch (Fig. 4.1). Multiple diagnostic tests can be used to assist in diagnosing suprascapular nerve damage and entrapment (Table 4.3).

Table 4.3 Diagnostic criteria for suprascapular nerve neuropathy

Physical exam	Atrophy of supraspinatus and infraspinatus muscles Weakness with abduction/external rotation.
Ultrasound	Possible edema of the corresponding muscle or direct compression of nerve by a cyst
Electrodiagnostic studies	EMG showing axonal loss limited to SN distribution Motor NCVs showing reduced amplitude
MRI	Edema, atrophy, or fatty infiltration of supraspinatus or infraspinatus muscles

NCV Nerve conduction velocity, *EMG* electromyography

Patient Selection

A suprascapular nerve block (SNB) is used for perioperative and postoperative pain control after surgery. The block can also be utilized for chronic pain management and diagnostic purposes for shoulder pain. Pulsed radiofrequency of the suprascapular nerve in conjunction with physical therapy has been shown to accelerate the recovery from adhesive capsulitis.

Ultrasound Scanning

Two approaches exist for targeting the suprascapular nerve: posterior (distal) technique and the anterior (proximal) technique. The posterior approach targets the suprascapular nerve as it courses in the suprascapular fossa over the scapular spine (Figs. 4.1, 4.2, 4.3, 4.4, and 4.5). The less commonly used technique targets the

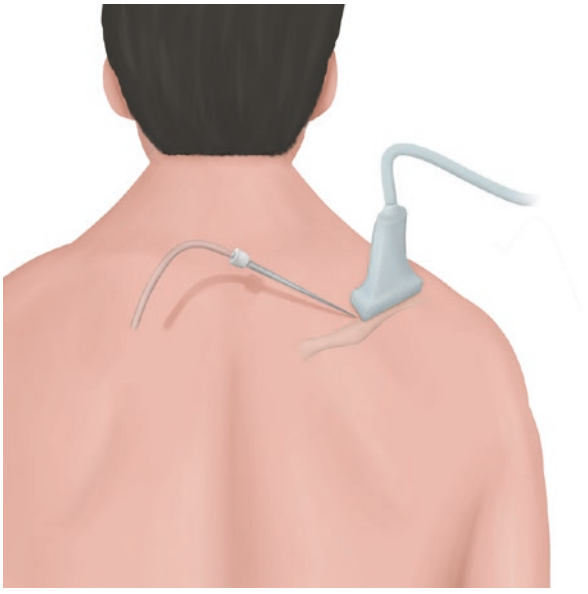

Fig. 4.2 Schematic drawing of the position of the ultrasound probe for a posterior approach ultrasound-guided suprascapular nerve block. (Reprinted with permission from Diagnostics and Interventional Care. Artwork by Zachary Pellis)

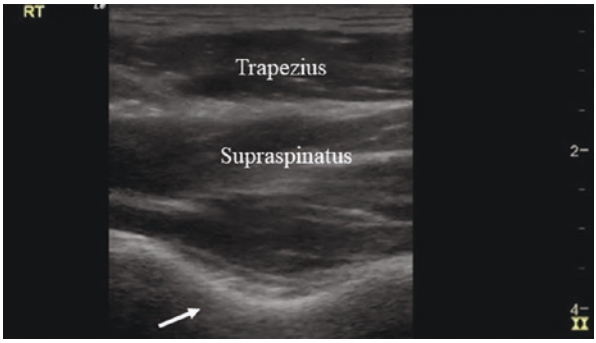

Fig. 4.3 An ultrasound image of the posterior approach for the ultrasound-guided suprascapular nerve block. The arrow identifies the spine of the scapula. (Reprinted with permission from Pain Diagnostics and Interventional Care)

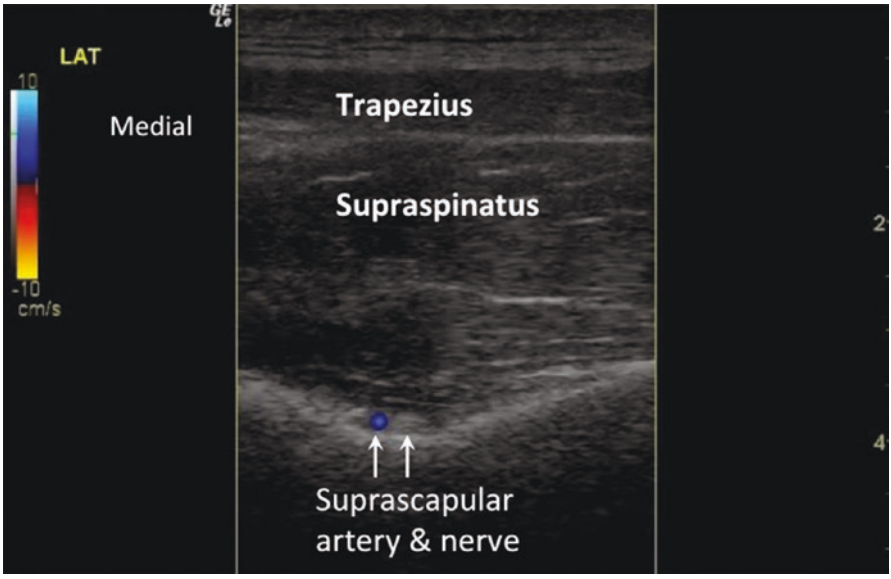

Fig. 4.4 An ultrasound image of the posterior approach for the ultrasound-guided suprascapular nerve block demonstrating the suprascapular artery at base of the spine of the scapula. (Reprinted with permission from Pain Diagnostics and Interventional Care)

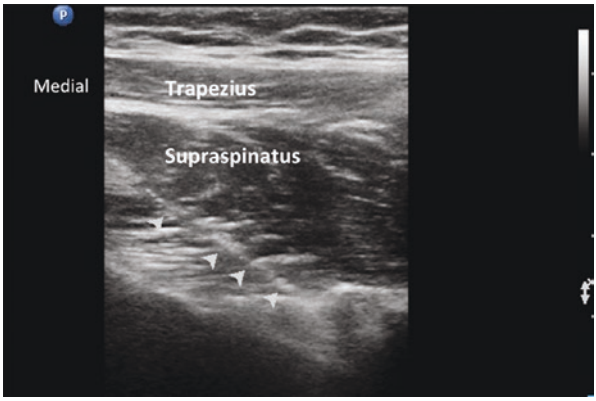

Fig. 4.5 An ultrasound image demonstrated needle (identified by arrow heads) placement for the posterior approach. The needle is being directed from medial to lateral. (Reprinted with permission from Pain Diagnostics and Interventional Care)

nerve anteriorly at its proximal origin. The nerve is blocked in the supraclavicular region, where it passes underneath the omohyoid muscle. Only the posterior approach is described here.

- Position: Sitting with the arm in the lap or with the hand of the side being blocked resting on the contralateral shoulder
- Alternatively, with the patient placed in a prone position with a pillow under his chest
- Probe: Linear 8–13 MHz

Scan 1

The spine of the scapula and the acromion are used as landmarks (Fig. 4.2). Ultrasound scanning is performed with a high-frequency linear ultrasound transducer placed in a coronal plane over the suprascapular fossa with a slight anterior tilt. In this position, a transverse section of the supraspinous fossa is visualized (Fig. 4.3).

Next, the supraspinous fossa region is identified from medial to lateral to determine the boundaries formed by the spine of the scapula.

Scan 2

Doppler (color or power) is used to identify vascular structures (Fig. 4.4).

Procedure

- Needle: 22G 3.5 or 4 inch needle
- Drugs: 1 ml of steroid preparation (e.g., 40 mg of triamcinolone or methylprednisolone)
  2–4 ml of local anesthetic

The initial US scan is performed as described in the above. The US probe is moved to visualize the suprascapular fossa. The transducer is used to identify the suprascapular nerve on the floor of the spine of the scapula between the suprascapular and spinoglenoid notches. In some cases, the nerve cannot be identified, and the area below the supraspinatus fascia just above the scapular spine is targeted.

Doppler is used to ensure blood vessels, including the suprascapular artery and vein, are not in the planned needle trajectory.

A 22-gauge needle is inserted in the longitudinal axis of the ultrasound beam (in-plane) and advanced under full ultrasound visualization until the needle tip is in proximity to the suprascapular nerve or spine of the scapula below the fascia of the

supraspinatus muscle (Fig. 4.5). The needle is advanced from medial to lateral. For specific cases, an echogenic needle tip can be helpful for visualization because of the steep trajectory of the needle.

The injection occurs under the distal fascial layer of the supraspinatus muscle.

Ultrasound-Guided Peripheral Nerve Stimulation of the Suprascapular Nerve

Chronic shoulder pain is the second most common musculoskeletal complaint after the knee. Although spinal cord and dorsal root ganglion stimulation are effective for managing regional pain syndromes, a more targeted approach is perhaps more appealing for discrete anatomical structures after appropriate diagnosis. The location of peripheral nerves is subject to anatomic variability, and precise imaging guidance is desirable.

Ultrasonography is an imaging tool used to localize the target nerve and to guide peripheral lead placement. Although limited by a small number of case reports and descriptive procedures, peripheral nerve stimulation of the suprascapular nerve may become a viable technique in the future to modulate pain. Large-scale studies are needed to verify safety and efficacy of the technique.

Proposed Procedure (Based on an Anatomical Study)

- A linear high-frequency ultrasound transducer is placed in the short-axis view.
- The SN is localized at the infraspinous fossa as it courses around the spinoglenoid notch.
- After obtaining the desired short-axis orientation to the SN, a stab incision is done 2–3 cm distally to the transducer. The skin and infraspinatus muscle are penetrated with 18-gauge Crawford needle. A guide probe is inserted and placed adjacent to the suprascapular nerve in an out-of-plane view.
- The needle is removed and the guide probe is advanced in the cephalad-medial direction. The transducer is shifted to the supraspinatus fossa. The guide is advanced parallel to the nerve, and its tip is identified as a bright hyperechoic signal at the supraspinous fossa.

Clinical Pearls

- The final ultrasound transducer position for the posterior approach should be more in the coronal plane, because, in the transverse plane, the structures in the supraspinous fossa are all obscured by the spine of the scapula.
- Two approaches have been described in the literature for performing an ultrasound-guided suprascapular nerve block: a posterior/distal technique and an anterior/proximal supraclavicular technique.

- The trapezius and supraspinatus will be clearly visualized deep to the subcutaneous tissue. The suprascapular artery can be confirmed with Doppler.
- For the posterior approach, the spine of the scapula is being targeted not the suprascapular notch.
- Complications for interventions targeting the suprascapular nerve include pneumothorax, direct needle trauma to the neurovascular bundle, intravascular injection, and infection. The spine of the scapula acts as an osseous safety border when performing this injection to avoid the risk of a pneumothorax.

Literature Review

Hand-shoulder syndrome (HSS) or complex regional pain syndrome (CRPS) type I (formerly known as reflex sympathetic dystrophy) affects up to 84% of the survivors at an early poststroke period and up to 47% after 1 year. This is a common cause of adhesive capsulitis in this population.

The cross-body adduction test described by Kopell and Thompson which is performed by having the patient elevate the arm to 90° and forcibly adduct the arm across their chest can tighten the spinoglenoid ligament and compress the nerve to reproduce the patient's symptoms clinically.

Use of the suprascapular injection for diagnosis as well as for treatment of conditions such as adhesive capsulitis (frozen shoulder) or chronic rotator cuff tears with atrophy may offer significant relief.

An anatomic study evaluating the posterior approach for the ultrasound-guided suprascapular nerve block found the suprascapular nerve on the spine of the scapula proximal to spinoglenoid notch. The block is not targeting the nerve in the suprascapular notch as routinely performed with fluoroscopy. The structure previously identified as the transverse scapular ligament in some publications describing the ultrasound-guided technique is actually the distal fascial layer of the supraspinatus muscle.

Entrapment proximally (anteriorly) at the suprascapular notch results in significant, sudden onset of shoulder pain due to compression of the deep sensory fibers innervating the glenohumeral and acromioclavicular joints.

Entrapment more distally (posteriorly), at the spinoglenoid notch, can result in isolated atrophy and weakness of the infraspinatus muscle. In this situation, pain is largely absent because the deep sensory fibers to the shoulder joint exit proximal to this entrapment site.

There is future promise for targeting the suprascapular nerve with the application of peripheral nerve stimulation; however, further randomized controlled trials are needed to accurately assess the long-term efficacy and safety of this treatment modality.

Suggested Reading

Bilfeld M, et al. Ultrasonography study of the suprascapular nerve. Diagn Interv Imaging. 2017;98:873–9.

Gofeld M, Agur A. Peripheral nerve stimulation for chronic shoulder pain: a proof of concept anatomy study. Neuromodulation. 2018;21(3):284–9.

Jezierski H, et al. The influence of suprascapular notch shape on the visualization of structures in the suprascapular notch region: studies based on a new four-stage ultrasonographic protocol. BioMed Res Int. 2017;2017:1–7, Article ID 5323628.

Laumonerie P, et al. Description and ultrasound targeting of the origin of the suprascapular nerve. Clin Anat. 2017;30:747–52.

Okur SC, et al. Ultrasound-guided block of the suprascapular nerve in breast cancer survivors with limited shoulder motion – case series. Pain Physician. 2017;20:E233–9.

Peng PW, Wiley MJ, Liang J, Bellingham GA. Ultrasound-guided suprascapular nerve block: a correlation with fluoroscopic and cadaveric findings. Can J Anaesth. 2010;57(2):143–8.

Picelli A, et al. Suprascapular nerve block for the treatment of hemiplegic shoulder pain in patients with long-term chronic stroke: a pilot study. Neurol Sci. 2017;38:1697–701.

Spinner D, Kirscher J, Herrera J. Atlas of ultrasound guided musculoskeletal injections. New York: Springer; 2015.

Trescott A. Suprascapular nerve entrapment: shoulder. In: Peripheral nerve entrapments. Cham: Springer; 2016.

Wu YT, Ho CW, Chen YL, Li TY, Lee KC, Chen LC. Ultrasound-guided pulsed radiofrequency stimulation of the suprascapular nerve for adhesive capsulitis: a prospective, randomized, controlled trial. Anesth Analg. 2014;119(3):686–92.

Intercostal Nerve Block

5

Yu M. Chiu and Amitabh Gulati

Introduction

In 1884, Halsted and Hall originated the nerve block by applying cocaine to specific nerves of the face, the brachial plexus, and the posterior tibial nerve. In 1902, Heinrich Braun first described nerve blocks as a treatment for acute and chronic pain of the posterior and anterior portions of the superficial thorax and upper abdomen.

Anatomy

The intercostal nerves are made up of twelve pairs of thoracic spinal nerves (T1–T12) and pass through the intervertebral foramina where they are divided into the ventral and dorsal rami. The ventral rami of T1–T11 form the intercostal nerves entering the intercostal spaces (Fig. 5.1). The ventral ramus of T12 forms the subcostal nerve that is located inferior to the corresponding 12th rib. The dorsal rami of T1–T12 travel posteriorly and innervate sensation to the skin, muscles, and bones of the back.

Each intercostal nerve is associated with an artery and vein of the corresponding level (Fig. 5.2). The aorta derives the intercostal arteries, while the azygous and hemiazygous veins derive the intercostal veins. The intercostal nerve courses inferior to both the vein and artery of the same segment.

The intercostal nerves are composed of dorsal horn sensory fibers, ventral horn motor efferent fibers, and postganglionic sympathetic nerves. The intercostal nerves

Y. M. Chiu (✉)
Department of Anesthesiology, Division of Pain Medicine, Medical College of Wisconsin, Milwaukee, WI, USA
e-mail: YMCHIU@mcw.edu

A. Gulati
Anesthesiology and Critical Care, Division of Pain Medicine, Memorial Sloan Kettering Cancer Center, New York, NY, USA

P. Peng et al. (eds.), *Ultrasound for Interventional Pain Management*,
https://doi.org/10.1007/978-3-030-18371-4_5

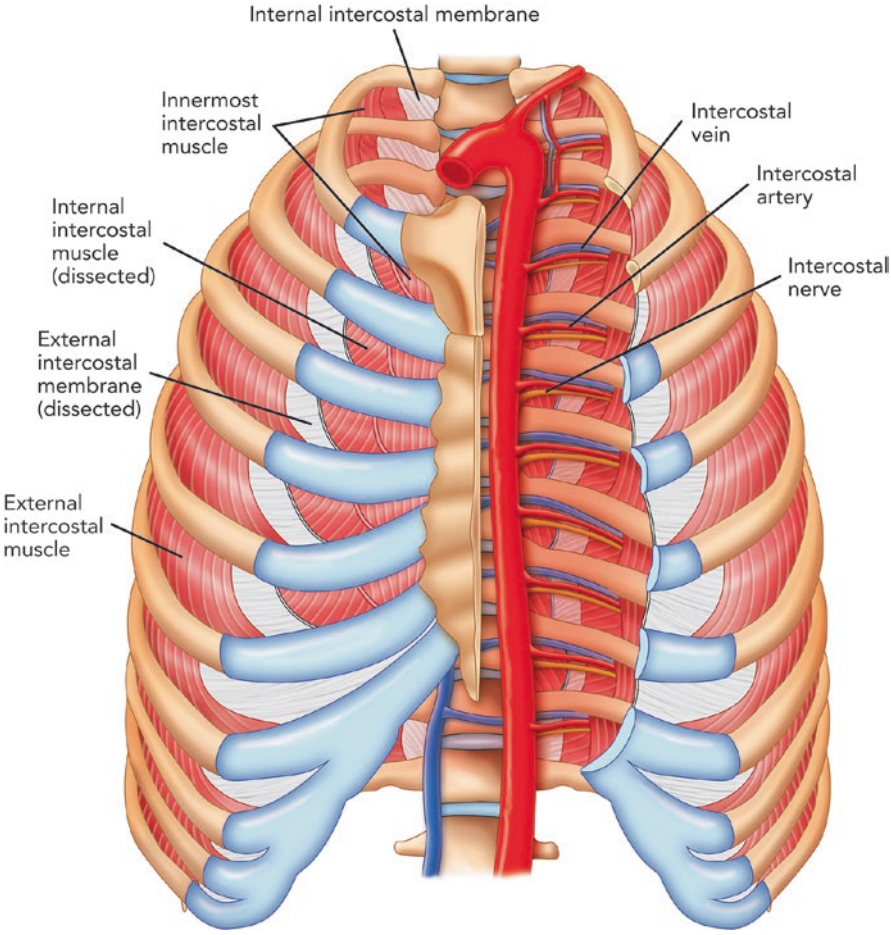

Fig. 5.1 Different layers of intercostal muscle. (Reprinted with permission from Philip Peng Educational Series)

divide into the anterior and lateral cutaneous branches that innervate the skin and intercostal muscles of each individual segment (Fig. 5.3). It is important to note that there is variable collateral innervation of the adjacent segment; therefore, it is necessary to block both the level above and below the desired level when performing an intercostal nerve block.

Additional Caveats

The subcostal nerve is a unique T12 intercostal nerve; it does not run as closely to the intercostal groove of its accompanying rib as other intercostal nerves do. The nerve supplies the lower abdominal wall and is not closely associated with the 12th rib. Instead, the subcostal nerve makes up the anterior ramus of spinal nerve T12 and is approximately 3 mm in diameter. It passes over the iliac crest by joining the

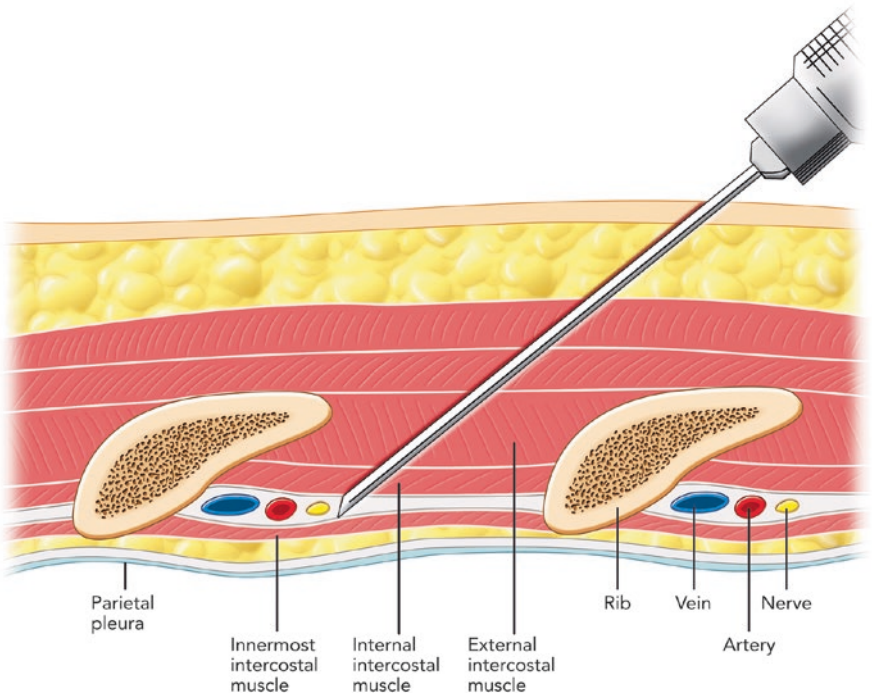

Fig. 5.2 Anatomy of the intercostal space. (Reprinted with permission from Philip Peng Educational Series)

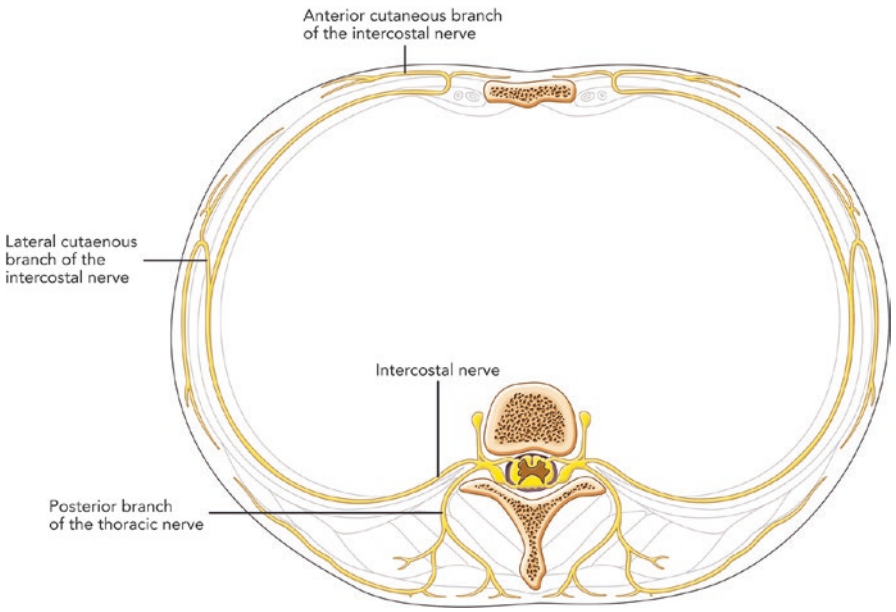

Fig. 5.3 Branches of intercostal nerve. (Reprinted with permission from Philip Peng Educational Series)

ventral ramus of L1, forming the iliohypogastric, ilioinguinal, and genitofemoral nerves. The remaining portion transects the transverse abdominis muscle and lies between that and the internal oblique muscle.

Patient Selection

Indications

Intercostal nerve blocks are useful in relieving pain from conditions including rib fractures, dislocation of costochondral joint, acute herpes zoster or postherpetic neuralgia, postoperative pain (i.e., thoracotomy, sternotomy, upper abdominal surgery), chronic intercostal nerve-related pain (i.e., post-thoracotomy pain), cancer-related pain of the chest wall, and idiopathic neuropathic pain of the intercostal nerve or serve as a diagnostic block to establish a diagnosis (Table 5.1).

Contraindications

The only absolute contraindications to intercostal nerve blocks are patient refusal of the procedure and active infection over the site of injection.

Extra caution must be taken in patients to whom a pneumothorax may be a life-threatening complication. These patients include those that have respiratory decompensation, single lung on the side of planned procedure, mechanically ventilated with positive-pressure ventilation, prior nerve injury, or neuromuscular disease involving area to be injected or postsurgical patients.

General relative contraindications include patients with blood dyscrasias, local or uncontrolled systemic infection, or unknown anatomical changes (i.e., unknown rib resection).

Other relative contraindications are allergy to local anesthetics, prior nerve injury or damage, inability of the patient to consent to procedure, and patients on anticoagulants or diagnosed with coagulopathy. Patient should be counseled on the expected results of the intercostal nerve block and pertinent potential complications (Table 5.2).

Table 5.1 Indications for intercostal nerve blocks

Indications	Intercostal nerve block mechanism
Diagnostic nerve block	Initial single-injection block to determine efficacy of temporary pain relief. A subsequent neurolytic block, cryoablation, radiofrequency ablation, or chemical neurolysis is then performed to relieve pain for an extended period.
Chest wall surgery	Relieves pain after upper abdominal or flank surgery
Chest wall trauma	Controls pain resulting from fractured ribs and other chest wall trauma
Shingles or postherpetic neuralgia	Acute herpes zoster infection results in inflammation of the intercostal nerves and dorsal root ganglion.
Chronic conditions	Manages pain associated with chest wall tumors, nerve entrapment syndromes, thoracic spine pain, and intercostal neuralgia

Table 5.2 Contraindications to intercostal nerve block

Contraindications	Related types
Absolute	Patient refusal or active infection over site of injection
Extra caution/special consideration	Respiratory decompensation, single lung on side of planned procedure, positive-pressure ventilation, postsurgical patients, prior nerve injury, neuromuscular disease involving area to be injected
General/relative/other	Blood dyscrasias, local or uncontrolled systemic infection, unknown anatomical changes (unknown rib resection), allergy to local anesthetics, prior nerve injury or damage, inability of patient to consent to procedure, on anticoagulants or diagnosed with coagulopathy

Advantages

The advantages of intercostal nerve blocks are associated with decreased need for parenteral or oral opioids. Decreasing use of oral and/or parental opioids may reduce the incidence of nausea, vomiting, urinary retention, itching, and hypotension. In thoracic surgery, the use of intercostal nerve blocks can lead to improved respiratory function in FEV1 and peak expiratory flow rate.

Complications

While complication rates vary, performing intercostal nerve block with ultrasound guidance may reduce some of the associated risks. These risks include bleeding along the path of the needle, hematoma, infection, toxicity to injectate (local anesthetic), pneumothorax, nerve damage, spinal cord injury due to epidural or spinal injection or uptake of alcohol from a neurolytic alcohol injection, and muscle trauma.

Ultrasound Scanning

- Patient Position: Prone; lateral decubitus, or sitting
- Probe: Linear high frequency

It is important to know your anatomic landmarks. By palpating the spine of the scapula or the inferior edge of the scapula, the physician can then infer spinous levels T4 and T7, respectively. However, T1 spinous process may be more reliably palpated (as compared to C7 spinous process which moves with rotation and flexion of the cervical spine), and thus thoracic vertebral levels can be more accurately determined.

The ultrasound probe is placed in the longitudinal axis parallel to the posterior midclavicular line, optimally at the angle of the rib. This approach allows for views of two ribs in a cross-sectional view (Fig. 5.4a, b). Note the orientation of the probe to align with the orientation of the internal intercostal muscle. With this view, one can identify external intercostal (EI) and internal intercostal (II) muscles.

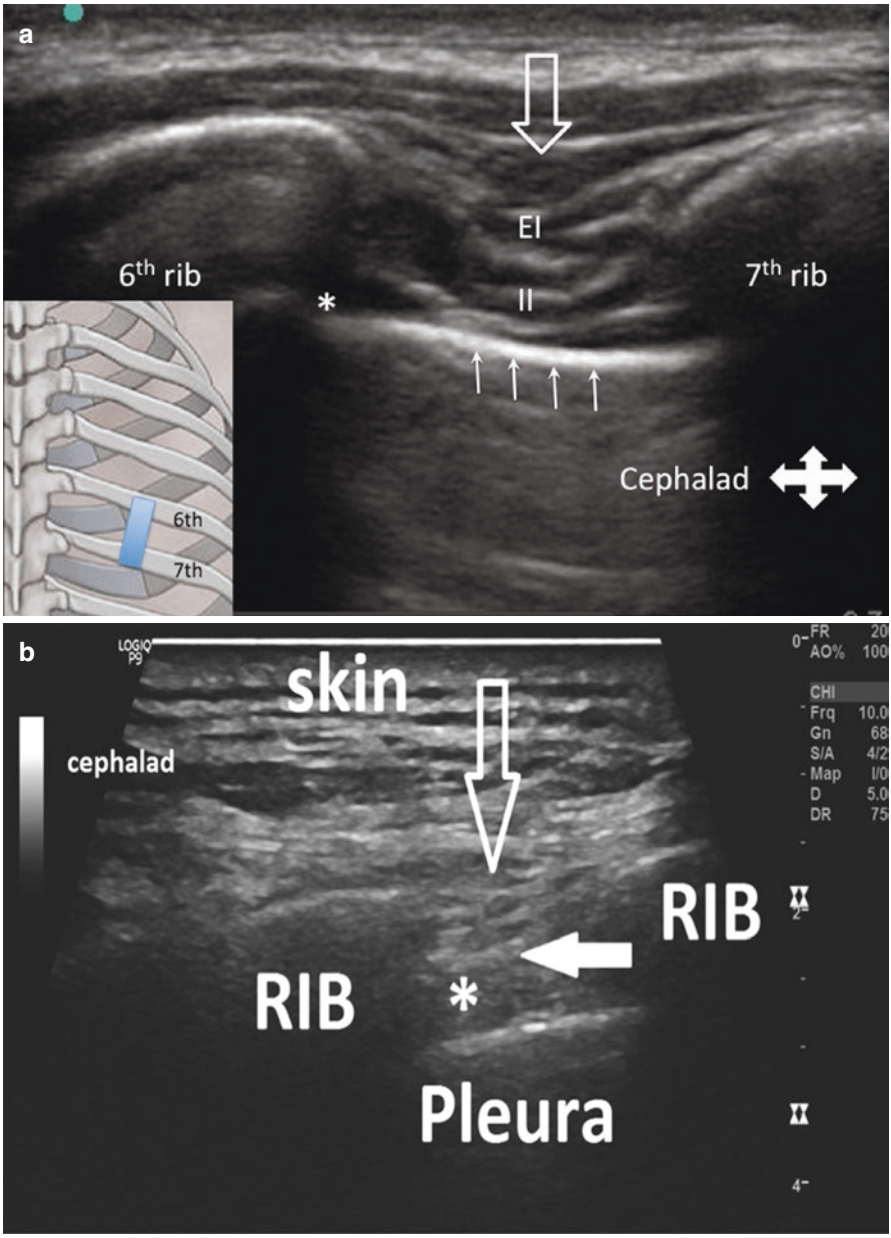

Fig. 5.4 (**a**) The intercostal muscles. EI external intercostal, II internal intercostal, pleura indicated by arrows. Bold arrow represents the fascia over the external intercostal muscle. (**b**) shows a similar sonogram in an obese patient. ∗ represents the target location for the fascial plane between the internal intercostal and innermost intercostal muscles, or deep to the internal intercostal when the innermost intercostal is not well visualized. (Reprinted with permission from Philip Peng Educational Series)

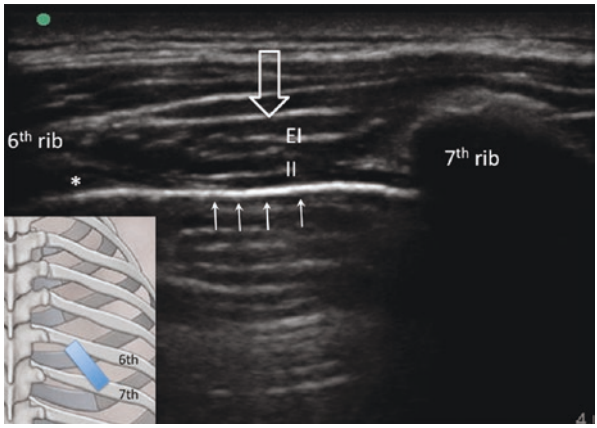

Fig. 5.5 The intercostal space in long axis. EI external intercostal, II internal intercostal; pleura, indicated by arrows. Bold arrow represents the fascia over the external intercostal muscle. ∗ represents the target location for the fascial plane between the internal intercostal and innermost intercostal muscles, or deep to the internal intercostal when the innermost intercostal is not well visualized. (Reprinted with permission from Philip Peng Educational Series)

The probe should then be placed in long axisacross the thoracic rib level desired. In this longitudinal view, one should be able to identify the EI and II during the rotation (Fig. 5.5).

Procedure

- Needles: 22- or 25-gauge 1.5- to 3.5-inch needle (echogenic needles may be preferable to visualize the needle tip); 5 mL syringe is typical.
- Drugs: Lidocaine 1–2%, ropivacaine 0.2–0.5%, or bupivacaine 0.25–0.5%.
- Steroids: common particulate steroids (e.g., triamcinolone) are used although not mandatory.

Please note that straight antiseptic technique is observed (i.e., sterile probe cover, glove, ultrasound gel, marker). Marking the rib edges and numbering them will help to position the probe.

The authors also suggest the availability of emergency equipment: sterile scalpel, chlorhexidine (or other skin prep agent), chest tube, wall suction, supplemental oxygen, stethoscope, and portable chest X-ray machine (Fig. 5.6).

An in-plane approach for needle placement is recommended for optimal visualization. Puncture site is initiated from the superior border of the rib inferior the intercostal nerve of interest (i.e., if T6 intercostal nerve is to be blocked, the superior border of T7 rib is the puncture site). Local anesthetic is given for skin anesthesia, and then a 22- or 25-gauge 1.5- to 3.5-inch needle is inserted at a 35–45° angle and directed to the inferior border of the corresponding rib. The needle can penetrate the internal intercostal muscle and can be visualized above the pleura and innermost

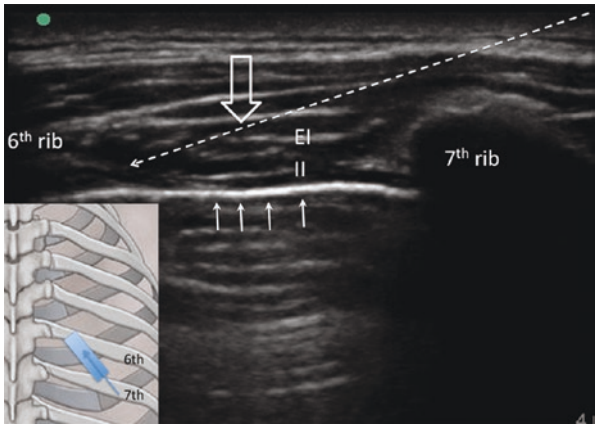

Fig. 5.6 Needle insertion for intercostal block. (Reprinted with permission from Philip Peng Educational Series)

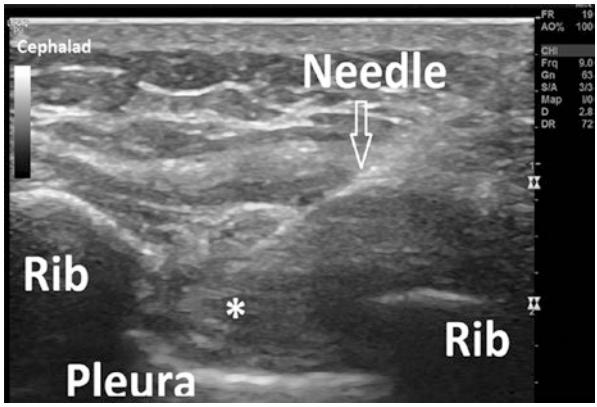

Fig. 5.7 Ice ball formation (∗) shows as a hypoechoic lesion at the approximate location of the intercostal nerve. (Reprinted with permission from Philip Peng Educational Series)

intercostal muscle. Usually the intercostal nerve is not visualized, but the spread of solution beneath the fascia of the internal intercostal muscle signifies a successful blockade of the intercostal nerve.

With similar technique, intercostal nerve cryoablation can be performed (Fig. 5.7).

Postprocedure Follow-Up and Pitfalls

- After completion of the procedure, an evaluation of the patient should be conducted. Auscultation using a stethoscope to confirm air movement in the chest wall is necessary to diagnose pneumothorax (Fig. 5.8).
- Alternatively, one can scan the patient at the site of needle entry with the patient in the same position. The pleura should appear as a discrete hyperechoic line freely gliding. B mode can be used and demonstrates seashore sign. Arrows indicate the pleura.
- If a mild pneumothorax is detected, supplemental oxygen may be necessary. For more severe tension pneumothorax, a chest tube may be needed to prevent pulmonary decompensation.

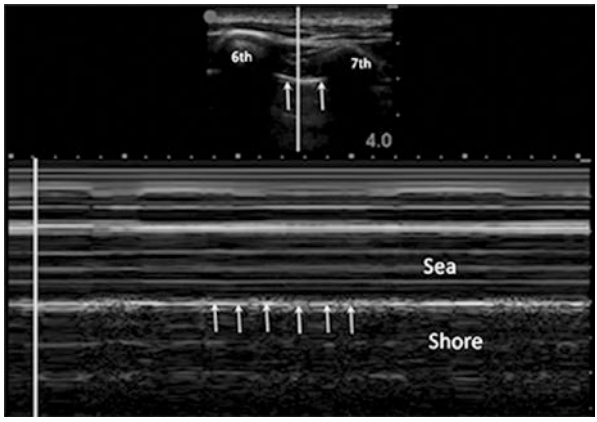

Fig. 5.8 M mode over the intercostal space. It showed the pleura (arrows), which divided the signal superficial to it (line pattern as "sea") and deep to it (grainy pattern as "shore"). This picture is known as the sea-shore sign. (Reprinted with permission from Philip Peng Educational Series)

- Local anesthetic toxicity should also be evaluated for both neurologic and cardiac complications, including arrhythmias and seizures.
- For lower thoracic intercostal nerve blocks, the peritoneum or retroperitoneum is at risk of being punctured. Hematoma or hemoperitoneum may be considered if abdominal or back pain ensues over time.

Clinical Pearls

- Patient positioning is important. Intercostal injections can be performed with patient in prone, lateral decubitus, or sitting position.
- Hydrodissection may be recommended to separate external and internal intercostal muscle injection. In Fig. 5.9, injection into the external intercostal (EI) muscle (∗) causes the lifting of external intercostal fascia.
- Visualization of the needle tip under ultrasonography and careful advancement of the needle to the neurovascular bundle under the rib, along with use of Doppler ultrasound, will further reduce iatrogenic pneumothorax/hemothorax.
- Intravascular or intravenous injection can be prevented by aspiration of syringe prior to injection. If blood is aspirated, reposition needle inferior to these vascular structures without advancing needle further.
- Tracking between the lower border of the ribs and the neurovascular bundle is not always matched. Discrepancies may be observed along the course of the rib.
- Postprocedure evaluation for pneumothorax is warranted. The chance of pneumothorax is ~50% and depends on the amount of aerated lung tissue traversed by the needle. It is important to note that patients with chronic obstructive lung disease and emphysema have a higher risk of pneumothorax.
- Intercostal blocks are best performed near the posterior angulation of the ribs. In this location, the nerves are shallow and relatively centrally located before branching occurs.

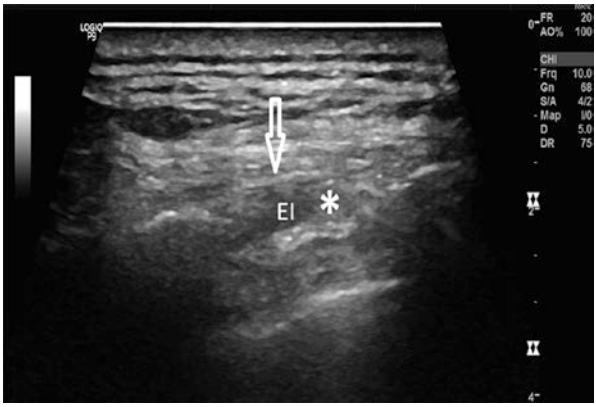

Fig. 5.9 External Intercostal (EI) muscle, Injectate (∗) causes the lifting of the external intercostal fascia

Literature Review

There is a relative dearth of publications in regard to intercostal nerve blocks utilizing ultrasound, HIFU, RFA, EtOH, and larger, randomized control trials, and more long-term studies are needed to truly elucidate the efficacy of these injection blocks (Tables 5.3 and 5.4).

Table 5.3 HIFU, RFA, EtOH, ICNB studies

References	Group (n)	Methods	Results	Conclusion	Limitations
Gulati et al. [3]	HIFU (4) RFA (4) EtOH lesions (4)	2 Yorkshire pigs (30–40 kg)	Pathology: HIFU (2) nerve intact (2) nerve lesioned RFA (2) nerve intact (2) nerve lesioned EtOH (4) nerve intact	HIFU may be used as a noninvasive neurolytic technique in swine. HIFU may have potential as a neuroablation technique for patients with chronic and cancer pain	Nonhuman study, not a survival study, no long-term follow-up
Byas-Smith and Gulati [2]	Cryoablation with N2O (1)	1 patient (50-year-old male)	Pain symptoms resolved within 1 hour postoperatively and absent at 2 months follow-up	Conclusive evidence of improved outcomes using ultrasound-guided techniques will require a prospective, randomized, controlled trial	Case study, no long-term follow-up

Table 5.3 (continued)

References	Group (n)	Methods	Results	Conclusion	Limitations
Zhu et al. [9]	Sufentanil (41) ICNB (40)	81 patients with moderate to severe pain after an Ivor Lewis esophagectomy	VAS scores at rest and on cough at 1, 2, and 4 hours after treatment were significantly decreased in ICNB group versus sufentanil group	Ultrasound-guided ICNB could provide effective and safe pain relief for patients who suffer from moderate to severe pain after esophagectomy in the PACU	No long-term follow-up
Wijayasinghe et al. [7]	ICBNB (6)	6 patients with persistent pain after breast cancer surgery (PPBCS)	All patients had preexisting areas of hypoesthesia, which decreased in size in 4/6 patients after block	Successful management of PPBCS patients using ultrasound-guided ICBNB	Pilot study, small sample size, no long-term follow-up
Wisotzky et al. [8]	ICBNB (3)	3 patients with intercostobrachial neuralgia in postmastectomy pain syndrome	All patients had pain relief after the ICBNB ranging from 2 weeks to 4 months	Ultrasound-guided perineural injection may provide a novel approach to control ICBN	Case series, small sample size, no long-term follow-up
Abd-Elsayed et al. [1]	RFA (2)	2 patients with resistant intercostal neuralgia	All patients responded to intercostal diagnostic nerve blocks, followed by RFA with improvement in pain ranging from 2 months to 1 year	Thermal RFA can be safely used to treat patients with resistant intercostal neuralgia	Case series, small sample size, no long-term follow-up

(continued)

Table 5.3 (continued)

References	Group (n)	Methods	Results	Conclusion	Limitations
Stone et al. [6]	ICNB (1)	1 patient (39 yo female) requiring chest tube for right PTX	Successful blockade prior to chest tube placement	Ultrasound guidance can greatly facilitate intercostal nerve blockade and improve patient comfort during tube thoracostomy placement. Ultrasound guidance offers distinct advantage over traditional anatomical landmark-based approach	Small sample size, no long-term follow-up

High-intensity focused ultrasound (HIFU), standard ultrasound-guided radiofrequency ablation (RFA) and/or alcohol lesion (EtOH), intercostal nerve block (ICNB), intercostal brachial neuralgia block (ICBNB)

Table 5.4 Pneumothorax after ICNB (no ultrasound used)

References	Type of study	Methods	Results	Conclusion	Limitations
Shanti et al. [5]	Retrospective chart review (1996–1999)	161 patients with rib fractures received 249 ICNB procedures (no ultrasound used)	Overall incidence of PTX was 8.7% per patient. Incidence of PTX per ICNB was 5.6%. Incidence of PTX for each individual ICNB was 1.4%	The incidence of PTX per individual ICNB is low and can be an effective form of analgesia and for most patients with rib fractures	
Holzer et al. [4]	Case report	1 patient (57 yo F) underwent ICNB T3–8 for interstitial radiotherapy (no ultrasound used)	A severe PTX occurred requiring chest tube placement	Extra caution should be used in applying ICNB to patients with underlying chronic lung disease, especially on the affected side	Case study

References

1. Abd-Elsayed A, Lee S, Jackson M. Radiofrequency ablation for treating resistant intercostal neuralgia. Ochsner J. 2018;18(1):91–3.
2. Byas-Smith M, Gulati A. Ultrasound-guided intercostal nerve cryoablation. Anesth Analg. 2006;103(4):1033–5.
3. Gulati A, Loh J, Gutta NB, et al. Novel use of noninvasive high-intensity focused ultrasonography for intercostal nerve neurolysis in a Swine model. Reg Anesth Pain Med. 2014;39(1):26–30.
4. Holzer A, Kapral S, Hellwagner K, et al. Severe pneumothorax after intercostal nerve blockade: a case report. Acta Anesthesiol Scand. 1998;42(9):1124–6.
5. Shanti CM, Carlin AM, Tyburski JG. Incidence of pneumothorax from intercostal nerve block for analgesia in rib fractures. J Trauma. 2001;51:536–9.
6. Stone MB, Carnell J, Fischer JW, et al. Ultrasound-guided intercostal nerve block for traumatic pneumothorax requiring tube thoracostomy. Am J Emerg Med. 2011;29(6):697. E1–2.
7. Wijayasinghe N, Duriaud H, Kehlet H, Andersen KG. Ultrasound guided intercostobrachial nerve blockade in patients with persistent pain after breast cancer surgery: a pilot study. Pain Physician. 2016;19:E309–17.
8. Wisotzky EM, Saini V, Kao C. Ultrasound-guided intercostobrachial nerve block for intercostobrachial neuralgia in breast cancer patients: a case series. PMR. 2016;8(3):273–7.
9. Zhu M, Gu Y, Sun X, et al. Ultrasound-guided intercostal nerve block following esophagectomy for acute postoperative pain relief in the postanesthesia care unit. Pain Pract. 2018;18:879–83. [Epub ahead of print].

Suggested Reading

Baxter CS, Fitzgerald BM. Nerve block, intercostal. [Updated 2018 Feb 7]. In: StatPearls [Internet]. Treasure Island: StatPearls Publishing; 2018.

Braun H. Operations of the spinal column and thorax. Local anesthesia, its scientific basis and practical use. 3rd ed. Cincinnati: Lea & Febiger; 1914. p. 278–82.

Cousins MJ, Carr DB, Horlocker TT, Bridenbaugh PO. Intercostal, intrapleural, and peripheral blockade of the thorax and abdomen. In: Harmon DC, Shorten GD, editors. Cousins and Bridenbaugh's neural blockade in clinical anesthesia and pain medicine. 4th ed. Philadelphia: Lippincott Williams and Wilkins; 2009. p. 386–90.

Dowling R, Thielmeier K, Ghaly A, Barber D, Dine A. Improved pain control after cardiac surgery: results of a randomized, double-blind, clinical trial. J Thorac Cardiovasc Surg. 2003;126(5):1271–9.

Gulati A. Chapter 57: Intercostal nerve block. In: Diwan S, Staats P, editors. Atlas of pain medicine procedures. New York: McGraw-Hill Education; 2014.

Gulati A. Precision pain medicine: can we deliver targeted pain therapies for the oncologic patient in the 21st century? Pain Med. 2017;18(7):1207–8. https://doi.org/10.1093/pm/pnx082.

Moore KL, Agur AMR. Essential clinical anatomy. Philadelphia: Lippincott Williams & Wilkins; 2006.

Mulroy MF, Bernards CM, McDonald SB, Salina FV. Intercostal and terminal nerve anesthesia of the trunk. In: Mulroy MF, editor. Regional anesthesia. 4th ed. Baltimore: Lippincott Williams & Wilkins; 2009. p. 137–46.

Ilioinguinal and Iliohypogastric Nerves

6

Pranab Kumar and Philip Peng

Introduction

The ilioinguinal (II) and iliohypogastric (IH) nerves are the primary nerves providing sensory innervation to the skin bordering the thigh and abdomen. Together with genitofemoral nerves, they are called "border nerves." Injury to the II and IH nerves is a known risk in open appendectomy, inguinal herniorrhaphy, cesarean section and hysterectomy [low Pfannenstiel incisions], and trocar insertion for laparoscopic or robotic surgeries of the abdomen and pelvis.

The lumbar plexus is formed by the ventral rami of nerves L1 to L3 and majority of the ventral ramus of L4, with a contribution from the T12 (subcostal) nerve. Branches of the lumbar plexus include the iliohypogastric, ilioinguinal, and genitofemoral nerves, lateral femoral cutaneous nerve of the thigh, and femoral and obturator nerves (Fig. 6.1). The IH and II nerves arise as a single trunk from the ventral ramus of nerve L1. Either before or soon after emerging from the lateral border of the psoas major muscle, this single trunk divides into the IH and II nerves.

The IH nerve emerges along the upper lateral border of the psoas major and passes across the ventral surface of quadratus lumborum muscle, travelling in the fascia lumborum towards the iliac crest. Midway between the iliac crest and twelfth rib pierces the transversus abdominis muscle to lie between it and the internal oblique muscles (Fig. 6.2).The IH nerve then runs inferomedially, piercing the internal oblique muscle above the anterior superior iliac spine (ASIS). From this point, the nerve runs between the internal oblique and external oblique muscles,

P. Kumar
Department of Anesthesia & Pain, Toronto Western Hospital, Toronto, ON, Canada

P. Peng (✉)
Department of Anesthesia and Pain Management, Toronto Western Hopsital and Mount Sinai Hospital, University of Toronto, Toronto, Ontario, Canada
e-mail: Philip.peng@uhn.ca

P. Peng et al. (eds.), *Ultrasound for Interventional Pain Management*,
https://doi.org/10.1007/978-3-030-18371-4_6

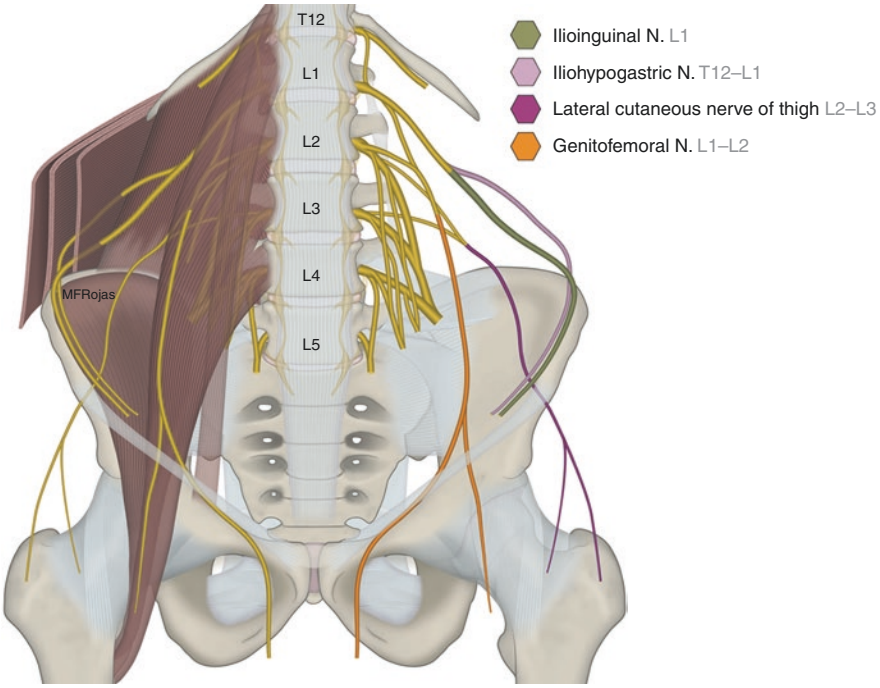

Fig. 6.1 The lumbar plexus showing the ilioinguinal, iliohypogastric, lateral femoral cutaneous, and genitofemoral nerve. (Reprinted with permission from Dr. Maria Fernanda Rojas)

piercing the external oblique aponeurosis approximately 1 inch above the superficial inguinal ring.

The IL nerve is *smaller* and emerges along the lateral border of the psoas major, running a similar course that is more *oblique* and *inferior* to the IH nerve. It pierces the transversus abdominis and then the internal oblique at its lower border and *enters the inguinal canal*, emerging through the superficial inguinal ring anterior to the spermatic cord.

It supplies the skin of the posterolateral gluteal region and the pubic region over the lower region of the rectus abdominis muscles (Fig. 6.3). Throughout the course, it also supplies branches to the abdominal musculature.

The nerve provides sensory innervation to the skin over the root of the penis and the anterior surface of the scrotum in men (mons pubis and lateral labium majora in women) and superomedial thigh region, although the sensory innervation is variable. Throughout the course, it also supplies branches to the abdominal musculature.

The border nerves anatomic variations are well documented as one or more of the nerves are frequently absent in dissections. There are free communications between all these nerves and they innervate common dermatomes. The inguinal course of the II and IH may be consistent with the classic textbook description in only 42% of the

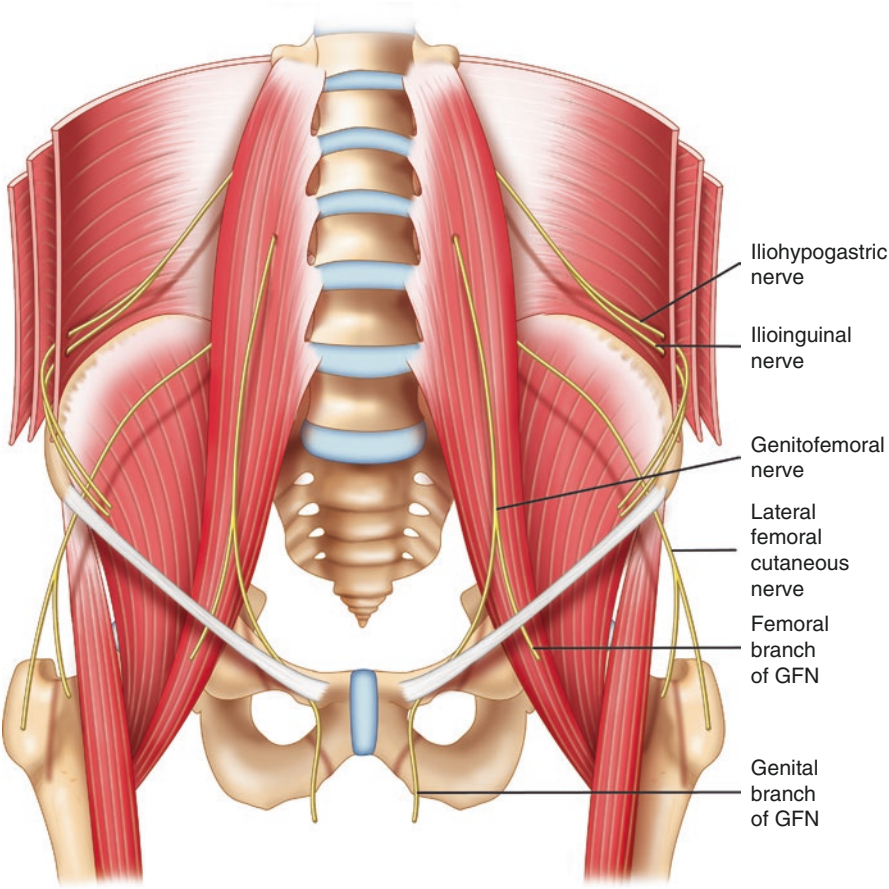

Fig. 6.2 The relationship of the ilioinguinal nerve, iliohypogastric nerve, and abdominal wall muscle. (Reprinted with permission from Philip Peng Educational Series)

dissections. Rab et al. delineate four different types of branching patterns in these nerves, and only 20% correspond to the normal distribution of the nerves. However, the location of II and IH nerves is quite consistently lateral and superior to the ASIS where the nerves are found between the transversus abdominis and internal oblique muscle layers (90%).

Patient Selection

Most of the patients have a previous history of surgery and a small subset of patients with no history of trauma. Involvement of II or IH nerves causes pain in the lower abdominal wall, which sometimes radiates to the genital area. There are two patterns

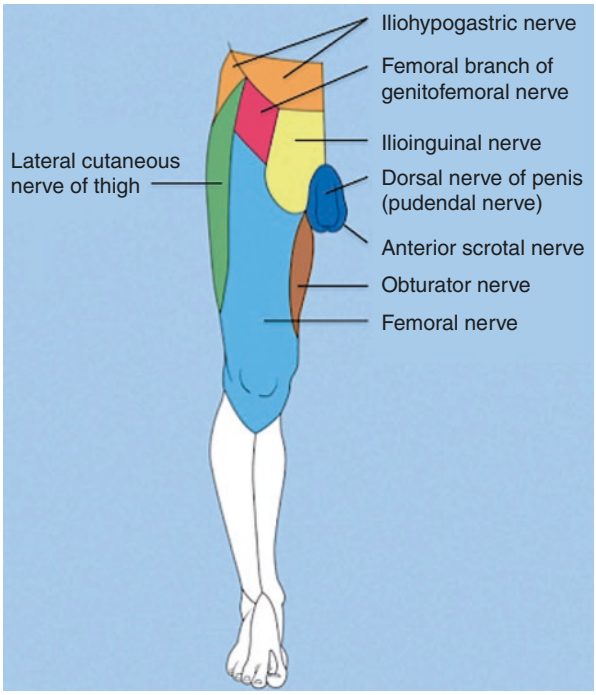

Fig. 6.3 Skin region innervated by different nerves in the thigh region. (Reprinted with permission from Dr. Danilo Jankovic)

related to previous trauma: early and late. The early is self-explanatory. The late presentation may be related to reduced mobility of the nerves, which are used to glide between muscle and fascia planes with movement. With scarring, the mobility decreases which contributes to microtrauma of the nerves.

The diagnosis remains primarily clinical. There is no pathognomonic imaging and laboratory and electrophysiology investigation for inguinal neuralgia. The clinician has to differentiate this from the visceral pain that is deep seated and poorly localized. Sensory change with objective signs is sometimes present. Other physical signs include a discrete tender spot, abnormal pain sensitivity (allodynia and hyperalgesia), and Tinel's sign.

The block serves both diagnostic and therapeutic roles. If the patient responds well to the analgesic injection with effects lasting for a few weeks, it is worthwhile to repeat the injections. Because of the potential systemic effects of steroids, it is prudent to avoid frequent repeated injections. The alternative options are pulsed radiofrequency, surgical nerve exploration and release (triple neurectomy), or implantation of peripheral nerve stimulator.

Ultrasound Scanning

- Position: Supine
- Probe: Linear 6–13 MHz

Step 1. Position of the probe

1. The key landmark is ASIS. Place the probe 2–3 fingerbreadths posterior to the ASIS (Fig. 6.4). At this level, all three layers of abdominal muscles can be easily visualized and the IH and II are quite consistently located between the transversus abdominis and internal oblique muscle.
2. Put the probe in short axis to the nerve.
3. Make sure the probe is perpendicular to the tangential plane of the skin.
4. Make sure the lateral part of the probe is on the iliac crest as the IH and II are usually located within 1.5 cm from the iliac crest.
5. Put more pressure on the medial part of the probe (toe-in) to allow better contact of probe to the three layers of muscle.

With this position, the left sonogram showed clearly the three layers of muscle: external oblique, internal oblique, and transversus abdominis (Fig. 6.5). A clear fascia expansion is where the IH nerve is. Quite commonly another fascia expansion is also seen but much further away from the iliac crest. It is the subcostal nerve as the

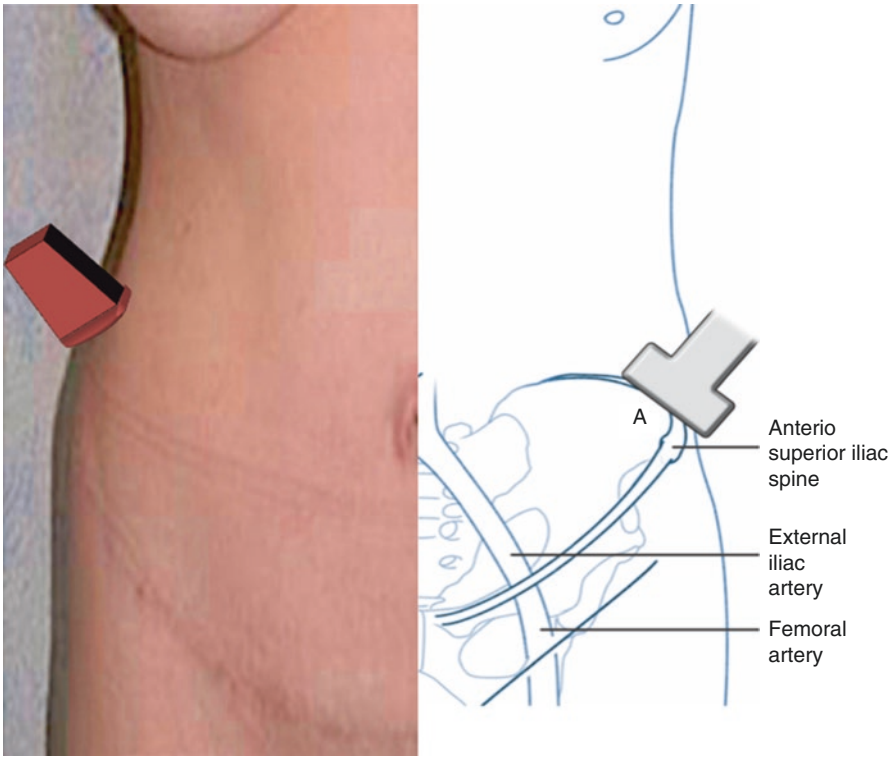

Fig. 6.4 The ultrasound probe position. (Reprinted with permission from Philip Peng Educational Series)

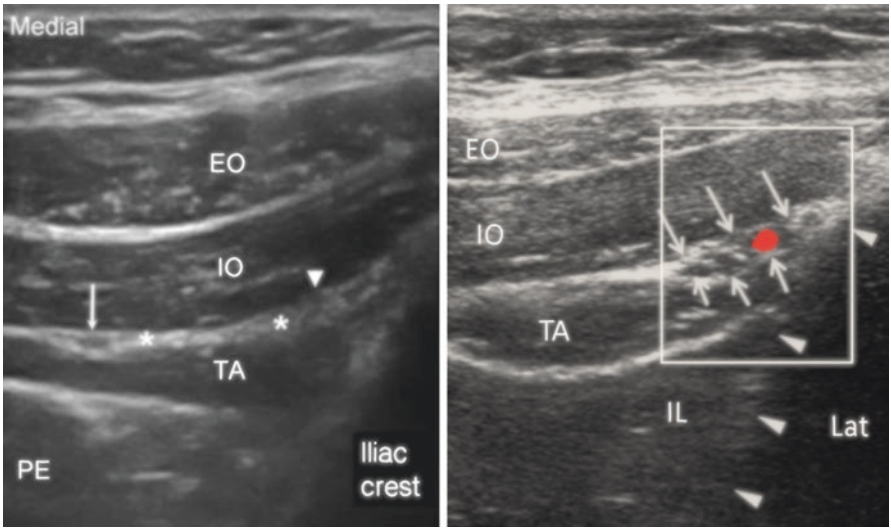

Fig. 6.5 Sonography of the abdominal muscles and ilioinguinal and iliohypogastric nerves. Fascia expansion (arrowhead) indicated where the ilioinguinal and iliohypogastric nerves are (∗). The right sonography showed the Doppler scan. The deep circumflex femoral artery is shown with the fascial expansion (arrows) between the IO and TA. Arrow indicated the subcostal nerve. EO external oblique, IO internal oblique, TA transversus abdominis, PE peritoneum. (Reprinted with permission from Philip Peng Educational Series)

nerve in the cephalad region is seen in more medial location in this scan. The right sonogram showed the Doppler scan and the deep circumflex iliac artery is seen in this fascia expansion.

Procedure

Equipment and Drugs

- Needles: 25G 1.5- or 3.5-inch needle (out of plane) – *preferred approach.*
  22G or 25G 3.5-inch needle (in plane)
- Drugs: 5 mL of local anesthetic (0.25% plain bupivacaine)
  1 mL steroid (40 mg Depo-Medrol)

Out of plane is the preferable technique as it causes less patient discomfort due to needle depth and trajectory (Fig. 6.6). The in-plane approach is performed from *medial to lateral* direction. Once the tip of the needle passes the internal oblique, hydrolocation with normal saline is important to recognize the fascial plane between IO and TA. The left sonogram highlighted the fascial plane (arrows) after injection of 0.5 mL injectate. Note the expansion of injectate within the fascial plane in the right sonogram with resultant compression of the TA. The steroid of the injectate (∗) casts a dense hyperechoic shadow.

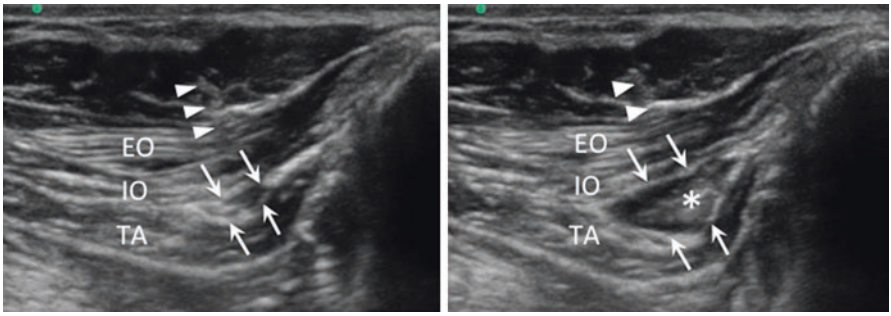

Fig. 6.6 Sonography showing the needle insertion. The needle was inserted out of plane and indicated by arrowheads. The injectate was indicated by ∗ within the fascia expansion (arrows). EO external oblique, IO internal oblique, TA transversus abdominis. (Reprinted with permission from Philip Peng Educational Series)

Clinical Pearls

1. When scanning at the level of ASIS, make sure the ultrasound probe is along the short axis of the inguinal canal.
2. Keep the iliac crest always in view.
3. Perfect alignment of the probe is lateral inward tilting of the probe towards the ilium.
4. Both out-of-plane technique and in-plane technique can be used, but the *authors' preferred approach is the out-of-plane*, which is easier and presents less discomfort to the patient.
5. Avoid mistaking the subcostal nerve for IH nerves, especially when the transducer position is too cephalad.
6. EO is often present as an aponeurosis when the ultrasound imaging is performed in the lower abdominal regions below the ASIS; hence instead of 3 layers typically seen in the abdominal wall, 2 layers will be seen at this location.
7. Epinephrine-containing local anesthetic is unnecessary as the injectate volume is low.

Literature Review

II and IH blocks serve both diagnostic and therapeutic purposes. The most consistent location of the II and IH nerves is lateral and superior to the ASIS where the nerves are found between the transversus abdominis and internal oblique muscle layers (90%). Besides anatomical landmark techniques and ultrasound approach, these blocks have not been performed under CT scan or X-ray.

All landmark techniques suggest the needle entry point medial to the ASIS. As mentioned above, there is a high degree of anatomic variability in not only the course of the nerves but also their branching pattern, areas of penetration of the

fascial layers, and dominance patterns. The sites at which the II and IH nerves pierce the abdominal wall muscle layers are significantly variable. Hence the failure rate of the blind technique lies in the range of 10–40%. In addition, there are other understandable risk of complications that include inadvertent femoral nerve block, colonic puncture, and vascular injury. Ultrasound provided an excellent imaging technique to visualize the three layers of abdominal muscles, and ultrasound-guided nerve block has been validated in a cadaver study with 95% accuracy in localizing nerves.

Suggested Reading

Aasvang E, Kehlet H. Chronic postoperative pain: the case of inguinal herniorrhaphy. Br J Anaesth. 2005;95:69–76.

Al-Dabbagh AKR. Anatomical variations of the inguinal nerves and risks of injury in 110 hernia repairs. Surg Radiol Anat. 2002;24:102–7.

Brandsborg B, Nikolajsen L, Kehlet H, Jensen TS. Chronic pain after hysterectomy. Acta Anaesthesiol Scand. 2008;52:327–31.

Can Schoor AN, Boon JM, Bosenbery AT, Abrahams PH, Meiring JH. Anatomical considerations of the pediatric ilioinguinal/iliohypogastric nerve block. Paediatr Anaesth. 2005;15:371–7.

Chan CW, Peng PWH. Ultrasound guided blocks for pelvic pain. In: Nauroze S, editor. Atlas of ultrasound-guided procedures in interventional pain management. 1st ed. Amherst: Springer; 2011. p. 207–26.

Eichenberger U, Greher M, Kirchmair L. Ultrasound –guided blocks of the ilioinguinal and iliohypogastric nerve: accuracy if a selective new technique confirmed by anatomical dissection. Br J Anaesth. 2006;97:238–43.

Mandelkor H, Loeweneck H. The iliohypogastric and ilioinguinal nerves. Distribution in the abdominal wall, danger areas in surgical incisions in the inguinal and pubic regions and reflected visceral pain in their dermatomes. Surg Radiol Anat. 1988;10:145–9.

Nagpal AS, Moody ES. Interventional Management for Pelvic Pain. Phys Med Rehabil Clin N Am. 2017;28:621–46.

Peng PWH. Peripheral application of ultrasound for chronic pain. In: Benzon H, Huntoon M, Narouze S, editors. Spinal injections and peripheral nerve blocks: interventional and neuromodulatory techniques for pain management (Deer T; Series editor). 1st ed. Philadelphia: Elsevier; 2012. p. 101–20.

Peng PWH, Narouze S. Ultrasound-guided interventional procedures in pain medicine: a review of anatomy, sonoanatomy and procedures. Part I: Non-axial structures. Reg Anesth Pain Med. 2009;34:458–74.

Peng PWH, Tumber PS. Ultrasound-guided interventional procedures for patients with chronic pelvic pain – a description of techniques and review of the literature. Pain Physician. 2008;11:215–24.

Rab M, Ebmer J, Dellon AL. Anatomic variability of the ilioinguinal and genitofemoral nerve: implications for the treatment of groin pain. Plast Reconstr Surg. 2001;108:1618–23.

Genitofemoral Nerve

7

Athmaja R. Thottungal and Philip Peng

Introduction

Genitofemoral neuralgia is a common cause of abdominopelvic pain. It may be caused by blunt trauma; compression along the course of the nerve; lower abdominal, groin, or pelvic surgery; injury to nerve following hernia repair especially laparoscopic surgery (12–43%) or spontaneous.

The genitofemoral nerve (GFN) arises from the L1 and L2 spinal nerves predominantly. It is part of the lumbar plexus. It is mainly a sensory nerve except for motor fibers of the cremasteric muscle. The GFN lies on top of the psoas muscle and crosses the ureter on descent. It divides into the genital and femoral branches which could happen anywhere during its course above the inguinal ligament (Fig. 7.1).

The femoral branch, a sensory branch, courses below the inguinal ligament and supplies the triangular dermatomal part over the femoral triangle. The area supplied by the genital branch is in the inguinal area inferior to that supplied by the ilioinguinal nerve (Fig. 7.2).

The genital branch crosses the inferior epigastric artery (IEA) at its lower end lateral to the junction between the external iliac artery (EIA) and IEA and enters the inguinal canal through the deep inguinal ring (Fig. 7.3). It travels along with other contents of the inguinal canal along with the spermatic cord in men and the round ligament of the uterus in women. The canal also contains the ilioinguinal nerve and testicular vessels in men or the vessel following the round ligament of the uterus in females.

A. R. Thottungal
Department of Anaesthesia & Pain, Kent and Canterbury Hospital, Canterbury, UK

P. Peng (✉)
Department of Anesthesia and Pain Management, Toronto Western Hopsital and Mount Sinai Hospital, University of Toronto, Toronto, Ontario, Canada
e-mail: Philip.peng@uhn.ca

P. Peng et al. (eds.), *Ultrasound for Interventional Pain Management*,
https://doi.org/10.1007/978-3-030-18371-4_7

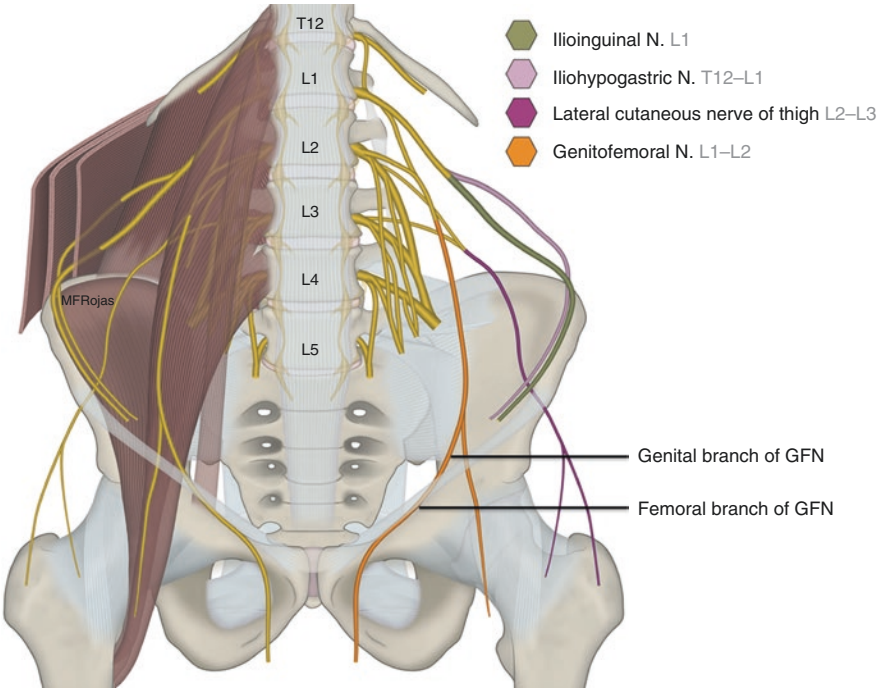

Fig. 7.1 The genital and femoral branches of the genitofemoral nerve. (Reprinted with permission from Dr. Maria Fernanda Rojas)

Fig. 7.2 Skin innervated by the genital and femoral branches of the genitofemoral nerve. (Reprinted with permission from Dr. Danilo Jankovic)

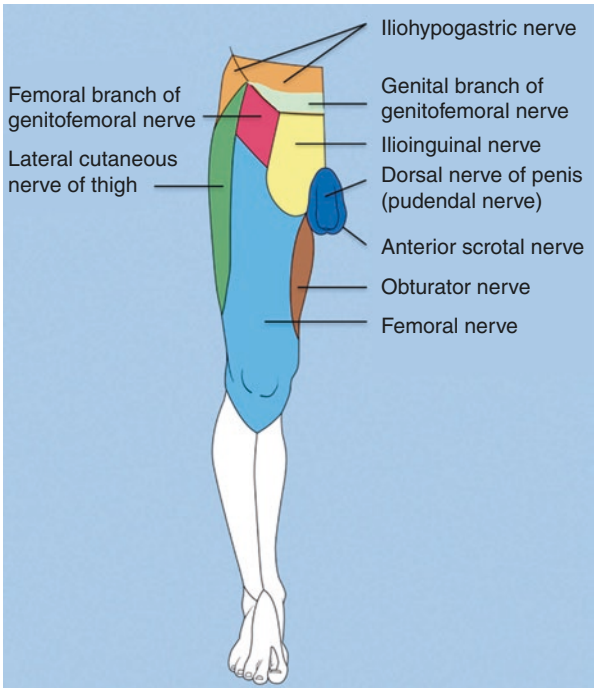

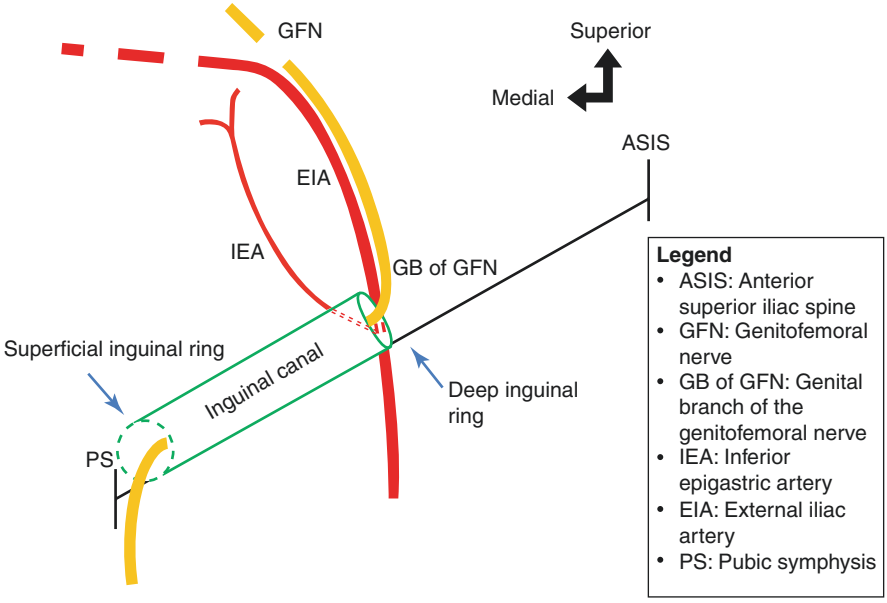

Fig. 7.3 Schematic diagram showing relationship of the genital branch (GB) of the genitofemoral nerve (GFN) to the external iliac artery (EIA) and inferior epigastric artery (IEA). (Reprinted with permission from Philip Peng Educational Series)

Patient Selection

Select patients with suspected genitofemoral neuralgia. Diagnosis is mainly clinical based on the history and the dermatomal distribution of pain, which is mainly neuropathic in nature (burning, paresthesia, or numbness in the lower abdomen radiating to medial thigh and into the labia majora in women and the anterior surface of the scrotum in men). Patients tend to hold a "novice skier's" position to relieve the strain on the nerves. Spinal extension tends to exacerbate the pain. Physical examination reveals cutaneous neuropathic sensory changes and Tinel's sign may be present on tapping along the inguinal ligament. Cremasteric reflex may be absent.

Ultrasound Scanning

There are three different methods to scan and identify the genital branch of the genitofemoral nerve (GFN). No validated standardized technique has been described yet. Two methods are already described in the literature and the third one (method 1) is from author's clinical experience especially from scanning female patients.

- Position: Supine
- Probe: High-frequency linear probe (6–13 MHz).

Method 1

Scan 1

Place the probe in transverse plane just below the inguinal ligament and identify the femoral artery and place it at the middle of the screen (Fig. 7.4).

Scan 2

The probe is then rotated to long axis to visualize the femoral artery (FA) longitudinally and moved cranially to identify the FA that becomes the external iliac artery (EIA) and dives deep into the abdomen (Fig. 7.5).

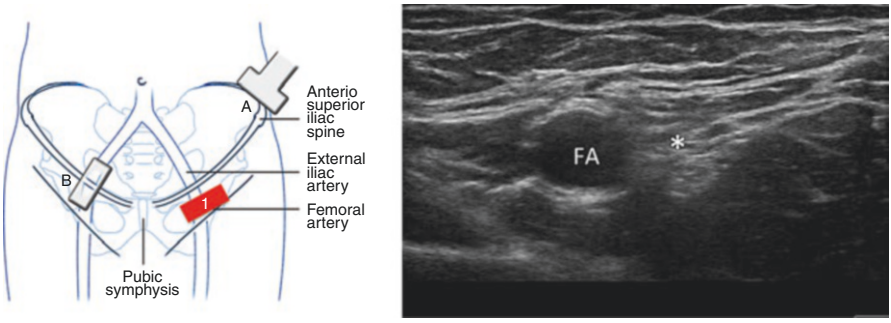

Fig. 7.4 Figure showing the position of the ultrasound transducer (red square 1) and the corresponding sonography. FA femoral artery, ∗ femoral nerve. (Reprinted with permission from Philip Peng Educational Series)

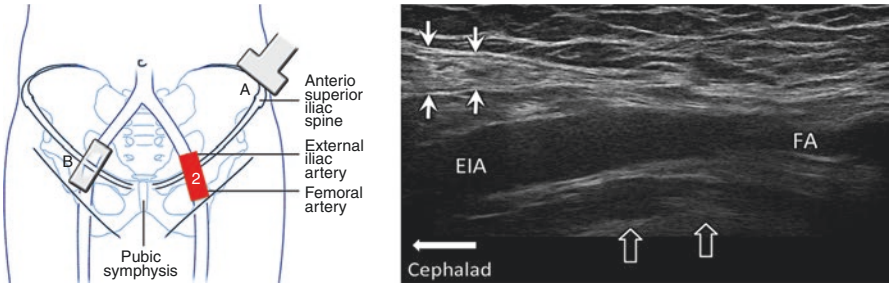

Fig. 7.5 Figure showing the position of the ultrasound transducer (red square 2) and the corresponding sonography. Line bold arrow, pubic ramus; arrows, inguinal canal, FA femoral artery, EIA external iliac artery. (Reprinted with permission from Philip Peng Educational Series)

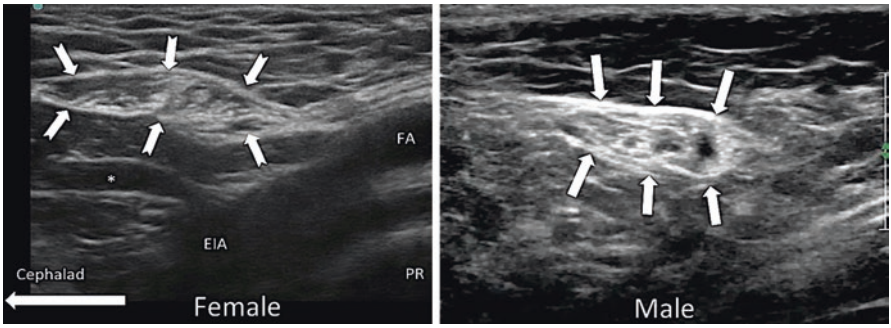

Fig. 7.6 Sonography of inguinal canal for female (left) and male (right). EIA external iliac artery, FA femoral artery, PR pubic ramus, ∗ inferior epigastric artery. (Reprinted with permission from Philip Peng Educational Series)

Scan 3

At this point, the inguinal canal appears as an oval structure (bold arrows) superficial to the FA with the round ligament (left) of the uterus or spermatic cord (right) (Fig. 7.6). Note the spermatic cord is a structure with multiple tubular structures inside (vas deferens, arteries, and vein). The probe is moved medially tracing these structures to move away from the FA.

Method 2

Ultrasound Scanning

Scan 1

This technique is mainly used for male. The initial probe position is to scan the spermatic cord next to the superficial inguinal ring around the pubic tubercle (PT) (upper panel of Fig. 7.7).

Scan 2

Scan laterally toward the external iliac artery. The spermatic cord (arrows) will become apparent as a structure with multiple lumens (lower panel of Fig. 7.7).

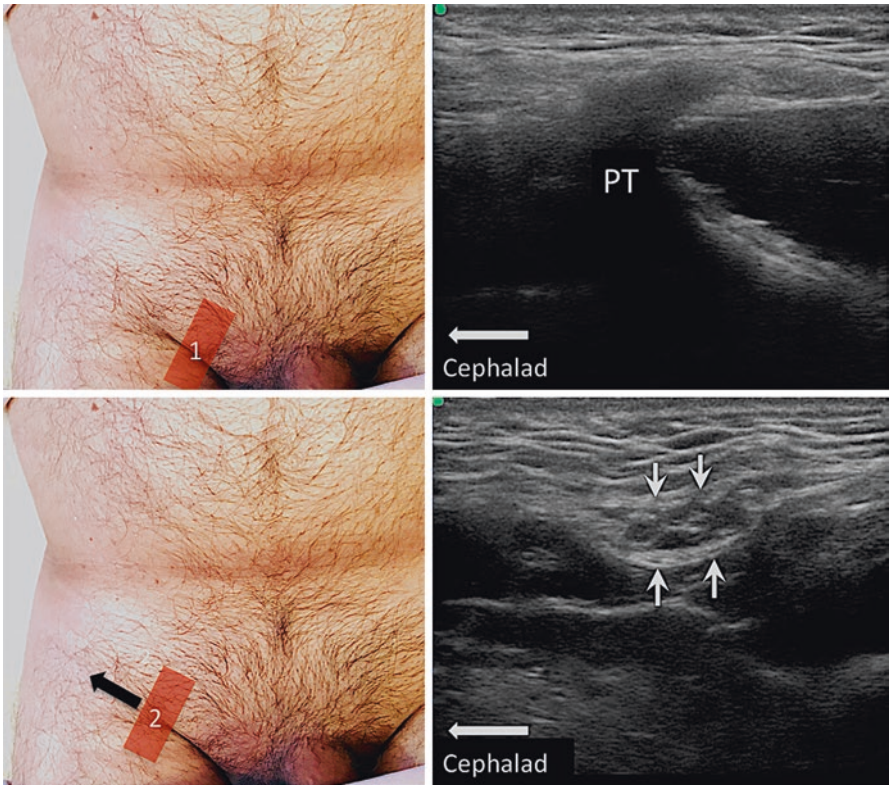

Fig. 7.7 Position of ultrasound probe at and lateral to the pubic tubercle (PT) and the corresponding sonography. The spermatic cord was outlined with arrows. (Reprinted with permission from Philip Peng Educational Series)

Method 3

This is from the author's (AT) clinical experience.

Scan 1

Upper panel. Start scanning the rectus abdominis (RA) muscle at the lower abdomen in transverse plane and identify the inferior epigastric artery (IEA) (Fig. 7.8).

Lower panel. Continue scanning caudally following the IEA till the junction of the IEA with the external iliac artery (EIA) is identified (Fig. 7.8).

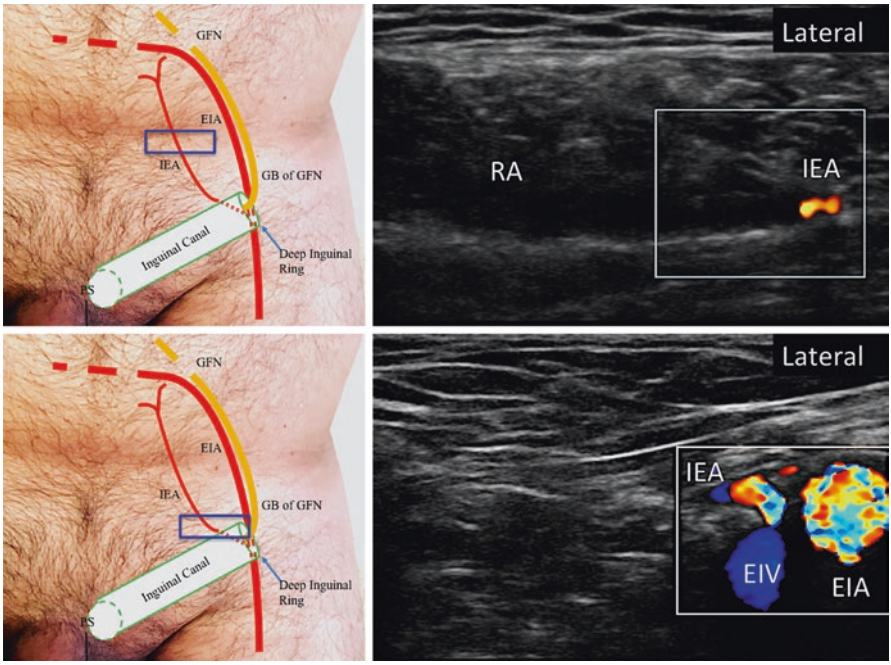

Fig. 7.8 Position of ultrasound probe and the corresponding sonography. GB genital branch of the genitofemoral nerve (GFN), EIA external iliac artery, IEA inferior epigastric artery, PS pubic symphysis, RA rectus abdominis. (Reprinted with permission from Philip Peng Educational Series)

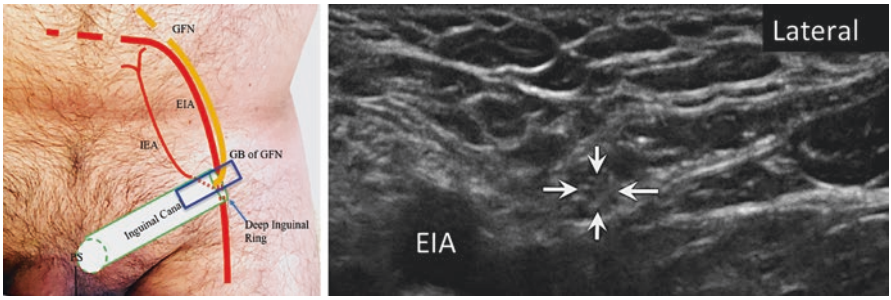

Fig. 7.9 Position of ultrasound probe and the corresponding sonography revealing the genital branch of the genitofemoral nerve (arrows). EIA external iliac artery. (Reprinted with permission from Philip Peng Educational Series)

Scan 2

Tilt the lateral part of the probe slightly cranially to make the probe position parallel to the inguinal ligament. Lateral to the EIA is the genital branch of GFN entering into the inguinal canal (Fig. 7.9).

Procedure

- Needles: 22G/25G, 35- or 50-mm echogenic needle
- Drugs: 2–4 ml of 0.25–0.5% levo or plain bupivacaine with 1 ml (3.8 mg) dexamethasone or 40 mg Depo-Medrol injected inside the inguinal canal and another 2–4 ml given inside the spermatic cord.

The needle is advanced as out of plane (Fig. 7.10). The initial injection (left sonogram) is inside the spermatic cord outlined by the arrowheads. It is important to observe the spread of the local anesthetic (∗) as this is a very vascular structure. The needle is pulled back to deport the medication outside the spermatic cord but inside the inguinal canal (arrows) in the right sonogram. This sonogram highlighted the spread of the local anesthetic around the spermatic cord. Inject twice because the GFN may travel outside or within the spermatic cord in the inguinal canal.

The injection can be performed as an in-plane approach with the needle (arrow) inserted in caudal to cranial direction. The inguinal canal is highlighted with arrowheads. ∗ local anesthetic (Fig. 7.11).

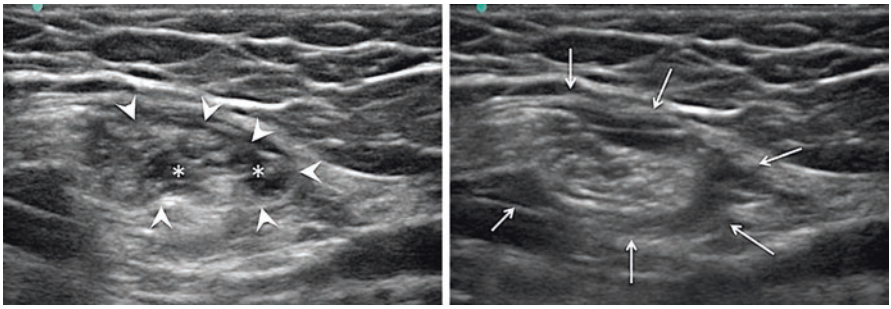

Fig. 7.10 Sonography of inguinal canal and the effect of the injectate. (Reprinted with permission from Philip Peng Educational Series)

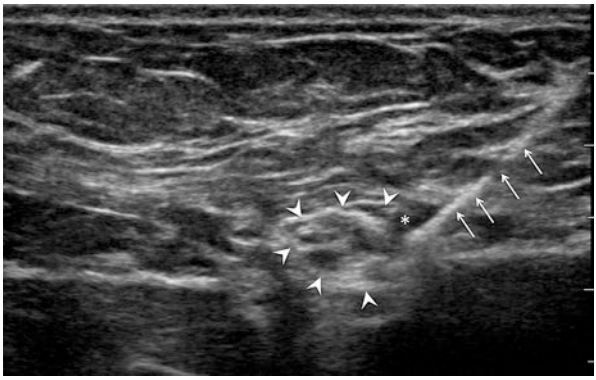

Fig. 7.11 Needle insertion to the genital branch of genital femoral nerve. (Reprinted with permission from Philip Peng Educational Series)

Clinical Pearls

1. Both method 1 and method 3 are useful for both male and female patients, any age group and size. In men it is easier to use method 2 as the spermatic cord is easy to identify.
2. Method 3 is also a better position for neuromodulatory techniques like pulsed radiofrequency denervation.
3. In-plane needling is preferred as EIA and FA are close by and can avoid bleeding.
4. Always use color Doppler prior to injection to identify testicular vessels and EIA pulsations.
5. GFN is a nerve of huge anatomical variation. It could also be originating from T12 or L3. L2 contribution tends to be more consistent.
6. The division of the genital and femoral branches is very variable and can happen anywhere during the course of the nerve.
7. There is overlap between the dermatomal supply of the ilioinguinal nerve (IIN) and GFN. So checking IIN is also important when GFN pathology is suspected.
8. Do not use local anesthetic with epinephrine for this block if injected around the spermatic cord.

Literature Review

Genitofemoral neuralgia can be a debilitating condition and is difficult to treat due to anatomical variability and difficulty identifying the nerve reliably. So it is not performed commonly by many physicians. The conventional description of the blockade of the genital branch of the GF nerve relies on palpating the pubic tubercle and injecting lateral to that or requires direct injection into the inguinal canal while performing surgery. When performed with landmark guidance, the pubic tubercle, inguinal ligament, inguinal crease, and femoral artery had been used as reference landmark, and the needle is inserted into the inguinal canal to block the genital branch. As one can appreciate from the sonoanatomy described above, the needle is likely to enter the spermatic cord or even the peritoneum, resulting in trauma of the structures inside the spermatic cord or bowel.

The genital branch is a small nerve and the technique described above is mainly a compartment block putting a volume of local anesthetic to reach the nerve. These techniques (methods 1 and 2) are not applicable to the radiofrequency or cryoablation as the precise anatomy is required. More research is required on the precise anatomy of the nerve. The method has not been validated and is based on one of the author's (AT) experience.

Suggested Reading

Alfieri S, Amid PK, Campanelli G, et al. International guidelines for prevention and management of post-operative chronic pain following inguinal hernia surgery. Hernia. 2011;15(3):239–49.

Bellingham GA, Peng PWH. Ultrasound guided interventional procedures for chronic pelvic pain. Tech Reg Anesth Pain Manang. 2009;13:171–8.

Broadman LM. Complications of pediatric regional anesthesia. Reg Anesth. 1996;21(6 Suppl):64–70.

Campos NA, Chiles JH, Plunkett AR. Ultrasound-guided cryoablation for genitofemoral nerve for chronic inguinal pain. Pain Physician. 2009;12(6):997–1000.

Chan CW, Peng PWH. Ultrasound guided blocks for pelvic pain. In: Nauroze S, editor. Atlas of ultrasound guided procedures in interventional pain management. 1st ed. New York: Springer; 2011. p. 207–26.

Conn D, Nicholls B. Regional Anesthesia. In: Wilson IH, Allman KG, editors. Oxford handbook of anaesthesia. 2nd ed. New York: Oxford University Press; 2006. p. 1055–104.

Liu WC, Chen TH, Shyu JF, et al. Applied anatomy of the genital branch of genitofemoral nerve in open inguinal herniorrhaphy. Eur J Surg. 2002;168(3):145–9.

Nienhuijs SW, Staal JF, Strobbe LJA, Rosman C, Groenewoud JMM, Bleichrodt RP. Chronic pain after mesh repair of inguinal hernia: a systemic review. Am J Surg. 2007;194:394–400.

Peng PW, Tumber PS. Ultrasound-guided inter- ventional procedures for patients with chronic pelvic pain—a description of techniques and review of literature. Pain Physician. 2008;11(2):215–24.

Rab M, Ebmer J, Dellon AL. Anatomic variability of the ilioinguinal and genitofemoral nerve: implications for the treatment of groin pain. Plast Reconstr Surg. 2001;108(6):1618–23.

Waldman SD. Atlas of pain management injection techniques. 3rd ed. Philadelphia: Elsevier Saunders; 2013. p. 340–1.

Pelvic Muscles

8

Anuj Bhatia and Philip Peng

Introduction

Chronic pelvic pain (CPP) is defined as noncyclic pain of at least 6 months duration, severe enough to cause disability or seek medical attention, and occurring in locations such as the pelvis, anterior abdominal wall at or below the umbilicus, lower back, or buttocks. The pathophysiology of CPP is complex. The pain generator may include the viscera (e.g., bladder, bowel), neuromuscular system (e.g., pudendal neuralgia, piriformis syndrome), or gynecological system (e.g., endometriosis). In this chapter, we will discuss three muscles that can be pain generators in patients with deep pelvic pain syndromes: piriformis, obturator internus, and quadratus femoris.

Piriformis Muscle

Piriformis syndrome, an etiology related to prolonged or excessive contraction of the piriformis muscle and its close relationship to the sciatic nerve and the inferior gluteal artery, is associated with pain in the buttocks, hip, and lower limb (Fig. 8.1). Pain aggravated on sitting, external tenderness near the greater sciatic notch, pain on any maneuver that increases piriformis muscle tension, and limitation of straight leg raising are features commonly observed in this syndrome. Injections of local anesthetics, steroids, and botulinum toxin into this muscle using anatomic landmarks,

A. Bhatia · P. Peng (✉)
Department of Anesthesia and Pain Management, Toronto Western Hopsital and Mount Sinai Hospital, University of Toronto, Toronto, Ontario, Canada
e-mail: Philip.peng@uhn.ca

P. Peng et al. (eds.), *Ultrasound for Interventional Pain Management*,
https://doi.org/10.1007/978-3-030-18371-4_8

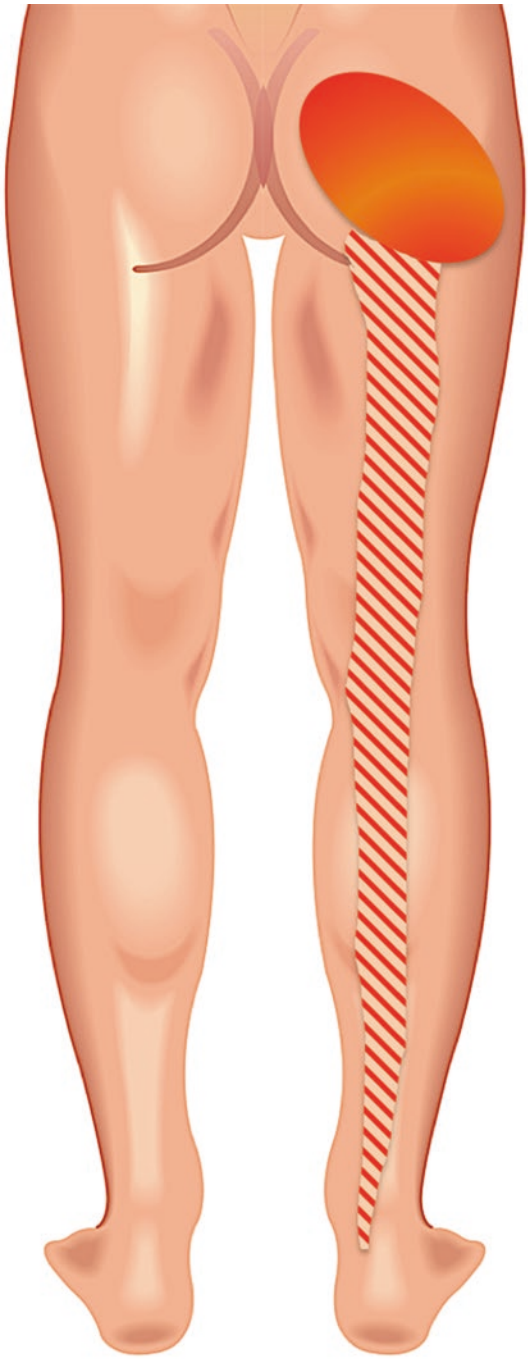

Fig. 8.1 The area of pain in patients with piriformis syndrome. (Reprinted with permission from Philip Peng Educational Series)

electrical stimulation, fluoroscopy, and ultrasound for guidance are often performed for diagnostic and therapeutic purposes.

The piriformis functions as an external rotator of the lower limb in the erect position, an abductor when supine, and a weak hip flexor when walking. It originates from the ventral surface of the S2 to S4 vertebrae. Running laterally anterior to the sacroiliac joint, this muscle exits the pelvis through the greater sciatic foramen. At this point the muscle becomes tendinous inserting into the upper border of the greater trochanter as a round tendon. All neurovascular structures exiting the pelvis to the buttock pass through the greater sciatic foramen (Fig. 8.2). The superior gluteal nerve and artery pass superior to the piriformis. Inferior to the piriformis lie the inferior gluteal artery and nerve, the internal pudendal artery, the pudendal nerve, obturator internus nerve, posterior femoral cutaneous nerve, quadratus lumborum nerve, and sciatic nerve.

The anatomical relationship between the piriformis muscle and sciatic nerve is variable. Most commonly, the sciatic nerve passes below the piriformis muscle (83%). There are five other variations as shown in Fig. 8.3.The close relationship of the piriformis muscle to the sciatic nerve explains why patients experiencing piriformis syndrome may also experience symptoms of sciatic nerve irritation.

Patient Selection

Piriformis syndrome is an uncommon cause of pain occurring in the back, buttock, or hip. Typically, pain is felt in the region of the sacroiliac joint, greater sciatic notch, and piriformis muscle with radiation down the lower limb similar to sciatica. The pain is exacerbated by walking, stooping, or lifting. On physical examination

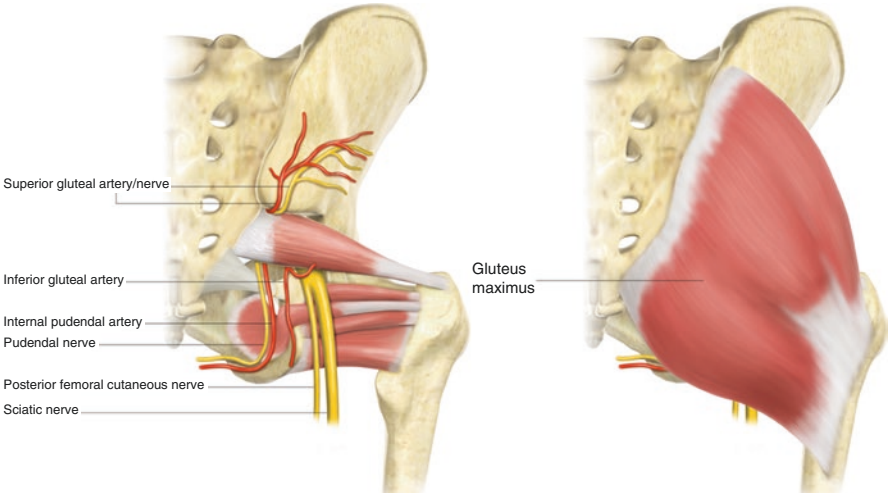

Fig. 8.2 Piriformis muscle and the neurovascular structures in the vicinity. (Reprinted with permission from Philip Peng Educational Series)

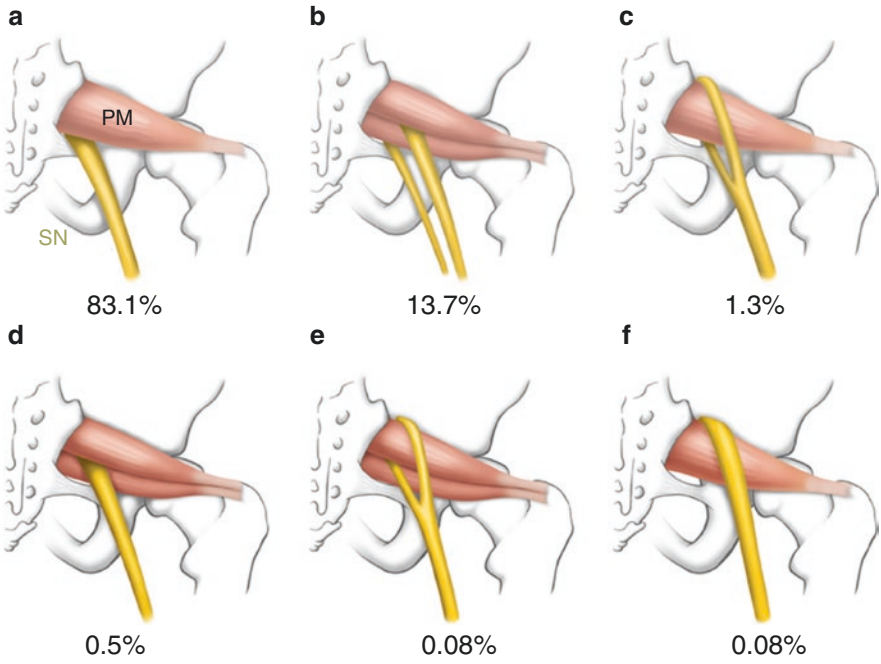

Fig. 8.3 The variation of the anatomical relationship between the piriformis muscle and sciatic nerve. The most common variation is shown in (**a**), where the sciatic nerve passes below the piriformis muscle (83%). The sciatic nerve can appear as two trunks passing between and inferior to the piriformis (**b**), superior and inferior to piriformis (**c**), or above and between the piriformis muscle (**e**). Rarely, it appears as one trunk passing between the piriformis (**d**), or superior to the piriformis muscle (**f**)

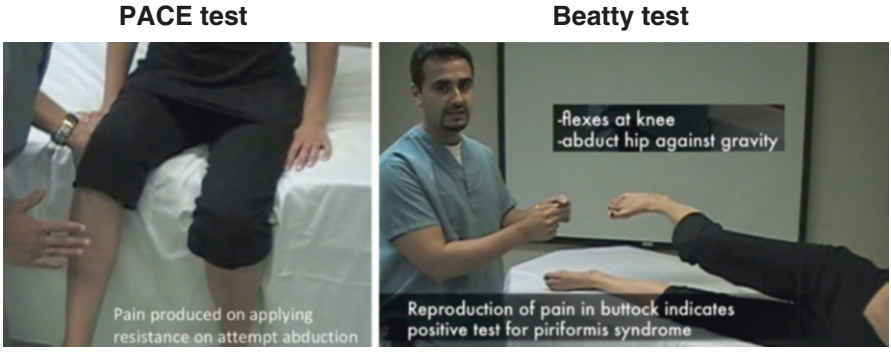

Fig. 8.4 PACE and Beatty test

there may be gluteal atrophy and tenderness on palpation and pain on stretching of the piriformis muscle.

A few clinical tests can be helpful (Figs. 8.4 and 8.5). Often, it is a diagnosis of exclusion with clinical assessment and investigations necessary to rule out pathology of the lumbar spine, hip, and sacroiliac joint.

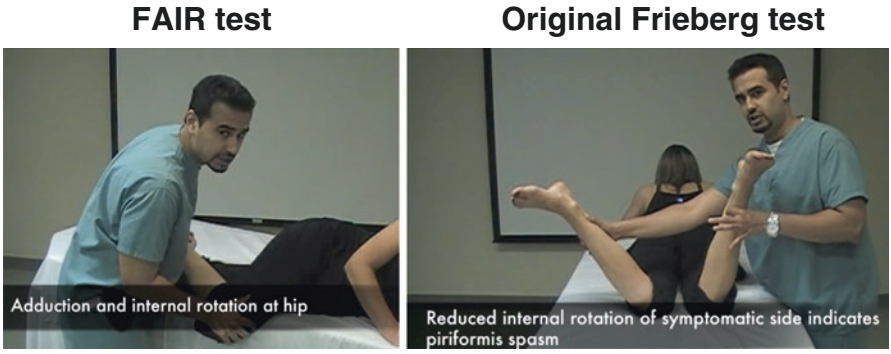

Fig. 8.5 FAIR and Freiberg test (original). (Reprinted with permission from Philip Peng Educational Series)

Ultrasound Scan

- *Patient position*: Prone
- *Probe*: Curvilinear (2–6 MHz)

Scan 1

First, locate the posterior superior iliac spine (PSIS). (approximated by the dimple of Venus). Then, place the ultrasound probe over the gluteal region with the medial part of the probe over PSIS (left upper figure position A in Fig. 8.6). The sonograph showed the iliac crest and the gluteus maximus (G Max) muscle (left lower figure).

Scan 2

The probe is moved in the caudal direction to the greater sciatic notch (left upper diagram position B in Fig. 8.6) when the curved hyperechoic shadow of the ischium appears (right upper sonogram). The scan can be optimized by aligning the probe with the long axis of the piriformis and tilting the probe in medial orientation.

It is important to optimize the scan by titling so as to identify the superficial and deep border of the piriformis (Pi) and the sciatic nerve (arrowheads). The latter is located deep to the piriformis medial to the ischium. By applying the Doppler (right lower sonogram), the branch of inferior gluteal artery can be seen accompanying the sciatic nerve.

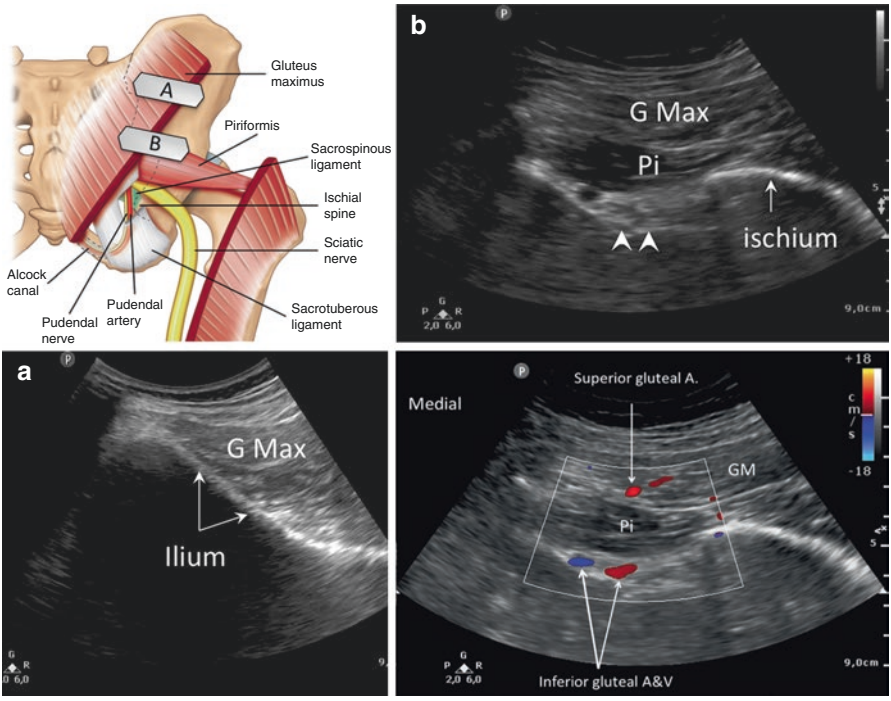

Fig. 8.6 The positions of the ultrasound probe (A and B) are shown in left upper diagram. (**a**) When the probe is placed at the iliac crest, the illum and gluteus maximus (*G Max*) is well seen. (**b**) Sliding the probe in the position B which is at the level of the greater sciatic notch, piriformis muscle (*Pi*) is seen deep to the gluteus maximus (*G Max*). Please note the sciatic nerve (*arrowheads*) and the curve shape of ischium (*arrow*). Right lower diagram is the Doppler scan when the probe is placed in position B. The artery between the gluteus maximus (*GM*) and piriformis is the superior gluteal artery, while the artery deep to the piriformis is the inferior gluteal artery and vein (A and V)

Procedure

- *Needle*: 22 or 25 G, 3.5- or 5-inch needle (preferably echogenic)
- *Drugs*: 1–2 cc of one of the following:
  - Local anesthetic (0.25% bupivacaine)
  - Local anesthetic with methylprednisolone 40 mg
  - Botulinum 50–100 units

The target is the muscle belly of the piriformis. The needle is inserted in-plane with the entry point 2 cm away from the medial edge of the probe (Fig. 8.7).

Clinical Pearls

- To enhance the visualization of the needle, one can insert the needle 2 cm away from the medial edge of the probe or tilt the probe more medially to allow a shallower angle of the needle.

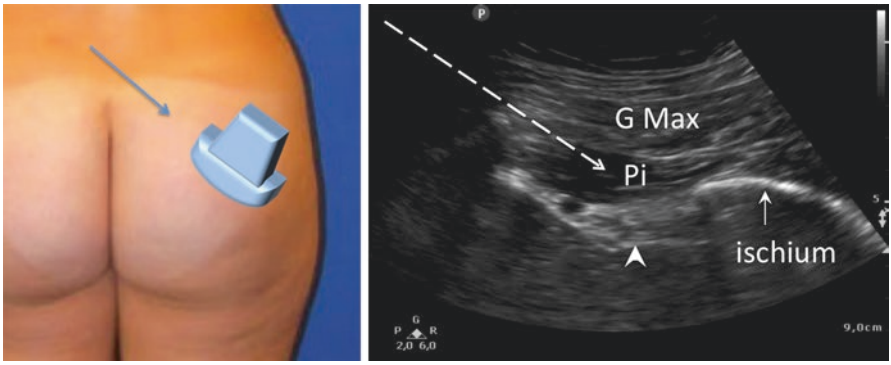

Fig. 8.7 Left figure showing position of the needle and the probe and right figure showed the corresponding sonography. (Reprinted with permission from Philip Peng Educational Series)

- Start scanning from the iliac crest and move the probe slowly in the caudal direction to avoid confusion with muscles in the lesser sciatic notch.
- When tilting the probe medially to optimize the scan, quite often the authors will also place the probe on the lateral aspect of gluteal regional and "push" the probe medially as well as the medial tilt action.
- Observe the slight curvature of the ischium deep to the lateral part of the piriformis. Straightening of the ischium suggests US scan is at the level of the ischial spine and the sacrospinous ligament – this is the boundary between the greater and lesser sciatic notches and caudal to the inferior border of the piriformis.

Literature Review

Involvement of the piriformis muscle in sciatic neuropathy has been supported by evidence from computed tomography (CT), magnetic resonance imaging (MRI), scintigraphy, and ultrasound (US). Proximity of the piriformis muscle to the sciatic nerve, inferior gluteal artery, and vein makes landmark- or fluoroscopy-based infiltration risky. Electrical stimulation of the muscle (in the absence of contraction of muscles innervated by the sciatic nerve) suggests that the needle tip is in the muscle belly, but there is significant variation in the needle-to-nerve distance for presence or absence of muscle twitches to be regarded as a reliable indicator of needle tip position. A study in cadavers showed that only 30% of fluoroscopy-guided injections were accurate with majority of incorrect injections in the gluteus maximus. Ultrasound allows visualization of the muscle and the surrounding neurovascular structures, thereby enhancing both accuracy and safety. Comparison of local anesthetic against a combination of local anesthetic with steroids as injectates to treat piriformis syndrome indicates that the combination does not confer any analgesic benefit over local anesthetic alone for a period of 3 months following the injections.

Obturator Internus Muscle

The obturator internus (OI) is one of the short external rotators of the thigh at the hip (Fig. 8.2). The other muscles that have the same action include the piriformis, superior and inferior gemelli, and quadratus femoris. Pathology of this muscle can present with gluteal pain and symptoms similar to piriformis syndrome. Important anatomical relationships include the Alcock's canal medially that contains the pudendal neurovascular bundle and is formed by splitting of the muscle's fascia into a medial and lateral layer – this canal underlies the plane of levator ani. Pathology in (tears or tendinitis) or around this muscle (bursitis) results in gluteal pain that is retrotrochanteric. This is often referred to as the "deep gluteal syndrome." Acute strain, chronic overuse, myofascial pain, contusions, tendinopathy, calcific tendinitis, or bursitis may be responsible for pain originating in the OI.

OI is partly a hip muscle and partly an intrapelvic muscle. It originates from within the pelvis along the obturator foramen and membrane, exits through the lesser sciatic foramen by curving around the posterior ischium, and courses laterally deep to the sciatic nerve toward its common insertion with the superior and inferior gemelli as the tricipital tendon on the medial greater trochanter (Fig. 8.2). The OI may be subjected to stress during its sharply angulated exit from the pelvis, as evidenced by the presence of a cartilaginous region on the posterior ischium over which the OI tendon glides. The OI bursa is located medially between the OI and posterior ischial cartilage and reduces frictional stresses in this region.

Patient Selection

Pain is present in the mid-buttock region and tenderness on palpation of the interval between the piriformis muscle and the ischial tuberosity can be elicited. Patients often report pain on sitting – apart from the OI, the hamstring-ischial bursa complex is another source for this pain.

Physical examination to elicit pain from OI requires maneuvers similar to those for stressing the piriformis muscle. Pain in innervation territory of the pudendal and/or sciatic nerves due to dynamic compression of the nerve by the OI muscle and tendon is an unusual presentation. Injecting the OI sheath, muscle, or bursa can relieve the pain depending on the site of the pathology.

Ultrasound Scan

- Patient position: Prone
- Probe: Curvilinear (2–6 MHz)

Scan 1

The scan sequence is similar to the scanning of piriformis, starting from the iliac crest, the greater sciatic notch, and then ischial spine (Fig. 8.8). The change of the

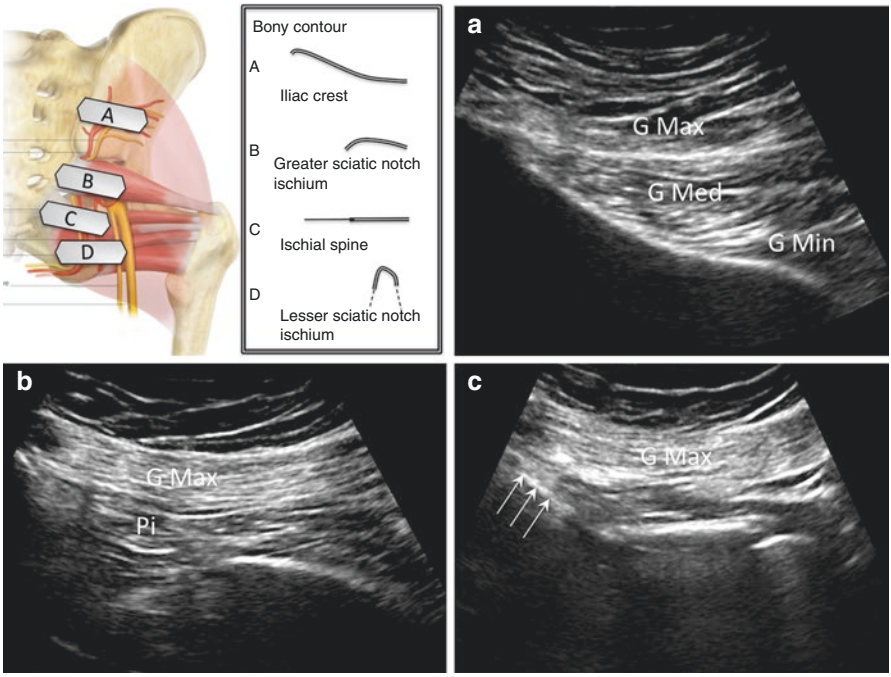

Fig. 8.8 The left upper diagram shows the positions of the ultrasound probe at different level of pelvis (A-D) and the typical appearances of the bony contour (A-D). Only the corresponding sonograms from A to C are shown here and D will be discussed in Fig. 8.9. (**a**) At iliac crest (scan A), the bony contour is continuous and three gluteus muscles: maximus (*G Max*), medius (*G Med*) and minimus (*G Min*) can be displayed in the same scan. (**b**) At great sciatic notch (*scan B*), both gluteus maximus (*G Max*) and piriformis (*Pi*) muscles can be seen. (**c**) At the level of ischial spine (*scan C*), the bony contour is straight and is seen in continuity with sacrospinous ligament (*arrows*)

contour of the bone is shown in the left upper figure. At the iliac crest, three gluteus muscles (right upper sonogram) can be visualized. At the greater sciatic fossa, the piriformis muscle (Pi) is seen. At the ischial spine level, the bony contour is straight and a hyperechoic line on the medial side of the ischial spine is the sacrospinous ligament (arrows in right lower figure). G Max, G Med, and G Min stand for gluteus maximus, medius, and minimus, respectively.

Scan 2

From the ischial spine level, further caudal movement of the probe will reach the lesser sciatic notch (Fig. 8.9). Please note the bony contour. Because the orientation of the bone and OI muscle is close to 90° to the ultrasound probe, the OI appears as a hypoechoic structure. If the clinician carefully observes the structures transitioned from the ischial spine to the less sciatic notch, the sacrotuberous ligament continues to be observed and the pudendal neurovascular bundle will move close to the OI in Alcock's canal. Deep to the sacrotuberous ligament, two pelvic floor muscles can be seen: coccygeus (labeled blue deep to the sacrotuberous ligament) and iliococcygeus muscle (outlined by dark blue line).

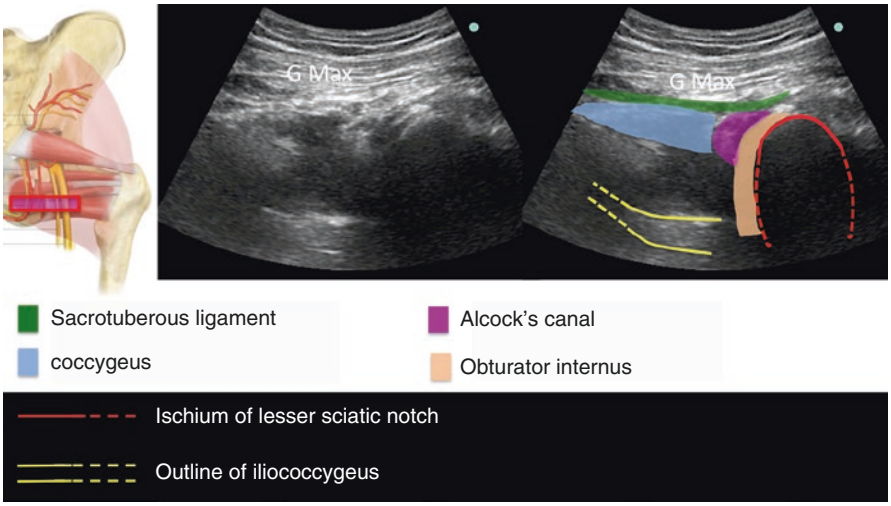

Fig. 8.9 Figure showing the ultrasound probe and the corresponding sonography. (Reprinted with permission from Philip Peng Educational Series)

Procedure

- Needle: 22 or 25 G, 3.5- or 5-inch needle (preferably echogenic)
- Medication: For OI muscle, 1–2 cc of either local anesthetic with methylprednisolone 40 mg or botulinum 50–100 units; for OI tendon sheath or bursa, 3–5 mL of local anesthetic (bupivacaine 0.25%) and methylprednisolone 40 mg

OI Muscle

Most of the author's practice is the injection into the muscle. Because it is a deep structure, a long and echogenic needle is preferred if available. The needle is inserted in-plane from medial to lateral (Fig. 8.10). Attention is paid to the pudendal neurovascular bundle in the Alcock's canal which is usually found in the region between the sacrotuberous ligament (green) and OI (orange). The needle angle is usually steep. Once the bony contact is encountered, hydrolocation is performed. Because of the deep location, one can use the Doppler to detect the location of the injectate (arrowheads).

Peritendon or Bursa Injection

Sometimes, the target is peritendinous sheath or bursa (Fig. 8.10). For the latter, the target is deep to the tendon (**). The needle is inserted in-plane as described above but at a shallower angle to the space between the OI tendon and the ischium. Medial to lateral direction is preferred to avoid the sciatic nerve. For peritendinous injection, the needle is simply directed superficial to the tendon.

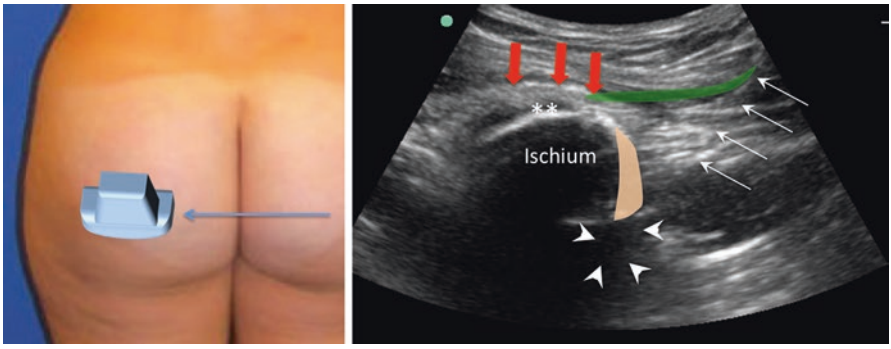

Fig. 8.10 Figure showing the ultrasound probe and needle position on the left side and the corresponding sonography on the right side. Obturator internus muscle, solid beige color; obturator internus tendon, bold red arrows; **, obturator internus bursa; sacrotuberous ligament, green color; line arrows, needle; arrowheads, injectate. (Reprinted with permission from Philip Peng Educational Series)

Clinical Pearls

- Insert needle 2 cm away from the edge of the probe.
- Start scanning from the iliac crest and move the probe in caudal direction following the change in the contour of the bone. The OI is also the only muscle with an intrapelvic belly and it wraps around the posterior ischium. Therefore, the hypoechoic shadow on the medial aspect of the ischium is the OI.
- Once at the ischial spine level, turn on the Doppler to visualize the pudendal vessel and then move caudally. This will help to identify the Alcock's canal.
- The hydrolocation of OI intramuscular injection can be assisted with Doppler.

Literature Review

The small size and deep location of the OI and its proximity to neurovascular structures and other muscles make it almost impossible to do accurate and safe landmark- or fluoroscopy-based injections. MRI, CT, and US have been used to perform these injections, but US has the advantage of allowing a dynamic scan, portability, and avoiding radiation. A cadaveric study of 10 transverse or longitudinal US-guided injections into the OI tendon sheath, muscle belly, and bursa reported 100% accuracy for deposition of the injectate, and there was no evidence of injury to sciatic nerve or gluteal arteries.

Quadratus Femoris

Quadratus femoris (QF) is a flat, quadrilateral muscle located posterior to the hip joint. It is an external rotator and adductor of the thigh. Pathology in this muscle can result in groin pain from inflammation of the tendon of the QF. Another manifestation is gluteal pain from ischiofemoral impingement (IFI), a syndrome characterized by decreased distance between the lesser trochanter of the femur and the ischial tuberosity.

The quadratus femoris originates on the lateral border of the ischial tuberosity and inserts on to the posterior surface of the head of the femur (Fig. 8.11). The inferior gemellus lies immediately cephalad and the adductor magnus is caudal. A bursa is often found between the QF muscle and the lesser trochanter. The obturator externus muscle lies deep to the QF and cannot be seen in the figure.

Patient Selection

Patients, often middle-aged and elderly women, present with buttock or hip pain that can be worsened with hip flexion. MRI of the gluteal region shows compression of the QF accompanied by tears, edema, or atrophy of this muscle and a narrowed ischiofemoral space. Compression of the sciatic nerve may result in radicular pain in the lower limb. Total hip arthroplasty, proximal femoral osteotomy, and abduction injury to the hip can cause IFI but there may not be a history of any

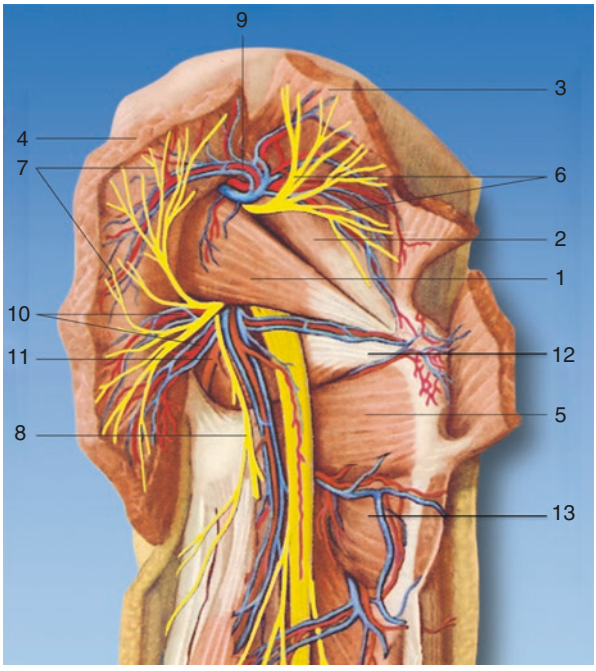

Fig. 8.11 The figure shows the muscles in the deep gluteal space. 1 the piriformis muscle, 2 gluteus minimus, 3 gluteus medius, 4 gluteus maximus, 5 quadratus femoris, 6 superior gluteal nerve, 7 inferior gluteal nerve, 8 posterior cutaneous femoral nerve, 9 superior gluteal artery, 10 inferior gluteal artery and vein, 11 internal pudendal artery, 12 inferior gemellus, 13 adductor magnus. (Reprinted with permission from Dr. Danilo Jankovic)

inciting surgery or trauma. Physical examination often reproduces focal tenderness at a point midway between the ischial tuberosity and the greater trochanter. Internal rotation, adduction, and extension of the hip will increase the pain.

Ultrasound Scan

- Patient position: Prone
- Probe: Curvilinear 2–6 MHz

Place the probe in the lower gluteal region to reveal the ischial tuberosity (IT) and greater trochanter (GT). Optimize the picture and the gluteus maximus (G Max) muscle can be seen overlying the two bony structures. The sciatic nerve (arrows) is identified deep to the gluteus maximus and superficial to the quadratus femoris (QF) (Fig. 8.12).

Procedure

- Needle: 22 or 25 G, 3.5- or 5-inch needle (preferably echogenic)
- Injectate: 1–2 mL of one of the following:
  - Local anesthetic (1% lidocaine or 0.25% bupivacaine)
  - Local anesthetic with methylprednisolone 40 mg
  - Botulinum 50 units

Both out-of-plane and in-plane are reasonable methods, depending on the experience and skill of the practitioner. The most important issue is to plane the needle trajectory so as to avoid the sciatic nerve.

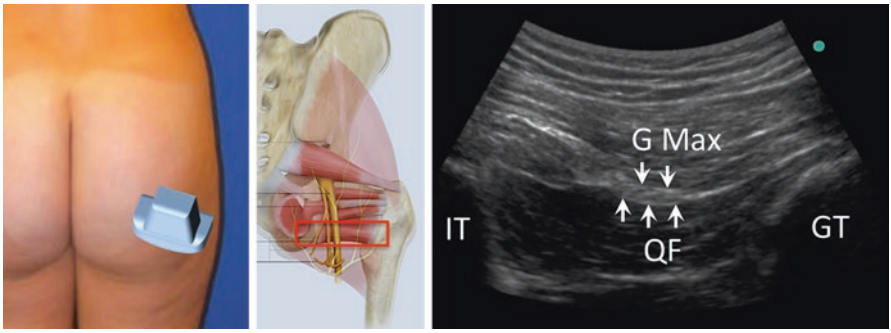

Fig. 8.12 Figure showing the ultrasound probe position and the corresponding sonography. *G Max* gluteus maximus, *QF* quadratus femoris, *IT* ischial tuberosity, *GT* greater trochanter. Sciatic nerve is indicated by arrows. (Reprinted with permission from Philip Peng Educational Series)

Literature Review

Fluoroscopy- and CT-guided injections into the QF muscle have been reported as conferring analgesic benefit in patients with IFI syndrome and/or those who had trigger points in the location of this muscle. US-guided injections of steroids into the QF muscle for patients with IFI syndrome produce better pain relief for 2 weeks following the injection as compared to noninterventional treatment. Proximity of the sciatic nerve and the inferior gluteal artery also suggests that US-guided injections are likely to decrease the probability of damage to the neurovascular structures during injection into the QF.

Suggested Reading

American College of Obstetricians and Gynecologists. Chronic pelvic pain: ACOG practice bulletin no 51. Obstet Gynecol. 2004;103:589–605.

Backer MW, Lee KS, Blankenbaker DG, Kijowski R, Keene JS. Correlation of ultrasound-guided corticosteroid injection of the quadratusfemoris with MRI findings of ischiofemoral impingement. AJR Am J Roentgenol. 2014;203:589–93.

Beason LE, Anson BJ. The relation of the sciatic nerve and its subdivisions to the piriformis muscle. Anat Rec. 1937;70:1–5.

Benzon HT, Katz JA, Enzon HA, Iqbal MS. Piriformis syndrome anatomic considerations, a new injection technique, and a review of the literature. Anesthesiology. 2003;98(6):1442–8.

Chan CW, Peng PWH. Ultrasound guided blocks for pelvic pain. In: Nauroze S, editor. Atlas of ultrasound-guided procedures in interventional pain management. 1st ed. Amherst: Springer; 2011. p. 207–26.

Durrani Z, Winnie AP. Piriformis muscle syndrome: an underdiagnosed cause of sciatica. J Pain Symptom Manag. 1991;6(6):374–9.

Fall M, Baranowski AP, Elniel S, et al. EAU guidelines on chronic pelvic pain. Eur Urol. 2010;57:35–48.

Finnoff JT, Hurdle MF, Smith J. Accuracy of ultrasound-guided versus fluoroscopically guided contrast-controlled piriformis injections: a cadaveric study. J Ultrasound Med. 2008;27:1157–63.

Hallin RP. Sciatic pain and the piriformis muscle. Postgrad Med. 1983;74(2):69–72.

Hopayian K, Danielyan A. Four symptoms define the piriformis syndrome: an updated systematic review of its clinical features. Eur J Orthop SurgTraumatol. 2018;28(2):155–64.

Jankiewicz JJ, Hennrikus WL, Houkom JA. The appearance of the piriformis muscle syndrome in computed tomography and magnetic resonance imaging. A case report and review of the literature. Clin Orthop Relat Res. 1991;262:205–9.

Karl RD Jr, Yedinak MA, Hartshorne MF, et al. Scintigraphic appearance of the piriformis muscle syndrome. Clin Nucl Med. 1985;10:361–3.

Kim DH, Yoon DM, Yoon KB. Ultrasound-guided quadratusfemoris muscle injection in patients with lower buttock pain: novel ultrasound-guided approach and clinical effectiveness. Pain Physician. 2016;19:E863–70.

Macfarlane AJ, Bhatia A, Brull R. Needle to nerve proximity: what do the animal studies tell us? Reg Anesth Pain Med. 2011;36:290–302.

Misirlioglu TO, Akgun K, Palamar D, Erden MG, Erbilir T. Piriformis syndrome: comparison of the effectiveness of local anesthetic and corticosteroid injections: a double-blinded, randomized controlled study. Pain Physician. 2015;18:163–71.

Murata Y, Ogata S, Ikeda Y, Yamagata M. An unusual cause of sciatic pain as a result of the dynamicmotion of the obturatorinternusmuscle. Spine J. 2009;9:e16–8.

Papadopoulos EC, Khan SN. Piriformis syndrome and low back pain: a new classification and review of the literature. Orthop Clin N Am. 2004;35(1):65–71.

Peng PH. Piriformis syndrome. In: Peng PH, editor. Ultrasound for pain medicine intervention: a practical guide. Volume 2. Pelvic pain. Philip Peng educational series. 1st ed. iBook, CA: Apple Inc.; 2013.

Peng PWH, Tumber PS. Ultrasound-guided interventional procedures for patients with chronic pelvic pain – a description of techniques and review of the literature. Pain Physician. 2008;11:215–24.

Shafik A, Doss SH. Pudendal canal: surgical anatomy and clinical implications. Am Surg. 1999;65:176–80.

Smith J, Hurdle MF, Locketz AJ, Wisniewski SJ. Ultrasound-guided piriformis injection: technique description and verification. Arch Phys Med Rehabil. 2006;87:1664–7.

Smith J, Wisniewski SJ, Wempe MK, Landry BW, Sellon JL. Sonographically guided obturatorinternus injections: techniques and validation. J Ultrasound Med. 2012;31:1597–608.

Yue SK. Morphological findings of asymmetrical and dystrophic psoas and piriformis muscles in chronic lower back pain during CT guided botulinum toxin injections (abstract). Reg Anesth Pain Med. 1998;23(3 Suppl):104.

Pudendal and Inferior Cluneal Nerve

9

Geoff A. Bellingham and Philip Peng

Introduction

Pudendal Entrapment Neuropathy

Pudendal neuralgia is defined as chronic perineal pain in the distribution of the pudendal nerve territory. When the clinical features are caused by the entrapment of pudendal nerve, it is referred to as pudendal entrapment neuropathy (PNE).

The pudendal nerve arises from the anterior rami of the second, third, and fourth sacral nerves (S2, S3, and S4). At the level of the ischial spine, the pudendal nerve travels ventrally between the sacrospinous (SP) and sacrotuberous (ST) ligaments (Fig. 9.1). The course between these ligaments is referred to as the interligamentous plane (ILP).

It gives off three terminal branches: the dorsal nerve of the penis or clitoris, inferior rectal nerve, and the perineal nerve (Fig. 9.2). Common sites of compression are at the ILP and within the Alcock's canal.

The pudendal nerve contains both motor and sensory fibers. The inferior rectal nerve supplies the external anal sphincter (Fig. 9.3). The remaining portion of the pudendal nerve trunk becomes the perineal nerve, which continues to supply sensation of the skin of the penis (clitoris), perianal area, and the posterior surface of the scrotum or labia majora. The perineal nerve also provides motor supply to the deep muscles of the urogenital triangle.

G. A. Bellingham
Department of Anesthesia & Perioperative Medicine, St. Joseph's Health Care London, London, ON, Canada

P. Peng (✉)
Department of Anesthesia and Pain Management, Toronto Western Hopsital and Mount Sinai Hospital, University of Toronto, Toronto, Ontario, Canada
e-mail: Philip.peng@uhn.ca

P. Peng et al. (eds.), *Ultrasound for Interventional Pain Management*,
https://doi.org/10.1007/978-3-030-18371-4_9

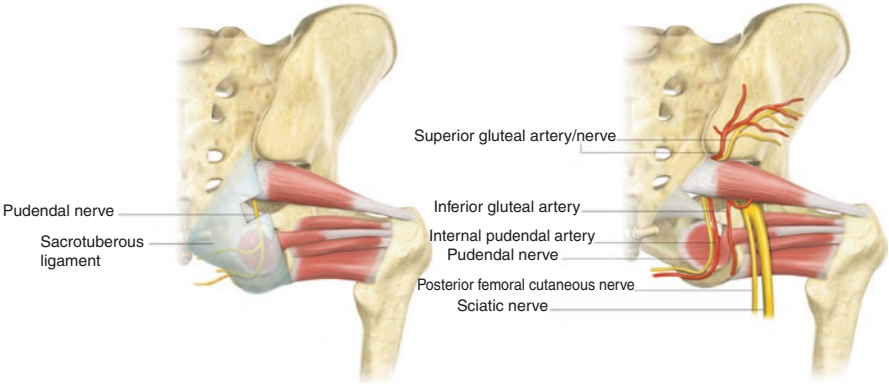

Fig. 9.1 Pudendal nerve between sacrospinous and sacrotuberous ligament. (Reprinted with permission from Philip Peng Educational Series)

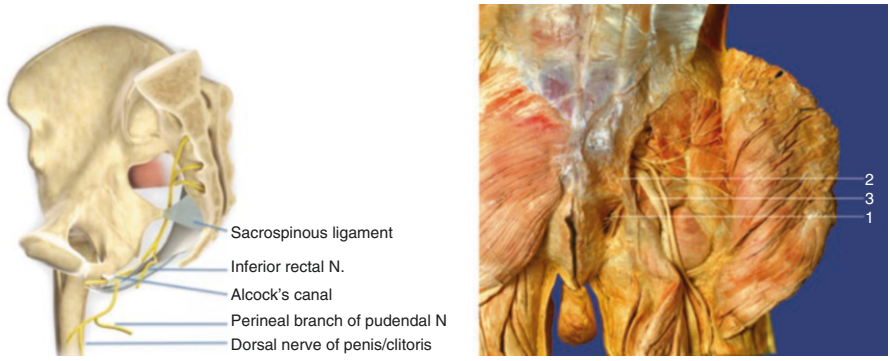

Fig. 9.2 The left diagram showed the course of pudendal nerve around the ischial spine and Alcock's canal and the three terminal branches of the pudendal nerve. (Reprinted with permission from Philip Peng Educational Series) The right diagram showed the pudendal and its close proximity with sciatic nerve. (1) Pudendal nerve and vessel, (2) sacrotuberous ligament, (3) sciatic nerve. (Reprinted with permission from Dr. Danilo Jankovic)

Inferior Cluneal Neuralgia

Patient with pain from inferior cluneal nerve (ICN) entrapment typically presents with pain in the lower buttock associated with perineal pain. On detailed assessment, the perineal pain is mainly in the lateral perineum. The ICN is a branch from posterior femoral cutaneous nerve of the thigh and shares the common trunk with perineal ramus (PR). It should be considered as one of the differential diagnoses of pudendal neuralgia.

The PR branch runs a horizontal course following the inferior edge of the ischial tuberosity to reach the perineum. In its course under the ischium and behind the

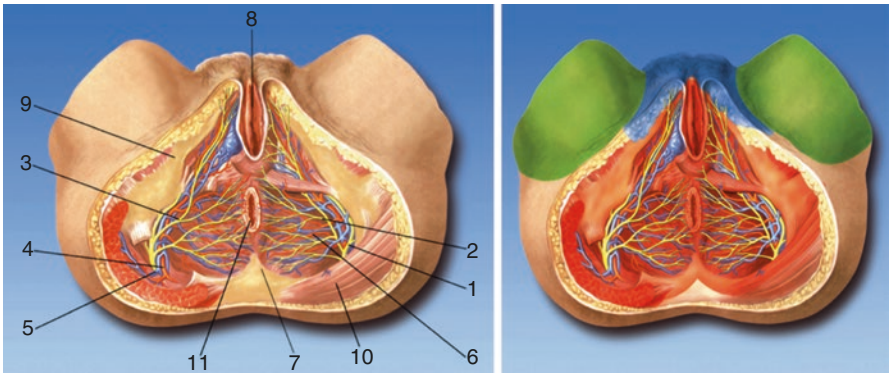

Fig. 9.3 (1) Pudendal nerve, (2) inferior rectal nerves, (3) perineal nerves, (4) internal pudendal artery, (5) internal pudendal veins, (6) inferior rectal artery, (7) ischiorectal fossa, (8) vaginal orifice, (9) ischial tuberosity, (10) gluteus maximus muscle, and (11) the anus. (Reprinted with permission from Dr. Danilo Jankovic)

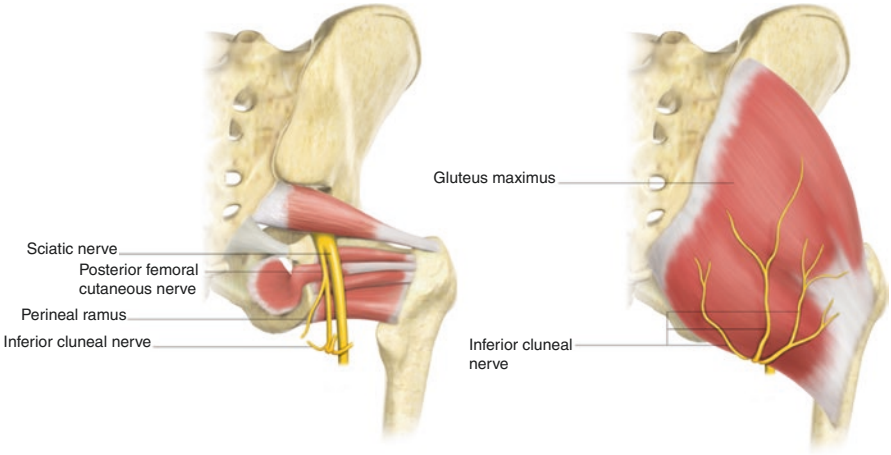

Fig. 9.4 Inferior cluneal nerve and perineal ramus. (Reprinted with permission from Philip Peng Educational Series)

hamstring muscles, the PR moved along in a fatty and fibrous corridor, which is susceptible to entrapment or injury. Also, injury to hamstring origin may cause irritation to this nerve as well. From there, the PR divides into branches to the lateral part of the anal margin and the labia majora or scrotum (left sonogram). The ICN follows the deep surface of the gluteus maximus muscle, and at the lower border of the same muscle, it perforates the gluteus maximus fascia and spreads out inside it and reaches the skin of the lower gluteal region to supply the lower buttock region (Fig. 9.4).

Patient Selection

Pudendal Entrapment Neuropathy

The diagnosis of PNE remains primarily clinical. There are no pathognomonic imaging and laboratory or electrophysiology investigations available for confirmation. Clinical criteria (Nantes criteria) have been established but are not accepted universally. The Nantes criteria are composed of four domains: essential criteria for the diagnosis of pudendal neuralgia, complementary diagnostic criteria, exclusion criteria, and associated signs not excluding the diagnosis. From the essential criteria, diagnostic nerve block plays an important role in the diagnosis.

Essential criteria
Pain in the territory of the pudendal nerve: from the anus to the penis or clitoris.
Pain is predominantly experienced while sitting.
The pain does not wake the patient at night.
Pain with no objective sensory impairment.
Pain relieved by diagnostic pudendal nerve block.

Inferior Cluneal Neuralgia

Patient with ICN entrapment is diagnosed on clinical ground with the use of diagnostic nerve block. The typical presentation is burning pain aggravated by sitting in the lower and medial aspect of buttock, the posterior and proximal aspect of the thigh, the lateral part of anal margin, and the skin of the labia majora/the scrotum. Detailed assessment may reveal sensory changes in the lower buttock and the pain restricted to the lateral part of perineum, at least in the initial presentation. Pressure on the ischial tuberosity provokes pain in similar region. Some patient may have pathology in hamstring origin as the PR courses the hamstring before innervating the perineum.

This is differentiated from pudendal neuralgia in that these pains are caused by the sitting position on a *hard* seat and provoked by the compression of the nerves against the ischial tuberosity and the hamstring muscle insertions. Pain in pudendal neuralgia is in the perineum (anus, penis, clitoris), aggravated by the sitting position on a *soft* seat or a bicycle seat and provoked by the compression of the soft parts of the perineum or against the Alcock's canal and ishcial spine.

Ultrasound Scan (Pudendal Nerve)

- Position: Prone
- Probe: Curvilinear 2–6 MHz

Scan 1: Over the iliac crest

The key landmark is the posterior superior iliac spine (PSIS). The structures will be iliac crest with three layers of gluteus muscles in view (Fig. 9.5).

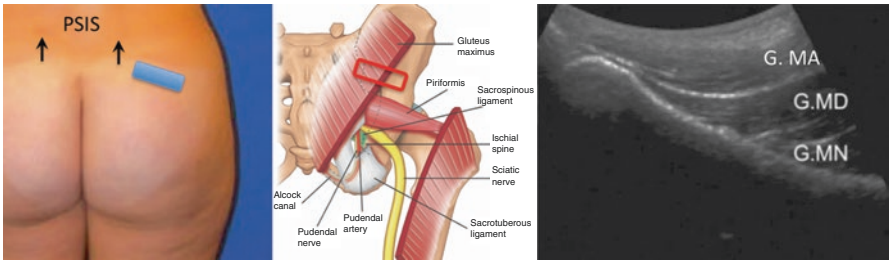

Fig. 9.5 Position of the ultrasound probe over the iliac crest and the pertinent anatomy and sonoanatomy. PSIS, posterior superior iliac spine; arrow, dimple of Venus approximating the position of PSIS; G. MA, gluteus maximus; G. MD, gluteus medius; G. MN, gluteus minimus. (Reprinted with permission from Philip Peng Educational Series)

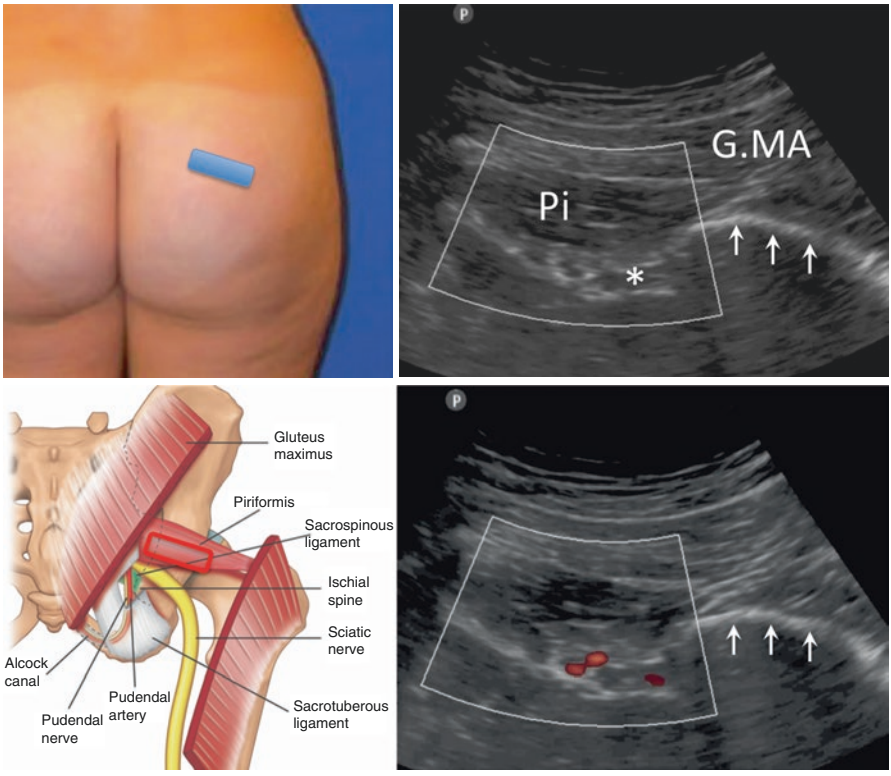

Fig. 9.6 Position of the ultrasound probe over the greater sciatic notch and the pertinent anatomy and sonoanatomy. G MA, gluteus maximus; Pi, piriformis; ∗, the sciatic nerve; branch of inferior gluteal artery, red in color Doppler; the ischium is indicated by arrows. (Reprinted with permission from Philip Peng Educational Series)

Scan 2: At the sciatic notch

The ischium appears as curved structure (arrows) as it forms the posterior wall of the acetabulum. Two layers of muscles are seen in this scan-gluteus maximus

covering the piriformis (Fig. 9.6). Deep to the piriformis, the sciatic nerve is seen and is always accompanied by the branch of inferior gluteal artery (red in color Doppler).

Scan 3: At the ischial spine

Moving the probe from the above scan position in the caudal direction, four changes will be observed (Fig. 9.7):

1. The ischium (IS) becomes longer and straighter.
2. Piriformis will disappear.
3. Medial to the ischium, a hyperechoic structure, sacrospinous ligament (SSL), appears.
4. Appearance of pudendal artery (PA).

Difference between the hyperechoic ischium and SSL is that the former casts an anechoic shadow (∗).

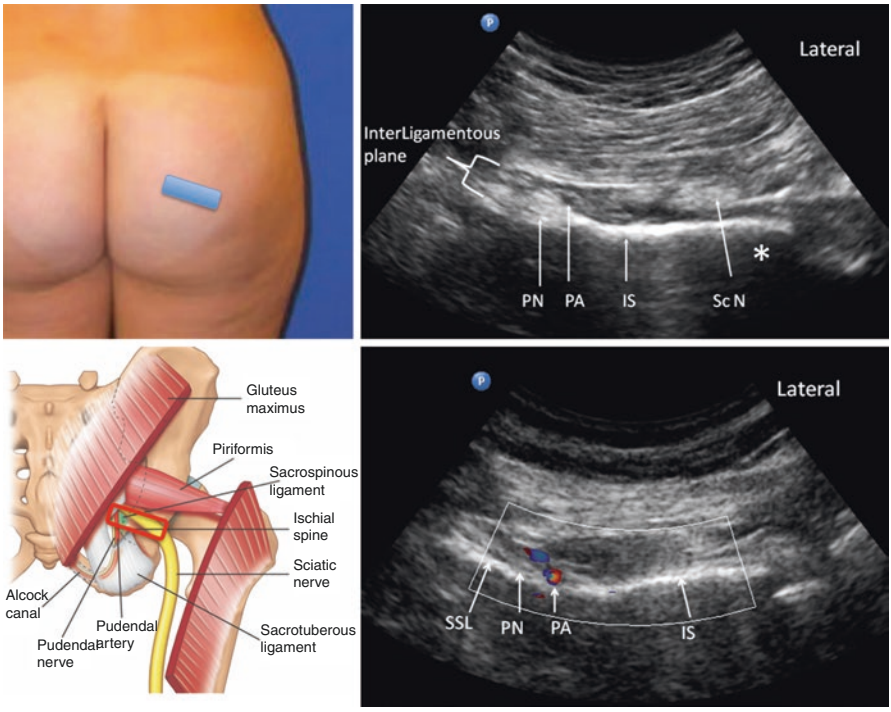

Fig. 9.7 Position of the ultrasound probe at the ischial spine (IS) and the pertinent anatomy and sonoanatomy. SCN, sciatic nerve; PA and PN, pudendal artery and pudendal nerve; SSL, sacrospinous ligament; ∗, anechoic shadow cast by the ischium. (Reprinted with permission from Philip Peng Educational Series)

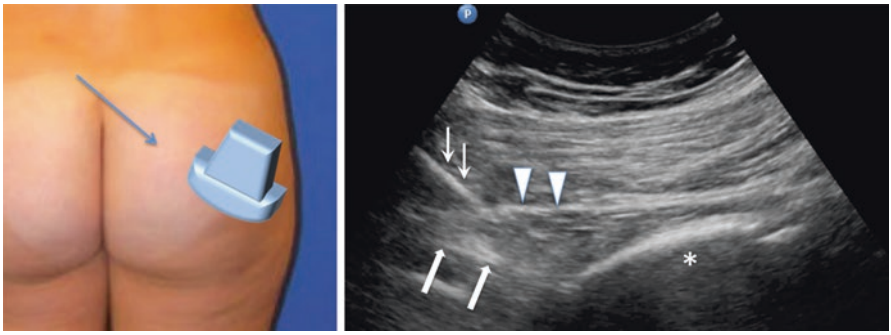

Fig. 9.8 Needle insertion into the interligamentous plane. Line arrow, needle; bold arrow, sacrospinous ligament; arrow heads, sacrotuberous ligament; ∗, ischium. (Reprinted with permission from Philip Peng Educational Series)

The pudendal nerve (PN) is mostly on the medial side of PA inside the interligamentous plane formed by SSL and sacrotuberous ligament (deep to the gluteus maximus). Sciatic nerve (ScN) is on the lateral aspect of the tip of ischial spine.

Procedure (Pudendal Nerve)

Equipment and Drugs

- Needles: 22G 3.5 inch needle
- Drugs: 4 mL of local anesthetic (0.25% plain bupivacaine)
  1 mL steroid (depomedrol)

In-plane approach is recommended from medial to lateral with the insertion point 2 cm away from the ultrasound probe (Fig. 9.8). Once the tip of the needle (arrows) passes the sacrotuberous ligament (arrowheads), hydrolocation of normal saline is important to ensure the spread of the injectate between the sacrospinous ligament (bold arrows) and sacrotuberous ligament.

Ultrasound Scan (Inferior Cluneal Nerve)

- Position: Probe
- Probe: Curvilinear 2–5 MHz

Scan 1

Upper sonogram of Fig. 9.9. Place the probe in the gluteal region to visualize both greater trochanter (GT) and ischial tuberosity (IT). The sciatic nerve (arrows) is seen between the gluteus maximus (G Max) and quadratus femoris (QF).

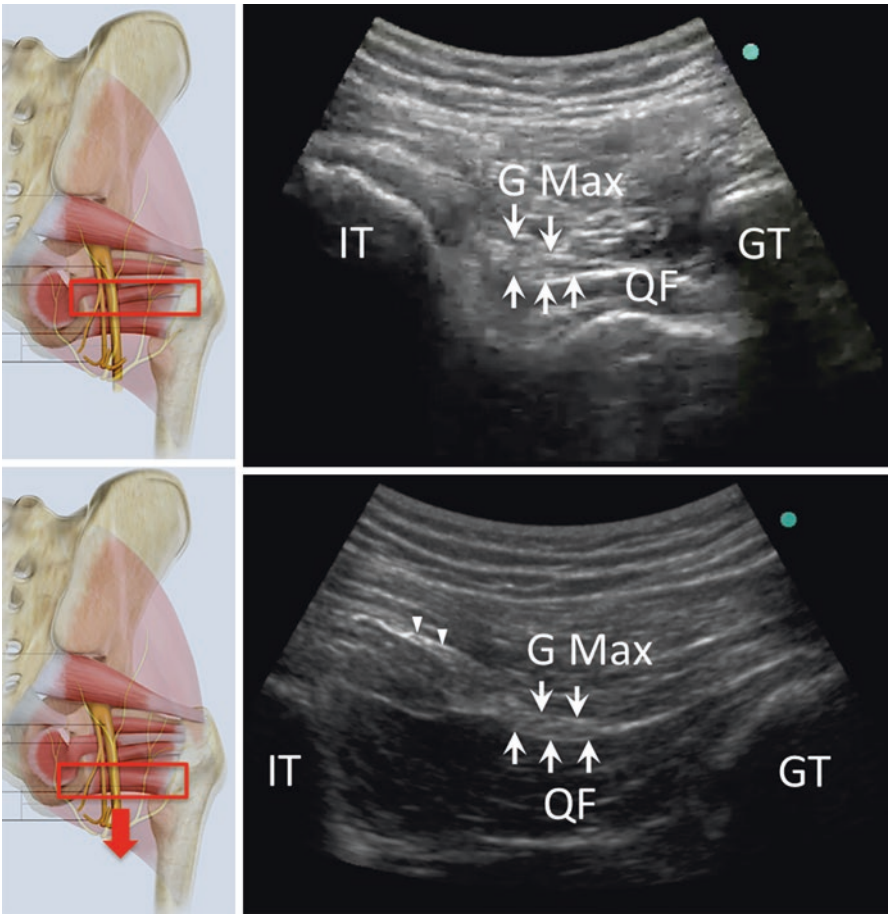

Fig. 9.9 Position of ultrasound probe and the corresponding sonography for the inferior cluneal nerve. Arrow, sciatic nerve; arrow heads, inferior cluneal nerve; G Max, gluteus maximus; QF, quadratus femoris. (Reprinted with permission from Philip Peng Educational Series)

Scan 2

Lower sonogram of Fig. 9.9. Pay attention to the details of the sciatic nerve and scan in the caudal direction. A few small nerves (arrowheads) move away from the sciatic nerve and move medially. They are the inferior cluneal nerve (ICN). Moving further in caudal direction, the ICN will course deep to the undersurface of the G Max and emerge at the lower border to the subcutaneous plane. However, at this level, the PR moves further medial and crosses the hamstring origin to the perineum. These are fine branches, especially the PR, and are not easy to visualize with curvilinear probe. Therefore, this is the plane which is ready for injection.

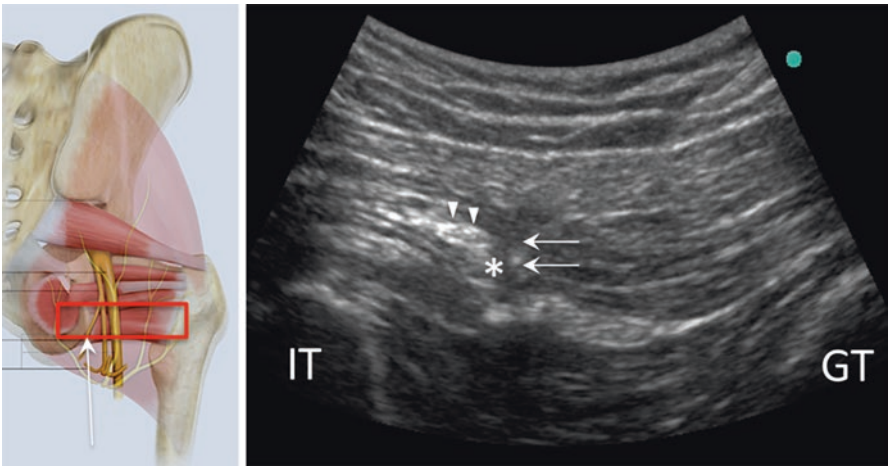

Fig. 9.10 Injection around the inferior cluneal nerve (arrow heads). GT, greater trochanter; IT, ischial tuberosity. ∗, injectate. (Reprinted with permission from Philip Peng Educational Series)

Procedure (Inferior Cluneal Nerve)

- Needle: 22G 3.5 inch spinal needle (longer for large patient)
- Drugs: Depo-Medrol 40 mg with 3 mL of normal saline or very diluted local anesthetic (0.5% lidocaine)

The inferior cluneal nerve is a deep structure (arrowheads), and a long needle (3.5 inch) is required. Both out-of-plane and in-plane techniques can be used. The sonogram showed the needle insertion with out-of-plane technique (Fig. 9.10). Local anesthetic is not desirable as the target is so close to the sciatic nerve. The authors prefer only normal saline and steroid.

Clinical Pearls

1. When scanning at the level of sciatic notch, make sure that the ultrasound probe is along the axis of piriformis muscle and the probe is tilted "medially" as the greater sciatic notch is tilted "laterally".
2. Keeping the needle insertion point 2 cm away is important as the needle will form a steep angle with the probe.
3. Avoid using epinephrine-containing local anesthetic to avoid jeopardizing the circulation of the compressed pudendal nerve.
4. Perfect alignment of the needle with the probe at the ischial spine level is key to success for the pudendal nerve block.

5. When the artery is seen "lateral" to the tip of ischial spine, it is likely that the artery is inferior gluteal artery which accompanies the sciatic nerve.
6. During the injection, make sure to avoid the lateral spread of injectate to the vicinity of the sciatic nerve.
7. A reason for an unsuccessful block may include anatomical variation of the nerve. The nerve can divide into its terminal branches early in its course and these branches may lie medial and lateral to the pudendal artery at the level of the ischial spine.
8. The PR may not be visualized in every patient. In that case, the target is simply medial to the sciatic nerve in the plane between the gluteus maximus and quadratus femoris.

Literature Review

Pudendal nerve block serves both diagnostic and therapeutic purposes. It targets at two sites of possible nerve compression: the ILP and Alcock's canal. At these sites, the compartments are defined by fascial plane. CT scan allows the visualization of both compartments but is not readily accessible to pain physician and subjects the patient to a high dose of radiation. A fluoroscopic technique has been described which uses the ischial spine as a surrogate marker for the ILP. Recently, the sonoanatomy of the pudendal nerve at the ILP was defined, and a feasibility study of an ultrasound-guided injection was established. A comparison study showed the ultrasound-guided injection is as effective as a fluoroscopy-guided injection. However, use of ultrasound allows visualization of the sciatic nerve and pudendal artery and potentially minimizes the risk of injury to these structures.

The literature on inferior cluneal nerve and its implication in pelvic pain is scant. Robert and Labat group are the first one to detail the anatomy and the possible implication of the ICN and PR in perineal pain. More clinical work needs to be done to characterize the clinical entity.

Suggested Reading

Bellingham GA, Bhatia A, Chan CW, Peng PW. Randomized controlled trial comparing pudendal nerve block under ultrasound and fluoroscopic guidance. Reg Anesth Pain Med. 2002;37:262–6.

Chan CW, Peng PWH. Ultrasound guided blocks for pelvic pain. In: Nauroze S, editor. Atlas of ultrasound-guided procedures in interventional pain management. 1st ed. Amherst: Springer; 2011. p. 207–26.

Darnis B, Robert R, Labat JJ, Riant T, Gaudin C, Hamel A, Hamel O. Perineal pain and inferior cluneal nerves: anatomy and surgery. Surg Radiol Anat. 2008;30:177–83.

Hough DM, Wittenberg KH, Pawlina W, et al. Chronic perineal pain caused by pudendal nerve entrapment: anatomy and CT-guided perineural injection technique. AJR Am J Roentgenol. 2003;181:561–7.

Labat JJ, Riant T, Robert R, Amarenco G, Lefaucheur JP, Rigaud J. Diagnostic criteria for pudendal neuralgia by pudendal nerve entrapment (Nantes criteria). Neurourol Urodyn. 2008;27:306–10.

Peng P, Narouze S. Ultrasound-guided interventional procedures in pain medicine: a review of anatomy, sonoanaotmy and procedures. Part I: non-axial structures. Reg Anesth Pain Med. 2009;34:458–74.

Peng PWH, Tumber PS. Ultrasound-guided interventional procedures for patients with chronic pelvic pain – a description of techniques and review of the literature. Pain Physician. 2008;11:215–24.

Peng PWH, Antolak SJ, Gordon AS. Pudendal neuralgia. In: Goldstein I, Pukall C, Goldstein A, editors. Female sexual pain disorders: evaluation and management. 1st ed. Oxford: Wiley-Blackwell; 2009. p. 112–8.

Robert R, Prat-Pradal D, Labat JJ, et al. Anatomic basis of chronic perineal pain: role of the pudendal nerve. Surg Radiol Anat. 1998;20:93–8.

Rofaeel A, Peng PWH, Chan VWS. Feasibility of real-time ultrasound for pudendal nerve block inpatients with chronic perineal pain. Reg Anesth Pain Med. 2008;33:139–45.

Sedy J, Nanka O, Belisova M, Walro JM, et al. Sulcus nervi dorsalis penis/clitoridis: anatomic structure and clinical significance. Eur Urol. 2006;50:1079–85.

Lateral Femoral Cutaneous Nerve

10

Ashutosh Joshi and Philip Peng

Introduction

Meralgia paresthetica (MP), derived from the Greek words "meros" and "algos" meaning thigh and pain, is a mononeuropathy of the lateral femoral cutaneous nerve (LFCN) that can lead to significant disability. The incidence in the primary care setting was estimated at 4.3 per 10,000 person-years.

The lateral femoral cutaneous nerve (LFCN) is a purely sensory nerve from L2 and L3 nerve roots. Emerging from the lateral border of the psoas major muscle, LFCN runs across the iliacus muscle toward the anterior superior iliac spine (ASIS) and passes deep into the inguinal ligament (Fig. 10.1). Before it reaches the level of ASIS, it crosses under the deep circumflex artery.

The LFCN usually emerges from under the inguinal ligament (IL) medial to ASIS at a variable distance (average 29 mm; range 0–73 mm) (Fig. 10.2). A few anatomical variations that one should bear in mind in scanning the LFCN: it may course over or through the IL rather than under it, it may branch before crossing the IL in up to 28% of cases, and it may pass over or posterior the ASIS in 4–29%. The average diameter of LFCN was found to be 3.2 ± 0.7 mm although there is no established normal value for cross-sectional area. Once the LFCN passes under the IL, it usually enters the thigh superficial to the sartorius muscle confined by the fascia lata, although in 22% of cases the LFCN may pass through the sartorius muscle or at times medial to it. Thereafter the LFCN is visualized consistently in a "fatty groove" between the tensor fascia lata muscle and the sartorius muscle. It will

A. Joshi
Department of Anaesthesia, Khoo Teck Puat Hospital, Singapore, Singapore

P. Peng (✉)
Department of Anesthesia and Pain Management, Toronto Western Hopsital and Mount Sinai Hospital, University of Toronto, Toronto, Ontario, Canada
e-mail: Philip.peng@uhn.ca

P. Peng et al. (eds.), *Ultrasound for Interventional Pain Management*,
https://doi.org/10.1007/978-3-030-18371-4_10

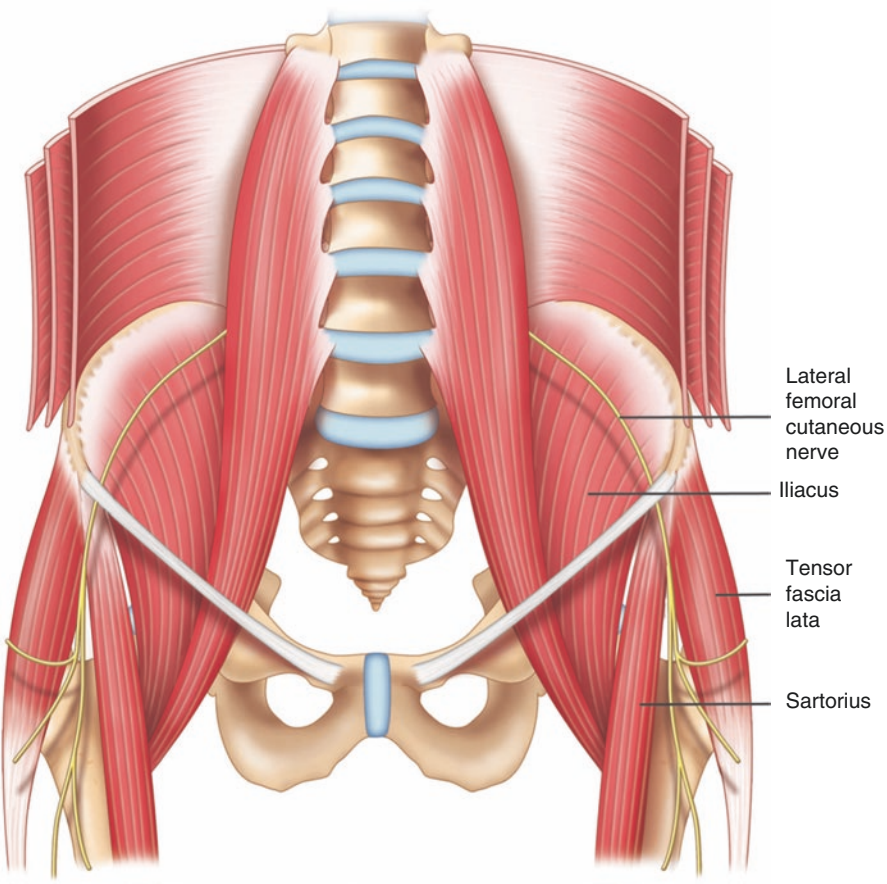

Fig. 10.1 Schematic diagram showing the pathway of a typical course of lateral femoral cutaneous nerve. (Reprinted with permission from Philip Peng Educational Series)

normally divide into an anterior and a posterior branch and will pierce the fascia lata in order to innervate the skin. The skin innervated by the LCFN has been characterized in details, covering the lateral aspect of the thigh approximately 8 cm below the greater trochanter and above the tibiofemoral joint line (Fig. 10.3).

Patient Selection

The diagnosis of MP is mainly on clinical ground. The most common presentation is a burning and tingling sensation on the anterior and lateral aspects of the thigh as far as the knee. Numbness is a late sign and is rarely the only presentation,

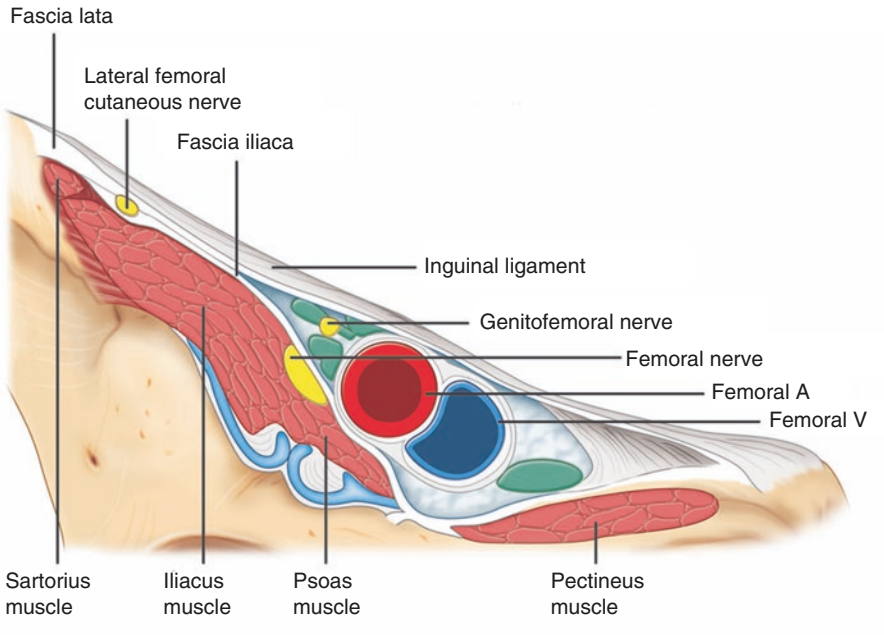

Fig. 10.2 Nerves at the inguinal area. (Reprinted with permission from Philip Peng Educational Series)

the presence of which theoretically disqualifies the use of the term of meralgia. Bilateral presentation is uncommon (20%). Pain or unpleasant tingling sensation can be aggravated by standing and hip extension and relieved by sitting.

Physical examination may reveal tenderness over the lateral aspect of the inguinal ligament with Tinel sign elicited at the site of entrapment. Hypoesthesia over the area innervated by the LFCN is commonly found with or without allodynia. Clues suggestive of the etiology may be revealed during the examination, such as the surgical scars, raised intra-abdominal pressure or low rise jean (hip-hugger). Because the LFCN is a sensory nerve, the presence of dermatomal sensory loss and motor and sphincter dysfunctions should alert the clinicians to the spinal etiology. In that case, spine imaging (magnetic resonance imaging) should be arranged. The presence of red flags such as weight loss and appetite change and acute onset of severe pain on pressure may suggest metastasis at the iliac crest or avulsion fracture of ASIS respectively.

In the situation of uncertainty, both electrophysiological test and diagnostic nerve block can be useful. Limitation of nerve conduction test is that it evaluates mainly large myelinated axons and the test can be normal in patients whose condition principally affects the small myelinated A δ and C fibers.

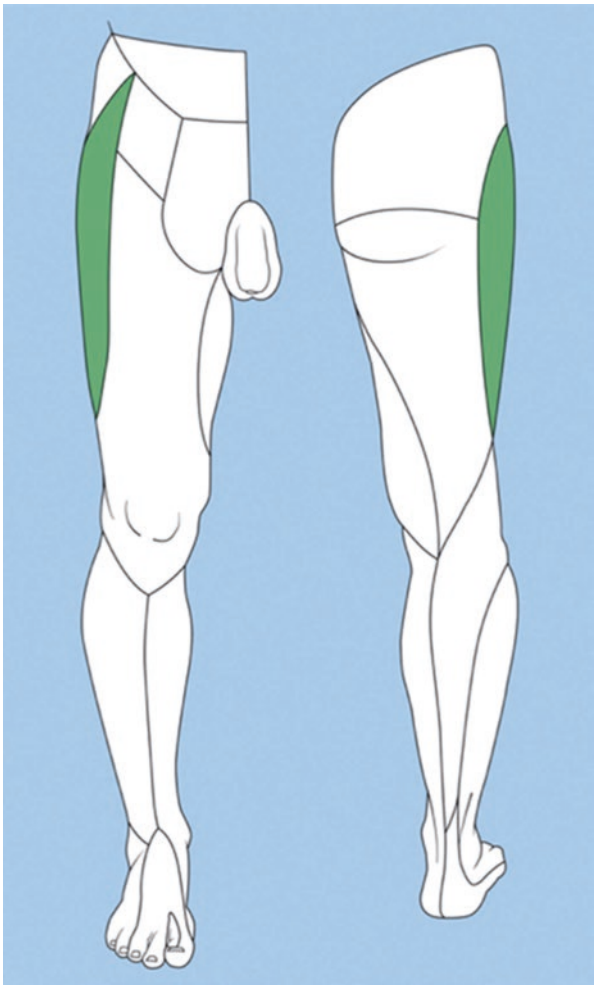

Fig. 10.3 The skin area supplied by LFCN. (Reprinted with permission from Dr. Danilo Jankovic)

Ultrasound Scanning

- Position: Supine.
- Probe: High-frequency linear 6–18 MHz use the highest for slim individual.

Scan 1

One of the starting points is the fat-filled groove between the sartorius (SAR) and tensor fascia lata (TFL) (Fig. 10.4). At this site, the LFCN is consistently

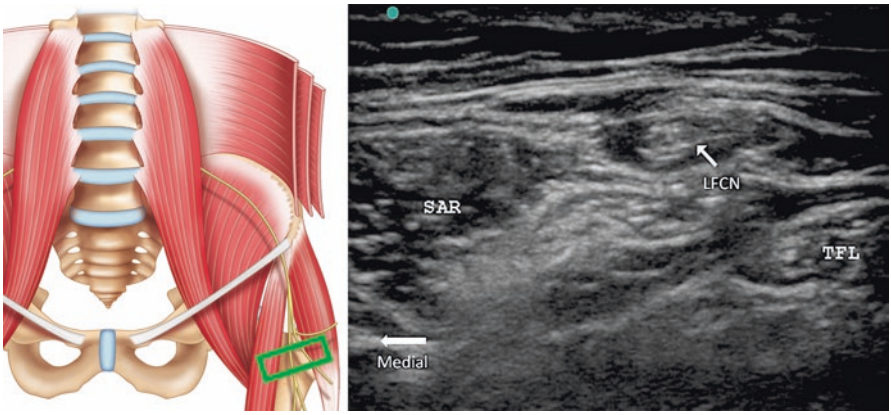

Fig. 10.4 Scanning at the fat-filled grove between sartorius and tensor fascia lata. (Reprinted with permission from Philip Peng Educational Series)

found approximately10cm distal to ASIS. Because the adipose tissue is typically hypoechoic, the nerve with the connective tissue can be easily seen in this region.

Scan 2

There are two drawbacks of the technique described above. First, injection even with 5 mL at this location will miss the proximal branches. While this can be remedied by injecting higher volume or advancing the needle proximally during injection to enhance proximal spread, the injection site is supposedly at or close to the site of pathology, i.e., inguinal ligament, in chronic pain setting. Second, pulsed radiofrequency lesion is commonly used to prolong the analgesic duration and this requires the precise location of the nerve at or close to the site of pathology.

Hence, the authors suggest to trace the nerve as proximal as possible. In patient with meralgia paresthetica, it is feasible as the LFCN is usually enlarged distal to the site of compression. The sonogram showed the tracing of the nerve (Fig. 10.5). The LFCN was found at the fat-filled grove (left upper sonogram). It was traced and the LFCN became to approach the surface of the sartorius muscle (right upper and lower two sonograms).

Please note a couple of variations (Fig. 10.6). The LFCN can branch into 2–5 branches over the sartorius (left sonogram). It may also pass through sartorius muscle between the fascia lata and the fascia overlying the sartorius (right sonogram).

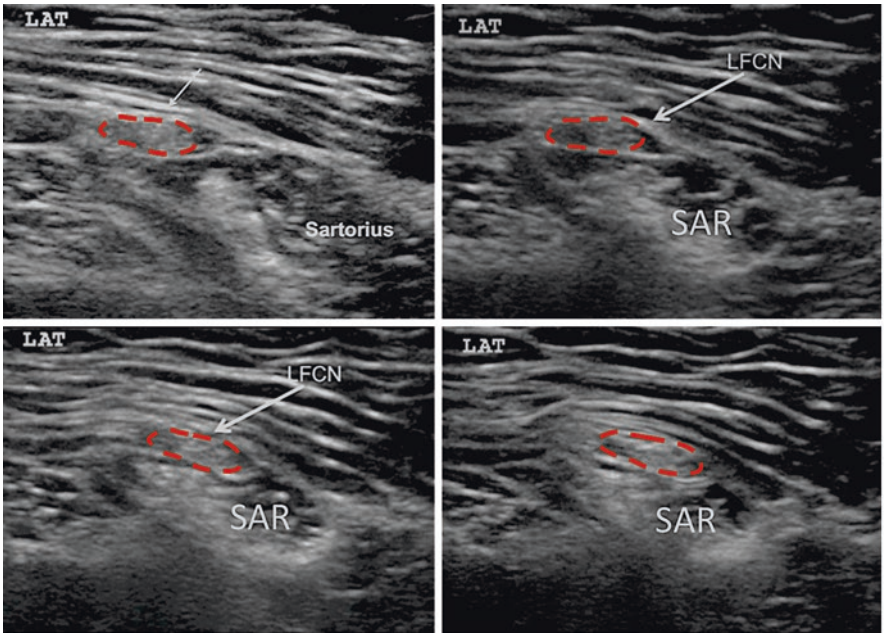

Fig. 10.5 Tracing the lateral femoral cutaneous nerve (LCFN) proximally. The LFCN can be seen moving medially toward the sartorius muscle. (Reprinted with permission from Philip Peng Educational Series)

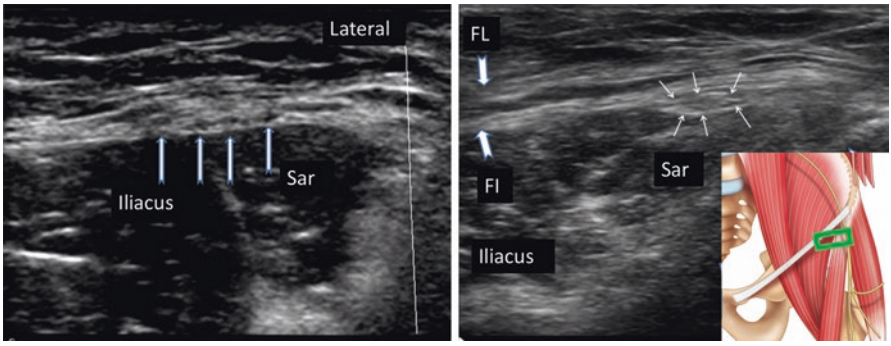

Fig. 10.6 Variation of appearance of LFCN. Sar sartorius, FL fascia lata, Fi fascia iliaca or fascia over the sartorius. (Reprinted with permission from Philip Peng Educational Series)

Procedure

- Needle: 25G 1.5-inch needle (except very obese patient with 22G 3.5-inch needle)
- Bupivacaine 0.25% 3 mL with 40 mg Depomedrol

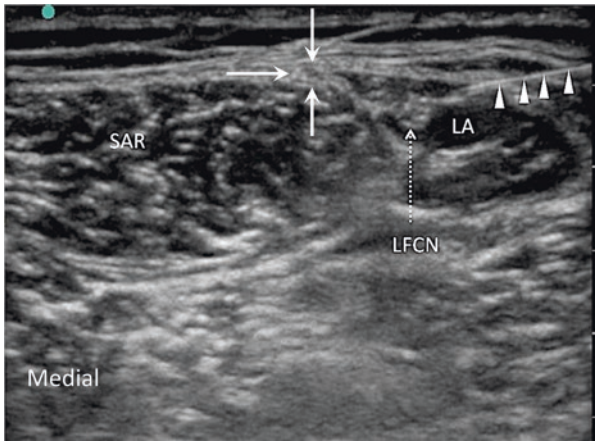

Fig. 10.7 Injection of LCFN. The needle is outlined with arrowheads and local anesthetic (LA) is injected. (Reprinted with permission from Philip Peng Educational Series)

Using a linear array transducer with the highest frequency (6–18 MHz), the LCFN is traced as proximal as possible (Fig. 10.7). Both in-plane and out-of-plane technique can be used. Even with large body habitus, a 1.5-inch needle should reach the target with out-of-plane technique. The sonogram showed an enlarged LFCN over the lateral edge of the sartorius (SAR). The needle is outlined with arrowheads and local anesthetic (LA) is injected. Interestingly, another branch of LFCN (arrows) is seen between the sartorius muscle and the overlying fascia. This is better seen after the injection of local anesthetic.

Clinical Pearls

1. A sound knowledge of anatomy of the course and direction of the LFCN as well as the structures around LFCN help to appreciate location of the nerve (sartorius muscle, tensor fascia lata muscle, and fascia lata).
2. The nerve is better appreciated with dynamic scanning or sweeping view because of the size of the nerve and its proximity with fascia layer.
3. The LFCN nerve may appear as hyperechoic, hypoechoic, or mixed structure, depending on the course of the nerve itself (under or through the inguinal ligament or over the iliac crest), the special tissue architecture in the corresponding area (surrounded by fatty tissue in the plane between sartorius and tensor fascia lata muscle), and the frequency of the transducer used (higher-frequency probe likely produces artifacts).
4. The LFCN in a patient with severe or advanced symptoms of MP is likely to be swollen or enlarged (pseudoneuroma) and is likely to be picked up by ultrasonography.
5. The common locations that the LFCN can be found are usually in the infrainguinal region, either superficial to the sartorius muscle or between sartorius and tensor of fascia lata muscles. In the latter case, it is a fat-filled space.

Literature Review

The technique of application of ultrasound to the LFCN blockade has been well published. Validation study demonstrated greater accuracy in identifying the LFCN with ultrasound in both cadavers and volunteers. With the method of identifying the LFCN in the fat-filled grove, the identification is 100% in cadavers, as opposed to 5% with landmark-based technique. Tagliafico et al. described a series of 20 patients who underwent US-guided injections of local anesthetic and steroid for treatment of meralgia paresthetica. The authors reported a significant reduction in visual analog scale pain scores in all patients at 2 months after the procedure. However, relatively large volumes (9 mL) of injectate were used, and 4 of the 20 patients had required a repeat US-guided LFCN block procedure at 1 week.

Suggested Reading

Aszmann OC, Dellon ES, Dellon AL. Anatomical course of the lateral femoral cutaneous nerve and its susceptibility to compression and injury. Plast Reconstr Surg. 1997;100(3):600–4.

Bodner G, Bernathova M, Galiano K, Putz D, Martinoli C, Felfernig M. Ultrasound of the lateral femoral cutaneous nerve: normal findings in a cadaver and in volunteers. Reg Anesth Pain Med. 2009;34(3):265–8.

Dias Filho LC, Valença MM, Guimarães Filho FA, et al. Lateral femoral cutaneous neuralgia: an anatomical insight. Clin Anat. 2003;16(4):309–16.

Harney D, Patijn J. Meralgia paresthetica: diagnosis and management strategies. Pain Med. 2007;8(8):669–77.

Hui GK, Peng PW. Meralgia paresthetica: what an anesthesiologist needs to know. Reg Anesth Pain Med. 2011;36(2):156–61.

Kosiyatrakul A, Nuansalee N, Luenam S, Koonchornboon T, Prachaporn S. The anatomical variation of the lateral femoral cutaneous nerve in relation to the anterior superior iliac spine and the iliac crest. Musculoskelet Surg. 2010;94:17–20.

Mallik A, Weir AL. Nerve conduction studies: essential and pitfalls in practice. J Neurol Neurosurg Psychiatry. 2005;76(Suppl):2. ii23-31.

Moritz T, Prosch H, Berzaczy D, et al. Common anatomical variation in patients with idiopathic meralgia paresthetica: a high resolution ultrasound case-control study. Pain Physician. 2013;16(3):E287–93.

Murata Y, Takahashi K, Yamagata M, Shimada Y, Moriya H. The anatomy of the lateral femoral cutaneous nerve, with special reference to the harvesting of iliac bone graft. J Bone Joint Surg Am. 2000;82(5):746–7.

Neilsen T, Morigl B, Barckman J, et al. The lateral femoral cutaneous nerve. Description of the sensory territory and a novel ultrasound-guided nerve block technique. Reg Anesth Pain Med. 2018;43:357–66.

Ng I, Vaghadia H, Choi PT, Helmy N. Ultrasound imaging accurately identifies the lateral femoral cutaneous nerve. Anesth Analg. 2008;107(3):1070–4.

Nouraei SAR, Anand B, Spink G, O'Neill KS. A novel approach to the diagnosis and management of meralgia paresthetica. Neurosurgery. 2007;60(4):696–700.

Seror P, Seror R. Meralgia paresthetica: clinical and electophysiological diagnosis in 120 cases. Muscle Nerve. 2006;33(5):650–4.

Tagliafico A, Serafini G, Lacelli F, Perrone N, Valsania V, Martinoli C. Ultrasound-guided treatment of meralgia paresthetica (lateral femoral cutaneous neuropathy): technical description and results of treatment in 20 consecutive patients. J Ultrasound Med. 2011;30:1341–6.

Trummer M, Flaschka G, Unger F, Eustacchio S. Lumbar disc herniation mimicking meralgia paresthetica: case report. Surg Neurol. 2000;54(1):80–1.
Van Slobbe AM, Bohnen AM, Bernsen RM, Koes BW, Bierma-Zeinstra SM. Incidence rates and determinants in meralgia paresthetica in general practice. J Neurol. 2004;251(3):294–7.
Zhu J, Zhao Y, Liu F, Huang Y, Shao J, Hu B. Ultrasound of the lateral femoral cutaneous nerve in asymptomatic adults. BMC Musculoskelet Disord. 2012;13:227.

Erector Spinae Plane Block (ESP Block)

11

Mauricio Forero, Vicente Roqués,
and Nestor Jose Trujillo-Uribe

Introduction

Erector spinae plane (ESP) block is an interfacial plane block which was first described in 2016 by Forero et al. This novel technique was initially applied in the management of thoracic neuropathic pain secondary to various conditions such as postoperative pain following thoracic surgery, metastasis, and mal-union of rib. Following this initial brief technical report, a plethora of interest in this block followed with around 100 reports published in the subsequent 19 months, most of which demonstrated efficacy for acute and chronic pain syndromes in the thoracoabdominal region. However, it has also been reported for analgesia of the brachial and the lumbar plexus.

Its multiple indications are linked to its spread to paravertebral region, taking advantage of the distribution of the erector spinae muscle from the neck to the lumbar region. Another potential advantage of ESP block is that the needle can be inserted away from the target, relying on the spread of injectate to reach the desired spinal level. This is particularly useful when the site of insertion is not readily accessible, e.g. covered by dressing or too sensitive for insertion.

M. Forero (✉)
Department of Anesthesia, McMaster University, Hamilton, ON, Canada

V. Roqués
Department of Anesthesia, Intensive Care and Pain Treatment, University Hospital Virgen de la Arrixaca, Murcia, Spain

N. J. Trujillo-Uribe
Universidad Autónoma de Bucaramanga, Bucaramanga, Colombia

Department of Anesthesia and Pain Medicine, Fundación Oftalmológica de Santander, Clínica Carlos Ardila Lule, Clínica del Dolor y Cuidado Paliativo ALIVIAR LTDA, Floridablanca, Colombia
e-mail: ntrujillo@unab.edu.co

P. Peng et al. (eds.), *Ultrasound for Interventional Pain Management*,
https://doi.org/10.1007/978-3-030-18371-4_11

The target of the ESP block is between the most anterior and deepest layer of the erector spinae muscle and the tip of the transverse process (Fig. 11.1). The erector spinae muscle is surrounded by fasciae that contain multiple layers (Fig. 11.2). The architecture of the erector spinae muscle is complex, with three muscle layers distributing in the lumbar, thoracic, and cervical area (brief explanation below).

The aim of the ESP block is to penetrate the most anterior layer of the erector spinae muscle and deposit the injectate between this layer and the tip of the transverse process. The plane allows cranial-caudal spread in multiple spinal segments (Fig. 11.3). The injectable is placed in close relation to the inter-transverse connective soft tissue, which allows the infiltration of the local anesthetic to the paravertebral space, through its porous surfaces or through the foramen where the dorsal ramus of the spinal nerve leaves the intervertebral foramen to innervate back structures.

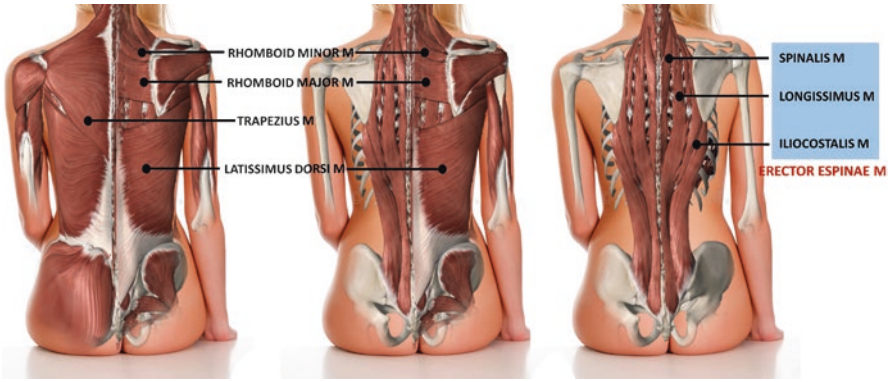

Fig. 11.1 Paraspinal muscles. (Reprinted with permission from Dr. Vicente Roques from imedar.com)

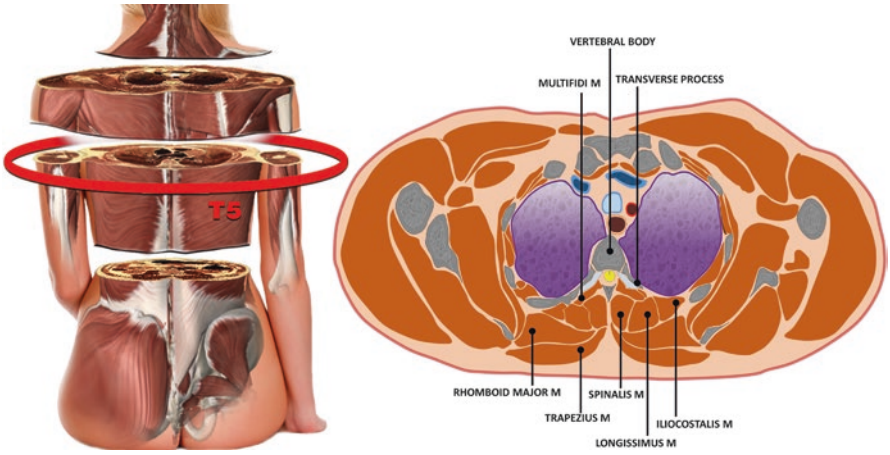

Fig. 11.2 Cross section of the paraspinal muscle at T5. (Reprinted with permission from Dr. Vicente Roques from imedar.com)

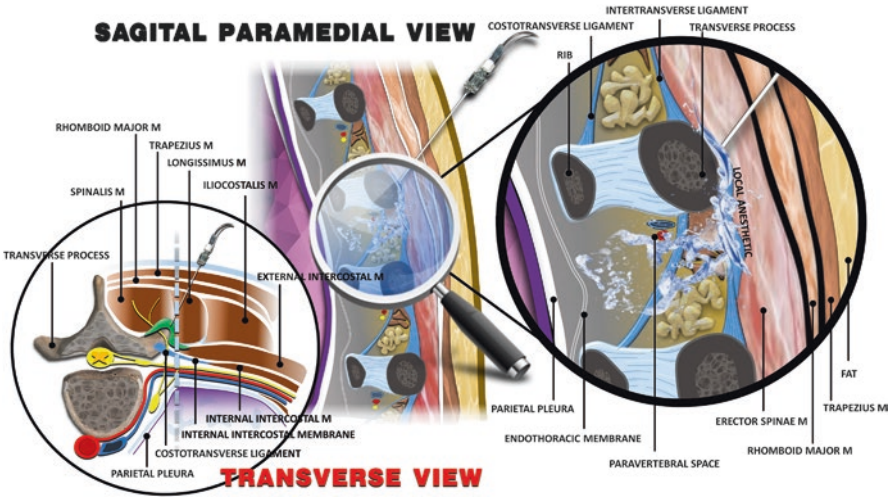

Fig. 11.3 Target of erector spinae plane block. (Reprinted with permission from Dr. Vicente Roques from imedar.com)

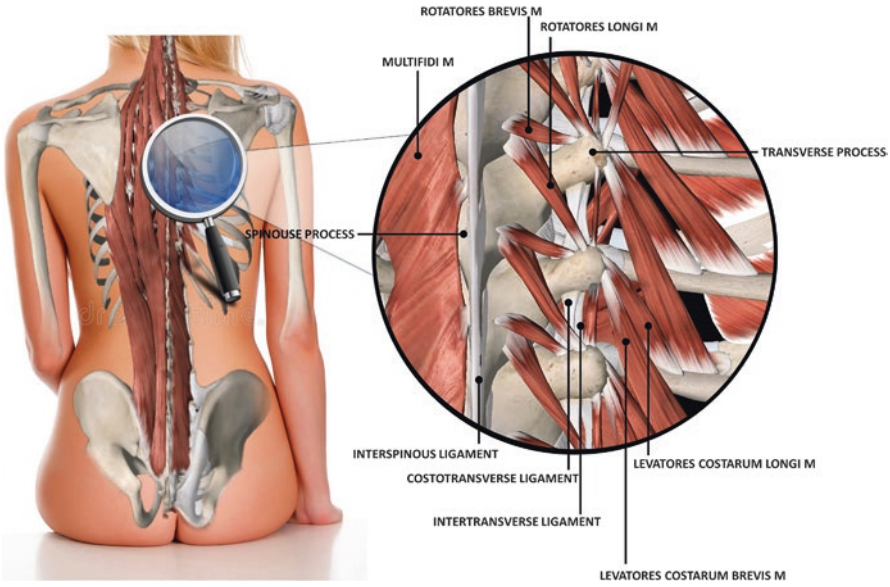

Fig. 11.4 Ligaments and muscles around the erector spinae plane. (Reprinted with permission from Dr. Vicente Roques from imedar.com)

The erector spinae plane is surrounded by soft tissues: ligaments (inter-transverse ligament, costotransverse ligament), muscles (levatores costarum, rotatores costarum, and external intercostal muscles), and fat (Fig. 11.4).

The mechanism of action has been examined through clinical (contrast spread) and cadaveric (imaging and dissection) studies. Following a single injection (usually

20 mL), the injectate spreads in paravertebral space in multiple segments over an average of 6 spinal segments, reaching the ventral and dorsal ramus of the spinal nerve along with the sympathetic ramus communicans at the intervertebral foramen level (Figs. 11.5 and 11.6). Epidural spread has been noticed as well. Spread to the intervertebral spinal foramen typically results in analgesic effect only even when anesthetic concentration of local anesthetic is used, although two reports had been published on the use of ESP block for mastectomy and ventral hernia repair with minimum sedation.

The ESP block has characteristics of differential blockade. The small amount of local anesthetic reaching the paravertebral space through the foramen provides sufficient local anesthetic mass to block small A delta and non-myelinated C fibers (pain and sympathetic fibers) but is not able to block large myelinated sensory and motor fibers. Analgesia without motor block along discernable cutaneous sensory block is consistent with the findings in most ESP literature.

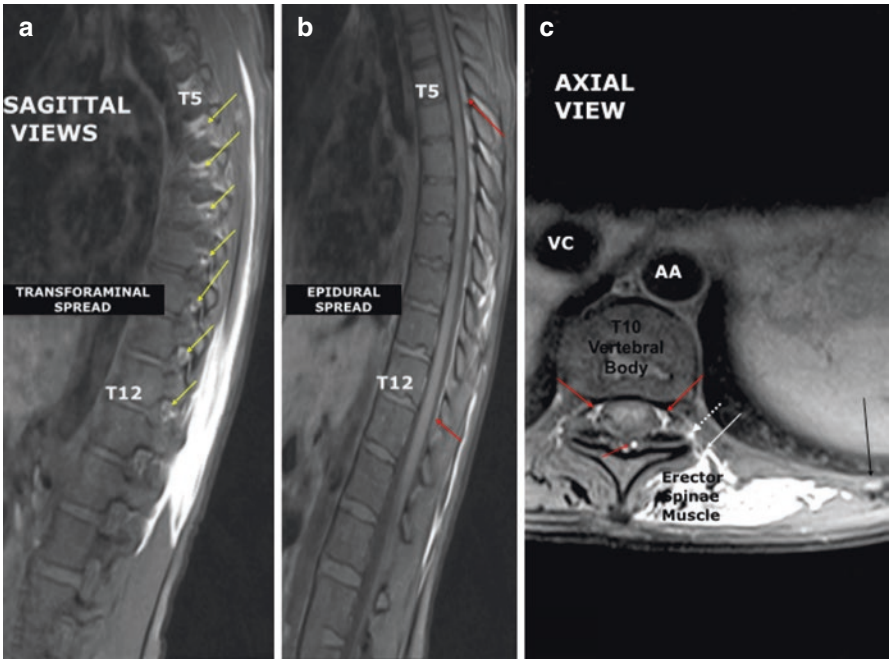

Fig. 11.5 Magnetic resonance imaging with gadolinium contrast added to bupivacaine erector spinae plane block (30 mL total volume) injected at the left T10 level. (**a**) Sagittal view at the level of the intervertebral foraminae showing transforaminal spread of the gadolinium from T5 to T12 of the left side (yellow arrows). (**b**) Sagittal view of the spinal canal depicting epidural spread (red arrows) of the contrast from T5 to T12. (**c**) Axial view at the T12 level demonstrating the spread of gadolinium from the erector spinae plane through paravertebral space (dashed white arrow) transiting the intervertebral foramina (yellow arrow) to spread circumferentially (red arrows) within the epidural space. Some venous uptake of gadolinium is also noted. (Modified, with permission, from the original unpublished image in the Philip Peng Educational Series collection (Toronto, ON, Canada))

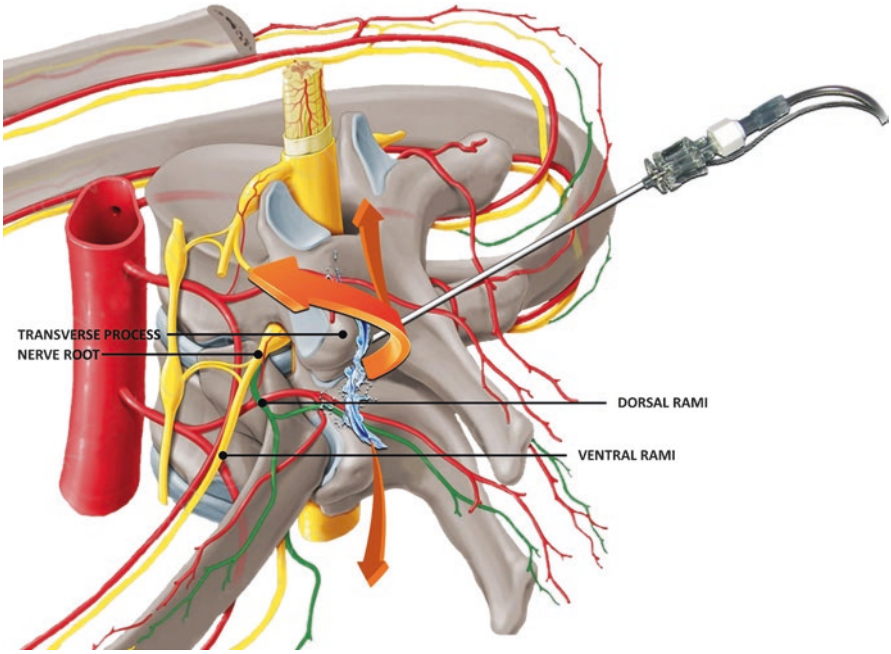

Fig. 11.6 Schematic diagram showing the spread of injectate following an ESP block. (Reprinted with permission from Dr. Vicente Roques from imedar.com)

Patient Selection and the Choice of Level

The ESP block has been published extensively in the upper thoracic level (thoracic indications) and the lower thoracic level (abdominal-pelvic indications). At these levels, the erector spinae muscle is located over the paraspinal gutter which consists of three muscular layers from medial to lateral: (1) spinalis, (2) longissimus, (3) iliocostalis (Figs. 11.1 and 11.2). When performing an ESP block at the thoracic level, the thoracic longissimus is the muscle in the needle path before the needle in contact with the tip of the transverse process, which is the target of ESP block. Usually, the level chosen for thoracic indications is between T2 and T5, and for abdominal pelvic indications between T7 and T10.

The cervical portion of erector spinae muscle is formed by semispinalis cervicis, longissimus cervicis, and iliocostalis cervicis, which inserts onto the transverse processes of C2–C6, extending the ESP plane from the upper thoracic region to the neck to reach cervical foraminae. This anatomic arrangement is the rationale for

performing the ESP block at the upper thoracic area to provide analgesic effect to cervical nerve roots (shoulder analgesia).

The thickness of erector spinae muscle in the lumbar level is thicker than in the thoracic area, making lumbar ESP block under ultrasound technically more challenging. However, same rationale applied to the cervical region can be applied here to the lumbar levels. Lower thoracic ESP block to reach lumbar nerve roots is recommended either by a single injection or by placing a catheter for interfascial infusion.

The various levels for the ESP blocks are summarized in Table 11.1.

Table 11.1 Area of blockade for erector spinae plane block in different surgeries

Spine region	Indications	Catheter after single shot	Single shot volume
High thoracic T2 or T3	Chronic shoulder pain syndrome	Unilateral	20 cc
	Post-surgical shoulder pain	Unilateral	
Mid thoracic T4 to T6	Rib fracture (midpoint of level of ribs fracture)	Unilateral or bilateral	20 cc
	Open thoracotomy and Vats lobectomy(T5)	Unilateral	
	Rescue after TE failure for thoracic surgery(T5)	Unilateral	
	Cardiac surgery – sternotomy (T5)	Bilateral	
	Breast surgery with axillary lymph node dissections (T3)	Unilateral	
	Chronic post-herpetic neuralgia (level of segments involved)	Unilateral	
	Chronic post-thoracotomy pain (level of segments involved)	Unilateral	
	Metastatic ribs cancer (level of segments involved)	Unilateral	
Low thoracic T7 to T12	Nephrectomies (T8)	Unilateral	20 cc
	Hysterectomies (T10)	Bilateral	
	Laparoscopic ventral hernia repair with mesh (T7)	Bilateral	
	Laparotomies (T7)	Bilateral	
	Chronic post-herpetic neuralgia (level of segments involved)	Unilateral	
	Chronic abdominal pain syndrome (T7 to T10)	Bilateral or unilateral	
	Chronic pelvic pain syndrome (T10)	Bilateral or unilateral	
Lumbar (L4)	Vertebral surgery (mid-point of levels involved)	Bilateral	20 cc
	Post-surgical hip replacement pain management (L4)	Unilateral	

Ultrasound Scanning

- *Position*: Sitting/lateral decubitus/prone; depending on the operator's and patient's comfort (Fig. 11.7).
- *Probe*: Usually a linear probe (7–12 MHz) is sufficient. For high BMI a curvilinear (2–6 MHz) is advised.

Scan 1 *Find the tip of transverse process using transverse view*

Place the probe in transverse orientation over the spinous process in the midline and transverse process laterally (Fig. 11.8). Just lateral to the spinous process is the lamina, a flat hyperechoic structure covered by ESM. Lateral to the lamina is the tip of transverse process which is a well-defined hyperechoic flat structure more superficial to the lamina. Mark the target on the skin (tip of transverse process) and then rotate the probe in cranio-caudal orientation, keeping the tip of transverse process on the middle of the ultrasound scream.

Scan 2 *Find the tip of transverse process using cranio-caudal probe orientation*, moving from RIBS to TRANSVERSE PROCESS.

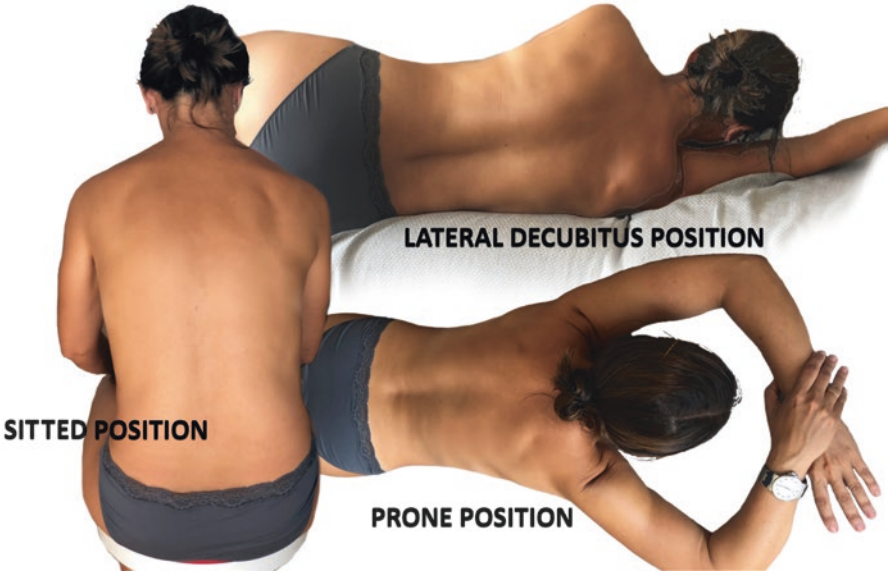

Fig. 11.7 Various positions for the performance of ESP block. (Reprinted with permission from Dr. Vicente Roques from imedar.com)

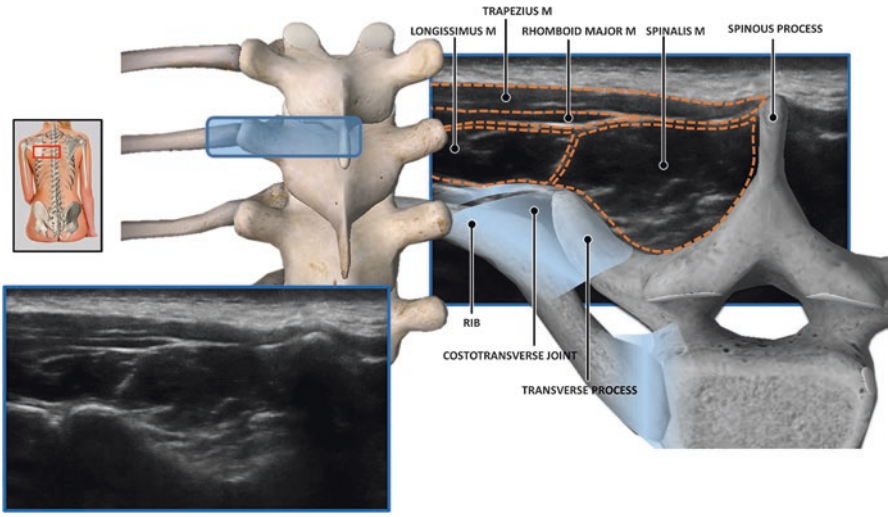

Fig. 11.8 Initial scan. (Reprinted with permission from Dr. Vicente Roques from imedar.com)

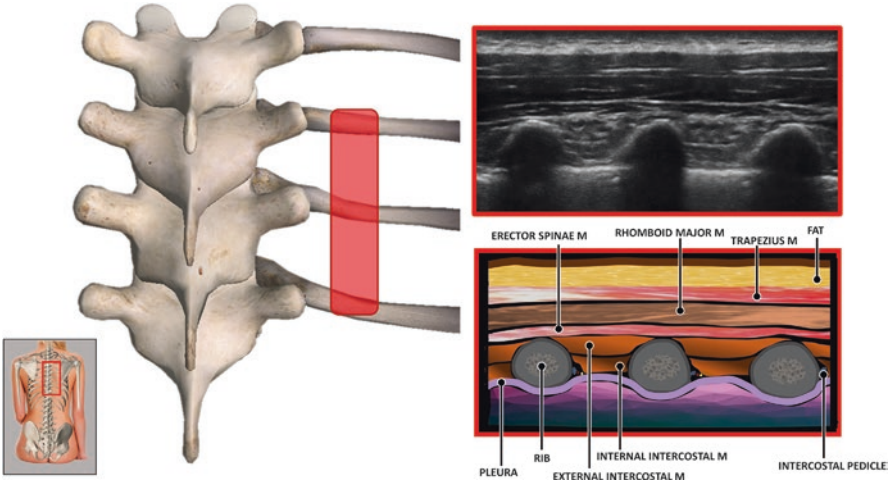

Fig. 11.9 Cranio-caudal probe orientation over the rib. (Reprinted with permission from Dr. Vicente Roques from imedar.com)

Scan 2a Cranio-caudal probe orientation over the rib in the selected spinal level (for instance the diagram depicts T5 level).

The structures from superficial to deep: TM (trapezius muscle), RM (rhomboid major), ESM (erector spinae muscle), rib (R) which is a rounded hyperechoic structure with clear underling hyperechoic linear pleura, external intercostal muscle (EIM), internal intercostal muscle (IIM), and pleura (P) (Fig. 11.9).

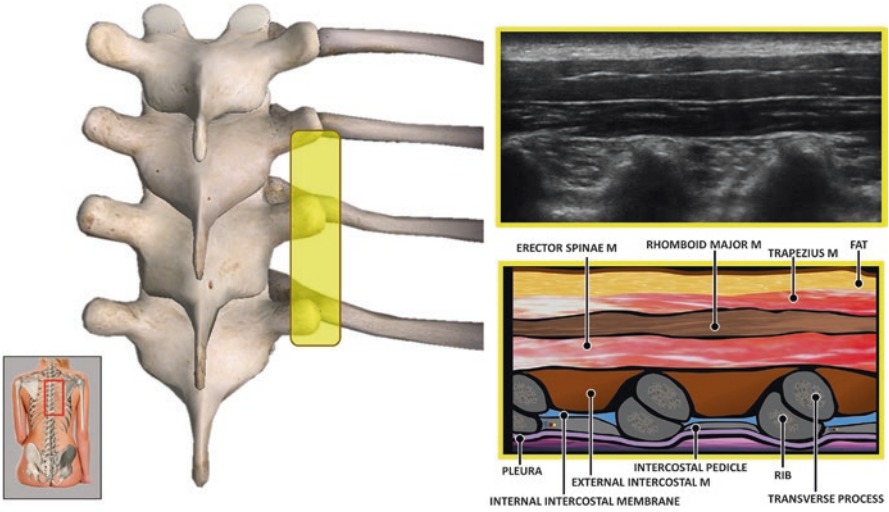

Fig. 11.10 Between the ribs and the tips of transverse process. (Reprinted with permission from Dr. Vicente Roques from imedar.com)

Scan 2b Move the ultrasound probe medially from rib towards the target (Tip of Transverse process).

Between the ribs and the tip of transverse process, a triangular-shaped structure is visualized (costo-transverse union) (Fig. 11.10).

Scan 2c Move the ultrasound probe slightly from the costo-transverse union to the tip of transverse process (TTP).

A clear transition from the deeper triangular structure (costo-transverse union) to a slightly more superficial FLAT hyperechoic structure (tip of transverse process) (Fig. 11.11). The diagram depicts sonoanatomy at the level of T5, which is the tip of the transverse process in the middle of ultrasound scan. This is the target for ESP injection. Please note the tip of the transverse process which is a FLAT hyperechoic structure.

Scan 2d Over the vertebral lamina

If ultrasound probe is moved further medially from the tip of the transverse process, the structures found are the ESM (erector spinae muscle) which is thicker than the portion covering the tip of the transverse process. The hyperechoic bone shadow is the vertebral laminae, deeper than the tip of the transverse process (Fig. 11.12).

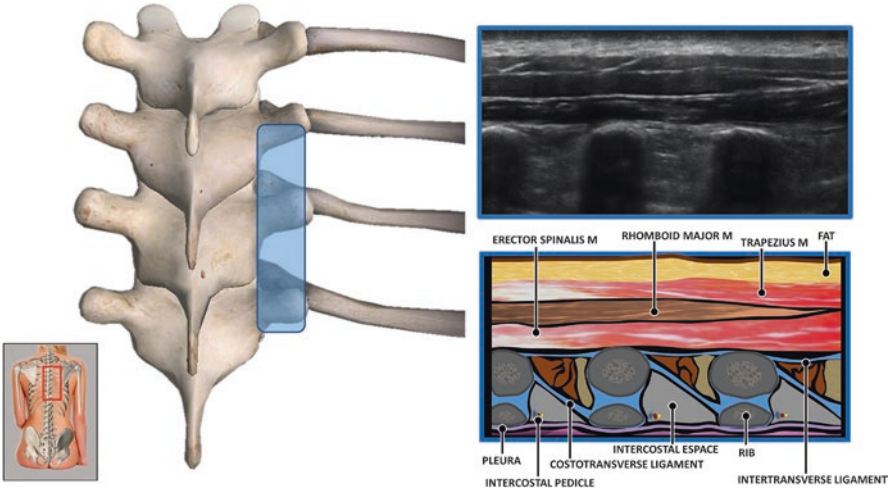

Fig. 11.11 Tip of the transverse process (target of the ESP block). (Reprinted with permission from Dr. Vicente Roques from imedar.com)

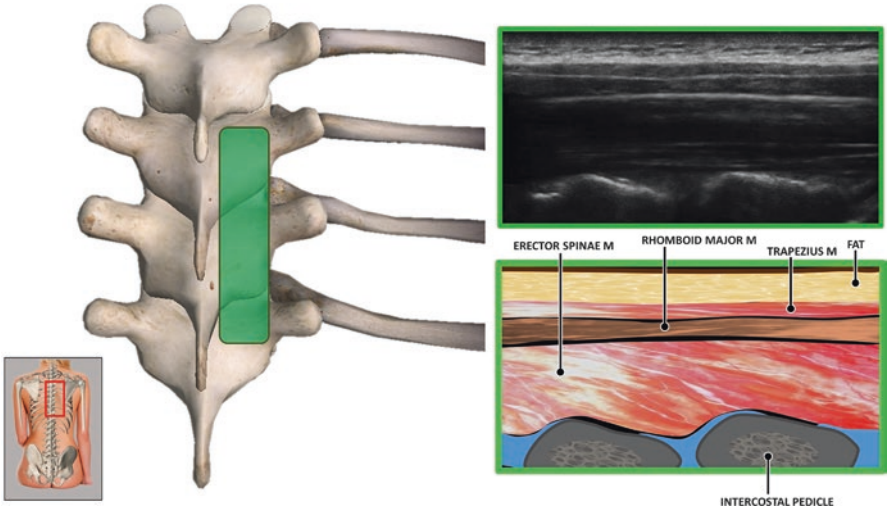

Fig. 11.12 Over the vertebral lamina. (Reprinted with permission from Dr. Vicente Roques from imedar.com)

Procedure

Single-Shot Injection

Equipment

- Needle: Usually an echogenic needle is advised; 22G 5–8 cm depending on the BMI of the patient
- Drugs: Long-acting local anesthetics, e.g. bupivacaine 0.5% (unilateral) or 0.25% (bilateral) with 2.5 mcgs per cc of epinephrine. Volume: please refer to Table 11.1.

In-plane approach is recommended either from cranial to caudal or caudal to cranial (both approaches have been published but the author prefers cranial to caudal except when performing at the upper thoracic level where caudal to cranial approach is preferred due to the operator comfort and the propensity of injectate to spread cranially to cervical roots). The needle insertion point is 1 cm away from the ultrasound probe (Fig. 11.13). Once the tip of the needle approaches the TTP in its distal end, hydrolocation of normal saline is important to ensure the spread anterior to the anterior fascia of the erector spinae muscle (AFESM) and posterior to the tip of the transverse process. Following confirmation of appropriate cranio-caudal spread, the total volume of local anesthetic is deposited.

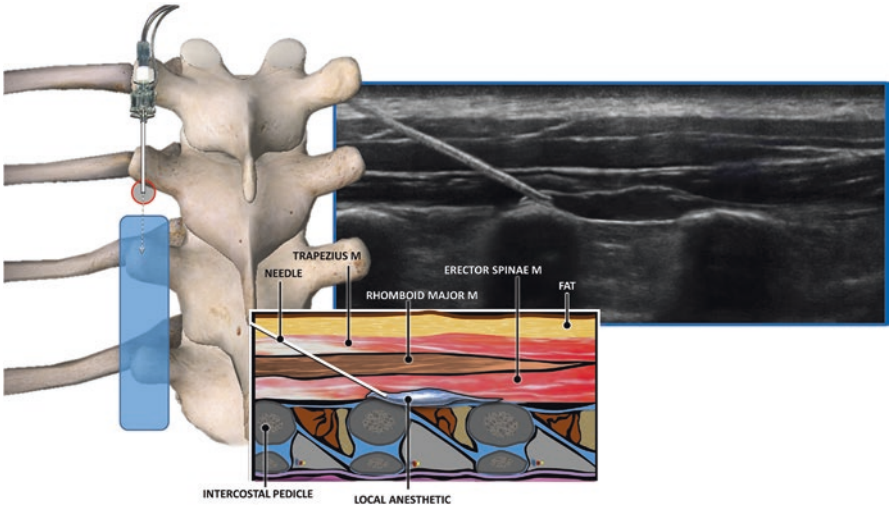

Fig. 11.13 Needle insertion in ESP block. (Reprinted with permission from Dr. Vicente Roques from imedar.com)

Catheter Placement

Equipment

- Needle/catheter: Catheter through needle (regular 18 G Tuohy needle) and regular epidural catheter (19 G) or catheter over needle can be used.
- Drugs: For unilateral infusions, bupivacaine 0.2%; for bilateral infusions, bupivacaine 0.125% at a rate that varies from 8 cc to 13 cc per catheter per hour.

Usually continuous infusion of 12 cc per hour provides sensory block to around 6 spinal levels**.** The most common infusion methods are continuous infusion plus patient-controlled analgesia. A typical example will be bupivacaine 0.2%: continuous infusion 5–8 cc/h plus PCA (5 cc lockout interval 60 minutes). Intermittent programmed boluses (IPB) also have been used. An example will be bupivacaine 0.2%: continuous infusion 5 cc/h plus IPB (10 cc/2 h). The most appropriate method of infusion has not been determined yet. However, IPB is lately gaining popularity due to the fact that pressure during injection appears to play an important role to improve analgesia during ESP continuous infusion.

Following the administration of the initial bolus (usually 20 cc), a catheter can be inserted and placed 5 cm beyond the tip of the needle (Fig. 11.14). Different catheters have been successfully used (catheter over needle or catheter through needle). The preference of the author is to use the later due to the fact that the catheter can be advanced and securely left into the erector spinae muscle.

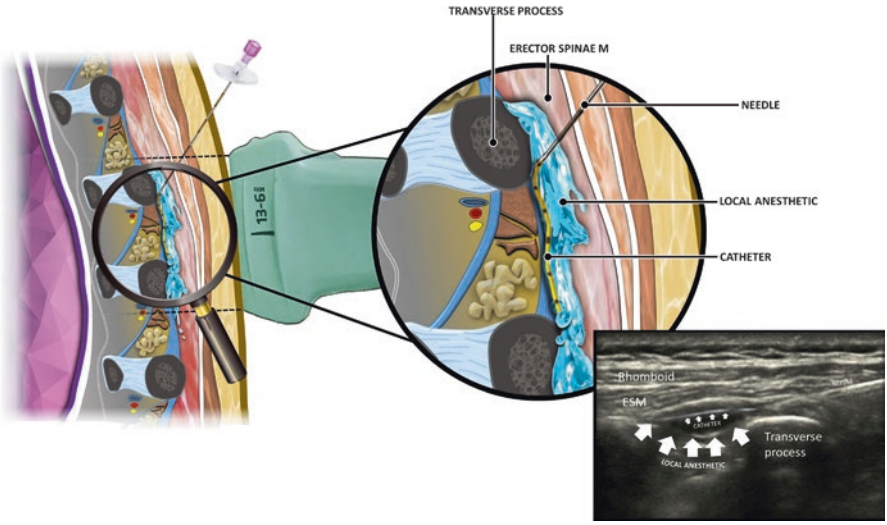

Fig. 11.14 Catheter insertion in ESP. (Reprinted with permission from Dr. Vicente Roques from imedar.com)

Clinical Pearls

1. When scanning you can find the target (tip of the transverse process, TTP) moving either from medial to lateral (lamina to TTP) or from lateral to medial (rib to TTP). The authors find it easier to identify the TTP moving from lamina which is a flat and deeper bony structure 2–3 cm medial to the TTP.
2. The authors recommend to place the target (TTP) in the middle of your ultrasound screen. Make sure that the needle entry point in 1 cm away from the ultrasound to avoid steep needle entry angle. The needle must be aligned with the axis of ultrasound probe. Hydrolocation and tissue movement help to visualize the needle when target deeper than 3 cm.
3. When having issues to see the shaft of the needle, hydrolocation can be used until reaching the target (TTP). The authors recommend to hold the ultrasound probe steady over tip of transverse process and redirect the needle to be visualized. In other words, "don't move your probe to find the needle."
4. The success of ESP block fully depends on the appropriate spread of the injectable during the injection. Careful and detailed hydrolocation must ensure that the injectable is located between the most anterior fascia layer of the erector spinae muscles and the TTP. Usually, after appropriate hydrolocation with volume as low as 5 cc of normal saline, the spread will be seen in cranial and caudal direction in at least 3 spinal levels. After confirmation of appropriate spread, the total of injectable can be delivered in aliquots of 3 cc following safety maneuver during injection to avoid intravascular depositions.
5. The ESP block is a paravertebral block where large volumes of local anesthetic are used; so patients must be under monitoring and IV in place during the intervention.
6. Patients must be under monitoring for at least 30 minutes after injection to rule out late local anesthetic toxicity episodes.
7. We advise to use local anesthetic containing epinephrine (2.5 mcg/mL) to rule out intravascular injections. If during injection the heart rate increases more than 15 beats per minute the injection must be stopped and revaluation of needle position and spread must be undertaking.
8. We advise to use catheter through needles (author preference); however, catheter over needles have also been successfully used. We recommend to place the catheter after initial single shot bolus (usually 20 cc) to open up the space before threading the catheter. If one finds resistance to advance the catheter, it is usually because the needle tip is facing the bony transverse process; so make sure that your needle tip is facing the operator during the catheter insertion. Also, we recommend to avoid steep needle angle when aiming the transverse process and this will facilitate to move your catheter out from the needle.

Literature Review

First described by Forero et al. in 2016, ESP block performed between erector spinae muscle and transverse process at T5 provided analgesia and discernable thoracoabdominal sensory block after a single injection of 20 mL of local anesthetic over 8 dermatomes innervated by the ventral and dorsal ramus. In this brief technical report, the authors also described the feasibility of prolongation of analgesic effect by inserting an interfacial catheter.

Following the initial report, approximately 100 publications including 4 randomized controlled trials (RCT) were published in the following 2 years. The findings of those reports are summarized:

1. The ESP can be applied to not just thoracoabdominal surgery but also upper and lower limb surgeries including hip and shoulder operations (see Table 11.1).
2. The efficacy in abdominal cavity procedure (gastric bypass) suggested the potential mechanism of visceral blockade in addition to the somatic blockade.
3. The defined interfascial plane and the thickness of erector muscle allow secure anchoring of the catheter. One case report even described the use of catheter for local anesthetic administration in a patient with malignant mesothelioma for 66 days without complication.
4. Extension of application to chronic pain emerges in the case report.
5. Because the target is away from the neuraxial compartment and thoracic cavity, the ESP block is used increasingly in procedure previously considered for paravertebral block. Furthermore, avoiding the neuraxial area and the superficial location of the target makes the ESP a more attractive alternative to patient on anticoagulants.
6. A few articles published in 2018 inspire further insights of the mechanism of how ESP block works. This has been discussed in the introduction.
7. In average the volume used is of 20 ml, with varying doses between 20 ml and maximum of 35 per side.
8. The block has been reported to be performed before surgery with patient under mild sedation and also right after general anesthesia induction either before surgical incision or at the end of the surgery. Preferred patient positioning after general anesthesia induction are lateral decubitus and prone. Before general anesthesia induction, the author prefers sitting position when performing the block in the upper thoracic and prone when performing it at the lower thoracic level, mostly related to the patient and operator comfort.
9. Extension to application to pediatrics (different ages including new born), when varying volumes have been used ranging from 0.2 cc to 0.4 cc per kg, adjusting the dose to avoid maximum recommended dose of local anesthetic used.
10. Regarding adjuvants the most common one reported is dexamethasone in the postoperative settings and methylprednisolone in the chronic pain setting.

11. The needle orientation to perform the block has been reported either from cranial to caudal or caudal to cranial (single shots). Apparently needle orientation does not significantly change the clinical effect (number of cranial or caudal dermatomes with sensory block); however when continuous ESP block, there is a tendency to orientate needle tip targeting the most potential painful dermatome to leave a catheter for interfacial infusion.
12. As similar as other interfacial blocks (TAP block), the ESP block has been reported to be effective as rescue block after surgery in the thoracic-abdominal cavity, shoulder and lower extremities above the knee.
13. Regarding safety, only two reports of either complication or unexpected clinical effect have been published. One reported pneumothorax and the second reported transient motor block. However, the authors recommended careful administration of local anesthetic following safety maneuvers under monitoring to avoid or detect intravascular administration and local anesthetic toxicity events.

In a short history of 2 years, it is encouraging to see four RCTs published. One RCT by Siva N. Krishna et al. demonstrated that bilateral single shot ESP block at T6 performed before general anesthesia induction provided superior analgesia to a multimodal intravenous analgesic regimen consisting of paracetamol and tramadol in patients undergoing elective cardiac surgery with cardiopulmonary bypass. The main outcome was VAS score and ESP block group results in significant lower pain scores at 6, 8, 10, and 12 hours post-extubation. Positive bilateral sensory block in anterior-lateral and posterior hemithorax was considered as successful ESP block. Patients in whom the block was unsuccessful were excluded from the study. In another RCT, Nagaraja et al. compared continuous bilateral ESP block with continuous thoracic epidural (TEA) for perioperative pain management in cardiac surgery. Comparable VAS scores were attained at 0-3-6-12 hours post-extubation at rest and coughing in both groups. The group of ESP block had significant less pain at 24-36-48 hours. However, mean VAS scores were less than 4 out of 10 in both groups. The conclusion from this study was that ESP block had a comparable pain scores with TEA, and provided an effective alternative to TEA in adult cardiac surgery for the perioperative pain management and fast tracking. In another randomized controlled study, Yavuz Gurkan et al. compared single shot ESP block at the level of T4 with no intervention in breast cancer surgery. The ESP group had significant less morphine consumption at 1-6-12-24 hours than the control group. As a result, the ESP group had 65% less morphine consumption at 24 hours. There was no statistically significant difference between the groups in terms of numeric rating score (NRS) in pain. The fourth RCT by Serkan Tulgar et al. was on the postoperative pain in abdominal procedure (laparoscopic cholecystectomy). They demonstrated bilateral T9 single shot ESP added to a multimodal analgesic regimen of IV-PCA of tramadol and IV paracetamol significantly reduced tramadol and paracetamol consumption at 24 hours. Fentanyl requirement was significantly lower in the recovery room for the ESP group while the NRS was lower in the ESP group during the first 3 hours.

Suggested Reading

Adhikary SD, Bernard S, Lopez H, Chin KJ. Erector spinae plane block versus retrolaminar block: a magnetic resonance imaging and anatomical study. Reg Anesth Pain Med. 2018;43:756–62.

Adhikary SD, Pruett A, Forero M, Thiruvenkatarajan V. Erector spinae plane block as an alternative to epidural analgesia for post-operative analgesia following video-assisted thoracoscopic surgery: a case study and a literature review on the spread of local anaesthetic in the erector spinae plane. Indian J Anaesth. 2018;62(1):75–8.

Adhikary SD, Prasad A, Soleimani B, Chin KJ. Continuous erector spinae plane block as an effective analgesic option in anticoagulated patients after left ventricular assist device implantation: a case series. J Cardiothorac Vasc Anesth. 2019;33:1063–7. pii: S1053-0770(18)30257-X.

Ahiskalioglu A, Alici HA, Ciftci B, Celik M, Karaca O. Continuous ultrasound guided erector spinae plane block for the management of chronic pain. Anaesth Crit Care Pain Med. 2017. https://doi.org/10.1016/j.accpm.2017.11.014. pii: S2352-5568(17)30357-0.

Aksu C, Gürkan Y. Opioid sparing effect of erector spinae plane block for pediatric bilateral inguinal hernia surgeries. J Clin Anesth. 2018;50:62–3.

Aksu C, Gürkan Y. Ultrasound-guided bilateral erector spinae plane block could provide effective postoperative analgesia in laparoscopic cholecystectomy in paediatric patients. Anaesth Crit Care Pain Med. 2019;38:87–8. pii: S2352-5568(18)30084-5.

Chin KJ, Malhas L, Perlas A. The erector spinae plane block provides visceral abdominal analgesia in bariatric surgery. A report of 3 cases. Reg Anesth Pain Med. 2017;42(3):372–6.

Chin KJ, Adhikary S, Sarwani N, Forero M. The analgesic efficacy of pre-operative bilateral erector spinae plane (ESP) blocks in patients having ventral hernia repair. Anaesthesia. 2017;72(4):452–60.

Cornish PB. Erector spinae plane block: the "happily accidental" paravertebral block. Reg Anesth Pain Med. 2018;43(6):644–5.

De Cassai A, Marchet A, Ori C. The combination of erector spinae plane block and PECS blocks could avoid general anesthesia for radical mastectomy in high risk patients. Minerva Anestesiol. 2018;84:1420–1.

De Cassai A, Stefani G, Ori C. Erector spinae plane block and brachial plexus. J Clin Anesth. 2018;45:32.

De la Cuadra-Fontaine JC, Concha M, Vuletin F, Arancibia H. Continuous erector spinae plane block for thoracic surgery in a pediatric patient. Paediatr Anaesth. 2018;28(1):74–5.

El-Boghdadly K, Pawa A. The erector spinae plane block: plane and simple. Anaesthesia. 2017;72(4):434–8.

Forero M, Adhikary SD, Lopez H, Tsui C, Chin KJ. The erector spinae plane block. A novel analgesic technique in thoracic neuropathic pain. Reg Anesth Pain Med. 2016;41(5):621–7.

Forero M, Rajarathinam M, Adhikary S, Chin KJ. Erector spinae plane (ESP) block in the management of post thoracotomy pain syndrome: a case series. Scand J Pain. 2017;17:325–9.

Forero M, Rajarathinam M, Adhikary S, Chin KJ. Continuous erector spinae plane block for rescue analgesia in thoracotomy after epidural failure: a case report. A A Case Rep. 2017;8(10):254–6.

Forero M, Rajarathinam M, Adhikary SD, Chin KJ. Erector spinae plane block for the management of chronic shoulder pain: a case report. Can J Anaesth. 2018;65(3):288–93.

Gürkan Y, Aksu C, Kuş A, Yörükoğlu UH, Kılıç CT. Ultrasound guided erector spinae plane block reduces postoperative opioid consumption following breast surgery: a randomized controlled study. J Clin Anesth. 2018;50:65–8.

Hamilton DL, Manickam B. The erector spinae plane block. Reg Anesth Pain Med. 2017;42(2):276.

Hannig KE, Jessen C, Soni UK, Børglum J, Bendtsen TF. Erector spinae plane block for elective laparoscopic cholecystectomy in the ambulatory surgical setting. Case Rep Anesthesiol. 2018;2018:5492527.

Ilker I, Zafeer KM, Tetsuya S. Ultrasound guided erector spinae plane block for bilateral lumbar transverse process fracture: a new or a pushing indication? Am J Emerg Med. 2019;37:557. pii: S0735-6757(18)30627-2.

Ivanusic J, Konishi Y, Barrington MJ. A cadaveric study investigating the mechanism of action of erector spinae blockade. Reg Anesth Pain Med. 2018;43(6):567–71.
Kimachi PP, Martins EG, Peng P, Forero M. The erector spinae plane block provides complete surgical anesthesia in breast surgery: a case report. A A Pract. 2018;11:186–8.
Kose HC, Kose SG, Thomas DT. Lumbar versus thoracic erector spinae plane block: similar nomenclature, different mechanism of action. J Clin Anesth. 2018;48:1.
Krishna SN, et al. Bilateral erector spinae plane block for acute post-surgical pain in adult cardiac surgical patients: a randomized controlled trial. J Cardiothorac Vasc Anesth. 2019;33:368–75. pii: S1053-0770(18)30383-5.
Kumar A, Hulsey A, Martinez-Wilson H, Kim J, Gadsden J. The use of liposomal bupivacaine in erector spinae plane block to minimize opioid consumption for breast surgery: a case report. A A Pract. 2018;10(9):239–41.
Muñoz F, Cubillos J, Bonilla AJ, Chin KJ. Erector spinae plane block for postoperative analgesia in pediatric oncological thoracic surgery. Can J Anaesth. 2017;64(8):880–2.
Nagaraja PS, et al. Comparison of continuous thoracic epidural analgesia with bilateral erector spinae plane block for perioperative pain management in cardiac surgery. Ann Card Anaesth. 2018;21(3):323–7.
Ramos J, Peng P, Forero M. Long-term continuous erector spinae plane block for palliative pain control in a patient with pleural mesothelioma. Can J Anaesth. 2018;65(7):852–3.
Restrepo-Garces CE, Chin KJ, Suarez P, Diaz A. Bilateral continuous erector spinae plane block contributes to effective postoperative analgesia after major open abdominal surgery: a case report. A A Case Rep. 2017;9(11):319–21.
Schwartzmann A, Peng P, Maciel MA, Forero M. Mechanism of the erector spinae plane block: insights from a magnetic resonance imaging study. Can J Anaesth. 2018;65:1165–6.
Selvi O, Tulgar S. Ultrasound guided erector spinae plane block as a cause of unintended motor block. Rev Esp Anestesiol Reanim. 2018;65:589–92. pii: S0034-9356(18)30110-5.
Sieben JM, van Otten I, Lataster A, Froeling M, Nederveen AJ, Strijkers GJ, Drost MR. In vivo reconstruction of lumbar erector spinae architecture using diffusion tensor MRI. Clin Spine Surg. 2016;29(3):E139–45.
Tsui BCH, Navaratnam M, Boltz G, Maeda K, Caruso TJ. Bilateral automatized intermittent bolus erector spinae plane analgesic blocks for sternotomy in a cardiac patient who underwent cardiopulmonary bypass: a new era of cardiac regional anesthesia. J Clin Anesth. 2018;48:9–10.
Tsui BCH, Mohler D, Caruso TJ, Horn JL. Cervical erector spinae plane block catheter using a thoracic approach: an alternative to brachial plexus blockade for forequarter amputation. Can J Anaesth. 2019;66:119–20.
Tulgar S, Senturk O. Ultrasound guided low thoracic erector spinae plane block for postoperative analgesia in radical retropubic T prostatectomy, a new indication. J Clin Anesth. 2018;47:4.
Tulgar S, Kapakli MS, Senturk O, Selvi O, Serifsoy TE, Ozer Z. Evaluation of ultrasound-guided erector spinae plane block for postoperative analgesia in laparoscopic cholecystectomy: a prospective, randomized, controlled clinical trial. J Clin Anesth. 2018;49:101–6.
Tulgar S, Thomas DT, Deveci U. Erector spinae plane block provides sufficient surgical anesthesia for ileostomy closure in a high-risk patient. J Clin Anesth. 2018;48:2–3.
Tulgar S, Selvi O, Ozer Z. Clinical experience of ultrasound-guided single and bi-level erectorspinae plane block for postoperative analgesia in patients undergoing thoracotomy. J Clin Anesth. 2018;50:22–3.
Tulgar S, Selvi O, Senturk O, Ermis MN, Cubuk R, Ozer Z. Clinical experiences of ultrasound-guided lumbar erector spinae plane block for hip joint and proximal femur surgeries. J Clin Anesth. 2018;47:5–6.
Ueshima H. Pneumothorax after the erector spinae plane block. J Clin Anesth. 2018;48:12.
Ueshima H, Otake H. Similarities between the retrolaminar and erector spinae plane blocks. Reg Anesth Pain Med. 2017;42(1):123–4.
Ueshima H, Otake H. Limitations of the Erector Spinae Plane (ESP) block for radical mastectomy. J Clin Anesth. 2018;51:97.

Wilson JM, Lohser J, Klaibert B. Erector spinae plane block for postoperative rescue analgesia in thoracoscopic surgery. J Cardiothorac Vasc Anesth. 2018;32:e5–7. pii: S1053-0770(18)30472-5.

Wong J, Navaratnam M, Boltz G, Maeda K, Ramamurthi RJ, Tsui BCH. Bilateral continuous erector spinae plane blocks for sternotomy in a pediatric cardiac patient. J Clin Anesth. 2018;47:82–3.

Yang HM, Choi YJ, Kwon HJ, O J, Cho TH, Kim SH. Comparison of injectate spread and nerve involvement between retrolaminar and erectorspinae plane blocks in the thoracic region: a cadaveric study. Anaesthesia. 2018;73:1244–50.

Ultrasound-Guided Cervical Nerve Root Block

12

Samer Narouze and Philip Peng

Introduction

Cervical transforaminal injections have been traditionally performed with the use of fluoroscopy or computed tomography (CT). However, there have been few reports of fatal complications in the literature as a result of vertebral artery injury, and/or infarction of the spinal cord and the brain stem. The mechanism of injury was believed to be vasospasm or embolus formation after inadvertent intra-arterial injection of the particulate steroid injectate.

Anatomy

The cervical spinal nerve occupies the lower part of the foramen with the epiradicular veins in the upper part (Figs. 12.1 and 12.2). The radicular arteries arising from the vertebral, ascending cervical and deep cervical arteries lie in close approximation to the spinal nerve.

In a cadaver study, Huntoon showed that the ascending and deep cervical arteries may contribute to the anterior spinal artery along with the vertebral artery (Fig. 12.2). In 20% of the foramina dissected, the ascending cervical artery or deep cervical artery branches within 2 mm of the needle path for a cervical transforaminal procedure. One-third of these vessels entered the foramen posteriorly potentially forming a radicular or a segmental feeder vessel to the spinal cord, making it vulnerable to inadvertent injury or injection even during correct needle placement.

S. Narouze
Center for Pain Medicine, Western Reserve Hospital, Cuyahoga Falls, OH, USA

P. Peng (✉)
Department of Anesthesia and Pain Management, Toronto Western Hopsital and Mount Sinai Hospital, University of Toronto, Toronto, Ontario, Canada
e-mail: Philip.peng@uhn.ca

P. Peng et al. (eds.), *Ultrasound for Interventional Pain Management*,
https://doi.org/10.1007/978-3-030-18371-4_12

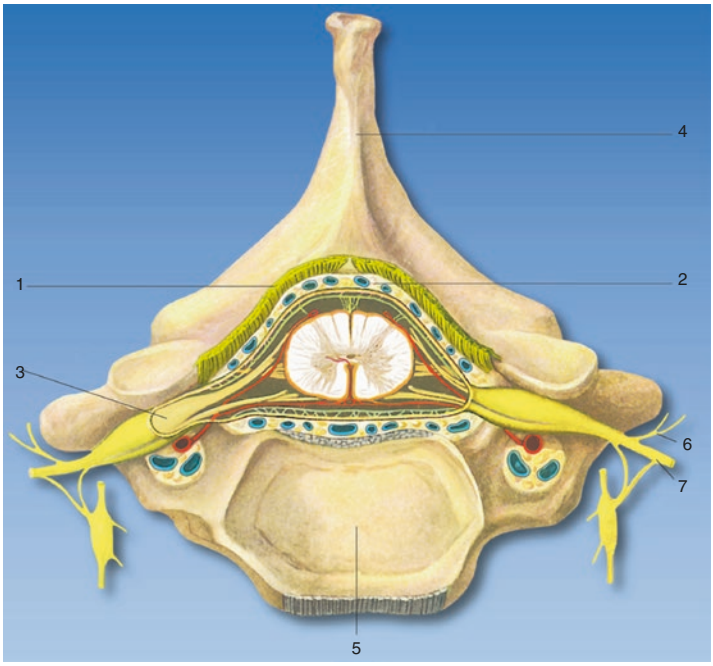

Fig. 12.1 Cross section of cervical epidural space. 1. Ligamentum flavum, 2. epidural space with venous plexus, 3. spinal ganglion, 4. spinous process, 5. body of vertebra, 6. dorsal branch of spinal nerve, 7. ventral branch of spinal nerve. (Reprinted with permission from Dr. Danilo Jankovic)

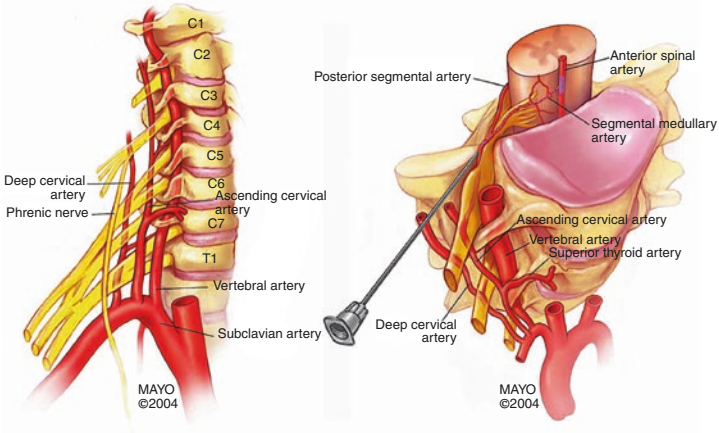

Fig. 12.2 The left diagram demonstrated the ascending cervical and deep cervical arteries anastomosing with the vertebral artery posterior to the spinal nerves. Note that the ascending cervical artery enters the foramen at C3-4 or C4-5, whereas the deep cervical artery enters the more distal C5-6, C6-7, or C7-T1 foramina. The right diagram showed a cervical transforaminal needle cannulating a segmental artery contributed by the ascending cervical artery. Steroid particles (purple) are shown coalescing in the anterior spinal artery. (Reprinted with permission of Mayo Foundation for Medical Education and Research)

In another cadaver study, Hoeft et al. showed that radicular artery branches from the vertebral artery lie over the most anteromedial aspect of the foramen, while those that arise from the ascending or deep cervical arteries are of greatest clinical significance as they must course medially throughout the entire length of the foramen.

Patient Selection

Cervical nerve root block/transforaminal epidural injections are indicated in cervical radicular pain not responsive to conservative therapy. Cervical epidural injections can be performed using an interlaminar or a transforaminal approach. As cervical radicular pain is frequently caused by foraminal stenosis, transforaminal approach can maximize the concentration of steroid delivered to the affected nerve roots while reducing the volume of injectate required and was shown to be effective in relieving radicular symptoms.

Ultrasound Scan

Patient position: Lateral decubitus position with injection side up.
Probe: Linear, high resolution 6–18 MHz

Scan 1: Identification of the cervical spine level

The ultrasound probe is placed in the short axis of the spine at the level of cricoid. At this level, the probe is moved in cephalad and caudal direction until the cervical tubercles are identified. The character of fifth to seventh cervical spine is illustrated below (Figs. 12.3, 12.4 and 12.5).

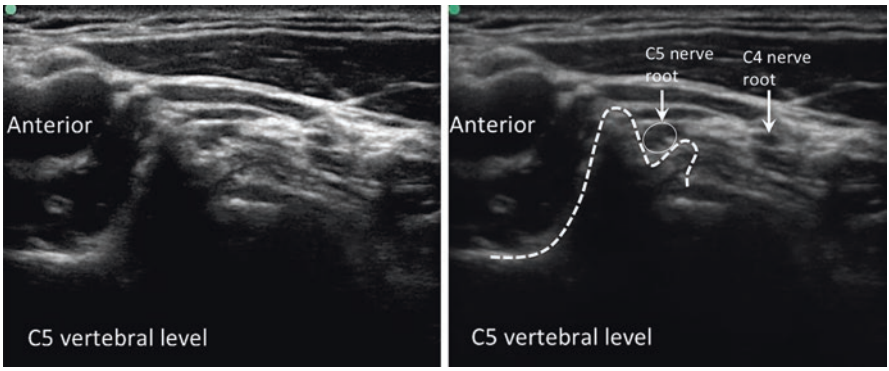

Fig. 12.3 Cervical 5th nerve root. Note the anterior and posterior tubercles are similar in size and give the impression of the double camel hump. (Reprinted with permission from Philip Peng Education Series)

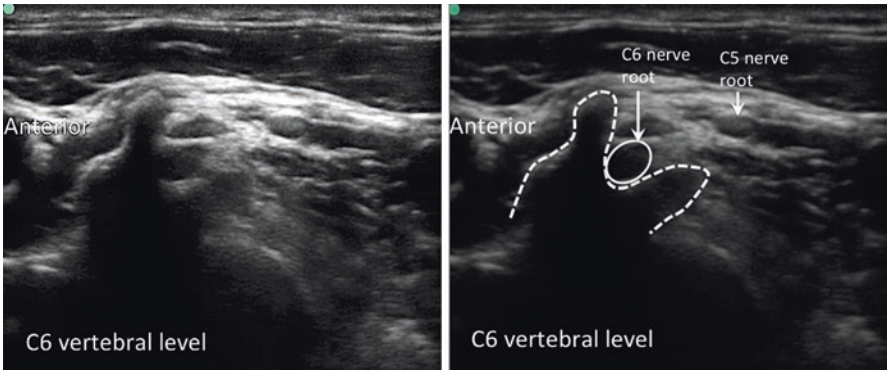

Fig. 12.4 Cervical 6th nerve root. Note the prominent anterior tubercle (Chassaignac's tubercle). (Reprinted with permission from Philip Peng Education Series)

Fig. 12.5 Cervical 7th nerve root. Note the presence of posterior tubercle while the anterior is either absent or vestigial. The vertebral artery is in close proximity to the nerve root. (Reprinted with permission from Philip Peng Education Series)

Scan 2: Identification of the target nerve root and associated vessel

Once the level is counted, the probe is tilted to optimize the visualization of nerve root. The clinician should minimize the use of pressure to reveal the pulsation of the vessel in the vicinity of the nerve root (Fig. 12.6).

Procedure

- Needles: 22G blunt-tip needle if available
- Drug: 1–2 ml Bupivacaine 0.25% for diagnostic blocks; 1–2 ml Bupivacaine 0.25% and 4 mg Dexamethasone for therapeutic injections

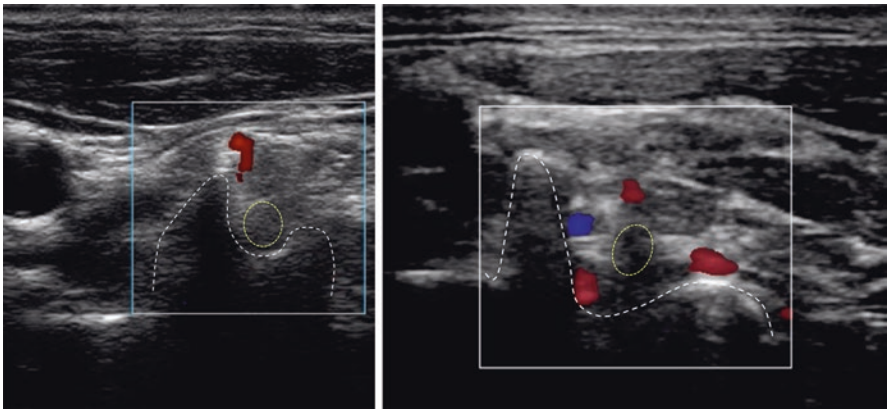

Fig. 12.6 The left sonogram showed the typical location of the vessel in the ventral aspect of the C6 nerve root. The right sonogram showed the rich presence of the vessel in both the ventral and dorsal aspect of the nerve root. (Reprinted with permission from Philip Peng Education Series)

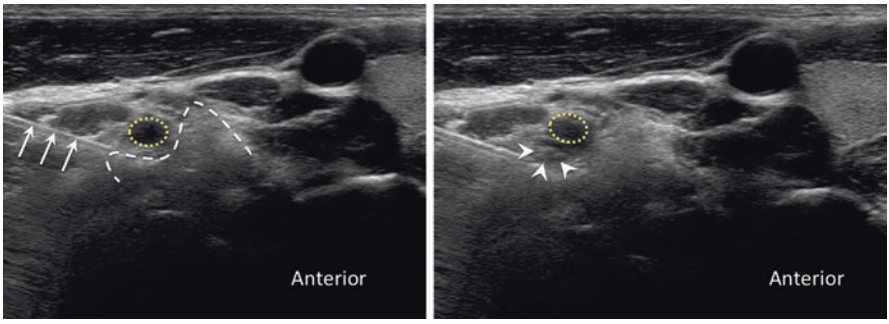

Fig. 12.7 Injection around the nerve root. The left sonography showed the needle inserted on the dorsal side of the nerve root. The right sonography showed the injectate. The nerve root was highlighted with yellow dotted line

The needle is introduced under real-time ultrasound guidance from posterior to anterior with an in-plane technique to target the corresponding cervical nerve root (from C3 to C8) at the external foraminal opening between the anterior and posterior tubercles of the transverse process (Fig. 12.7).

One can successfully monitor the spread of the injectate around the cervical nerve with real-time ultrasonography, and the absence of such spread around the nerve root may suggest unsuspected or inadvertent intravascular injection. However, it is difficult to monitor the spread of the injectate through the foramen into the

epidural space because of the bony drop out artifact of the transverse process. We therefore refer to this approach as a "cervical selective nerve root block" rather than cervical transforaminal epidural injection.

Clinical Peals

1. It is recommended to perform the initial ultrasound-guided cervical nerve root injection with the use of fluoroscopy. Correct level determination with ultrasound as described above may be difficult in the beginning.
2. The author believes that visualization of such small vessels (radicular arteries) may be very challenging especially in obese patients and requires special training and expertise. Real-time fluoroscopy with contrast injection and digital subtraction—when available—should still be used with ultrasound as an adjunct to help identify blood vessels in the vicinity of the foramen.

Literature Review

Currently, the guidelines for cervical transforaminal injection technique involve introducing the needle under fluoroscopic guidance into the posterior aspect of the intervertebral foramen just anterior to the superior articular process (SAP) in the oblique view to minimize the risk of injury to the vertebral artery or the nerve root. Despite the strict adherence to these guidelines, adverse outcomes have been reported. A potential shortcoming of the described fluoroscopic-guided procedure is that the needle may puncture a critical contributing vessel to the anterior spinal artery in the posterior aspect of the intervertebral foramen. Here the ultrasonography may come to play; as it allows for visualization of soft tissues, nerves and vessels and the spread of the injectate around the nerve; thus it may be potentially advantageous to fluoroscopy. Ultrasound allows identification of vessels before they are punctured, while fluoroscopy recognizes intravascular injection only after the vessel has been punctured.

Galiano et al. first described ultrasound-guided cervical periradicular injections in cadavers. However they were not able to comment on the relevant blood vessels in the vicinity of the vertebral foramen.

Narouze et al. reported a pilot study of 10 patients who received cervical nerve root injections using ultrasound as the primary imaging tool with fluoroscopy as the control. The radiologic target point was the posterior aspect of the intervertebral foramen just anterior to the SAP in the oblique view, and at the mid-sagittal plane of the articular pillars in the anteroposterior view (the target point for transforaminal injection). The needle was exactly at the target point in 5 patients in the oblique view and in 3 patients in the AP views. The needle was within 3 mm in all patients in the lateral oblique view and in 8 patients in the AP view. In the other 2

patients the needle was within 5 mm from the radiologic target as intentionally the needle was not introduced into the foramen but rather just outside the foramen as the goal was to perform selective nerve root injection and not a transforaminal injection. In four patients they were able to identify vessels at the anterior aspect of the foramen, while two patients had critical vessels at the posterior aspect of the foramen, and in one patient this artery continued medially into the foramen most likely forming a segmental feeder artery. In these 2 cases, such vessels could have been injured easily in the pathway of a correctly placed needle under fluoroscopy.

Yamauchi et al. were able to show the analgesic efficacy of this technique in the clinical subjects as far as 30 days. By using fluoroscopy in clinical subjects and dye spread followed by dissection in cadavers, they also confirmed the needle-to-nerve root accuracy. However, the spread pattern tended to be extraforaminal. Lee et al. examined a cohort of 59 patients with ultrasound-guided periradicular steroid injection and found a significant reduction of pain in 78% of the patients up to 3 months, and the outcome was dependent on the spread pattern.

The efficacy and safety of the ultrasound and fluoroscopy-guided cervical nerve root block were compared in a randomized trial involving 120 patients. Jee et al. demonstrated that the treatment effects and functional improvement were comparable at 2 and 12 weeks. In a prospective randomized trial, Obernauer et al. evaluated and compared the accuracy, performance efficiency, safety, and pain relief between ultrasound-guided and CT scan-guided cervical nerve root injections. The mean time for final needle placement in the ultrasound group was much shorter than CT scan group (2:21 ± 1:43 min versus 10:33 ± 02:30 min, respectively). The accuracy of ultrasound-guided injections was 100%. Both groups resulted in significant improvement in pain with difference between these two groups.

Compared with fluoroscopy-guided injection, the ultrasound technique offers the recognition of the periradicular vessels before the needle injection and a shorter performance time while the analgesia efficacy is comparable.

Suggested Reading

Baker R, Dreyfuss P, Mercer S, Bogduk N. Cervical transforaminal injections of corticosteroids into a radicular artery: a possible mechanism for spinal cord injury. Pain. 2003;103:211–5.

Beckman WA, Mendez RJ, Paine GF, Mazzilli MA. Cerebellar herniation after cervical transforaminal epidural injection. Reg Anesth Pain Med. 2006;31:282–5.

Brouwers PJ, Kottink EJ, Simon MA, Prevo RL. A cervical anterior spinal artery syndrome after diagnostic blockade of the right C6-nerve root. Pain. 2001;91:397–9.

Galiano K, Obwegeser AA, Bodner G, Freund MG, Gruber H, Maurer H, Schatzer R, Ploner F. Ultrasound-guided periradicular injections in the middle to lower cervical spine: an imaging study of a new approach. Reg Anesth Pain Med. 2005;30:391–6.

Hoeft MA, Rathmell JP, Monsey RD, Fonda BJ. Cervical transforaminal injection and the radicular artery: variation in anatomical location within the cervical intervertebral foramina. Reg Anesth Pain Med. 2006;31:270–4.

Huntoon MA. Anatomy of the cervical intervertebral foramina: vulnerable arteries and ischemic neurologic injuries after transforaminal epidural injections. Pain. 2005;117:104–11.

Jee H, Lee JH, Kim J, Park KD, Lee WY, Park Y. Ultrasound-guided selective nerve root block versus fluoroscopy-guided transforaminal block for the treatment of radicular pain in the lower cervical spine: a randomized, blinded, controlled study. Skelet Radiol. 2013;42(1):69–78.

Kolstad F, Leivseth L, Nygaard OP. Transforaminal steroid injections in the treatment of cervical radiculopathy: a prospective outcome study. Acta Neurochir. 2005;147:1065–70.

Lee SH, Kim JM, Chan V, Kim HJ, Kim HI. Ultrasound-guided cervical periradicular steroid injection for cervical radicular pain: relevance of spread pattern and degree of penetration of contrast medium. Pain Med. 2013;14(1):5–13.

Martinoli C, Bianchi S, Santacroce E, Pugliese F, Graif M, Derchi LE. Brachial plexus sonography: a technique for assessing the root level. AJR Am J Roentgenol. 2002;179:699–702.

Matula C, Trattnig S, Tschabitscher M, Day JD, Koos WT. The course of the prevertebral segment of the vertebral artery: anatomy and clinical significance. Surg Neurol. 1997;48:125–31.

Muro K, O'Shaughnessy B, Ganju A. Infarction of the cervical spinal cord following multilevel transforaminal epidural steroid injection: case report and review of the literature. J Spinal Cord Med. 2007;30:385–8.

Narouze S, Peng PWH. Ultrasound-guided interventional procedures in pain medicine: a review of anatomy, sonoanaotmy and procedures. Part II: axial structures. Reg Anesth Pain Med. 2010;35:386–96.

Narouze S, Vydyanathan A, Kapural L, Sessler D, Mekhail N. Ultrasound-guided cervical selective nerve root block: a fluoroscopy-controlled feasibility study. Reg Anesth Pain Med. 2009;34:343–8.

Obernauer J, Galiano K, Gruber H, Bale R, Obwegeser AA, Schatzer R, Loizides A. Ultrasound-guided versus computed tomography-controlled periradicular injections in the middle and lower cervical spine: a prospective randomized clinical trial. Eur Spine J. 2013;22(11):2532–7.

Rathmell JP, Aprill C, Bogduk N. Cervical transforaminal injection of steroids. Anesthesiology. 2004;100:1595–600.

Rozin L, Rozin R, Koehler SA, Shakir A, Ladham S, Barmada M, Dominick J, Wecht CH. Death during transforaminal epidural steroid nerve root block (C7) due to perforation of the left vertebral artery. Am J Forensic Med Pathol. 2003;24:351–5.

Slipman CW, Lipetz JS, Jackson HB, Rogers DP, Vresilovic EJ. Therapeutic selective nerve root block in the nonsurgical treatment of atraumatic cervical spondylotic radicular pain: a retrospective analysis with independent clinical review. Arch Phys Med Rehabil. 2000;81:741–6.

Tiso RL, Cutler T, Catania JA, Whalen K. Adverse central nervous system sequelae after selective transforaminal block: the role of corticosteroids. Spine J. 2004;4:468–74.

Wallace MA, Fukui MB, Williams RL, Ku A, Baghai P. Complications of cervical selective nerve root blocks performed with fluoroscopic guidance. AJR. 2007;188:1218–21.

Yamauchi M, Suzuki D, Niiya T, Honma H, Tachibana N, Watanabe A, Fujimiya M, Yamakage M. Ultrasound-guided cervical nerve root block: spread of solution and clinical effect. Pain Med. 2011;12:1190–5.

Cervical Medial Branch and Third Occipital Nerve Blocks

13

John-Paul B. Etheridge and Roderick Finlayson

Abbreviations

AP	Articular pillars
CMBBs	Cervical medial branch blocks
LA	Local anesthetic
SSC	Semispinalis capitis muscle
TON	Third occipital nerve
TP	Transverse process
USG	Ultrasound-guided

Introduction

Indication

Cervical medial branch blocks and third occipital nerve blocks are commonly used in the diagnosis and treatment of chronic neck pain and headaches related to cervical facet joints.

J.-P. B. Etheridge (✉)
Department of Anesthesia, Kelowna General Hospital, Kelowna, BC, Canada

R. Finlayson
Alan Edwards Pain Management Unit, McGill University Health Centre, Montreal, Quebec, Canada

P. Peng et al. (eds.), *Ultrasound for Interventional Pain Management*,
https://doi.org/10.1007/978-3-030-18371-4_13

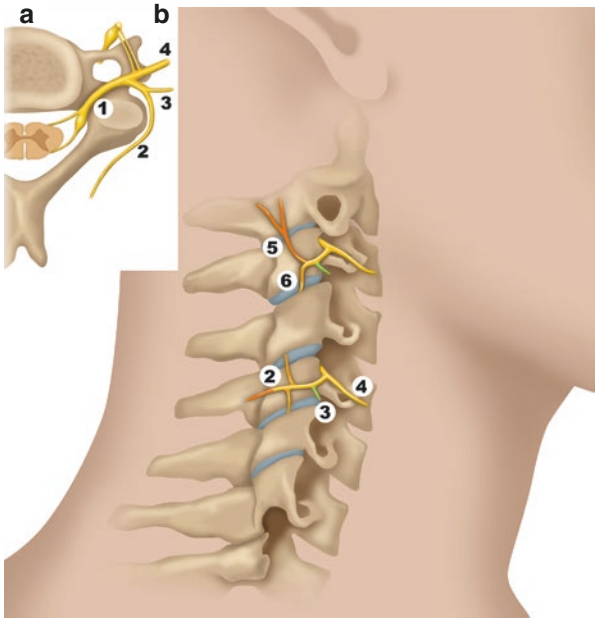

Fig. 13.1 Anatomy of cervical medial branch and third occipital nerve (TON). (Reprinted with permission from Philip Peng Educational Series)

Anatomy

Each zygapophyseal joint is innervated by the medial branch above and below it, except for the C2/C3 level, which is solely innervated by the TON (Fig. 13.1).

(**a**) Transverse view of a C5 vertebra demonstrating the spinal nerve anatomy. Spinal nerve (1); medial branch of posterior ramus (2); lateral branch of posterior ramus (3); ventral ramus (4).
(**b**) Lateral view of a cervical spine model demonstrating the course of the cervical medial branches. A cervical medial branch traverses the articular pillar, supplying the zygapophyseal joint above and below (2); The C2/C3 joint is unique as it is innervated solely by the third occipital nerve (5), which emerges from the posterior ramus along with the medial branch of C3 (6). The latter innervates the C3/C4 joint with the C4 medial branch.

Patient Selection

Facet joints are the most commonly implicated structure in chronic neck pain. Levels to be treated are determined by known pain referral patterns (Fig. 13.2).

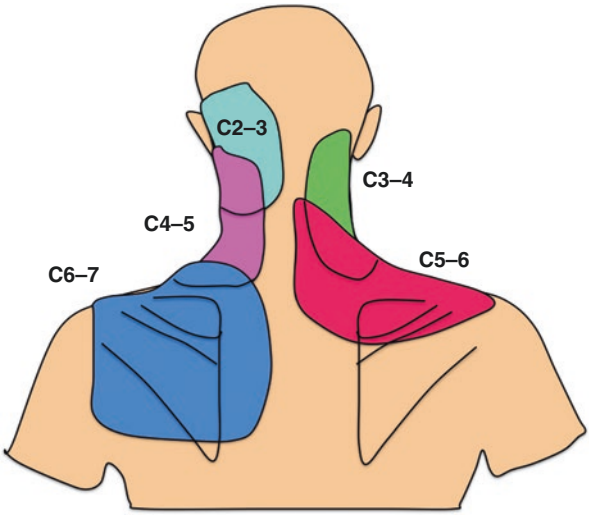

Fig. 13.2 Segmental pain referral patterns for cervical zygapophyseal joints. (Adapted from Dwyer A, Aprill C, Bogduk N. Cervical zygapophyseal joint pain patterns I: A study in normal volunteers. *Spine* 1990;15:453–457). (Reprinted with permission from Philip Peng Educational Series)

Ultrasound Scan

- Probe: linear 15-8 MHz
- Position: lateral decubitus, neck in neutral position.

Coronal (Long Axis) Scan

This view is used for level confirmation in both the upper and lower cervical spines. In the long axis, the AP appear as a series of peaks (zygapophyseal joints lines) and valleys (convex shapes of the APs).

Figure 13.3 shows the coronal scan of the cervical spine demonstrating the articular pillars (AP) of C4, C5 and C6, as well as the inferior articular process (IAP) of C2. This view is used for level and needle position confirmation. The medial branches (mb) of C3, C4 and C5 can be seen, as well as the third occipital nerve (TON).

Above the C2–C3 joint, the slope of the inferior articular process of C2 creates a characteristic drop-off with the vertebral artery visible immediately cephalad to it (Fig. 13.4).

In the lower cervical spine, the TP of C7, which can be found anterior to the AP, provides a reference for needle positioning (Fig. 13.5).

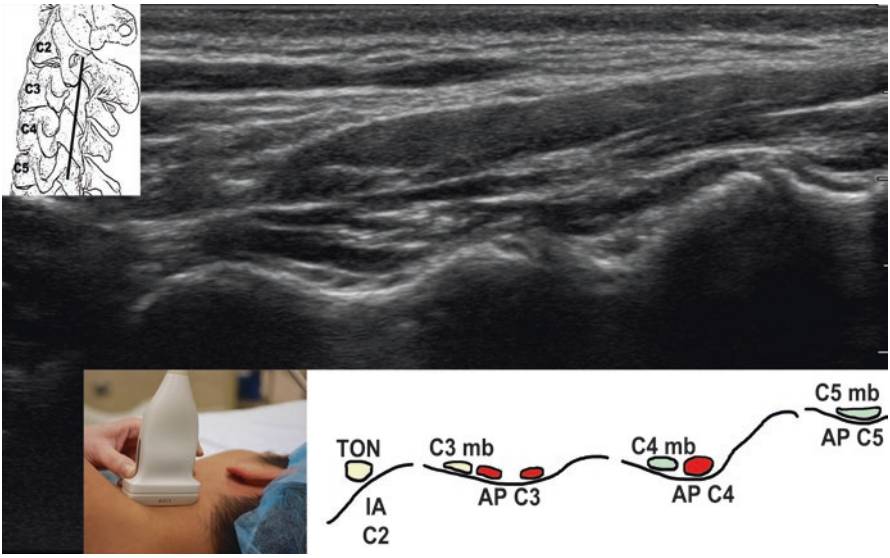

Fig. 13.3 Coronal scan of the cervical spine. (Reprinted with permission from Philip Peng Educational Series)

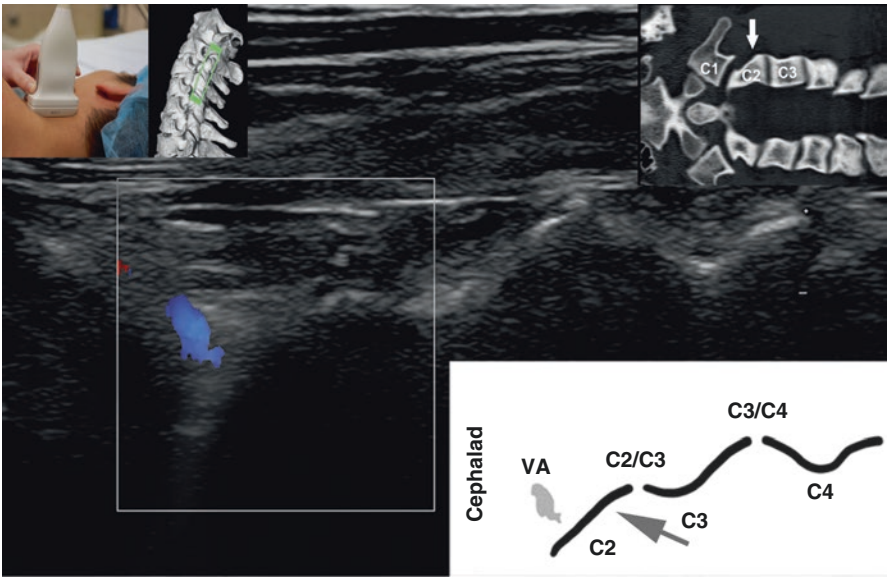

Fig. 13.4 Coronal scan of the upper cervical spine demonstrating the drop-off formed by the inferior articular process of C2 (grey arrow in right lower inset), the vertebral artery (VA) can be imaged with duplex Doppler immediately cephalad. This view facilitates identification of the C2/C3 joint which is used as a landmark during third occipital nerve blocks. The right upper inset is a coronal CT scan of the cervical spine demonstrating the drop-off formed by the inferior articular process of C2 (grey arrow). (Reprinted with permission from Philip Peng Educational Series)

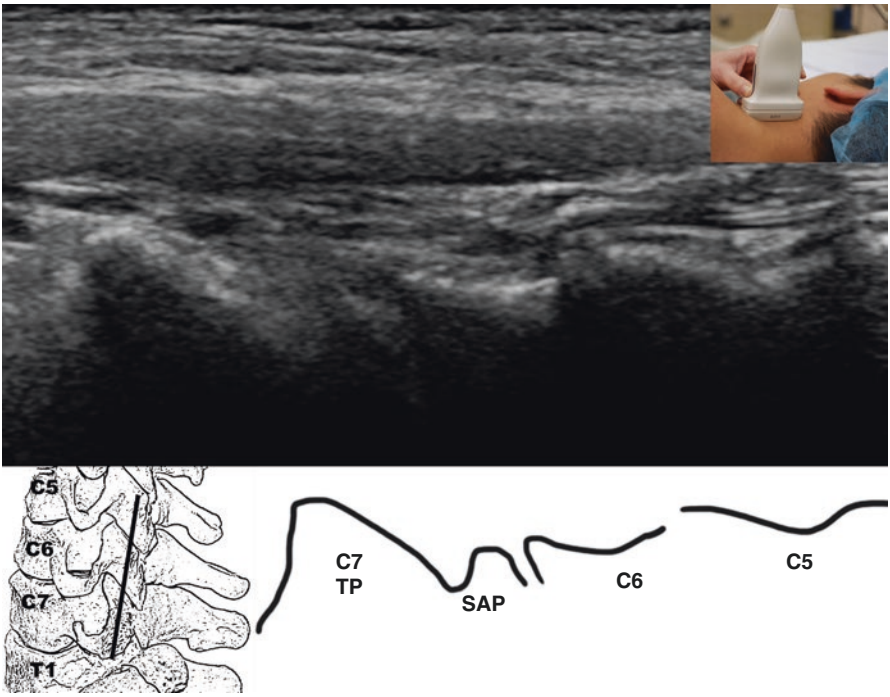

Fig. 13.5 Coronal scan of the lower cervical spine. (Reprinted with permission from Philip Peng Educational Series)

Figure 13.5 shows a coronal scan of the lower cervical spine demonstrating the transverse process of C7 (C7 TP); superior articular process of C7 (SAP); articular pillar of (C5) and (C6). This view is used to confirm appropriate needle positioning for blocks of the lower cervical medial branches.

Transverse (Short Axis) Scan

This view is used for needle placement (Fig. 13.6). The targets are the C2–C3 zygapophyseal joint (TON) and the centroid aspect of the AP (C3–C6 medial branches MB). The latter appears as a distinctive flat hyperechoic line that can be appreciated when moving the probe in a cephalo-caudal direction. In contrast, the joints present a rounded and less echogenic contour (Fig. 13.7).

Figure 13.6 shows a transverse scan of the cervical spine at the level of C6. The centroid of the articular pillar (AP) forms a distinct flat hyperechoic line and constitutes the target for cervical medial branch blocks. The semispinalis capitis muscle (SSC) inserts on the posterior tubercle of the transverse process (PT) and courses over the AP. Further anterior, the nerve root (NR) and anterior tubercle (AT) can be seen. A CT overlay of the same bony landmarks is depicted in the right lower inset.

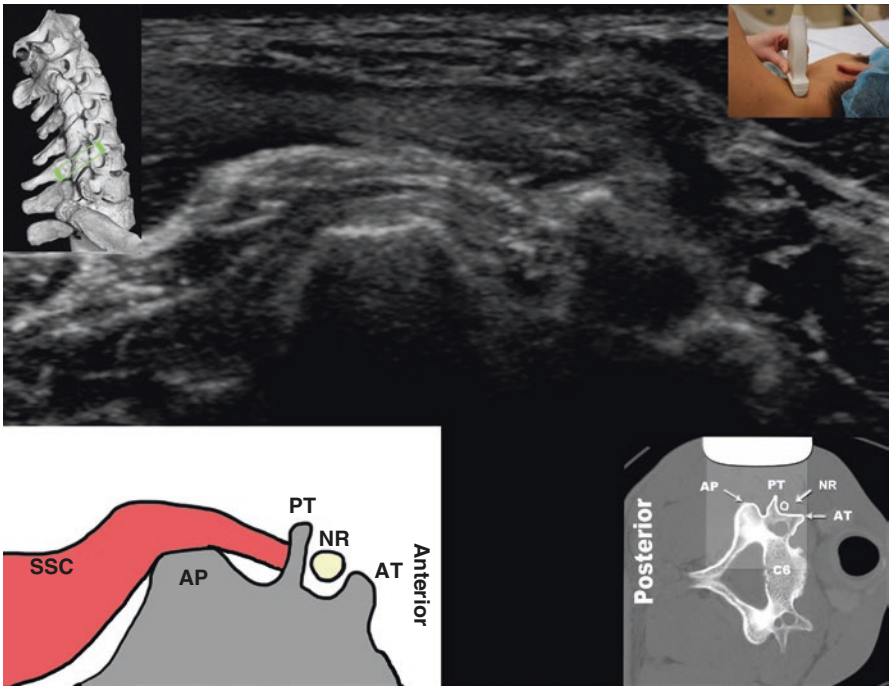

Fig. 13.6 Transverse scan of the cervical spine at the level of C6. (Reprinted with permission from Philip Peng Educational Series)

When performing a cervical medial branch block, the injectate should be deposited along the periosteum of the AP, beneath the SSC.

A useful landmark in the lower cervical spine is the narrow TP of C7, which has no anterior tubercle: this permits its differentiation from the TPs of other cervical levels and the wider square shape of the more posterior T1 TP (Fig. 13.8).

(**a**) The T1 transverse process (T1 TP) can be recognized because of its typical wide and square contour. Further confirmation can be obtained by tilting the probe caudally and imaging the pleura.

(**b**) When scanning cephalad in a transverse plane from T1, the C7 transverse process (C7 TP) can be found anterior to that of T1. Visualizing this posterior to anterior translation (black arrow in upper inset) is a reliable way to identify the C7 TP, which can be differentiated from that of C6 (depicted in Fig. 13.6) because it lacks an anterior tubercle. The brachial plexus (BP), nerve root of C7 (NR) and vertebral artery (VA) can be imaged anterior to the C7 TP.

(**c**) The C7 superior articular process (C7 SAP) is targeted when performing C7 medial branch blocks (black star). It can be found immediately cephalad to the C7 transverse process (TP) and appears as a small hyperechoic line with the C6 inferior articular process (C6 IAP) and C6/C7 joint forming posteriorly. The nerve root of C6 can be seen anteriorly (NR).

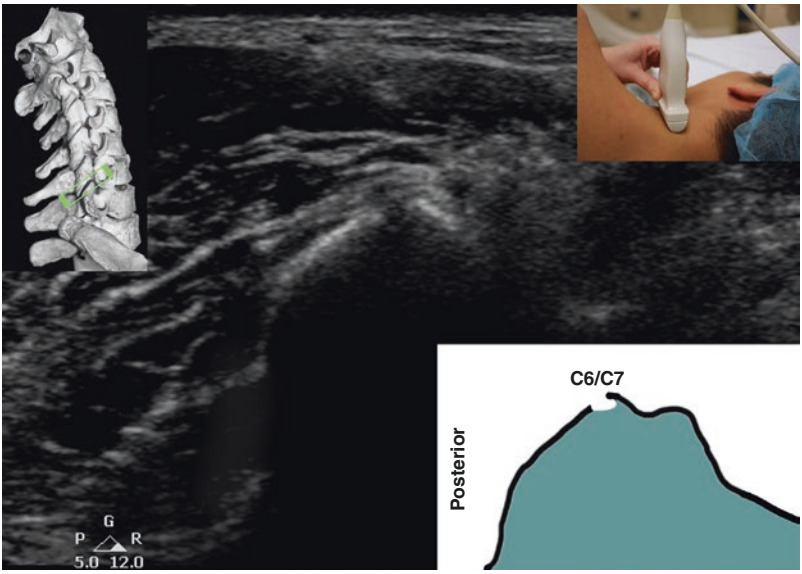

Fig. 13.7 Transverse scan at the level of the (C6/C7) zygapophyseal joint. (Reprinted with permission from Philip Peng Educational Series)

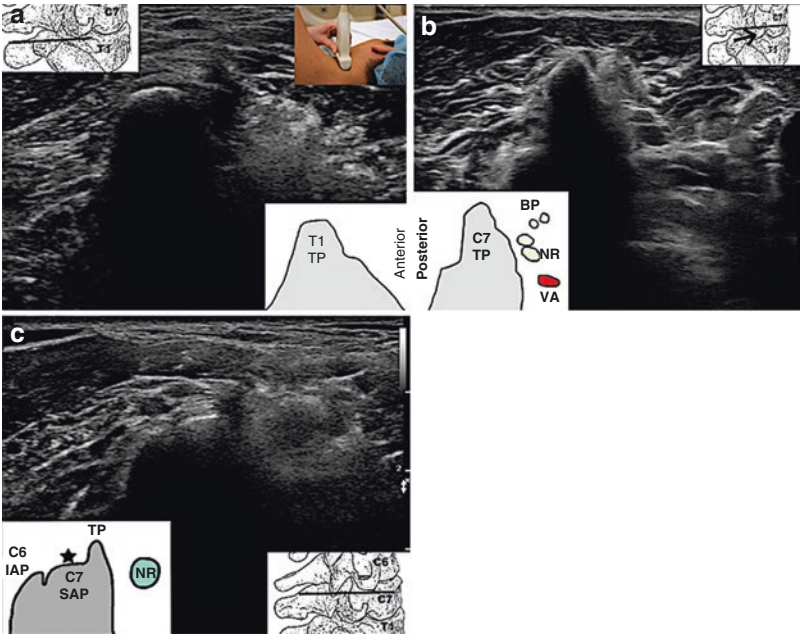

Fig. 13.8 Transverse scan of C7 and T1. (Reprinted with permission from Philip Peng Educational Series)

Procedure

- Needle: 2.5 inch, 22- or 25-gauge block needle
- Drugs: Lidocaine 2%. Volumes used for diagnostic blocks are 0.3 mL (MB C3–C6), 0.6 mL (MB C7) and 0.9 mL (TON). Steroids appear to have limited value when added to local anesthetics for CMBB.

TON, C3, C4 Medial Branches

The neck is first scanned in the coronal plane along the posterior edge of the AP in order to identify the drop-off at the C2–C3 level (Figs. 13.3 and 13.4).

The probe is then rotated to a transverse plane, and the C2–C3 zygapophyseal joint identified for the TON block. A needle (N) is then inserted to the (C2/C3) zygapophyseal joint using an in-plane technique and posterolateral approach (Fig. 13.9).

From this point, the probe is moved caudally to the target points on the C3 and C4 APs.

C5, C6 Medial Branches

The base of the neck is scanned in the transverse plane and the TP of T1 identified. As the probe is moved cephalad from this point, the more anterior TP of C7 is localized (Fig. 13.8), followed by the targets on the AP of C6 and C5 (Figs. 13.6 and 13.10).

(**a**) transverse scan of the lower neck demonstrating a needle (N) that has been placed on the C5 articular pillar (C5) using an in-plane technique and a

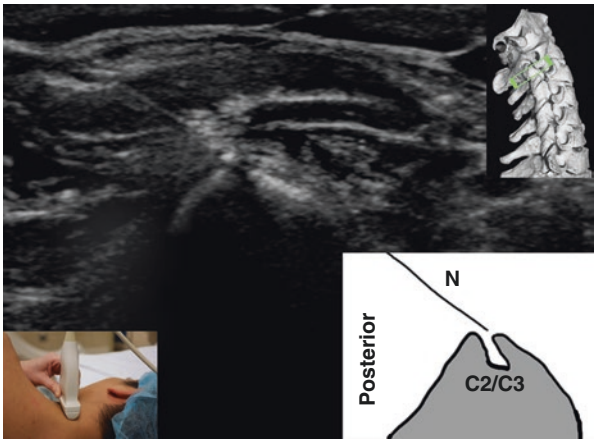

Fig. 13.9 Needle insertion at C2–C3. (Reprinted with permission from Philip Peng Educational Series)

posterolateral approach during the performance of a C5 medial branch block. Posterior tubercle (PT).

(**b**) coronal scan of the needle placement illustrated in (a). The needle (N) can be seen appropriately positioned in the middle of the (C5) articular pillar. The articular pillars of (C3), (C4) and (C6) are also visible, as well as the zygapophyseal joints (black stars).

C7 Medial Branch

The base of the neck is scanned in the transverse plane and the TP of T1 identified. As the probe is moved cephalad from this point, the more anterior TP of C7 is localized (Fig. 13.8). The superior articular process of C7 can be imaged cephalad to the TP of C7 (Fig. 13.8c).

Needle placement after target level has been identified Once the target has been identified in the transverse plane, pressure on the probe is reduced and the color Doppler mode engaged to detect potential blood vessels in the needle path. A posterolateral in-plane approach is used and the needle is advanced until contact with the periosteum (Fig. 13.10a). The probe is then rotated to obtain a coronal scan and the needle confirmed to be in the middle of the targeted AP (Fig. 13.10b).

Returning to a transverse view, LA is then injected under real-time visualization; if necessary, the position of the needle tip is adjusted to obtain an LA spread under the semispinalis capitis muscle that covers the anteroposterior diameter of the AP or joint (TON). The sonogram shows a transverse scan of the lower neck demonstrating a needle (N) that has been placed on the C6 articular pillar (AP) using an in-plane technique and a posterolateral approach during the performance of a C6

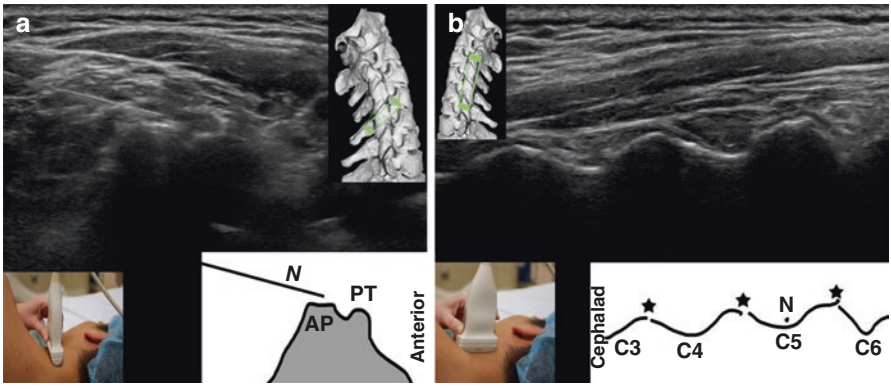

Fig. 13.10 Needle insertion at C5. (Reprinted with permission from Philip Peng Educational Series)

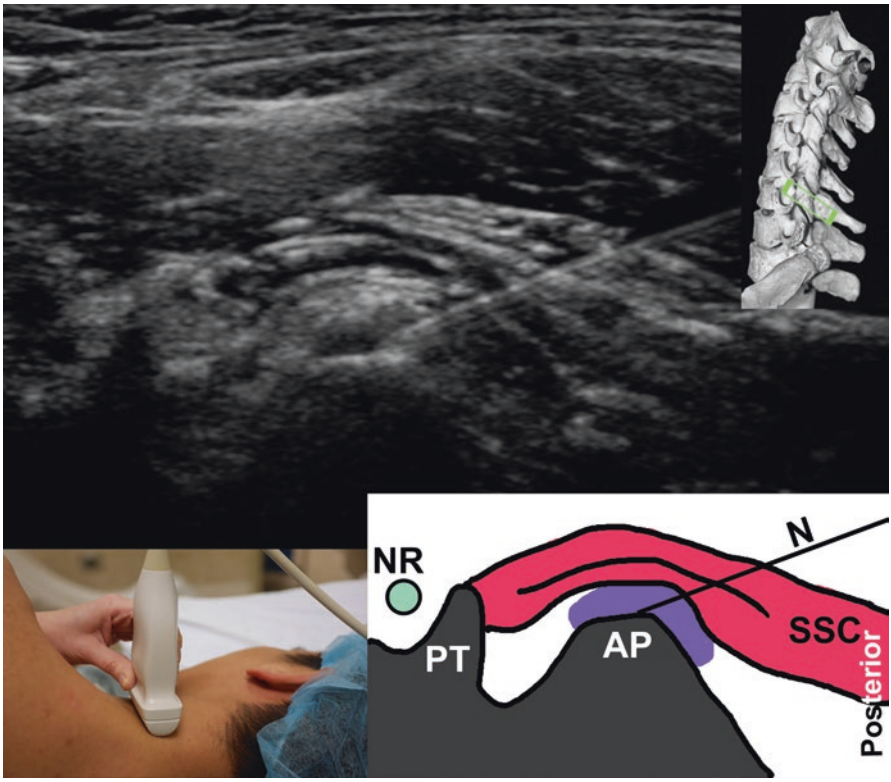

Fig. 13.11 Needle insertion at C6 level. The injectate can be seen spreading under the semispinalis capitis muscle (SSC). Posterior tubercle (PT); nerve root of C6 (NR). (Reprinted with permission from Philip Peng Educational Series)

medial branch block (Fig. 13.11). The injectate can be seen spreading under the semispinalis capitis muscle (SSC).

When performing a TONB, needle placement can be further refined by placing the tip next to the nerve as it can often be imaged near the C2–C3 joint in the coronal plane (Fig. 13.3). The C7 MB, because of its variable anatomy, requires 2 injections, with half the volume deposited on the superior articular process of C7 and the remainder 3 mm lateral to it.

Clinical Pearls

1. An in-plane needle placement using a posterolateral approach is preferred over a needle out-of-plane one, as it allows the operator to avoid blood vessels and reduces the risk of needle misdirection.
2. Using a bi-planar technique (inserting the needle in a transverse plane and confirming its position in a coronal view) is critical to maximize accuracy.

3. Scanning the intended needle path using color Doppler will help identify and avoid vulnerable vessels.
4. The spread of local anesthetic can be evaluated in the coronal plane as it forms a hypoechoic artifact along the articular pillars.
5. When scanning it is important to keep the probe at a 90-degree angle to the sagittal plane in order to properly visualize bony landmarks. In addition, when scanning in the transverse plane, rotating the probe slightly so that it is parallel with the facet joint lines (see left upper inset in Fig. 13.6) will help identify the injection targets on the articular pillars.
6. Tilting the probe caudally in the lower neck to visualize the pleura and tracing the first rib back to the T1 transverse process can help with level identification.
7. Identifying the target for a C7 medial branch blocks (superior articular process of C7) can be difficult if the transverse process occupies the entire cephalocaudal dimension of the articular pillar. In these situations, it may be necessary to inject over the C6/C7 joint.

Literature Review

An emerging body of literature supports the use of ultrasound imaging for CMMBs. Compared to fluoroscopy, the latter provides similar accuracy but reduces performance time and the number of required needle passes. In addition, USG CMBBs are associated with the same short- and long-term clinical effects (pain reduction, improved functional status) as their fluoroscopy-guided counterparts. Although several trials have reported a lower incidence of vascular breach in patients assigned to ultrasound guidance, further prospective studies involving larger numbers of patients are required to determine whether US can reduce procedural complications.

Suggested Reading

Finlayson RJ, Gaurav G, Alhujairi M, Dugani S, Tran DHQ. Cervical medial branch block: a novel technique using ultrasound guidance. Reg Anesth Pain Med. 2012;37:219–23.

Finlayson RJ, Etheridge JP, Vieira L, Gupta G, Tran DQH. A randomized comparison between ultrasound- and fluoroscopy-guided third occipital nerve block. Reg Anesth Pain Med. 2013;38:212–7.

Finlayson RJ, Etheridge JP, Tiyaprasertkul W, Nelems B, Tran DQH. A prospective validation of bi-planar ultrasound imaging for C5-C6 medial branch blocks. Reg Anesth Pain Med. 2014;39:160–3.

Finlayson RJ, Etheridge JP, Tiyaprasertkul W, Nelems B, Tran DQH. A randomized comparison between ultrasound- and fluoroscopy-guided C7 medial branch blocks. Reg Anesth Pain Med. 2015;40:52–7.

Thonnagith A, Elgueta MF, Chalermkitpanit P, Tran DQ, Finlayson RJ. Ultrasound-guided cervical medial branch blocks, a technical review. Int J Phys Med Rehabil. 2016.

Lumbar Medial Branches and L5 Dorsal Ramus

14

Manfred Greher and Philip Peng

Introduction

Low back pain (LBP) is ranked as the single leading cause of disability worldwide. The prevalence rate of chronic low back pain in the United States is 19%, and other industrialized nations reported similar rates, ranging from 13% to 28%. To provide appropriate treatment, a definitive diagnosis of the source of pain is important, although it is not always possible. Potential sources of low back pain are many, but those amenable for treatment include intervertebral discs, nerve roots, facet joints, and sacroiliac joints. The contribution of lumbar facets to low back pain ranges between 25% and 45%. The innervation to the facet joint is the target for diagnostic block and for radiofrequency ablation.

Anatomy

The facet joint of the lumbar spine is a small synovial joint with a joint space of about 1–1.5 mL. Each facet receives dual innervation from the medial branches of the dorsal rami from the same vertebral level and from the vertebral level above. For example, L2–3 facet joint receives innervations from both the L1 and L2 medial branches (Fig. 14.1). The medial branches of the L1–L4 dorsal rami all typically

M. Greher
Department of Anesthesiology, Intensive Care and Pain Therapy, Herz-Jesu Krankenhaus GmbH (Hospital of the Sacred Heart of Jesus), Vienna, Austria

P. Peng (✉)
Department of Anesthesia and Pain Management, Toronto Western Hopsital and Mount Sinai Hospital, University of Toronto, Toronto, Ontario, Canada
e-mail: Philip.peng@uhn.ca

P. Peng et al. (eds.), *Ultrasound for Interventional Pain Management*,
https://doi.org/10.1007/978-3-030-18371-4_14

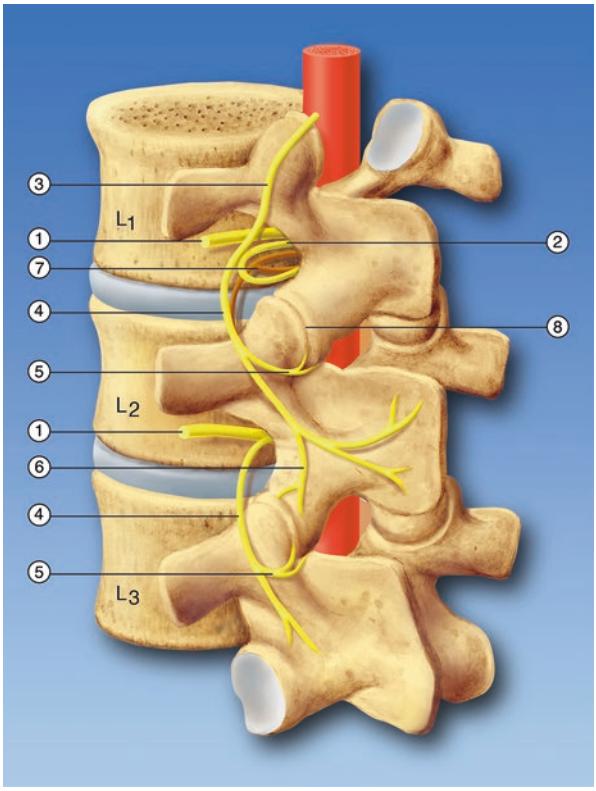

Fig. 14.1 Dual neural supply of the facet joint. Oblique parasagittal view of overlapping segmental innervation of the facet joint. (*1*) Ventral branch of spinal nerve, (*2*) dorsal branch of spinal nerve, (*3*) ascendant branch of dorsal ramus, (*4*) medial branch of dorsal ramus, (*5*) distal branch of medial ramus to facet joint, (*6*) proximal branch of medial ramus to facet joint, (*7*) posterior ramus (sinuvertebral nerve of Luschka), (*8*) facet joint. (Reproduced with permission from Dr. Danilo Jankovic)

cross in a groove formed by the junction of the transverse process (TP) and superior articular process (SAP) of the vertebral level below (e.g., L1 crosses the transverse process of L2).

From there, they run beneath the mamilloaccessory ligament before they innervate the multifidus muscle, interspinous ligament, and the periosteum of the neural arch.

The L5 dorsal ramus differs from the other lumbar dorsal rami, in that it *itself* runs along the junction of the sacral ala and superior articular process of the sacrum and gives off the medial branch only as it reaches the caudal aspect of the L5–S1 zygapophyseal joint. Therefore, the target for injection or ablation at this level is the dorsal rami.

Patient Selection

No clinical or radiological test is specific enough to enable reliable diagnosis of low back pain of facetogenic in origin. Diagnosis of facetogenic pain can only be established by pain reduction and mobility improvement after the local anesthetic blocks.

Pain of facetogenic origin typically presents as unilateral or bilateral back pain with or without nondermatomal leg pain above the knee. Hyperextension and lumbar rotation are often painful in those individuals as well as local paraspinal tender points upon pressure. Motor function and reflexes are usually preserved and straight leg raise test is negative. Referred pain patterns from the upper lumbar joints can extend into the flank, hip, and upper lateral thighs. Groin pain can also be caused by L3–S1 facet joints. In very rare cases, pain from the lower lumbar joints may also extend into the lower lateral leg and even to the foot. The facet joint L5/S1 is the single one most commonly affected. After lumbar stabilization operations, facet joints of the adjacent segments can often be pain generators.

Ultrasound Scanning

- Position: Prone;
- Probe: Curvilinear 2–6 MHz

Five Basic Views

To understand the sonoanatomy of the lumbar spine, one can start with the five basic views of spine sonogram described by Chin, Karmakar, and Peng.

Paramedian Sagittal Transverse Process View

This is a sagittal view but not in the midline (median) but paramedian plane (Fig. 14.2). The transducer is placed 3–5 cm away from the midline. Two to three hyperechoic bone shadows of transverse process (TP) are seen deep to the erector spinae muscle (ESM) with open windows to reveal psoas muscles (PM) deep to TP. Deep to the psoas muscle, the peritoneum (P-indicated by arrows) can be seen.

Paramedian Sagittal Articular Process View

Moving the transducer medially 1–2 cm reveals an image with continuous hyperechoic bone shadow (no gap) from the articular process (AP) (Fig. 14.3).

Paramedian Sagittal Oblique View

Maintaining the transducer in the same position as Fig. 14.3 but tilting it medially will yield a view that reveals the interlaminar window (Fig. 14.4). Through this window, the intrathecal space (ITS) can be seen between the laminae (L). The

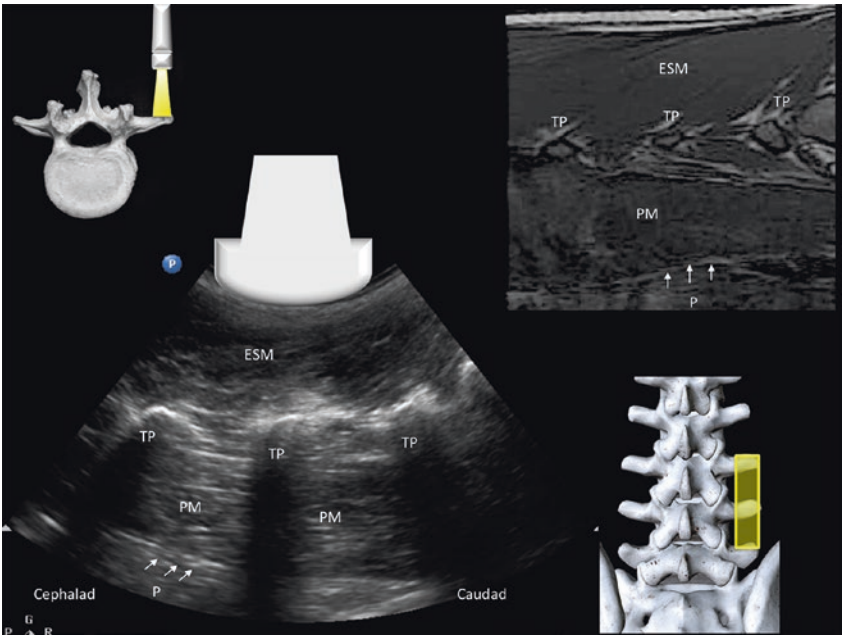

Fig. 14.2 Paramedial sagittal transverse process view. (Reprinted with permission from Philip Peng Educational Series)

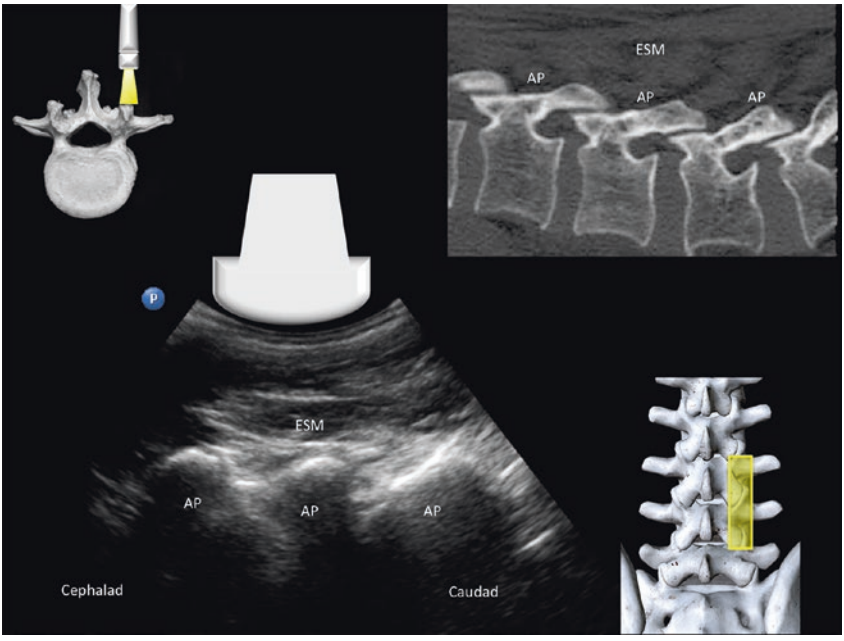

Fig. 14.3 Paramedian sagittal articular process view. (Reprinted with permission from Philip Peng Educational Series)

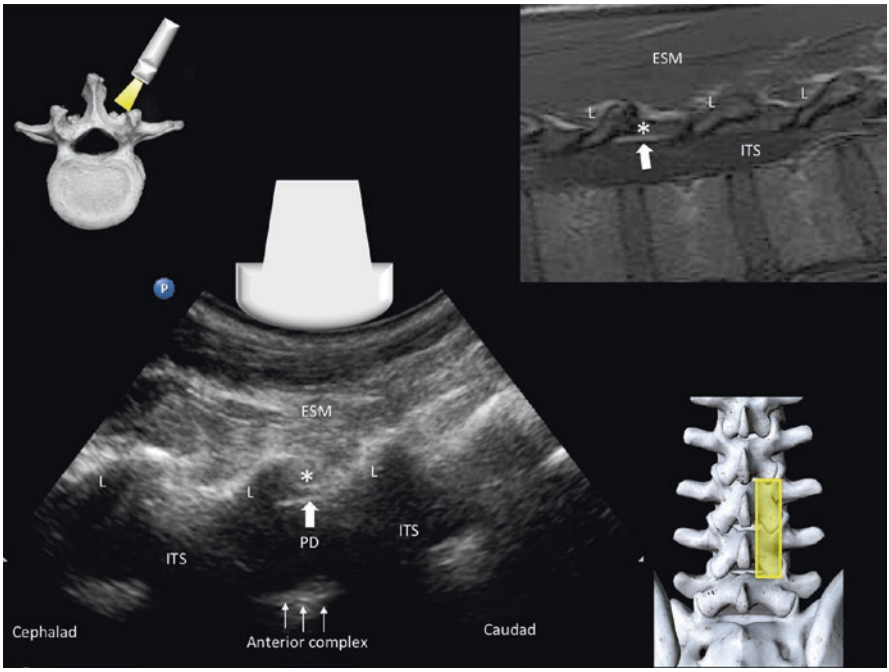

Fig. 14.4 Paramedian sagittal oblique view. (Reprinted with permission from Philip Peng Educational Series)

ligamentum flavum (∗) is usually not clearly seen due to the orientation of the structure relative to the transducer but the posterior dura (PD) can be usually seen clearly in young patient. The other side of the ITS reveals a dense hyperechoic shadow from the posterior cortex of the vertebra, posterior longitudinal ligament, and anterior dura. Since the three structures cannot be differentiated in ultrasound, they are termed anterior complex.

Transverse Spinous Process View

By placing the transducer behind the spinous process (SP), the structures deep in the spine will not be seen (Fig. 14.5).

Transverse Interlaminar View

This is the most useful view (Fig. 14.6). The transducer is placed behind the interspinous ligament (ISL) which allows a window to reveal the intrathecal space (ITS). Typically, inferior articular process (IAP) is closer to the midline than the superior articular process (SAP), the hyperechoic shadow of which is seen

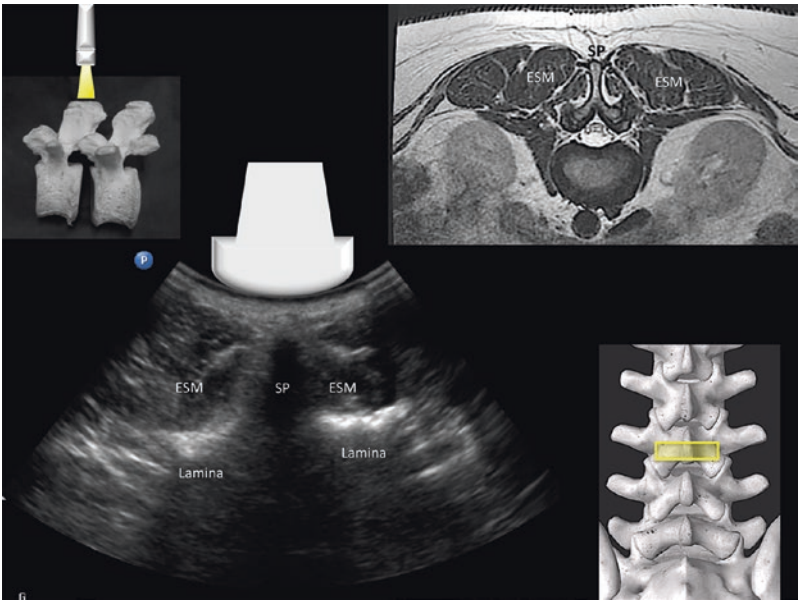

Fig. 14.5 Transverse spinous process view. ESM-erector spinae muscle. (Reprinted with permission from Philip Peng Educational Series)

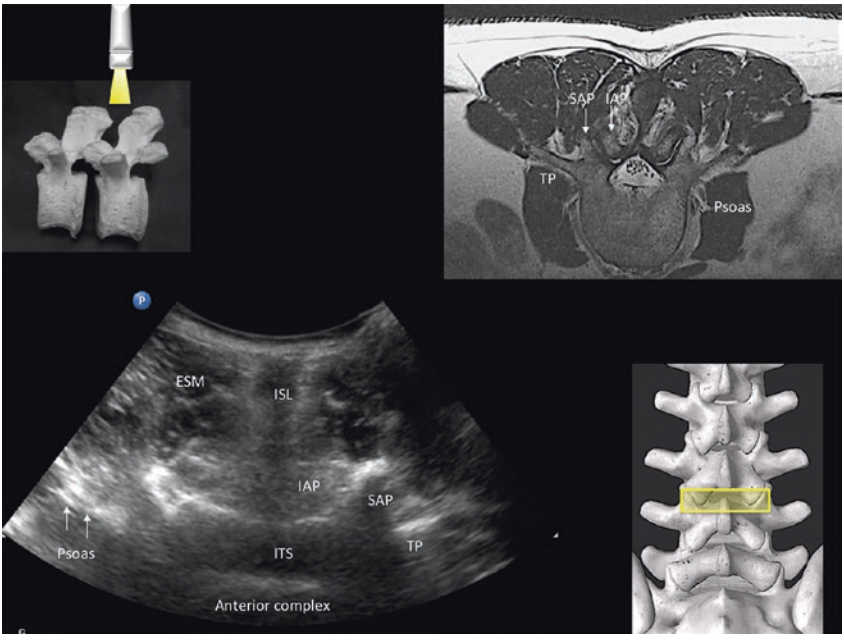

Fig. 14.6 Transverse interlaminar view. (Reprinted with permission from Philip Peng Educational Series)

continuous to the transverse process laterally (right side of Fig. 14.6). Practitioner should be careful in discerning the difference between TP and intertransverse ligament (line arrows) which is the ligament joining the transverse process dorsal to the psoas muscle.

How to Count the Level

- Equipment
- A marking pen
- A towel to wipe the gel before marking (otherwise, the pen cannot mark after used once)

There are two methods. In the authors' opinion, both methods are used to accurately count the level.

Method 1 Sagittal View

First, the interlaminar levels are indicated with paramedian sagittal oblique view including the sacrum (upper right). The interlaminar levels are then marked on the skin (yellow lines) (Fig. 14.7).

Second, the paramedian sagittal transverse process view is obtained (lower right). The transverse process are counted and marked on the skin (red lines). The cephalad level of the sacrum is also marked. Quite often, there is a gap in the sacrum and practitioner may mistake that as the L5S1 junction. This is first sacral foramen (S1) (Reprinted with permission from Philip Peng Educational Series).

Method 2 Transverse View

Transverse scan is used throughout the counting (Fig. 14.8). The transducer is placed close the posterior superior iliac spine (PSIS) and a typical transverse view of sacrum with median crest (MC) in the midline is revealed (yellow line).

Moving the transducer in cephalad direction will reveal the intrathecal space (ITS) and dura. This is the L5S1 (orange line).

Moving the transducer further cephalad and lateral, a transverse interlaminar view with transverse process and superior articular process (TP & SAP) is revealed (red line).

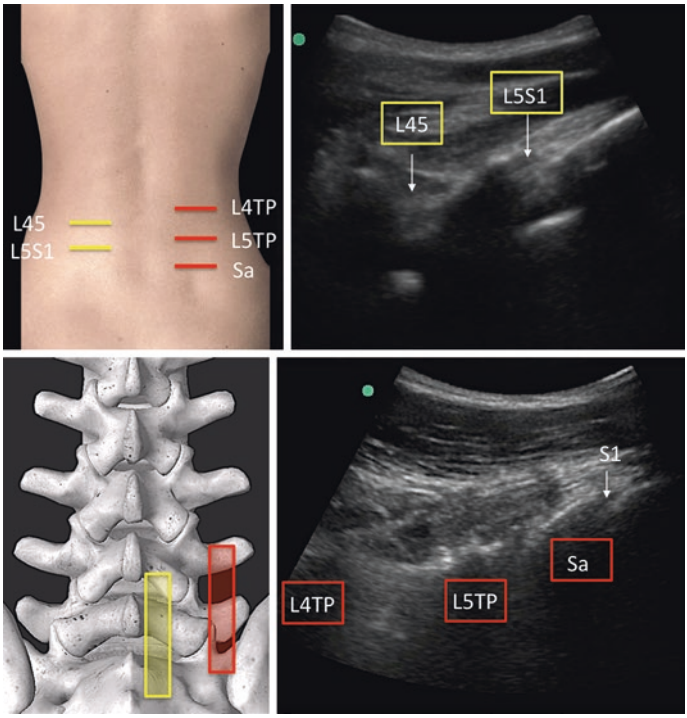

Fig. 14.7 Spine counting in sagittal view. (Reprinted with permission from Philip Peng Educational Series)

Determining the Target for Medial Branch L1–4

The target for medial branch is the junction of SAP with the cephalad border of TP. The most important exercise here is to understand the sonographic feature of transverse process (TP) and how to determine the most cephalad border (Fig. 14.9). TP is bone and cast an anechoic shadow deep in the scan (orange line and box). If one is not sure, move the transducer cephalad and one can tell the difference. In between the transverse process, a bright hyperechoic line can be cast by the inter-transverse ligament and the fascia overlying the psoas. However, it allows the psoas to be seen (red line and box). Mistaking the later shadow with TP allows the needle to advance to the foramen.

Determining the Target for L5 Dorsal Ramus

First, perform the paramedian sagittal transverse process view to determine the cephalad part of sacrum (Fig. 14.10a).

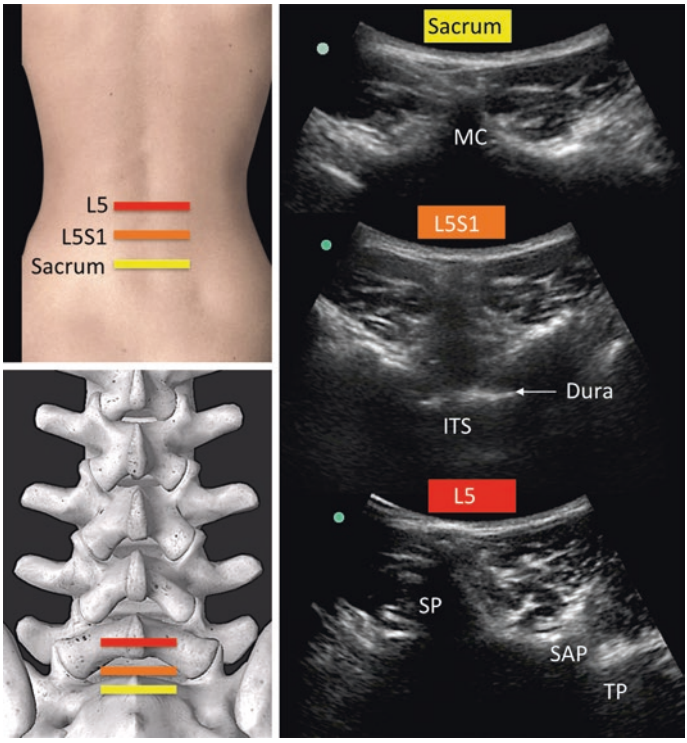

Fig. 14.8 Spine counting in transverse view. (Reprinted with permission from Philip Peng Educational Series)

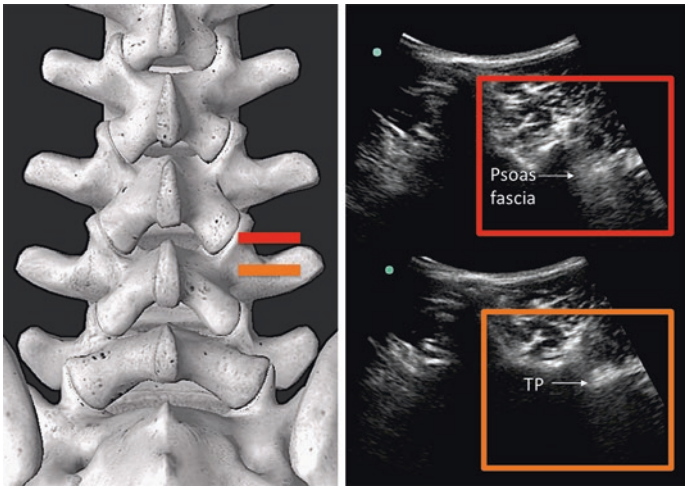

Fig. 14.9 Determination of transverse process. (Reprinted with permission from Philip Peng Educational Series)

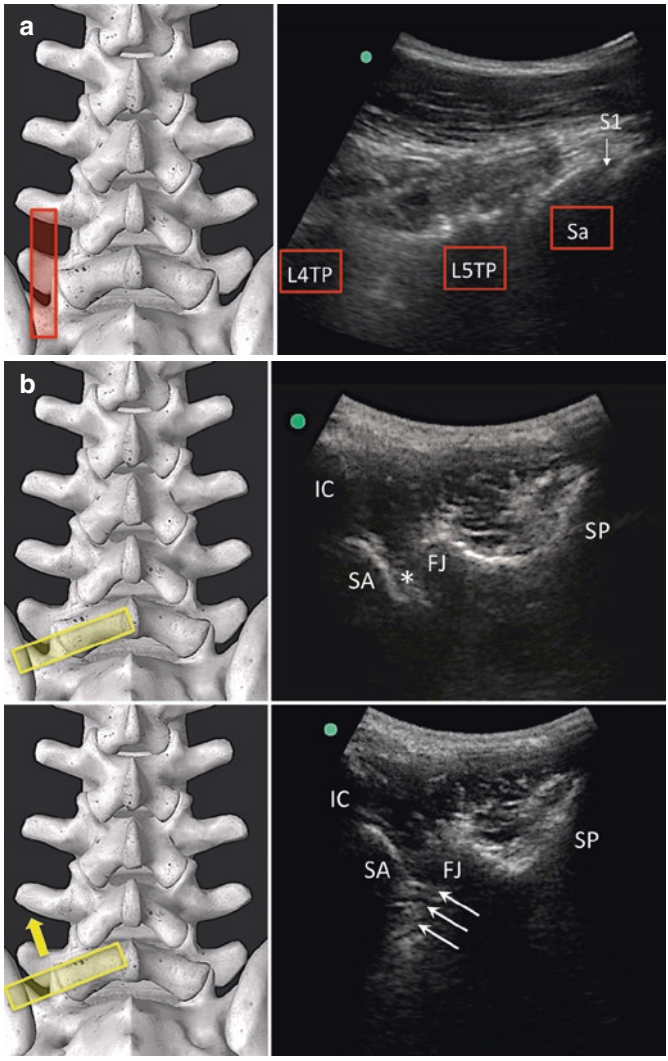

Fig. 14.10 (**a**) Paramedian sagittal transverse process of lumbosacral junction. (**b**) Oblique view of lumbosacral junction. (Reprinted with permission from Philip Peng Educational Series)

Second, rotate the transducer approximately 90 degrees with the medial part slightly cephalad to the lateral part (upper part of Fig. 14.10b). This results in a view with all the necessary bony landmarks in a continuous hyperechoic line. They are (from medial to lateral) spinous process (SP) of L5, facet joint (FJ), sacral ala (SA), and iliac crest (IC). The junction between the SA and FJ is the target. To make sure the transducer is at the right location, simply move the transducer in cephalad position (lower part of Fig. 14.10b). A discontinuation of the hyperechoic shadow will appear (line arrows).

Procedure

Equipment and Drugs

- Needles: 22G, 8 cm echogenic needle
- Drugs: 1 ml of local anesthetic (0.25% plain bupivacaine or 1% plain lidocaine)

Lumbar Medial Branch (L1–4) Block

First, in-plane needle (arrow) approach from lateral to medial with the tip (asterisk) at the upper edge of the transverse process (TP) in the groove just lateral to the superior articular process of the adjacent facet joint (FJ) (Fig. 14.11).

Second, rotate the transducer to the paramedian sagittal transverse process view to check the needle (arrow) at the target point (asterisk), which should be at the cephalad edge of the transverse process (TP) (Fig. 14.12).

L5 Dorsal Ramus Block

First, the needle is inserted with an oblique out-of-plane (arrow) approach with the tip (asterisk) at the upper edge of the sacral ala (SA) medial to the iliac crest (IC) in the groove just lateral to the superior articular process of the L5/S1 facet joint (FJ) (Fig. 14.13).

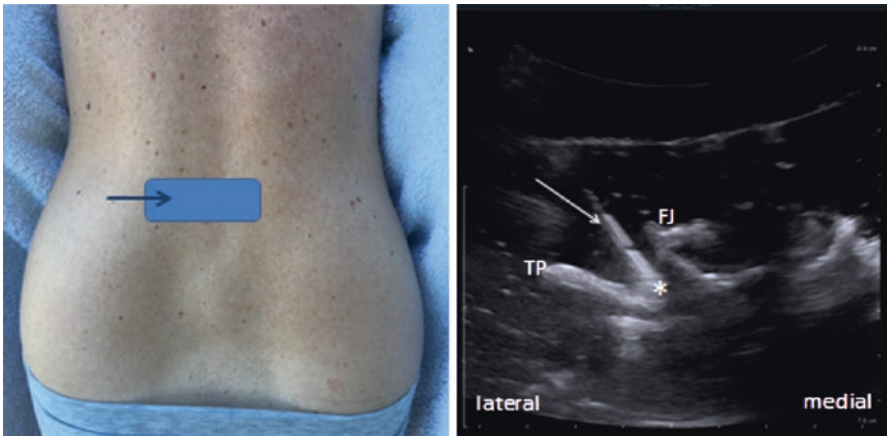

Fig. 14.11 Needle insertion at the target. (Reprinted with permission from Philip Peng Educational Series)

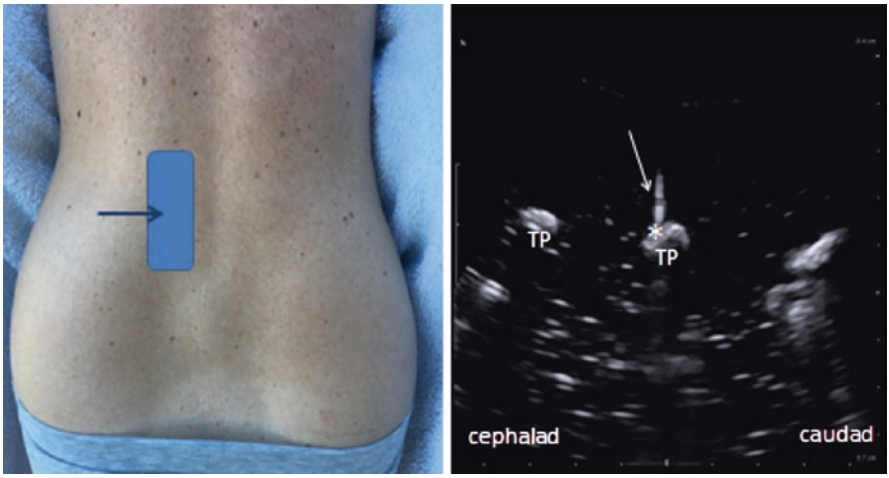

Fig. 14.12 Checking the needle position in the paramedian sagittal transverse process view. (Reprinted with permission from Philip Peng Educational Series)

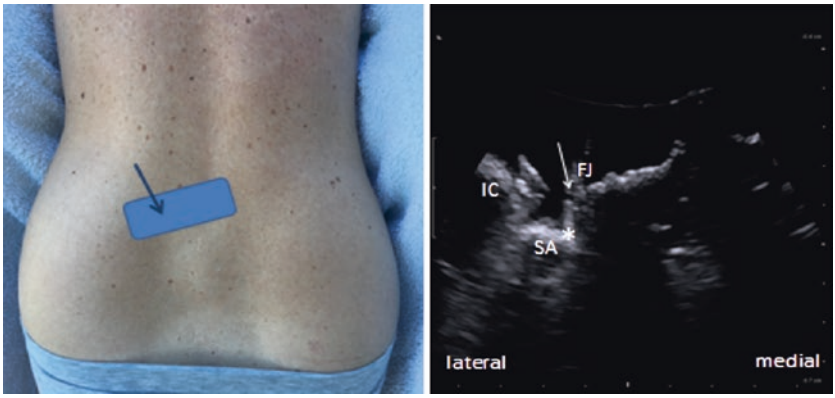

Fig. 14.13 Needle insertion for the L5 dorsal ramus block. (Reprinted with permission from Philip Peng Educational Series)

Second, the ultrasound transducer is placed in paramedian sagittal transverse process view to check the needle position (arrow) at the target point (asterisk),which should be at the cephalad edge of the sacrum ala (SA) caudal to the transverse process of L5 (TP) (Fig. 14.14).

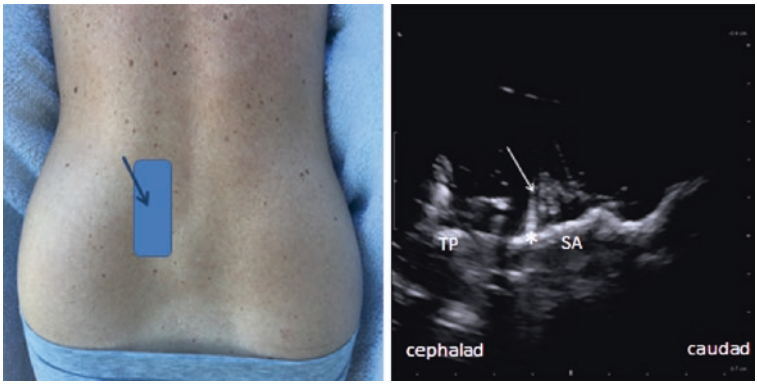

Fig. 14.14 Confirming the needle position with paramedian sagittal view. (Reprinted with permission from Philip Peng Educational Series)

Clinical Pearls

1. Before the use of ultrasound guide facet nerve injection, always check the X-rays to account for lumbarization or sacralization (important for counting) and the presence of spondylolisthesis (which affect the accuracy of target localization).
2. Select your patient. The accuracy of the block under ultrasound guidance substantially diminished when the body mass index is high.
3. Always use sterile covered curvilinear probes with appropriate focus zone setting and optimal frequency as possible. A small footprint probe can be advantageous for the procedure.
4. For lumbar medial branch block, after needle placement with an in-plane technique, always try to verify the correct needle tip position on the cephalad part of the transverse process by turning the transducer 90 degrees in long axis of the spine.
5. The best way to be sure that you are seeing the most cephalad part of the transverse process is to move the transducer further cephalad to find the psoas muscle and intertransverse ligament. Mistaking the intertransverse ligament as transverse process may lead to needle entry to the neuroforamen.
6. While observing the needle entry in plane to the junction of SAP to TP, failure to have bony contact when the needle tip reaches the junction signifies that the needle and the transducer are not in the same plane.
7. For L5 dorsal ramus block, after needle placement with an oblique out-of-plane technique, rotate the transducer 90 degrees in long axis to the spine to verify correct needle tip position, which is the cephalad part of the sacrum.
8. Always check for vessels with Power Doppler and observe volume spread at the needle tip during injection.

Literature Review

Lumbar medial branch and L5 dorsal ramus blocks are mainly performed for diagnostic purposes to select patients for radiofrequency denervation. This is the reason why volumes of 1 ml or lower are used to achieve the necessary specificity. It is recommended to perform repeated test blocks because single blocks have a very high false-positive rate up to one third of the cases. A concordant response on a short (lidocaine)- and long (bupivacaine)-acting local anesthetic with 80% pain reduction is an excellent predictor for subsequent successful radiofrequency procedures, while diagnostic intraarticular injections show a little lower correlation. Ultrasound-guided lumbar medial branch blocks have initially been described by our study group in 2004 followed by a publication of a special technique for the L5 dorsal ramus block in 2015. Clinical studies with fluoroscopy or CT scan control supported the feasibility and high accuracy of the medial branch block, especially in nonobese patients. Increased bed-side and office practicability, availability at remote locations as well as total avoidance of ionizing radiation are clear advantages of ultrasound compared to fluoroscopy. Radiofrequency denervation (cooled tip) has been shown to be feasible under ultrasound guidance combined with magnetic positioning in one cadaver study so far. Therefore, the ultrasound-guided technique serves as an alternative to fluoroscopy-guided one for diagnostic block only.

Suggested Reading

Chin KJ, Karmakar MK, Peng PWH. Ultrasonography of the adult thoracic and lumbar spine for central neuraxial blockade. Anesthesiology. 2011;114:1459–85.

Cohen SP, Raja SN. Pathogenesis, diagnosis, and treatment of lumbar zygapophysial (facet) joint pain. Anesthesiology. 2007;106:591–614.

Gofeld M, Brown MN, Bollag L, Hanlon JG, Theodore BR. Magnetic positioning system and ultrasound guidance for lumbar zygapophysial radiofrequency neurotomy: a cadaver study. Reg Anesth Pain Med. 2014;39:61–6.

Greher M, Scharbert G, Kamolz LP, et al. Ultrasound-guided lumbar facet nerve block: a sonoanatomic study of a new methodologic approach. Anesthesiology. 2004a;100:1242–8.

Greher M, Kirchmair L, Enna B, et al. Ultrasound-guided lumbar facet nerve block: accuracy of a new technique confirmed by computed tomography. Anesthesiology. 2004b;101:1195–200.

Greher M, Moriggl B, Peng PW, Minella CE, Zacchino M, Eichenberger U. Ultrasound-guided approach for L5 dorsal ramus block and fluoroscopic evaluation in unpreselected cadavers. Reg Anesth Pain Med. 2015;40(6):713–7.

Han SH, Park KD, Cho KR, Park Y. Ultrasound versus fluoroscopy-guided medial branch block for the treatment of lower lumbar facet joint pain: a retrospective comparative study. Medicine (Baltimore). 2017;96(16):e6655.

Jung H, Jeon S, Ahn S, Kim M, Choi Y. The validation of ultrasound-guided lumbar facet nerve blocks as confirmed by fluoroscopy. Asian Spine J. 2012;6:163–7.

Rauch S, Kasuya Y, Turan A, Neamtu A, Vinayakan A, Sessler DI. Ultrasound-guided lumbar medial branch block in obese patients: a fluoroscopically confirmed clinical feasibility study. Reg Anesth Pain Med. 2009;34:340–2.

Schwarzer AC, Aprill CN, Derby R, Fortin J, Kine G, Bogduk N. Clinical features of patients with pain stemming from the lumbar zygapophysial joints. Is the lumbar facet syndrome a clinical entity? Spine. 1994a;19:1132–7.

Schwarzer AC, Aprill CN, Derby R, Fortin J, Kine G, Bogduk N. Clinical features of patients with pain stemming from the lumbar zygapophysial joints. Is the lumbar facet syndrome a clinical entity? Spine (Phila Pa 1976). 1994b;19:1132–7.

Shim JK, Moon JC, Yoon KB, Kim WO, Yoon DM. Ultrasound-guided lumbar medial-branch block: a clinical study with fluoroscopy control. Reg Anesth Pain Med. 2006;31:451–4.

Turk DC, Theodore BR. Epidemiology and economics of chronic and recurrent pain. In: Lynch ME, Craig K, Peng PWH, editors. Clinical pain management: a practical guide. Oxford: Wiley-Blackwell; 2011. p. 6–13.

Vos T, Flaxman AD, Naghavi M, et al. Years lived with disability (YLDs) for 1160 sequelae of 289 diseases and injuries 1990-2010: a systematic analysis for the Global Burden of Disease Study 2010. Lancet. 2012;380(9859):2163–96.

Sacroiliac Joint and Sacral Lateral Branch Blocks

15

Roderick Finlayson and María Francisca Elgueta Le-Beuffe

Abbreviations

FL	Fluoroscopic guidance
PSN	Posterior sacral neural network
SIJ	Sacroiliac joint
SLB	Sacral lateral branch
USG	Ultrasound guidance

Introduction

Indication

Sacroiliac joint and sacral lateral branch blocks are used for the management of SIJ and posterior complex pain, respectively.

Anatomy

The SIJ is innervated anteriorly by the anterior rami of L4 and L5, whereas a PSN, which originates from the S1 to S3 levels (and occasionally the S4 and L5 levels), supplies the dorsal aspect of the SIJ. Most of the nerves contributing to the PSN cross the lateral sacral crest between the second and third transverse sacral tubercles; however a superior lateral branch can also innervate the SIJ at the S1 level in

R. Finlayson (✉)
Alan Edwards Pain Management Unit, McGill University Health Centre, Montreal, Quebec, Canada

M. F. E. Le-Beuffe
Department of Anesthesia, Pontificia Universidad Católica de Chile, Santiago, Chile

P. Peng et al. (eds.), *Ultrasound for Interventional Pain Management*,
https://doi.org/10.1007/978-3-030-18371-4_15

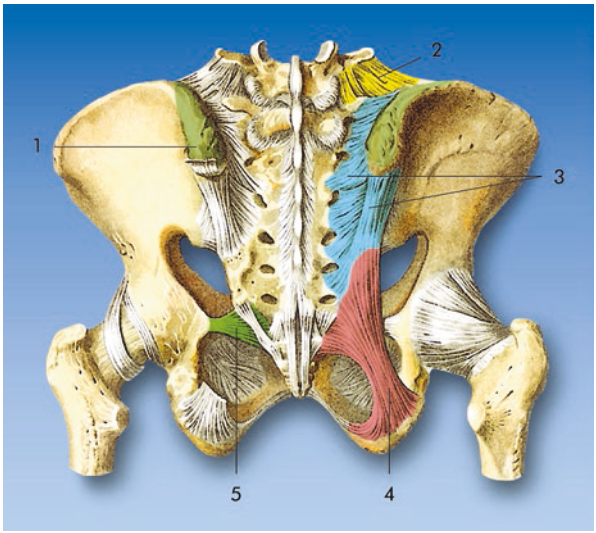

Fig. 15.1 Illustration of the posterior sacral ligaments: posterior superior iliac spine (1); iliolumbar ligament (2); interosseous and dorsal sacroiliac ligaments (3); sacrotuberous ligament (4); sacrospinous ligament (5). (Reprinted with permission from Dr. Danilo Janovic)

up to 40% of subjects. Sacral lateral branches are increasingly targeted for the treatment of posterior complex pain, which involves the dorsal ligaments as well as the posterior aspect of the joint itself (Fig. 15.1).

Patient Selection

The SIJ plays a causative role in up to 30% of patients with chronic low back pain. Afflicted patients will typically have back pain below the L5 level with radiation to the buttocks or lower extremities. Provocative physical exam tests can be used to identify likely candidates, and the findings of 3 or more positive tests have been found to have a modest predictive power (sensitivity 91%, specificity 78%) in relation to controlled comparative SIJ blocks. Key tests include distraction, compression, thigh thrust, Gaenslen's, sacral thrust, and Patrick's FABER. However, their ability to detect posterior complex pain has not been evaluated.

Ultrasound Scanning

- Probe: C5-2 MHz curved transducer.
- Position: prone

Transverse Plane Scan

This is the primary view for procedures targeting the SIJ. Accurate identification of the various landmarks depends on a methodical scan which begins at the sacral hiatus and progresses cephalad to the posterior S1 foramen (Fig. 15.2).

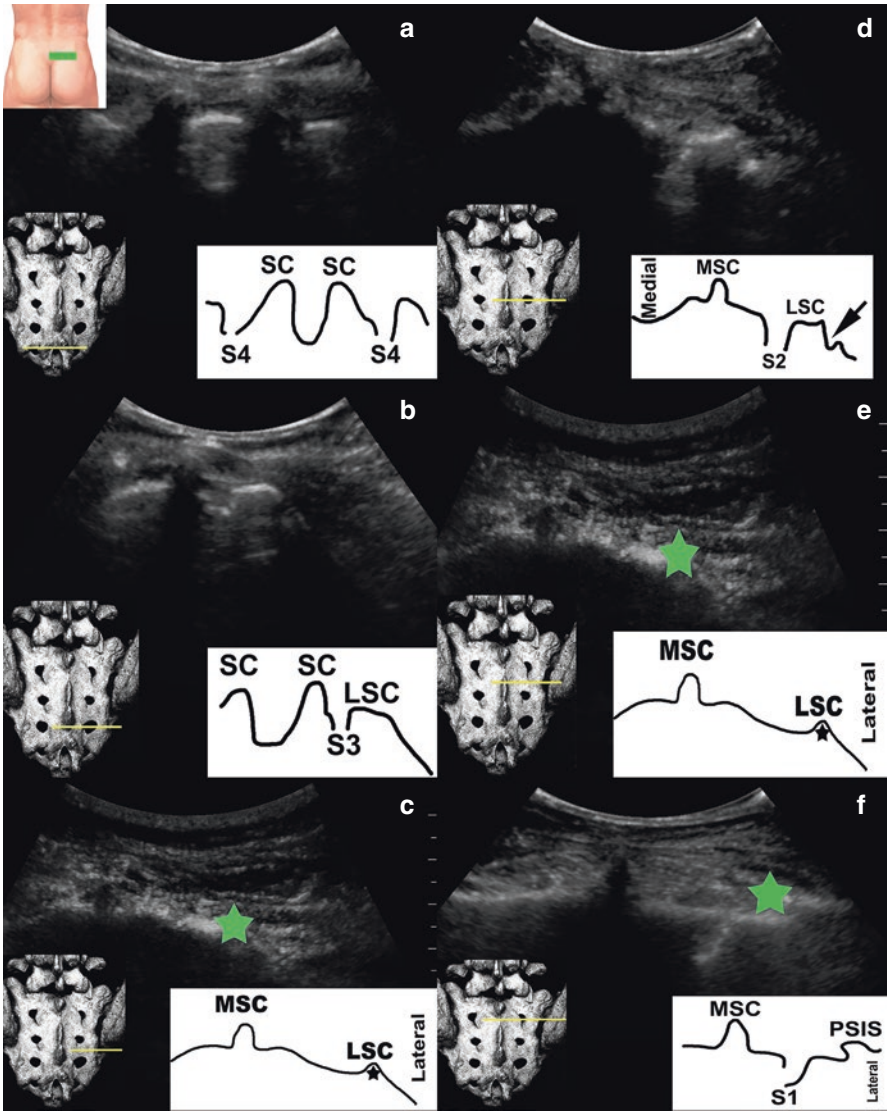

Fig. 15.2 Sonographic images of the posterior sacrum depicting the various views required for the performance of an ultrasound-guided sacral lateral branch block. The three injection points on the sacral lateral crest are marked by a star (★); probe placement on the skin surface is illustrated in the upper left inset of panel (**a**); scan lines are illustrated on a skeletal model in the left lower insets. (**a**) transverse sonographic view of the lower sacrum demonstrating the sacral cornu (SC) and posterior foramen of S4 (S4); (**b**) sacral cornu (SC), posterior foramen of S3 (S3), lateral sacral crest (LSC); (**c**) median sacral crest (MSC), lateral sacral crest (LSC), yellow star indicates injection target; (**d**) median sacral crest (MSC), posterior foramen of S2 (S2), lateral sacral crest (LSC), black arrow indicates caudal aspect of sacroiliac joint; (**e**) median sacral crest (MSC), lateral sacral crest (LSC), yellow star indicates injection target; (**f**) median sacral crest (MSC), posterior foramen of S1 (S1), yellow star indicates injection target, posterior superior iliac spine (PSIS). (Reprinted with permission from Philip Peng Educational Series)

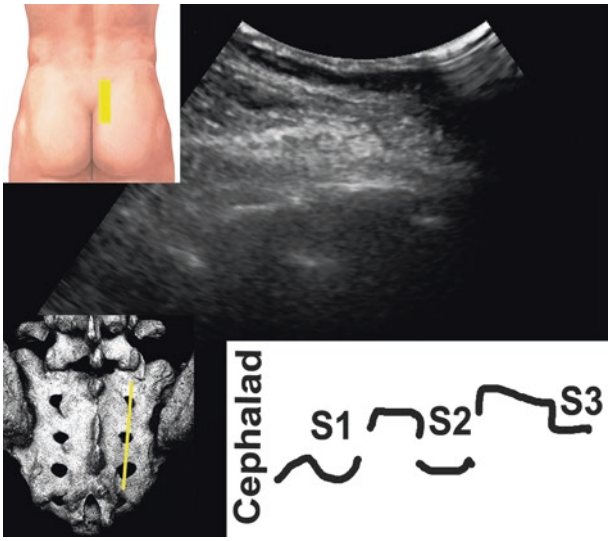

Fig. 15.3 Parasagittal scan of the sacrum demonstrating the posterior sacral foramen. This view is used to confirm needle placement. Probe placement on the skin surface is illustrated in the upper left inset. The posterior foramen of S1, S2, and S3 are visible. (Reprinted with permission from Philip Peng Educational Series)

Sagittal Plane Scan

This view is used for needle placement verification during SLB block procedures (Fig. 15.3).

Procedure

- Needle: 3.5 inch, 22- or 25-gauge block needle
- Drugs: 2% lidocaine

Sacroiliac Joint Block

The lower third of the SIJ is identified at the level of S2 by scanning cephalad from the sacral hiatus (Fig. 15.2a–d) and a needle is then advanced into the joint cleft (Fig. 15.4). The choice of technique (in-plane medial to lateral or out-of-plane) is determined by the optimal angle of approach. Volumes of 2–4 mL of a mixture of local anesthetic and steroid are typically injected. In addition, color duplex Doppler can be used to facilitate visualization of the injectate and confirm spread in the joint cleft (Fig. 15.4b).

Sacral Lateral Branch Blocks

Key landmarks are identified by scanning the sacrum in the transverse plane, cephalad from the sacral hiatus (Fig. 15.2). Three injections of local anesthetic are performed on the sacral lateral crest by advancing the needle in-plane from a medial to

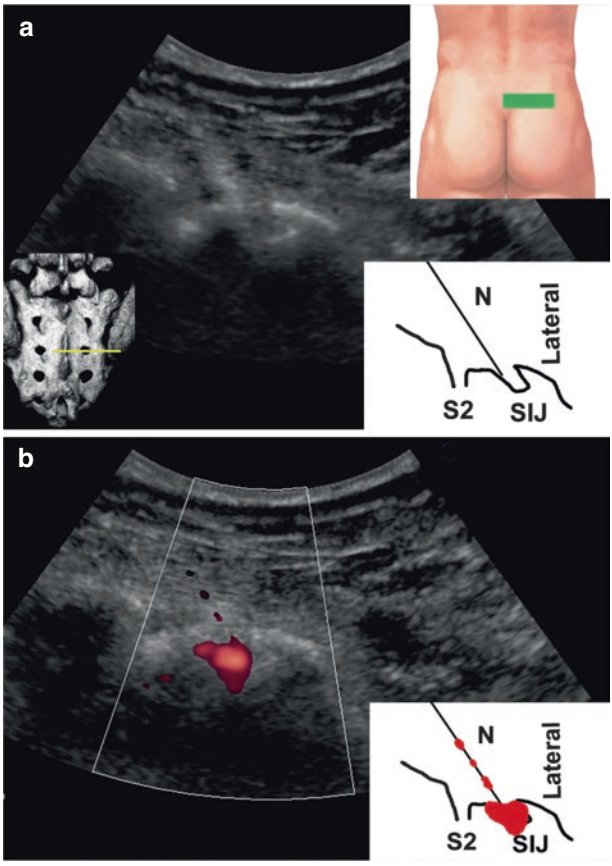

Fig. 15.4 Needle placement for a sacroiliac joint injection. (**a**) right upper inset illustrates the probe placement on the skin surface; left lower inset illustrates the scan line on a skeletal model. Needle (N), S2 posterior foramen (S2), sacroiliac joint (SIJ). (**b**) color duplex Doppler scan during injection demonstrating spread of injectate in the joint cleft. Reprinted with permission from Philip Peng Educational Series

lateral direction: 1.5 mL between S2 and S3, 0.5 mL between S2 and S3, and 0.5 mL lateral to S1. After each needle placement, a sagittal scan is performed to confirm needle position in the cephalocaudal dimension (Fig. 15.3).

Clinical Pearls

1. If an eventual SLB radiofrequency ablation procedure is being contemplated, a SLB block may be of greater value than an SIJ block, as the latter can also relieve pain originating from the anterior joint and is therefore not diagnostic of posterior complex pain.
2. Greater attention to needle placement technique is required above S2, as sacral angulation can significantly increase skin to target distance.
3. The posterior sacral foramina can be confused with the more lateral SIJ cleft, particularly at the S2 level. Further confirmation can be sought by scanning cephalad in the transverse plane and identifying the posterior

superior iliac spine. The SIJ cleft should be visible immediately below its inferior border, whereas the S2 foramen is found more medially.
4. Vascular breach is a common occurrence during injection procedures targeting the sacral area and can be prevented by identifying vulnerable vessels in the projected needle path using duplex color Doppler.
5. A prominent median sacral crest can hinder needle placement and require a more lateral needle insertion point and a steeper angle of approach.

Literature Review

Ultrasound-guided and fluoroscopically guided sacroiliac joint injections have been compared in two randomized controlled trials (RCT). A first study by Jee et al. found that USG provided lower accuracy than fluoroscopy (87.3% vs 98.2%, respectively), but no intergroup differences were found in measures of pain and disability over a 3-month follow-up period. Echoing these findings, Soneji et al. found a lower, but not statistically significant, difference in the incidence of intraarticular spread in the USG group (50% vs 65% for FL) and similar improvement in post-block clinical measures. A single RCT has compared USG SLB blocks to the FL multisite multi-depth technique. Finlayson et al. found that USG was associated with significantly shorter performance time, fewer needle passes, and a lower incidence of vascular breach, while providing the same analgesic effect.

Suggested Reading

Cohen SP, Chen Y, Neufeld NJ. Sacroiliac joint pain: a comprehensive review of epidemiology, diagnosis and treatment. Expert Rev Neurother. 2013;13:99–116.

Finlayson RJ, Etheridge JP, Elgueta MF, Thonnagith A, Nelems B, Tran DQH. A randomized comparison between ultrasound- and fluoroscopy-guided sacral lateral branch blocks. Reg Anesth Pain Med. 2017;42:400–6.

Jee H, Lee JH, Park KD, Ahn J, Park Y. Ultrasound-guided versus fluoroscopy-guided sacroiliac joint intra-articular injections in the noninflammatory sacroiliac joint dysfunction: a prospective, randomized, single-blinded study. Arch Phys Med Rehabil. 2014;95:330–7.

King W, Ahmed SU, Baisden J, Patel N, Kennedy DJ, MacVicar J, Duszynski B. Diagnosis and treatment of posterior sacroiliac complex pain: a systematic review with comprehensive analysis of the published data. Pain Med. 2015;16:257–65.

Roberts SL, Burnham RS, Ravichandiran K, Agur AM, Loh E. Cadaveric study of sacroiliac joint innervation: implications for diagnostic blocks and radiofrequency ablation. Reg Anesth Pain Med. 2014;39:456–64.

Soneji N, Bhatia A, Seib R, Tumber P, Dissanayake M, Peng PW. Comparison of fluoroscopy and ultrasound guidance for sacroiliac joint injection in patients with chronic low back pain. Pain Pract. 2016;16:537–44.

Sacroiliac Joint Radiofrequency Ablation

16

Eldon Loh and Robert S. Burnham

Introduction

When pain originating from the sacroiliac joint is inadequately managed by other modalities (e.g., sacroiliac joint intra-articular injection), radiofrequency ablation may be a reasonable option for relief. Radiofrequency ablation interrupts the transmission of nociceptive signals to the central nervous system through the denervation of putative pain generating structures, such as the sacroiliac joint.

Anatomy

Posteriorly, the sacroiliac joint is innervated by the posterior sacral network (PSN), which is formed by nerves originating from the lateral branches of the first through third sacral roots, with occasional contributions from the L5 dorsal ramus and the S4 sacral root (Fig. 16.1).

E. Loh (✉)
Department of Physical Medicine and Rehabilitation, Schulich School of Medicine and Dentistry, Western University, London, ON, Canada

Parkwood Institute, St. Joseph's Health Care London, London, ON, Canada
e-mail: eldon.loh@sjhc.london.on.ca

R. S. Burnham
Central Alberta Pain & Rehabilitation Institute, Lacombe, AB, Canada

P. Peng et al. (eds.), *Ultrasound for Interventional Pain Management*,
https://doi.org/10.1007/978-3-030-18371-4_16

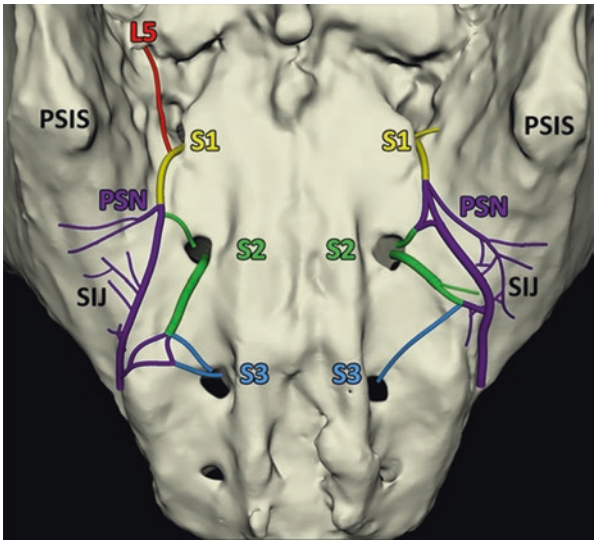

Fig. 16.1 Posterior innervation of the sacroiliac joint from the posterior sacral network. S1, S2, and S3 indicate the S1, S2, and S3 posterior sacral foramen. The lateral branches from these levels (S1, yellow; S2, green; and S3, blue) contribute to the posterior sacral network (purple). Occasionally, a branch from the L5 dorsal ramus (red) and/or the S4 lateral branches (not pictured) also contribute to the network. (Reprinted with permission from Wolters Kluwer Health, Inc.)

The PSN courses over the periosteum and traverses the lateral sacral crest, primarily between the second and third transverse sacral tubercles. In some cases, an S1 lateral branch contributes directly to the innervation of the joint (Fig. 16.2).

Patient Selection

Sacral lateral branch blocks are preferred over intraarticular sacroiliac joint injections when selecting patients for radiofrequency ablation, as the latter targets structures not innervated by the PSN. Eligible patients should demonstrate at least 50% pain relief after the block.

Ultrasound Scanning

- Probe: C5-2 MHz curved transducer.
- Position: prone

A transverse scan of the sacrum is performed in a caudad to cephalad direction to identify transverse sacral tubercles (TST) 1–4 which serve as landmarks during radiofrequency lesioning procedures of the PSN (Fig. 16.3).

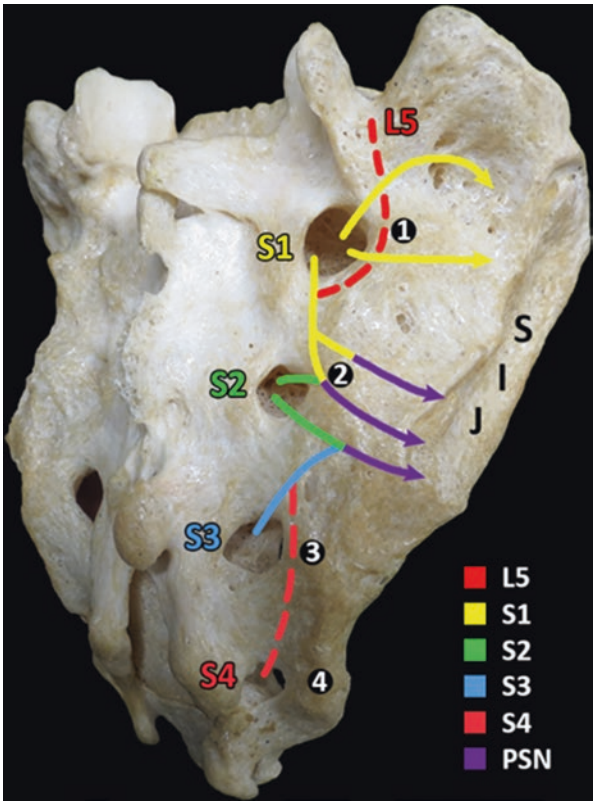

Fig. 16.2 Model illustrating the course of the posterior innervation (lateral branches of S1 – yellow, lateral branches of S2 – green, lateral branches of S3 – blue, branches from L5 dorsal ramus and lateral branches of S4 – dotted red, posterior sacral network – purple) to the sacroiliac joint relative to the transverse sacral tubercles (circled numbers). In one anatomic study, 80% of cadaveric specimens had a posterior sacral network that was bordered by the second and third transverse sacral tubercles. Twenty percent of specimens had a proximal border that extended superior to the second transverse sacral tubercle but below the first transverse sacral tubercle. A short, separate S1 lateral branch that innervated the sacroiliac joint was present below the first transverse sacral tubercle in 32% of specimens, and superior to the first transverse sacral tubercle in 8% of specimens. (Reprinted with permission from Wolters Kluwer Health, Inc.)

Radiofrequency Ablation Technique

After marking the skin at the TST1 and TST3 levels, a line overlying the lateral sacral crest is drawn between those two points. The latter is marked at intervals which are determined by the radiofrequency technique used; the goal is to generate a continuous strip lesion from the first to third transverse sacral tubercle that captures the posterior sacral network (Fig. 16.4).

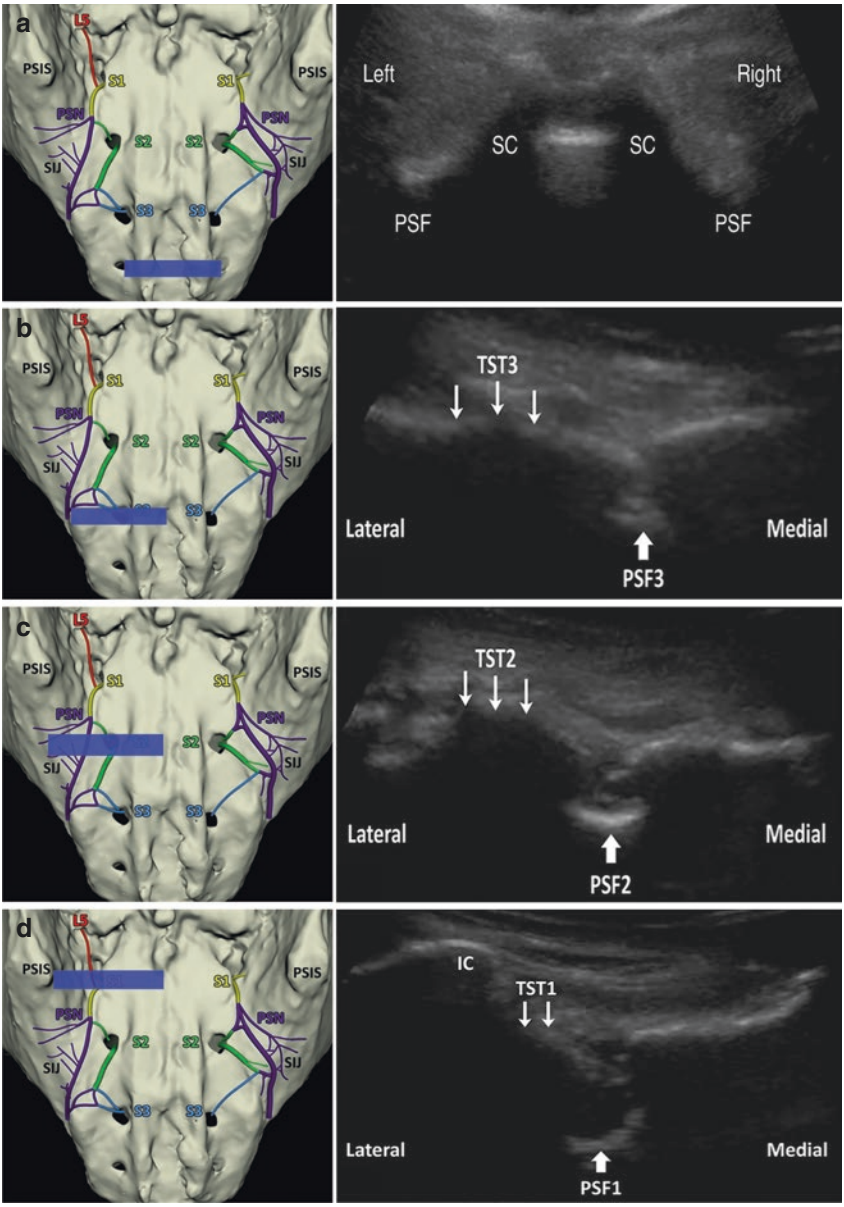

Fig. 16.3 Caudad to cephalad scan of the sacrum in the transverse plane illustrating the landmarks used to perform a radiofrequency lesioning procedure of the posterior sacral network. (**a**) Once the sacral cornua (SC) are identified, the probe is moved laterally over the side of interest and the fourth transverse sacral tubercle as well as the fourth posterior sacral foramen (PSF) (not pictured) are visualized. Further cephalad along the lateral sacral crest (LSC), (**b**) the third transverse sacral tubercle (TST3) and the third posterior sacral foramen (PSF), (**c**) the second transverse sacral tubercle (TST2) and the second posterior sacral foramen (PSF), and (**d**) the first transverse sacral tubercle (TST1), first posterior sacral foramen (PSF), and iliac crest (IC) are seen

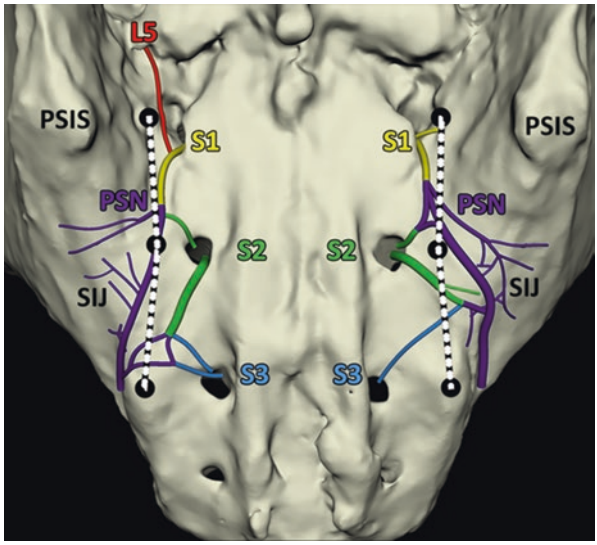

Fig. 16.4 Illustration of bilateral strip lesion (dotted lines) extending from the first to third transverse sacral tubercle along the lateral crest. The extent of this lesion should capture the posterior innervation of the sacroiliac joint. (Reprinted with permission from Wolters Kluwer Health, Inc.)

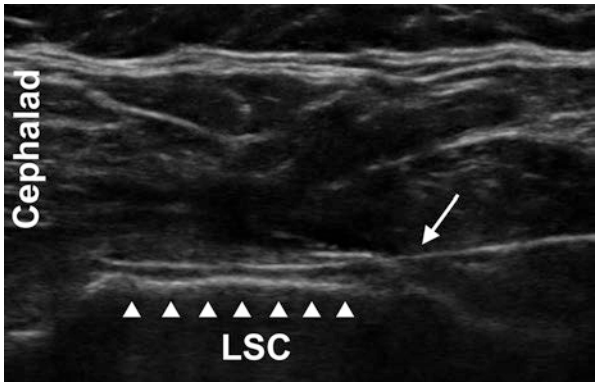

Fig. 16.5 Sagittal scan of the sacrum illustrating a cannula (arrow) in place along the lateral sacral crest (LSC) (block arrows)

When performing bipolar ablations, the marks should be 0.7 cm and 1–1.5 cm apart for standard and multi-tined cannulas, respectively. Using an out-of-plane approach and a transverse sonographic view, the cannulae are inserted sequentially at a perpendicular angle to the periosteum along the lateral sacral crest employing the skin markings as a spacing guide. Care should be taken to keep the cannula parallel to each other to optimize the lesion configuration. An alternative technique involves placing a cannula with a long (20 mm) bare tip using a sagittal view and advancing it along the lateral sacral crest to create a continuous lesion (personal communication Dr. John-Paul Etheridge) (Fig. 16.5).

Clinical Pearls

1. When using a multipolar approach, place the needles as parallel to each other as possible to ensure that the distance measured at the skin is maintained at the level of the periosteum.
2. A prominent iliac crest can hinder cannula placement at the level of TST1 and may require a medial to lateral insertion angle instead of a perpendicular approach. This may lead to a suboptimal strip lesion between TST1 and TST2 when using a multipolar technique.
3. As cadaveric studies have shown that the nerves of the posterior sacral network are most commonly found between TST2 and TST3, particular attention should be paid to this area when performing denervation procedures.

Literature Review

Although procedural efficacy is dependent on appropriate patient selection and technique, the optimal approach to both these aspects has not been determined. Clinical success following radiofrequency ablation targeting the posterior innervation of the sacroiliac joint has been limited; a systematic review that evaluated fluoroscopy-guided procedures estimated that 50% of patients achieved 50% relief at 3 months. Recent anatomical knowledge concerning the distribution of the posterior sacral network and the use of ultrasound guidance to facilitate cannula placement may lead to better results. Cadaveric studies have found that radiofrequency ablation techniques differ significantly in their ability to target the posterior innervation and currently described techniques were estimated to capture 49.6–99.7% of the posterior innervation. Ex vivo evaluations of lesion morphology have found that perpendicular bipolar techniques are superior to currently described monopolar techniques, as they are estimated to capture 93.4–99.7% compared to 49.6–99.1% of the posterior innervation. In addition, ultrasound-guided approaches targeting the lateral crest and those using the palisade technique were found to have the highest capture rates.

Suggested Reading

King W, Ahmed SU, Baisden J, Patel N, Kennedy DJ, MacVicar J, Duszynski B. Diagnosis and treatment of posterior sacroiliac complex pain: a systematic review with comprehensive analysis of the published data. Pain Med. 2015;16(2):257–65.

Roberts SL, Burnham RS, Ravichandiran K, Agur AM, Loh EY. Cadaveric study of sacroiliac joint innervation: implications for diagnostic blocks and radiofrequency ablation. Reg Anesth Pain Med. 2014;39(6):456–64.

Roberts SL, Burnham RS, Agur AM, Loh EY. A cadaveric study evaluating the feasibility of an ultrasound-guided diagnostic block and radiofrequency ablation technique for sacroiliac joint pain. Reg Anesth Pain Med. 2017;42(1):69–74.

Roberts SL, Stout A, Loh EY, Swain N, Dreyfuss P, Agur AM. Anatomical comparison of radiofrequency ablation techniques for sacroiliac joint pain. Pain Med. 2018;19(10):1924–43.

Robinson TJG, Roberts SL, Burnham RS, Loh E, Agur AM. Sacro-iliac joint sensory block and radiofrequency ablation: assessment of bony landmarks relevant for image-guided procedures. Biomed Res Int. 2016;2016:1432074.

Caudal Canal Injections

17

Juan Felipe Vargas-Silva and Philip Peng

Introduction

Caudal canal injections refer to the administration of medications (usually local anesthetics and steroids) into the epidural space via the sacral hiatus. Success of caudal epidural injections depends on the appropriate placement of a needle into the epidural space. Without image guidance, the success rate could be as low as 75% even in experienced hands. With ultrasound guidance, the accuracy in caudal epidural needle placement is 100%. However, ultrasound cannot provide information to its depth of the needle as the needle (or catheter) cannot be visualized beyond the sacral hiatus.

The sacral hiatus occurs by a natural defect in the fusion between S4 and S5, and is bordered by the sacral cornu laterally and covered by superficial posterior sacrococcygeal ligament, which is attached to the margins of the hiatus (Figs. 17.1 and 17.2).

The sacral hiatus contains lower sacral and coccygeal nerve roots (passing through the sacral hiatus), filum terminale externa, and fibro-fatty tissue (Fig. 17.3). The coccygeal plexus is formed as an anastomosis between S4, S5, and coccygeal nerve. Depending on age, the termination of the thecal sac varies between the lower border of the S1 foramen in adults and the S3 foramen in children. In 1–5% of patients, the dural sac terminates at S3 or below, an important fact to remember when placing the epidural needle to avoid dural puncture. Variations in the anatomy of the sacrococcygeal area (up to 10%) or even total absence of the posterior wall of the sacral canal can make the identification of anatomy in this region challenging.

J. F. Vargas-Silva
Department of Surgery and Image Guided Therapy, Pain Clinic, Hospital Pablo Tobón Uribe, Medellin, Colombia

P. Peng (✉)
Department of Anesthesia and Pain Management, Toronto Western Hopsital and Mount Sinai Hospital, University of Toronto, Toronto, Ontario, Canada
e-mail: Philip.peng@uhn.ca

P. Peng et al. (eds.), *Ultrasound for Interventional Pain Management*,
https://doi.org/10.1007/978-3-030-18371-4_17

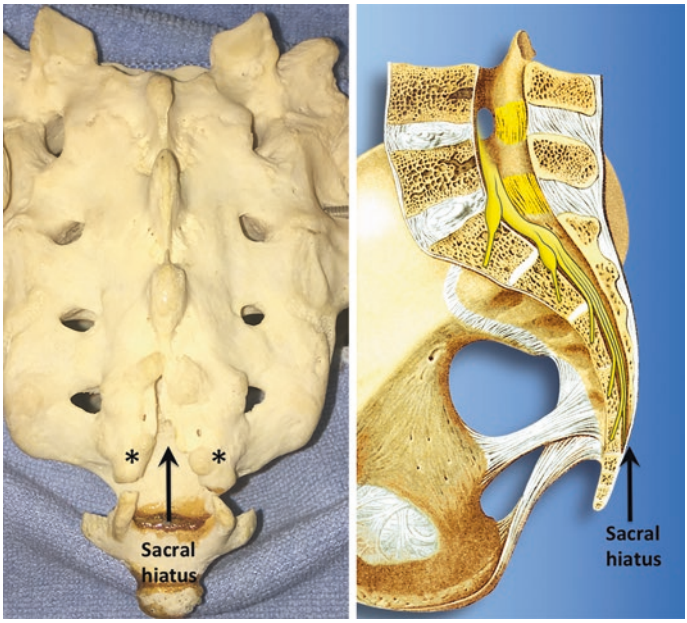

Fig. 17.1 Sacral hiatus (arrow) with the sacral cornu (∗). (Reproduced with permission from Dr. Danilo Jankovic)

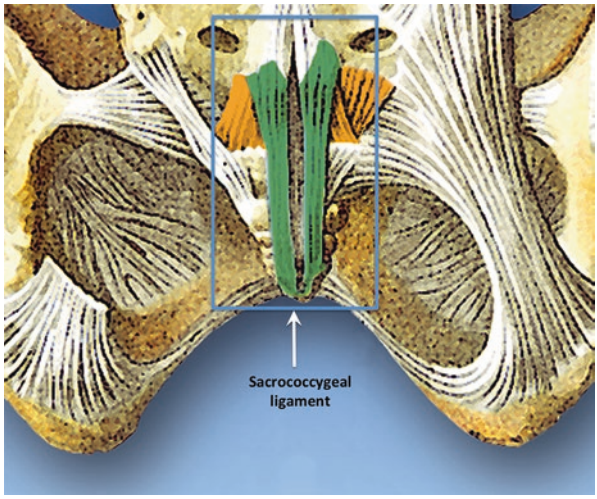

Fig. 17.2 Sacral hiatus covered by sacrococcygeal ligament. (Reproduced with permission from Dr. Danilo Jankovic)

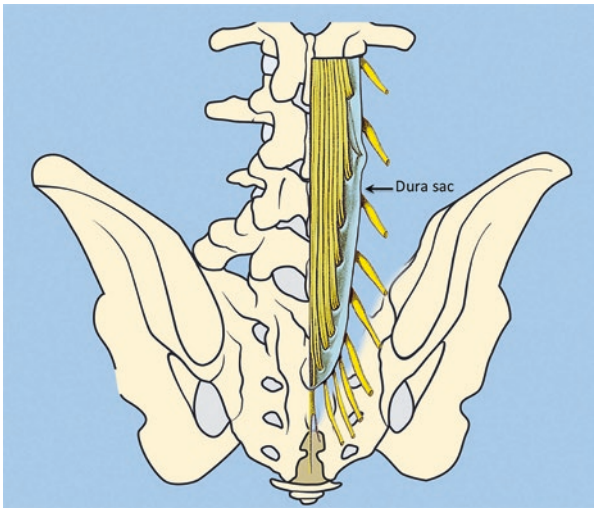

Fig. 17.3 Filum terminale and dura in sacral canal. (Reproduced with permission from Dr. Danilo Jankovic)

Patient Selection

Chronic low back pain with radicular pain secondary to disc herniation or radiculitis not responding to conservative treatment can be considered for caudal canal injection. It is especially useful when there is difficult anatomy in the lumbar spine, such as previous lumbar surgery or degenerative changes, limiting transforaminal or interlaminar access to the epidural space.

Ultrasound Scan

- Position: Prone or Kraske position with the buttocks separated.
- Probe: Linear probe is generally used. A convex probe rarely is needed, except in some cases of obese patients.

Scan 1

Figure 17.4 Upper panel. A transverse scan is performed first and the structures need to be identified are the sacral cornua (SC), the apex of the sacral hiatus (indicated with bold arrows), and the sacrococcygeal ligament (line arrows). The caudal epidural space (***) is the hypoechoic area in between the surface of the sacrum and the sacrococcygeal ligament.

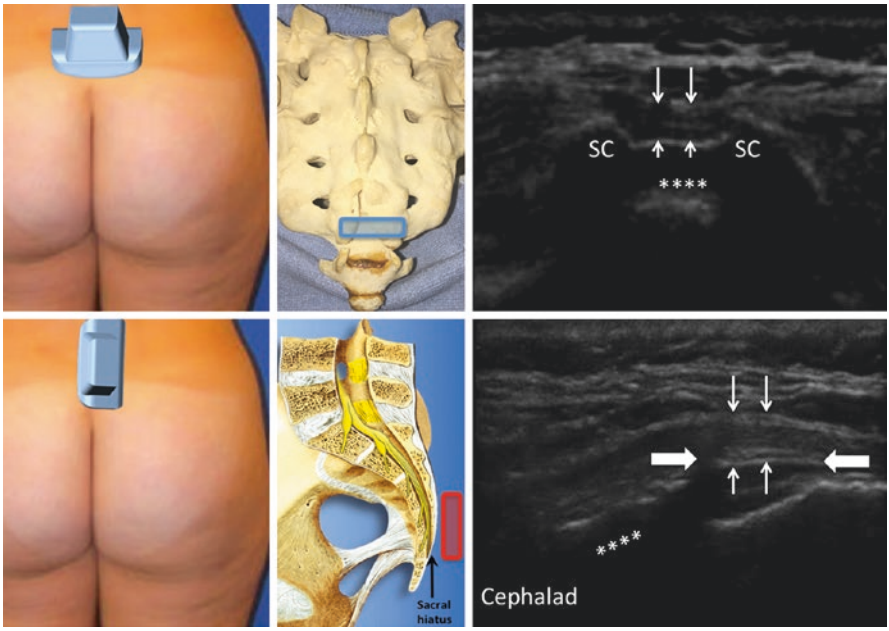

Fig. 17.4 Short-axis (upper panel) and long-axis (lower panel) scan of the caudal canal. (Reprinted with permission from Philip Peng Educational Series)

Scan 2

Figure 17.4 Lower panel. The transducer is turned 90 degrees to have long-axis view of the sacral canal. The sacral canal (***) and the entrance (bold arrows) covered by the thick sacrococcygeal ligament (line arrows) are well appreciated.

Procedure

- Needles: 17G Tuohy epidural needle (when catheter insertion is planned); or a 3.5-inch 22G spinal needle
- Drugs: Volume 10–20 mL with diluted local anesthetic and 40 mg Depo-Medrol (volume depending on using catheter or not)

Both in-plane and out-of-plane techniques have been described. The out-of-plane technique is performed with the short-axis view of the sacral canal and needle is inserted into the canal in caudal to cephalad direction. However, the authors prefer in-plane technique, as the angle of entry is very shallow (Fig. 17.5).

With the sacral area fully prepped and the buttock is open with tape or both leg internally rotated, the transducer, covered with sterile sheath, is placed in long axis as described in the scanning section. Following local anesthetic infiltration of the

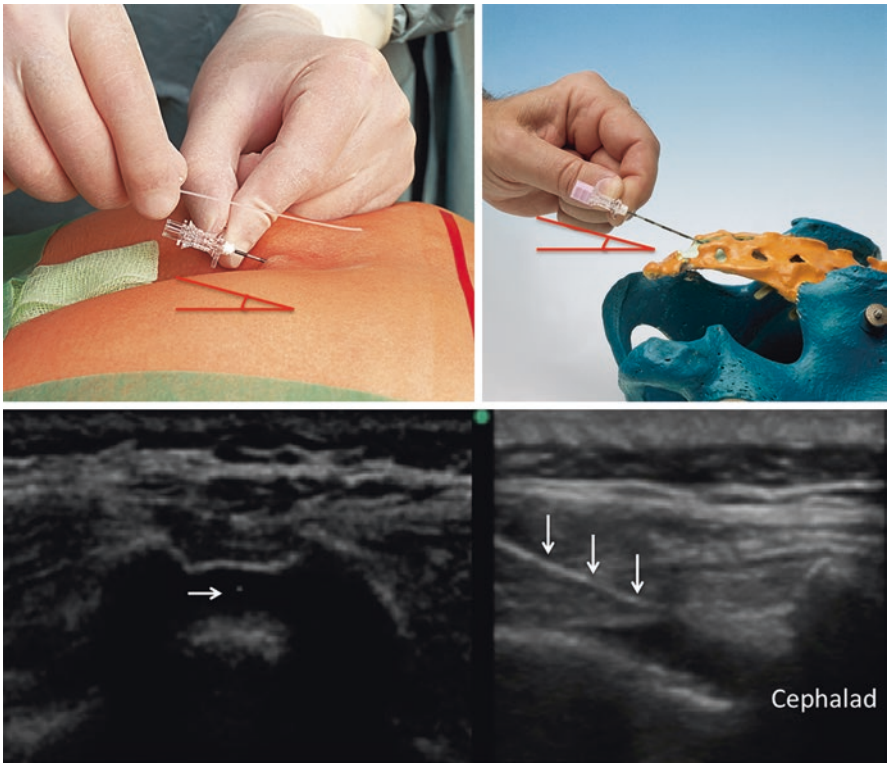

Fig. 17.5 Upper panel. The steep angle of entry to caudal canal. Lower panel. Sonographic images of the needle in short axis (left lower) and long axis (right lower). (Reproduced with permission from Philip Peng Educational Series)

skin, the needle is inserted in cephalad direction at a very shallow angle. Once the needle passes inside the sacral canal, the needle cannot be seen due to the acoustic shadow from the dorsal wall of sacral canal. A high volume of injectate (20 mL) can be administered.

Difficult entrance is encountered in patients with small AP diameter of sacral hiatus at apex (<1.6 mm). Intravascular or intraosseous injection may lead to toxicity of local anesthetic, which is reduced by confirming the needle location with contrast injection under fluoroscopy (Fig. 17.6).

Quite often, a catheter is inserted and the position is confirmed with fluoroscopy and contrast. If the catheter is advanced to L5-S1 level, a lower volume (10 mL) can be administered.

Complications

Direct needle damage to spinal cord and spinal nerve, massive subdural spread, incidental dural puncture (especially in the presence of cystic structures or abnormally low termination of the dural sac), epidural hematoma, infection or epidural

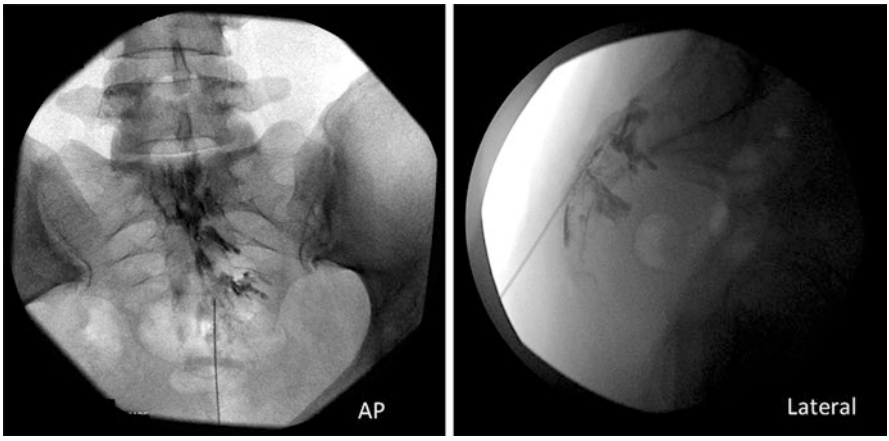

Fig. 17.6 The fluoroscopy image showed spread of contrast leaking through foramen and gives rise to "Christmas tree" appearance. (Reproduced with permission from Philip Peng Educational Series)

abscess, anterior spinal anterior syndrome, and ischemia could be caused by a caudal approach. Injury to sacral nerve(s) is rare during caudal epidural steroid injection. Postinjection pain at the sacral hiatus entry site may be prolonged (up to 6 months when present).

Clinical Pearls

- Remove the excess prep solution or let the solution dry completely (chlorhexidine) to avoid inadvertent introduction of the prep solution into the epidural space which may result in arachnoiditis.
- Once the needle is advanced inside the sacral canal, one should be able to see both the long-axis view of the canal and needle. If this is not the case, the needle is unlikely in the sacral canal.
- Place the medication just piercing the sacrococcygeal ligament or use fluoroscopic guidance to advance the needle or threaten a catheter cephalad to the sacral hiatus. When using a catheter, the volume for injection is dependent on the level of catheter tip.
- Avoid advancing the needle too deep into the sacral canal to prevent inadvertent dural puncture or vascular injections.
- Contemplate in advance, the possible variations in the anatomy of the sacral hiatus.

Literature Review

Literature showed that caudal epidural steroid injection demonstrated similar efficacy in reducing pain and functional improvement compared to transforaminal approaches in the management of lumbosacral radicular pain. Ultrasound has been shown to prevent vascular injection, reduce needle passes, and improve the accuracy of needle placement into the epidural space up to 100%.

Suggested Reading

Bagheri H, Govsa F. Anatomy of the sacral hiatus and its clinical relevance in caudal epidural block. Surg Radiol Anat. 2017;39(9):943–51.

Chen CP, Tang SF, Hsu T, Tsai W, Liu H, Chen MJ, et al. Ultrasound guidance in caudal epidural needle placement. Anesthesiology. 2004;101(1):181–4.

Colimon FJ, Villalobos FJ. Epidural steroid injections: evidence and technical aspects. Tech Reg Anesth Pain Manag. 2010;14(3):113–9.

Fukazawa K, Matsuki Y, Ueno H, Hosokawa T, Hirose M. Risk factors related to accidental intravascular injection during caudal anesthesia. J Anesth. 2014;28(6):940–3.

Liu J, Zhou H, Lu L, Li X, Jia J, Shi Z, et al. The effectiveness of transforaminal versus caudal routes for epidural steroid injections in managing lumbosacral radicular pain: a systematic review and meta-analysis. Medicine (Baltimore). 2016;95(18):e3373.

Ogoke BA. Caudal epidural steroid injections. Pain Physician. 2000;3(3):305–12.

Parr AT, Manchikanti L, Hameed H, et al. Caudal epidural injections in the management of chronic low back pain: a systematic appraisal of the literature. Pain Physician. 2012;15:E159–98.

Rho ME, Tang C. The efficacy of lumbar epidural steroid injections: transforaminal, interlaminar, and caudal approaches. Phys Med Rehabil Clin N Am. 2011;22(1):139–48.

Woon JT, Stringer MD. Clinical anatomy of the coccyx: a systematic review. Clin Anat. 2012;25(2):158–67.

General Principle of Musculoskeletal Scanning and Intervention

18

David A. Spinner and Anthony J. Mazzola

Ultrasound has become the gold standard for most non-axial interventions as it allows the practitioner to view a live dynamic image of the target structure as the needle is guided to a precise location while avoiding vulnerable structures and by enabling visualization of the spreading injectate. In regional anesthesia this translates to a block that has a faster onset, longer duration, decreased patient discomfort, and greater quality utilizing less local anesthesia. In musculoskeletal pathologies this translates into safer interventions with improved outcomes.

Ultrasound in the hands of an experienced user provides excellent image quality of soft tissues. Currently ultrasound guidance is used for most joint, nerve, muscle, ligament, bursa, and ganglion injections. More advanced applications with ultrasound include cryoablation, peripheral nerve stimulators, regenerative medicine, viscosupplementation, and sclerosing agents. Although ultrasound can be limited by its impaired penetration through bone and decreased resolution as depth increases, ultrasound has been successfully used for spinal injections including facet joint, medial branch blocks, and caudal and sacroiliac joint injections.

Advantages of Ultrasound

Musculoskeletal pain is a common symptom that often limits a patient's function and worsens their quality of life. Improvements in ultrasound technology along with increased use by practitioners have led to a growing field of ultrasound-guided interventions focused on pain reduction. Overall the practice of ultrasound to evaluate non-spine joint disease has been increasing. For instance, musculoskeletal

D. A. Spinner (✉) · A. J. Mazzola
Department of Rehabilitation and Human Performance, Mount Sinai Hospital, New York, NY, USA
e-mail: David.Spinner@mountsinai.org

P. Peng et al. (eds.), *Ultrasound for Interventional Pain Management*,
https://doi.org/10.1007/978-3-030-18371-4_18

Table 18.1 Comparison of the imaging modalities for intervention

	Fluoroscopy	CT scan	Ultrasound
Soft tissue scanning	Poor	Excellent	Good to excellent
Radiation risk	+−++	+−+++	0
Cost of equipment	+++	+++++	+−++
Portability of equipment	+	0	++−+++
Requirement of infrastructure	++	++++	0
Real-time guidance	++	0−+ (↑radiation)	++
Bone imaging	Excellent	Excellent	Limited
Deep structure scanning	Fairly reliable	Reliable	Unreliable

Reprinted with permission from Philip Peng Educational Series

Medicare ultrasound imaging increased by 347% compared to only a 53% growth in MRI imaging from 2003 to 2015.

Ultrasound proves superior to other imaging modalities in portability and safety. Risk is minimized: ultrasound has no contraindications and provides no harmful radiation. Ultrasound has been shown to decrease procedure time and enhance accuracy of injections by enabling the dynamic visualization of needle course and injectate spread (Table 18.1).

Ultrasound Scanning

Ultrasound provides a dynamic instant image of structures directly under the transducer. It is ideal to align the probe in a perpendicular manner to the structure of interest. Image quality directly correlates with the frequency of the transducer. High-frequency waves provide excellent superficial tissue resolution, while low-frequency waves provide better visualization for deeper structures.

Ultrasound scanning should include visualizing the target in long axis and short axis when applicable. First, use knowledge of anatomical landmarks to guide orientation. Next, it is important to minimize artifact, especially anisotropy, by ensuring the structure of interest is directly perpendicular to the transducer. When the sound beam is perpendicular to bone, the cortex will appear hyperechoic and well defined. The final step is analyzing the image for pathology. Ultrasound imaging can be performed over any area of concern. When evaluating tears in muscles, tendons, or ligaments, the structure in question can be actively and passively engaged to characterize the severity. A force can be applied to examine for joint space widening. Furthermore, a limb can be moved in various planes to mimic and reproduce symptoms under real-time image analysis.

Hyperechoic images are bright and can be visualized at the interfaces between bone and soft tissue as the sound beam is strongly reflected back to the transducer. Low or weak sound reflection produces hypoechoic or darker images. Deep to the bone is anechoic and appears completely black because no sound waves penetrate. Isoechoic is the term to describe a structure that is of similar echogenicity to adjacent tissue.

Anisotropy is the term used to describe ultrasound artifact that occurs secondary to the amount of sound beam that is reflected back to the transducer based on the angle the beam reflects off the structure of interest. Changing the angle as few as 2–3 degrees relative to the perpendicular can result in a hyperechoic structure (expected healthy tendon) appearing hypoechoic (pathologic) as fewer sound waves are reflected to the transducer.

Ultrasound takes advantage of the Doppler effect to distinguish objects moving away and toward the probe. Use this color flow feature before injecting to highlight vasculature.

Setting Up Injection

Injections can be performed either with the needle in-plane (parallel) or out-of-plane (perpendicular) to the transducer. Some injections based on physical anatomy and location will have a preferred orientation. Overall, in-plane allows optimal viewing of the needle course through structures completely to the target as well as uninterrupted identification of the needle tip.

The needle is best visualized directly parallel to and under the transducer. Therefore, when possible a shallow needle angle is preferred. Overall the needle is hyperechogenic and the image is diminished as depth increases. To improve visualization, rotate the bevel, inject fluid looking for spread, or cautiously move the needle in and out.

Out-of-plane involves the needle being entered perpendicular to probe. This allows a larger field of vision; however it impairs the ability to identify the tip of the needle from the shaft as the complete path of the needle cannot be tracked. When injecting out-of-plane, a "walk-down" approach can be utilized to track the needle tip by stepwise sliding the probe and then further advancing the needle. By repeating this technique, the tip of the needle is followed directly to the target.

Ultrasound Utilization

All injections should be performed in an aseptic manner. Glucocorticoids create an anti-inflammatory environment, which temporarily helps to decrease pain generators with diminishing returns often starting after 5 weeks and culminating around 24 weeks. Sclerosing agents are postulated to reduce pain either by limiting neovascularization or by impairing adjacent nerve endings. Studies have shown excellent pain reduction lasting up to 2 years when treating tendinopathies. Another treatment for tendinopathies involves ultrasound-guided scarification and autologous blood injection into affected tendons and ligaments stimulating the production of granulation tissue. In a comparable manner, platelet-rich plasma injections help to stimulate growth factors in tendinopathies and joints. Hyaluronic acid injections act by lubricating and separating the joint space. Ozone injections have been used to treat

Table 18.2 Comparing ultrasound for musculoskeletal (MSK) vs. regional anesthesia procedure

	Ultrasound in MSK	Regional anesthesia
Target structures	Nerve Joint and bone Ligament Muscle Bursa Tendon Ganglion/cyst Fat pad Fascia plane Retinaculum	Nerve Fascia plane
Scanning interest	Normal structures Abnormal (pathology diagnosis) Dynamic scanning[a]	Normal structures
Intervention	Nerves Perineural Fascia plane Nerve release Intraneural injection[b] Radiofrequency (RF) ablation Pulsed RF lesion Cryoablation Tendon/muscle Fenestration Barbotage[c] Ganglion/cyst Aspiration Retinaculum Release[d]	Perineural or fascia plane injection
Injectate	Local anesthetic Adjuvant (e.g., steroid) Viscosupplement Dextrose (prolotherapy) Platelet-rich plasma/blood Botox Biologic agent (e.g., stem cells)	Local anesthetic Adjuvant (e.g., steroid)

Reprinted with permission from Philip Peng Educational Series

[a]Important in diagnosing certain pathology such as rotator cuff impingement or snapping hip syndrome

[b]For Morton's or stump neuroma

[c]Barbotage is used for treatment in calcific tendinitis

[d]Release of carpal tunnel retinaculum for median nerve compression

painful small joints or localized disease. Ozone is postulated to decrease free radical production. Normal saline can be injected to dissolve intratendinous calcifications and to wash away inflammatory compounds. Needle selection varies based on characteristics of the target (Table 18.2).

Ultrasound technology continues to progress allowing for improved imaging which has increased its scope of practice. Three-dimensional ultrasound enables reconstruction at any image plane and can be used to quantify volume. Fusion

imaging superimposes the dynamic ultrasound image on previous CT or MRI imaging and has been used for sacroiliac joint injections. Sonoelastography allows one to quantify the elasticity of structures such as tendons.

Similarly, as medical technology advances, new applications for ultrasound have the potential to be developed. Mastering the principles of musculoskeletal scanning and intervention affords one the opportunity to be at the forefront of medical advancement as innovative techniques including neuromodulation, regional anesthesia, and regenerative medicine are further perfected.

Clinical Pearls

1. Use anatomical landmarks to target the structure of interest.
2. Scan for any pathology prior to injection.
3. Be aware of anisotropy: adjust transducer angle when evaluating structures.
4. Advance needle directly under the probe for optimal visualization.
5. Only advance needle when the location of the tip is known.
6. If unable to locate the hyperechoic needle, hold needle in place and slide probe to scan for needle.
7. If unable to visualize structures under the needle due to reverberation, perform a step-off maneuver by changing probe angle.
8. Use color flow to highlight vasculature that is to be avoided.
9. Only inject when the needle tip has been identified at target site, and observe for spread of injectate.
10. In most interventions, the tendon or nerve should not be directly injected. If resistance is felt while delivering medication, retract or advance needle [2].

Suggested Reading

1. Spinner DA, Kirschner JS, Herrera JE, editors. Atlas of ultrasound guided musculoskeletal injections. Chapter 1. New York: Springer; 2014.
2. Jacobson JA. Fundamentals of musculoskeletal ultrasound. Chapter 2. 3rd ed. Philadelphia: Elsevier; 2018.
3. Robotti G, Canepa MG, Bortolotto C, Draghi F. Interventional musculoskeletal US: an update on materials and methods. J Ultrasound. 2013;16(2):45–55.
4. Peng PW, Narouze S. Ultrasound-guided interventional procedures in pain medicine: a review of anatomy, sonoanatomy, and procedures: part I: nonaxial structures. Reg Anesth Pain Med. 2009;34(5):458–74.
5. Narouze S, Peng PW. Ultrasound-guided interventional procedures in pain medicine: a review of anatomy, sonoanatomy, and procedures. Part II: axial structures. Reg Anesth Pain Med. 2010;35(4):386–96.
6. Peng PW, Cheng P. Ultrasound-guided interventional procedures in pain medicine: a review of anatomy, sonoanatomy, and procedures. Part III: shoulder. Reg Anesth Pain Med. 2011;36(6):592–605.

7. Peng PW. Ultrasound-guided interventional procedures in pain medicine: a review of anatomy, sonoanatomy, and procedures. Part IV: hip. Reg Anesth Pain Med. 2013;38(4):264–73.
8. Peng PW, Shankar H. Ultrasound-guided interventional procedures in pain medicine: a review of anatomy, sonoanatomy, and procedures. Part V: knee joint. Reg Anesth Pain Med. 2014;39(5):368–80.
9. Soneji N, Peng PW. Ultrasound-guided interventional procedures in pain medicine: a review of anatomy, sonoanatomy, and procedures: part VI: ankle joint. Reg Anesth Pain Med. 2016;41(1):99–116.
10. Soneji N, Peng PW. Ultrasound-guided pain interventions - a review of techniques for peripheral nerves. Korean J Pain. 2013;26(2):111–24.
11. Niazi AU, Peng PW, Ho M, Tiwari A, Chan VW. The future of regional anesthesia education: lessons learned from the surgical specialty. Can J Anaesth. 2016;63(8):966–72.
12. Griffin J, Nicholls B. Ultrasound in regional anaesthesia. Anaesthesia. 2010;65 Suppl 1:1–12.
13. Kanesa-Thasan RM, Nazarian LN, Parker L, Rao VM, Levin DC. Comparative trends in utilization of MRI and ultrasound to evaluate nonspine joint disease 2003 to 2015. J Am Coll Radiol. 2018;15(3 Pt A):402–7.

Shoulder

19

Jennifer Kelly McDonald and Philip Peng

Abbreviations

AC	acromioclavicular
CHL	coracohumeral ligament
GH	glenohumeral
GT	greater tuberosity
HA	hyaluronic acid
LHB	long head of biceps
LT	lesser tuberosity
RCT	randomized control trial
SASD	subacromial subdeltoid
SGHL	superior glenohumeral ligament
THL	transverse humeral ligament
US	ultrasound

Introduction

With a lifetime prevalence of 70%, shoulder pain is a ubiquitous complaint. Encouragingly, shoulder pain often improves with conservative management strategies, including activity modification, physical therapy, and medications. When required, injections can be very helpful.

J. K. McDonald
The Ottawa Hospital, Physical Medicine and Rehabilitation, The Ottawa Hospital Rehabilitation Centre, Ottawa, ON, Canada

P. Peng (✉)
Department of Anesthesia and Pain Management, Toronto Western Hopsital and Mount Sinai Hospital, University of Toronto, Toronto, Ontario, Canada
e-mail: Philip.peng@uhn.ca

P. Peng et al. (eds.), *Ultrasound for Interventional Pain Management*,
https://doi.org/10.1007/978-3-030-18371-4_19

The shoulder consult can be formidable due to the multiple potential pain generators (Table 19.1).

The relevant shoulder girdle anatomy and corresponding pain generators will be briefly reviewed.

The glenohumeral (GH) joint is a synovial ball-and-socket joint consisting of the humeral head and shallow glenoid fossa. The fibrocartilaginous glenoid labrum and surrounding ligamentous structures are instrumental in stabilizing the joint (Fig. 19.1). Chronic pain localizing to the GH joint is often related to degenerative labral pathology and/or cartilage loss (GH joint osteoarthritis).

Table 19.1 Common shoulder pain generators

Structure	Associated pathology
GH joint	GH osteoarthritis
Rotator cuff/SASD bursa	Supraspinatus tendinopathy/partial tear, SASD bursitis
Long head of biceps tendon	Biceps tendinopathy, biceps tendon instability
GH joint capsule/ligaments	Frozen shoulder
AC joint	AC osteoarthritis

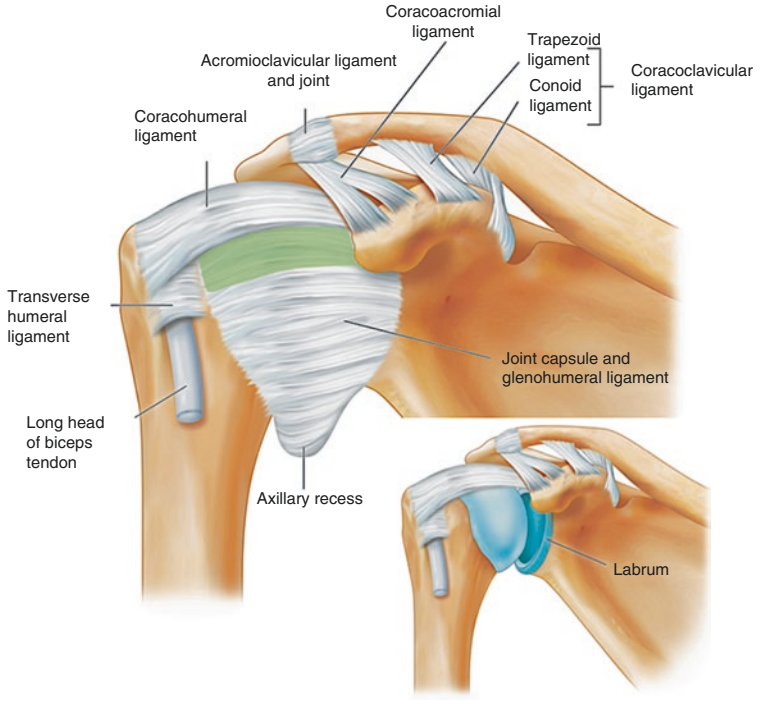

Fig. 19.1 The GH joint capsule and surrounding ligaments are pictured. Notably, the coracohumeral ligament (CHL) is a thick fibrous band arising from the coracoid process and inserting on the greater and lesser tuberosities of the humerus. The CHL assists with reinforcing the joint capsule and stabilizing the LHB tendon. Outlined in green, the superior fibers of the glenohumeral ligament are called the superior glenohumeral ligament (SGHL). The CHL and SGHL are important structures within the rotator interval, discussed below. The acromioclavicular joint and associated stabilizing ligaments are also pictured. The inset picture shows the joint's articular surface, glenoid and labrum. (Reproduced with permission from Philip Peng Educational Series)

The four rotator cuff muscles, which create a tight layer of tendons around the GH joint, also play an important role in joint stabilization (Fig. 19.2). The rotator cuff helps to keep the humeral head centered on the glenoid during arm elevation. The subacromial subdeltoid (SASD) bursa lies sandwiched between the deeper rotator cuff tendons and the superficial deltoid muscle and coracoacromial arch. The SASD bursa allows the rotator cuff tendons to glide smoothly under the deltoid and arch. Subacromial impingement, an important clinical sign, occurs when the superior aspect of the humeral head and rotator cuff tendons impinge on the undersurface of the coracoacromial arch. The clinical finding of subacromial impingement is often seen together with the clinical diagnoses of rotator cuff pathology and SASD bursitis.

The long head of biceps (LHB) tendon originates at the superior aspect of the glenoid and labrum. The intra-articular proximal tendon travels over the anterosuperior humeral head and then takes a sharp turn to become extra-articular within the bicipital groove of the humerus (Fig. 19.3a, b). LHB tendinopathy and/or instability are additional causes of shoulder pain. Isolated LHB tendon pathology is rare. Biceps tendinopathy is often associated with other shoulder pathology, especially superior labral tears and anterosuperior rotator cuff tears in the region of the rotator interval.

The rotator interval is a triangular space where the anterior supraspinatus fibers and lateral subscapularis fibers border the intra-articular portion of the biceps

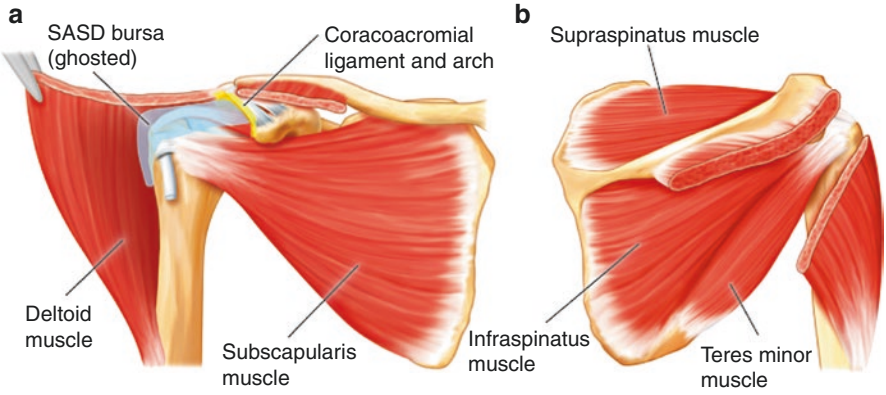

Fig. 19.2 There are four rotator cuff muscles: supraspinatus, infraspinatus, subscapularis, and teres minor. The supraspinatus passes under the coracoacromial arch (outlined in yellow), which consists of the bony acromion and coracoid process bridged by the coracoacromial ligament. The SASD bursa is a synovium-lined potential space located deep to the acromion and deltoid muscle and superficial to the supraspinatus and infraspinatus tendons. The clinical finding of subacromial impingement is often associated with poor shoulder biomechanics, rotator cuff tendinopathy/tears, SASD bursitis, and/or abnormal coracoacromial arch anatomy. (**a**) Anterior view of the rotator cuff muscles with anterior deltoid muscle reflected away. (**b**) Posterior view of the rotator cuff muscles with posterior deltoid muscle partially resected. (Reproduced with permission from Philip Peng Educational Series)

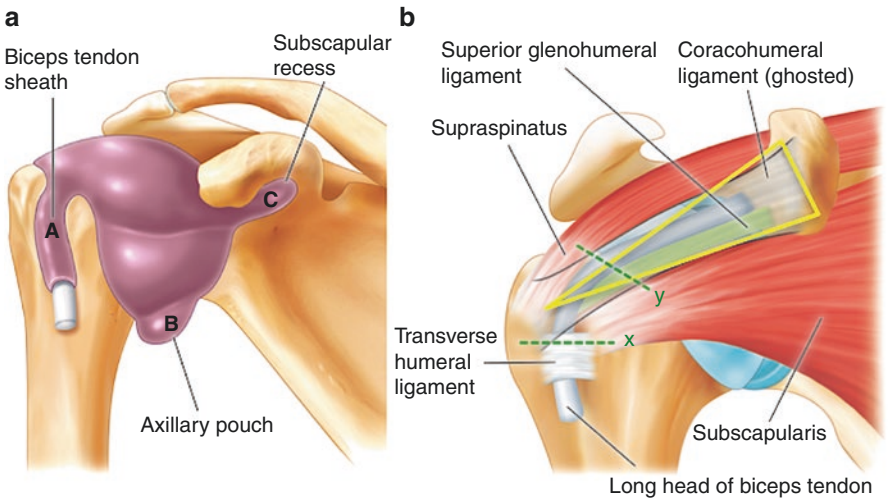

Fig. 19.3 The joint capsule (not pictured) extends from the medial glenoid cavity and base of the coracoid process to the anatomic neck of the humerus. The synovial membrane lines the deep surface of the capsule and the outer surface of the biceps tendon. As one of three main synovial recesses, the biceps tendon sheath extends along the extra-articular portion of the LHB tendon. The rotator interval is a triangular space (outlined in yellow) located in the anterosuperior portion of the GH joint with complex anatomical relationships. The boundary is defined superiorly by the supraspinatus tendon, inferiorly by the subscapularis tendon, and medially, at its base, by the coracoid process. The rotator interval contains the CHL, SGHL, LHB tendon, and rotator interval joint capsule. (**a**) The three main synovial membrane recesses are pictured. (**b**) Diagram of the rotator interval. Slices x and y mark ultrasound positions applicable to Figs. 19.6a and 19.6b. (Reproduced with permission from Philip Peng Educational Series)

tendon (Fig. 19.3a, b). Frozen shoulder, another common cause of shoulder pain and stiffness, is thought to be related to inflammation and thickening of the rotator interval structures.

The acromioclavicular (AC) joint, located at the superior aspect of the shoulder complex, is a small synovial joint between the lateral aspect of the clavicle and the acromion process of the scapula (Fig. 19.4). It has limited range of motion. A wedge-shaped fibrocartilaginous disk separates the articular surfaces of the joint. Several surrounding ligaments reinforce the AC joint capsule. Chronic AC joint pain is often related to degenerative changes with cartilage loss and bone spurring.

Patient Selection

One of the more challenging aspects of ultrasound-guided shoulder injections is choosing the appropriate patient and anatomical target. The clinical history is an important part of the shoulder pain consult and provides clues about the primary pain generator. Associated with each of the major shoulder pain diagnoses, a few key symptoms are often elicited on history (Table 19.2). Pain with sleeping,

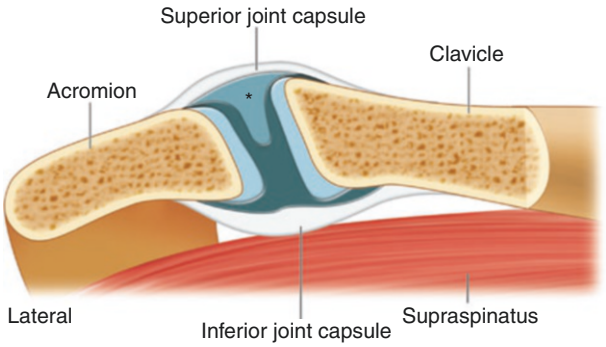

Fig. 19.4 The acromioclavicular joint is a synovial joint with the articular surfaces separated by a wedge-shaped fibrocartilaginous disk (asterisk). The inferior surface of the joint is in direct contact with the subacromial bursa and supraspinatus muscle and may play a role in the development of the impingement syndrome. (Reproduced with permission from Philip Peng Educational Series)

Table 19.2 Clues on shoulder history

Diagnosis	Pertinent history
GH joint osteoarthritis	Advanced age, associated stiffness, pain with putting on a seat belt and reaching behind the back
Frozen shoulder	Middle age, progressive marked stiffness, pain with putting on a seat belt and reaching behind the back
Rotator cuff pathology/SASD bursitis	Pain referral to lateral upper arm, pain with overhead activities
Long head of biceps tendinopathy/instability	Anterior shoulder pain, pain with putting on a seat belt and reaching behind the back
AC joint osteoarthritis	Superior shoulder pain, variable referral pattern, pain with reaching across the chest and overhead

Table 19.3 Shoulder physical examination special tests

Test	Site of pathology	Description
Cross-body adduction	AC joint	Arm flexed 90°, forced into horizontal adduction, pain localizes over AC joint
Speed's	LHB tendon	Arm flexed 90°, elbow extended and forearm supinated (palm up), downward force applied Pain localizes over the bicipital groove
Empty can	Supraspinatus	Arm flexed 90° in scapular plane (relatively abducted), internally rotated (thumb pointing down), downward force applied
O'Brien's	Labrum	Arm flexed 90°, horizontally adducted 15°, internally rotated (thumb pointing down), downward force applied

especially when lying on the affected shoulder, is often reported and is a nonspecific finding.

The shoulder physical examination can also be challenging. Most of the special tests are not sensitive or specific. A simplified algorithm is provided to assist the pain physician in interpreting the physical examination findings (Fig. 19.5). A simple explanation of the included tests is seen in Table 19.3. In many cases, the

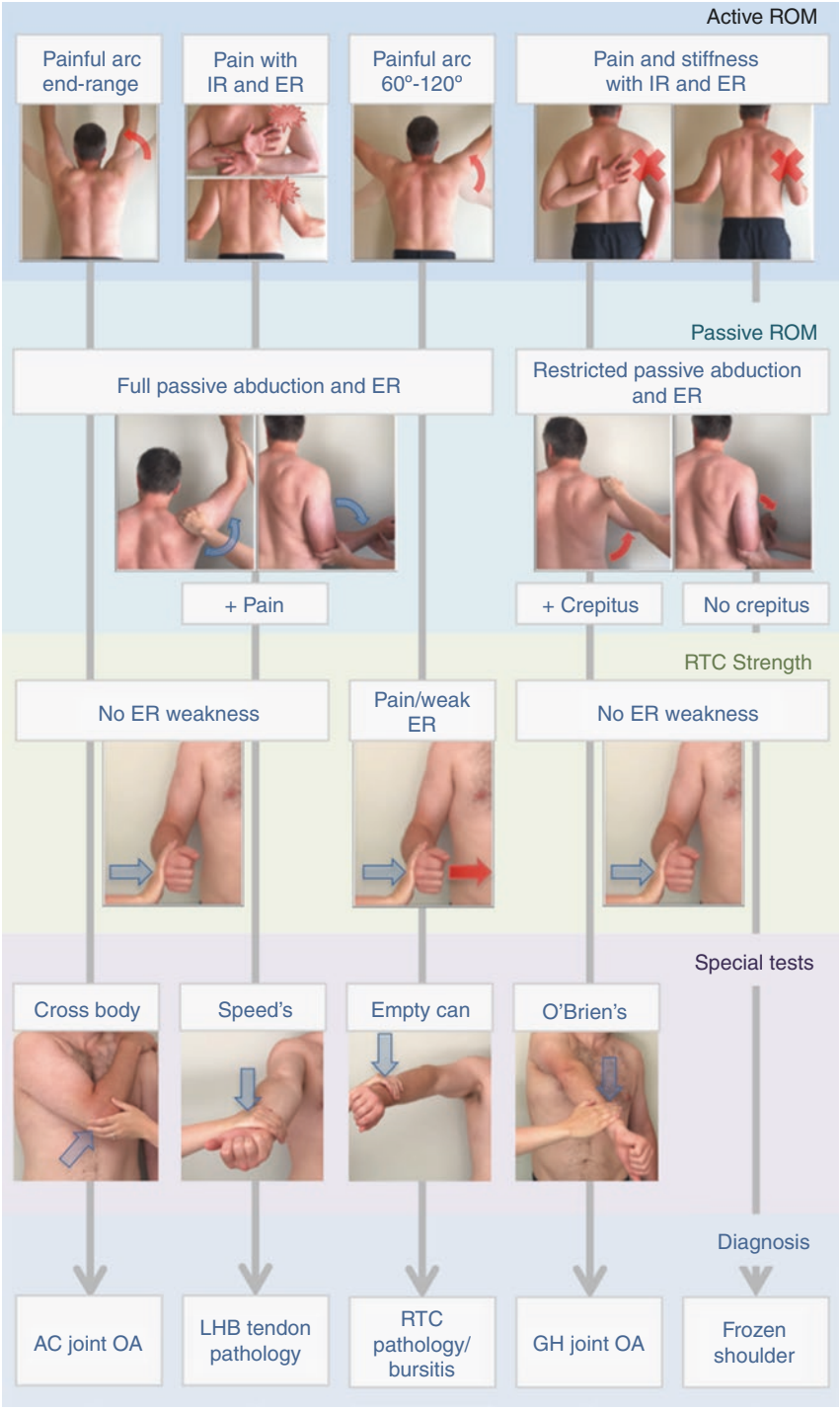
Active ROM
Painful arc end-range
Pain with IR and ER
Painful arc 60°-120°
Pain and stiffness with IR and ER
Passive ROM
Full passive abduction and ER
Restricted passive abduction and ER
+ Pain
+ Crepitus
No crepitus
RTC Strength
No ER weakness
Pain/weak ER
No ER weakness
Special tests
Cross body
Speed's
Empty can
O'Brien's
Diagnosis
AC joint OA
LHB tendon pathology
RTC pathology/ bursitis
GH joint OA
Frozen shoulder

Fig. 19.5 A simplified algorithm is provided to guide the reader through the physical examination of the shoulder. Palpation is omitted because tenderness of various structures, especially the LHB tendon, is common and non-specific. AC joint tenderness worse on the affected side and that reproduces the patient's typical pain supports a diagnosis of AC joint pathology. If marked stiffness and pain is apparent on range of motion examination in a middle-aged adult, the diagnosis of frozen shoulder is likely. In this case, the remaining exam can be abbreviated, as most of the provocative maneuvers will be painful and non-specific. A normal x-ray to rule out early osteoarthritis or bony pathology essentially confirms the diagnosis of frozen shoulder. ROM, range of motion; RTC, rotator cuff; ER, external rotation; IR, internal rotation; OA, osteoarthritis. (Reproduced with permission from Dr. Jennifer McDonald)

primary pain generator will remain unclear despite a detailed history and physical. In these instances, US-guided injection of the most likely target with local anesthetic can assist with diagnostic clarification.

A simple explanation of the tests is seen in Table 19.3.

When in doubt, or if the injection is not providing the expected benefit, seeking the opinion of a shoulder surgeon or musculoskeletal medicine specialist for diagnostic clarification is recommended. In addition, clinical findings suggestive of acute trauma, marked weakness, instability, or significant mechanical symptoms (i.e., locking) should trigger a referral for diagnostic clarification and to rule out the need for surgical management.

Ultrasound Scan

LHB tendon and rotator interval	
Position:	Supine, arm supinated
Probe:	Linear, 5–13 MHz

Scan 1: Extra-articular LHB tendon, transverse view (Fig. 19.6a). Probe position corresponds to Fig. 19.3 slice "x." Note the greater and lesser tuberosities (GT and LT, respectively) of the humerus and LHB tendon within the bicipital groove. Depicted in purple, the synovial-lined biceps tendon sheath surrounds the tendon and is the target (marked by a star) for injection. The accompanying ascending branch of the anterior circumflex artery should also be located. The transverse humeral ligament (THL), an extension of the subscapularis tendon, is the roof of the bicipital groove.

Scan 2: Rotator cuff interval view of LHB tendon (Fig. 19.6b). From scan 1, the probe is translated just cephalad and rotated slightly to remain perpendicular to the LHB tendon. Probe position corresponds to Fig. 19.3 slice "y." Note the now convex shape of the humeral head. The joint capsule with trace GH joint fluid (hypoechoic on US, purple on drawing) surrounds the oval hyperechoic LHB tendon. The CHL

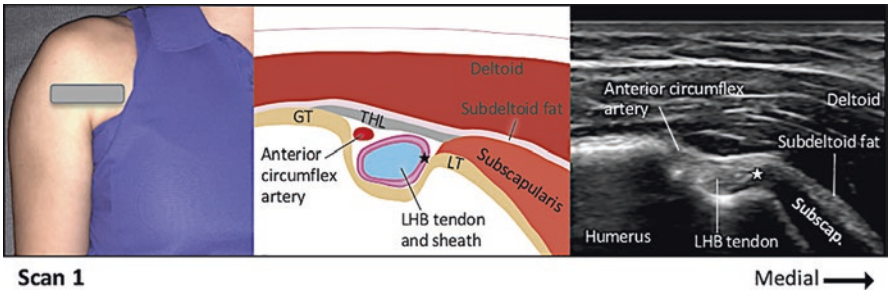

Fig. 19.6a Short-axis scan of long head of biceps (LHB). (Figure reproduced with permission from Jennifer McDonald)

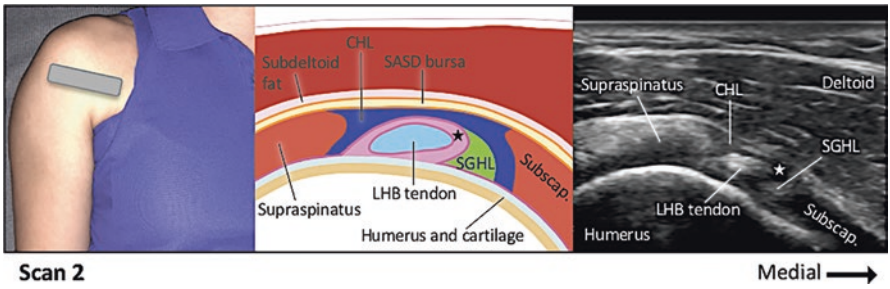

Fig. 19.6b Rotator cuff interval. (Figure reproduced with permission from Jennifer McDonald)

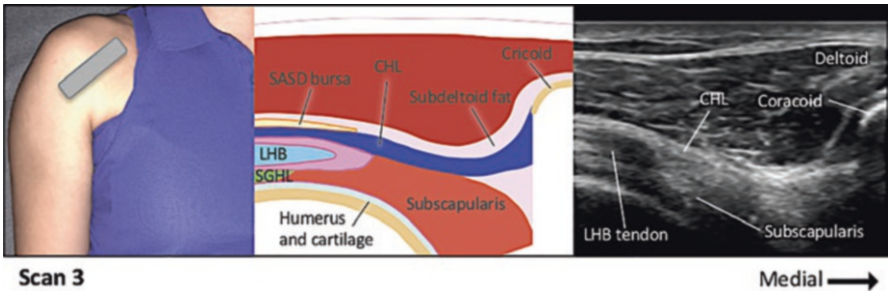

Fig. 19.6c Coracoid and longitudinal CHL view. (Reproduced with permission from Jennifer McDonald)

overlies the LHB tendon. The star marks the target for intra-articular GH joint injection via the rotator interval. The subscapularis tendon appears hypoechoic on the US image due to anisotropy.

Scan 3: Coracoid and longitudinal CHL view (Fig. 19.6c). From scan 2, moving medially and rotating the probe, the CHL can be followed to its origin at the coracoid process of the scapula. The underlying LHB tendon and subscapularis muscle are visible. Externally rotating the shoulder will bring more of the subscapularis into view and tighten the CHL.

Posterior GH joint	
Position:	Lateral, ipsilateral shoulder facing up with arm touching contralateral shoulder
Probe:	Linear, 5–13 MHz Curvilinear (2–6 MHz) is used for scanning large body mass index and is sometimes preferred for injection due to steep needle trajectory

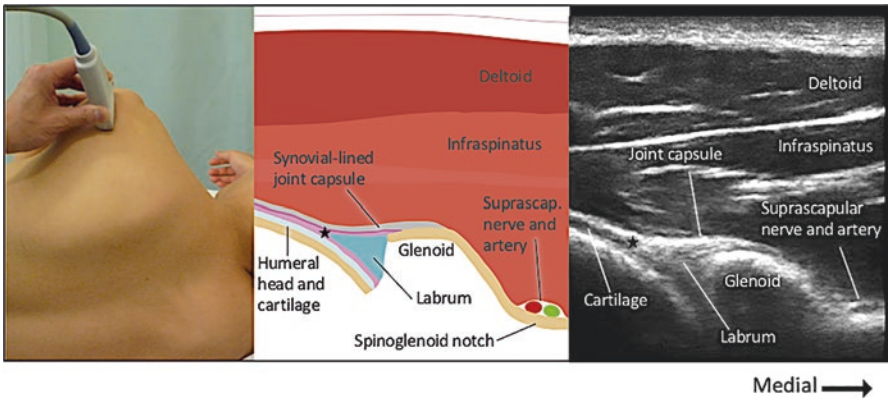

Fig. 19.7 Posterior view of glenohumeral joint. (Photo and ultrasound image reproduced with permission from Philip Peng Educational Series. Illustration by Jennifer McDonald)

Scan 1: Infraspinous view (Fig. 19.7). The spine of the scapula is palpated laterally toward the acromion. The probe is placed parallel and directly caudal to the scapular spine. Deep to the deltoid muscle, fibers of the infraspinatus muscle can be seen overlying the humeral head and glenoid. Note the hypoechoic hyaline cartilage along the surface of the humeral head and hyperechoic triangular labrum. These structures should be avoided during injection. Just medial to the glenoid, the bony spinoglenoid notch cradles the suprascapular nerve and artery. The star marks the target for posterior intra-articular GH joint injection.

Supraspinatus tendon and SASD bursa	
Position:	Seated, modified Crass position (arm supinated and extended, as if the hand is in the back pocket)
Probe:	Linear, 5–13 MHz

Scan 1: LHB tendon, longitudinal view (Fig. 19.8, upper panel). Starting with the rotator interval view (Fig. 19.6b), the probe is centered on the LHB tendon and then carefully rotated so that the biceps tendon appears as elongated as possible. The LHB tendon will have a typical fibrillar pattern when viewed in the long axis.

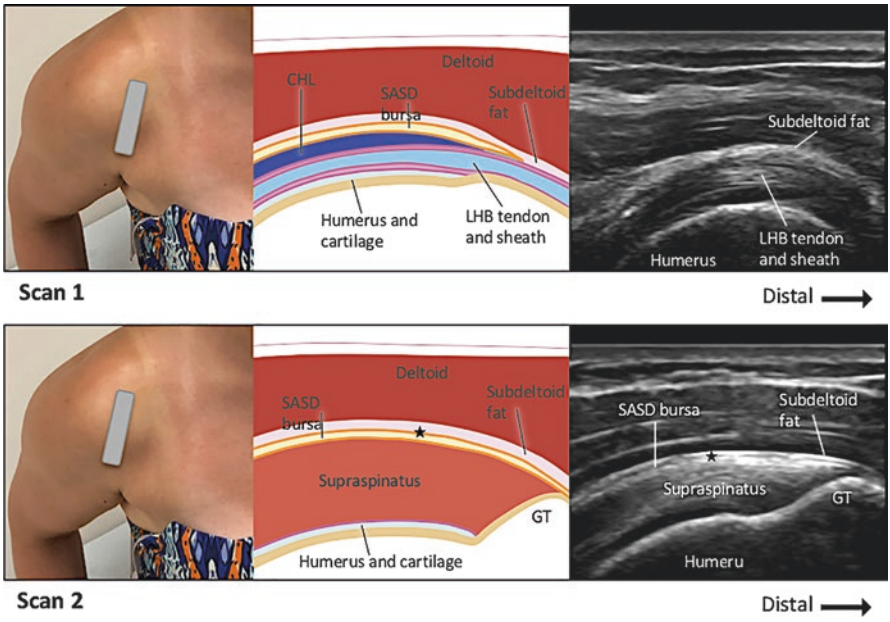

Fig. 19.8 Upper panel. Long-axis view of LHB. Lower panel. Long-axis view of supraspinatus tendon. (Figure reproduced with permission of Jennifer McDonald)

Scan 2: Supraspinatus tendon, longitudinal view (Fig. 19.8, lower panel). From Scan 1, the probe is translated just lateral to bring the supraspinatus tendon into view. The supraspinatus tendon inserts onto the beak-shaped greater tuberosity (GT). Note the hypoechoic hyaline cartilage along the humeral head. The SASD bursa can be identified as a thin hypoechoic line flanked by the hyperechoic supraspinatus tendon and subdeltoid fat. When bursitis is present, this bursal space will be fluid-filled with thickening of the peribursal fat. The star marks the target for SASD bursa injection.

AC joint	
Position:	Seated, arm at side
Probe:	Linear, 5–13 MHz

Scan 1: AC joint, coronal plane (Fig. 19.9a). The AC joint is located by palpating along the concave lateral third of the clavicle to its lateral edge where it articulates with the acromion. The probe is centered over the joint in the coronal plane. Note the superior joint capsule and intra-articular wedge-shaped fibrocartilaginous disk. The SASD bursa and supraspinatus tendon lie immediately inferior to the joint. The star marks the target for AC joint injection using an out-of-plane approach.

Scan 2: Acromion, sagittal plane (Fig. 19.9b). From Scan 1, the probe is rotated 90 degrees and translated laterally over the acromion. The superficial bony acromion is visualized in the sagittal plane. This is the starting point for locating the AC joint in short-axis view (Fig. 19.9d).

Scan 3: Clavicle, sagittal plane (Fig. 19.9c). From Scan 2, the probe is translated medially past the AC joint space (Fig. 19.9d) to the superficial bony clavicle in short axis. McDonald.

Scan 4: AC joint, short-axis view (Fig. 19.9d). To find the AC joint, the probe is moved between the Scan 2 and Scan 3 positions. The AC joint is found when the bone shadows of the clavicle and acromion are not visible and the superficial capsule of the AC joint and underlying bursa and supraspinatus tendon come into view. The star marks the target for AC joint injection using an in-plane approach.

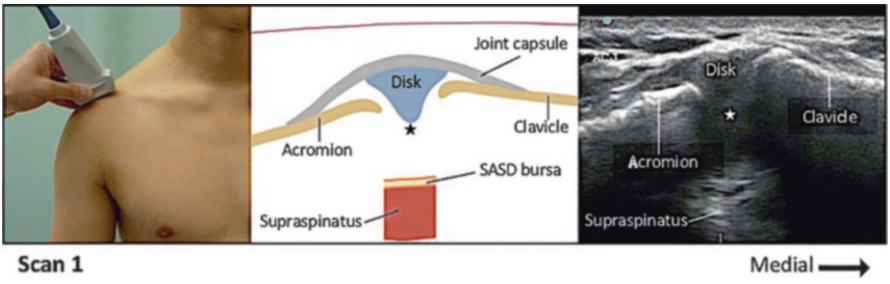

Fig. 19.9a AC joint coronal plane. (Photo and ultrasound image reproduced with permission from Philip Peng Educational Series. Illustration by Jennifer McDonald)

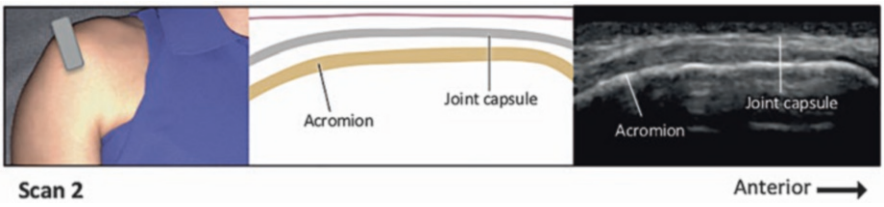

Fig. 19.9b Acromion, sagittal plane. (Photo and ultrasound image reproduced with permission from Philip Peng Educational Series. Illustration by Jennifer McDonald)

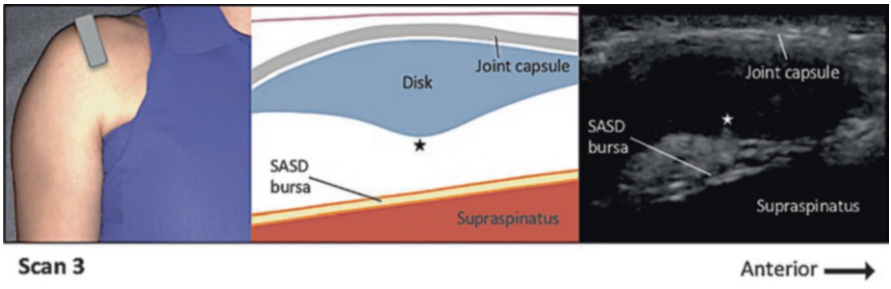

Fig. 19.9c Clavicle, sagittal plane. (Photo and ultrasound image reproduced with permission from Philip Peng Educational Series. Illustration by Jennifer McDonald)

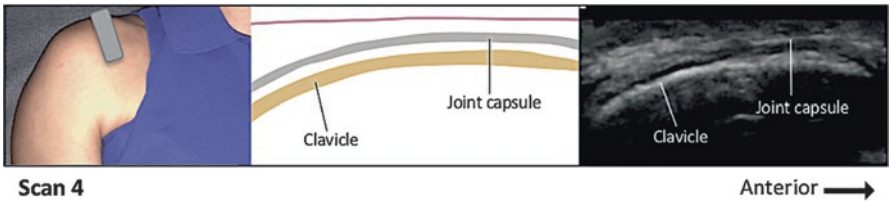

Fig. 19.9d AC joint, short-axis view. (Photo and ultrasound image reproduced with permission from Philip Peng Educational Series. Illustration by Jennifer McDonald)

Ultrasound Procedure

LHB tendon	
Needles:	25G 1.5-inch needle
Drugs:	2–4 mL local anesthetic with steroid (0.25% bupivacaine and 20–40 mg Depo-Medrol)
Approach:	Out-of-plane or in-plane

The target is the biceps tendon sheath (Fig. 19.10). The needle tip is positioned medial to the hyperechoic biceps tendon deep to the transverse humeral ligament. The lateral anterior circumflex artery should be avoided. (a) Correct position of ultrasound probe and needle for out-of-plane technique. (b) Corresponding US image post-injection. Black arrow marks the anterior circumflex artery. White arrowheads outline the local anesthetic within the biceps tendon sheath.

Clinical Pearls

1. LHB tendon pathology is rarely present in isolation, and localized tenderness on examination is not a specific finding. Before targeting the biceps tendon, consider rotator cuff pathology or GH joint pathology with an effusion tracking down the biceps tendon sheath.
2. Doppler examination is helpful to localize the anterior circumflex artery and to assess for increased vascularity (aka hyperemia), representing inflammation.
3. Intratendinous injection should be avoided. If the tendon begins to swell, stop the injection, and redirect the needle tip to the tendon sheath.

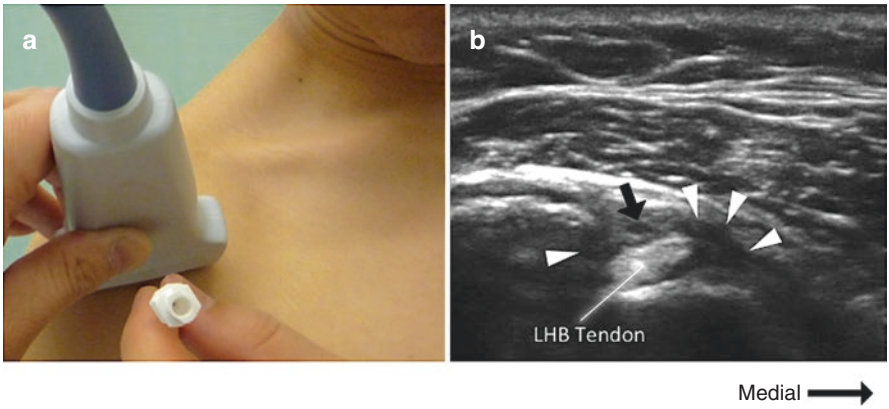

Fig. 19.10 Needle insertion for LHB. (Reproduced with permission from Philip Peng Educational Series)

Literature Review

The target site for biceps tendon disease is the tendon sheath with avoidance of intratendinous injection. This is difficult to achieve with blind technique. A study comparing blind injection to US-guided technique, using CT scan as the validating tool, revealed accurate injection in all of the US-guided injections but only two-thirds of the blind injections. US-guided technique also results in better outcome. A prospective randomized trial revealed improved pain and function scores in the US-guided injection group compared to the blind injection group.

Anterior GH joint approach via rotator interval with capsular distension	
Needles:	22G 2-inch needle or 22 G 3.5-inch spinal needle
Drugs:	10 mL local anesthetic with steroid (1% lidocaine and 40–80 mg Depo-Medrol)
Approach:	In-plane from medial aspect of probe

The needle tip is positioned adjacent to the intra-articular portion of the LHB tendon, deep to the CHL (Fig. 19.11). The fluid will fill the synovial recess, which is continuous with the GH joint, and distend the rotator interval capsule. (a) Correct position of ultrasound probe and needle for in-plane technique. (b) Corresponding US image post-injection. The white line marks the needle trajectory, and white arrowheads outline the local anesthetic within the synovial recess. Some injectate commonly leaks back into the subdeltoid bursal space (marked by asterisk) due to the high pressure.

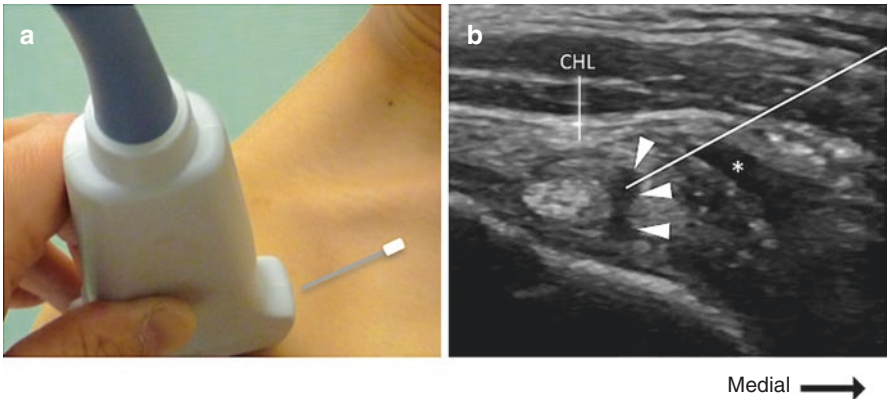

Fig. 19.11 Anterior approach to GHJ. (Reproduced with permission from Philip Peng Educational Series)

Clinical Pearls

1. High resistance will be encountered during the injection of the frozen shoulder due to thickening of the CHL and SGHL. Thus, proper localization of the needle tip is critical to avoid intratendinous injection, which will also provide high resistance.
2. If a sudden loss of resistance is encountered, check that the needle tip has not slipped out into the subdeltoid bursal space. If this has occurred, stop the injection, and redirect the needle tip to the correct target site.
3. A home stretching routine, with a focus on passive range of motion of the GH joint, is recommended when the pain settles, approximately 1-week post-injection.

Literature Review

Frozen shoulder or adhesive capsulitis is a particularly painful shoulder disorder most often impacting adults in their 50s. Given the presence of inflammation and thickening in region of the rotator interval in individuals with frozen shoulder, many have theorized that a steroid injection targeting the rotator interval capsule would be more beneficial than other injection techniques. Thus, the intra-articular GH joint space is accessed through the synovial recess and the rotator interval capsule distended with 10 mL total volume. While there are currently no published RCTs studying this approach, the authors have noted positive outcomes in clinical practice.

A recent systematic review concluded that corticosteroid injections provide short-term efficacy in frozen shoulder. There is currently no evidence to support a particular approach (SASD bursa, posterior GH joint, rotator interval) or the use of ultrasound over blind technique.

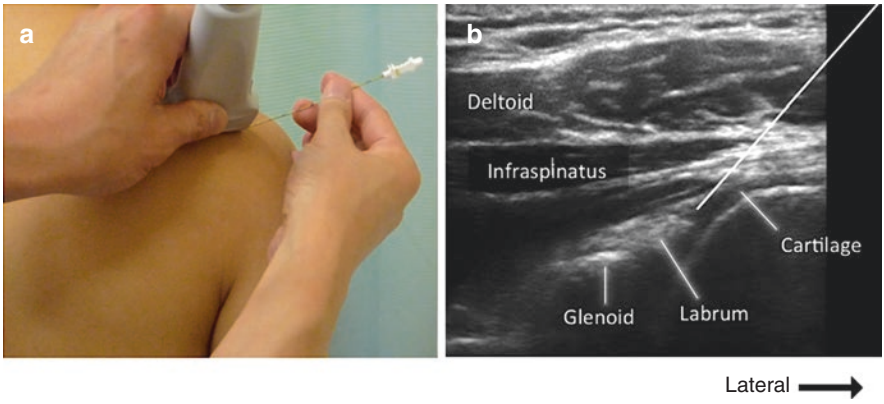

Fig. 19.12 Posterior approach to GHJ. (Reproduced with permission from Philip Peng Educational Series)

A recent meta-analysis of 11 randomized control trials (RCTs) did not show superiority of capsular distension (accessed via posterior GH joint injection) over intra-articular steroid injection alone for long-term improvement in shoulder function.

Posterior approach GH joint	
Needles:	22G 2-inch needle or 22G 3.5-inch spinal needle
Drugs:	4 mL local anesthetic with steroid (1–2% lidocaine and 40 mg Depo-Medrol)
Approach:	In-plane from lateral aspect of probe

The needle tip is positioned adjacent to the triangular labrum, just deep to the joint capsule (Fig. 19.12). The cartilage and labrum should be avoided. With proper needle tip placement, the posterior capsule will distend. (a) Correct position of ultrasound probe and needle for in-plane technique. (b) Corresponding US image. The white line marks the needle trajectory. A successful injection will result in transient capsular distension and medial spread of medication into the joint.

Clinical Pearls

1. In order to clear the humeral head and access the narrow target, the needle trajectory can be quite steep. To improve needle visualization, a curvilinear probe can be used and heeled in toward the needle. Gel can be heaped under the toe of the probe to improve contact with the skin.
2. If resistance is encountered during the injection, turn the bevel 90 degrees or withdraw the needle slightly.
3. The hypoechoic hyaline cartilage lining the humeral head should not be mistaken for fluid within the joint space and should be avoided during injection.

Literature Review

The accuracy of blind GH joint injection ranges 27% to 100% in the literature. This is compared to an accuracy rate of 87%–100% with US guidance. Comparison studies of US-guided versus fluoroscopically guided GH joint injections by experienced radiologists revealed 100% accuracy in both groups, but less time and patient discomfort in the US group. There is no evidence to support or refute the use of GH joint steroid injections in the treatment of GH joint osteoarthritis. The American Academy of Orthopedic Surgeons 2011 guidelines on the treatment of GH osteoarthritis were unable to recommend for or against steroid injections and recommended the use of hyaluronic acid (HA) injections as an option, citing weak evidence. A 2017 non-blinded RCT comparing HA injection and physical therapy to physical therapy alone in patients with GH osteoarthritis found a statistically significant reduction in pain at 6 months in the HA group.

Many surgeons will wait 6–12 months between an intra-articular steroid injection and shoulder arthroplasty for the treatment of advanced osteoarthritis because of the theoretical risk of infection. A 2015 matched cohort study revealed no statistically significant relationship between preoperative steroid injection and postoperative infection.

Subacromial subdeltoid (SASD) bursa	
Needles:	25G 1.5-inch or 22G 2-inch needle
Drugs:	4 mL local anesthetic with steroid (0.25% bupivacaine and 40 mg Depo-Medrol)
Approach:	In-plane from distal aspect of probe

The target is the subdeltoid portion of the SASD bursa, which lies just deep to the subdeltoid fat and is continuous with the subacromial bursa (Fig. 19.13). (a) Correct position of ultrasound probe and needle for in-plane technique. (b) Corresponding

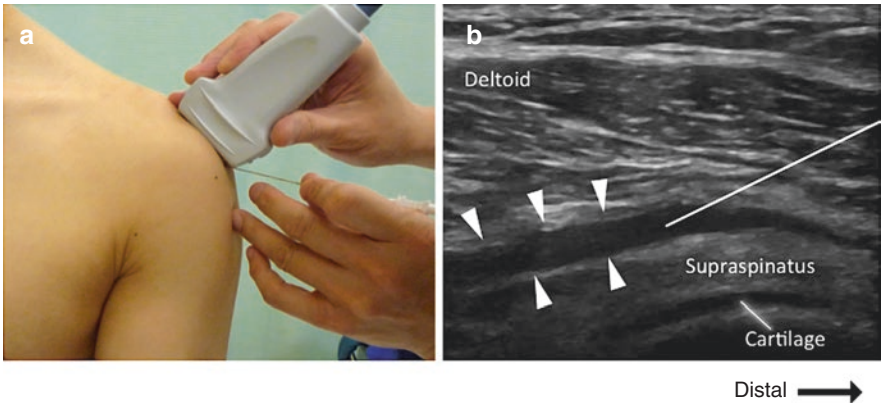

Fig. 19.13 Subacromial bursa injection. (Reproduced with permission from Philip Peng Educational Series)

US image post-injection. The white line marks the needle trajectory. The white arrowheads outline the local anesthetic within the SASD bursal space.

Clinical Pearls

1. Correct needle location within the bursal space is confirmed by rapid expansion of the bursa with small volume (0.5 mL) hydrodissection.
2. Partial rotator cuff tears are common incidental findings on shoulder US and MRI in healthy adults. Thus, imaging findings alone should not be used to determine the pain generator.

Literature Review

The success rate of landmark-based SASD bursa injection ranges 29–100% in clinical studies. The success rate was similar irrespective of approach, experience, and/or confidence level. A study of US-guided injection, with MRI validation, revealed an accuracy of 100%. A systematic review of nine RCTs studying SASD bursa steroid injections for treatment of rotator cuff disease concluded that there was no benefit. None of the reviewed studies used US-guided technique. A recent RCT revealed improved pain and function in the short-term post subacromial steroid injection, but no difference when compared to exercise alone at 3 and 6 months post-injection.

Acromioclavicular (AC) joint	
Needles:	25G 1.5-inch needle
Drugs:	1.5–2 mL local anesthetic with steroid (2% lidocaine and 10–20 mg Depo-Medrol)
Approach:	Out-of-plane or in-plane

The target is just deep to the AC joint capsule (Fig. 19.14). Out-of-plane technique is often used for this superficial structure. (a) Correct position of ultrasound probe and needle for out-of-plane technique. (b) Corresponding US image with out-of-plane needle (solid arrow) and superior joint capsule (white arrowheads) highlighted.

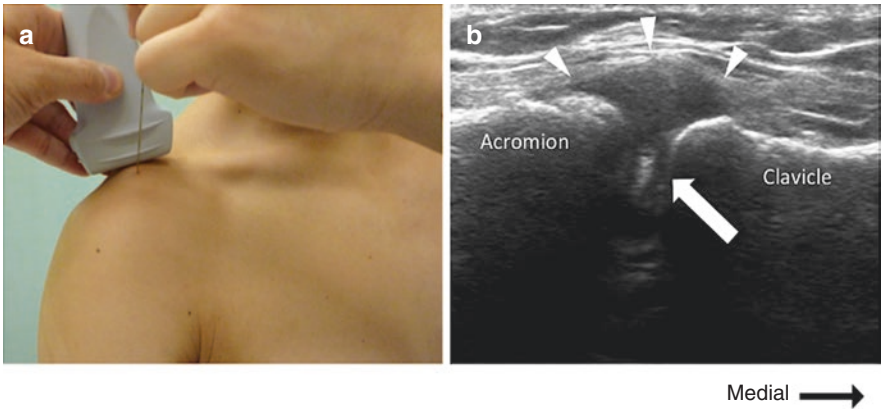

Fig. 19.14 AC joint injection. Reproduced with permission from Philip Peng Educational Series

Clinical Pearls

1. The AC joint is very shallow. The needle tip should be inserted no more than 1 cm deep. If the needle is too deep, the injectate will be deposited within the underlying subacromial bursa or supraspinatus tendon.
2. AC joint pathology often mimics other pain generators of the shoulder. If the AC joint is the suspected pain generator, repeating provocative maneuvers on examination post-injection with local anesthetic can be very helpful.

Literature Review

The accuracy of ultrasound-guided AC joint injection is significantly better than blind injection (95–100% versus 39–50%). The therapeutic role of AC joint injection is unclear as RCTs are lacking.

Suggested Reading

Cadogan A, Laslett M, Hing WA, McNair PJ, Coates MH. A prospective study of shoulder pain in primary care: prevalence of imaged pathology and response to guided diagnostic blocks. BMC Musculoskelet Disord. 8 ed. BioMed Central. 2011;12(1):119.

Crawshaw DP, Helliwell PS, Hensor EMA, Hay EM, Aldous SJ, Conaghan PG. Exercise therapy after corticosteroid injection for moderate to severe shoulder pain: large pragmatic randomised trial. BMJ. BMJ Publishing Group. 2010;340(jun28 1):c3037–7.

Di Giacomo G, de Gasperis N. Hyaluronic acid intra-articular injections in patients affected by moderate to severe glenohumeral osteoarthritis: a prospective randomized study. Joints. 2017;5(3):138–42.

Hashiuchi T, Sakurai G, Morimoto M, Komei T, Takakura Y, Tanaka Y. Accuracy of the biceps tendon sheath injection: ultrasound-guided or unguided injection? A randomized controlled trial. J Shoulder Elb Surg. 2011;20(7):1069–73.

Hutchinson M, Brukner P, Khan K, Ben Clarsen, McCrory P, Cools A, et al. Brukner & Khans clinical sports medicine injuries. McGraw-Hill Education; 2017. 1 p.

Izquierdo R, Voloshin I, Edwards S, Freehill MQ, Stanwood W, Wiater JM, et al. American academy of orthopaedic surgeons clinical practice guideline on: the treatment of glenohumeral joint osteoarthritis. J Bone Joint Surg Am. 2011;93(2):203–5.

Koester MC, Dunn WR, Kuhn JE, Spindler KP. The efficacy of subacromial corticosteroid injection in the treatment of rotator cuff disease: a systematic review. J Am Acad Orthop Surg. 2007;15(1):3–11.

Peck E, Lai JK, Pawlina W, Smith J. Accuracy of ultrasound-guided versus palpation-guided acromioclavicular joint injections: a cadaveric study. PM R. 2010;2(9):817–21.

Peng PWH, Cheng P. Ultrasound-guided interventional procedures in pain medicine: a review of anatomy, sonoanatomy, and procedures. Part III: shoulder. Reg Anesth Pain Med. 2011;36(6):592–605.

Rashid A, Kalson N, Jiwa N, Patel A, Irwin A, Corner T. The effects of pre-operative intra-articular glenohumeral corticosteroid injection on infective complications after shoulder arthroplasty. Shoulder Elbow. SAGE PublicationsSage UK: London. 2015;7(3):154–6.

Rockwood CA Jr, Matsen FA III, Wirth MA, Lippitt SB, Fehringer EV, Sperling JW. Rockwood and Matsen's the shoulder: Elsevier Health Sciences; 2016. 1 p.

Rutten MJCM, Collins JMP, Maresch BJ, Smeets JHJM, Janssen CMM, Kiemeney LALM, et al. Glenohumeral joint injection: a comparative study of ultrasound and fluoroscopically guided techniques before MR arthrography. Eur Radiol. Springer-Verlag. 2009;19(3):722–30.

Sabeti-Aschraf M, Lemmerhofer B, Lang S, Schmidt M, Funovics PT, Ziai P, et al. Ultrasound guidance improves the accuracy of the acromioclavicular joint infiltration: a prospective randomized study. Knee Surg Sports Traumatol Arthrosc. Springer-Verlag. 2011;19(2):292–5.

Schaeffeler C, Brügel M, Waldt S, Rummeny EJ, Wörtler K. Ultrasound-guided intraarticular injection for MR arthrography of the shoulder. Rofo. © Georg Thieme Verlag KG Stuttgart · New York. 2010;182(3):267–73.

Wu W-T, Chang K-V, Han D-S, Chang C-H, Yang F-S, Lin C-P. Effectiveness of glenohumeral joint dilatation for treatment of frozen shoulder: a systematic review and meta-analysis of randomized controlled trials. Sci Rep. Nature Publishing Group. 2017;7(1):10507.

Xiao RC, Walley KC, DeAngelis JP, Ramappa AJ. Corticosteroid injections for adhesive capsulitis: a review. Clin J Sport Med. 2016.

Zhang J, Ebraheim N, Lause GE. Ultrasound-guided injection for the biceps brachii tendinitis: results and experience. Ultrasound Med Biol. 2011;37(5):729–33.

Ultrasound-Guided Injections for Elbow Pain

20

Marko Bodor, Sean Colio, Jameel Khan, and Marc Raj

Introduction

Chronic elbow pain can be seen among patients at primary care and specialty clinics. The most frequent causes include common extensor and flexor tendinopathy, lateral and medial epicondylosis (tennis and golfer's elbow), and radio-humeral and humero-ulnar joint osteoarthritis. Intervention in these areas requires a sound knowledge of the anatomy (Figs. 20.1, 20.2, 20.3, and 20.4).

M. Bodor (✉)
Physical Medicine and Rehabilitation, University of California Davis, and Bodor Clinic, Napa, CA, USA
e-mail: mbodormd@sbcglobal.net

S. Colio · J. Khan · M. Raj
Bodor Clinic, Napa, CA, USA

P. Peng et al. (eds.), *Ultrasound for Interventional Pain Management*,
https://doi.org/10.1007/978-3-030-18371-4_20

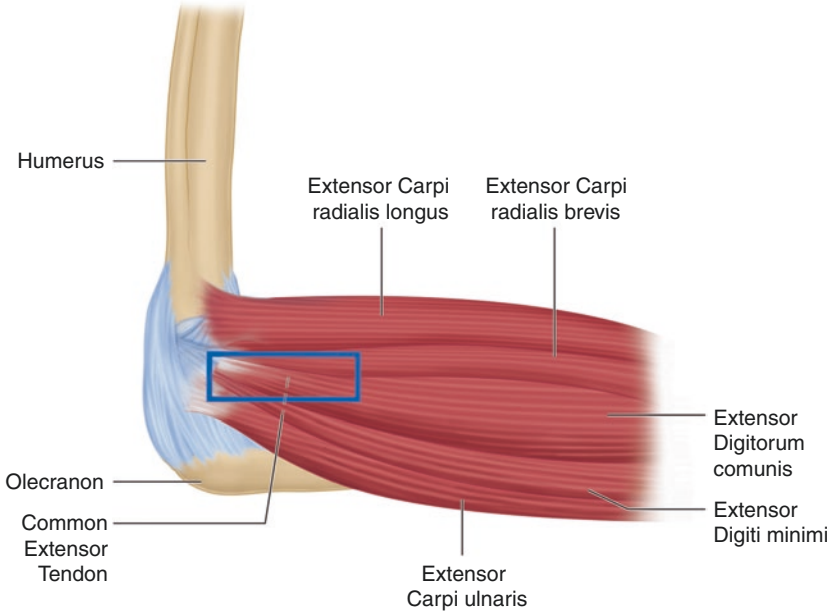

Fig. 20.1 Anatomy of the lateral elbow. The blue box is the region of the common extensor tendon and area of interest for ultrasound scanning

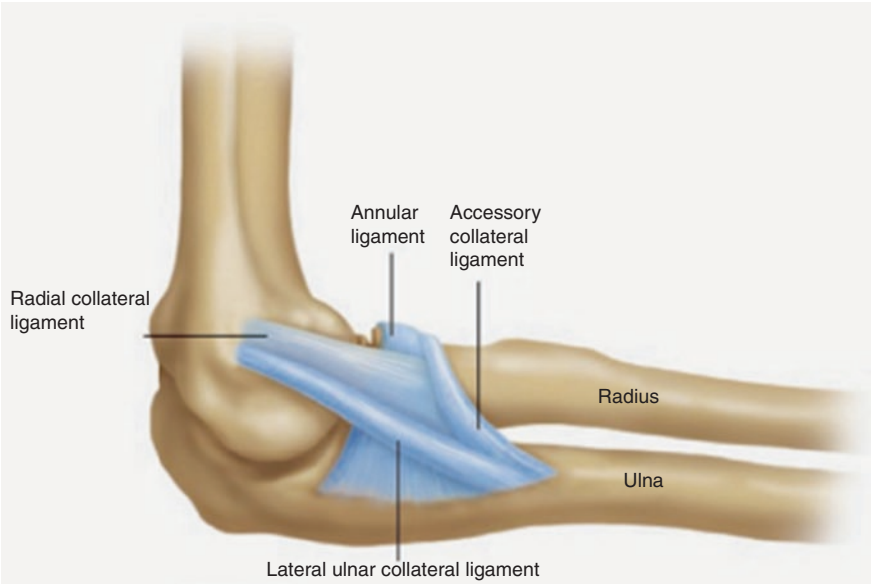

Fig. 20.2 The ligaments in the lateral elbow. (Reprinted with permission from Philip Peng Educational Series)

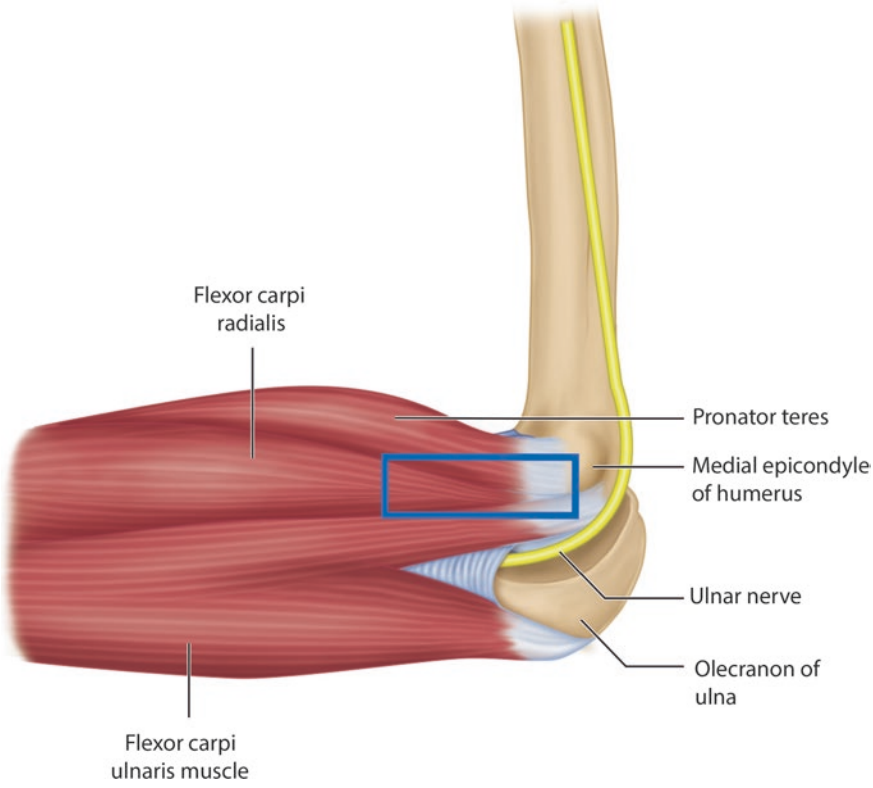

Fig. 20.3 Anatomy of the medial elbow. The blue box is the region of the common flexor tendon and area of interest for ultrasound scanning

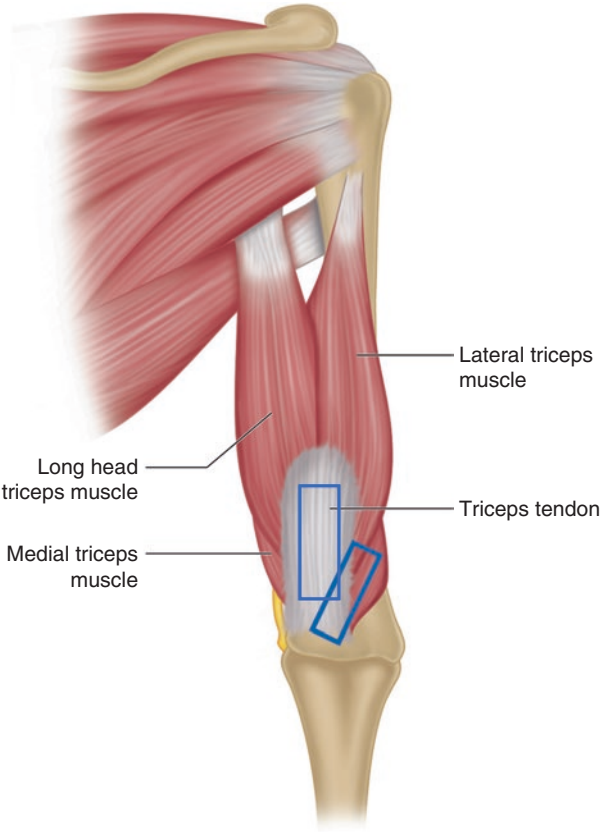

Fig. 20.4 Anatomy of the posterior elbow. The blue boxes are the area of interest for ultrasound scanning

Patient Selection

Common extensor and flexor tendinopathies are diagnosed based on pain and tenderness at the lateral and medial epicondyles and pain on resisted wrist extension or flexion. Relative rest, activity modifications, and physical therapy should be considered before an injection. Injections can be done using local anesthetic (e.g., ropivacaine) with or without steroid, platelet-rich plasma (PRP), or whole blood. The possibility of an underlying radial collateral ligament injury should be considered among patients with chronic lateral epicondylosis who have failed previous treatment, particularly corticosteroid injections. Humero-ulnar and radio-humeral (also known as radio-capitellar) joint arthritis is diagnosed on the basis of focal tenderness, painful movement, ultrasound findings of an effusion, or radiographic abnormalities.

Ultrasound Scan

- Position: Seated or supine
- Probe: Linear 5–12 MHz

Lateral Elbow

The key landmark is the lateral epicondyle (LE), the origin of the common extensor tendon (CET). Additional structures include the radio-capitellar joint (J) between head of the radius (R) and capitellum (C) of the humerus, and the radial collateral ligament (RCL) (Fig. 20.5).

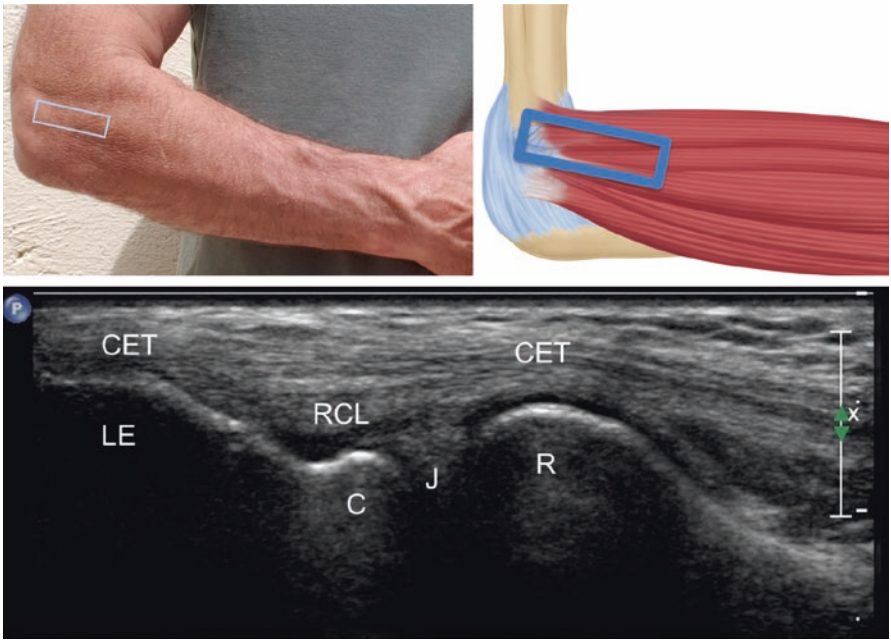

Fig. 20.5 Sonoanatomy of the lateral elbow

Medial Elbow

Medial elbow scan 1: The key landmark is the medial epicondyle (ME), from which the common flexor tendon (CFT) originates (Fig. 20.6).

Medial elbow scan 2: Short-axis views of the ulnar nerve (UN) in its usual retrocondylar position (Fig. 20.7a) and subluxed over the medial epicondyle (ME) of the humerus where it could be injured during an injection (Fig. 20.7b). Additional structures include the olecranon of ulna (U) and the triceps muscle (TM).

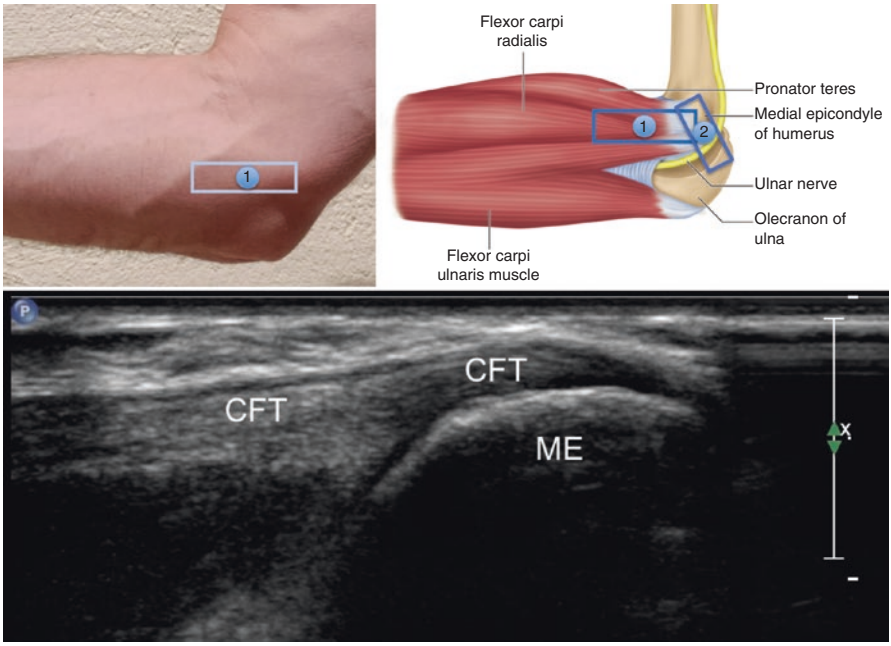

Fig. 20.6 Sonoanatomy of medial elbow with the ultrasound probe in scan position 1

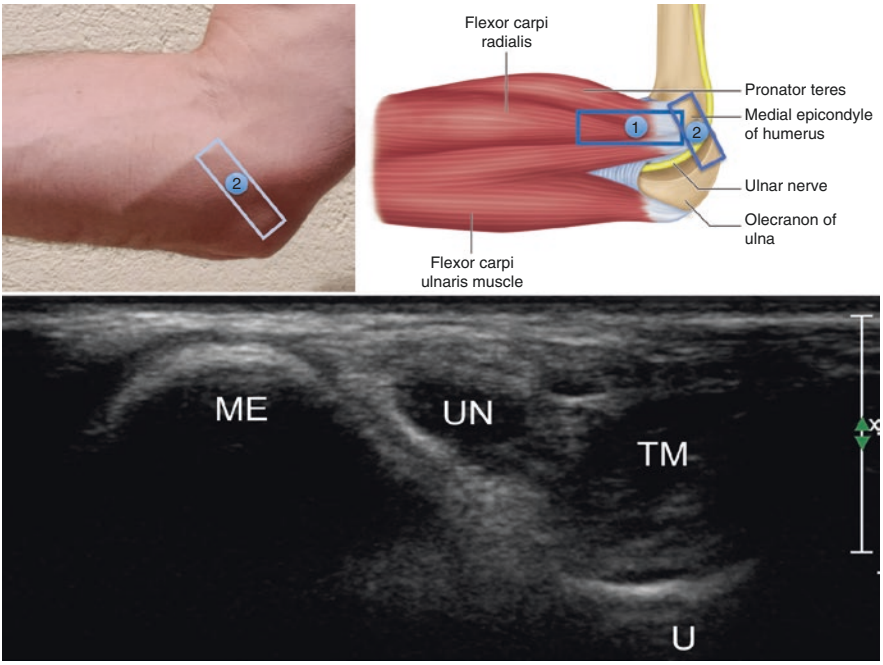

Fig. 20.7a Sonoanatomy of the medial elbow with the ultrasound probe in scan position 2

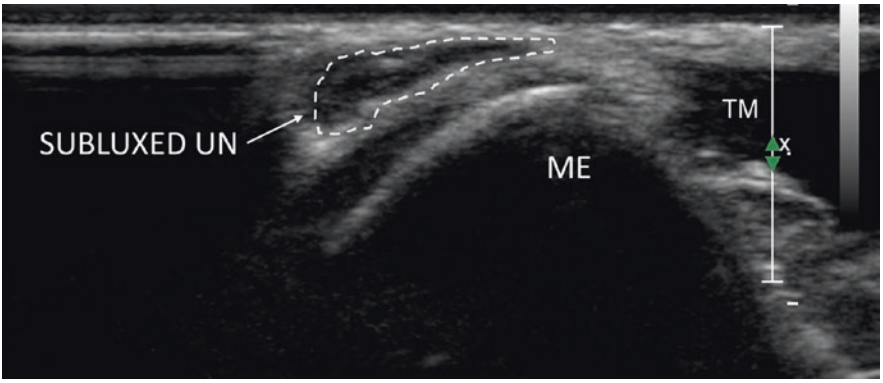

Fig. 20.7b Sonograph showed the ulnar nerve (UN) subluxed on the other side of medial epicondyle (ME)

Posterior Elbow

Posterior elbow scan 1. The position is shown in scan position 1. The key landmark is the olecranon (O) of the ulna and the triceps muscle (TM) and triceps tendon (TT). Humero-ulnar joint (HUJ) is seen between the humerus (H) and olecranon (O) (Fig. 20.8).

Keeping one end of the transducer over the olecranon while rotating the other end laterally, reveals the humero-ulnar joint (HUJ). Additional structures include the triceps muscle (TM), triceps tendon (TT), and distal humerus (H) (Fig. 20.9).

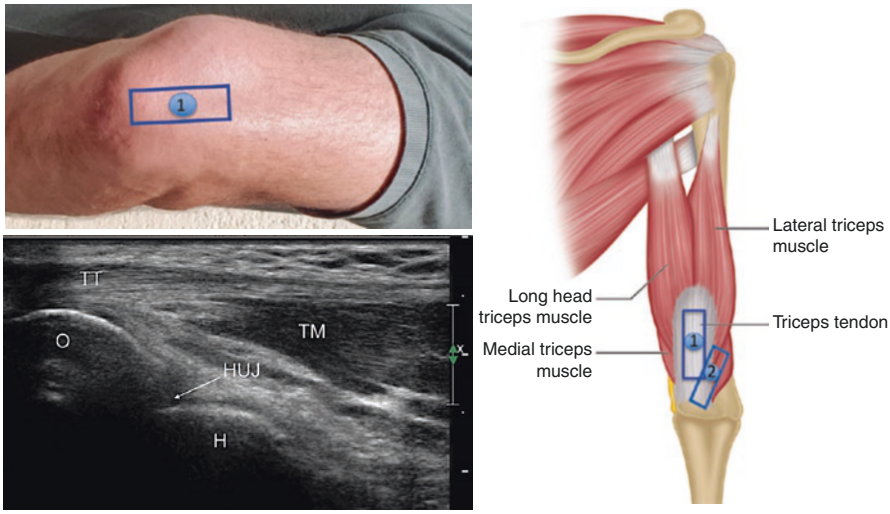

Fig. 20.8 Sonoanatomy of the posterior elbow with the ultrasound probe in the scan position 1

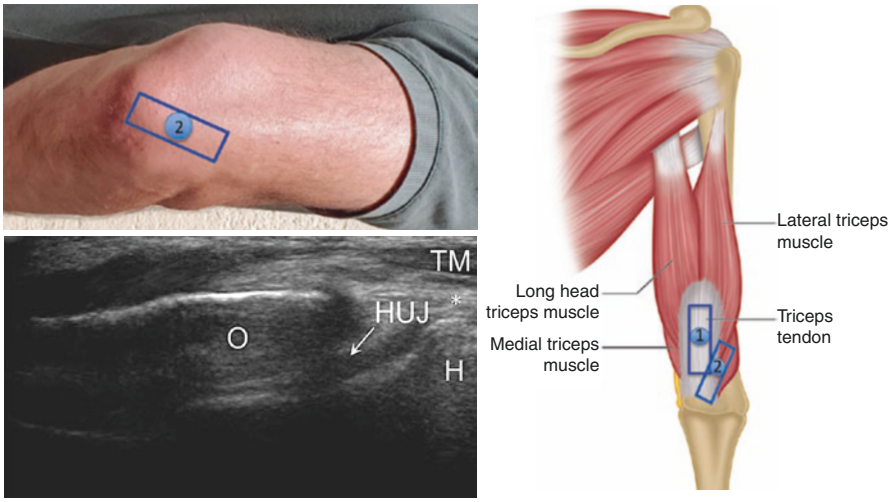

Fig. 20.9 Sonoanatomy of the posterior elbow with the ultrasound probe in the scan position 2

Procedure

- Needles: 27G 1.25-inch needle.
- Drugs: 1–2 ml of local anesthetic (0.5% plain ropivacaine) with or without 0.5–1.0 ml of steroid (triamcinolone acetonide 10 mg/ml), 1–2 ml of platelet-rich plasma (PRP) or whole blood.

Injection for Common Extensor Tendon

For the lateral epicondyle/common extensor tendon, injections can be done in-plane or out-of-plane (Fig. 20.10).

Injection for Common Flexor Tendon

For the medial epicondyle/common flexor tendon, an in-plane distal to proximal approach is preferred (Fig. 20.11).

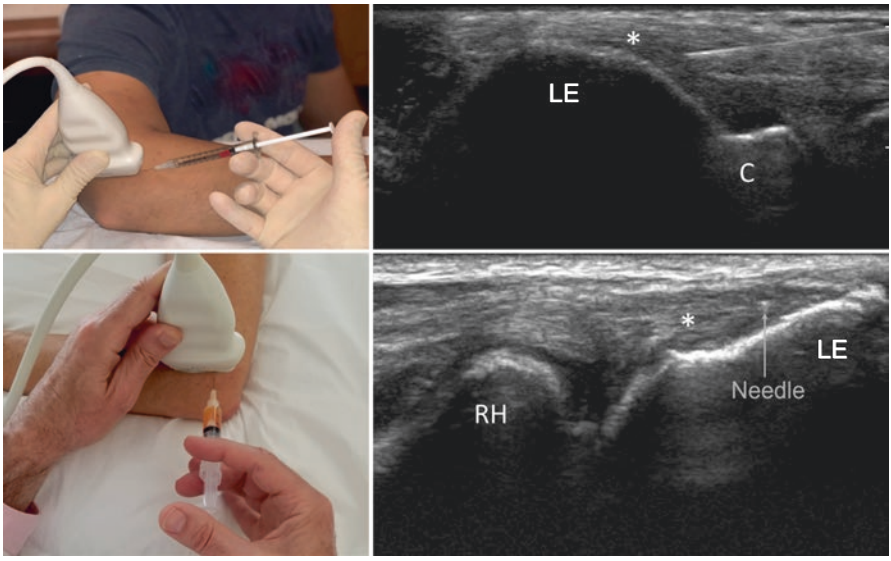

Fig. 20.10 Upper panel. In-plane injection. Lower panel. Out-of-plane injection. LE, lateral epicondyle; C, capitellum; RH, radial head; ∗, common extensor tendon

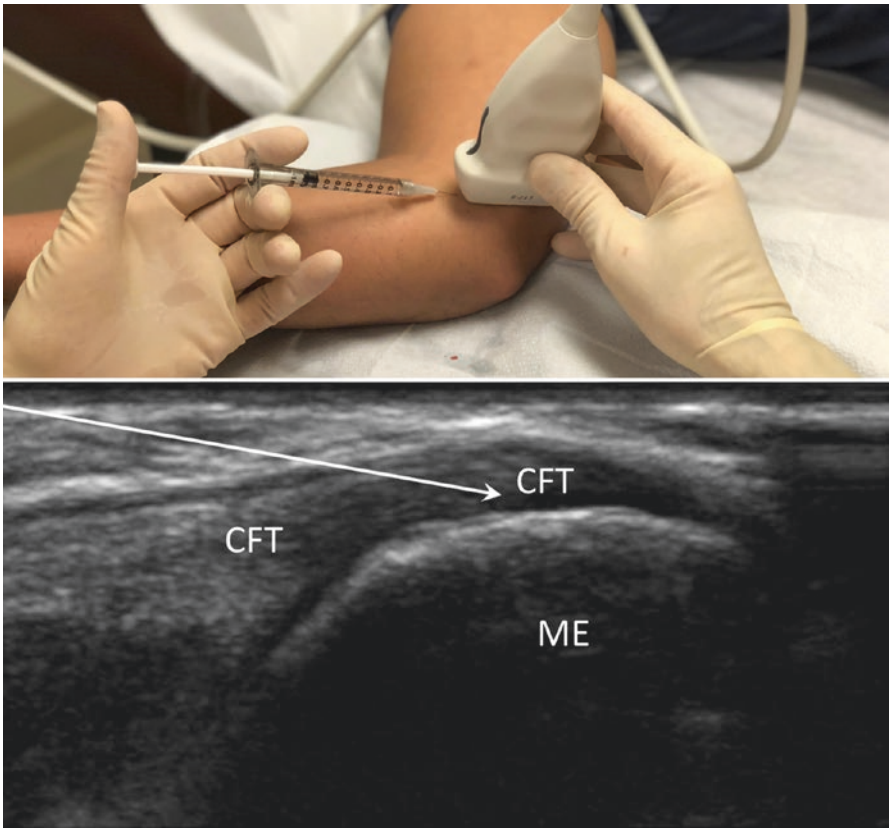

Fig. 20.11 Sonograph showing the needle trajectory for common flexor tendon injection

Elbow Joint Injection

For the radio-capitellar joint, an out-of-plane approach is best (Fig. 20.12 upper panel). For the humero-ulnar joint, an in-plane approach can be done by positioning one end of the transducer over the distal olecranon and then rotating the other end 30° laterally to bring the joint into view (Fig. 20.12 lower panel). The transducer is then moved a bit distally to bring the joint opening closer to the needle entry site.

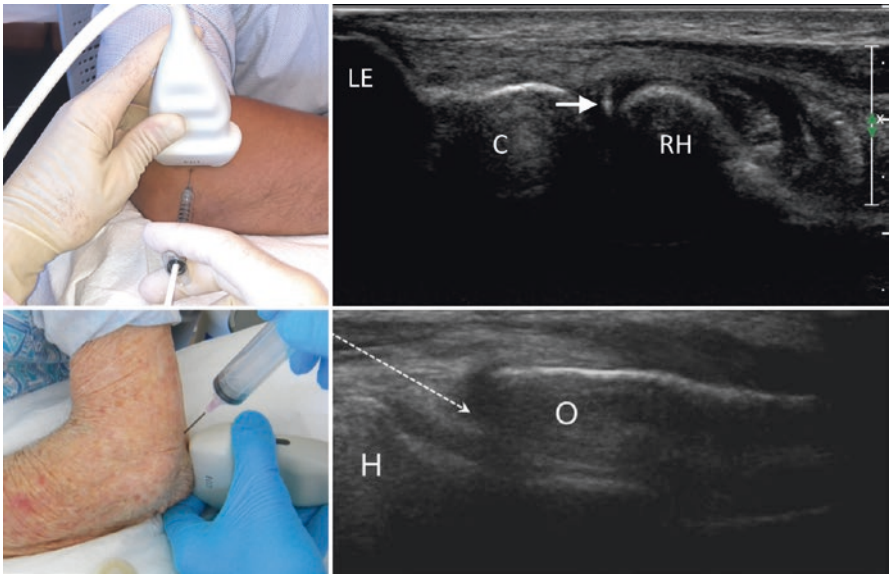

Fig. 20.12 Upper panel. Radio-capitellar joint injection. Arrow indicated the needle. Lower panel. Humero-ulnar injection. C, capitellum; LE, lateral epicondyle; RH, radial head; O, olecranon; H, humerus

Clinical Pearls

1. When injecting tendons, the position of the needle and flow of injectate should be seen in two planes to ensure injectate spreads where intended.
2. When injecting the common flexor tendon, check to make sure the ulnar nerve is not subluxed over the medial epicondyle and in the path of the needle.
3. When injecting steroid into the common extensor tendon, make sure the needle does not go too deep and into the radial collateral ligament.
4. When injecting the radio-capitellar joint, note that the joint is quite superficial and the needle depth should not exceed 1–2 cm.
5. When injecting steroids, use the lowest possible doses and volumes because of the potential for steroid-induced weakening of tendons, ligaments, and cartilage.

Literature Review

Coombes et al. randomized 165 patients with lateral epicondylalgia of at least 6 weeks duration to corticosteroid or anesthetic injection groups and found that the corticosteroid injection group had a lower rate of complete recovery compared to the anesthetic-only group (83% versus 96%) at 1 year [1]. Mishra et al. randomized 230 patients with lateral epicondylalgia of at least 3 months duration to needling plus bupivacaine or needling plus leukocyte-rich PRP groups with 68% and 84%, respectively, reporting successful outcomes at 6 months [2]. Suresh et al. injected whole blood in a series of 20 patients with chronic (median of 12 months) medial epicondyle pain and noted improvement of average VAS scores from 6 to 1 at 10 months [3]. In a prospective study of 19 patients with chronic (greater than 6 months) elbow tendinosis, Barnes et al. performed ultrasound-guided percutaneous ultrasonic tenotomy instead of open surgery and noted improvement of average VAS scores from 6.4 to 0.7 at 1 year [4].

Suggested Reading

1. Coombes BK, Bisset L, Brooks P, et al. Effect of corticosteroid injection, physio- therapy, or both on clinical outcomes in patients with unilateral lateral epicondylalgia: a randomized controlled trial. JAMA. 2013;309(5):461–9.
2. Mishra AK, Skrepnik NV, Edwards SG, et al. Platelet-rich plasma significantly improves clinical outcomes in patients with chronic tennis elbow a double-blind, prospective, multicenter, controlled trial of 230 patients. Am J Sports Med. 2014;42(2):463–71.
3. Suresh SP, Ali KE, Jones H, et al. Medial epicondylitis: is ultrasound guided autologous blood injection an effective treatment. Br J Sports Med. 2006;40(11):935–9.
4. Barnes DE, Beckley JM, Smith J. Percutaneous ultrasonic tenotomy for chronic elbow tendinosis: a prospective study. J Shoulder Elbow Surg. 2015;24(1):67–73.
5. Jacobson JA, Chiavaras MM, Lawton JM, Downie B, Yablon CM, Lawton J. Radial collateral ligament of the elbow: sonographic characterization with cadaveric dissection correlation and magnetic resonance arthrography. J Ultrasound Med. 2014;33(6):1041–8.
6. Cunnington J, Marshall N, Hide G, et al. A randomized, double-blind, controlled study of ultrasound-guided corticosteroid injection into the joint of patients with inflammatory arthritis. Arthritis Rheum. 2010;62(7):1862–9.
7. Kim TK, Lee JH, Park KD, et al. Ultrasound versus palpation guidance for intra-articular injections in patients with degenerative osteoarthritis of the elbow. J Clin Ultrasound. 2013;41(8):479–85.
8. Sussman WI, Williams CJ, Mautner K. Ultrasound-guided elbow procedures. Phys Med Rehabil Clin N Am. 2016;27(3):573–87.
9. Bodor M, Lesher J, Colio S. Chap. 23 - Ultrasound-guided hand, wrist, and elbow injections. In: Atlas of ultrasound-guided procedures in interventional pain management. Springer; 2011.

10. Krogh TP, Bartels EM, Ellingsen T, et al. Comparative effectiveness of injection therapies in lateral epicondylitis: a systematic review and network meta- analysis of randomized controlled trials. Am J Sports Med. 2013;41(6):1435–46.
11. Krogh TP, Fredberg U, Stengaard-Pedersen K, et al. Treatment of lateral epicondylitis with platelet-rich plasma, glucocorticoid, or saline: a randomized, double-blind, placebo-controlled trial. Am J Sports Med. 2013;41(3):625–35.
12. Edwards SG, Calandruccio JH. Autologous blood injections for the refractory lateral epicondylitis. J Hand Surg Am. 2003;28(2):272–8.
13. Stahl S, Kaufman T. Ulnar nerve injury at the elbow after steroid injection for medial epicondylitis. J Hand Surg Br. 1997;22(1):69–70.
14. McShane JM, Shah VN, Nazarian LN. Sonographically guided percutaneous needle tenotomy for treatment of common extensor tendinosis in the elbow: is a corticosteroid necessary? J Ultrasound Med. 2008;27:1137.

Intervention on Wrist and Hand

21

David A. Spinner and Anthony J. Mazzola

Median Nerve (Carpal Tunnel Syndrome)

Introduction

Median nerve neuralgia can produce pain and paresthesias in the distribution of the median nerve. When untreated, weakness and atrophy of the flexor pollicis brevis, opponens pollicis, and abductor pollicis brevis may occur. Carpal tunnel syndrome is caused by compression of the median nerve as it passes through the carpal tunnel at the volar aspect of the wrist.

The median nerve arises at the brachial plexus with origins from the medial and lateral cords (encompassing nerve roots C5-T1). The median nerve travels in the anterior compartment, medial to the humerus down to the forearm, and enters into the hand by passing through the carpal tunnel. At the forearm, it gives off two branches: the anterior interosseous nerve and palmar cutaneous nerve. After passing through the carpal tunnel, it gives off an additional two branches: the recurrent branch (provides motor to the thenar muscles) and digital cutaneous branch (provides sensory to the lateral three and half digits and provides motor to the lumbricals) (Figs. 21.1 and 21.2). Of note, the palmar branch (provides sensory to the palm) is often spared as it comes off proximally and then travels superficially to the flexor retinaculum.

Patient Selection

Diagnosis begins with a complete history characterizing the type of pain and its location. The history should correlate with expected findings of median nerve compression as it passes through the tunnel at the wrist. These include burning pain associated

D. A. Spinner (✉) · A. J. Mazzola
Department of Rehabilitation and Human Performance, Mount Sinai Hospital, New York, NY, USA
e-mail: David.Spinner@mountsinai.org

P. Peng et al. (eds.), *Ultrasound for Interventional Pain Management*,
https://doi.org/10.1007/978-3-030-18371-4_21

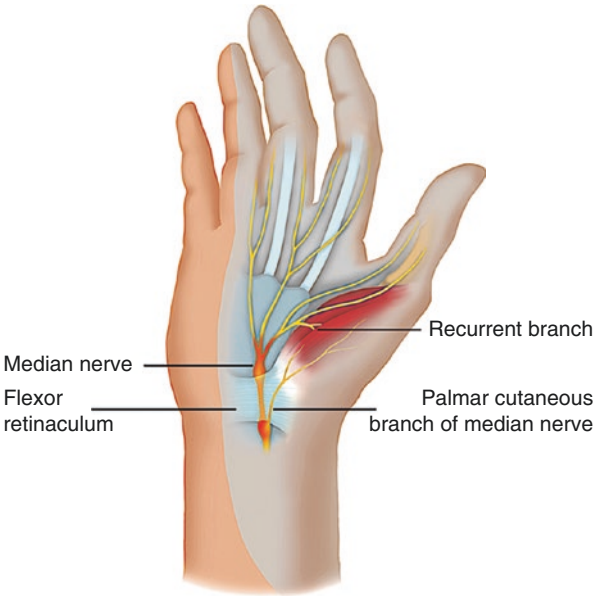

Fig. 21.1 Carpal tunnel. Please note the recurrent branch and palmar cutaneous branch of median nerve. (Reprinted with permission from Philip Peng Educational Series)

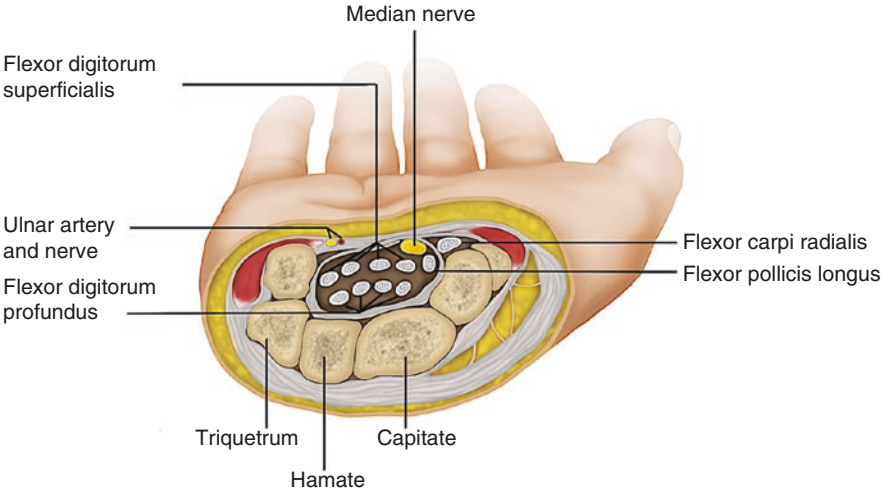

Fig. 21.2 Cross-sectional view of the wrist at carpal tunnel. (Reprinted with permission from Philip Peng Educational Series)

with numbness and tingling of the volar surface of the thumb, index finger, middle finger, and radial half of the ring finger. The palm and little finger are often spared. Symptoms often worsen at night and after repeated use. Traditional physical exam maneuvers to reproduce nerve compression including Tinel's sign and Phalen's test are neither highly sensitive nor specific. Thenar atrophy can help to rule in. Diagnostic testing includes electrodiagnostic studies (nerve conduction and electromyography) and ultrasound measurements of median nerve cross-sectional area.

Ultrasound Scan

- Position: Seated with forearm supinated with hand resting comfortably on the table. Rolled towel can support wrist in mild extension.
- Probe: High-frequency linear array transducer (10 MHz+); Hockey stick linear probe is preferred.

Short axis over the distal wrist crease (Fig. 21.3)

The borders of the tunnel seen are the scaphoid and trapezium laterally and the hamate and pisiform medially. The roof of the tunnel is the flexor retinaculum (marked with ∗). Identify the flexor carpi radialis (FCR) and the palmaris longus (PL) located superficial to the flexor retinaculum. The median nerve (MN) will appear honeycomb-like in the tunnel along with the hypoechoic tendons of the flexor digitorum profundus (flexor tendons), flexor digitorum superficialis (flexor tendons), and flexor pollicis longus (FPL). To clearly identify the nerve, scan proximally and distally. The ideal injection will have the median nerve identified at the level of the pisiform under the transverse carpal ligament. Use color flow to mark the location of the ulnar artery (UA) as in the right lower diagram. The left diagram shows the position of the probe and the underlying structures.

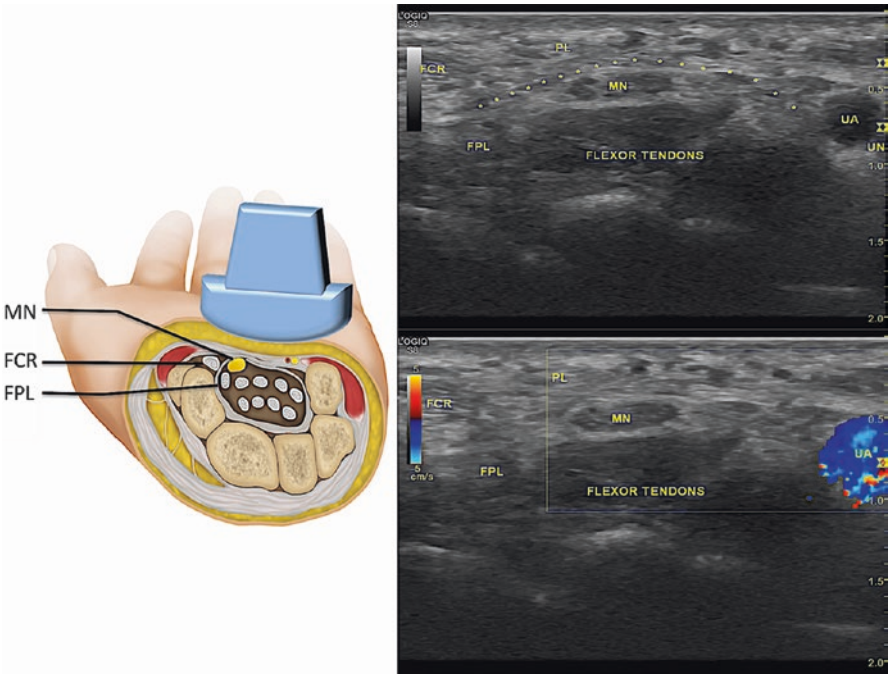

Fig. 21.3 Sonograph of the carpal tunnel. (Reprinted with permission from Philip Peng Educational Series)

Procedure

1. In-Plane Injection

- Needles: 25G–27G 1.5 inch needle
- Drugs: 1–3 mL local anesthetic (0.25% plain bupivacaine)
  0.5 mL steroid (depomedrol)

In-plane approach is performed from ulnar to radial inserting the needle 1–3 cm away and parallel to probe just radial or deep to the ulnar nerve and artery at a shallow angle (Fig. 21.4). The needle (arrows) will be visualized in the canal. Here, the needle is next to and under the median nerve (MN). The injectate can now be administered. As the space is enclosed, the medicine will spread and saturate the nerve.

2. Out-of-Plane Injection

Short axis over the distal wrist crease (Fig. 21.5). With the probe target just ulnar to the median nerve, an out-of-plane approach is performed by inserting needle perpendicular to the probe at a steep angle directed just off to the ulnar side of the median nerve (MN). A small hyperechoic dot will be seen on the ulnar side of the nerve (needle tip depicted by arrowhead). Use caution with out-of-plane injections to ensure tip is under the transducer. Inject next to the nerve.

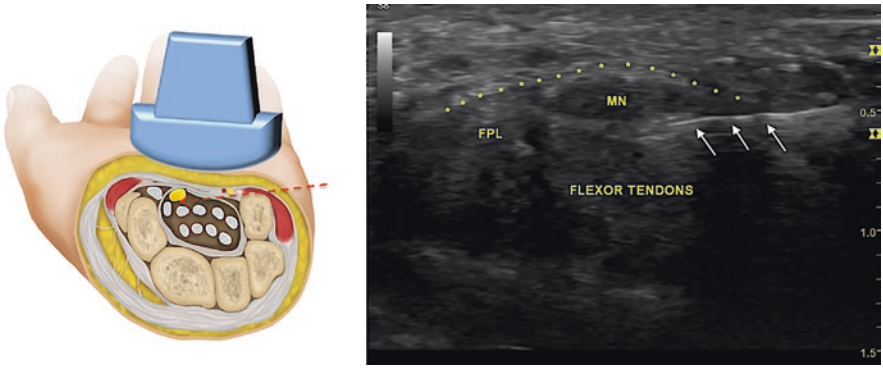

Fig. 21.4 In-plane needle insertion. FPL-flexor pollicis longus. (Reprinted with permission from Philip Peng Educational Series)

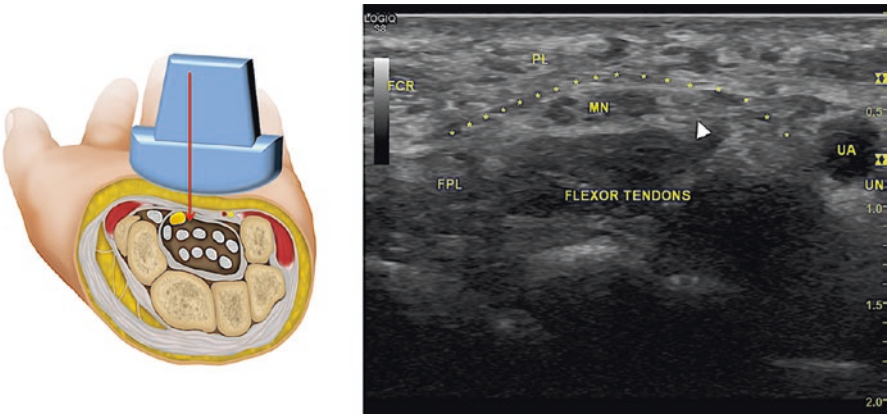

Fig. 21.5 Out-of-plane needle insertion. (Reprinted with permission from Philip Peng Educational Series)

Clinical Pearls

1. To visualize the median nerve, isolate a relatively hypoechoic area surrounded by hyperechoic tendons in cross-sectional view.
2. Tilt/angle the probe or have patient flex and extend their hand: the nerve will remain relatively unchanged because the tendons are more subject to anisotropy.
3. Look for adhesions, which can be treated by hydrodissection.
4. Track nerve proximally up the arm if difficult to visualize.
5. Use gel standoff technique if wrist is too small to achieve a shallow needle trajectory.
6. Use color flow to aid in identifying vascular structures such as a persistent medial artery.
7. Advise patients to refrain from driving secondary to possible temporary hand numbness/weakness.

Literature Review

Ultrasound-guided injections at the carpal tunnel allow the practitioner to visualize the median nerve, assess for any structural abnormalities or masses, and ultimately place medicine in the correct position without damaging the nerve. Median nerve blocks are proven to provide pain relief in patients suffering from carpal tunnel syndrome. Ultrasound-guided corticosteroid injections targeting the median nerve are more accurate over direct approach and demonstrate significant improvements

in post-injection monofilament testing, sensory nerve conduction velocity, and digit-4 comparison study (comparing ulnar to medial sensory latency at the dually innervated fourth digit). The American Academy of Orthopedic Surgeons suggests the use of local steroid injections prior to considering surgery for carpal tunnel syndrome. Recent studies demonstrate that in-plane ulnar approach proves to be superior over out-of-plane injection.

De Quervain's Tenosynovitis

Introduction

Pain or tenderness in the first extensor compartment of the radial wrist at the styloid process produced by a tendinopathy of the abductor pollicis longus (APL) and extensor pollicis brevis (EPB) is known as De Quervain's tenosynovitis (Fig. 21.6). These tendons are involved in radial abduction and extension of the thumb. Through progressive rubbing, these tendons become irritated causing symptoms.

Locate the abductor pollicis longus and extensor pollicis brevis tendon at the first dorsal compartment at the radial styloid process (Fig. 21.7). The APL originates at the ulna and inserts at the base of the metacarpal of the first digit. The EPB originates at the lower third of the radius and inserts at the base of the proximal phalanx of the first digit.

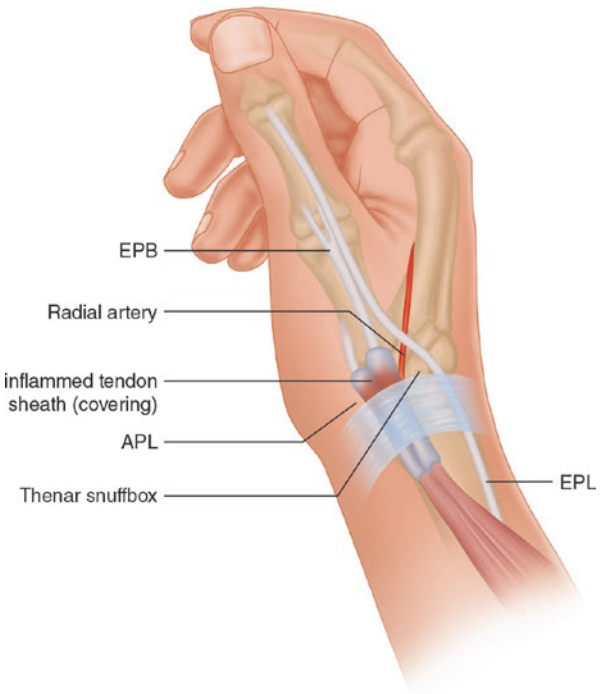

Fig. 21.6 Anatomical snuff box. EPB, extensor pollicis brevis; APL, abductor pollicis longus; EPL, extensor pollicis longus

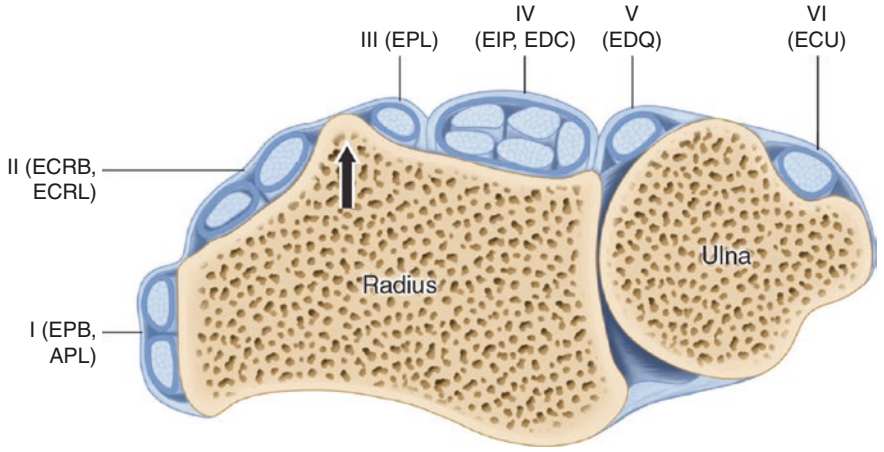

Fig. 21.7 Six compartments of the extensor tendons in the wrist. First compartment, abductor pollicis longus (APL) and extensor pollicis brevis (EPB); second compartment, extensor carpi radialis longus (ECRL) and extensor carpi radialis brevis (ECRB); third compartment, the extensor pollicis longus (EPL); fourth compartment, extensor indicis proprius (EIP) and extensor digitorum (EDC); fifth compartment, the extensor digiti quinti (EDQ); sixth compartment, extensor carpi ulnaris (ECU). Lister tubercle (arrow) separates the second from the third compartment

Fig. 21.8 Finkelstein maneuver. (Reprinted with permission from Philip Peng Educational Series)

Patient Selection

Patients present with radial sided wrist pain at the thumb base with histories of overuse often without direct acute trauma. There is a higher prevalence in the dominant wrist. Tenderness is common over the location of the APL and EPB tendons.

Classically, the Finkelstein maneuver will reproduce symptoms as the two thumb tendons are elongated by flexing the thumb and ulnar deviating the wrist (Fig. 21.8). Imaging is not routinely useful as x-rays are expected to be unremarkable. With ultrasound, one can demonstrate a thickened extensor retinaculum indicating possible synovitis.

Ultrasound Scanning

- Position: Seated with elbow flexed with radial styloid facing up and arm resting comfortably on the table
- Probe used: High-frequency linear array transducer (10 MHz+); Hockey stick probe is preferred.

Scan 1

Short-Axis View

Over the radial styloid process, the transducer is placed transversely, short axis to visualize the first extensor compartment (Fig. 21.9). The abductor pollicis longus (APL) and extensor pollicis brevis (EPB) are seen. Extensor retinaculum (outlined by ∗) lies superficially to tendons and radius (RAD) is seen deep to tendons. Note location of the radial artery prior to injection.

Scan 2

Longitudinal View of Radial Styloid and APL Tendon

Over the radial styloid process, the transducer is rotated longitudinally (Fig. 21.10). Abductor pollicis longus (APL) and extensor pollicis brevis (EPB) are seen along their long axis above the radius.

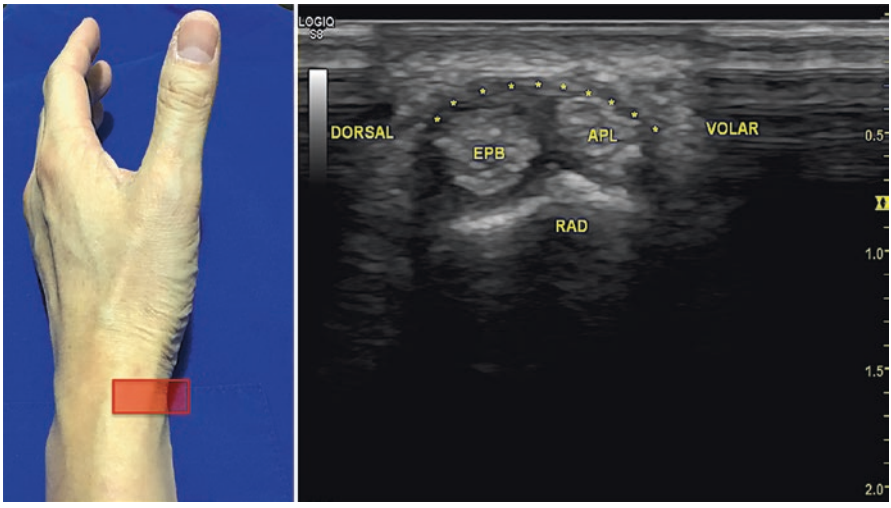

Fig. 21.9 Sonograph of the first extensor compartment. (Reprinted with permission from Philip Peng Educational Series)

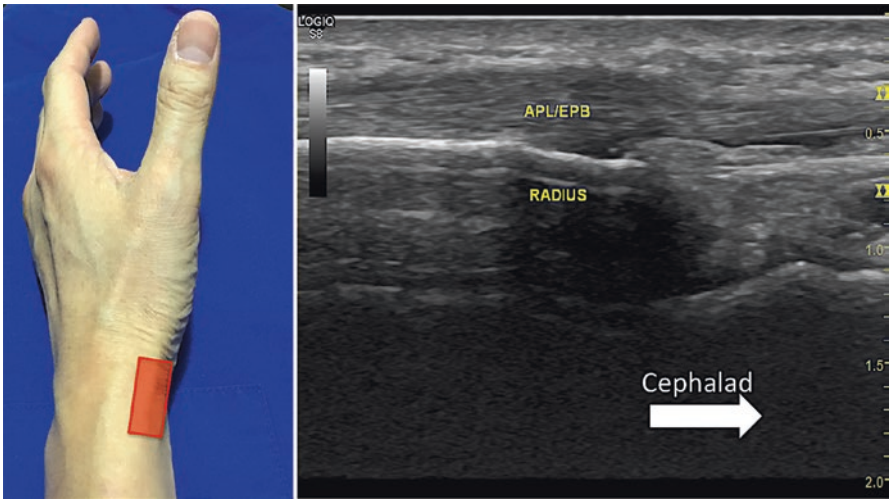

Fig. 21.10 Long-axis view of the first extensor compartment. (Reprinted with permission from Philip Peng Educational Series)

Procedure

- Needles: 25G 1.5 inch needle
- Drugs: 1–3 mL local anesthetic (0.25% plain bupivacaine)
  0.5 mL steroid (depomedrol)

1. In-Plane Injection

Place the probe short axis over the abductor pollicis longus (APL) and extensor pollicis brevis (EPB) adjacent to radial styloid process. In-plane injection is performed from dorsal to volar with insertion point 1–3 cm away from the probe (Fig. 21.11). Deliver injectate when the needle (arrows) tip is visualized near the tendon sheath above the APL and EPB.

2. Out-of-Plane Injection

Place the probe short axis over the abductor pollicis longus (APL) and extensor pollicis brevis (EPB) adjacent to radial styloid process. Note the radial artery that will be located toward the volar surface. Using an out-of-plane approach, steeply insert needle adjacent and centered to the transducer (Fig. 21.12). Keeping the needle superficial, visualize a small hyperechoic dot approaching the target (needle tip depicted by arrowhead) of the tendon sheath before injecting. Reprinted with permission from Philip Peng Educational Series.

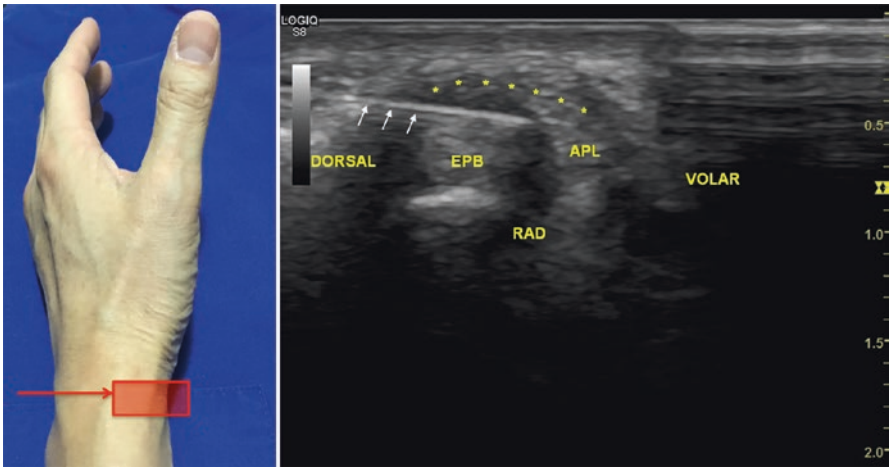

Fig. 21.11 In-plane needle insertion. (Reprinted with permission from Philip Peng Educational Series)

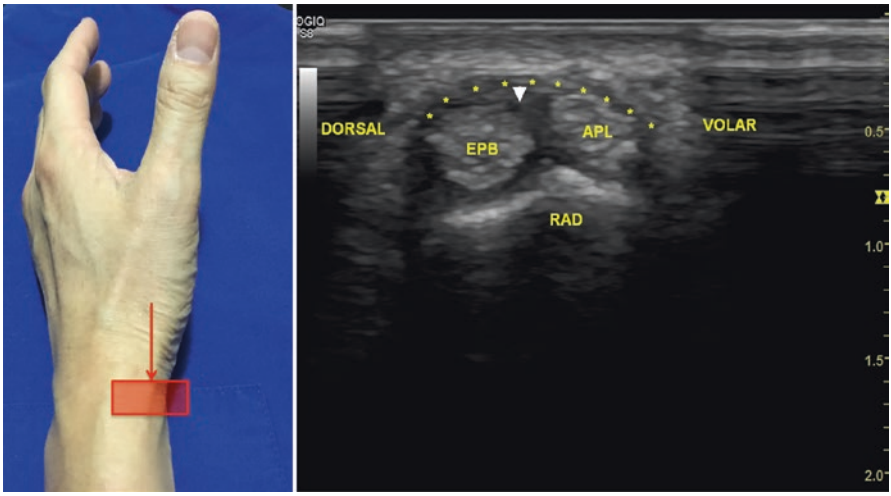

Fig. 21.12 Out-of-plane needle insertion. (Reprinted with permission from Philip Peng Educational Series)

Clinical Pearls

1. On longitudinal view thickening of the tendon sheath may be noted suggesting synovitis.
2. Scan distally from the radial styloid to visualize the insertions of the tendons.
3. Use color flow to visualize vascular structures and identify the radial artery.
4. If the probe is too large, consider utilizing a gel standoff technique or complete a long-axis in-plane approach for improved needle visualization.
5. As the superficial branch of the radial nerve often lies over the first dorsal compartment patient may have symptoms of radial nerve block.
6. Be aware of risk for bleeding, tendon rupture, and decreased functional scores. If using corticosteroid be aware of local depigmentation and scooping at the base of the thumb.
7. If a septum is visualized, each compartment should be injected to allow for complete dispersion of medication.

Literature Review

Ultrasound-guided injection of the first extensor compartment allows the practitioner to visualize the EPB and APL ensuring correct needle placement. Compared to landmark-guided technique, utilizing ultrasound allows improved accuracy. Ultrasound-guided injections to the first extensor compartment provide significant relief, improving pain and function, when utilizing steroid injectate. A combination of steroids and hyaluronic acid proved to have significantly greater symptom relief. Only under ultrasound guidance can the presence of a septum creating unique compartments be visualized. If separate compartments are visualized, injectate should be placed in each compartment. Moderate evidence supports the combination of corticosteroid injection followed by wearing of a thumb splint for increased effectiveness.

Trigger Finger

Introduction

Trigger finger also known as stenosing tenosynovitis causes irregular flexion and extension of the digits with palmar pain around the metacarpophalangeal (MCP) joint. These symptoms originate from the catching of the flexor tendon as the tendon glides through the hand/finger pulley system. This trapping is often related to a thickening of the pulley system and secondary entrapment of the tendon at the first annular pulley (A1). Pain is caused when an inflamed flexor tendon becomes mechanically stuck proximally to the tendon sheath often locking the finger in flexion.

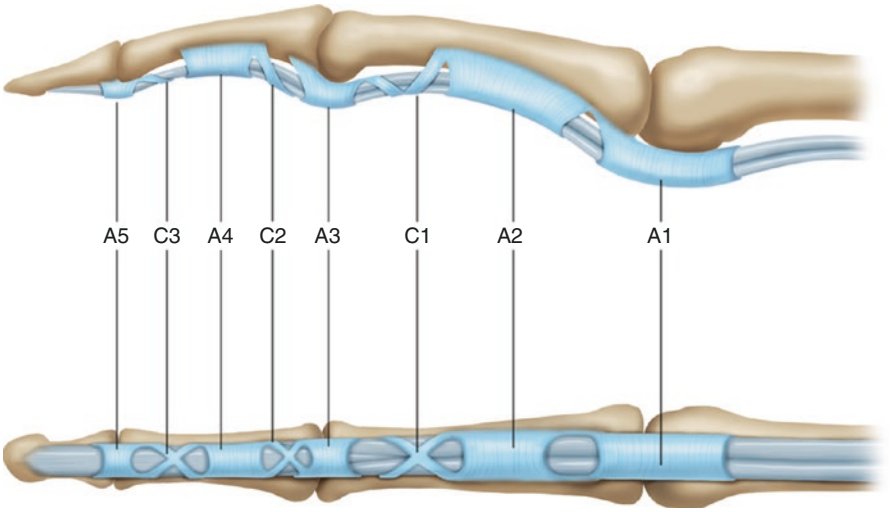

Fig. 21.13 Annular (A1–A5) and cruciform (C1–C3) pulleys. The proximal aspect of the A1 pulley is at the level of the distal metacarpal bone. (Reprinted with permission from Philip Peng Educational Series)

The two tendons of the flexor digitorum profundus (FDP) and the flexor digitorum superficialis (FDS) travel down the volar aspect of the finger through the retinacular pulley system that allows the tendons to glide back and forth. The FDP attaches at the base of the distal phalanx in digits 2–5 and works to flex the distal phalanges (Fig. 21.13). The FDS attaches to the bodies of the middle phalanges of digits 2–5 and acts to flex the middle phalanges at the proximal interphalangeal joint and the proximal phalanges at the MCP joint. At the MCP joint is the first annular pulley.

Patient Selection

Patients often present with history of locking or catching of the affected finger in flexion that can progress to pain over the volar aspect of the MCP. Pain may radiate to the tip of the digit affected or to the palm. Examine for thickening of the tendon pulley system just proximal to the MCP. Have the patient flex and extend their fingers to feel for asymmetry in motion or to replicate the locking symptoms. Ultrasound can be utilized to demonstrate a hypoechoic thickened pulley and a nodular tendon. While utilizing ultrasound, flex and extend the fingers to view dynamic abnormalities. Those with higher grades of locking symptoms are found on ultrasound to have greater thickening of the tendon and pulley system.

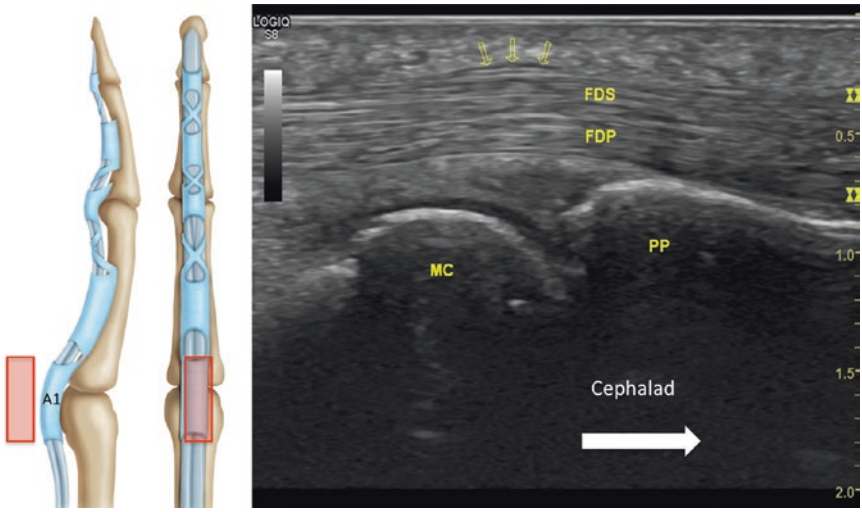

Fig. 21.14 Long-axis scan of the digit. (Reprinted with permission from Philip Peng Educational Series)

Ultrasound Scan

- Position: Hand palm up and resting comfortably on a table
- Probe used: High-frequency linear array transducer (10 MHz+); Hockey stick probe is preferred.

Scan 1: Over the MCP Joint Longitudinally

The A1 pulley (yellow arrows) is superficial and proximal to the joint. The metacarpal head (MC) is hyperechoic and the proximal phalanx (PP) is deep (Fig. 21.14). The tendons of the flexor digitorum profundus (FDP) and the flexor digitorum superficialis (FDS) lay over the phalanx, superficially to deep, respectively. Reprinted with permission from Philip Peng Educational Series.

Scan 2: Rotate the Probe to Highlight the A1 Pulley System in Short Axis

The flexor digitorum superficialis (FDS) and the flexor digitorum profundus (FDP) and the metacarpal bone (MC) are visualized (Fig. 21.15). Superficial to the FDS is the tendon sheath (marked with ∗). Use color flow to highlight the digital arteries (A). Reprinted with permission from Philip Peng Educational Series.

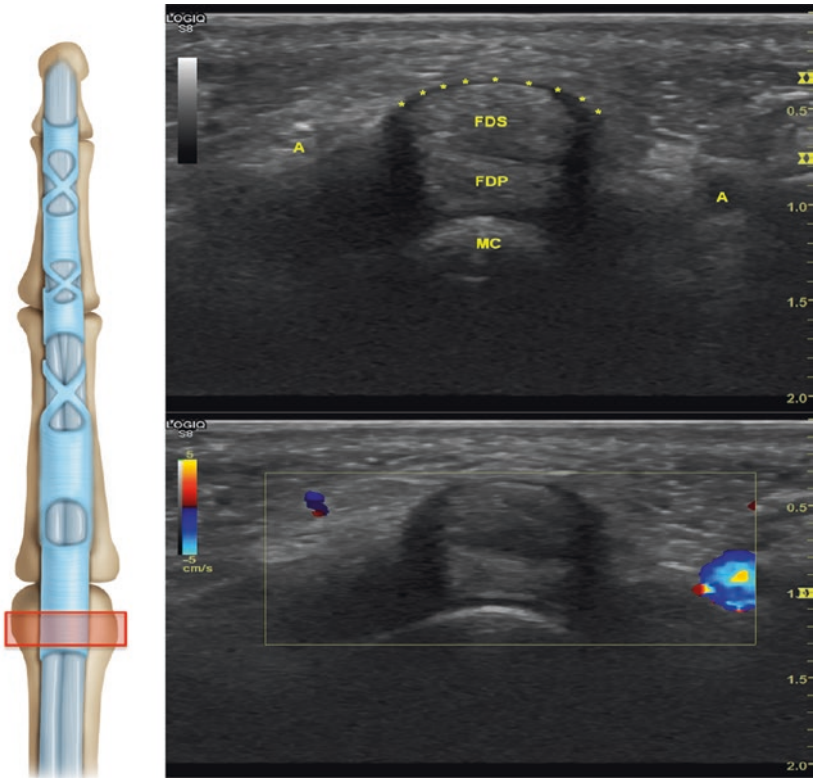

Fig. 21.15 Short-axis view of the A1 pulley. (Reprinted with permission from Philip Peng Educational Series)

Procedure

- Needles: 25G 0.5 inch needle
- Drugs: 1 mL local anesthetic (0.25% plain bupivacaine)
  0.5 mL steroid (depomedrol)

In short-axis view, the A1 pulley lies above the flexor digitorum superficialis (FDS) and the flexor digitorum profundus (FDP). The probe is centered precisely over the FDS, FDP, and metacarpal bone. Using out-of-plane approach and steep angle, insert the needle (dotted red arrow) adjacent to the probe and aim toward the midpoint of the transducer (Fig. 21.16). Avoid the arteries (A). When the hyperechoic dot is seen by target (needle tip depicted by arrowhead), the injectate is given. Reprinted with permission from Philip Peng Educational Series.

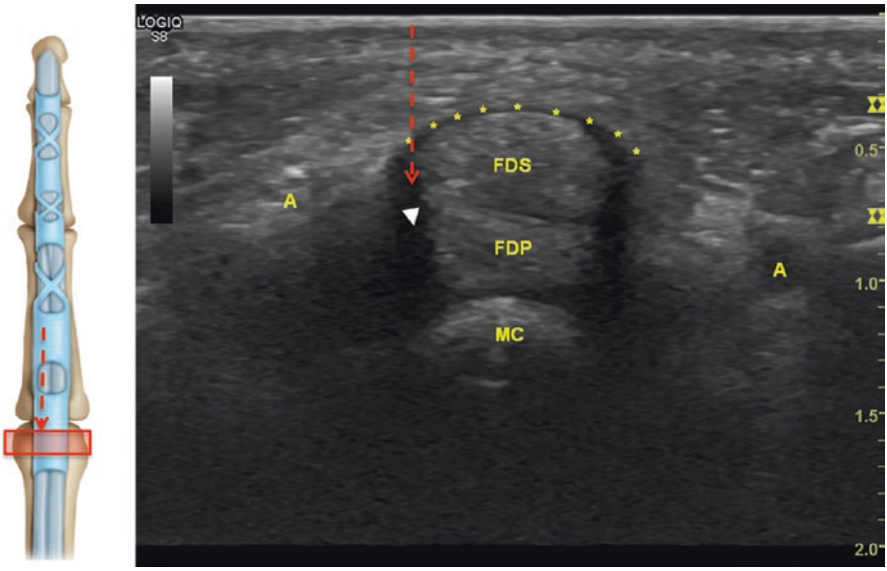

Fig. 21.16 Out-of-plane injection of trigger finger. (Reprinted with permission from Philip Peng Educational Series)

Clinical Pearls

1. Identify the digital arteries and nerves to avoid puncture.
2. Flex and extend the patient's fingers to aid in identifying a nodule.
3. A pathologic A1 pulley will appear hypoechogenic.
4. Retract needle slightly if resistance is felt to avoid injecting tendons.

Literature Review

Ultrasound-guided intra-sheath trigger finger injections have been shown to provide pain relief and improve function. Studies show that a combination of corticosteroid and lidocaine improved pain greater at 1- and 4-week follow-up compared to local anesthetic alone. Ultrasound assessment at 1-month post-steroid injection demonstrated decreased thickness of the A1 pulley and the flexor tendons. Furthermore, the precision of ultrasound-guided injections minimizes risk of tendon injury or rupture. Recent success in pain control and improved motion has been obtained by following a corticosteroid injection with a hyaluronic acid injection 10–15 days later which helps to stretch the pulley system and to improve sliding.

Carpometacarpal Joint

Introduction

The first carpometacarpal (CMC) joint is a saddle joint that provides stability and allows motion of the thumb in various planes. The joint space is created distally by the metacarpal and proximally by the trapezium (Fig. 21.17). The dominant pain generator at this site originates from degenerative disease and joint instability.

The thumb consists of the distal phalanges and the proximal phalanges that connect proximally to the first metacarpal bone. Proximal to the metacarpal bone is the trapezium. This articulation forms the CMC joint. This joint's movements include flexion/extension and abduction/adduction. Combining flexion and abduction allows for opposition. Combining extension and adduction allows for reposition.

Patient Selection

Consider first CMC joint pathology when pain is exacerbated through movements of the thumb especially pinching or grasping motions. In addition, weakness and reduced thumb motions are possible.

Perform a provocative grind test by providing axial load and rotating the CMC joint or lever test by holding the base of metacarpal with index and thumb and lever the CMC in both radial and ulnar direction (Fig. 21.18).

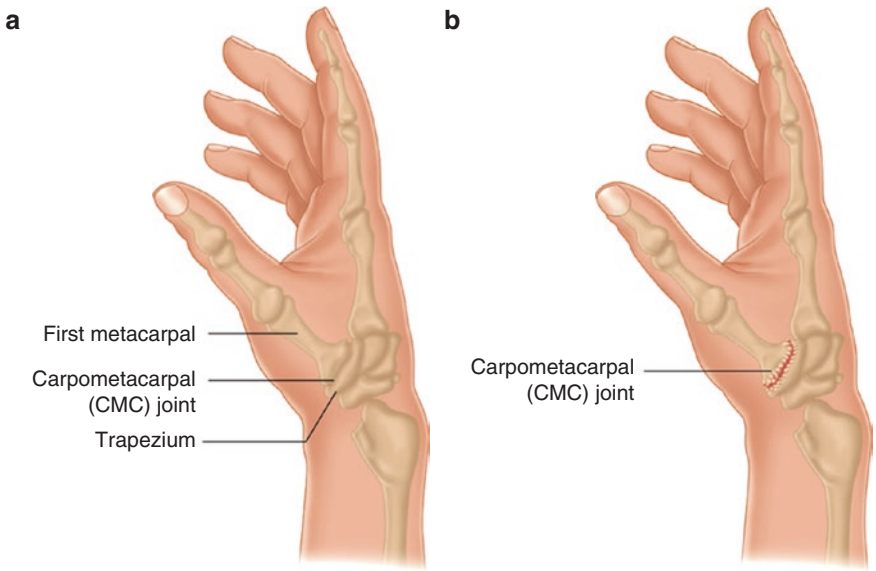

Fig. 21.17 (**a**) First carpometacarpal joint (CMC) is formed between the first metacarpal and trapezium. (**b**) Osteoarthritis of the CMC joint

Fig. 21.18 Grind and lever test. (Reprinted with permission from Philip Peng Educational Series)

Crepitus or sharp pain is suggestive of pathology. Plain radiographs may show degenerative changes. Ultrasound evaluation can demonstrate degenerative changes including osteophytes, loss of joint space, thickening of the synovium, or joint effusion. Injections are indicated when pain or weakness impedes function.

Ultrasound Scan

- Position: Hand thumb side up in a neutral position and resting comfortably on a table
- Probe used: High-frequency linear array transducer (10 MHz+), Hockey stick probe preferred

Place transducer long axis over the thumb to identify the first metacarpal bone and the trapezium (Fig. 21.19). The abductor pollicis longus and extensor pollicis brevis tendons can be visualized as they cross over the first CMC joint. The joint space will be seen between the trapezium and the first metacarpal. Evaluate for any bony joint abnormalities. Identify the location of the radial artery prior to injecting. Reprinted with permission from Philip Peng Educational Series.

Procedure

- Needles: 25G 1.5 inch needle
- Drugs: 1 mL local anesthetic (0.25% plain bupivacaine)
  0.5 mL steroid (depomedrol)

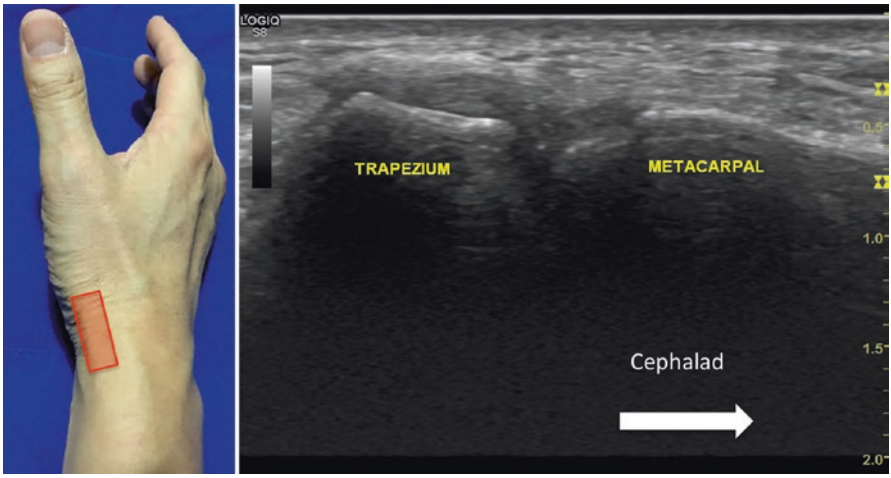

Fig. 21.19 Sonograph of the CMC joint. (Reprinted with permission from Philip Peng Educational Series)

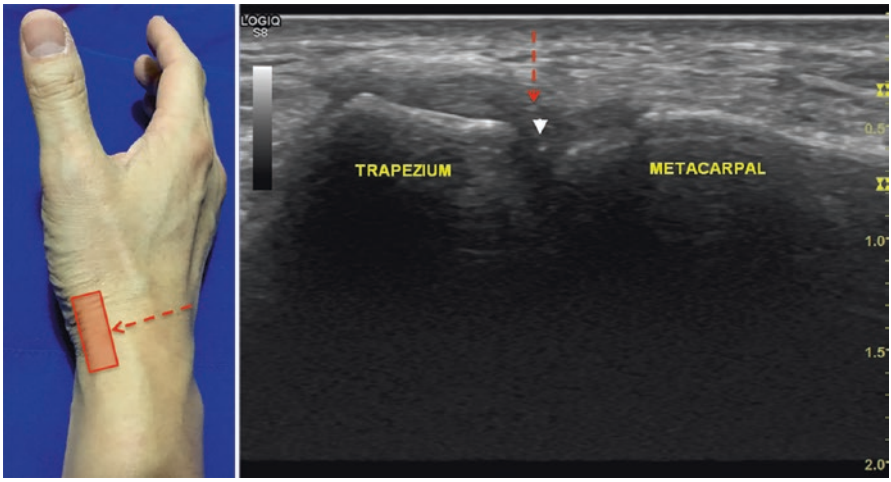

Fig. 21.20 Needle insertion. (Reprinted with permission from Philip Peng Educational Series)

With the probe long axis over the CMC joint, utilize an out-of-plane approach (Fig. 21.20). Advance the needle adjacent to probe with a steep angle (red arrow) until a hyperechoic needle tip is visualized within the joint space (needle tip depicted by arrowhead). Injectate should be visualized spreading within the joint. Reprinted with permission from Philip Peng Educational Series.

Clinical Pearls

1. Flex the thumb to open the CMC joint.
2. Avoid injecting into the tendons.

Literature Review

Ultrasound-guided intra-articular corticosteroid injections are shown to provide effective short-term relief. Ultrasound assistance aids in the accuracy of the desired intervention. A combination of injection with thumb spica splint can improve pain symptoms. Ultrasound is essential in providing correct needle placement in cases of advanced osteoarthritis and joint space narrowing or abnormality. Corticosteroid CMC injections with ultrasound guidance have been shown to predict future surgery incidence. Patients with ongoing pain 1 week post-injection were more likely to require surgery within a 1-year period. Hyaluronic acid injections utilizing ultrasound have been demonstrated to reduce pain with both activity and rest, while also reducing NSAID use.

Suggested Reading

General

Chopra A, Rowbotham EL, Grainger AJ. Radiological intervention of the hand and wrist. Br J Radiol. 2016;89(1057):20150373.

Huisstede BM, Gladdines S, Randsdorp MS, Koes BW. Effectiveness of conservative, surgical, and postsurgical interventions for trigger finger, Dupuytren disease, and De Quervain disease: a systematic review. Arch Phys Med Rehabil. 2018;99:1635–49. pii: S0003-9993(17)31018-3.

Jacobson JA. Fundamentals of musculoskeletal ultrasound. 3rd ed. Chapter 5. Philadelphia: Elsevier; 2018.

Orlandi D, Corazza A, Silvestri E, Serafini G, Savarino EV, Garlaschi G, Mauri G, Cimmino MA, Sconfienza LM. Ultrasound-guided procedures around the wrist and hand: how to do. Eur J Radiol. 2014;83(7):1231–8.

Spinner DA, Rosado MI. Wrist and hand. In: Spinner D, Kirschner J, Herrera J, editors. Atlas of ultrasound guided musculoskeletal injections. Musculoskeletal Medicine. New York: Springer; 2014.

Specific Procedures

Median Nerve

Cartwright MS, Hobson-Webb LD, Boon AJ, Alter KE, Hunt CH, Flores VH, Werner RA, Shook SJ, Thomas TD, Primack SJ, Walker FO, American Association of Neuromuscular and Electrodiagnostic Medicine. Evidence-based guideline: neuromuscular ultrasound for the diagnosis of carpal tunnel syndrome. Muscle Nerve. 2012;46(2):287–93.

Chen PC, Wang LY, Pong YP, Hsin YJ, Liaw MY, Chiang CW. Effectiveness of ultrasound-guided vs direct approach corticosteroid injections for carpal tunnel syndrome: a double-blind randomized controlled trial. J Rehabil Med. 2018;50(2):200–8.
Chopra A, Rowbotham EL, Grainger AJ. Radiological intervention of the hand and wrist. Br J Radiol. 2016;89(1057):20150373.
Drake RL, Vogl W, Mitchell AWM, Gray H. Gray's anatomy for students. 3rd. ed, international edition. Philadelphia: Churchill Livingstone Elsevier; 2015.
Lee JY, Park Y, Park KD, Lee JK, Lim OK. Effectiveness of ultrasound-guided carpal tunnel injection using in-plane ulnar approach: a prospective, randomized, single-blinded study. Medicine (Baltimore). 2014;93(29):e350.
Spinner DA, Rosado MI. Wrist and hand. In: Spinner D, Kirschner J, Herrera J, editors. Atlas of ultrasound guided musculoskeletal injections. Musculoskeletal Medicine. New York: Springer; 2014.

De Quervain's

Huisstede BM, Gladdines S, Randsdorp MS, Koes BW. Effectiveness of conservative, surgical, and postsurgical interventions for trigger finger, Dupuytren disease, and De Quervain disease: a systematic review. Arch Phys Med Rehabil. 2018;99:1635–49. pii: S0003-9993(17)31018-3.
Kang JW, Park JW, Lee SH, Park JH, Han SB, Park SY, Jeong WK. Ultrasound-guided injection for De Quervain's disease: accuracy and its influenceable anatomical variances in first extensor compartment of fresh cadaver wrists. J Orthop Sci. 2017;22(2):270–4.
Orlandi D, Corazza A, Silvestri E, Serafini G, Savarino EV, Garlaschi G, Mauri G, Cimmino MA, Sconfienza LM. Ultrasound-guided procedures around the wrist and hand: how to do. Eur J Radiol. 2014;83(7):1231–8.
Orlandi D, Corazza A, Fabbro E, Ferrero G, Sabino G, Serafini G, Silvestri E, Sconfienza LM. Ultrasound-guided percutaneous injection to treat de Quervain's disease using three different techniques: a randomized controlled trial. Eur Radiol. 2015;25(5):1512–9.

Trigger Finger

Mifune Y, Inui A, Sakata R, Harada Y, Takase F, Kurosaka M, Kokubu T. High-resolution ultrasound in the diagnosis of trigger finger and evaluation of response to steroid injection. Skeletal Radiol. 2016;45(12):1661–7.

CMC

McCann PA, Wakeley CJ, Amirfeyz R. The effect of ultrasound guided steroid injection on progression to surgery in thumb CMC arthritis. Hand Surg. 2014;19(1):49–52.
Neumann DA, Bielefeld T. The carpometacarpal joint of the thumb: stability, deformity, and therapeutic intervention. J Orthop Sports Phys Ther. 2003;33(7):386–99.
Salini V, De Amicis D, Abate M, Natale MA, Di Iorio A. Ultrasound-guided hyaluronic acid injection in carpometacarpal osteoarthritis: short-term results. Int J Immunopathol Pharmacol. 2009;22(2):455–60.

Hip

22

Agnes Stogicza

Introduction

Hip pain is common (14.3%) among individuals over 60 years and also affects 12% of patients after total hip arthroplasty. Intraarticular hip injection is often the first interventional pain procedure performed to alleviate hip pain. Recognition of enthesopathies and tendinosis is important as they may be amendable to specific minimally invasive procedures. Pain at the greater trochanter has been classically identified as bursitis; however, tendinopathy of the muscles around the greater trochanteric region is common and plays a more important role in the pain symptomatology in greater trochanteric pain syndrome. Anterior hip pain may be the result of iliopsoas dysfunction and enthesopathy, which often accompanies intraarticular hip pathologies. A variety of etiologies causing hip pain are summarized in Table 22.1.

Anatomy

Bones, Cartilage, and Ligamentous Structures

The hip joint consists of the acetabulum (ilium, ischium, and pubis), the femoral head and neck, the labral fibrocartilage that deepens the socket of the acetabulum, and the iliofemoral, ischiofemoral, and pubofemoral ligaments.

A. Stogicza (✉)
Anesthesiology and Pain Management, Saint Magdolna Private Hospital, Budapest, Hungary

P. Peng et al. (eds.), *Ultrasound for Interventional Pain Management*,
https://doi.org/10.1007/978-3-030-18371-4_22

Table 22.1 Hip pain etiologies

Intraarticular pathologies	Hip osteoarthritis (OA) Intraarticular cartilage degeneration Labral tears Loose bodies Femoro-acetabular impingement (FAI) Synovitis
Extraarticular pathologies	Greater trochanteric (GT) complex enthesopathies, greater trochanteric bursitis, iliotibial tract tendinopathy *(lateral/posterior hip pain)* Iliopsoas tendonitis, snapping hip *(anterior hip pain)* Femoral neck stress fracture *(pain on weight-bearing)* Deep gluteal syndrome (includes piriformis syndrome), sacroiliac joint pain, athletic pubalgia (trochanteric-pelvic impingement, ischiofemoral impingement, and subspine impingement) *(lateral/posterior hip pain)* Myofascial pain *(anterior and posterior pain)*
Referred pain	Lumbosacral spine disorders and sacroiliac joint arthropathy Knee pathologies Intraabdominal pathologies
Others	Fibromyalgia, rheumatoid diseases, avascular necrosis of the femoral head *(clinically similar to advanced hip OA)*

Musculature

Table 22.2 summarizes the core hip muscles and their attachments and functions.

Blood supply: Medial and lateral circumflex artery that are branches of the deep femoral artery.

Innervation: The posterior hip capsule is innervated by branches from the superior gluteal and sciatic nerves, while the anterior capsule is innervated by the articular branches of the obturator nerve, accessory obturator, and femoral nerve (Fig. 22.1). These anterior articular branches have been well studied and implied to be clinically relevant in hip pain and hip denervation. Further details are discussed in Chap. 27 (Hip and Knee joint denervation).

Hip Intraarticular Injection

Patient Selection

Injection is indicated in patients with pain from intraarticular hip pathologies (as listed in Table 22.1) lasting longer than 3 months, nonresponsive to pharmacologic and physical therapy. Osteoarthritis (OA) of different stages (II–IV) may be considered but clinical success is less likely with advanced conditions especially "bone-on-bone" situation. Imaging is only recommended in case of atypical presentation or rapid progression of OA.

Table 22.2 Core hip muscles and their attachments and functions

Muscle	Principal group Subgroups	Origin	Insertion	Primary action/ secondary action
Inferior gemelli	Gluteal region (hip-joint stability) Deep	Ischial tuberosity	Greater trochanter	Femur: lateral rotation
Obturator externus	Gluteal region (hip-joint stability) Deep	Obturator membrane (external surface)	Greater trochanter	Femur: lateral rotation
Obturator internus	Gluteal region (hip-joint stability) Deep	Obturator membrane (internal surface)	Greater trochanter	Femur: lateral rotation
Piriformis	Gluteal region (hip-joint stability) Deep	Anterior aspect of the sacrum	Greater trochanter (superior aspect)	Femur, lateral rotation/femur, abduction
Quadratus femoris	Gluteal region (hip-joint stability) Deep	Ischial tuberosity	Intertrochanteric crest (quadrate tubercle)	Femur: lateral rotation
Superior gemelli	Gluteal region (hip-joint stability) Deep	Ischial spine	Greater trochanter	Femur: lateral rotation
Gluteus maximus	Gluteal region (hip-joint stability) Superficial	Ilium, sacrum, and coccyx	Gluteal tuberosity of femur and iliotibial tract	Hip: extension
Gluteus medius	Gluteal region (hip-joint stability) Superficial	Outer surface of ileum, between top two gluteal lines	Greater trochanter (lateral)	Anterior fibers: Femur: abduction and internal rotation Posterior fibers: Femur: abduction and external rotation
Gluteus minimus	Gluteal region (hip-joint stability) Superficial	Outer surface of ilium, between bottom two gluteal lines	Greater trochanter (anterior)	Femur: abduction and internal rotation
Iliopsoas	Thigh, anterior	Psoas: lumbar vertebrae, transverse processes Iliacus: iliac crest and inner plate of ilium	Lesser trochanter of femur	Hip flexion

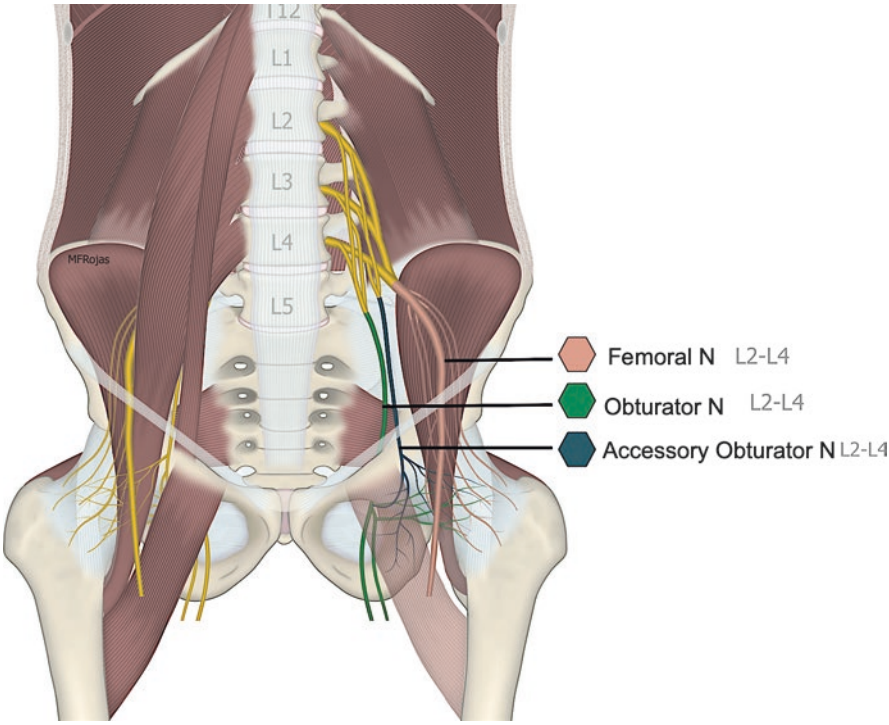

Fig. 22.1 Articular branches to the anterior hip joint. (Reprinted with permission from Dr. Maria Fernanda Rojas)

Ultrasound Scanning

The hip joint can be easily accessed through the anterior synovial recess (***) in an anterior approach under ultrasound guidance (Fig. 22.2). Lateral approach to the hip joint is commonly performed for fluoroscopy-guided injection and endoscopy procedures but can be implemented with ultrasound guidance as well. Both approaches are described below.

Anterior Approach

- Position: Supine
- Probe: Curvilinear 2–6 MHz, linear 5–16 MHz in low BMI patients

Scan 1

Operator stands on the affected side of the patient. Place probe perpendicular to the femur at the upper third of the thigh; it shows the femoral shaft in short axis as a dome-shaped hyperechoic structure (Fig. 22.3).

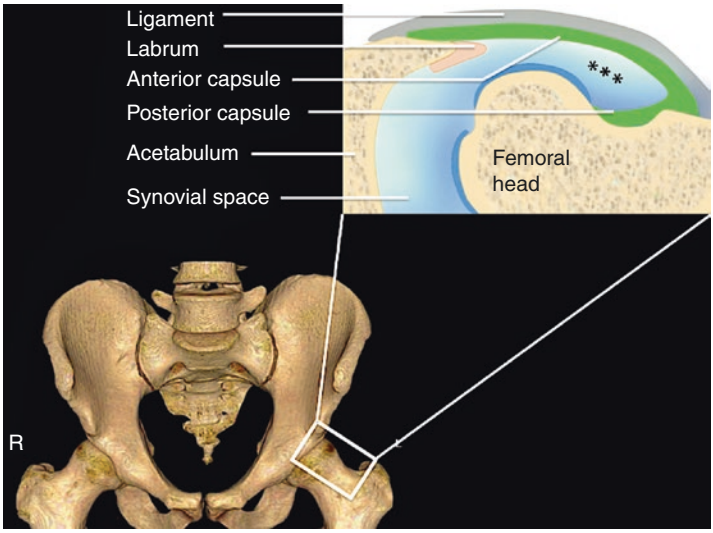

Fig. 22.2 Anterior recess of hip. (Figure reprinted with permission from Philip Peng Educational Series)

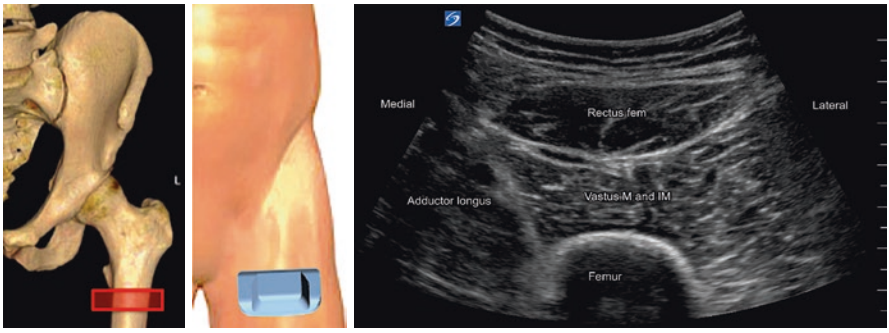

Fig. 22.3 Short-axis view of femur. (Reprinted with permission from Dr. Agnes Stogicza)

Scan 2

Scan cephalad without changing the angle of the probe, until femoral bone is no longer dome-shaped, but flattens out. The flat bone marks the anterior surface of the greater trochanter (arrows) (Fig. 22.4).

Rotate the probe toward the femoral neck and head (Fig. 22.5). Slide probe toward the femoral head to optimize image to visualize the femoral neck, femoral head, acetabulum, capsule (arrows), and anterior recess (∗∗).

Color Doppler helps identify and avoid the ascending branch of the lateral femoral circumflex artery between iliopsoas and rectus femoris muscles when injecting (Fig. 22.6).

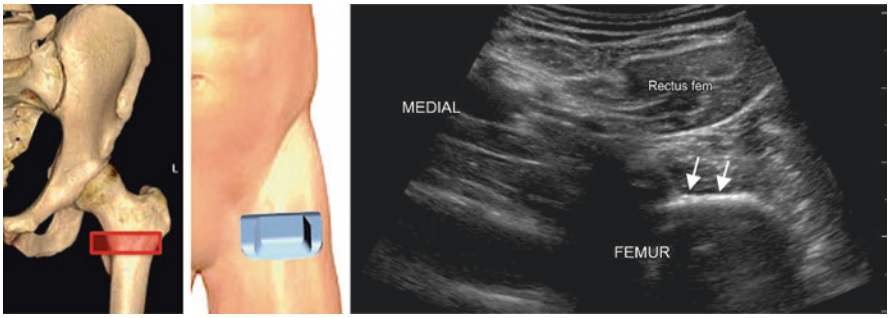

Fig. 22.4 Ultrasound scan in the trochanteric area. (Reprinted with permission from Dr. Agnes Stogicza)

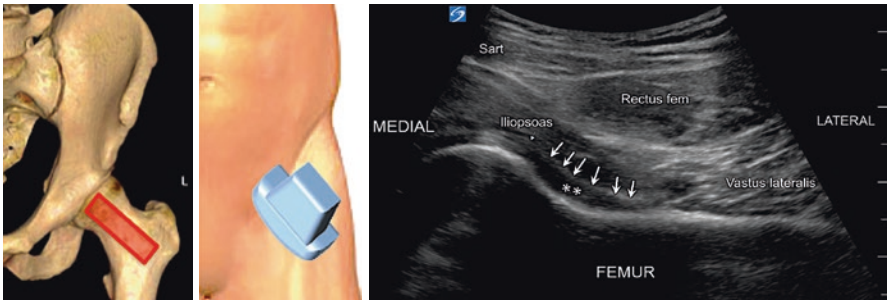

Fig. 22.5 Ultrasound scan over the anterior recess. (Reprinted with permission from Dr. Agnes Stogicza)

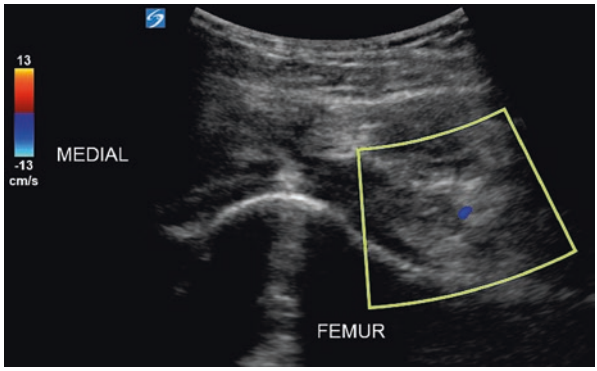

Fig. 22.6 Color Doppler scan of the potential needle path. (Reprinted with permission from Dr. Agnes Stogicza)

Lateral Approach

- Position: Lateral decubitus, affected side up
- Probe: Curvilinear 2–6 MHz, linear 5–16 MHz in low BMI patients

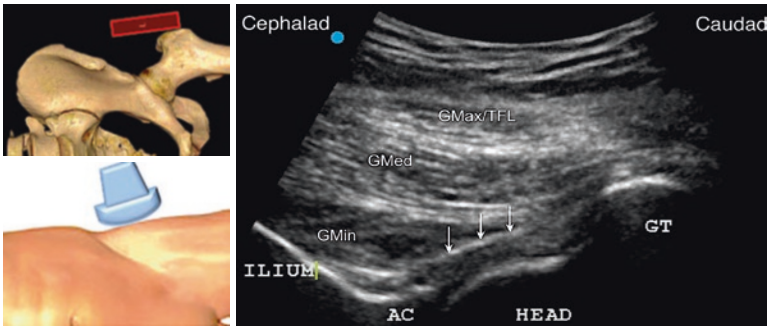

Fig. 22.7 Long-axis view of the greater trochanteric area. (Reprinted with permission from Dr. Agnes Stogicza)

Operator stands behind the patient. Palpate the greater trochanter (GT), and then place the probe over it, oriented toward the anterior superior iliac spine (ASIS). This allows immediate visualization of the GT, femoral neck, femoral head, acetabulum (AC), hip capsule (arrows), and overlaying muscles (Fig. 22.7). The deepest muscle is the gluteus minimus (GMin) and then gluteus medius (GMed), and the most superficial layer is the tensor fascia lata (TFL) or the gluteus maximus (GMax) if scanned slightly posteriorly.

Procedure

- Needles: 22G, 3.5–5 inch needle, depending on patient size
- Drugs: 4–8 mL of local anesthetic (0.25% plain bupivacaine). Mixed with 1 mL depo steroid (40 mg methylprednisolone or triamcinolone)
- Alternative injectate: 5 mL hyaluronic acid; 3–6 mL platelet-rich plasma/bone marrow aspirate; or 4–8 mL 25% dextrose with 0.5% lidocaine

Anterior Approach

In-plane approach is recommended from lateral to medial with the insertion point 2 cm away from the ultrasound probe to allow a shallow needle path (Fig. 22.8 left panel). Once the tip of the needle (arrows) reaches the junction of the femoral head (FH) and neck (FN) inside the anterior recess (bold arrows), injection of normal saline for hydrolocation or color Doppler (right figure) is used to ensure the spread of the injectate under the hip capsule.

Lateral Approach

Out-of-plane approach is recommended, where needle passes parallel to the US beam, aiming at the femoral head/neck junction. Once the tip of the needle passes the capsule (arrow), injection of normal saline for hydrolocation or color Doppler is used to ensure the spread of the injectate under the hip capsule (Fig. 22.9).

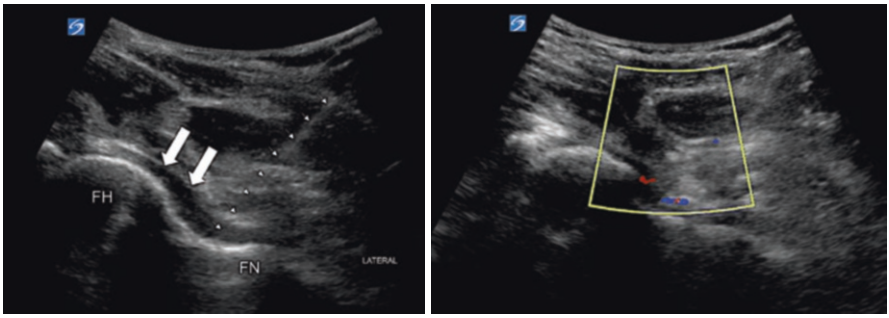

Fig. 22.8 Left panel: In-plane needle insertion for anterior approach of hip joint injection. Right panel: Fluid spread under the hip capsule as shown by color Doppler. (Reprinted with permission from Dr. Agnes Stogicza)

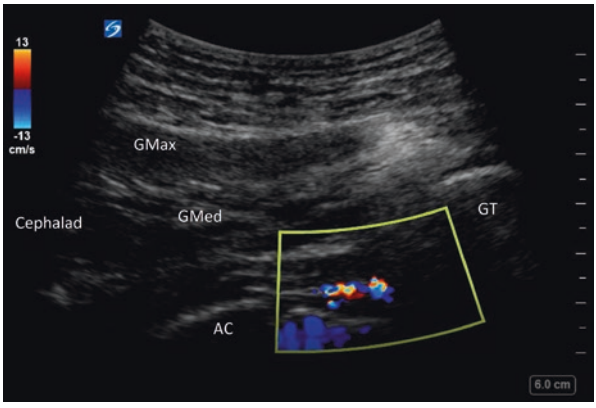

Fig. 22.9 Out-of-plane injection in lateral approach. The needle cannot be visualized in this picture. Once the needle passes the capsule and contacts bone, the tip is confirmed with color Doppler. AC-acetabulum, GT-greater trochanter, GMax- gluteus maximus, GMed-gluteus medius (Reprinted with permission from Dr. Agnes Stogicza)

Clinical Pearls

- For anterior approach, identify the vessels with Doppler. The trajectory of the needle can be adjusted by tilting the probe in cephalad direction to avoid inadvertent puncture and hematoma formation.
- A successful injection will result in capsular distension and cephalad migration of medication. If this is not seen, rotate or withdraw the needle slightly. If it fails after these attempts, the needle can be repositioned closer toward the head but avoiding the labrum and cartilage.

Greater Trochanteric Complex and Bursae

The greater trochanteric (GT) complex comprises several muscles and their tendons (Table 22.2). Understanding their attachments and function is key if specific, targeted injection is performed. Figure 22.10 showed the four facets of the greater trochanter and Fig. 22.11 showed the three different gluteus muscles in relationship to their attachments.

The gluteus minimus (GMin) attaches at the anterior facet for the GT, while the gluteus medius attaches to the inferior aspect of lateral facet and posterosuperior facet of the GT. This supports their function as abductors, hip stabilizers, with the GMin slightly internally and the GMed slightly externally rotating the hip. The gluteus maximus GMax does not attach directly on the GT, as it attaches in the iliotibial band and fibers at the femoral shaft, below the GT. The tensor fascia lata (TFL)/iliotibial band (ITB) passes over the GMed and GMin attachments. The piriformis, the gemelli and the obturator internus muscles attach at the posterior, inner surface of the GT, contributing to external rotation and hip stabilization when walking. There are various bursae at each muscle attachment/tendon.

Fig. 22.10 Different facets of greater trochanter. (Reprinted with permission from Philip Peng Educational Series)

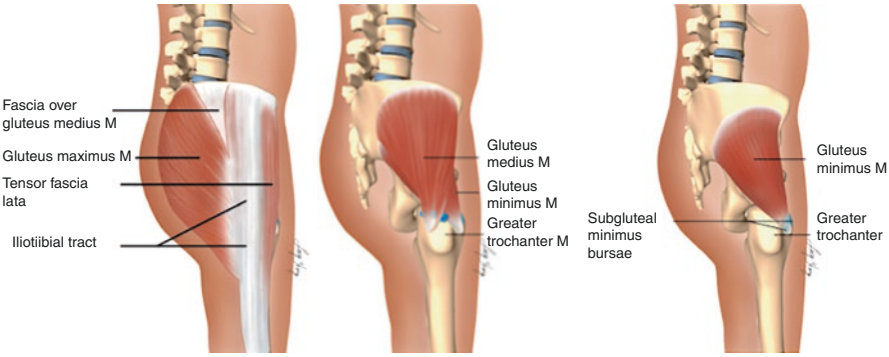

Fig. 22.11 The gluteus muscles. (Reprinted with permission from Philip Peng Educational Series)

Patient Selection

Patients with greater trochanteric pain syndrome who are nonresponsive to conservative therapies.

Clinically, the patient presents with pain in the lateral hip and cannot sleep while lying on the painful side. Difficulty with getting up from sitting, then pain usually decreases when walking. Physical exam shows tenderness at the greater trochanter. Specific palpation usually allows distinguishing between various enthesopathies of the GMin, GMed, piriformis, and quadratus femoris (QF), with probably GMed being the most commonly found. MRI may show tendinosis, tendon tears, fluid-filled bursae, or calcification of these entheses. Ultrasound exam is sensitive to calcifications, and uneven bony surfaces, which are signs of enthesopathy. In spite of imaging support, the diagnosis still remains mainly clinical.

Ultrasound Scanning and Procedure

Gluteus Medius and Gluteus Minimus Attachment and Bursae

- Position: Lateral decubitus, affected side up, legs comfortably straight or slightly bent
- Probe: Linear 5–12 MHz or curvilinear in larger BMI patients

Equipment and Drugs

- Needles: 22G 3.5–5 inch needle
- Drugs:
- Bursa injection: 1–3 mL of local anesthetic (0.25% plain bupivacaine). Mixed with 1 mL depo steroid (40 mg methylprednisolone or triamcinolone)
- Anterior Hip: Iliopsoas Muscle Belly, Bursa, and Tendon
- Alternatively, injection toward the enthesis (fenestration): 1–2 mL platelet-rich plasma/bone marrow aspirate at each enthesis or 1–2 mL 15% dextrose with 0.5% lidocaine at each enthesis.

Short-Axis Approach

After palpation, place the probe over the greater trochanter (GT), oriented in short axis to femur. This allows immediate visualization of the "ridge" which divides the anterior and lateral facets (AF & LF, respectively) of GT, the tendon attachments of the gluteus minimus (GMin), and gluteus medius (***), respectively, the iliotibial

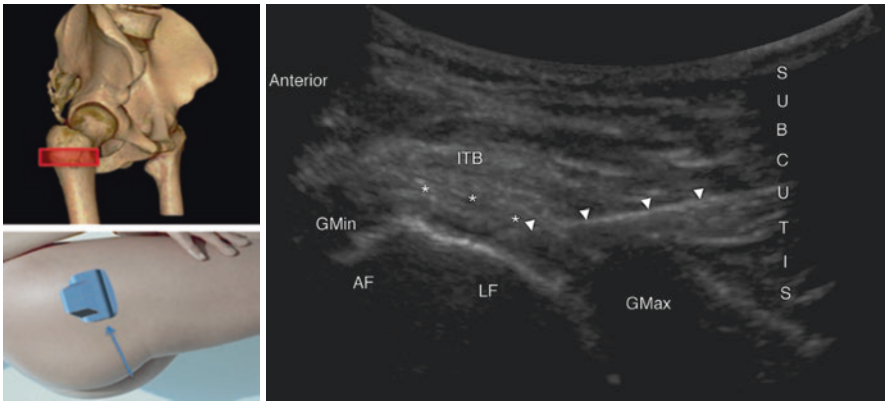

Fig. 22.12 Short-axis view of greater trochanter. (Reprinted with permission from Dr. Agnes Stogicza)

band (ITB). In-plane approach is the suggested approach, and the needle (arrowheads) is inserted from posterior to anterior for gluteus medius tendon prolotherapy or PRP injection (Fig. 22.12) or just superficial to it for bursa injection. Anterior to posterior approach allows access to the Gmin tendon, deep to the tensor fascia lata. Bursae of the GMin or GMed are usually slightly cephalad, and well visualized in long axis view of the GT area, as shown on Fig. 22.7. This approach allows clear needle visualization even in patients with high BMI.

Long-Axis Approach

Place the probe over the greater trochanter (GT), oriented toward the anterior superior iliac spine as shown in Fig. 22.9. This allows immediate visualization of the GT, femoral neck, femoral head (FH), acetabulum (AC), hip capsule, and overlaying muscles. Aligning in the lateral facet in this position, the gluteus medius (GMed) can be visualized as the tendon deep to the tensor fascia lata/ITB (white arrows).

Needle is inserted in an in-plane approach (yellow arrows). It is usually easier to approach from caudal to cephalad (Fig. 22.13).

Anterior Hip: Iliopsoas Muscle Belly, Bursa, and Tendon

The iliacus muscle originates at the iliac crest and inner plate of the ilium, and the psoas muscle attaches at the transverse processes of the five lumbar vertebrae. The iliacus and psoas form the iliopsoas and they attach together at the lesser trochanter (Fig. 22.1).

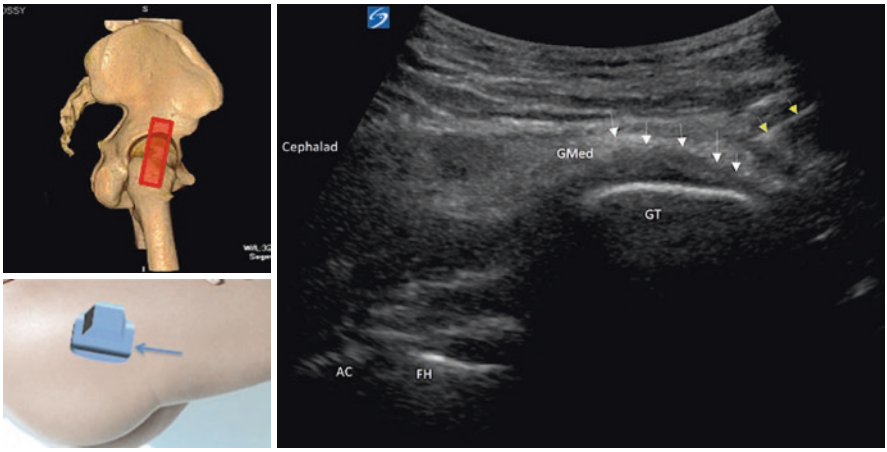

Fig. 22.13 Injection of trochanteric bursa. (Reprinted with permission from Dr. Agnes Stogicza)

Patient Selection

Patients with iliopsoas origin pain that is nonresponsive to conservative treatments.

Psoas and iliacus shortening is very common with a sedentary lifestyle. Patients present with decreased hip extension, lumbar facet pain, anterior hip pain, anterior thigh pain, and/or snapping hip syndrome, in which the iliopsoas tendon snaps over underlying bony prominences, such as the iliopectineal eminence or the anterior aspect of the femoral head. MRI or dynamic ultrasound scan can confirm the diagnosis.

Ultrasound Scan

- Position: Supine patient, thigh slighly externally rotated
- Operator on the affected side of the patient

Scan 1

Place the probe in a way similar to scanning the anterior recess (Fig. 22.5). The muscle that runs immediately anterior to the femoral head is the iliopsoas.

Scan 2

Rotating the probe along the femur as shown in the upper diagram position 1, the iliopsoas and its fibers visualize well in long axis (Fig. 22.14 position 1).

Scan 3

Once the caudal end of iliopsoas is identified, the probe is again rotated to view the muscle in short axis and its attachment on the lesser trochanter (LT) as in position 2 in the lower diagram (Fig. 22.14 position 2). One can confirm being at the LT by

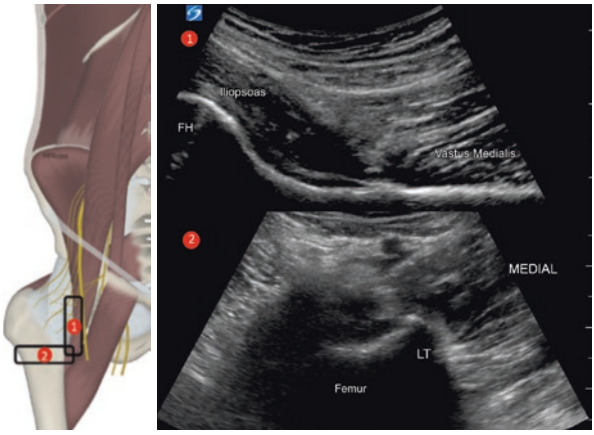

Fig. 22.14 Scanning of iliopsoas. (The left diagram is modified with the permission from Dr. Maria Fernanda Rojas, and the sonogram on the right is reprinted with permission from Dr. Agnes Stogicza)

scanning cephalad and caudad and visualizing the typical dome shape of the femoral shaft, without the widening caused by the LT.

Procedure

Needles: 22G 3.5–5 inch needle
Drugs:

1. For the bursa: 1–3 mL of local anesthetic (0.25% bupivacaine). Mixed with 1 mL depo steroid (40 mg methylprednisolone or triamcinolone)
2. For trigger point injection: 3 mL 1% lidocaine for the psoas muscle belly
3. For the entheses: 1–2 mL platelet-rich plasma/bone marrow aspirate
4. For the entheses: 1–3 mL 15% dextrose with 0.5% lidocaine

The needle is inserted in plane lateral to medial to the target which can be the muscle belly, the bursa, or the attachment. Note that the bursa may extend to the iliopectineal eminence (well explained in chap. 27) and may be injected there, depending on the exam findings.

Literature Review

Hip pain is common among individuals over 60 years old and also affects 12% of patients post hip arthroplasty.

Hip intraarticular injection serves both diagnostic and therapeutic purposes. Anterior, lateral, and posterior approaches are available with US guidance, the anterior being the most commonly used and studied. Lateral approach avoids all major vessels and nerves, which makes it a safe technique. Anterior approach has been shown to have similar precision to fluoroscopy guidance. Intraarticular steroid and

hyaluronic acid provide 3 and 6 months relief, respectively, but neither of them has disease-modifying effect in hip OA. Regenerative medicine approaches possibly have positive effects in hip OA, and the preclinical literature shows an overall support toward the use of PRP. An intraarticular injection does not just target cartilage; instead, PRP might influence the entire joint environment, leading to clinical improvement.

The greater trochanteric complex, also referred to as "rotator cuff of the hip," often presents itself with injury of these "rotators" and is a common complaint among patients seeking help with MSK conditions. Tendinopathies and enthesopathies occur with overuse, repetitive motion injury, and with trauma as well.

Ultrasound is a useful diagnostic tool both to evaluate enthesopathies and tendon injuries: it can identify disruption in the normal fibrillar echotexture of the tendon, thickening, or calcification. It also allows precise needle placement to various tendons for needle fenestration, steroid injection, or injection of PRP.

Suggested Reading

Backer MW, Lee KS, Blankenbaker DG, Kijowski R, Keene JS. Correlation of ultrasound-guided corticosteroid injection of the quadratus femoris with MRI findings of ischiofemoral impingement. AJR Am J Roentgenol. 2014;203(3):589–93.

Balog TP, Rhodehouse BB, Turner EK, Slevin JM, Bush LA, Grassbaugh JA, et al. Accuracy of ultrasound-guided intra-articular hip injections performed in the orthopedic clinic. Orthopedics. 2017;40(2):96–100.

Bhatia A, Hoydonckx Y, Peng P, Cohen SP. Radiofrequency procedures to relieve chronic hip pain: an evidence-based narrative review. Reg Anesth Pain Med. 2018;43(1):72–83.

Birnbaum K, Prescher A, Hessler S, Heller KD. The sensory innervation of the hip joint--an anatomical study. Surg Radiol Anat. 1997;19(6):371–5.

Chaiban G, Paradis T, Atallah J. Use of ultrasound and fluoroscopy guidance in percutaneous radiofrequency lesioning of the sensory branches of the femoral and obturator nerves. Pain Pract. 2014;14(4):343–5.

Chi AS, Long SS, Zoga AC, Read PJ, Deely DM, Parker L, et al. Prevalence and pattern of gluteus medius and minimus tendon pathology and muscle atrophy in older individuals using MRI. Skelet Radiol. 2015;44(12):1727–33.

Cvitanic O, Henzie G, Skezas N, Lyons J, Minter J. MRI diagnosis of tears of the hip abductor tendons (gluteus medius and gluteus minimus). AJR Am J Roentgenol. 2004;182(1):137–43.

Ebell MH. Osteoarthritis: rapid evidence review. Am Fam Physician. 2018;97(8):523–6.

Fernandes L, Hagen KB, Bijlsma JW, Andreassen O, Christensen P, Conaghan PG, et al. EULAR recommendations for the non-pharmacological core management of hip and knee osteoarthritis. Ann Rheum Dis. 2013;72(7):1125–35.

Filardo G, Kon E, Roffi A, Di Matteo B, Merli ML, Marcacci M. Platelet-rich plasma: why intra-articular? A systematic review of preclinical studies and clinical evidence on PRP for joint degeneration. Knee Surg Sports Traumatol Arthrosc. 2015;23(9):2459–74.

Gardner E. The innervation of the hip joint. Anat Rec. 1948;101(3):353–71.

Hoeber S, Aly AR, Ashworth N, Rajasekaran S. Ultrasound-guided hip joint injections are more accurate than landmark-guided injections: a systematic review and meta-analysis. Br J Sports Med. 2016;50(7):392–6.

Jernick M, Walker Gallego E, Nuzzo M. Retrospective analysis of the accuracy of ultrasound-guided magnetic resonance arthrogram injections of the hip in the office setting. Orthop J Sports Med. 2017;5(12):2325967117743915.

Jo H, Kim G, Baek S, Park HW. Calcific tendinopathy of the gluteus medius mimicking lumbar radicular pain successfully treated with barbotage: a case report. Ann Rehabil Med. 2016;40(2):368–72.

Kapural L, Jolly S, Mantoan J, Badhey H, Ptacek T. Cooled radiofrequency neurotomy of the articular sensory branches of the obturator and femoral nerves – combined approach using fluoroscopy and ultrasound guidance: technical report, and observational study on safety and efficacy. Pain Physician. 2018;21(3):279–84.

Kim DH, Yoon DM, Yoon KB. Ultrasound-guided quadratus femoris muscle injection in patients with lower buttock pain: novel ultrasound-guided approach and clinical effectiveness. Pain Physician. 2016;19(6):E863–70.

Kingzett-Taylor A, Tirman PF, Feller J, McGann W, Prieto V, Wischer T, et al. Tendinosis and tears of gluteus medius and minimus muscles as a cause of hip pain: MR imaging findings. AJR Am J Roentgenol. 1999;173(4):1123–6.

Lindner D, Shohat N, Botser I, Agar G, Domb BG. Clinical presentation and imaging results of patients with symptomatic gluteus medius tears. J Hip Preserv Surg. 2015;2(3):310–5.

Musick SR, Bhimji SS. Snapping hip syndrome. Treasure Island: StatPearls Publishing LLC.; 2018.

Nikolajsen L, Brandsborg B, Lucht U, Jensen TS, Kehlet H. Chronic pain following total hip arthroplasty: a nationwide questionnaire study. Acta Anaesthesiol Scand. 2006;50(4):495–500.

Sakellariou G, Conaghan PG, Zhang W, Bijlsma JWJ, Boyesen P, D'Agostino MA, et al. EULAR recommendations for the use of imaging in the clinical management of peripheral joint osteoarthritis. Ann Rheum Dis. 2017;76(9):1484–94.

Segal NA, Felson DT, Torner JC, Zhu Y, Curtis JR, Niu J, et al. Greater trochanteric pain syndrome: epidemiology and associated factors. Arch Phys Med Rehabil. 2007;88(8):988–92.

Short AJ, Barnett JJG, Gofeld M, Baig E, Lam K, Agur AMR, et al. Anatomic study of innervation of the anterior hip capsule: implication for image-guided intervention. Reg Anesth Pain Med. 2018;43(2):186–92.

Ultrasound-Guided Knee Intervention

23

Thiago Nouer Frederico and Philip Peng

Introduction

Knee pain is a common complaint during life. It may happen in different populations and ages like in young athletes with overuse injuries, and in elders that already developed arthritis. Knee pain generators might be intra-articular, extra-articular, or the combination of both pathologies, what makes the correlation between the clinical picture (history and physical examination) and radiologic findings mandatory for choosing the right targets and types of intervention.

Consider a multidisciplinary approach to manage the knee pain, and it includes weight loss and pharmacologic and physical therapy. Patients not responding to conservative management are usually offered injections, which may be performed blindly or with image guidance, either fluoroscopy or ultrasound. Ultrasound guidance has provided an additional diagnostic value and improves accuracy over landmark technique, without the harmful effects of radiation. Application of ultrasound can be used for extra-articular interventions for pain generators such as tendons and bursae.

The objective of this chapter is to briefly review the most common knee pathologies and how to do the intervention under ultrasound guidance without discussing the solution injected in each intervention. The most common approach are the anti-inflammatory injections using local anesthetics and steroids, but many other solutions like hyaluronic acid, platelet-rich plasma, stem cells are being used with good outcomes providing pain relief and possibly regeneration properties.

T. Nouer Frederico
Department of Anesthesia & Pain, Hospital Sirio Libanes, Sao Paulo, Brazil

P. Peng (✉)
Department of Anesthesia and Pain Management, Toronto Western Hopsital and Mount Sinai Hospital, University of Toronto, Toronto, Ontario, Canada
e-mail: Philip.peng@uhn.ca

P. Peng et al. (eds.), *Ultrasound for Interventional Pain Management*,
https://doi.org/10.1007/978-3-030-18371-4_23

Ultrasound-Guided Knee Intra-Articular Injection

Patient Selection

Osteoarthritis
Can be used for other arthritis conditions

Ultrasound Scan

- Position: Supine with support underneath the knee to keep it slightly flexed
- Probe: Linear 6–13 MHz

The target is suprapatellar recess SPR (◆), which is a recess that connects with the knee joint and is bounded by the suprapatellar (★) and prefemoral (★★) fat pad (Fig. 23.1).

Scan 1

The ultrasound probe is placed in long axis to the femur just on the superior border of the patella (Fig. 23.2). This will reveal the SPR (∗∗). When there is difficulty in visualizing the recess, applying pressure in the parapatellar space to squeeze the synovial fluid to the SPR may help when there is no large effusion.

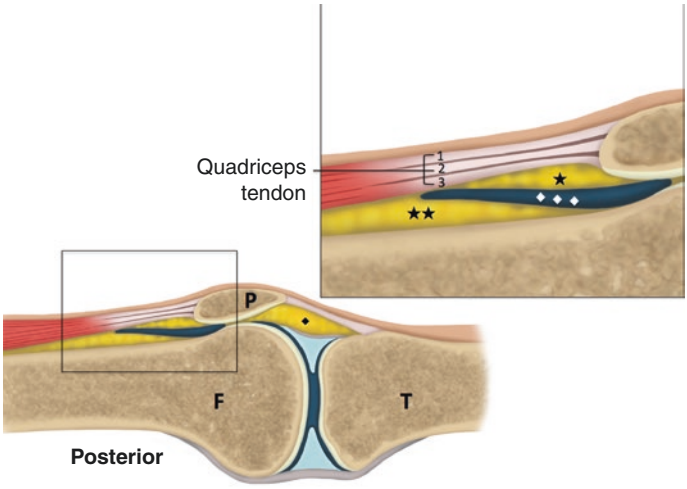

Fig. 23.1 Suprapatellar recess (SPR). (Reprinted with permission from Philip Peng Educational Series)

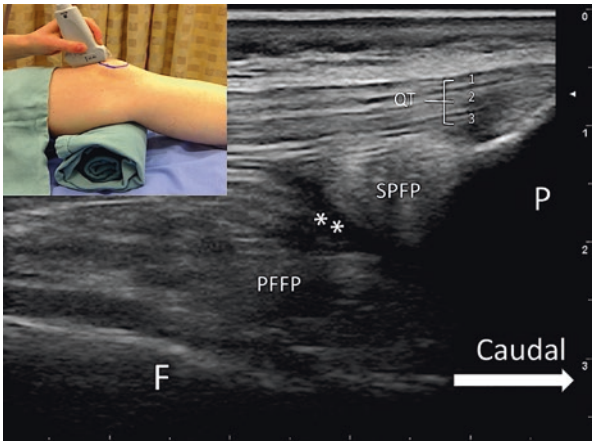

Fig. 23.2 Sonographic image of the suprapatellar recess. The position of ultrasound probe is shown in the left upper insert. PFFP, prefemoral fat pad; SPFP, suprapatellar fat pad; QT, trilaminar quadriceps tendon; F, femur; P, patella. (Reprinted with permission from Philip Peng Educational Series)

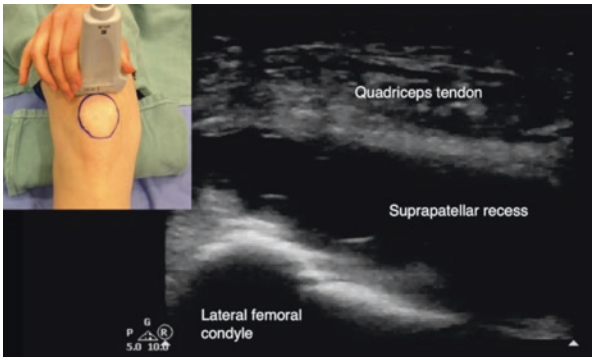

Fig. 23.3 Sonographic image of the probe position ready for injection. (Reprinted with permission from Philip Peng Educational Series)

Scan 2

Once the SPR is seen, the ultrasound probe is rotated 90° above the patella (Fig. 23.3). A 20- or 22-gauge needle is inserted from lateral to medial in-plane toward the SPR. Alternatively, the ultrasound probe is rotated 45 degrees with the cephalad end directed to the lateral side (Fig. 23.4). The rotation of the probe is to avoid needle trauma to the quadriceps tendon. The red square indicates the probe position.

Procedure

- Needle: 1.5-inch 25G or 3-inch 22G needle
- Drugs: 5 mL of mixture of steroid and local anesthetic or viscosupplement or platelet-rich supplement

Before injection, it is always advisable to aspirate the joint fluid as much as possible. In-plane technique is used with the needle inserted from lateral to medial (Fig. 23.5).

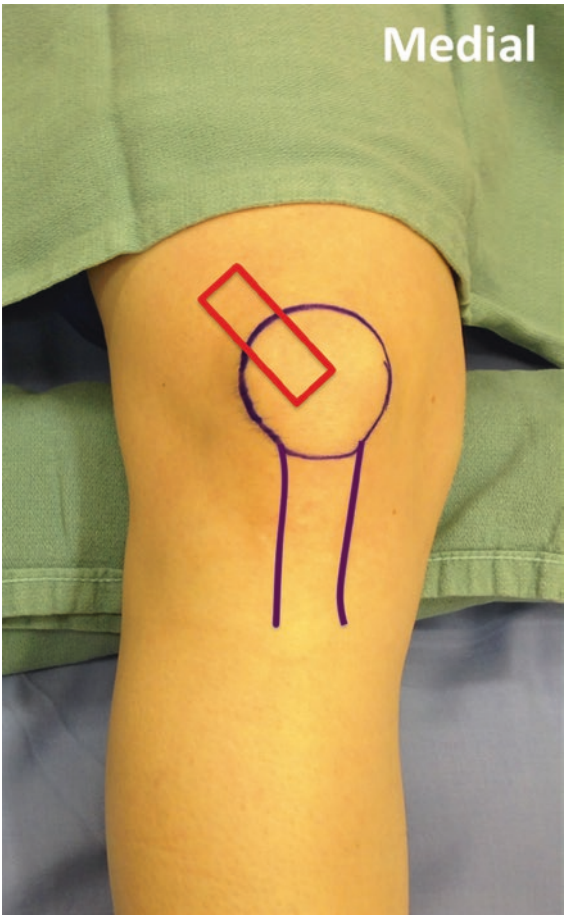

Fig. 23.4 Superolateral approach with ultrasound probe rotated to 45° to long axis of femur. (Reprinted with permission from Philip Peng Educational Series)

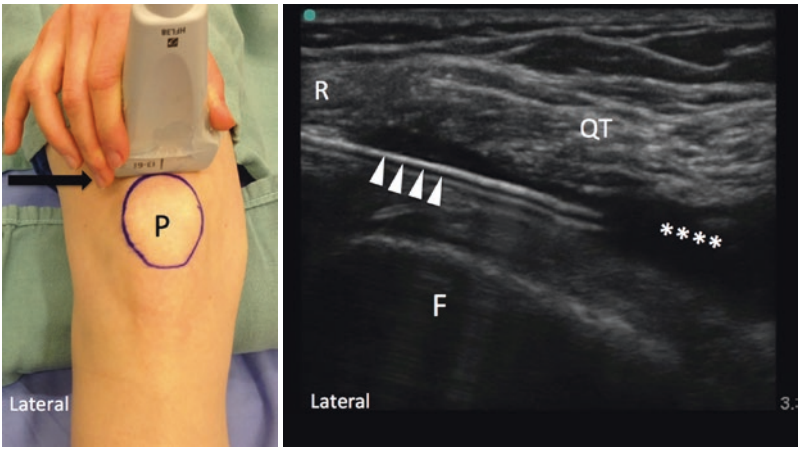

Fig. 23.5 Sonographic image of needle insertion. Needle indicated by arrow. ***, suprapatellar recess; F, femur; QT, quadriceps tendon. (Reprinted with permission from Philip Peng Educational Series)

Table 23.1 Comparison of various injectate for knee

	Steroid	Viscosupplement	Platelet-rich plasma
Mechanism	Anti-inflammatory	Supplementation of synovial fluid	Restore joint hemostasis
Duration	<3 weeks	<3 months	<12 months
Comments	Accelerate cartilage loss	Less effect for end-stage OA	Less effect for end-stage OA

Reprinted with permission from Philip Peng Educational Series

Literature Review

Ultrasound improves the accuracy of knee intra-articular injection. The pool data from the literature suggested that the accuracy of landmark-guided injection is approximately 79% and is inferior to the ultrasound-guided injection even in experienced hand. Injection into the fat pad accounts for most of the inaccuracies from the landmark-guided technique.

A lot of studies were published on the efficacy of intra-articular (IA) steroid, viscosupplement, and platelet-rich plasma. In general, the duration of IA steroid is short (<3 weeks), but repeated injection recently showed acceleration of cartilage loss. Both viscosupplement and platelet-rich plasma result in longer duration of effect and in general are not very effective in advanced osteoarthritis (see Table 23.1).

Ultrasound-Guided Popliteal (Baker's) Cyst Aspiration, Fenestration, and Injection

Popliteal cyst or Baker's cyst is commonly located in the posteromedial aspect of the popliteal fossa. Technically, it is a nonmalignant, fluid-filled swelling formed by distention of the semimembranosus-gastrocnemius bursa.

A Baker's cyst can be classified as a primary cyst if the distended semimembranosus-gastrocnemius bursa arises independently without communication to the knee joint or a secondary cyst if there is an open communication between the bursa and the knee joint cavity (Fig. 23.6). Whereas most of Baker's cysts are secondary cysts and associated with degenerative knee joint diseases, primary cysts are less common and occur primarily in children.

Ultrasound Scan

- Position: Prone
- Probe: Linea 6–15 MHz

Scan 1: Normal Knee

Palpate the semitendinosus (ST) tendon by slightly flex the knee. Put the ultrasound probe over the ST tendon and a "cherry on the cake" appearance with the ST tendon (arrow head) as the cherry and semimembranosus (SM) as the cake (Fig. 23.7).

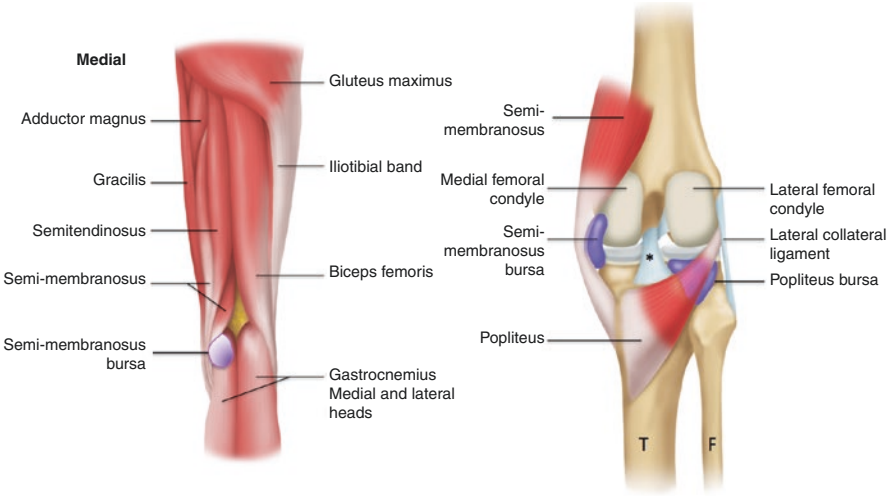

Fig. 23.6 Baker's cyst or semimembranosus-gastrocnemius bursa. (Reprinted with permission from Philip Peng Educational Series)

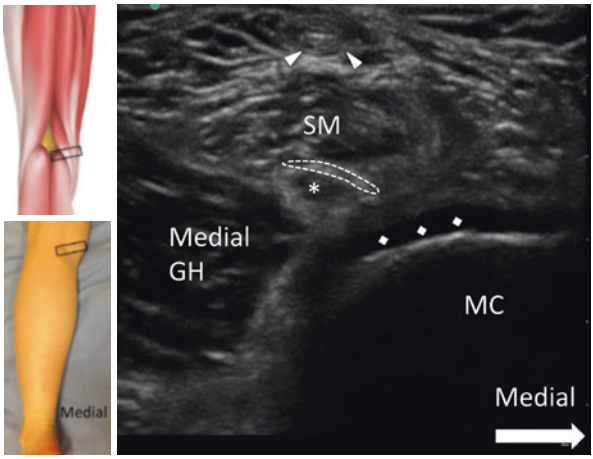

Fig. 23.7 Sonographic image of semimembranosus-gastrocnemius bursa. (Reprinted with permission from Philip Peng Educational Series)

Deep to the SM, medial condyle (MC) is seen on the medial side and medial head of the gastrocnemius (GH) on the lateral side. The semimembranosus-gastrocnemius bursa (outlined by dotted line) appears between the tendon of the GH (∗) and SM. Because of lack of fluid in normal state, one should apply very light pressure to the ultrasound probe to reveal its presence. The cartilage is denoted by ◆.

Scan 2: Abnormal knee with Baker's Cyst

In patient with Baker's cyst, fluid collection can be seen between the semimembranosus and medial head of gastrocnemius (Fig. 23.8a, b). Scan carefully and mark the pedicle of Baker's cyst.

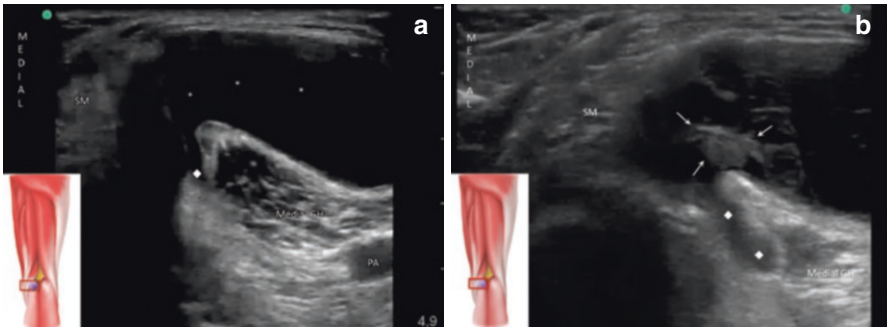

Fig. 23.8 (**a**) Baker's cyst filled with fluid (∗). (**b**) Baker's cyst filled of dense fluid and debris (arrows) that might make aspiration difficult or impossible. GH, head of gastrocnemius; PA, popliteal artery; SM, semimembranosus; ◆, pedicle of Baker's cyst with articular communication. (Reprinted with permission from Philip Peng Educational Series)

Procedure

- Needles: 16G needle
- Approach: Linear probe in plane medial to lateral

Step 1

After obtaining a short-axis view of the semimembranosus and medial head of gastrocnemius, the sonogram should reveal the cyst and pedicle which connect to the knee joint. A 16G needle (arrows) is advanced in plane to the pedicle (∗) of the cyst deep to semimembranosus tendon trying to mark the location of the pedicle place without piercing the cyst, because it can be difficult to identify it after aspiration of the fluid (Fig. 23.9).

Step 2

Then another needle (bold arrow) is inserted inside the cyst, in plane or out of plane, to perform the aspiration and fenestration (Fig. 23.10). Remember to evaluate the nature of the fluid (serous or particulate) in order to choose the appropriate size of the needle capable of fluid aspiration (18G or higher).

Step 3

After aspiration, a possible strategy is to fenestrate the capsule in attempt to induce a fibrosis of the cyst wall and thus obliterate the cyst (Fig. 23.11). Fenestration of the cyst pedicle is performed for the same purpose, trying to interrupt the communication with the joint. Note the cyst is empty at this stage (Fig. 23.12).

Step 4

Finally, injection of steroid into the intra-articular space is performed through the anterior approach described before, as most of the cyst is secondary to the

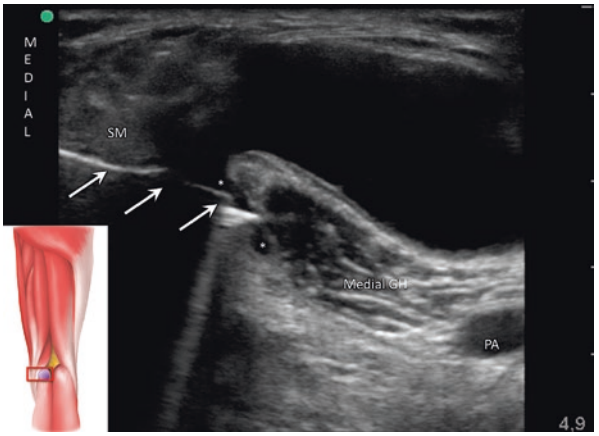

Fig. 23.9 Needle (arrow) marking the pedicle of Baker's cyst which communicates with the joint. The insert showed the position of the probe. PA, popliteal artery. (Reprinted with permission from Philip Peng Educational Series)

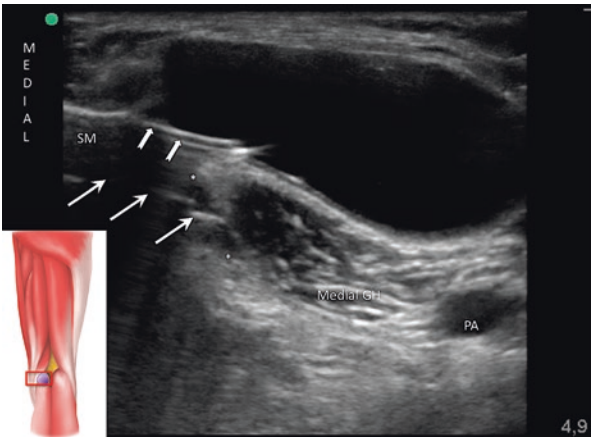

Fig. 23.10 Second needle (bold arrow) insertion into the cyst to perform the aspiration and fenestration. (Reprinted with permission from Philip Peng Educational Series)

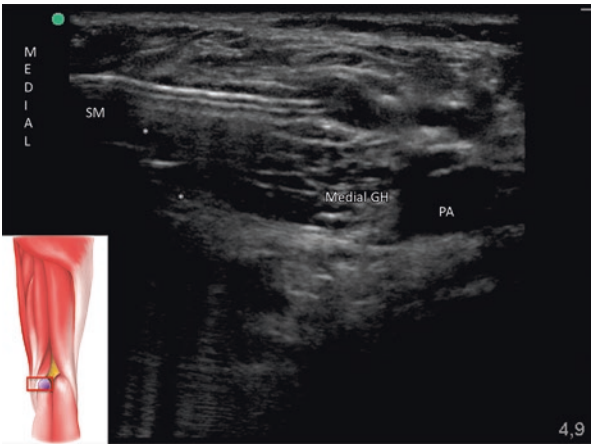

Fig. 23.11 Aspiration and fenestration of the cyst. (Reprinted with permission from Philip Peng Educational Series)

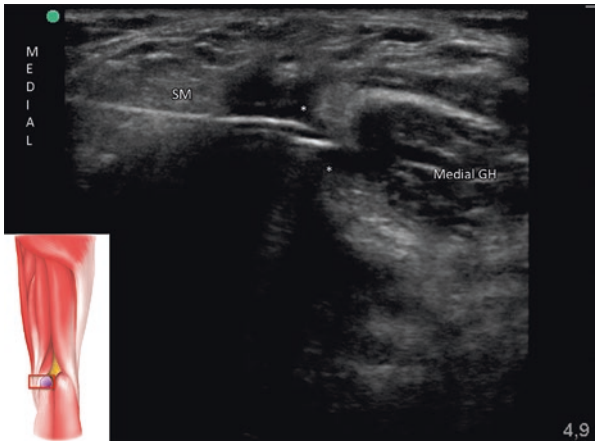

Fig. 23.12 Fenestration of the pedicle of the cyst. (Reprinted with permission from Philip Peng Educational Series)

intra-articular pathology. The purpose of the IA steroid is to reduce articular effusion and thus the increase in pressure of the IA compartment leading to the joint fluid leak through the weakness between semimembranosus and medial head of gastrocnemius. However, if the cyst is primary from semimembranosus bursa, steroid should be injected into the cyst instead.

After procedure the patient is advised to wear a moderate or strong compression elastic knee brace for 4 weeks to keep cyst and pedicle walls together and keep same pressure in anterior and posterior knee.

Literature Review

The incidence of concomitant intra-articular disorders with popliteal cysts is high (94%). Underlying meniscal, ligamentous, and osteochondral derangements result in joint effusion that overflow through the weakness between gastrocnemius and the semimembranosus which works as a valve opening during high pressure in the joint and closes entrapping the fluid when pressure is decreased. Ultrasound is excellent in the diagnosis of the popliteal cyst formation in adults as the sensitivity, specificity, and accuracy are 100% and allow different approaches for treatment, like aspirations, fenestrations, cyst injections, intra-articular injections, or the combination of those.

Ultrasound-Guided Pes Anserinus Bursa and Peritendon Injection

Pes anserinus is the anatomic name given to the conjoined tendons inserted onto the anteromedial aspect of the proximal tibia. Its name comes from the webbed-foot appearance of the tendons of sartorius, gracilis, and semitendinous insertion onto the tibia. Between the tibia (medial collateral ligament) and the conjoined tendons,

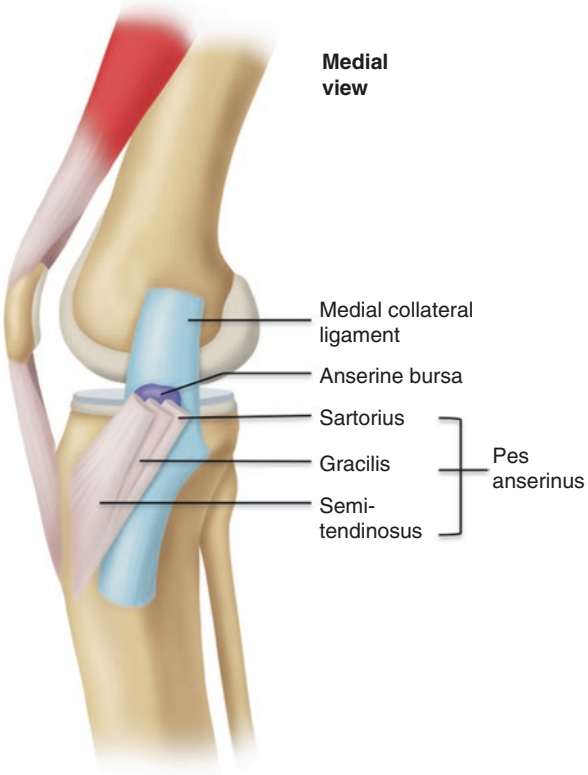

Fig. 23.13 Anserine bursa. (Reprinted with permission from Philip Peng Educational Series)

there is a bursa that allows the tendon slides freely during flexion and extension of the knee (Fig. 23.13). Both pes anserinus tendons and bursa can be injured in valgus deformities and medial compartment osteoarthritis deformities and it can be a very important source of extra-articular pain generator.

Ultrasound Scan

- Position: Supine with the knee flex and hip externally rotated, assuming "Figure of 4" position
- Probe: Linear 6–15 mHz

With the patient in figure of 4 position, the transducer is placed in long axis in relation of the tibia with the caudal end tilt in anterior direction (Fig. 23.14). The bursa can be seen as a thin hypoechoic line in the plane between the medial collateral ligament (black arrow head) and the pes anserinus tendons (arrows). The right upper panel showed the sonoanatomy in a normal individual. The right low panel showed a pathological bursa (∗∗) which is easier to visualize and the tendons are bigger and more hypoechoic than normal (when compared with the medial collateral ligament).

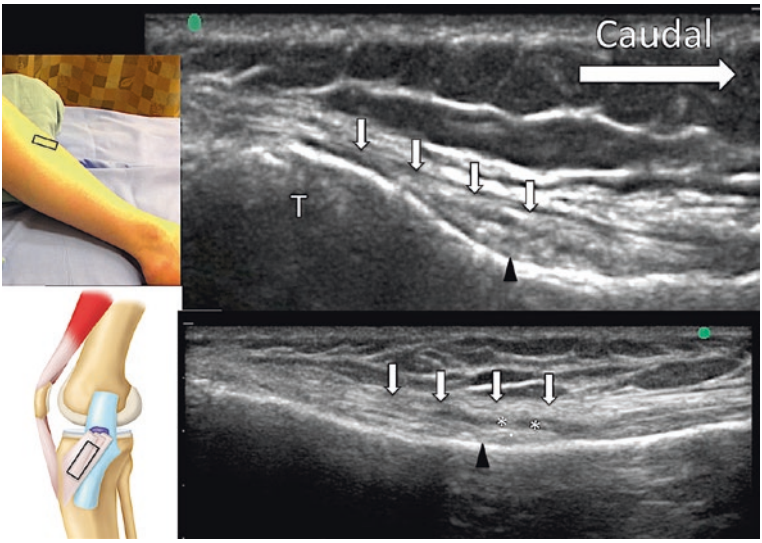

Fig. 23.14 Sonographic images of pes anserinus (marked by bold arrows in upper panel) and anserine bursa (∗ in lower panel). Black arrow head-medial collateral ligament. (Reprinted with permission from Philip Peng Educational Series)

Procedure

- Needle: 25G 1.5-inch needle
- Drugs: 3 mL 20 mg Depo-Medrol mixed with bupivacaine 0.25

Pes anserinus bursa injection is performed in plane targeting the fascial plane between the medial collateral ligament and the pes anserinus conjoint tendons (arrows) (Fig. 23.15). A linear pattern of spread is seen during the injection expanding the fascial plane with no changing in the echogenicity of the tendon (implying intratendinous injection). The lower two panel showed the positions of the probe and needle. Alternatively, the bursa can be injected when the probe is in short axis to the pes anserinus tendon (Fig. 23.16).

Ultrasound-Guided Distal Iliotibial Band Bursa Injection

The iliotibial band is a thick strip of dense connective tissue located on lateral thigh from ilium to tibia. It arises at its proximal end from the tendons of the tensor fasciae latae and gluteus maximus muscles and travels along the lateral side of the thigh to insert in Gerdy's tubercle (Fig. 23.17), a bony prominence between the fibula and tibia tubercle.

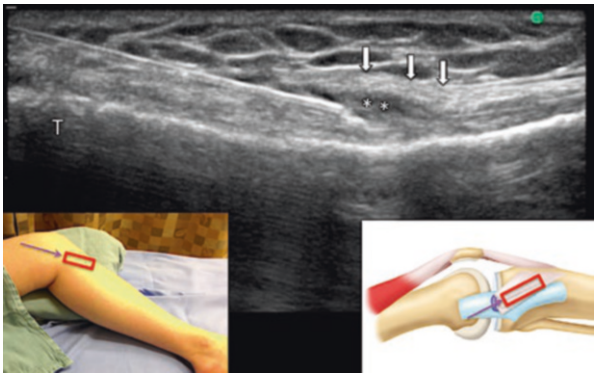

Fig. 23.15 In-plane injection of anserine bursa (∗) in long axis. T, tibial. (Reprinted with permission from Philip Peng Educational Series)

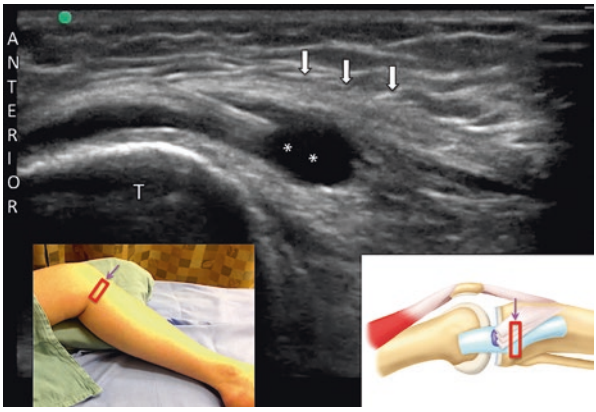

Fig. 23.16 In-plane injection of anserine bursa (∗) in short axis. (Reprinted with permission from Philip Peng Educational Series)

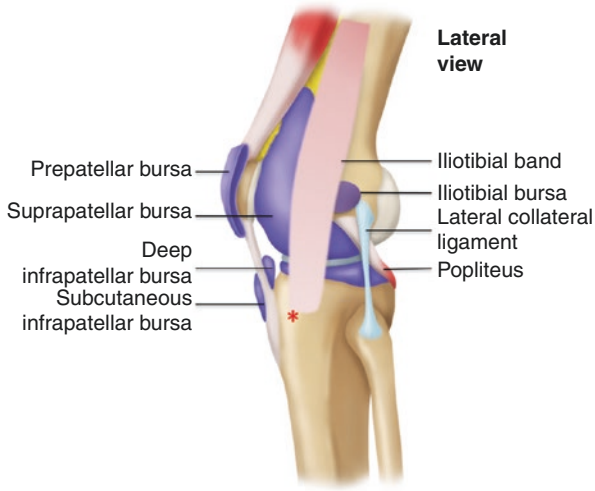

Fig. 23.17 Iliotibial band and its bursa. The Gerdy tubercle is marked by *. (Reprinted with permission from Philip Peng Education Series)

Iliotibial band (ITB) syndrome is an overuse injury usually observed in the active athletic population, but can happen in patients with varus deformity and or lateral compartment osteoarthritis. The main reason of this pathology is related to the friction of ITB against the lateral femoral epicondyle during flexion and extension, resulting in compression of the fat and connective tissue deep to the ITB, and chronic inflammation of the ITB bursa. Most of affected patients complain lateral side knee pain associated with repetitive activities. ITB syndrome is diagnosed mainly on clinical ground based on characteristic history and physical examination.

Ultrasound Scan

- Position: In lateral or semi-lateral position with the scan area in the non-dependent side
- Ultrasound probe: Linear 6–15 MHz

Scans 1 and 2

Scanning of iliotibial band (outlined by arrows) is initially performed in long axis to appreciate the structure from distal femur to the insertion into Gerdy's tubercle (GT) (Fig. 23.18). Normally the bursa between the ITB and the distal femur is not easily visible or appears as a hypoechoic thin line between the femur and the band. Compare the ITB of the contralateral side to appreciate the ITB thickness and echogenicity. Fluid collection can be seen when the bursa is filled with liquid (Fig. 23.19).

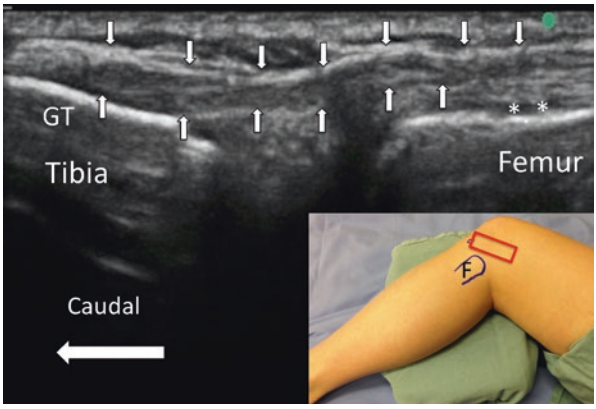

Fig. 23.18 Sonographic image of normal iliotibial band (ITB). (Reprinted with permission from Philip Peng Education Series)

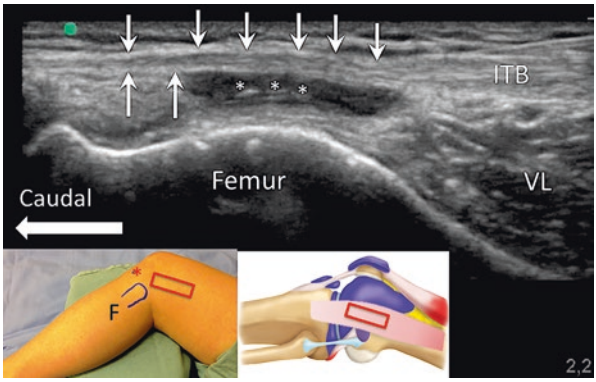

Fig. 23.19 ITB with bursitis. In patient with ITB syndrome, the ITB (arrows) may appear thickened with fluid collection in the bursa (**). VL, vastus lateralis. (Reprinted with permission from Philip Peng Education Series)

Procedure

- Needle: 25G 1.5-inch needle
- Drugs: 3–5 mL of Depo-Medrol (20 mg) mixed with 0.25% bupivacaine

A 25G needle is inserted in-plane from cephalad direction through the ITB to reach the bursal space (Fig. 23.20). Then, 3–5 mL of solution is slowly injected and visualization of the distension of bursa is observed.

Another approach is to inject the bursa in short axis of the ITB using a 22-gauge needle (arrow) inserted from posterior direction to avoid causing damage or piercing the ITB (Fig. 23.21).

Literature Review

The mainstay of treatment is the nonsurgical approach for symptom improvement of ITB syndrome. Oral nonsteroidal anti-inflammatory drugs and corticosteroid injection can be used to treat the acute inflammatory response. Although corticosteroid injections have shown significant pain improvement compared to placebo injections, there are few studies showing corticosteroid injection by the ultrasound.

Ultrasound-Guided Patellar Tendon Injections

Patellar tendinopathy ("jumper's knee") is a painful and disabling condition caused by chronic repetitive stress of the proximal patellar tendon at its origin from the inferior pole of the patella. It is particularly prevalent in athletic populations, affecting 40–50% of persons in those sports requiring repetitive, explosive power from

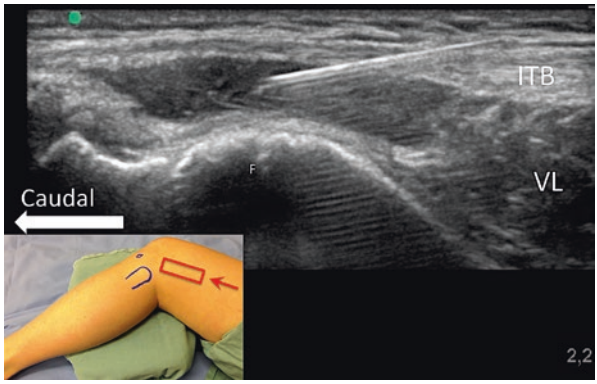

Fig. 23.20 In-plane needle insertion of ITB bursa in long axis. (Reprinted with permission from Philip Peng Education Series)

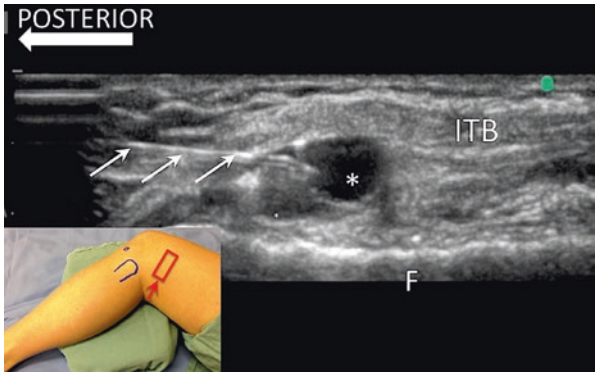

Fig. 23.21 In-plane needle insertion of ITB bursa in short axis. ∗, the bursa. (Reprinted with permission from Philip Peng Education Series)

the knee extensors, including basketball, volleyball, soccer, and track and field. Patellar tendinopathy is associated with significant impact on quality of life, loss of function and changes on ultrasound imaging of the tendon.

Ultrasound Scan

- Position: Supine with knee slight flexed
- Probe: Linear 6–15 MHz

Scan 1

Normal patella tendon (Fig. 23.22 left upper panel). The patella tendon is scan in long axis with the cephalad end of the probe on the lower patella. The patella tendon (bold arrow) is revealed. Please note the presence of the crura fascia (line arrow) and Hoffa fat pad (∗). TT, tibial tubercle. Right upper panel: Position of the ultrasound probe. Left lower panel: Abnormal patella tendon. Ultrasonographic imaging of

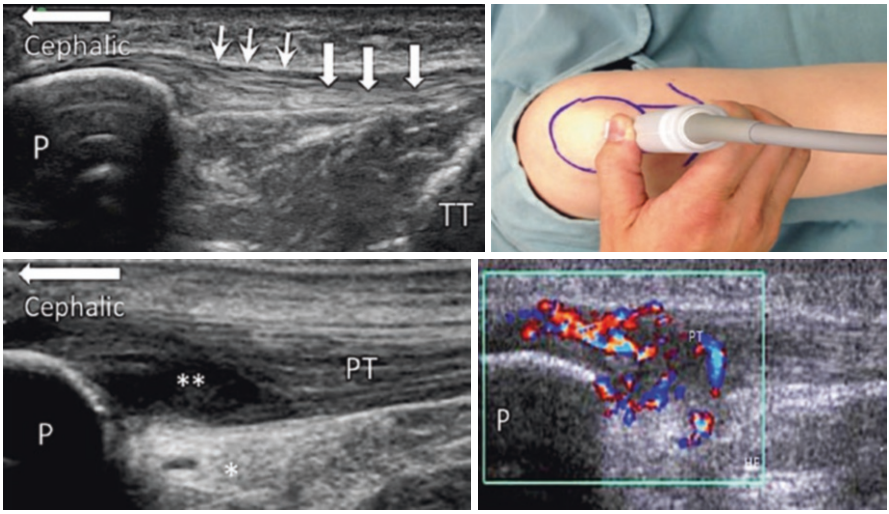

Fig. 23.22 Sonographic images of patella tendon. (Reprinted with permission from Philip Peng Education Series)

patella tendon (PT) typically reveals decreased echogenicity, increased thickness (∗∗), focal sonolucent regions (cysts), and intratendinous calcification. Right lower panel: Neovascular infiltration suggesting inflammation can be seen using Doppler ultrasound (lower panel) and graded on ordinal scales. ∗, Hoffa fat pad.

Procedure

Different types of ultrasound interventions have been described for this pathology, including high-volume image-guided injections, steroid peritendon injection, needle fenestration tenotomy, dextrose prolotherapy, and platelet-rich plasma intratendinous injection.

- Needle: 25G 1.5-inch needle (peritendon injection); 20–22G needle (fenestration)
- Drug: Depo-Medrol 20 mg mixed with 3 mL of bupivacaine 0.25% (peritendon injection) and mixed with 20 mL dextrose 5% for high-volume injection

The ultrasound probe is place in short axis to the patella tendon and the needle (arrow) is inserted in-plane from the lateral position (Fig. 23.23a). For high-volume injection, the needle is inserted in the plane deep to the patella tendon (PT). Hydrolocation is performed to visualize the posterior displacement of the Hoffa fat pad (HFD). #, injectate. Please note the intrasubstance tear (bold arrow) with the PT.

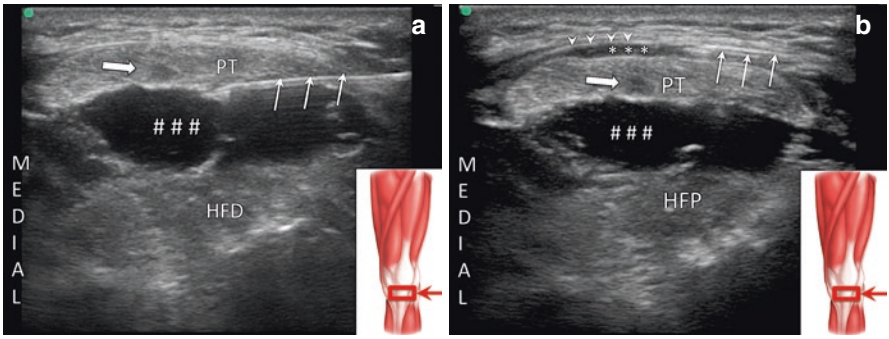

Fig. 23.23 Needle insertion (arrows) in short axis to patella tendon (**a**) deep to the patella tendon (PT), #-injectate, (**b**) between the PT and the crura fascia (arrow head). *-injectate (Reprinted with permission from Philip Peng Education Series)

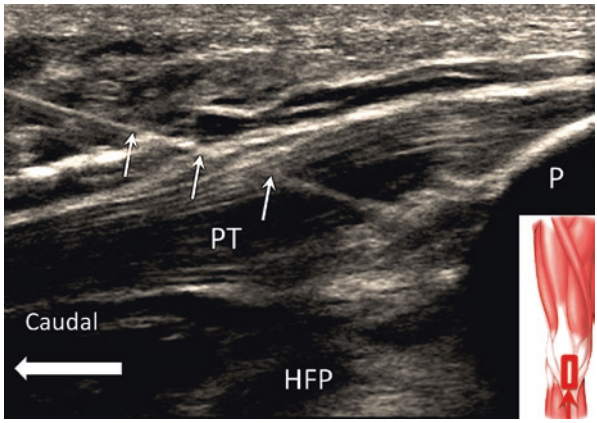

Fig. 23.24 Long-axis in-plane injection of the patella tendon. (Reprinted with permission from Philip Peng Education Series)

Peritendon injection between the patella tendon (PT) and the crura fascia (arrow head) (Fig. 23.23b). ∗, injectate.

Long-axis view of patellar tendon is used for intratendinous procedures as needle fenestration tenotomy and/or injection of platelet-rich plasma and other regenerative strategies (Fig. 23.24).

Suggested Reading

Acebes JC, Sánchez-Pernaute O. Ultrasonographic assessment of Baker's cysts after intra-articular corticosteroid injection in knee osteoarthritis. J Clin Ultrasound. 2006;34:113–7.

Bandinelli F, Fedi R, Generini S, et al. Longitudinal ultrasound and clinical follow-up of Baker's cysts injection with steroids in knee osteoarthritis. Clin Rheumatol. 2012;31:727–31.

Berkoff DJ. Clinical utility of ultrasound guidance for intra-articular knee injections: a review. Clin Interv Aging. 2012;7:89–95.

Chen CK, Lew HL, Liao RI. Ultrasound-guided diagnosis and aspiration of Baker's cyst. Am J Phys Med Rehabil. 2012;91(11):1002–4.

Crisp T. High volume ultrasound guided injections at the interface between the patellar tendon and Hoffa's body are effective in chronic patellar tendinopathy: a pilot study. Disabil Rehabil. 2008;30(20–22):1625–34.
Curtiss HM. Accuracy of ultrasound-guided and palpation-guided knee injections by an experienced and less-experienced injector using a superolateral approach: a cadaveric study. PM&R. 2011;3:507–15.
Daley EL. Elbow, knee, and shoulder: does injection site and imaging make a difference? A systematic review. Am Sports Med. 2011;39:656–62.
Ellis R. Iliotibial band friction syndrome—a systematic review. Man Ther. 2007;12:200–8.
Ferrero G. Ultrasound-guided injection of platelet-rich plasma in chronic Achilles and patellar tendinopathy. J Ultrasound. 2012;15(4):260–6.
Finnoff JT. Accuracy of ultrasound-guided versus unguided pes anserinus bursa injections. PM&R. 2010;2(8):732–9.
Gunter P. Local corticosteroid injection in iliotibial band friction syndrome in runners: a randomised controlled trial. Br J Sports Med. 2004;38:269–72.
Hong JH. Diagnosis of iliotibial band friction syndrome and ultrasound guided steroid injection. Korean J Pain. 2013;26(4):387–91.
Kanaan Y. Sonographically guided patellar tendon fenestration: prognostic value of preprocedure sonographic findings. Ultrasound Med. 2013;32(5):771–7.
Lueders DR. Ultrasound-guided knee procedures. Phys Med Rehabil Clin N Am. 2016;27(3):631–48.
Peng PW, Shankar H. Ultrasound-guided interventional procedures in pain medicine: a review of anatomy, sonoanatomy, and procedures. Part V: knee joint. Reg Anesth Pain Med. 2014;39(5):368–80.
Sarah M. High volume image-guided Injections for patellar tendinopathy: a combined retrospective and prospective case series. Muscles Ligaments Tendons J. 2014;4(2):214–9.
Smith MK. Treatment of popliteal (Baker) cysts with ultrasound-guided aspiration, fenestration, and injection long-term follow-up. Sports Health. 2015;7(5):409–14.
Strauss EJ. Iliotibial band syndrome: evaluation and management. J Am Acad Orthop Surg. 2011;19:728–36.
Ward EE, Jacobson JA, Fessell DP, Hayes CW, van Holsbeeck M. Sonographic detection of Baker's cysts: comparison with MR imaging. AJR Am J Roentgenol. 2001;176:373–80.
Worp MP. Iliotibial band syndrome in runners: a systematic review. Sports Med. 2012;42:969–92.

Ankle Joint and Nerves

24

Neilesh Soneji and Philip Peng

Introduction

Foot and ankle pain is a common reason for patients to present to their primary care doctor. It is clinically challenging to identify the etiology of foot and ankle pain because the region is anatomically complex. Two of the most common musculoskeletal causes of foot and ankle pain include tibiotalar and subtalar joint pathology such as osteoarthritis. In addition foot pain may be neuropathic in nature. The peripheral nerves of the foot may be injured or entrapped, which can cause pain in specific nerve distributions.

The ankle joint is formed from three primary articulations: the tibiotalar joint, the subtalar joint, and the distal tibiofibular joint (Fig. 24.1). The tibiotalar joint is formed by the articulation between the tibia and fibula with the talus. It is a hinged synovial joint, which allows for flexion and extension. The subtalar joint is formed by the articulation of the talus and the calcaneous. The subtalar joint has an anterior and posterior component. The tibiotalar and subtalar joints communicate in approximately 10–20% of people.

There are five peripheral nerves which innervate the foot: the superficial peroneal nerve (SPN), deep peroneal nerve (DPN), saphenous nerve (SaN), tibial nerve (TB), and sural nerve (SuN).

The SPN and DPN are branches of the common peroneal nerve . The SPN provides sensation to the majority of dorsum of the foot, apart from the webspace of the first and second toe, which is supplied by the DPN (Fig. 24.2). The SPN usually emerges below

N. Soneji
Department of Anesthesia, University of Toronto, Toronto, ON, Canada

Department of Anesthesia and Pain Management, University Health Network – Toronto Western Hospital, Women's College Hospital, Toronto, ON, Canada

P. Peng (✉)
Department of Anesthesia and Pain Management, Toronto Western Hopsital and Mount Sinai Hospital, University of Toronto, Toronto, Ontario, Canada
e-mail: Philip.peng@uhn.ca

P. Peng et al. (eds.), *Ultrasound for Interventional Pain Management*,
https://doi.org/10.1007/978-3-030-18371-4_24

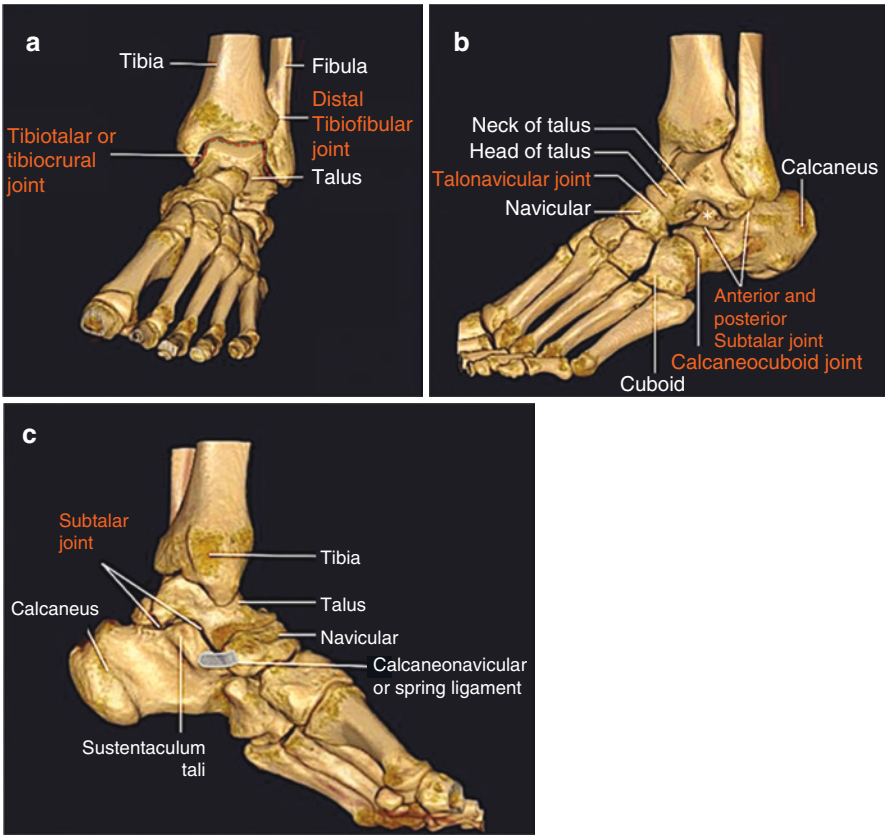

Fig. 24.1 Ankle anatomy. (**a**) Anterior view. (**b**) Lateral view. (**c**) Medial view. (Reprinted with permission from the Philip Peng Educational Series)

the knee in the middle third of the leg in the fascial plane between the peroneus muscles and the extensor digitorum longus muscle (Fig. 24.3). The terminal branches are sensory. Above the level of the ankle joint the DPN lies lateral to the anterior tibial artery between the extensor digitorum longus and extensor hallucis longus tendons.

On the medial aspect of the ankle, the SaN provides sensation to the region around the medial malleolus and the medial aspect of the foot (Fig. 24.4). The SaN runs adjacent to the greater saphenous vein in the distal lower extremity. It commonly bifurcates 3 cm above the medial malleolus into an anterior and posterior division.

The TN provides sensation to the plantar aspect of the foot. The TN runs in the tarsal tunnel adjacent to the posterior tibial artery (Fig. 24.5). The TN gives off a calcaneal branch proximal to the medial malleolus and then continues to terminate in the medial and lateral branches.

The SuN provides sensation to the lateral aspect of the distal leg and the lateral aspect of the foot. In the distal leg, the SuN runs adjacent to the lesser saphenous vein between the Achilles tendon and the peroneus tendons (Fig. 24.6).

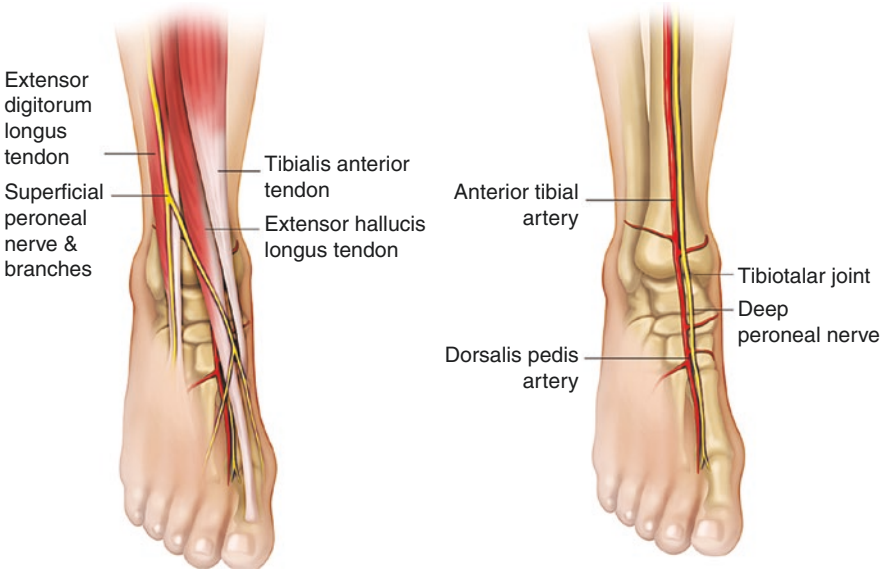

Fig. 24.2 Anterior view of the ankle. (**a**) Superficial peroneal nerve. (**b**) Deep peroneal nerve and tibiotalar joint. (Reprinted with permission from the Philip Peng Educational Series)

Patient Selection

Injection of the tibiotalar and subtalar joints can be valuable for diagnostic and therapeutic purposes. Joint injections with local anesthetic can help to clarify the articular contribution of pain and may be used for surgical planning for arthrodesis. Joint injections can also provide symptomatic relief for osteoarthritis, rheumatoid arthritis, and ankle impingement. Perineural injections around the foot and ankle nerves may be offered for patients with neuropathic pain, particularly in the context of peripheral nerve injury or entrapment.

Ultrasound Scan for Ankle Nerves

Sural and Superficial Peroneal Nerve

- Position: Supine, tilted contralateral side, affected leg nondependent position
- Probe: Linear 6–15 MHz

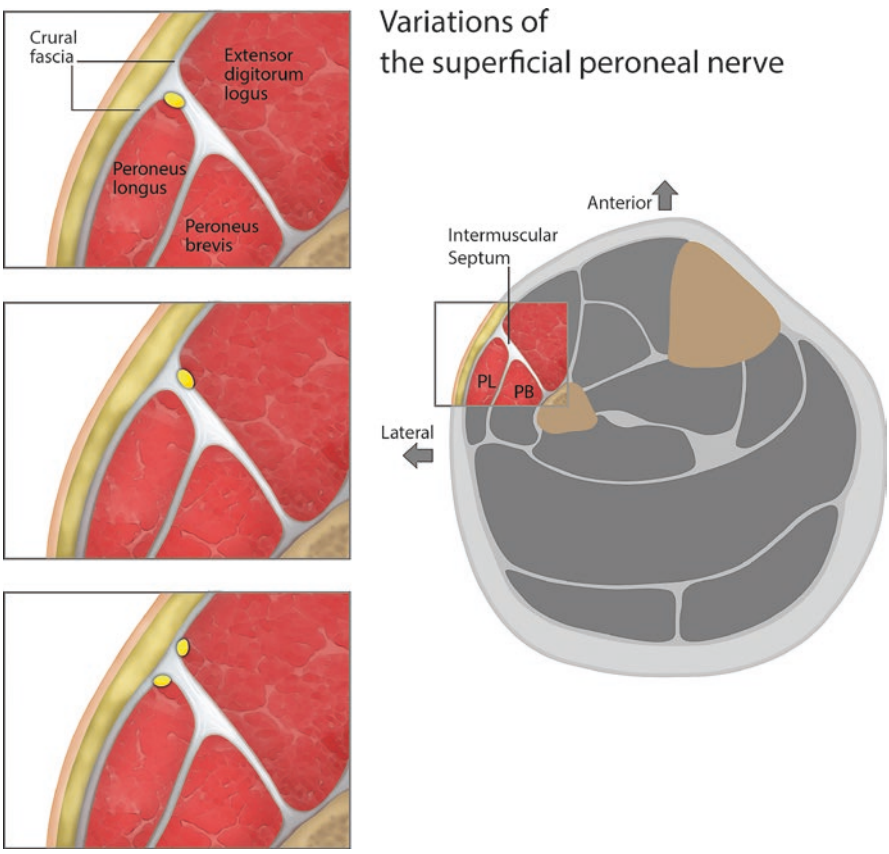

Fig. 24.3 Superficial peroneal nerve in middle third of leg. (Reprinted with permission from the Philip Peng Educational Series)

Scan 1

The author suggests to place the probe initially at the lower one-third of the leg over the fibula (F) and extensor digitorum longus (EDL) (Fig. 24.7 upper panel). SPN is deep to the crural fascial (bold arrow). The SPN (arrow) can be located at the junction of the intermuscular septum (between the peroneus muscle and EDL as indicated by the arrow heads) and the crural fascia.

Scan 2

By moving the probe in the caudal direction, the SPN (arrow) can be seen within the crural fascia (bold arrows) in the middle figure (Fig. 24.7 middle panel).

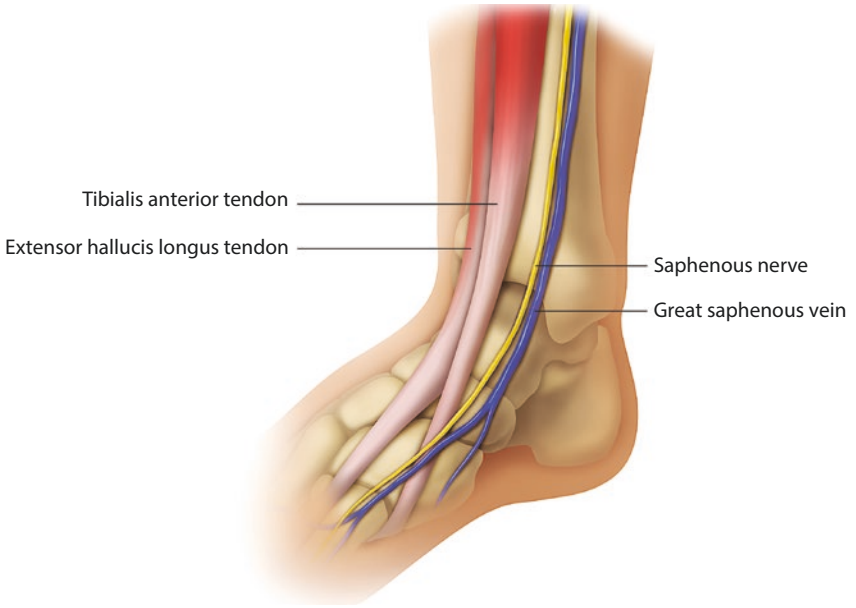

Fig. 24.4 Anteromedial view of the ankle. Saphenous nerve. (Reprinted with permission from the Philip Peng Educational Series)

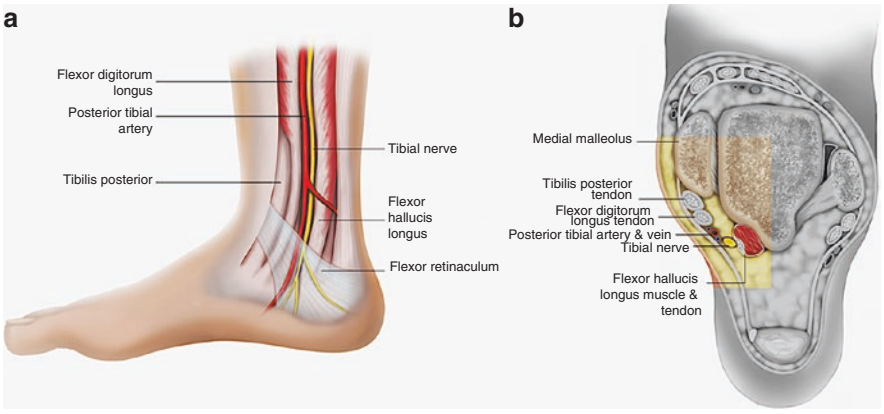

Fig. 24.5 Medial view of the ankle. (**a**) Medial view tibial nerve. (**b**) Cross-sectional view of the ankle. (Reprinted with permission from the Philip Peng Educational Series)

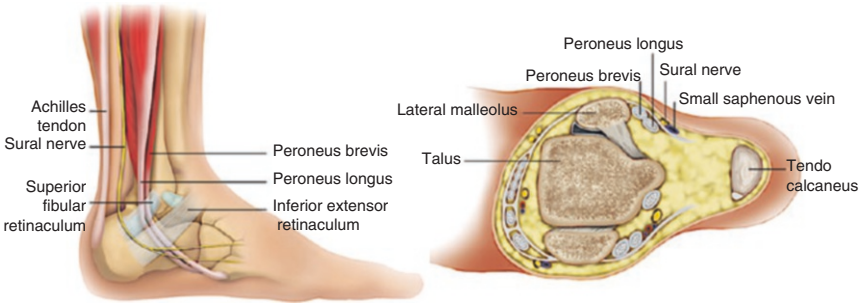

Fig. 24.6 Lateral view of the ankle. (**a**) Lateral view of sural nerve. (**b**) Cross-sectional view of the ankle. (Reprinted with permission from the Philip Peng Educational Series)

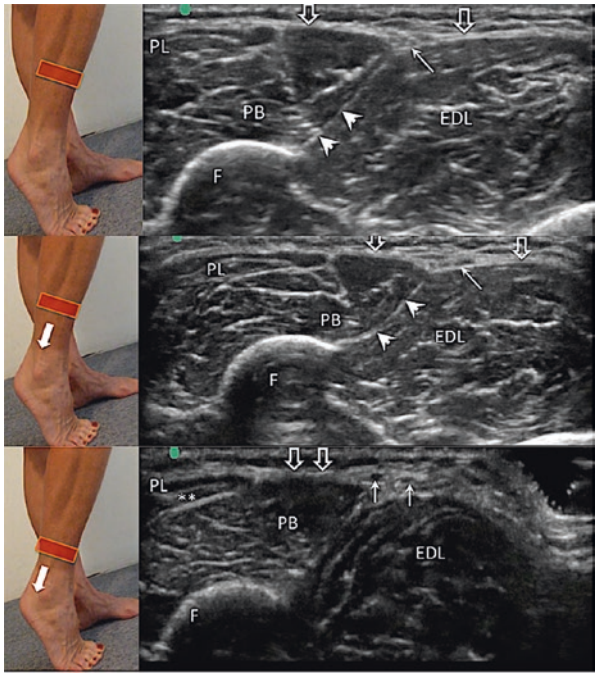

Fig. 24.7 Sonoanatomy of the superficial peroneal nerve at different locations in the lower extremity. (Reprinted with permission from the Philip Peng Educational Series)

Scan 3

Further caudal movement of the probe, the SPN (arrows) is now superficial to the crural fascia (bold arrows) (Fig. 24.7 lower panel). PB and PL, peroneus brevis and longus; **, PB tendon; F, fibula.

Placing the probe between the lateral malleolus and Achilles tendon (TA), a fascia plane (bold arrows) can be appreciated (Fig. 24.8). Sural nerve (arrow) can be seen adjacent to the lesser saphenous vein (V) in this fascia plane.

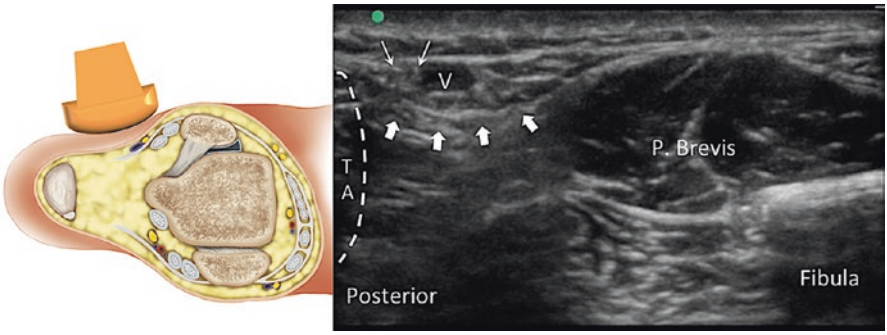

Fig. 24.8 Sonoanatomy of sural nerve. Line arrow, SuN. P. brevis, peroneus brevis. (Reprinted with permission from the Philip Peng Educational Series)

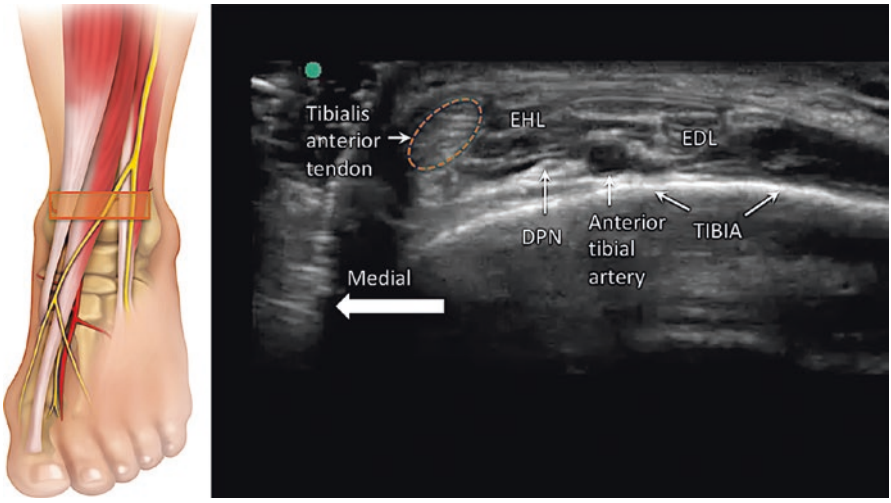

Fig. 24.9 Sonoanatomy of DPN. (Reprinted with permission from the Philip Peng Educational Series)

Deep Peroneal Nerve

- Position: Supine, knee flexed, foot on the examination table
- Probe: Linear 6–15 MHz

By placing the probe in short axis to the tendons just above the ankle joint, the most prominent tendon will be the tibialis anterior tendon (orange circle) (Fig. 24.9). Deep to the extensor hallucis longus (EHL) and extensor digitorum longus (EDL) tendon, the anterior tibial artery is seen. The DPN is in the fascia plane with the vessel.

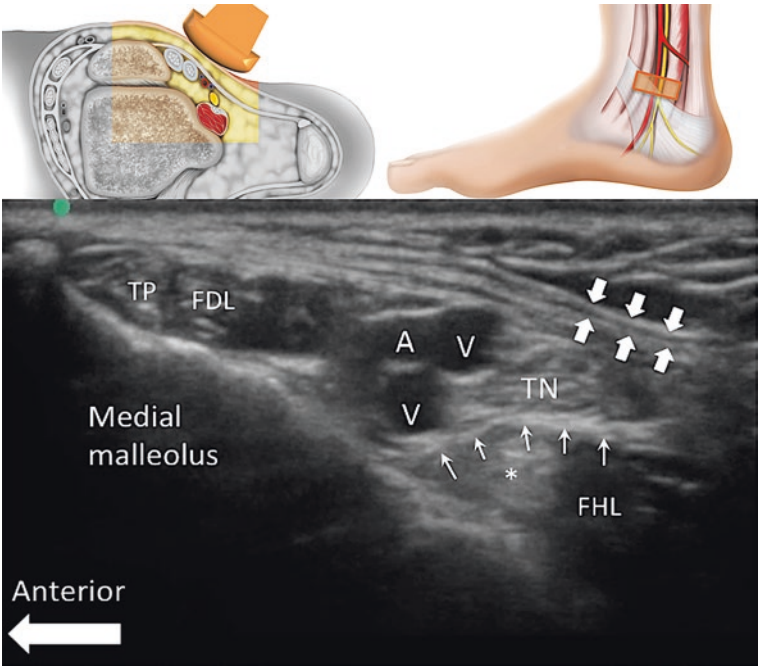

Fig. 24.10 Sonoanatomy of tibial nerve. TP, tibialis posterior tendon; FDL, flexor digitorum longus tendon; bold arrows, flexor retinaculum. (Reprinted with permission from the Philip Peng Educational Series)

Tibial and Saphenous Nerve

- Position: Supine, tilted ipsilateral side, knee flexed
- Probe: Linear 6–15 MHz

By placing the probe between the medial malleolus and Achilles tendon, the tarsal tunnel and its content are revealed (Fig. 24.10). The tibial nerve (TN) is visualized posterolateral to the posterior tibial artery over the flexor hallucis longus (FHL). By moving the big toe, the TN is seen resting on the fascia over the FHL (line arrows), and the tendon of FHL (∗) is seen as well.

Place the probe over the medial malleolus and apply very slight pressure (Fig. 24.11). The saphenous nerve (arrow) is seen beside the saphenous vein (SV). Quite often the nerve is small or is already divided into small branches and cannot be visualized at this level.

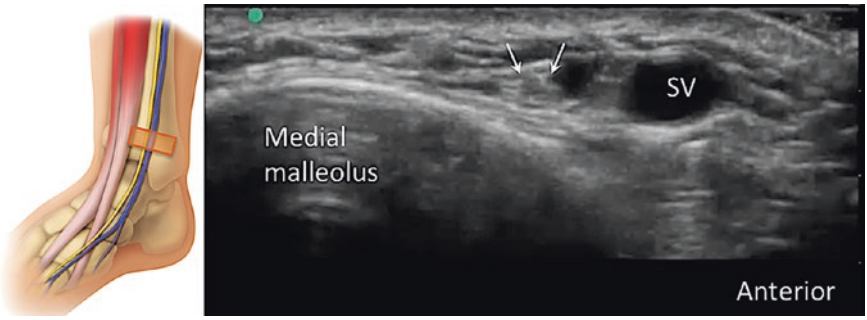

Fig. 24.11 Sonoanatomy of sural nerve. (Reprinted with permission from the Philip Peng Educational Series)

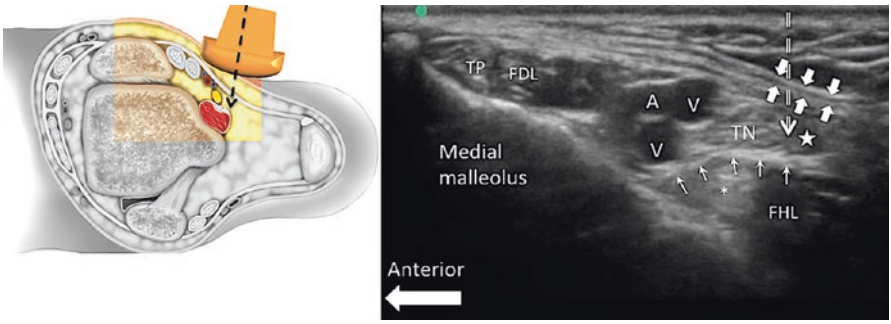

Fig. 24.12 Out-of-plane needle insertion to the space behind tibial nerve. (Reprinted with permission from the Philip Peng Educational Series)

Procedure for Ankle Nerves

- Drugs: Bupivacaine 0.25% 10 mL mixed with depo steroid (Depo-Medrol) 40 mg
- Needle: 25G 1.5-inch needle

For each site, 3–5 mL is sufficient, larger volume for TN. For TN, we prefer to direct the needle out-of-plane (dotted arrow) to target the space (★) posterior to TN formed by the retinaculum (bold arrow) and the fascia overlying the FHL (arrows) (Fig. 24.12). For SPN, SaN, and DPN, we suggest in-plane and SN out-of-plane.

Ultrasound Scan for Ankle Joints

Tibiotalar Joint

- Position: Supine, knee flexed, foot on the examination table
- Probe: Linear 6–15 MHz

Scan 1
Similar to Fig. 24.9, place the probe at distal tibia. Identify the tibialis anterior tendon.

Scan 2
Rotate the probe so as to view the long axis of tibialis anterior (TA) tendon (Fig. 24.13). The space between the TA tendon (arrow) and the medial malleolus is the entry where the anterior recess of the tibiotalar joint is visualized. It is covered by fat pad (*).

Subtalar Joint (Lateral Approach)

There are three approaches to the subtalar joint and the author prefer lateral approach.

- Position: Lateral position, affected leg nondependent position, rolled towel on the medial ankle to allow inversion of the ankle
- Probe: Linear 6–15 MHz

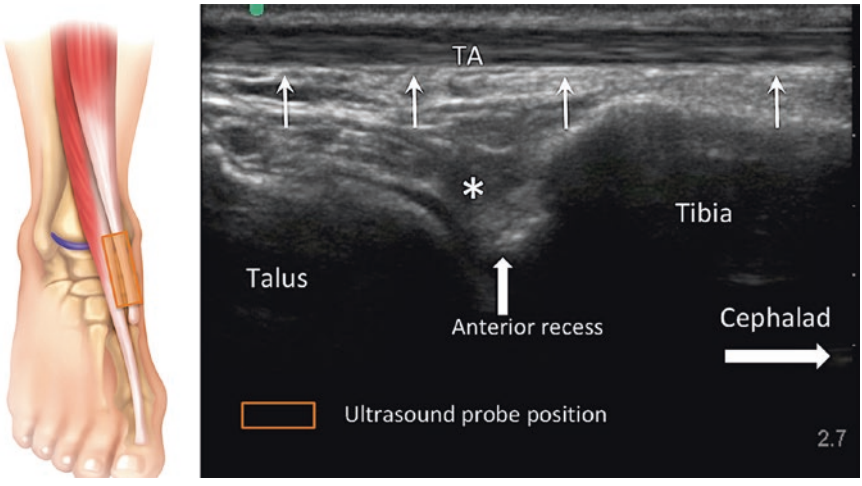

Fig. 24.13 Sonoanatomy of anterior to the tibiotalar joint. (Reprinted with permission from the Philip Peng Educational Series)

Fig. 24.14 Sonoanatomy of sinus tarsi. (Reprinted with permission from the Philip Peng Educational Series)

Scan 1

Palpate the sinus tarsi (a big "hollow" in the lateral ankle) and place the probe over it (Fig. 24.14). On the calcaneal side, the peroneus tendon (∗) can be seen.

Scan 1

Rotate the probe toward the lateral malleolus as much as possible, and the hyperechoic shadow of both calcaneus and talus will become superficial with a gap in between (bold arrow) (Fig. 24.15). This is the entrance to the subtalar joint. The peroneus tendon (∗) is on the calcaneus side.

Procedure

Tibiotalar Joint Injection—Anterior Joint Recess

- Needles: 22G 3.5-inch needle.
- Drugs: 3 mL of local anesthetic (2% plain bupivacaine)
- 1 mL steroid (40 mg Depo-Medrol)

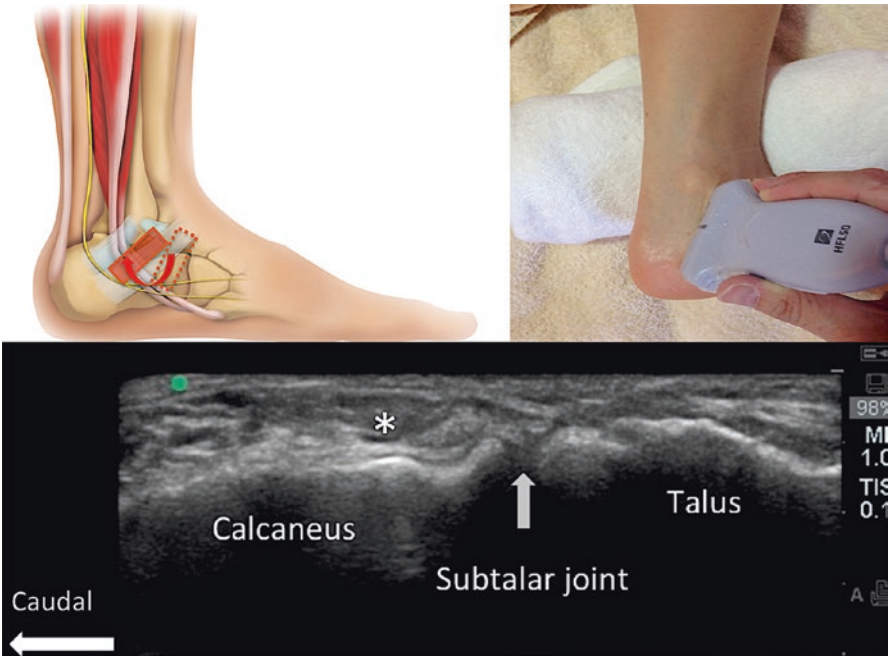

Fig. 24.15 Sonoanatomy of posterior subtalar joint. (Reprinted with permission from the Philip Peng Educational Series)

Both out-of-plane (Fig. 24.16a) and in-plane (Fig. 24.16b) approaches have been described. The authors prefer out-of-plane because of the ease and short distance to the target. Once the needle passes the anterior fat pad, hydrolocation with normal saline is used to ensure the spread of the injectate into the joint. A successful injection will result in rising of the fat pad.

Subtalar Joint Injection—Lateral Approach

Needles: 25G 1.5-inch needle.
Drugs: 2 mL of local anesthetic (2% plain lidocaine)
1 mL steroid (40 mg Depo-Medrol)

An out-of-plane technique is used. The linear probe is rotated posteriorly to visualize the subtalar joint (Fig. 24.17). The needle tip is passed between the calcaneous and talus using hydrolocation with saline. Thin arrows, needle direction with out of plane technique. Thick arrow, subtalar joint. Reprinted with permission from the Philip Peng Educational Series.

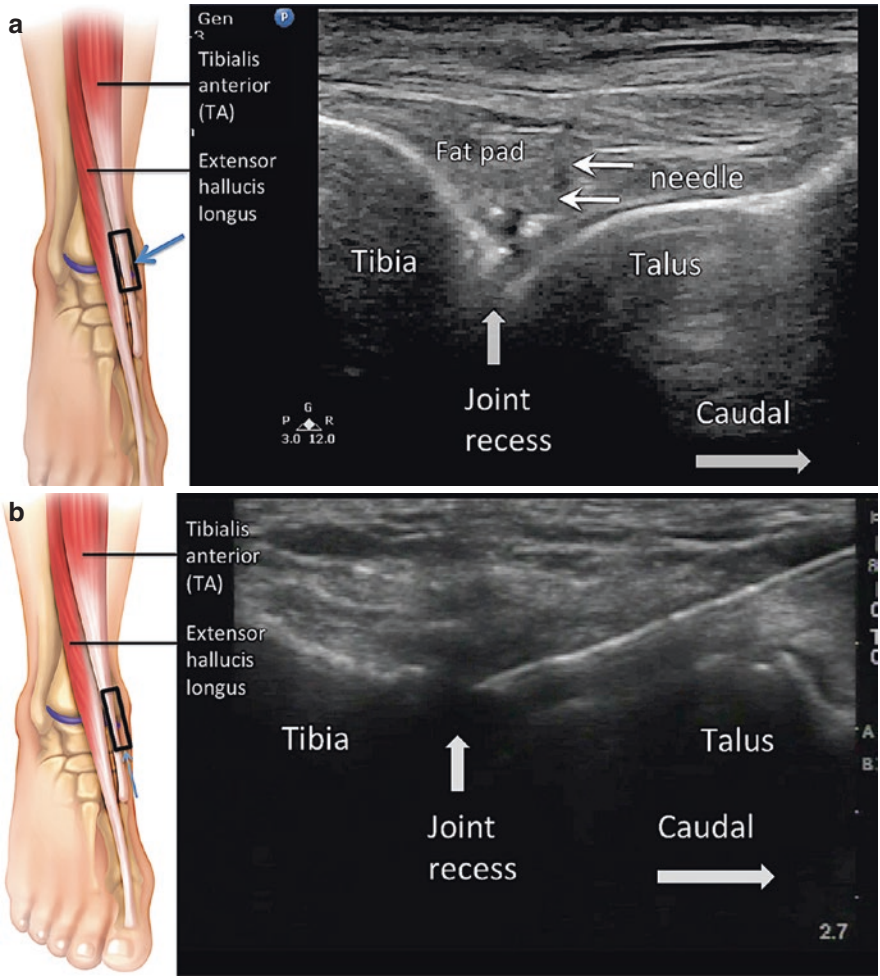

Fig. 24.16 (**a**) Out-of-plane needle insertion to tibiotalar joint. (**b**) In-plane approach to tibiotalar joint. (Reprinted with permission from the Philip Peng Educational Series)

Clinical Pearls

1. When scanning the anterior tibiotalar joint, ensure the patient's foot is flat on the examination table with the knee flexed. This opens the anterior joint recess.
2. When scanning the tibiotalar joint, start by scanning over the tibialis anterior tendon. The probe should then be shifted medially. Needle insertion medial to the tibialis anterior tendon will prevent injury to the deep peroneal nerve or dorsalis pedis artery.

3. When injecting the anterior tibiotalar joint, ensure the medication is not accumulating within the anterior fat pad.
4. The subtalar joint can be injected from the medial side, lateral side, or posterolateral side. The lateral approach is the preferred approach by the author as there is less risk to neurovascular structures in this region.
5. When scanning the lateral subtalar joint, start by scanning the sinus tarsi which can be palpated in most patients. Then rotate the distal aspect of the probe posteriorly and look for the peroneal tendons. The subtalar joint will be visualized adjacent to the peroneal tendons.

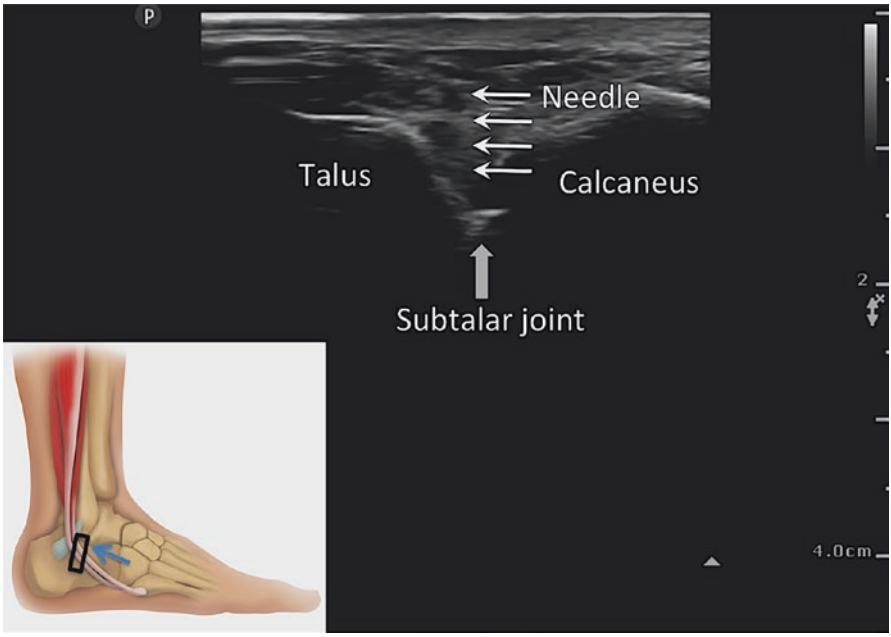

Fig. 24.17 Needle insertion to subtalar joint. (Reprinted with permission from the Philip Peng Educational Series)

Literature Review

Ultrasound guidance is a validated technique for tibiotalar and subtalar joint injections. Studies have shown 100% accuracy rates when ultrasound guidance is used for tibiotalar joint injections. Accuracy rates for subtalar joint injections also approach 100%. Due to the anatomy of the subtalar joint, extravasation of the injectate to surrounding structures occurs in approximately 20% of injections. Rates

of extravasation to areas such as the subtalar joint and peroneal tendons are similar between ultrasound and other injection techniques such as fluoroscopy and anatomic guidance. Foot and ankle joint injections with local anesthetic and steroid can be valuable for diagnostic purposes. Literature generally supports the correlation between response to local anesthetic and steroid and good surgical outcome. From a therapeutic standpoint, a limited number of studies demonstrate short-term benefit with foot and ankle injections with local anesthetic and steroid. Viscosupplementation is another viable option for ankle joint injections. A recent meta-analysis concluded that viscosupplementation for ankle arthritis can significantly reduce pain and is likely superior to reference therapy; however, the number of studies is limited. Larger good quality randomized studies are required to assess longer-term efficacy of foot and ankle injections.

Suggested Readings

Antonakakis JG, Scalzo DC, Jorgenson AS, et al. Ultrasound does not improve the success rate of a deep peroneal nerve block at the ankle. Reg Anesth Pain Med. 2010;35:217–21.

Chang KV, Hsiao MY, Chen WS, Wang TG, Chien KL. Effectiveness of intra-articular hyaluronic acid for ankle osteoarthritis treatment: a systematic review and meta-analysis. Arch Phys Med Rehabil. 2013;94:951–60.

Chen J, Lesser J, Hadzic A, Resta-Flarer F. The importance of the proximal saphenous nerve block for foot and ankle surgery. Reg Anesth Pain Med. 2013;38:372.

Chin KJ. Ultrasound visualization of the superficial peroneal nerve in the mid-calf. Anesthesiology. 2013;118:956–65.

Ducic I, Dellon AL, Graw KS. The clinical importance of variations in the surgical anatomy of the superficial peroneal nerve in the mid-third of the lateral leg. Ann Plast Surg. 2006;56:635–8.

Khosla S, Thiele R, Baumhauer JF. Ultrasound guidance for intra-articular injections of the foot and ankle. Foot Ankle Int. 2009;30:886–90.

Khoury NJ, el-Khoury GY, Saltzman CL, Brandser EA. Intraarticular foot and ankle injections to identify source of pain before arthrodesis. AJR Am J Roentgenol. 1996;167:669–73.

Lucas PE, Hurwitz SR, Kaplan PA, Dussault RG, Maurer EJ. Fluoroscopically guided injections into the foot and ankle: localization of the source of pain as a guide to treatment—prospective study. Radiology. 1997;204:411–5.

Newman JS. Diagnostic and therapeutic injections of the foot and ankle. Semin Roentgenol. 2004;39:85–94.

Papaliodis DN, Vanushkina MA, Richardson NG, Di Preta JA. The foot and ankle examination. Med Clin North Am. 2014;98:181–204.

Reach JS, Easley ME, Chuckpaiwong B, Nunley JA. Accuracy of ultrasound guided injections in the foot and ankle. Foot Ankle Int. 2009;30:239–42.

Redborg KE, Antonakakis JG, Beach ML, Chinn CD, Sites BD. Ultrasound improves the success rate of a tibial nerve block at the ankle. Reg Anesth Pain Med. 2009;34:256–60.

Ricci S, Moro L, Antonelli Incalzi R. Ultrasound imaging of the sural nerve: ultrasound anatomy and rationale for investigation. Eur J Vasc Endovasc Surg. 2010;39:636–41.

Smith J, Finnoff JT, Henning PT, Turner NS. Accuracy of sonographically guided posterior subtalar joint injections: comparison of 3 techniques. J Ultrasound Med. 2009;28:1549–57.

Smith J, Maida E, Murthy NS, Kissin EY, Jacobson JA. Sonographically guided posterior subtalar joint injections via the sinus tarsi approach. J Ultrasound Med. 2015;34:83–93.

Soneji N, Peng P. Ultrasound-guided interventional procedures in pain medicine: a review of anatomy, sonoanaotmy and procedures. Part VI: ankle joint. Reg Anesth Pain Med. 2016;41:99–116.

Thomas MJ, Roddy E, Zhang W, Menz HB, Hannan MT, Peat GM. The population prevalence of foot and ankle pain in middle and old age: a systematic review. Pain. 2011;152:2870–80.
Ward ST, Williams PL, Purkayastha S. Intra-articular corticosteroid injections in the foot and ankle: a prospective 1-year follow-up investigation. J Foot Ankle Surg. 2008;47:138–44.
Wisniewski SJ, Smith J, Patterson DG, Carmichael SW, Pawlina W. Ultrasound-guided versus nonguided tibiotalar joint and sinus tarsi injections: a cadaveric study. PM R. 2010;2:277–81.

Platelet-Rich Plasma

25

Dmitri Souza

Abbreviations

LP-PRP	Leukocyte-pure platelet-rich plasma
LR-PRP	Leukocyte-rich platelet-rich plasma
NSAIDs	Nonsteroidal anti-inflammatory drugs
PPP	Platelet-pure plasma
PRP	Platelet-rich plasma

Introduction

What Is PRP?

Platelet-rich plasma (PRP) denotes a supraphysiologic concentration of platelets in the serum. PRP injections represent one of the regenerative medicine instruments which gained popularity in managing certain musculoskeletal conditions. The basic research and clinical utilization of PRP, and, more inclusively regenerative medicine, are one of most innovative trends in treatment of musculoskeletal conditions and coexistent chronic pain. However, there is still paucity of high-quality clinical studies on this topic. This chapter will provide a brief overview of PRP and review the recent developments in PRP application in the treatment of chronic musculoskeletal painful conditions.

D. Souza (✉)
Ohio University, Heritage College of Osteopathic Medicine, Athens, OH, USA

Center for Pain Medicine, Western Reserve Hospital, Cuyahoga Falls, OH, USA
e-mail: ds241014@ohio.edu

P. Peng et al. (eds.), *Ultrasound for Interventional Pain Management*,
https://doi.org/10.1007/978-3-030-18371-4_25

How Does It Work?

PRP, similar to other regenerative medicine modalities, aims to repair damaged or worn-out tissue. The mechanisms of the repair continue to be explored. There is extensive body of data regarding basic research of PRP. It is established that the primary role of PRP is not replacement of the damaged or worn-off tissue, but, rather, facilitation of tissue recovery by signaling and recruiting mesenchymal stem cells, also called medicinal stem cells (MSC). It appears that PRP contains significantly more growth factors and other signaling molecules than are typically present in the affected tissue or, even, in the whole blood (Fig. 25.1 and Table 25.1).

The mechanisms of effects of PRP on repair are complex but appear to resemble a typical pattern of healing, facilitated with PRP (Figs. 25.2 and 25.3). There are a number of factors, producing impact on its effect, including volume of blood used for PRP preparation, PRP concentration, use of anticoagulant during PRP preparation, platelet count, white blood cell (WBC) count, type of injury or disease, PRP equipment used, number of PRP injections, interval between PRP injections, and many others (Table 25.2). The recent studies suggest that the release of PRP growth factors may be dependent on such remote factors and the microbiota and immune status of the host.

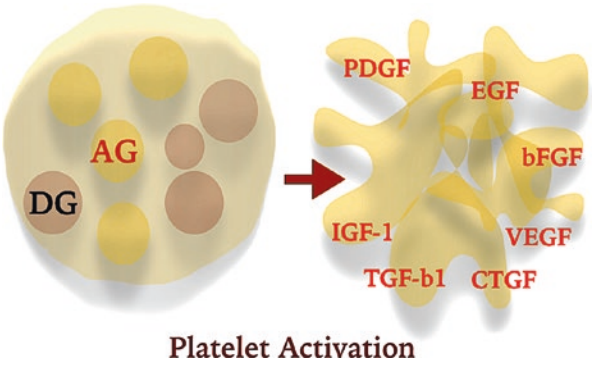

Fig. 25.1 Platelet physiology. Platelets are not cells, but rather 1–4 μm anucleated cytoplasmic fragments of megakaryocytes. Platelets contain dense granules and alpha granules. The latter contain adhesion molecules, coagulation and fibrinolytic factors, growth factors, cytokines, antibacterial proteins, and other factors, totaling more than 1000. These factors are released with platelet activation as shown on the schematics. ∗AG – Alpha granules, DG – Dense granules, PDGF – Platelet-derived growth factor, IGF-1 – Insulin-like growth factor-1, TGF-b1 – Transforming growth factor beta-1, CTGF – Connective tissue growth factor, VEGF – Vascular endothelial growth factor, b-FGF – Basic fibroblastic growth factor, EGF – Epidermal growth factor

Table 25.1 Platelet-rich plasma proteins

Biologically active proteins released from platelet-rich plasma and their effects on tissue repair
Platelet-derived growth factor (PDGF) – fibroblast production, chemotaxis, collagen production
Insulin-like growth factor-1 (IGF-1) – cell growth, differentiation
Transforming growth factor beta-1 (TGF-b1) angiogenesis, extracellular matrix formation, cell viability
Connective tissue growth factor (CTGF) – connective tissue growth
Vascular endothelial growth factor (VEGF) – new blood vessel growth and anti-apoptosis of blood vessel cells
Fibroblastic growth factor (b-FGF) – tissue repair, collagen production, myoblast proliferation
Epidermal growth factor (EGF) – cell recruitment, proliferation, differentiation, promotion of epithelial cells

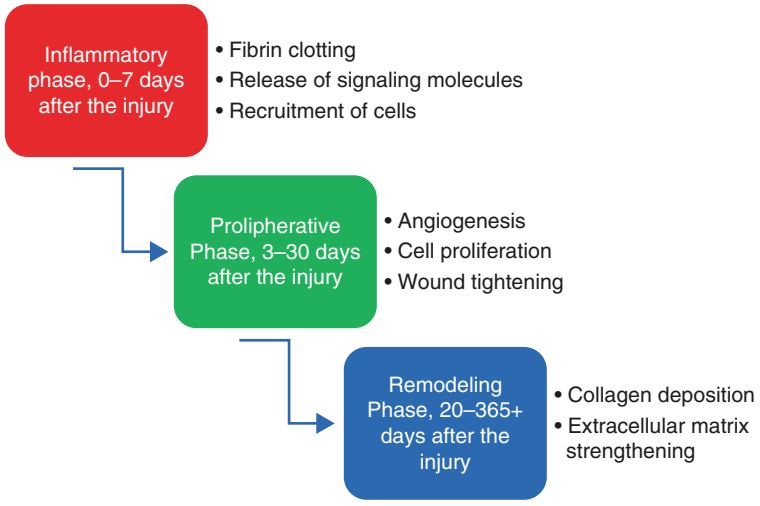

Fig. 25.2 Typical pattern of healing. An initial reaction to injury starts immediately with hemostasis. The inflammatory phase followed by proliferation and then remodeling. The healing of tissue may last more than a year

Regulatory Landscape

The regulatory landscape of regenerative is very complex and, in addition, is quickly evolving to reflect new developments. There are some fundamental rules, however. For example, the Code of Federal Regulations Title 21, 1271 (USA) suggests that autologous products must be "minimally manipulated" and used for a "homologous" purpose in order to be regulated solely under the Part 1271. Example of another rule which should be taken in consideration is the "Same Surgical Procedure" rule of

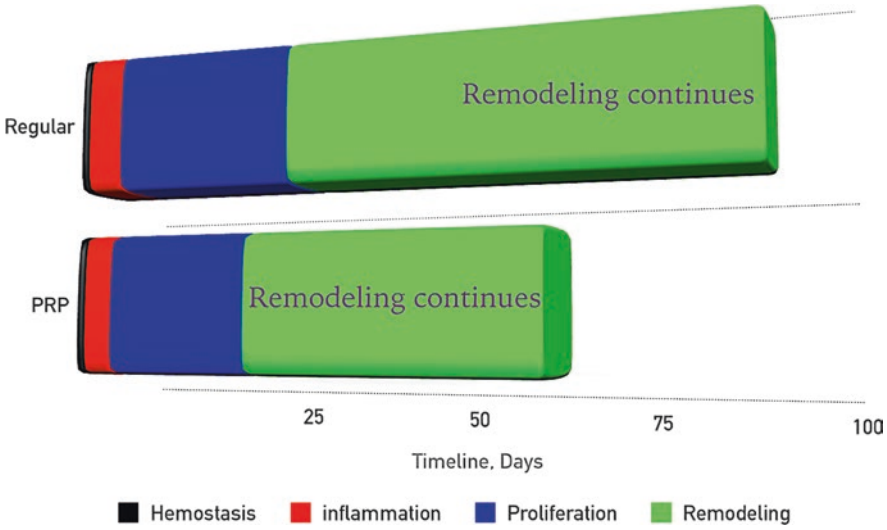

Fig. 25.3 Why use platelet-rich plasma (PRP)? The normal or physiologic platelet concentration in blood is 150–450,00 per μL. It is characteristically three to eight times greater in the PRP. Subsequently, the concentration of growth factors and other signaling molecules is significantly higher, which may potentially explain some of the mechanisms of accelerated tissue regeneration with platelet-rich plasma application. PRP seems to produce simultaneous anti-inflammatory and pro-inflammatory effects, which diverge it from corticosteroids, widely used to hold up inflammatory cascade, and from prolotherapy, which typically aggravates inflammatory reaction after its injection

Table 25.2 Factors influencing platelet-rich plasma effect

Factors affecting PRP injection outcomes
Volume of blood used for PRP preparation
PRP concentration
Use of anticoagulant
Pre-procedure platelet count
WBC count
Type of injury or disease treated with PRP
Equipment used in PRP preparation
Number of PRP injections
Interval between PRP injections
Host microbiota
Host immune status
Others

PRP Platelet-rich plasma

the Public Health Service Act. It describes removal of human cells or tissue product from an individual and implant it into the same individual during the same procedure. Pain practitioners, utilizing regenerative medicine techniques, should scrupulously explore, and follow the rules and regulations as they relate to the practice of regenerative medicine.

Clinical Applications of PRP and Patient Selection

Clinical applications of PRP include, but not limited to tendinopathies, ligament injuries, muscle injuries, cartilage pathology, subchondral bone disease, and bone injuries (Fig. 25.4). Treatment of tendinopathy is one of the most common applications of PRP.

Comparative effectiveness of PRP and other techniques is presented on Fig. 25.5. Recent developments in the field of regenerative medicine suggest that the different autologous blood products, namely, leukocyte-pure platelet-rich plasma (LP-PRP), leucocyte-rich platelet-rich plasma (LR-PRP), and platelet pure plasma (PPP), may affect musculoskeletal tissues differently (Table 25.3).

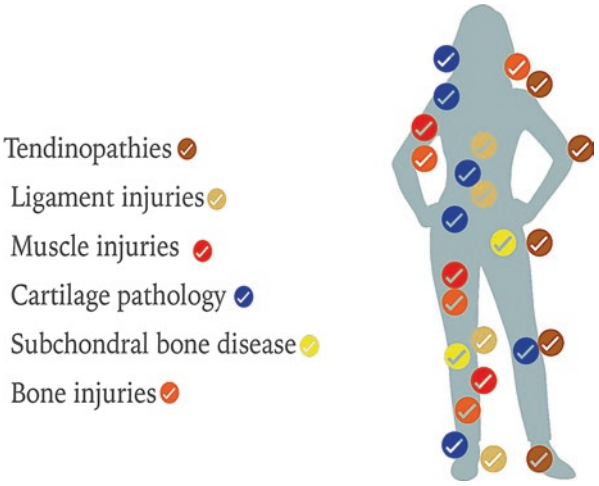

Fig. 25.4 Clinical application of platelet-rich plasma (PRP). There are more than 5000 publications related to PRP. Most common clinical applications are tendinopathy and osteoarthritis

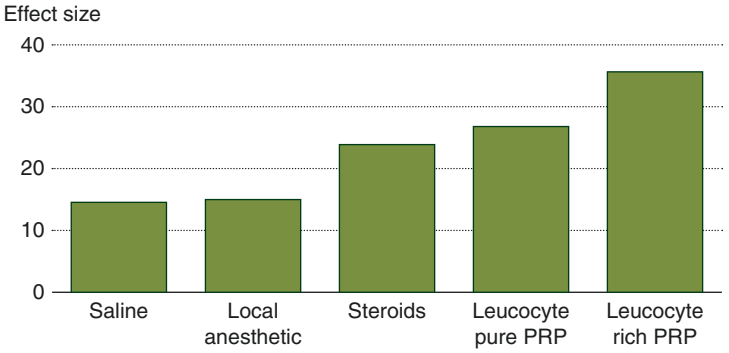

Fig. 25.5 Platelet-rich plasma (PRP) in the treatment of tendinopathy. This figure demonstrates the effect size of various injectates on tendinopathy based on a recent meta-analysis (Fitzpatrick J, Bulsara M, Zheng MH. The Effectiveness of Platelet-Rich Plasma in the Treatment of Tendinopathy: A Meta-analysis of Randomized Controlled Clinical Trials. Am J Sports Med. 2017;45(1):226-233)

Table 25.3 Effect of different platelet-rich plasma formulations on tissue regeneration

The outcomes of different tissue regenerations may depend on PRP formulation
LR-PRP appears to be more effective for tendon regeneration.
LP-PRP appears to be more effective for cartilage regeneration.
PPP appears to be more effective for tendon regeneration muscle repair.

PRP Platelet-rich plasma, *LR-PRP* Leucocyte-rich platelet-rich plasma, *LR-PRP* Leucocyte-pure platelet-rich plasma, *PPP* Platelet-pure plasma

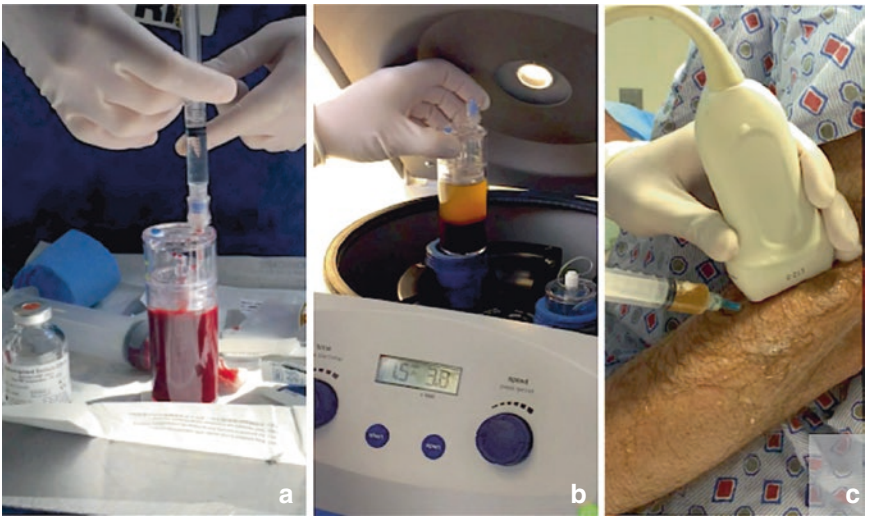

Fig. 25.6 Platelet-rich plasma preparation and injection. (**a**) Adding an anticoagulant to the blood sample. (**b**) Separation of red blood cells from plasma. (**c**) PRP injection. It is important to preserve aseptic conditions during the entire process: stating from blood draw, until the completion of the PRP injection

Most of the authors agree that PRP is not the first-line treatment. Indications for PRP injections should be carefully weighted against its risks. It is important to discuss limitations of treatment with PRP with patient and obtain a detailed informed consent. Absolute contraindications to PRP injection include, but not limited to patient rejection of the procedure, an uncontrolled systemic disease, skin lesions, or infection at the planned injection site. Relative contraindications include thrombocytopenia and concurrent cancer.

Platelet-Rich Plasma Preparation

PRP preparation consists of aseptic blood draw, adding anticoagulant and centrifuging the blood sample to concentrate platelets in the plasma (Fig. 25.6).

Clinical Pearls

1. An initial visit should consist of a detailed physical evaluation, diagnostic cell blood count, and others if needed.
2. It is advisable to discontinue NSAIDs and acetylsalicylic acid-containing medications in the doses exceeding 81 mg, 1 week prior to PRP treatment after getting permission from the doctor, prescribing acetylsalicylic acid, when appropriate.
3. It is advisable for patient to drink three to four glasses of water 1.5 hour prior to the procedure.
4. To produce the best outcomes, the LP-PRP should be injected into the synovial joints; the LR-PRP works better for ligament and tendon pathology, and PPP would possibly benefit muscle tissues the most.
5. A temporary restriction of movements in the treated area is advisable, except for the intra-articular injections.
6. It is advisable to hold NSAID, and acetylsalicylic acid-containing medications in the doses exceeding 81 mg, for 4 weeks after the PRP treatment after getting permission from the doctor, prescribing acetylsalicylic acid, when appropriate.

Literature Review

There is a significant interest of medical community to regenerative medicine treatment options. The number of publications on PRP increased dramatically over the last few years. There are high-quality clinical studies and systematic reviews suggesting that PRP is moderately effective for early knee osteoarthritis. The indications for other musculoskeletal pathology are still under development. There are recent advances in the PRP domain, suggesting that the different autologous blood products, namely, LP-PRP, LR-PRP, and PPP, are affecting musculoskeletal tissues differently. These advances would possibly lead to a body of new high-quality clinical data in the nearest future. The difficulties in normalizing biomaterials remain one of most challenging aspects of development of clinical applications. Another major challenge is related to diversity of clinical conditions treated with PRP. The priority – safety considerations – however, remains the same.

Suggested Readings

Cole BJ, Karas V, Hussey K, Pilz K, Fortier LA. Hyaluronic acid versus platelet-rich plasma: a prospective, double-blind randomized controlled trial comparing clinical outcomes and effects on intra-articular biology for the treatment of knee osteoarthritis. Am J Sports Med. 2017;45(2):339–46.

Fitzpatrick J, Bulsara M, Zheng MH. The effectiveness of platelet-rich plasma in the treatment of tendinopathy: a meta-analysis of randomized controlled clinical trials. Am J Sports Med. 2017;45(1):226–33.

Gormeli G, Gormeli CA, Ataoglu B, Colak C, Aslanturk O, Ertem K. Multiple PRP injections are more effective than single injections and hyaluronic acid in knees with early osteoarthritis: a randomized, double-blind, placebo-controlled trial. Knee Surg Sports Traumatol Arthrosc. 2017;25(3):958–65.

Joshi Jubert N, Rodríguez L, Reverté-Vinaixa MM, Navarro A. Platelet-rich plasma injections for advanced knee osteoarthritis: a prospective, randomized, double-blinded clinical trial. Orthop J Sports Med. 2017;5(2):2325967116689386.

Lana JF, Weglein A, Sampson SE, et al. Randomized controlled trial comparing hyaluronic acid, platelet-rich plasma and the combination of both in the treatment of mild and moderate osteoarthritis of the knee. J Stem Cells Regen Med. 2016;12:69–78.

Souzdalnitski D. Regenerative medicine: invigorating pain medicine practice. Tech Reg Anesth Pain Manag. 2015;19(1-2):1–6.

Souzdalnitski D, Narouze SN, Lerman IL. Platelet-rich plasma injections for knee osteoarthritis: systematic review of duration of clinical benefit. Tech Reg Anesth Pain Med. 2015;19(1-2):1 67–72.

Calcific Tendinitis Intervention

26

Sang Hoon Lee

Introduction

Calcific tendinosis, or calcific tendinopathy in rotator cuff (also referred to calcifying tendinitis), is caused by the deposition of loosely bonded carbonate-apatite crystals, most commonly in the critical zone of the supraspinatus tendon roughly 1 cm proximal to its insertion. Most of calcium deposits are remained in silent stage and can be detected on radiographs in 7.5–20% of asymptomatic adult. However, these deposits can become symptomatic in 50% of patients, causing acute or chronic pain. In this situation, minimal invasive treatments can be used for symptomatic calcific tendinosis: (1) barbotage (repeated alternating injection and aspiration of fluid with a syringe, lavage, and aspiration), (2) fenestration (creating new opening in calcium deposit by repeated needling procedure to stimulate natural absorption), and (3) steroid injection into the subacromial bursa.

Uhthoff and Loehr described three distinct stages in the disease process, namely, the precalcific, calcific, and postcalcific stages (Fig. 26.1). Depending on the phase of disease, the imaging appearance and physical consistency of the calcification differ significantly as do patient symptoms. The calcific stage consists of three phases: formative, resting, and resorptive.

The formative and resting phases are long-lasting asymptomatic stages (hard calcific phases) but may be associated with varying degrees of pain at rest or with movement. Many patients are asymptomatic if they are not large enough to induce impingement syndrome. These calcifications tend to be well circumscribed and discrete when examined radiographically and often produce significant acoustic shadowing by ultrasound scan (Fig. 26.2). It is difficult to aspirate the calcifications in these two phases because the calcifications are quite hard and chalklike. Most common indication of lavage at this stage is calcification over 1 cm in diameter, which commonly causes impingement syndrome.

S. H. Lee (✉)
Madi Pain Management Center, Jeonju, Republic of Korea

P. Peng et al. (eds.), *Ultrasound for Interventional Pain Management*,
https://doi.org/10.1007/978-3-030-18371-4_26

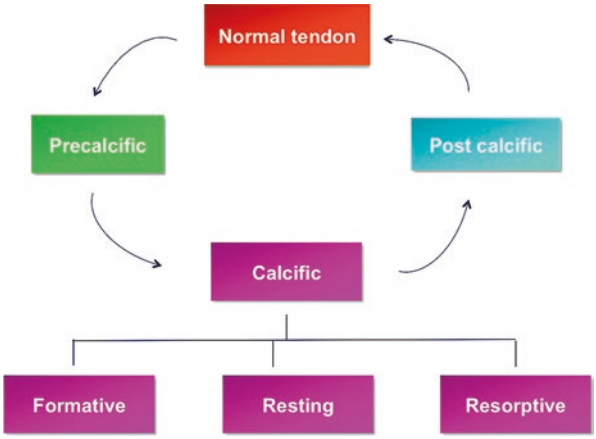

Fig. 26.1 The three phases of calcific tendinitis. (Reprinted with permission from Philip Peng Education Series)

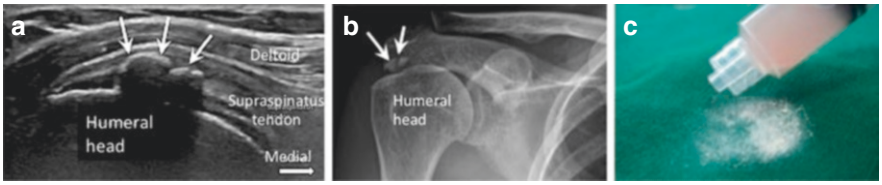

Fig. 26.2 Hard calcific phase: sonographic (**a**), radiographic image (**b**), and aspirated specimen (**c**). The arrows indicate the calcification. Note the anechoic shadow cast by the calcium in (**a**). (Reprinted with permission from Philip Peng Education Series)

Fig. 26.3 Soft calcific phase: sonographic (**a**), radiographic image (**b**), and aspirated specimen (**c**). The arrows indicate the calcification. Note the minimal echogenic shadow cast by the calcium in (**a**). (Reprinted with permission from Philip Peng Education Series)

The resorptive phase is the last phase in the calcific stage (soft or liquid calcium phase) and is the most symptomatic. Shedding of calcium crystals into the adjacent subacromial bursa may result in severe acute pain and restricted range of motion. This phase typically lasts for 2 weeks or longer. These calcifications appear ill-defined or well defined, but the opacity is homogeneous and less dense over hard calcific phase on radiographs, producing little or no acoustic shadowing by ultrasonography (Fig. 26.3). When aspirated, these calcified deposits typically are soft with toothpaste-like consistency. This stage is the most common indication for ultrasound-guided intervention.

Successful aspiration may not be possible in cases when the calcifications appear striated or small and diffusely scattered. In these cases, these calcifications can be grounded gently with the needle tip by rotating the syringe by fenestration technique.

Fenestration means the surgical creation of a new opening in a body part. For calcific tendinosis, new opening can be made by repeated needling procedure to stimulate natural absorption. This mechanical perturbation of the deposit is hypothesized to stimulate cell-mediated resorption. There is evidence in the surgical literature to support that calcific deposits need not be removed completely to achieve successful outcomes.

Patient Selection

Patient with painful arc and with radiologic evidence of calcium deposit in the tendon is usually the candidate. If the calcified tendinosis is noticed in patient with no symptoms, it is better to leave it alone as the procedure can cause pain. Dystrophic calcification is not included in the entity of calcific tendinosis and not a candidate for this procedure. This occurs in degenerative tissue and does not heal spontaneously. This is in contrast to the calcific tendinosis, which occurs in healthy tissue, is cell-mediated, and is self-limiting.

Ultrasound Scan and Procedure

- Position:
  - Supine or oblique supine position for subscapularis and supraspinous lesion opposite the affected side
  - Lateral decubitus position for infraspinatus lesion
- Probe: Linear 6–12 MHz
- Needles:
  - 26G 1.5 inch needle for local anesthetic infiltration
  - 18G 1.5 inch needle for calcium barbotage
  - 24G 3.5 inch needle for release of calcium plug obstructing the 18G needle or fragment the hard calcium before lavage
  - Several 5 mL lock syringes
- Drug:
  - 3 mL 1% lidocaine for irrigation (for filling in the several 5 mL syringes)
  - 3 mL lidocaine with 1 mL dexamethasone
- Approach: In-plane approach

One-Needle Barbotage Technique

First, identify the symptomatic calcification through full ultrasound examination. Place the transducer along the long axis of maximum calcium cavity (Fig. 26.4a). Target is the center of calcium cavity. Following skin infiltration with local anesthetic, advance the 18G needle until its tip is placed in the center of the calcification. Do not relocate or adjust the needle after inserting the needle in the calcium cavity. You have only one chance to insert the needle.

After bending the distal part of 6-cm-long 24G needle, pass the needle through into the lumen of 18G needle as a stylet for release of calcium plug obstructing the needle (Fig. 26.4b).

Push the stylet further over the 18G needle, and rotate the 18G needle to fragment or soften the hard calcium (Fig. 26.4c).

After withdrawal of the stylet, assemble the needle to a 5 cc lock syringe prefilled with 3 mL of lidocaine 1%. Initial step is very important. Push the plunger very gently to avoid rupture of the calcium cavity (Fig. 26.4d), which is the most common cause of the failure of the single needle technique, followed by release of pressure on the plunger.

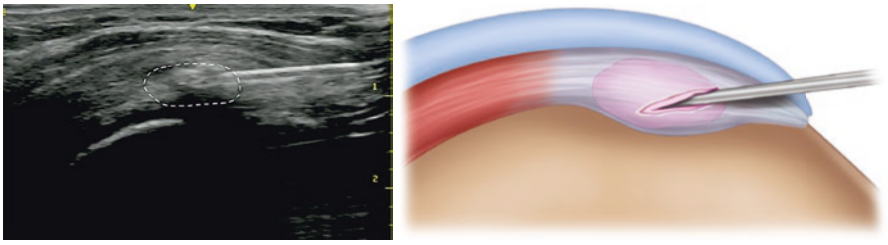

Fig. 26.4a Needle insertion into the center of calcium with in-plane method. (Reprinted with permission from Philip Peng Education Series)

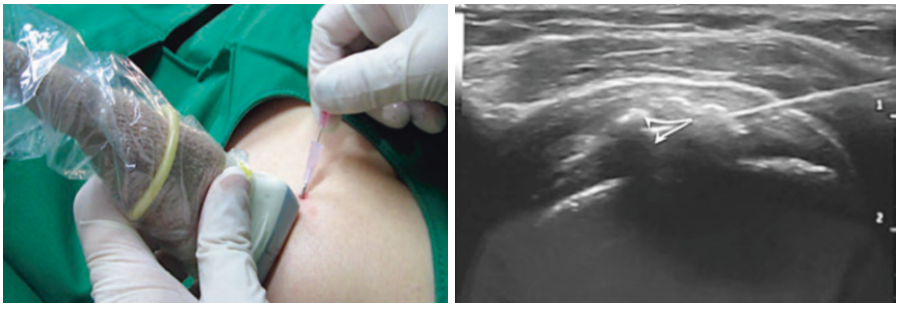

Fig. 26.4b Pass the 24G needle through into the lumen of 18G needle as a stylet for release of calcium plug obstructing the needle. (Reprinted with permission from Philip Peng Education Series)

Repeated slow and low-pressure injections several times, each followed by the release of pressure on the plunger (Fig. 26.4e). If successful, lidocaine and calcium fragments will evacuate into the syringe. Exchange new lidocaine-filled syringes until aspirates are clean. Barbotage should be continued until no more calcification can be aspirated.

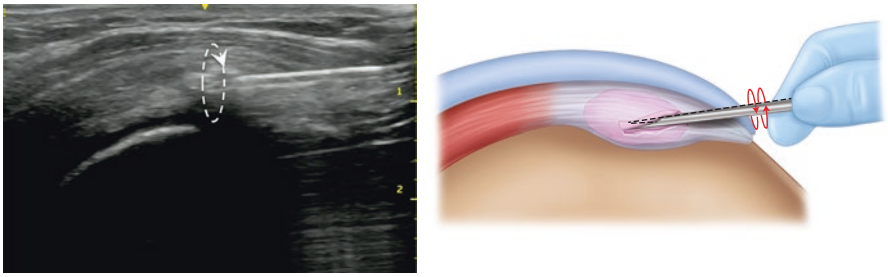

Fig. 26.4c Further push the stylet needle and rotate the needle to fragment. (Reprinted with permission from Philip Peng Education Series)

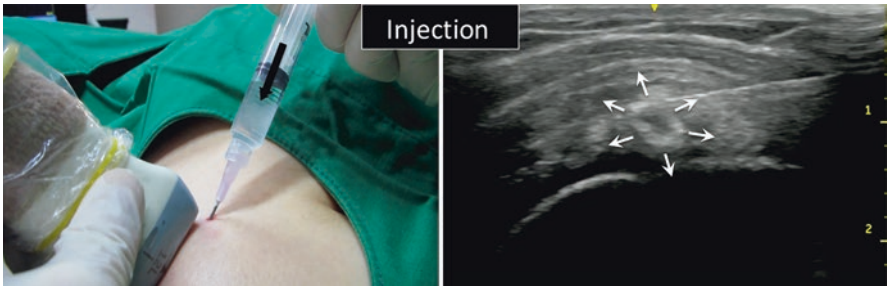

Fig. 26.4d Push the plunger very gently to avoid rupture of the calcium cavity. (Reprinted with permission from Philip Peng Education Series)

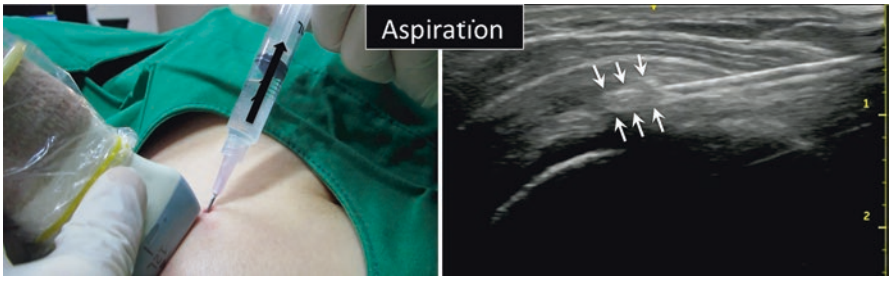

Fig. 26.4e The injection is followed by the release of pressure on the plunger. If successful, lidocaine and calcium fragments will evacuate into the syringe. (Reprinted with permission from Philip Peng Education Series)

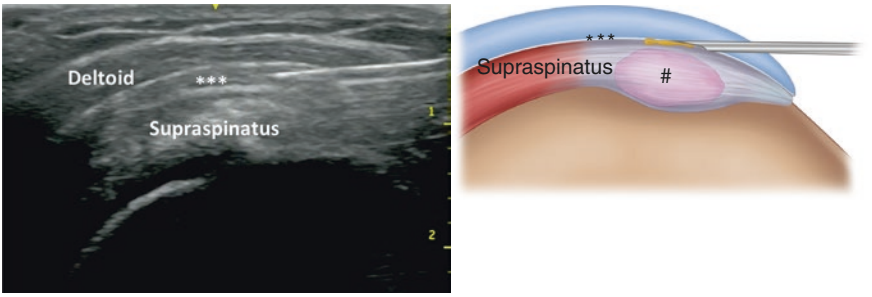

Fig. 26.4f Subacromial bursa injection of steroid. (Reprinted with permission from Philip Peng Education Series)

Withdraw the needle and insert it into the subacromial bursa (Fig. 26.4f). Once the needle is inside the bursa, inject a combination of 1 mL 2% lidocaine and 1 mL of dexamethasone palmitate to mitigate the risk of post-procedural bursitis.

Fenestration Technique

Targets for repeated fenestrations are usually symptomatic small hard calcification (Fig. 26.5). Identify the symptomatic calcification. Place the transducer along the long axis of the center of calcification. After administration of the local anesthetic, advance the fenestration needle until its tip is placed in the surface of the calcification. Fenestrate the calcification by repeated forward and backward movement or rotating movement until the calcification is softened, and crepitation is diminished. During repeated fenestration procedure, infiltrate the 1% of lidocaine or steroid solution. Withdraw the needle into the subacromial bursa, and deposit a combination of 1 mL 2% lidocaine and 1 mL of dexamethasone palmitate into the bursa.

Clinical Pearls

1. Identify the symptomatic calcification.
2. Target is the center of calcium cavity.
3. Do not relocate or adjust the needle after insertion of the needle.
4. Initial step is very important. Push the plunger very gently to avoid the calcium rupture, which is the most common cause of failure.
5. Subacromial bursal injection of steroid is important in minimizing the post-procedural bursitis.
6. Following treatment, the patient is advised to avoid heavy lifting and overhead movement for about 2 weeks. For post-procedure pain, a cold compress is applied over the shoulder. Prescribe analgesics including a combination of acetaminophen and nonsteroid anti-inflammatory drugs.

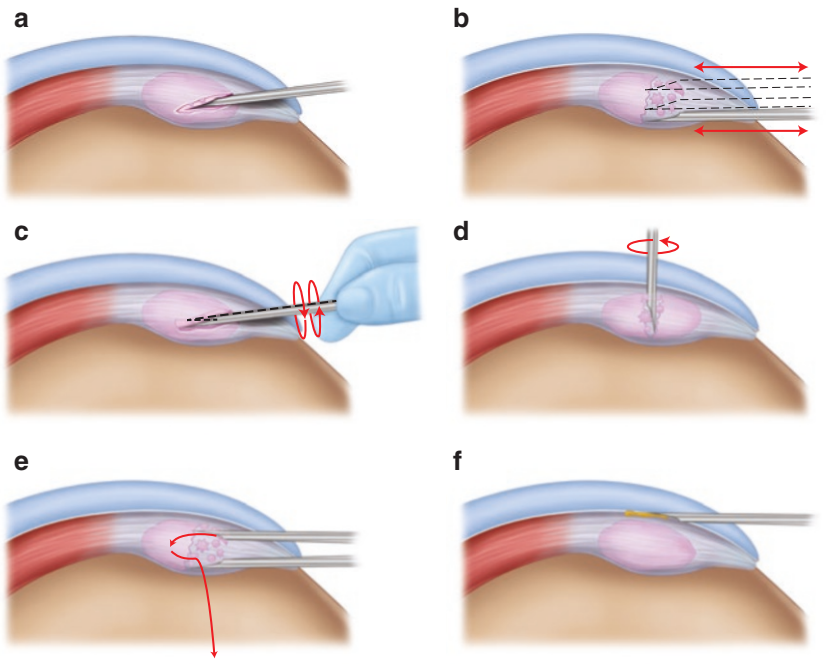

Fig. 26.5 (**a**) Needle insertion into the center of calcium with in-plane method. (**b**) Fenestration with backward and forward movement. (**c**) Fenestration with rotation. (**d**) Fenestration out-of-plane. (**e**) Fenestration with two needles. (**f**) Subacromial bursa injection of steroid. (Reprinted with permission from Philip Peng Educational Series)

Literature Review

Calcific tendinosis is usually a self-limited disease in which the calcification is resorbed after a period of worsening pain. However, in some patients, the condition can lead to chronic pain and functional impairment. The resolution of calcification correlates well with clinical improvement of symptoms, and, therefore, various treatments have been devised to promote their removal.

There is no conclusive evidence that intralesional steroid injection, acetic acid iontophoresis, or pulsed ultrasound therapy are effective in hard calcific phase. Extracorporeal shockwave lithotripsy uses acoustic waves to fragment calcium deposits, and substantial or complete clinical improvement has been reported in 66–91% of patients with chronic calcific tendinosis. However, it will aggravate the pain when it is used in resorptive phase or soft calcification. Furthermore, the therapy is relatively expensive.

Image-guided needle irrigation and aspiration (barbotage) of rotator cuff calcific tendinosis have been shown to be an effective minimally invasive technique and were first described three decades ago. In a recent study, del Cura and colleagues

reported that 91% of patients experienced significant or complete improvement in range of motion, pain, and disability when aspiration was performed under ultrasound guidance [5] Given the potential risks of surgery, percutaneous calcium aspiration should be considered after failure of medical therapy.

Successful aspiration may not be possible in cases in which the calcification appears striated because this is thought to represent calcification of the tendon fibers themselves. Also, clinical outcomes when attempting to remove numerous, diffuse, small (<5 mm) calcifications are only fair to poor, even when treated surgically. Fortunately, most of multiple small calcifications are asymptomatic.

If the pain is associated with the multiple small, scattered calcifications in distal insertional portion, these calcifications are degenerative calcification or a feature of the tendinosis. The prognosis in these situations is usually poor.

Suggested Reading

1. Hamada J, Ono W, Tamai K, Saotome K, Hoshino T. Analysis of calcium deposits in calcific periarthritis. J Rheumatol. 2001;28:809–13.
2. Sarkar K, Uhthoff HK. Ultrastructural localization of calcium in calcifying tendinitis. Arch Pathol Lab Med. 1978;102:266–9.
3. Speed CA, Hazleman BL. Calcific tendinitis of the shoulder. New Engl J Med. 1999;340:1582–4.
4. Hurt G, Baker CL Jr. Calcific tendinitis of the shoulder. Orthop Clin North Am. 2003;34:567–75.
5. del Cura JL, Torre I, Zabala R, Legorburu A. Sonographically guided percutaneous needle lavage in calcific tendinitis of the shoulder: short- and long-term results. AJR. 2007;189:W128–34.
6. Farin PU, Jaroma H, Soimakallio S. Rotator cuff calcifications: treatment with US-guided technique. Radiology. 1995;195:841–3.
7. Farin PU, Rasanen H, Jaroma H, Harju A. Rotator cuff calcifications: treatment with ultrasound-guided percutaneous needle aspiration and lavage. Skelet Radiol. 1996;25:551–4.
8. Giacomoni P, Siliotto R. Echo-guided percutaneous treatment of chronic calcific tendinitis of the shoulder. Radiol Med. 1999;98:386–90.
9. Lin JT, Adler RS, Bracilovic A, Cooper G, Sofka C, Lutz GE. Clinical outcomes of ultrasound-guided aspiration and lavage in calcific tendinosis of the shoulder. HSS J. 2007;3:99–105.
10. Yoo JC, Koh KH, Park WH, Park JC, Kim SM, Yoon YC. The outcome of ultrasound-guided needle decompression and steroid injection in calcific tendinitis. J Shoulder Elb Surg. 2010;19:596–600.
11. Comfort TH, Arafiles RP. Barbotage of the shoulder with image-intensified fluoroscopic control of needle placement for calcific tendinitis. Clin Ortho Relat Res. 1978;171:–178.
12. Cooper G, Lutz GE, Adler RS. Ultrasound-guided aspiration of symptomatic rotator cuff calcific tendonitis. Am J Phys Med Rehab. 2005;84:81.
13. Lee KS, Rosas HG. Musculoskeletal ultrasound: how to treat calcific tendinitis of the rotator cuff by ultrasound-guided single-needle lavage technique. AJR. 2010;195:638.
14. Uhthoff HK, Loehr JW. Calcific tendinopathy of the rotator cuff: pathogenesis, diagnosis, and management. J Am Acad Ortho Surg. 1997;5:183–91.
15. McKendry RJ, Uhthoff HK, Sarkar K, Hyslop PS. Calcifying tendinitis of the shoulder: prognostic value of clinical, histologic, and radiologic features in 57 surgically treated cases. J Rheumatol. 1982;9:75–80.
16. Gosens T, Hofstee DJ. Calcifying tendinitis of the shoulder: advances in imaging and management. Curr Rheumatol Rep. 2009;11:129–34.
17. Maier M, Schmidt-Ramsin J, Glaser C, Kunz A, Kuchenhoff H, Tischer T. Intra- and interobserver reliability of classification scores in calcific tendinitis using plain radiographs and CT scans. Acta Orthop Belg. 2008;74:590–5.

18. Ciccone CD. Does acetic acid iontophoresis accelerate the resorption of calcium deposits in calcific tendinitis of the shoulder? Phys Ther. 2003;83:68–74.
19. Speed CA, Richards C, Nichols D, et al. Extracorporeal shock-wave therapy for tendonitis of the rotator cuff. A double-blind, randomized, controlled trial. J Bone Joint Surg Br. 2002;84:509–12.
20. Farr S, Sevelda F, Mader P, Graf A, Petje G, Sabeti-Aschraf M. Extracorporeal shockwave therapy in calcifying tendinitis of the shoulder. Knee Surg Sports Traumatol Arthrosc. 2011;19:2085–9.
21. Gerdesmeyer L, Wagenpfeil S, Haake M, et al. Extracorporeal shock wave therapy for the treatment of chronic calcifying tendonitis of the rotator cuff: a randomized controlled trial. JAMA. 2003;290:2573–80.
22. Hsu CJ, Wang DY, Tseng KF, Fong YC, Hsu HC, Jim YF. Extracorporeal shock wave therapy for calcifying tendinitis of the shoulder. J Shoulder Elb Surg. 2008;17:55–9.
23. Louis LJ. Musculoskeletal ultrasound intervention: principles and advances. Radiol Clin N Am. 2008;46:515–33.
24. Chiou HJ, Hung SC, Lin SY, Wei YS, Li MJ. Correlations among mineral components, progressive calcification process and clinical symptoms of calcific tendonitis. Rheumatology. 2010;49:548–55.

Hip and Knee Joint Denervation

27

John Tran and Philip Peng

Introduction

Osteoarthritis (OA) is the most common type of arthritis and classically produces joint pain exacerbated by physical activity and alleviated with rest. OA of the hip and knee contributes the most to OA disease burden. Globally, hip and knee OA was ranked as the 11th highest contributor to global disability. The prevalence of radiographic and symptomatic osteoarthritis for hip was 19.6% [95% confidence interval (CI) = 16.7, 23.0%] and 4.2% (95% CI = 2.9, 6.1%), respectively, and for knee was 25.4% (95% CI = 24.1, 26.1) and 15.4% (95% CI = 14.2, 16.7), respectively.

The management strategies for OA consist of assistive devices, exercise and weight loss, self-management, pharmacologic, and interventional and surgical interventions. Various interventional techniques for joint pain are summarized in Table 27.1.

Radiofrequency ablation (RFA) of the knee and hip is an emerging technique that causes a lot of interest in interventionist. Two reviews on the RFA publications

Table 27.1 Comparison of interventions for osteoarthritis of major joint

Modality		Proposed mechanism
Intra-articular	Steroid	Anti-inflammatory
	Hyaluronic acid	Supplementation of synovial fluid
	Platelet-rich plasma	Restoration of joint hemostasis
Extra-articular	Radiofrequency ablation	Denervation of articular branches
	Peripheral nerve stimulation	Neuromodulation

J. Tran
Division of Anatomy, Department of Surgery, 1 King's College Circle, Toronto, ON, Canada

P. Peng (✉)
Department of Anesthesia and Pain Management, Toronto Western Hopsital and Mount Sinai Hospital, University of Toronto, Toronto, Ontario, Canada
e-mail: Philip.peng@uhn.ca

P. Peng et al. (eds.), *Ultrasound for Interventional Pain Management*,
https://doi.org/10.1007/978-3-030-18371-4_27

concluded more research to be done on those techniques including the anatomy of the articular branches discernable to the imaging modalities such as fluoroscopy or ultrasound. Since then, two seminal publications on the detailed anatomy of the articular branches of the anterior hip and knee have been published. Furthermore, we have two good-quality randomized controlled trials and one long-term (1 year) follow-up study on the application of RFA in knee OA. This chapter will summarize the pertinent anatomy, sonoanatomy, and technique pertinent to the RFA of hip and knee.

Hip

Articular Branches of the Hip

The sensory fibers for the anterior hip capsule are mainly nociceptive, while the fibers for posterior capsule are mainly proprioceptive. The three nerves supplying the anterior capsule are femoral, accessory obturator, and obturator nerves (Fig. 27.1).

The *femoral nerve* (FN) arises from the posterior divisions of the second, third, and fourth lumbar nerves (L2–L4). In the abdomen, the FN course inferolaterally posterior to the psoas muscle and anterior to the iliacus muscle. The sensory nerves

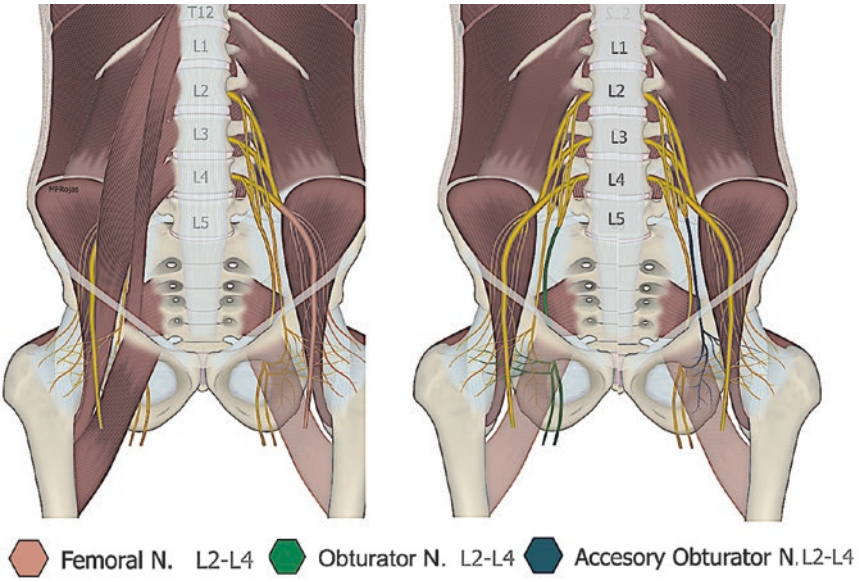

Fig. 27.1 Schematic diagram to show the articular branches to the anterior hip joint capsule. The femoral, obturator, and accessory obturator nerves are color coded. (Reprinted with permission from Philip Peng Educational Series. The original artwork was created and modified with the permission from Dr. Maria Fernanda Rojas, Bucaramanga, Colombia)

to the hip joint commonly branch out at L4–L5 level (high branches) and course intramuscularly through iliacus to reach the periosteal surface of the pubis between the anterior inferior iliac spine (AIIS) and the iliopubic eminence (IPE). At the level of the superior ramus of the pubis, the sensory branches continue to descend deep to the iliopsoas muscle and tendon to reach the anterior hip joint capsule. The main trunk of FN courses superficial to the iliopsoas and continues inferiorly passing beneath the inguinal ligament to enter the femoral triangle (Fig. 27.2).

The *accessory obturator nerve* (AON) arises as one branch usually from the posterior division of third and fourth lumbar nerves (L3–L4). In the abdomen, the AON courses inferiorly deep to the medial border of the psoas major. At the level of the superior ramus of pubis, the AON courses along the periosteal surface just medial to the iliopubic eminence (Fig. 27.3).

The *obturator nerve* (ON) articular branches were categorized as high or low according to their point of origin. High branches originated just proximal to or within the obturator canal and low branches from the posterior branch of ON (Fig. 27.4).

Thus, the important landmarks for the articular branches are AIIS, IPE, and inferomedial acetabulum. The distribution of these articular branches to the four different quadrants of the anterior hip capsule is shown in Fig. 27.5.

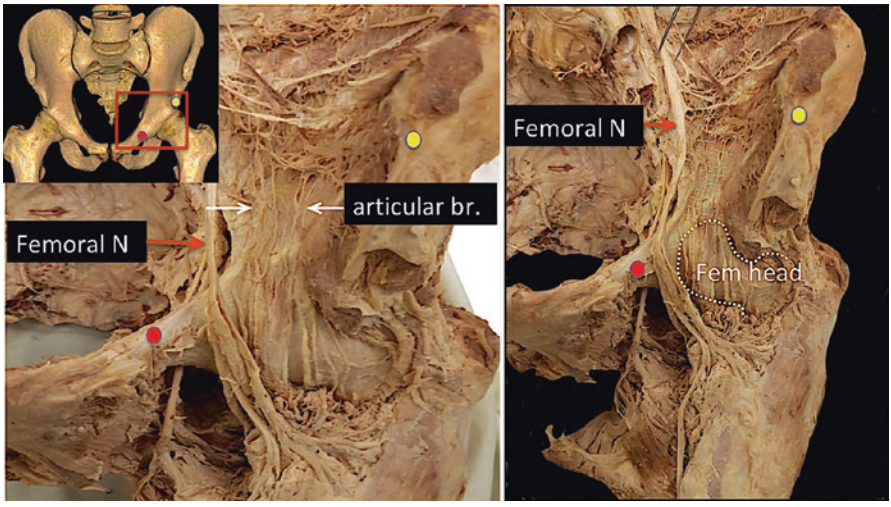

Fig. 27.2 The articular branches of the femoral nerve are classified as either high or low, corresponding to their origin superior or inferior to the inguinal ligament. High branches are much more prevalent than low branches. In this dissection photograph, the left iliopsoas had been removed, and the femoral nerve (orange arrow) was retracted medially to visualize the high articular branches (highlighted in green) supplying the anterior hip joint capsule. Left upper insert showed the region of interest of the left figure. Yellow dot, anterior inferior iliac spine; red dot, iliopubic eminence. The femoral is outlined in the right figure. (Reprinted with permission from Philip Peng Educational Series)

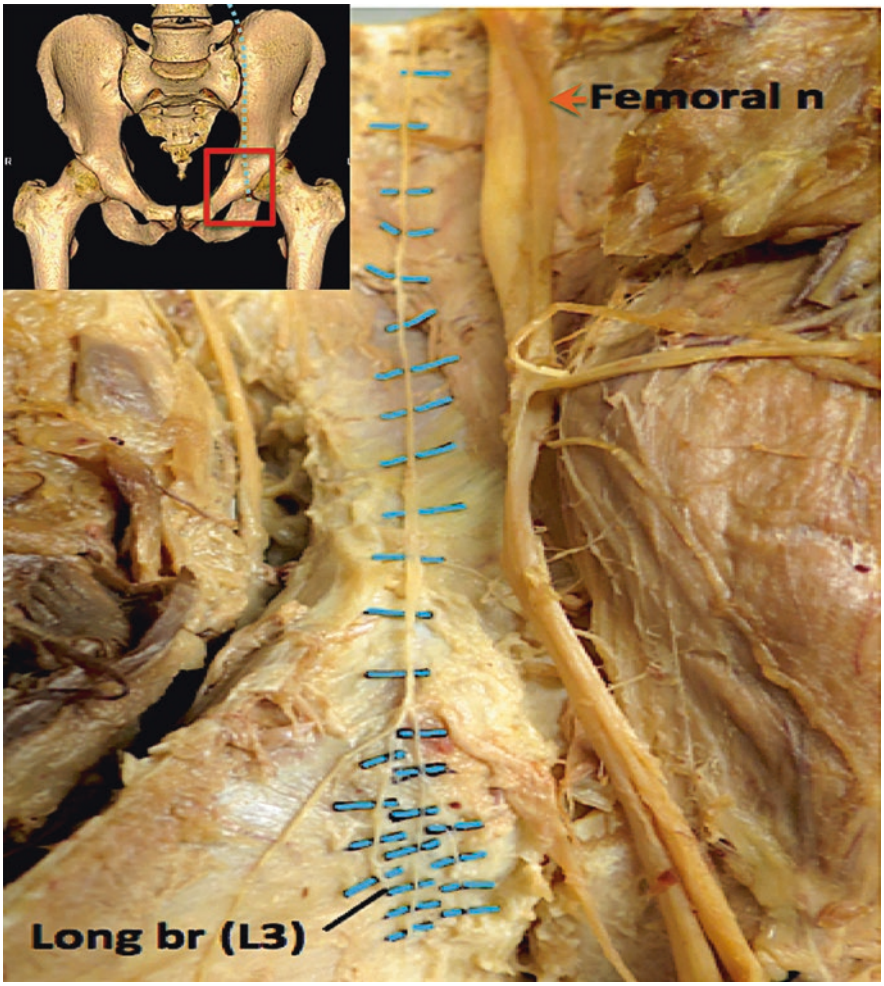

Fig. 27.3 The AON (highlighted in blue) descended into the anterior thigh region and supplied sensory branches to the medial aspect of the anterior hip joint capsule. Note in the dissection photograph, the iliopsoas had been removed to visualize the AON. The insert in the left upper corner showed the region of the photograph. (Reprinted with permission from Philip Peng Educational Series)

Patient Selection

The best candidate is a patient with moderate to severe pain from osteoarthritis with at least moderate degree of osteoarthritis changes in the radiograph. The patient with other types of arthritis is possible but the literature support is scant. The RFA is selected based on the appropriate response to the diagnostic test.

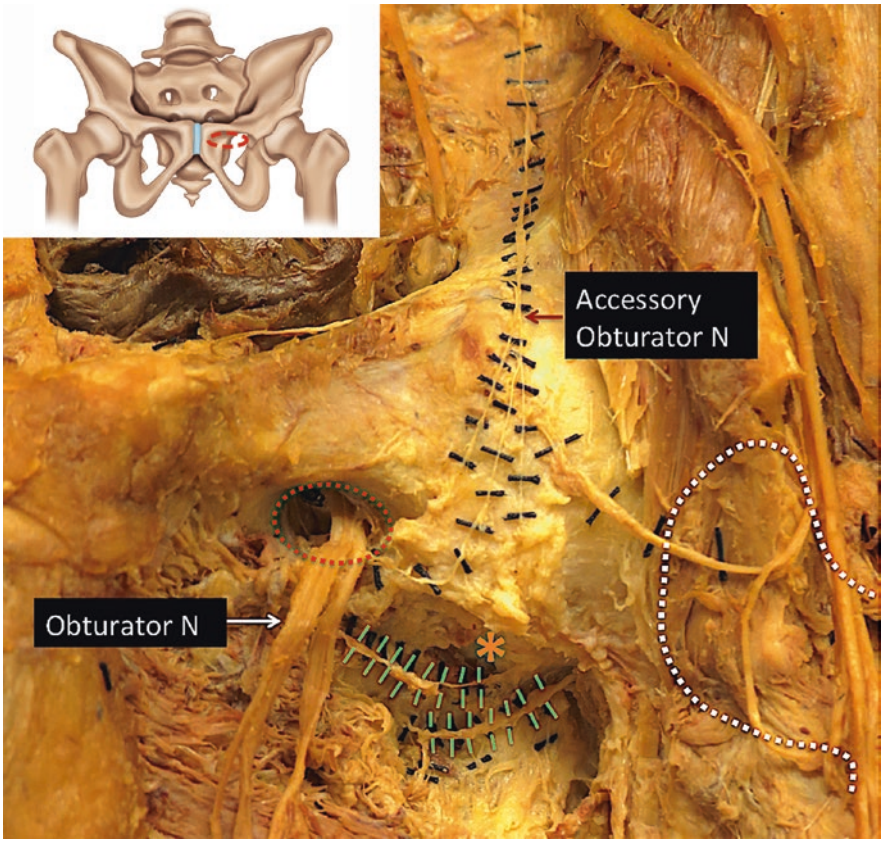

Fig. 27.4 In this figure, a low branch was shown. If a high branch was present, it usually consisted of a single nerve branch. The low branches, when present, were more numerous (green) and traveled either directly to the hip joint or formed a fine plexus that innervated the capsule. The obturator canal was outlined with red circle and the femoral head in white dotted line. The most consistent landmark for both high and low ON branches was the bone thickening of the inferomedial acetabulum (∗) that correlates to the previously described radiographic teardrop. (Reprinted with permission from Philip Peng Education Series)

Ultrasound Scan

- Position: Supine
- Probe: Linear 6–15 MHz or curvilinear 2–5 (the latter reserved for the patient with high BMI)

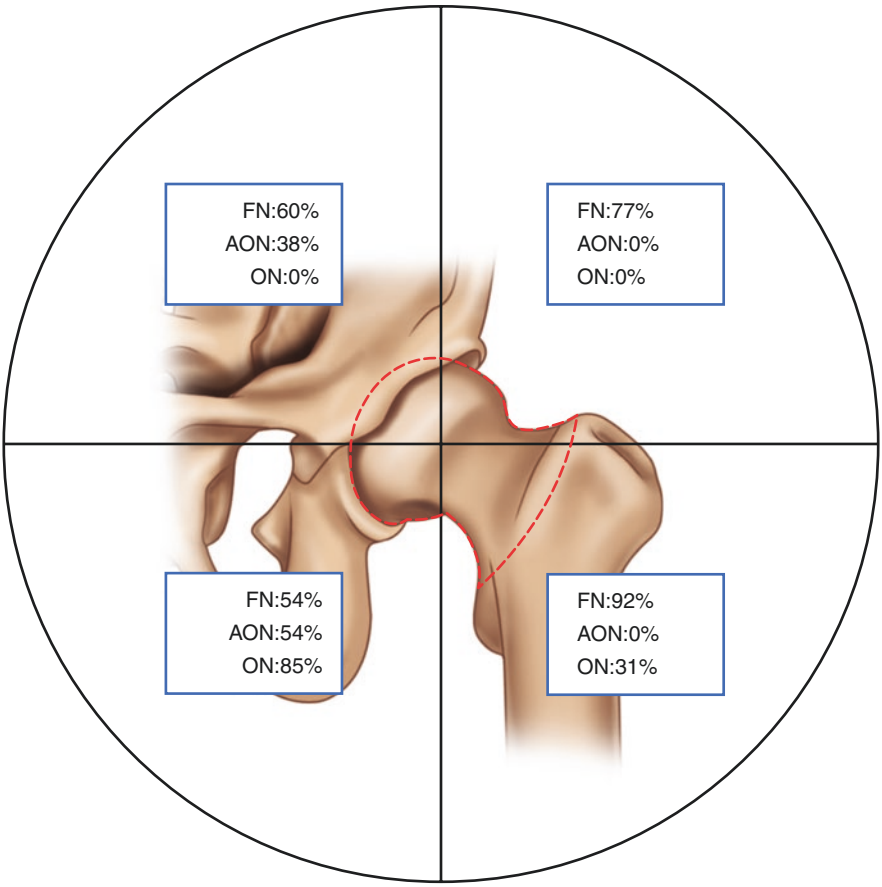

Fig. 27.5 The diagram summarized the contribution of various articular branches to the anterior hip capsule. The articular branches from femoral nerve (FN) contribute to all four quadrants including the weight-bearing superior (medial and lateral) quadrants. Articular branches from obturator nerve (ON) only contribute to the lower half and that from accessory obturator nerve (AON) to medial half of the anterior capsule. (Reprinted with permission from Philip Peng Education Series)

The First Target for AON and FN Is the Interval Between AIIS and IPE

Scan 1

Place the probe over ASIS (Fig. 27.6a).

Scan 2

Slide the probe in caudal direction to reveal the AIIS, which is deeper and medial in location compared with ASIS (Fig. 27.6b).

Scan 3

Rotate the probe to align the AIIS and IPE in the same scan. The articular branches of femoral and accessory obturator nerve can be located between AIIS and IPE deep to the psoas tendon which is hyperechoic (Fig. 27.6c).

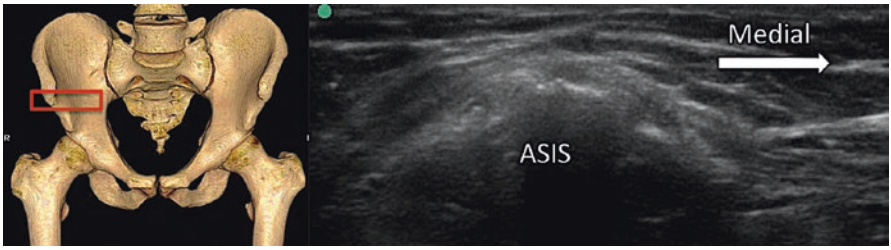

Fig. 27.6a Sonographic image of the anterior superior iliac spine (ASIS). (Reprinted with permission from Philip Peng Educational Series)

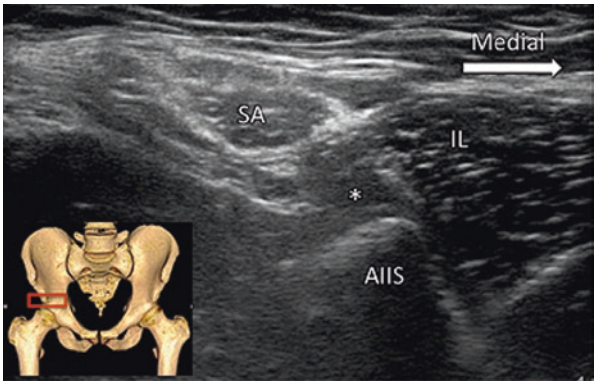

Fig. 27.6b Sonographic image of the anterior inferior iliac spine (AIIS). Sartorius (SA) and iliacus (IL) are seen superficial to AIIS, which is covered by the straight head of rectus femoris (∗). (Reprinted with permission from Philip Peng Educational Series)

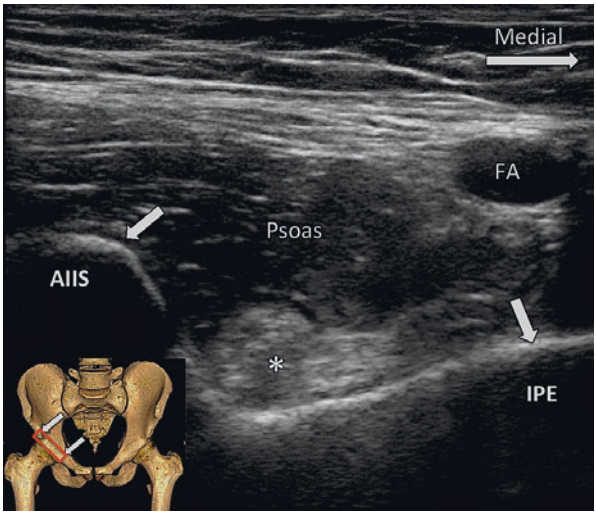

Fig. 27.6c Sonographic image when aligning the ultrasound probe with AIIS and IPE (both indicated by bold arrows). Psoas tendon is marked by the asterisk. FA, femoral artery. (Reprinted with permission from Philip Peng Educational Series)

Scan 4

Further caudal scan will reveal the femoral head (Fig. 27.6d). Please differentiate the fascia layer between the iliopsoas tendon from the iliofemoral ligament overlying the anterior joint capsule.

The Second Target Is the Obturator Articular Branch

At the present time, the author prefers a combined fluoroscopic and ultrasound technique. The bony target is the inferomedial acetabulum. Direct insertion of the needle under fluoroscopy will be at high risk to the femoral neurovascular bundle because of the close vicinity. Directing the needle initially under ultrasound scan guidance to the inferomedial acetabulum avoids the puncture of the femoral neurovascular bundle. The final position can be adjusted under fluoroscopy.

Scan 1

Similar to the scanning of the anterior recess for hip intra-articular injection, the probe is placed in the long axis of the femoral head and neck (Fig. 27.7 red rectangle).

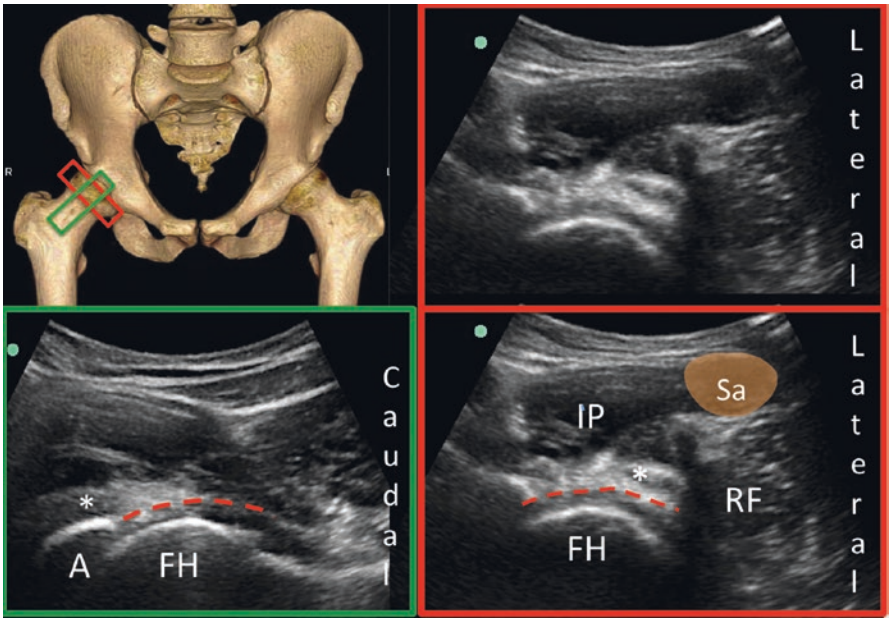

Fig. 27.6d Sonographic image when the ultrasound probe was placed just distal to the pubic rami as in Fig. 27.6c. Upper left showed the position of the probe. Red rectangle represented the sonographic image on the right upper and lower images without and with label, respectively. The green rectangle is the long-axis view of the femoral head and neck and was shown in the lower left image. IP, iliopsoas; SA, satorius; RF, rectus femoris; ∗, psoas tendon; red dotted line, iliofemoral ligament. (Reprinted with permission from Philip Peng Educational Series)

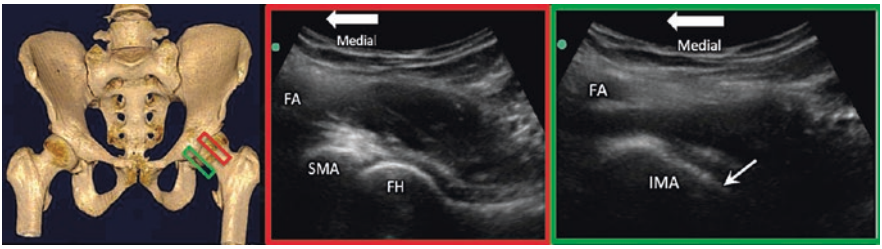

Fig. 27.7 Left figure showed the position of the ultrasound probe in both positions (red and green rectangles). The middle and right figures were the corresponding sonographic images in red and green rectangles, respectively. SMA, superomedial acetabulum; IMA, inferomedial acetabulum; FA, femoral artery; FH, femoral head; arrow, target of the obturator articular branches. (Reprinted with permission from Philip Peng Educational Series)

Scan 2

Moving the probe in the medial and inferior direction until the femoral head disappears, the part of the acetabulum is the inferomedial aspect of the acetabulum (Fig. 27.7 green rectangle).

Procedure

Diagnostic Block

- Needle: 22G 3.5 inch needle
- Drug: 3 mL 0.25% bupivacaine

For AON and FN articular branches, place the ultrasound probe as shown in the upper panel of Fig. 27.8. The needle is inserted in-plane from lateral to medial targeting toward the space between AIIS and IPE deep to the psoas tendon. The author prefers the needle closer to the IPE as it is where the AON articular branches are located. After confirming the needle position with hydrolocation, 3 mL of local anesthetic is injected. Optimal injection will result in a transient spread of injectate between the psoas tendon and the pubic bone.

In case the spread is not in the space between the psoas tendon and the periosteum, three maneuvers can be used:

1. Rotate the needle to pierce through the psoas tendon
2. Reposition the needle to another location
3. Choose the injection site as in Scan 4 (Fig. 27.6d), i.e., between the psoas tendon and the iliofemoral ligament

The needle insertion site is in the vicinity of the lateral femoral cutaneous nerve, and caution should be taken during needle insertion.

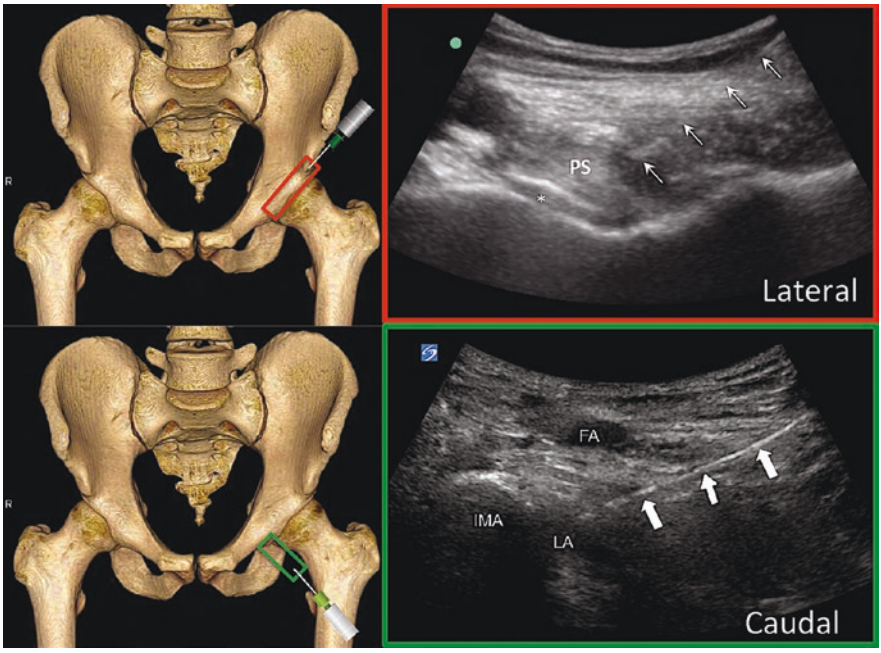

Fig. 27.8 Upper panel. The left diagram showed the needle insertion and the relevant landmark. The corresponding sonographic image was shown on the right with the spread of local anesthetic (∗) deep to the psoas tendon (PS). The needle was outlined by the arrows. Lower panel. The left diagram showed the needle insertion and the relevant landmark. The needle (bold arrows) was directed to the deep end of the inferomedial acetabulum (IMA) with the local anesthetic (LA) shown at the tip. FA, femoral artery. (Reprinted with permission from Philip Peng Educational Series)

For articular branches of ON, once the scan shows the inferomedial acetabulum, attention is paid to the vessel (femoral artery itself or the circumflex arteries) in the needle path (lower panel of Fig. 27.8). Once the optimal path is determined by "rocking" the ultrasound probe, the needle is inserted in-plane from lateral to medial to touch the periosteum. Fine-tuning the final needle position under the fluoroscopy to the "teardrop" before administering 3 mL of local anesthetic (Fig. 27.9).

Radiofrequency Ablation

- Needle: System providing large or palisade or strip lesion
- For example, cooled RF needle 17G 100mm length, 4 mm active tip; RF needle providing bipolar lesion, and the author prefers multi-tined needle (18G 100mm with 5 mm active tip) because this needle will give the maximum lesion size with the trajectory of the needle.

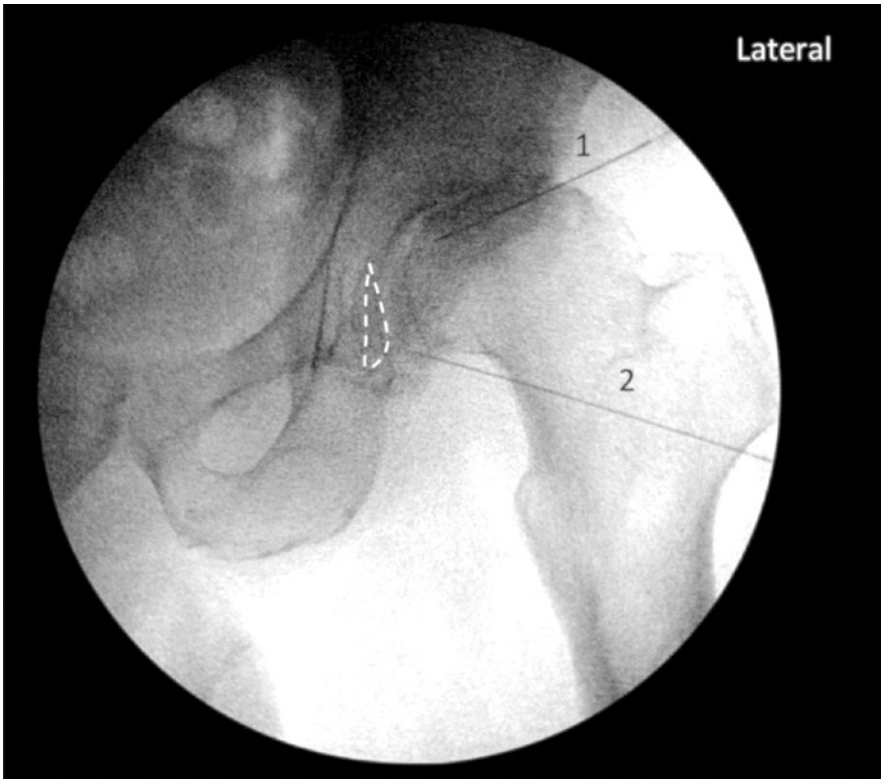

Fig. 27.9 Radiograph of the pelvis and hip joint in the anteroposterior (AP) view. Needle 1 was targeted to the femoral articular branches and needle 2 targeted to the inferomedial acetabulum or teardrops (white dotted line). (Reprinted with permission from Philip Peng Educational Series)

1. *AON and FN articular branches*

   If a single needle is placed (cooled RF system), the location is between AIIS and IPE deep to the psoas tendon. If multi-tined needles are used, a minimum of two needles is required separated by no more than 1 cm. One needle will be placed just lateral to the IPE and another within 1 cm to this needle. Depending on the size of the interval between AIIS and IPE, a third needle may be required.
2. *ON articular branches*

   The target size is small, and a single needle (whether it is cooled RF system or multi-tined system) is usually sufficient. Using the scan technique described above, the author starts with needle insertion in-plane from lateral to medial. However, the clinician must scan the needle trajectory and the vicinity for the vessel. If necessary, the distal end of the probe can be rotated while keeping the inferomedial acetabulum in view. Once the needle makes a bony contact, the tip position is further fine-tuned under fluoroscopy. The main obturator trunk is

closer to the medial half of the teardrop. Thus, the author prefers to put the needle on the lateral half of the teardrop. Sensory and motor test will add to the safety of the procedure.

Clinical Pearls

1. When inserting the needle for AON and FN, the needle entry site is close to the lateral femoral cutaneous nerve. Infiltrate the skin with a smaller needle, and if the patient complains of tingling sensation down the lateral thigh, it is an indication to reposition the needle.
2. Unlike the volume chosen for the diagnostic block of lumbar or cervical facet medial branch, the author prefers a larger volume of 3 mL as it covers a larger area of the periosteum from AIIS to IPE, and the volume is not sufficient to spill to femoral nerve which is in the plane superficial not deep to the psoas muscle.
3. In the literature, the well-accepted landmark for ON articular branches is the teardrop or inferomedial acetabulum. The study was designed to determine the landmark discernable by fluoroscopy. On inspection of the specimens dissected at the University of Toronto, we also confirmed that this was true. However, two important points need to be made: (1) a slight deviation to the medial side of this landmark will increase the risk of injury to the main trunk of ON; (2) the inferomedial joint capsule is also an excellent landmark to the articular branches of ON.

Literature Review

The literature on hip denervation is weak. A review on this subject was published in 2018 including six case reports and eight case series (five retrospective and three prospective) from 1993 to 2017. Articular branches from obturator and femoral nerve were the targets in all studies with the exception of two studies: one targeted femoral nerve and other obturator nerve only. Fluoroscopy was the mainstay of imaging modalities to target the obturator articular branches at the teardrop silhouette with three reports using ultrasound to direct the needle initially avoiding the puncture of femoral neurovascular bundle. The lateral acetabulum or the point medial and inferior to the AIIS was commonly adopted as the target for femoral nerve articular branches. One study described the ultrasound-guided ablation of femoral nerve articular branches, but the target nerve in the sonographic image was dubiously large for the articular branches. No studies mentioned the accessory obturator nerve as the target. Although one study targeted the nerves to the posterior capsule, a histological study suggested that the neural innervation to the posterior capsule was mainly proprioceptive not nociceptive.

All the 14 publications reported reduction in pain scores, ranging from 30% to greater than 90% from baseline scores, following RF procedures. However, the length of follow-up was very variable ranging from 8 days to 3 years. The improvement in functional outcome was poorly documented, and only a few studies used validated measures of hip function (e.g., WOMAC, Oxford Hip Score) for functional assessment.

Knee

Articular Branches of the Knee

The articular branches of the knee had recently been revealed in details in the literature with a frequency map (Fig. 27.10).

On the superomedial quadrant, the articular branches are superior medial genicular nerve, nerve to vastus medialis, and medial branch of the nerve to vastus intermedius and saphenous nerve. All branches are originated from femoral nerve including superior medial genicular nerve. With the exception of saphenous nerve, all contribute to the joint innervation consistently. Of all those articular branches, only the superior medial genicular nerve and medial branch of the nerve to vastus intermedius are close to the anteromedial periosteal surface and therefore amendable to the conventional RFA (Table 27.2).

On the superolateral quadrant, the superior lateral genicular nerve and lateral branch of the nerve to vastus intermedius are the conventional target for RFA.

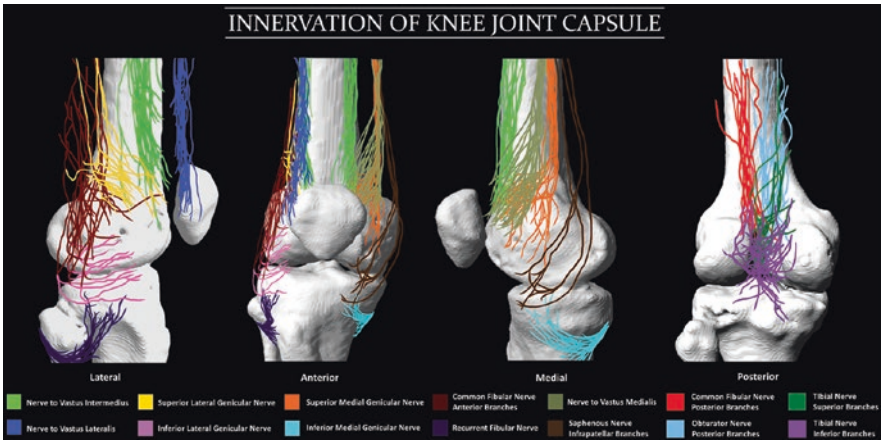

Fig. 27.10 Innervation of the knee joint capsule. (Reprinted with permission from Philip Peng Educational Series)

Table 27.2 Articular branches of the anterior knee capsule

Quadrants	Conventional RFA target	Non-conventional target	Reason
Superomedial	SMGN	NVM	Intermuscular plane
	Medial br. NVI		
Inferomedial	IMGN	IPBSN	Mainly cutaneous
Superolateral	SLGN, lateral br. NVI,	NVL,CFN anterior br.	Far away from target
Inferolateral		ILGN, rec fibular N	Close to CFN

SGMN superior medial genicular nerve, *NVI* nerve to the vastus intermedius, *NVM* nerve to the vastus medius, *IMGN* inferior medial genicular nerve, *IPBSN* infrapatellar branch of the saphenous nerve, *SLGN* superior lateral genicular nerve, *NVL* nerve to vastus lateralis, *CFN* common fibular nerve, *ILGN* inferior lateral genicular nerve; rec fibular N, recurrent fibular nerve

In the inferomedial quadrant, the inferior medial genicular branch is very consistent in the position for RFA. The articular branches in the inferolateral are not chosen for RFA because of the vicinity to the common fibular nerve.

It is important to highlight two points. First, there is no need for a complete denervation of all articular branches. As will be discussed in the literature review, a partial knee denervation is enough to produce analgesia for osteoarthritis of knee. The articular nerves are listed in Table 27.2 as "conventional RFA target" because they are close to the periosteal surface at the junction of diaphysis and epiphysis. The nerves listed "non-conventional target" can still be denervated with the advancement of the understanding of the sonoanatomy of those nerves (Table 27.2).

Patient Selection

The best candidate is a patient with moderate to severe pain from osteoarthritis with at least grade II Kellgren-Lawrence osteoarthritis changes in radiograph. Patient with other types of arthritis is possible but the literature support is scant. The RFA is selected based on the appropriate response to the diagnostic test.

Ultrasound Scan

- Position: Supine with the hip externally rotated (figure-of-four) position for the superomedial and inferomedial articular branches; semi-lateral away from the site of procedure for the uperolateral articular branches.
- Probe: Linear 6–15 MHz

Superomedial Articular Branches

Scan 1

With the leg in the figure-of-four position, it is easier to recognize the lateral plane of the femur. The ultrasound probe is placed in the plane as if one is taking a lateral X-ray of the knee (Fig. 27.11 upper left panel). The probe is also placed along the long axis of femur at the metaphysis approximately 2–3 cm proximal to the knee

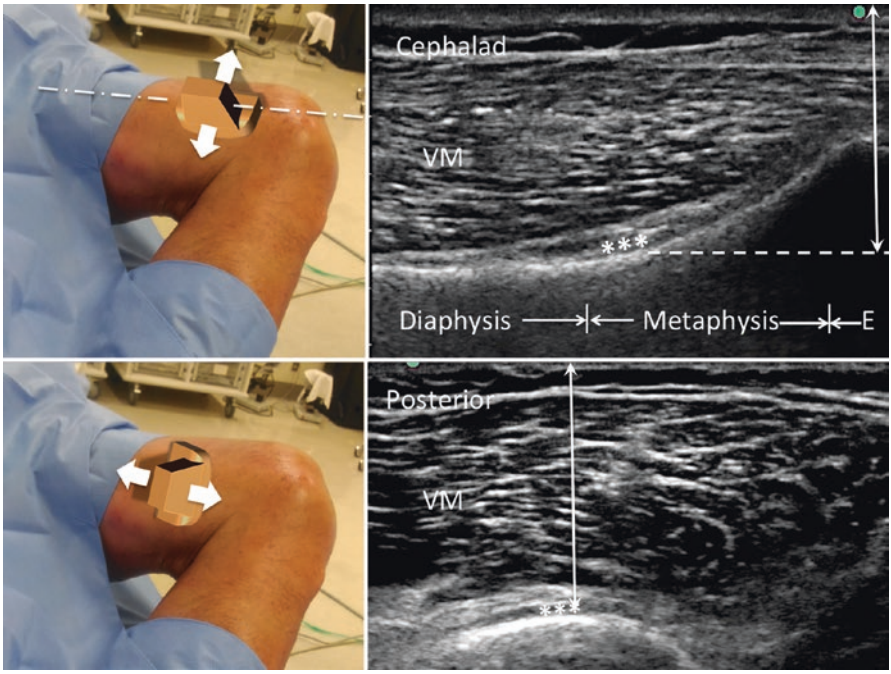

Fig. 27.11 Ultrasound imaging technique and the corresponding sonographic image of the superomedial knee. Upper left panel. The ultrasound probe was placed along the long axis of femur between the diaphysis and epiphysis. Upper right panel. A fascia expansion (***) deep to the vastus medial (VM) could be seen. E, epiphysis. Lower left panel. The ultrasound probe was then turned 90 °C to obtain a short-axis view of the femur. Move or align the probe in the cephalad-caudal direction until the target of the same depth as the long-axis view is obtained. It is important that the probe should not be tilted but aligned in cephalad-caudal direction. When the appropriate depth was found, the same fascia expansion (***) could be located. (Reprinted with permission from Philip Peng Educational Series)

joint. With this position, a fascia expansion is commonly seen between diaphysis and epiphysis, and this is the target for the RFA (Fig. 27.11 upper right panel). The scan can be optimized by moving in an anterior-posterior direction. Measure the depth of the target (Fig. 27.11 upper left panel).

Scan 2

Rotate the probe 90 °C to obtain a short-axis view of the femur (Fig. 27.11 lower left panel). Align the probe in the cephalad-caudal direction without tilting to obtain the target at the same depth as in the long-axis scan (Fig. 27.11 lower right panel).

Inferomedial Articular Branches

Scan 1

For inferomedial quadrant, the best starting point for scan is to scan over the medial joint line. Then slide the ultrasound probe in the caudal direction until the metaphysis is seen (Fig. 27.12). Optimize the scan until the medial collateral ligament and

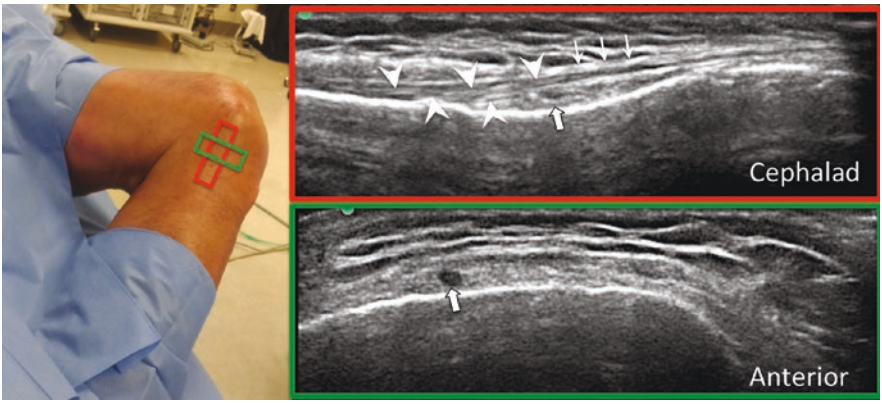

Fig. 27.12 Left panel. The two positions of the ultrasound probe just distal to the epiphysis of the tibia. Right upper panel in red rectangle. The ultrasound probe was in the long axis of the tibia. The inferior medial genicular nerve (IMGN) and vessel (bold arrow) are deep to the medial collateral ligament (arrowheads), which is deep to the crural fascia (arrows). Mark the depth of the bone hyperechoic shadow deep to the IMGN. Right lower panel in green rectangle. The ultrasound was rotated 90 °C and aligned in the cephalad-caudal direction so that the hyperechoic bone shadow is at the same depth as the previous scan. The neurovascular bundle (bold arrow) was seen again. (Reprinted with permission from Philip Peng Educational Series)

the neurovascular bundle of the inferior medial genicular nerve (IMGN) are seen (Fig. 27.12 right upper panel). Mark the depth of the bone hyperechoic shadow deep to the IMGN.

Scan 2

Rotate the ultrasound probe 90 °C and adjust the depth of the bone shadow by aligning the probe in cephalad-caudal direction (Fig. 27.12 lower panel). The same neurovascular bundle can be identified.

Superolateral Articular Branches

The patient is asked to turn away from the side of the procedure so that the lateral aspect of the thigh can be approached. The scanning technique will be the same as for the superomedial articular branches.

Procedure

Diagnostic Block

- Needle: 22G 3.5-inch needle for the superomedial and superolateral articular branches, 25G 1.5-inch for the inferomedial articular branches
- Drug: 2 mL 0.25% bupivacaine for the superomedial and superolateral articular branches, 1 mL for the inferomedial articular branches

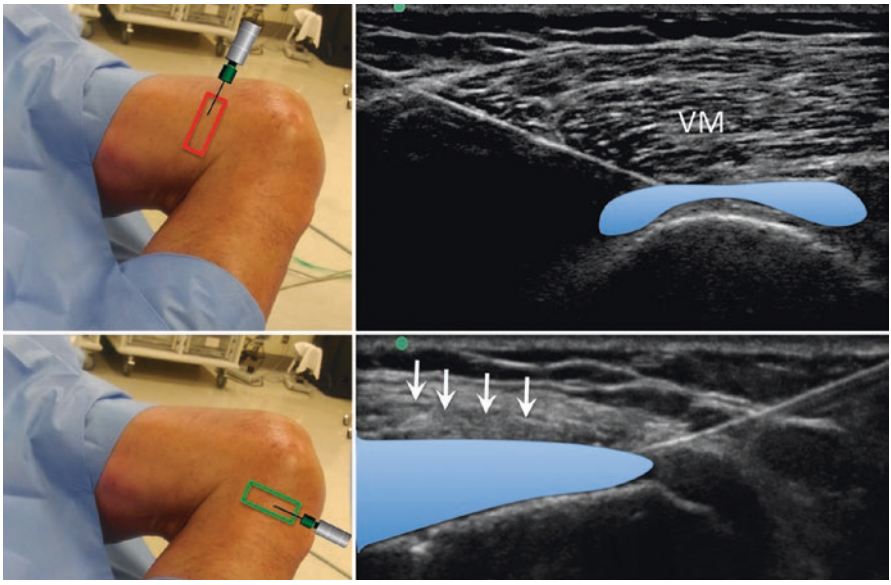

Fig. 27.13 Upper panel. The needle was inserted in-plane from anterior to posterior direction to the fascia expansion deep to the vastus medialis (VM). The injectate was shown in blue color. Lower panel. The needle was inserted in-plane from anterior to posterior direction to the fascia expansion deep to the medial collateral ligament (arrows). The injectate was shown in blue color. (Reprinted with permission from Philip Peng Educational Series)

The basic scan technique for all three diagnostic blocks is to put the ultrasound probe in the short axis to the femur or tibia (Fig. 27.13). Therefore, the needle is inserted in-plane from anterior to posterior direction. The trajectory of the needle is similar to the fluoroscopy-guided knee genicular branch injection.

A few important points are highlighted here. First, the author suggests a "90-degree rule." What this means is that the ultrasound probe is placed in the same alignment as it is for lateral X-ray. The probe will only be aligned or glided without tilting or rotating. The rationale behind is simple. This maneuver will allow the clinician to predict the final position of the needle tip reliably when one crosses reference the needle position with fluoroscopy. Second, our innervation study clearly showed the consistent presence of the medial and lateral branches of nerve to vastus intermedius in the anteromedial and anterolateral position of the fascia expansion. Since the needle insertion is from anterior to posterior, the author prefers the tip of the needle to be slightly anterior to the midline. Third, ultrasound allows the clinician to appreciate the fascia expansion which is a surrogate marker of the articular branches and their genicular arteries. For fluoroscopy-guided technique, the landmark is fixed at the metaphysis. As shown in Fig. 27.9, there are variations in the location of the articular branches. Ultrasound allows the clinician to appreciate the location of the genicular branches and their vessels by revealing the fascia expansion and arterial pulsation (Fig. 27.14). This may lead to a different location for the needle target.

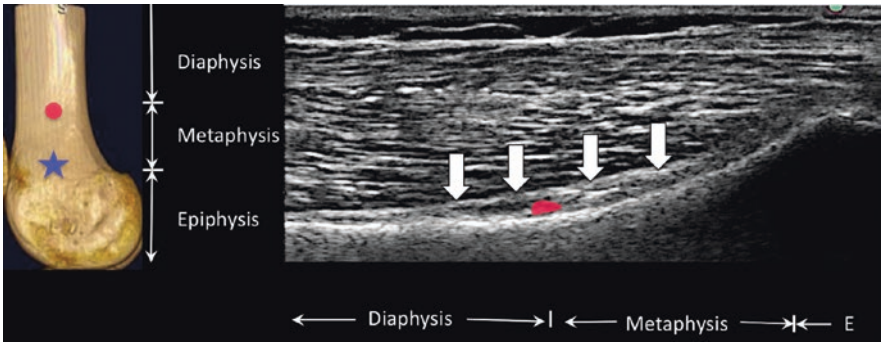

Fig. 27.14 The left panel showed the target for the fluoroscopy-guided injection (star). However, the ultrasound showed the fascia expansion (bold arrows) and the vessel at a more proximal location (red dot in the left panel). The red spot in the right panel is not a sign of Doppler but was artificially added to show the vessel, which was seen in the video. E, epiphysis. (Reprinted with permission from Philip Peng Educational Series)

Radiofrequency Ablation

- Needle: system providing large or palisade or strip lesion
- For example, cooled RF needle 17G 50–100 mm length, 4 mm active tip; RF needle providing bipolar lesion, e.g.,Trident 18G 50–100 mm with 5 m active tip.

1. *Superomedial and superolateral articular branches*

If a single needle is placed (cooled RF system), the location is guided by the thickest part of the fascia expansion in the midpoint of the femur in the anterior-posterior dimension. If a cooled RF system is not used, the author suggests a bipolar or even tripolar palisade lesion on the superomedial side, as most of the osteoarthritis pathology is on the medial tibiofemoral compartment (Fig. 27.15). The needles are inserted in-plane from anterior to posterior direction using the scanning technique described above with no more than 1 cm apart.

2. *Inferomedial articular branches*

The target size is small, and a single needle (whether it is cooled RF system or multi-tined system) is usually sufficient. Using the scan technique described above, the needle is inserted in-plane from anterior to posterior.

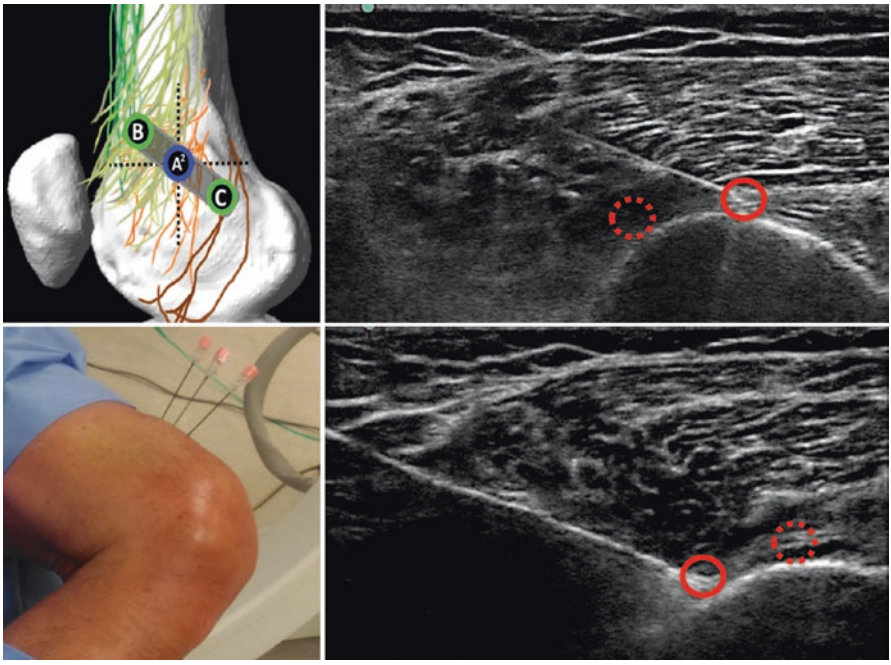

Fig. 27.15 Multiple needle insertion for the superomedial quadrant. If three needles are planned for insertion, the first needle is placed at the midpoint of the femur (position A in the left upper panel and solid red circle in the right upper panel). A second needle is placed in a slight cephalad and anterior position (position B in the left upper panel and solid red circle in the right lower panel). The left lower panel showed the arrangement of the three needles. (Reprinted with permission from Philip Peng Educational Series)

Clinical Pearls

1. When performing the RFA procedures, pay attention to the coronal plane of the femur and the handling of the probe with alignment only without tilting and rotating is important. This will give a very precise placement of the needle tip.
2. Prepping of the patient for RFA is important. The author suggests prepping the patient on both sides with extra drapes to avoid contamination of the field when one turns the patient for the superolateral procedure.

Literature Review

Since the publication of the RFA of "genicular nerves of knee" by Choi et al., there was an emerging interest in the RFA technique of the knee. In 2016, a review of the

radiofrequency procedures for chronic knee pain was published, and at that time there were 13 publications including the only 1 true randomized controlled trial (RCT) by Choi et al. All publications reported significant analgesia but follow-up period varied. Approximately half of those publications employed the use of RFA to the periarticular nerves, and pulsed RF procedures were used for others, including periarticular nerves and intra-articular targets. Since then, more publications were seen in the literature including another large multicenter RCT and a large prospective case series with 1-year follow-up.

Three studies will be discussed in details.

Choi et al. published the first RCT. Following a positive diagnostic block, 38 patients were randomized to receive RF "genicular neurotomy" under fluoroscopy guidance. The targets were periosteal areas connecting the shaft and both femoral condyles for the superomedial and superolateral areas and the shaft and medial tibial epicondyle for the inferomedial area. Their technique was widely adopted in the subsequent literature. Their RF system was conventional RF and maximum temperature was only 70 °C. The average body mass index (BMI) of their population was 26. The result was impressive with a significant reduction of the visual analogue score (VAS) up to 12 weeks which was their final assessment. Ten participants achieved >50% pain relief at 12 weeks, while none in the control group achieved this outcome. They used the Oxford Knee Score for functional outcome assessment, and the treatment group also achieved significant functional improvement for 12 weeks.

Davis et al. conducted a larger RCT recruiting 151 patients from 6 centers in the United States. The average BMI was 30, and they used cooled RF system adopting the same targets as in Choi study. The control group is intra-articular steroid (IAS). At the sixth month, 58 and 68 patients from cooled RFA and IAS group were completed for follow-up. The number of patients with complete relief was 13 vs. 3 in the treatment and control group, respectively. The percentages of patients with >50% relief were 74% vs. 16%. They used Oxford Knee Score and the treatment group also had a significant functional improvement over the control group at 6 months.

The third study that is noteworthy to discuss here is a single-center prospective study with 1-year long-term follow-up. There were only 25 patients in this study, but the percentages of patients with >50% pain relief were 88%, 64%, and 32% at 1, 6, and 12 months. The 6-month analgesia outcome is comparable with the US multicenter study, but this study showed that the analgesic benefit faded over time. Another interesting feature in this article was that they used ultrasound as their imaging modality for needle placement, contrast to the two articles discussed above.

Suggested Reading

Allen KD, Golightly YM. Epidemiology of osteoarthritis: state of the evidence. Curr Opin Rheumatol. 2015;27:276–83.

Bhatia A, Peng P, Cohen S. Radiofrequency procedures to relieve chronic knee pain: an evidence-based narrative review. Reg Anesth Pain Med. 2016;41:501–10.

Bhatia A, Hoydonckx Y, Peng P, Cohen S. Radiofrequency procedures to relieve chronic hip pain: an evidence- based narrative review. Reg Anesth Pain Med. 2018;43:72–83.

Choi WJ, Hwang SJ, Song JG, et al. Radiofrequency treatment relieves chronic knee osteoarthritis pain: a double-blind randomized controlled trial. Pain. 2011;152:481–7.

Cross M, et al. The global burden of hip and knee osteoarthritis: estimates from the Global Burden of Disease 2010 study. Ann Rheum Dis. 2014;73(7):1323–30.

Davis T, Loudermilk E, DePalma M. Prospective, multicenter, randomized, crossover clinical trial comparing the safety and effectiveness of cooled radiofrequency ablation with corticosteroid injection in the management of knee pain from osteoarthritis. Reg Anesth Pain Med. 2018;43:84–91.

Gerhardt M, Johnson K, Atkinson R, et al. Characterisation and classification of the neural anatomy in the human hip joint. Hip Int. 2012;22:75–81.

Giron-Arango L, Peng P, Chin KJ, Brull R, Perlas A. Pericapsular Nerve Group (PENG) block for hip fracture: a brief technical report. Reg Anesth Pain Med. 2018 Epub ahead of print.

Kapural L, Jolly S, Mantoan J, Badhey H, Ptacek T. Cooled radiofrequency neurotomy of the articular sensory branches of the obturator and femoral nerves – combined approach using fluoroscopy and ultrasound guidance: technical report, and observational study on safety and efficacy. Pain Physician. 2018;21:279–84.

Nelson AE, et al. A systematic review of recommendations and guidelines for the management of osteoarthritis: The Chronic Osteoarthritis Management Initiative of the U.S. Bone and Joint Initiative. Semin Arthritis Rheum. 2014;43(6):701–12.

Santana Pineda MM, Van linthout LE, Moreno Martin A, et al. Analgesic effect and functional improvement caused by radiofrequency treatment of genicular nerves in patients with advanced osteoarthritis of the knee until 1 year following treatment. Reg Anesth Pain Med. 2017;42:62–8.

Short AJ, Barnett JJG, Gofeld M, Baig E, Lam K, Agur AMR, Peng PWH. Anatomic study of innervation of the anterior hip capsule: implication for image guided intervention. Reg Anesth Pain Med. 2018;43:186–92.

Tran J, Peng P, Lam K, Baig E, Agur A, Gofeld M. Anatomical study of the innervation of anterior knee joint capsule: implication for image-guided intervention. Reg Anesth Pain Med. 2018;43:407–14.

Tran J, Peng PWH, Gofeld M, Chan V, Agur AMR. Anatomical study of the innervation of posterior knee joint capsule: implication for image-guided intervention. Reg Anesth Pain Med. (In press).

Index

P. Peng et al. (eds.), *Ultrasound for Interventional Pain Management*,
https://doi.org/10.1007/978-3-030-18371-4